Scuola Universitaria Superiore IUSS Pavia

Performance-Based Seismic Assessment and Retrofit of Existing RC Frame Buildings in Italy

A Thesis Submitted in Partial Fulfilment of the Requirements
for the Degree of Doctor of Philosophy in

EARTHQUAKE ENGINEERING AND ENGINEERING SEISMOLOGY

Obtained in the framework of the Doctoral Programme in
Understanding and Managing Extremes

by

Gerard J. O'Reilly

December, 2016

Scuola Universitaria Superiore IUSS Pavia

Performance-Based Seismic Assessment and Retrofit of Existing RC Frame Buildings in Italy

A Thesis Submitted in Partial Fulfilment of the Requirements
for the Degree of Doctor of Philosophy in

EARTHQUAKE ENGINEERING AND ENGINEERING SEISMOLOGY

Obtained in the framework of the Doctoral Programme in
Understanding and Managing Extremes

by

Gerard J. O'Reilly

Supervisor:
Prof. Timothy J. Sullivan – University of Canterbury, New Zealand

December, 2016

ABSTRACT

In recent decades, the seismic assessment of existing buildings has significantly developed from traditional objectives that have focused on ensuring life safety of the building. The economic impact of the 1994 Northridge earthquake in the US due to the extensive damage suffered by buildings, in addition to the overall disruption, highlighted the need for a paradigm shift in the way in which the performance of buildings ought to be defined. The performance of buildings during recent earthquakes in Italy have also emphasised this point where to this day, the city of L'Aquila remains in the process of recovery following the damage induced during the earthquake of 2009, with initial damage from the Rieti earthquake in 2016 showing a similar, if not greater, amount of damage. Such repercussions have highlighted the need for a more comprehensive deliberation of building performance during seismic assessment. Such a methodology that not only considers the life safety of the building occupants during extreme events but also appraises the potential economic consequences of the damage inflicted on the building's structural and non-structural elements during more frequent events has been developed into what is known as the PEER PBEE methodology. Through this methodology, the performance of buildings can be defined in terms of more meaningful metrics, such as direct economic losses, that can be better understood by a wider audience instead of quantifying the performance through a parlance of demand-capacity checks and verifications mostly familiar to seismic engineers.

This thesis focuses on the assessment of existing Italian reinforced concrete (RC) frame buildings with masonry infill, which were typically gravity load designed (GLD) prior to the introduction of seismic design provisions in the 1970's. The assessment of such GLD RC frames with masonry infill is discussed within a setting similar to that of the FEMA P58 guidelines which aim to provide practising engineers with the tools and procedures, both advanced and simplified, to quantify the performance of existing buildings in a more meaningful way that can be easily conveyed to decision makers. This is applied for these GLD building typologies through the calibration of a numerical modelling procedure in OpenSees to not only account for the non-linearity of the vulnerable components of the structure but also to account for the strength and stiffness degradation so as to appropriately represent the non-linear behaviour and collapse capacity of the building. Additional tools to perform building-specific loss assessment are outlined, where further developments with regard to the proper handling of torsional response, amongst other issues, in the damage and subsequent loss estimation steps of the PEER PBEE are discussed and implemented into a MATLAB based tool.

Using the numerical modelling approach calibrated to the available experimental test data collected from the literature, the uncertainty associated with the various modelling parameters is quantified via an extensive numerical study. This is done to quantify the propagation of this uncertainty in the modelling of the various structural elements to the overall dispersion of the demand parameters used in damage assessment, in addition to its impact on the collapse fragility function of such buildings. Using these results, empirical values of modelling uncertainty to be used in the assessment of GLD RC frames with masonry infill are quantified. Comparing these empirical values to those available in the literature, it is seen how the fundamental behaviour of the GLD frames differs to the extent that default values available in guidelines such as FEMA P58 cannot be reasonably adopted. Building on this study, extensive numerical analysis is carried out on a variety of case study buildings to quantify and benchmark the performance of such buildings, both in terms of expected demand and overall collapse capacity, where the impact of incorporating the potential shear failure in column members can result in a reduction of up to 20% of the median collapse intensity due to the interaction with the masonry infill, a failure mechanism that has been highlighted during past earthquakes in Italy. Furthermore, loss estimation studies are carried out on these case study buildings to not only quantify the expected losses but also investigate ways in which shrewd retrofitting can have maximum impact on the overall performance of the buildings. It is shown that when collapse safety of the existing structure is not an issue, as may be the case in areas of low to moderate seismicity in Italy, the performance defined in terms of expected annual loss (EAL) can be effectively reduced through astute retrofitting of the most vulnerable non-structural elements. On the contrary, adopting structural retrofitting schemes involving strengthening and/or stiffening of the structure in compliance with NTC 2008 requirements in these situations may actually lead to a worsening of the building performance defined in terms of EAL. This results due to the trade-off between reduced storey drifts and increased floor accelerations of the retrofitted frame in addition to potential increase in intensity for a given return period due to the shortening of the fundamental period. This observation was also observed in the 2016 earthquake in Ecuador, where excessive strengthening measures to existing hospital structures following the 1998 event resulted in extensive non-structural damage to hospital structures resulting in widespread loss of functionality of these essential services following the 2016 earthquake.

In light of the findings made in relation to the modelling and uncertainty in GLD frames, a new framework for the assessment of GLD RC frames with masonry infill similar to that outlined by FEMA P58 is established. This is described here as a multifaceted framework whereby the extensive approach described above can be adopted, or a more practice-oriented approach that allows simplified structural analysis in the form of displacement-based assessment (DBA) to be adopted. The results using the DBA methodology are compared to the results from refined analysis conducted here to show that although the general framework works quite well, some key ingredients to the DBA methodology are

required before a full proposal to GLD RC frames with infills can be made. Nevertheless, the framework is established whereby the median demand on the building can be computed using the completed DBA methodology in conjunction with empirical values of demand dispersion and correlation proposed as part of this study. Comparing this approach with an application to a real school building illustrated both facets of this framework outlined above, where the both the rigorous and simplified approaches are applied to illustrate how the empirical values for demand dispersion and correlations proposed here are to be adopted for such buildings. It is shown how those outlined in FEMA P58 are not representative and tend to underestimate the dispersion, overestimate the demand correlations and subsequently underestimate the expected loss and its associated variance to result in an overall underestimation of the EAL.

Lastly, the extension of the SAC/FEMA methodology for the computation of the mean annual frequency of exceedance of different limit states is investigated for the structures examined here, and it is shown that the exponent term b required in the demand-intensity relationship should not be taken as unity for GLD RC frames with infill, and instead a set of more appropriate values are proposed for use when masonry infills are present.

SOMMARIO

Nelle ultime decadi, la valutazione del comportamento sismico degli edifici è notevolmente progredita rispetto ai tradizionali obiettivi riguardanti principalmente la salvaguardia della vita. L'impatto economico e l'interruzione di attività nevralgiche a seguito dei considerevoli danni strutturali causati dal terremoto di Northridge negli Stati Uniti nel 1994 hanno evidenziato la necessità di un cambiamento nelle modalità di definizione delle prestazioni degli edifici. Le prestazioni esibite dagli edifici durante il sisma che ha colpito L'Aquila nel 2009, città ancora in fase di ricostruzione, e i report iniziali dei danni a seguito del sisma di Rieti nel 2016 hanno confermato l'esigenza di una valutazione del comportamento più ampia, non esclusivamente legata alla salvaguardia della vita degli occupanti. Questa valutazione integrata che considera anche le perdite economiche potenziali dovute al danneggiamento sia degli elementi strutturali che degli elementi non-strutturali è conosciuta come metodologia PEER PBEE. In questo modo le "performance" strutturali possono essere meglio descritte da strumenti come le perdite economiche dirette, attirando così l'interesse di un pubblico più vasto rispetto alle sole comunità di ingegneri e progettisti sismici.

Questa tesi ha come oggetto di studio la valutazione del comportamento sismico di edifici a telaio in cemento armato con tamponature di laterizio in Italia progettati esclusivamente per carichi gravatici fino all'introduzione delle prime norme antisismiche nel 1970. L'approccio allo studio di questa tipologia strutturale segue le linee guida suggerite da FEMA P58 il cui obiettivo è quello di fornire agli ingegneri progettisti, attraverso strumenti semplificati e avanzati, la possibilità di caratterizzare in maniera significativa il comportamento degli edifici e interagire in maniera più efficace con coloro che prendono decisioni. Il lavoro ha previsto la calibrazione di modelli numerici in OpenSees di questi telai, considerando non solo la non-linearità degli elementi critici della struttura ma anche la perdita progressiva di capacità e rigidezza caratterizzanti il comportamento a collasso di questa tipologia strutturale. Ulteriori strumenti necessari ad un'adeguata valutazione delle perdite sono stati indagati e implementati in una MATLAB routine, come le implicazioni legate alla risposta torsionale delle strutture per esempio.

Un dettagliato studio su questi modelli numerici, calibrati attraverso le prove sperimentali disponibili in letteratura, è stato condotto per poter quantificare l'incertezza legata ai vari parametri di modellazione. É stato possibile in questo modo considerare l'effetto di tale incertezza sulla dispersione globale della domanda e l'impatto sulle funzioni di fragilità a

collasso di questi edifici. Valori empirici di incertezza legata alla modellazione sono stati proposti per telai di calcestruzzo armato con tamponature. Comparando i risultati ottenuti è stato possibile osservare come i parametri proposti da FEMA P58 non possono essere utilizzati per la tipologia strutturale oggetto di studio. Le analisi realizzate su un numero di modelli tale da caratterizzare pienamente la risposta di questa tipologia strutturale in termini sia di domanda attesa che di capacità ultima, hanno evidenziato come considerare il potenziale collasso a taglio sui pilastri, dovuto all'interazione con la tamponatura, porta a una riduzione del 20% dell'intensità mediana a collasso. Il lavoro ha previsto inoltre non solo il calcolo delle perdite attese per le tipologie di edifici analizzati ma anche l'impatto positivo su perdite attese e performance strutturali legato ad efficaci interventi di miglioramento sismico. Si è evidenziato infatti, quando la sicurezza, in zone di bassa o moderata sismicità in Italia, le risposta in termini di EAL può essere notevolmente ridotta attraverso abili strategie di adeguamento sismico dei più vulnerabili elementi non strutturali. Al contrario si è evidenziato come strategie basate sull'irrigidimento e l'incremento della capacità ultima secondo le disposizioni NTC 2008 possano condurre ad un peggioramento della risposta strutturale in termini di EAL. Ciò è legato alla relazione fra ridotto spostamento interpiano e incremento dell'accelerazione di piano stessa delle strutture adeguate oltre al potenziale incremento dell'intensità di misura considerata dato un particolare periodo di ritorno e secondo l'intensità di misura considerata. Questo è stato confermato dalle osservazioni post-sisma seguenti l'evento verificatosi in Ecuador nel 2016, dove ospedali che avevano subito interventi di adeguamento basati sull'incremento di rigidezza e capacità ultima hanno evidenziato estesi danni a componenti non strutturali e ad apparecchiature cruciali inficiando la funzionalità e l'agibilità delle strutture stesse immediatamente dopo il sisma.

Il lavoro si inserisce nell'ambito delle metodologie di valutazione sismica proposte da FEMA P58, dove metodologie di analisi dettagliate descritte precedentemente sono affiancate a metodologie semplificate che non richiedono analisi numeriche come il DBA. La metodologia DBA è stata confrontata con metodologie di analisi avanzate per mostrare come, nonostante il metodo sembri funzionare abbastanza bene, ulteriori elementi debbano essere investigati prima di formulare una proposta finale di DBA per questa tipologia di edifici. In ogni caso lo studio svolto consente di calcolare la domanda mediana sull'edificio attraverso la metodologia DBA e la dispersione legata a tale domanda oltre che la correlazione fra i vari EDP attraverso ulteriori approfondimenti contenuti nella tesi. Il confronto tra metodologie di approccio avanzate e DBA applicate ad un edificio reale adibito a scuola ha mostrato come i valori empirici di dispersione proposti e la correlazione fra i vari parametri di domanda possono rappresentare in maniera soddisfacente la risposta di questi edifici. I valori proposti da FEMA P58 non possono essere considerati soddisfacenti in quanto sottostimano la dispersione della domanda, sovrastimano la correlazione fra i parametri di domanda sottostimando conseguentemente le perdite attese e la loro variabilità.

Infine la metodologia SAC/FEMA per il calcolo della la probabilità media annua di superamento di differenti stati limite, è stata sviluppata per questa tipologia strutturale, mostrando come il termine in potenza b nella relazione domanda-intensità, tipicamente assunto uguale a 1.0, non è rappresentativo di questa tipologia di telai. Valori più appropriati di b sono stati identificati per telai con tamponature.

ACKNOWLEDGEMENTS

There are many people to whom I owe a sincere thank you following the completion of this thesis, the first of whom is Tim Sullivan. I would like to express my immense gratitude to Tim for all he has done and helped me with throughout these past three years in Pavia. His advice and experience on many aspects of research, whether they be our initial adventures in steel EBF design or more recent work in existing RC structures, he has always been available to offer practical advice and insightful input.

The funding provided by the IUSS doctoral programme scholarship is gratefully acknowledged. The funding provided by the ReLUIS consortium in addition to the support provided by the CGIAM that contributed to the development of different aspects of this thesis is also gratefully acknowledged. I would also like to thank my two reviewers, Prof. Dimitrios Vamvatisikos and Prof. Luca Landi, for taking the time to review my thesis.

I would like to acknowledge the help and advice from Matteo Moratti who indirectly contributed to many aspects of this thesis during our numerous discussions at Studio Calvi and during our travels to different school buildings throughout Italy. I would also like to thank both André Filiatrault and Ricardo Monteiro for their help and advice during our time together working on Progetto Scuole.

The past three years have been probably one of the best experiences of my life to date. I have made close friends with people from every corner of the earth, learnt much about Italy and the world in general and above all about myself. It was a big decision to move here back in 2013 and luckily I can now say that it was the best decision I have ever made.

The first of these different groups of people is of course the "buffoon squad", composed of myself, David Welch, Rodolfo Danesi and Ricardo Roldán. The time spent with these lads was always great craic (an Irish word, nothing to do with narcotics!). To Dave, we did it man. We had some of the roughest days/nights of our lives in late October 2016 to get the thesis in on time, but we finally did it! There have been many unforgettable moments over the years, interrailing during the summer of 2014 is sure up there but one I will always remember are those nights down in Bitter Bar quoting Pulp Fiction. To Rody, we had a few unforgettable times in Italy, from the trip to Como to having the most budget ski trip ever in Barzio, but the one that will always make me smile is when I, an Irishman, during a game of football pulled off a "Maradona turn" and subsequently nutmegged you, an Argentine. I didn't score, though. To Ricky, what a great guy, it was because of you that I

learned that Costa Rica was a country in Central America and not some mythical, tropical paradise – although the more I learn it sure seems to be. Your performances at the WCEE in Lisbon are stuff of legend and you have been without a doubt been a great friend to have made. Pura vida, mae!

This leads to me another group to thank – the "DBD Squad", consisting of Dave and Ricky from above, Matt Fox, Cecilia Nievas and of course Tim Sullivan. There were some good times during our tea-time meetings at the EUCENTRE but my best memory will always be when we, a bunch of misfit foreigners, trounced the all-Italian Masonry team 7-3 in an interdepartmental 5-a-side game. The Italians are still making their excuses to this day, but have yet to request a rematch.

Another memory during my time in Pavia will, of course, be the days spent working at Car College, in the so-called CC. A lot of faces have come and gone over the years but more recently, a few notable ones have appeared and their support during the last few months is greatly acknowledged. From the zingers of Thanasis Papadopoulos to keep you on your toes or the email forwards of Julia Harrer to keep a smile on your face, there was never a dull day.

To all the lads from back home in Ireland, who are forever keeping my battery worn out from all the Whatsapp group messages, especially the CG lads James Corcoran, Richard Hession and Patrick Cullen. Who'd have thought back in our days as young lads playing hurling with Pat Duddy in Bawnmore I'd end up living in Italy. I certainly didn't.

To Pat Healy, who gave me an appreciation and understanding of both physics and mathematics during my years in St. Mary's College in Galway. What I learned from you during those days back in science block at Mary's initially led me down this path and has undoubtedly gotten me as far as I have today.

To the lads from NUIG – Kevin Flynn, Dan Coakley and Colm Kennelly, in particular, who are always great craic to see when I'm home.

To Mariamalia Rodríguez, who is always a delight with her tica positivity and outlook on life. She is one of the dearest friends to have and her support throughout these years is wholeheartedly acknowledged.

And of course, there are the countless friends I have made in Pavia over these past years who have made my time an absolute blast: Stefania Gatti, Antonella Pepe, Silvia Gabrieli, Antonio Castiello, Elena Canepari, Bibitz, Chicco, Barbara Ferma and of course, Umberto Tomassetti. I have had the time of my life here in Pavia with you all and you have even made me feel pseudo-Pavese – pheega! Between those nights on the steps of the Duomo,

evenings having aperitivo, feste di collegio or nights out at 50/60's night dancing in Portopeo, it has always been great fun.

I would be locked out of my apartment tonight if I didn't have a special mention for Umberto, who has not only been a great housemate to have over the past two years but also a great friend. I have to thank him for many things, his friendship first of all, teaching me about cooking real food (che sarebbe cibo Italiano, anzi Abruzzese) being another and also for teaching me Italian to the point where I have a strange Irish-Abruzzese accent.

Last but not least are my family back in Ireland. I have missed you all during the past three years. To my sister Paula and new brother-in-law Ger, my brothers Aidan, Conor and David and above all else to my Mam and Dad, Maura and Gerry, who have been there with me all the way. I finally made it and hope I have made you all proud.

Gerard J. O'Reilly

Pavia, Italy

December 2016

TABLE OF CONTENTS

LIST OF FIGURES

LIST OF TABLES

NOMENCLATURE

LIST OF ABBREVIATIONS

ASCE	= American Society of Civil Engineers
CLHS	= Correlation-Reduced Latin Hypercube Sampling
COM	= Centre of Mass
DBA	= Displacement-Based Assessment
DBD	= Displacement-Based Design
DBLE	= Displacement-Based Loss Estimation
DDBD	= Direct Displacement-Based Design
DOF	= Degree of Freedom
DS	= Damage State
DV	= Decision Variable
EAL	= Expected Annual Loss
EBF	= Eccentrically Braced Frame
EC8	= Eurocode 8
EDP	= Engineering Demand Parameter
EVD	= Equivalent Viscous Damping
FBD	= Force-Based Design
FEMA	= Federal Emergency Management Agency
GCCM	= General Crack Component Method
GLD	= Gravity-Load Designed
GM	= Ground Motion

IDA = Incremental Dynamic Analysis

IM = Intensity Measure

INGV = Istituto Nazionale di Geofisica e Vulcanologia

IP = In-Plane

LHS = Latin Hypercube Sampling

LS = Limit State

MAF = Mean Annual Frequency

MCE = Maximum Considered Earthquake

MCS = Monte Carlo Simulation

MCFT = Modified Compression Field Theory

MDOF = Multi Degree of Freedom

MSA = Multiple Stripe Analysis

NRHA = Non-Linear Response History Analysis

NTC = Norme Tecniche per le Costruzioni

OOP = Out-of-Plane

PACT = Performance Assessment Calculation Tool

PBEE = Performance-Based Earthquake Engineering

PEER = Pacific Earthquake Engineering Research Center

PFA = Peak Floor Acceleration

PGA = Peak Ground Acceleration

PSD = Peak Storey Drift

PSHA = Probabilistic Seismic Hazard Analysis

RC = Reinforced Concrete

ReLUIS = Rete dei Laboratori Universitari di Ingegneria Sismica

RV = Random Variable

TOMS = Tool for More Refined Seismic Loss Estimation

SDOF = Single Degree of Freedom

SEOAC = Structural Engineering Association of California

SLE = Serviceability Limit States (Stati Limite di Esercizio)

SLU = Ultimate Limit States (Stati Limite Ultimi)

SLO = Operational Limit State (Stato Limite di Operatività)

SLD = Damage Control Limit State (Stato Limite di Danno)

SLV = Life-Safety Limit-Sate (Stato Limite di salvaguardia della Vita)

SLC = Collapse Prevention (Stato Limit di prevenzione del Collasso)

SPO = Static Pushover

SRSS = Square Root Sum of the Squares

SS = Strong single – strong masonry infill modelled using single diagonal struts

SD = Strong double – strong masonry infill modelled using double diagonal struts

WS = Weak single – weak masonry infill modelled using single diagonal struts

WD = Weak double – weak masonry infill modelled using double diagonal struts

LIST OF SYMBOLS

Chapter 1

EAL = Expected annual loss

E[L] = Expected value of direct loss

P[A | B] = Probability of A given B

λ = Mean annual frequency of exceedance

Chapter 2

b = Section width

h = Section height

ν = Axial load ratio

M = Bending Moment

ϕ = Section curvature

ø = Bar diameter

ρ = Reinforcement ratio

ε = Strain

L_p = Plastic hinge length

d_{bL} = Longitudinal bar diameter

L_s = Shear span

f_{yL} = Yield strength of longitudinal reinforcement

θ_i = Ultimate chord rotation

f_c' = Concrete characteristic compressive strength

ϕ_u = Ultimate section curvature

μ_ϕ = Ultimate curvature ductility

K_{pp} = Post peak stiffness

a_{pp} = Post peak stiffness ratio

G = Elastic shear modulus

A_g = Gross section area

f_{cr} = Tensile cracking strength of concrete

N = Axial load

f_{yV} = Yield strength of shear reinforcement

s = Stirrup spacing

d = Depth to reinforcing bars in tension

d' = Depth to reinforcing bars in compression

θ = Shear crack angle

E_s = Steel elastic modulus

E_c = Concrete elastic modulus

γ = Joint shear deformation

$\varkappa$ = Joint shear strength coefficient

b_w = Equivalent masonry infill strut width

d_w = Equivalent masonry infill strut length

Chapter 3

λ = Mean annual frequency of exceedance

$E[A]$ = Expected value of A

$P[A|B]$ = Conditional probability of A given B

N_C = Number of damageable components

N_{DS} = Number of damage states

N_{EDP} = Number of EDPs

N_{LVL} = Number of levels

h_b = Beam height

L_b = Bay width

θ = Storey drift

X = Raw input demand data

Y = Natural logarithm of X

σ_Y = Variance of Y

Σ_{YY} = Covariance of Y

M_Y = Mean of Y

ρ_{YY} =Correlation of Y

Z = Sampled values of Y

Σ_{ZZ} = Covariance of Z

σ_Z = Variance of Z

β_{DU} = Modelling uncertainty in demand

Chapter 4

R_c = Median collapse intensity reduction factor

$\beta_{TOT,IM}$ = Total dispersion with respect to intensity

$\beta_{RC,IM}$ = Record-to-record variability with respect to intensity

$\beta_{UC,IM}$ = Modelling uncertainty with respect to intensity

$\beta_{D,\theta}$ = Total dispersion in peak storey drift demand

$\beta_{D,a}$ = Total dispersion in peak floor acceleration demand

$\beta_{DR,\theta}$ = Record-to-record variability in peak storey drift demand

$\beta_{DU,\theta}$ = Modelling uncertainty in peak storey drift demand

$\beta_{DR,a}$ = Record-to-record variability in peak floor acceleration demand

$\beta_{DU,a}$ = Modelling uncertainty in peak floor acceleration demand

Chapter 5

a = Maximum peak floor acceleration

A_c = Column area

b = Section width

h = Section height

$\widehat{IM}$ = Median intensity measure

N = Axial Force

s = Stirrup spacing

M = Bending moment

$P[C]$ = Probability of collapse

R_c = Median collapse intensity reduction factor

$S_a(T)$ = 5% damped spectral acceleration at a period T

$S_{a,2500yrs}$ = Spectral acceleration at 2500 year return period at condition period T^*

T = Period of vibration

T^* = Conditioning period

T_1 = First mode period of vibration

V_b = Base shear

$ø$ = Bar diameter

$\beta_{RC,IM}$ = Record-to-record variability with respect to intensity

$\beta_{UC,IM}$ = Modelling uncertainty with respect to intensity

$\beta_{D,\theta}$ = Total dispersion in peak storey drift demand

$\beta_{D,a}$ = Total dispersion in peak floor acceleration demand

$\beta_{DR,\theta}$ = Record-to-record variability in peak storey drift demand

$\beta_{DU,\theta}$ = Modelling uncertainty in peak storey drift demand

$\beta_{DR,a}$ = Record-to-record variability in peak floor acceleration demand

$\beta_{DU,a}$ = Modelling uncertainty in peak floor acceleration demand

Δ_{roof} = Roof displacement

θ = Maximum peak storey drift

σ = Stress

Chapter 6

$E[L]$ = Expected value of direct loss

EAL = Expected annual loss

$S_a(T)$ = 5% damped spectral acceleration at a period T

$S_{a,2500yrs}$ = Spectral acceleration at 2500 year return period at condition period T^*

T_R = Return period

T = Period of vibration

T^* = Conditioning period

T_1 = First mode period of vibration

V_{max} = Peak base shear of structure

V_y = Yield base shear of structure

θ = Maximum peak storey drift

Chapter 7

a = Demand-intensity relationship parameter

b = Demand-intensity relationship parameter

C_H = Hazard MAF adjustment factor

C_f = Response MAF adjustment factor

C_x = Confidence level MAF adjustment factor

$corr(X)$ = Correlation matrix of X

EAL = Expected annual loss

F_j = Equivalent lateral force at a level j

H_i = Elevation of floor i

H_e = Effective height of equivalent SDOF system

h_i = Height of storey i

h_c = Height of column

h_{cf} = Contraflexure height

k_0 = Second order hazard model fit parameter

k_1 = Second order hazard model fit parameter

k_2 = Second order hazard model fit parameter

K_e = Effective stiffness of equivalent SDOF system

L_b = Bay length

$M_{b,left}$ = Beam moment to the left of the joint extrapolated to the joint centre

$M_{b,right}$ = Beam moment to the right of the joint extrapolated to the joint centre

$M_{c,upper}$ = Column moment above the joint extrapolated to the joint centre

$M_{b,lower}$ = Column moment below the joint extrapolated to the joint centre

$M_{jt,i}$ = Minimum of the beam, column or joint moment capacities extrapolated to the joint centre

m_i = Mass at a floor level i

m_e = Effective mass of equivalent SDOF system

n_{fs} = Number of floors of separation

OTM = Overturning moment

P[C] = Probability of collapse

p' = Second order hazard model MAF modification factor (intensity-based)

$S_a(T)$ = 5% damped spectral acceleration at a period T

SD_i = Sway demand index of storey i

$S_{d,el}$ = Elastic spectral displacement at the effective period

S_i = Sway potential index of storey i

T = Period of vibration

T^* = Conditioning period

T_1 = First mode period of vibration

T_e = Effective period of equivalent SDOF system

V_b = Base shear at a given limit state

V_{crit} = Storey shear capacity at critical storey

$V_{i,D}$ = Storey shear demand at floor i

$V_{b,D}$ = Storey shear demand at base

$V_{i,R}$ = Storey shear resistance at floor i

$V_{b,R}$ = Storey shear resistance at base

V_0 = Base shear from governing mechanism

$V_{P\Delta}$ = Base shear adjustment to account for P-Delta effects

V_{max} = Peak base shear of structure

V_y = Yield base shear of structure

x = Confidence level

$\beta_{RC,IM}$ = Record-to-record variability with respect to intensity

$\beta_{UC,IM}$ = Modelling uncertainty with respect to intensity

$\beta_{DR,\theta}$ = Record-to-record variability in peak storey drift demand

$\beta_{DU,\theta}$ = Modelling uncertainty in peak storey drift demand

$\beta_{CR,\theta}$ = Record-to-record variability in peak storey drift capacity

$\beta_{CU,\theta}$ = Modelling uncertainty in peak storey drift capacity

$\beta_{DR,a}$ = Record-to-record variability in peak floor acceleration demand

$\beta_{DU,a}$ = Modelling uncertainty in peak floor acceleration demand

δ_i = Inter-storey displacement

Δ_{cap} = Displacement capacity of equivalent SDOF for a given limit state

Δ_i = Limit state displacement at floor level i

ε_y = Yield strain of reinforcement

η = Spectral displacement reduction factor

θ_y = Yield storey drift

λ = Mean annual frequency of exceedance

μ = Ductility

ξ = Equivalent viscous damping

ρ = Correlation coefficient between different demand parameters

$\rho_{\ln(\theta),\ln(\theta)}$ = Correlation coefficient between natural logarithm of PSD

$\rho_{\ln(a),\ln(a)}$ = Correlation coefficient between natural logarithm of PFA

$\rho_{\ln(\theta),\ln(a)}$ = Correlation coefficient between natural logarithm of PSD and PFA

ϕ' = Second order hazard model MAF modification factor (demand-based)

Chapter 8

EAL = Expected annual loss

E[L] = Expected value of direct loss

P[C] = Probability of collapse

$S_a(T)$ = 5% damped spectral acceleration at a period T

T = Period of vibration

T^* = Conditioning period

T_1 = First mode period of vibration

T_R = Return period

$t_{break\text{-}even}$ = Break-even time

V/W = Base shear coefficient

$\beta_{DR,\theta}$ = Record-to-record variability in peak storey drift demand

$\beta_{DR,a}$ = Record-to-record variability in peak floor acceleration demand

$\beta_{RC,IM}$ = Record-to-record variability with respect to intensity

1 INTRODUCTION

Significant developments have been made in the seismic assessment of existing buildings during recent decades, where traditional objectives tended to concentrate on ensuring the life safety of buildings in order to prevent loss of life. Despite the relatively limited number of lives lost, the economic losses and overall disruption caused by the 1994 Northridge earthquake in the US suggested that a more advanced approach was needed into how performance of structures should be defined. Such a change came about with the advent of the performance-based earthquake engineering (PBEE) in the latter half of the 1990's in the form of the "Vision 2000" document [SEAOC, 1995] that effectively related expected levels of building performance to different levels of earthquake intensity in order to consider not only life safety performance but also the functionality of the building as a whole, with additional consideration given to more frequent events at lower intensities. In the early 2000's, the idea of a PBEE loss assessment methodology began to emerge [Porter, 2003] that laid the foundations for what is now commonly referred to in the field as the pacific earthquake engineering research (PEER) PBEE methodology [Cornell and Krawinkler, 2000]. This approach represents a powerful methodology with which to quantify the building performance, as not only does it consider the overall life safety of the building but it also aims to quantify the damage induced in all elements of the building, both structural and non-structural. This way, the overall performance of the building can be quantified in terms of more meaningful metrics such as direct economic losses due to the cost of repairing the building, in addition to the anticipated downtime and other indirect sources of indirect loss associated with returning the building to full functionality. These performance metrics were categorised as the "3D's", which referred to death, dollars and downtime in an attempt to encompass the aspects of performance most relevant to the building owners or stakeholders. This represented a major step forward in earthquake engineering as it expresses performance in a way that is accessible to a wider audience, as opposed to quantifying the building's performance through a jargon of demand-capacity checks and verifications mostly familiar to seismic engineers.

In Italy, the overall impact of earthquakes is still quite substantial, where despite only accounting for 15.5% of the different types of natural disaster, they have been responsible for over 44% of the economic losses between the years 1990 and 2014 [Prevention Web, 2016]. This was further highlighted by the widespread damage and interruption by the more recent L'Aquila, Emilia-Romagna and more recent Rieti earthquakes in 2009, 2012 and 2016, respectively, with the damage and interruption following the Emilia-Romagna event amounting to almost 1% of the national GDP of Italy [Benvenuti, 2012]. In addition to the

economic impact of the earthquake, interruption of services and daily life have also been demonstrated to be very critical aspects, as demonstrated by the ongoing recovery of the city of L'Aquila following the 2009 event, where Jones [2016] describes the city's struggle to recover through many areas of the city as still being cordoned off. Combining this with how of the €21 billion earmarked for the reconstruction of L'Aquila, Jones [2016] notes how only approximately €7 billion of this has been spent to date citing the inefficient use of resources and many projects getting held back by administrative issues. It is clear that more resilient communities are required to better equip town and cities such as L'Aquila to recover from such earthquake events and for seismic design and assessment methodologies to focus on aspects beyond ensuring just life safety. Initial reconnaissance reports from the Rieti/Macerata/Perugia earthquake sequence at the time of writing in 2016 have illustrated further the need for more resilient communities. This aspect was touched on by Calvi *et al.* [2014] where a building classification framework was hypothesised with the intention of providing more resilient communities by limiting the annualised direct monetary losses expected from earthquake events.

The above remarks highlight how improved performance-based design and assessment methodologies are required in order to ensure more resilient communities that can not only ensure life safety during earthquake events of significant intensity but also provide adequate building performance during more moderate and frequent earthquakes. As such, this thesis focuses on the seismic assessment and retrofitting of existing reinforced concrete (RC) frame buildings with masonry infill built throughout Italy following the World War II and before the introduction of seismic design codes in the 1970's. This structural typology occupies over 30% of the building stock in Central and Southern Italy, of which over 23% was constructed during the construction boom period that followed the end of World War II and the introduction of seismic design provisions in Italy during the 1970's [ISTAT, 2011]. To illustrate the vulnerability of such structural typologies, Figure 1.1 shows the distribution of damage to RC frames following the 2009 L'Aquila earthquake, where a significant amount of heavy damage was recorded for these structures during this aforementioned construction period between 1946 and 1970.

The following sections will provide a brief overview of some of the past damage typically observed in these structures to illustrate some of the specific issues addressed in this thesis. This is followed by a brief review of the development and current state-of-the-art in performance-based assessment to give the reader an idea of some of the existing methods to be discussed in later chapters. Finally, a description of the scope of this thesis and the layout of the work is presented to set the stage for the chapters that follow.

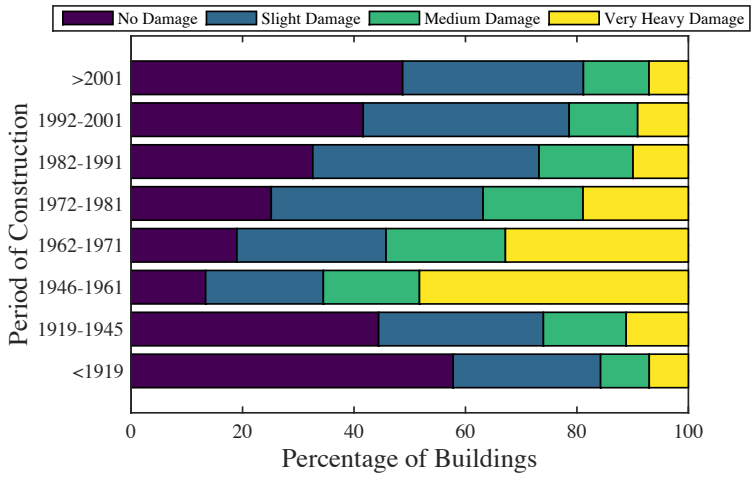

Figure 1.1. Distribution of observed damage to RC buildings following the 2009 L'Aquila earthquake disaggregated in terms of the period of construction (Adapted from Del Gaudio *et al.* [2016]).

1.1 Review of Damage to RC Frame Structures During Past Earthquakes in Italy

Upon reviewing the existing literature on the reconnaissance of recent earthquakes in Italy, several recurring observations of damage to RC frame structures constructed prior to the introduction of seismic design requirements in Italy in the 1970's are reported. These include the formation of column sway soft storey mechanisms due to a lack of capacity design, brittle shear failure in the columns due to overloading of the column by the masonry infills in addition to poor beam-column joint behaviour due to a lack of joint transverse shear reinforcement. Many of these failures can be attributed to a lack of proper seismic design and detailing due to the period in which these structures were built. Therefore, this section reports some of this observed damage to RC structures from past earthquake events in Italy. These events include the 2002 Molise earthquake, 2009 L'Aquila event, 2012 Emilia Romagna event and the more recent Rieti/Macerata/Perugia earthquake sequence from this year. Typical damage and observed mechanisms are grouped together and discussed separately to provide a general overview of the various types of damage mechanisms observed in such structures that will be the focus of much of this thesis.

1.1.1 Column Members

Among the numerous damage mechanisms reported from recent earthquake events, non-ductile response of column members was a frequently encountered observation. Modern seismic design codes require that RC frames be well detailed to ensure a ductile behaviour and to avoid non-ductile failure mechanisms. That is, beams are intended to yield in flexure

instead of a more brittle shear mechanism. This is typically prevented by providing stirrups at a certain spacing along the member such that the shear capacity is sufficiently high to ensure a shear failure is avoided and a more ductile flexural mechanism forms. Prior to the introduction of seismic provisions in Italian design codes, buildings were typically only designed for gravity loads, with no consideration of lateral seismic forces or the concept of ensuring stable and ductile lateral response. As such, many existing buildings in Italy possess column members that are susceptible to shear failure since as these were principally sized to meet axial load capacity requirements.

One of the more infamous cases of shear failure in RC frame structures in past seismic events in Italy occurred at the San Salvatore Hospital in L'Aquila. The failure of three columns (one of which is shown in Figure 1.2) along with the out-of-plane failure of masonry walls resulted in an evacuation of the hospital following the earthquake, which would have been otherwise critical in providing medical aid following the earthquake. While Augenti and Parisi [2010] note that the failure of the columns may have been due to the relatively large vertical excitation component recorded during the L'Aquila main shock, a lack of effective stirrups and poor confinement was evident and the resulting mechanism was a shear failure of the columns.

Figure 1.2. Column shear failure (left) at San Salvatore hospital in L'Aquila [Augenti and Parisi, 2010] in addition to shear cracking and rebar buckling in the column at Scuola Media G. Carducci in L'Aquila [Salvatore et al., 2009].

Salvatore *et al.* [2009] provide a summary of observed damage to six different school structures as a result of the L'Aquila earthquake. Figure 1.2 shows the shear cracking of a column member at one of these schools, the Scuola Media G. Carducci in L'Aquila. It is possible to observe the clear diagonal cracking typically associated with shear failure in

addition to buckling of one of the longitudinal reinforcement bars. The buckling of this bar indicates that the spacing between stirrups was sufficiently large to allow buckling, which also suggests that an insufficient transverse reinforcement ratio was provided to prevent the observed shear mechanism.

More recently in Emilia-Romagna during the 2012 event, further evidence of shear failures in column members was observed. Figure 1.3 shows the brittle cracking of the upper end of a column which could be as a result of the additional shear forces induced in the member from the masonry infill, which is noted to have collapsed. Ioannou *et al.* [2012] commented that the failure observed in Figure 1.3 maybe be also as a result of the relatively large spacing between transverse reinforcing bars, with these bars being closed at 90° instead of the current requirement of 135°.

Figure 1.3. Shear failure of ground floor column in Cavezzo following the Emilia Romagna, 2012 event where temporary steel columns have been placed to stabilise the building [Ioannou et al., 2012].

In addition, a number of additional shear failures have been reported that are a result of unanticipated shear forces acting on the member. Figure 1.4 shows what is typically termed the "short column effect", where a column is designed and detailed for a certain storey height, only to have a non-structural element such as an infill or parapet wall built in around it. This greatly affects the response of the column member as the effective length of the member is greatly reduced, where this reduced length implies a larger shear force for a constant flexural capacity. In addition to having large shear forces being generated in the column due to the presence of the wall, where it was not expected to be. As in the case with the shear failures observed previously, the mechanism is typically characterised by 45° cracks in the member, with the primary difference being that this failure mechanism is due to a non-structural element, whose strength and stiffness is typically ignored in design, inducing an unexpected large force into the column. Hence, the issue is not necessarily due to lack of member capacity but rather an improper consideration of the load path of the different structural and non-structural elements during design.

Figure 1.4. Short column effect on a circular column in L'Aquila [Ricci et al., 2011].

In addition to the presence of fully and partially infilled frames causing a short column effect, the presence of stairways can also cause problems. Salvatore *et al.* [2009] note that the ground floor columns at the Istituto Tecnico Commerciale L. Rendina in L'Aquila showed signs of shear cracking corresponding to the points at which the staircases were attached, which was again noted at the Scuola Media G. Carducci. This type of behaviour clearly visible from the reconnaissance report by Verderame *et al.* [2009], where Figure 1.5 shows the shear failure of a column due to the overloading by the stairway beams.

Figure 1.5. Shear failure of a column due to stairway overloading in L'Aquila [Verderame et al., 2009].

In addition to the shear damage to the column members previously highlighted, where damage was linked to either an insufficient shear capacity in the members or due to an unanticipated load path inducing large shear forces; considerable damage has been noted due to the flexural response of the column members as lack of capacity design considerations resulted in an unfavourable strong beam-weak column strength hierarchy in many buildings. Figure 1.6, for example, show the soft storey collapse of a four-storey RC frame structure.

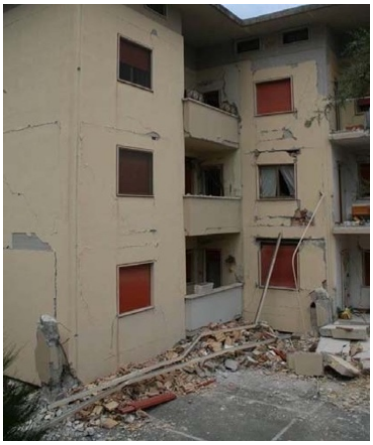

Figure 1.6. Soft storey collapse of a four-storey RC building in L'Aquila [Verderame et al., 2009].

Similarly, in Figure 1.7, a soft storey mechanism formed in the second storey of a residential structure in L'Aquila. Augenti and Parisi [2010] report how the floor completely collapsed in the building causing many fatalities. It was also observed how the columns showed very little evidence of a ductile mechanism.

Figure 1.7. Second storey collapse of a residential RC frame building in L'Aquila [Augenti and Parisi, 2010].

1.1.2 Beam-Column Joints

In addition to the poor performance of RC frame members, significant damage to beam-column joints has been observed during past earthquakes in Italy. This is typically as a result of considering the joints as rigid zones and not giving due consideration at the design stage to the forces it will need to transmit during loading. The most common shortcoming as a result of this is a lack of transverse shear reinforcement in the joint resulting in a susceptibility to concrete cracking and crushing due to a lack of the required shear reinforcement to transfer the force. Figure 1.8 shows some examples of beam-column joint failure from the L'Aquila event, where the concrete is seen to crack, spall and crush under the seismic demand. Figure 1.8(b) shows a typical example of this type of failure mechanism, where the principle tensile stress developed in the joint results in the concrete forming a diagonal crack, which is illustrated further in Figure 2.17. In addition to this, the lack of shear reinforcement in the joint can result in buckling of the longitudinal reinforcement, which is shown in Figure 1.8(a), leading to a loss of axial load carrying capacity as well as the shear capacity.

(a) Buckling of joint reinforcement.

(b) Diagonal cracking of the beam-column joint.

(c) Loss of cover concrete and a severe degradation of the concrete within the joint.

(d) Loss of cover concrete and damage to the joint.

Figure 1.8. Typical beam-column joint failure observed in L'Aquila, 2009 and Rieti, 2016 (Images (a) and (b) are adopted from Verderame et al. [2009], (c) is adopted from Bursi et al. [2009] and (d) is adopted from Celano *et al.* [2016]).

1.1.3 Masonry Infills

The use of masonry infills in RC frame structures is very common in the existing Italian building stock. Masonry infills have generally been considered non-structural elements and not considered part of the load resisting system. However, in the case of lateral loading the presence of these infills significantly modifies the behaviour of the structures through the stiffening and in turn, reducing the fundamental period of the structure. The additional

forces generated by the presence of these infills can be very problematic, such as the "short column" effect and shear failures of columns as a result of masonry infills discussed previously.

The images on the left and right of Figure 1.9 shows the cracking of a masonry infilled RC frame in Molise and Rieti. The actual damage to the infill is minor, but the surrounding plaster and painting of the structure have been affected such that it would require repair following the event. Similarly in the central image of Figure 1.9, the actual damage to the structure appears to be minimal, however, the damage to the infill walls means that such minor damage requires repair following the event. This type of damage doesn't typically affect immediate occupancy of the structure since it is not critical. However, it does mean that the time taken for the building to be restored fully is extended. In addition, the cost of repainting walls can be quite significant since the whole structure typically requires repainting, not just the affected areas.

Figure 1.9. The image on the left shows infill cracking following the event in Molise, 2002 [Decanini et al., 2004], whereas the image on the rights shows diagonal cracking observed in an apartment complex following the event in L'Aquila, 2009 [Verderame et al., 2009] and the image on the right shows the damage to the infill interface with the surrounding frame in Rieti, 2016 [Celano *et al.*, 2016].

In addition to the cracking of masonry infill, the excessive overloading in-plane of the infill can result in a number of in-plane failure modes, in addition to the out-of-plane failure of the infill. These types of failures of the masonry infills can be noted in Figure 1.10, where the infill walls of RC frame in Molise, L'Aquila and Rieti are seen to collapse out-of-plane, highlighting their importance in the assessment of older RC frames in Italy.

Figure 1.10. Infill collapse at an apartment complex (left), complete failure of infill walls at the upper floors of the San Salvatore hospital in L'Aquila, 2009 [Global Risk Miyamoto, 2009] and infill failure in Rieti, 2016 [Celano *et al.*, 2016].

Another well-known case of infill failure is that of the San Salvatore hospital in L'Aquila, which was previously mentioned. This hospital was closed following the earthquake as a result of the brittle damage observed in one of the columns, shown in Figure 1.10. In addition to the shear failure of the column, the masonry infill in the top level of the hospital completely failed and collapsed, as seen in Figure 1.10, and contributed to the decision to close the hospital following the earthquake.

1.2 REVIEW OF EXISTING PROCEDURES FOR THE SEISMIC ASSESSMENT OF RC FRAME BUILDINGS IN ITALY

The seismic assessment of buildings has been significantly developed over the past few decades, where traditional means of quantifying performance such as available strength or deformation capacity have been further developed to the point where the performance can now be described in terms of monetary losses, loss of life or downtime in what has been previously described as the "3D's" referring to deaths, dollars and downtime. This section presents a brief, but non-exhaustive, review of the procedures available for the assessment of existing buildings, where some of the earliest work is outlined to give the reader an appreciation of the developments made up to this point and background methodologies to present methodologies for the assessment of existing RC frame buildings in Italy.

The term PBEE has been used quite a lot in the field and has tended to refer to slightly different things depending on the context, but it's early origins and most basic definition are in the Structural Engineering Association of California's (SEAOC) "Vision 2000" document [SEAOC, 1995] that essentially linked expected levels of structural performance to various levels of seismic excitation, often illustrated by the performance matrix diagram and the "Joe's Bar" illustration, shown in Figure 1.11. In the early 2000's, the idea of PBEE probabilistic assessment methodology began to emerge (e.g. Porter [2003]) that laid the foundations for what is now commonly referred to as the PEER PBEE methodology. It can be argued that the general concept of PBEE is still unchanged, rather that the definition of performance was revised, where instead of speaking terms of maximum storey drift at

the maximum considered earthquake (MCE) the expected losses due to the induced damage in the building are described. Some of the developments in terms of loss estimation that were happening prior to the 2000's are examined here, leading up to the introduction of the aforementioned PEER PBEE methodology, and the subsequent development of methods since then.

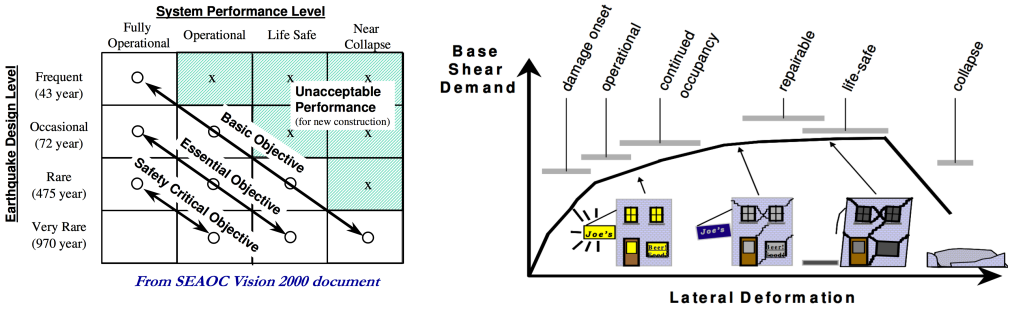

(a) PBEE Performance Matrix **(b) "Joe's Bar" Illustration of Performance**

Figure 1.11. Illustration of "Vision 2000" definition of PBEE [SEAOC, 1995].

The PhD thesis of Carlos Ramirez at Stanford University in 2009 [Ramirez and Miranda, 2009] provides a review of the developments in building-specific loss estimation and this is summarised in the following text. It was noted how one of the first building-specific loss estimation studies was performed by Scholl *et al.* [1982] who assessed the damage to a building on a component by component basis and used experimental data for elements typically found in high-rise buildings to determine the central tendency and variability of exceeding different DSs. The structural analysis was estimated using linear elastic analysis and the results were presented in terms of a mean damage factor, which was defined as the ratio of the expected repair costs from earthquake damage to the replacement value of the building. However, Ramirez and Miranda [2009] note that this approach was carried out for just a single earthquake intensity. Such an approach was further developed by Gunturi and Shah [1993] who performed non-linear response history analysis (NRHA) considering three intensities of peak ground acceleration (PGA). Although no probabilistic aspects were considered in relation to the intensity levels chosen by Gunturi and Shah [1993], it may be considered to be one of the earliest forms of the PEER PBEE loss methodology as it is known today, since the building's damageable components were separated in terms of structural and non-structural elements in addition to building contents; and the loss ratios were calculated at a number of intensities. Singhal and Kiremidjian [1996] furthered this approach by considering the influence of ground motions (GMs) by using sets of artificially

simulated records and defining the intensity of each GM set in terms of the modified Mercalli intensity scale, although no consideration of non-structural elements was included in the study. Fast forward to 2000, when Cornell and Krawinkler [2000] identified the fully probabilistic framework described in Equation 1.1 and illustrated in Figure 1.12 that would become the foundation of the PEER PBEE probabilistic assessment methodology. The general approach is described by:

$$\lambda[DV|D] = \iiint p[DV|DM, D]\, p[DM|EDP, D] p[EDP|IM, D] \lambda[IM|D] dIM dEDP dDM$$

Equation 1.1

where p[A | B] is the conditional probability of A given B, λ represents the mean annual frequency (MAF) of exceedance for the decision variable (DV), which can be defined in terms of the aforementioned performance measures, such as monetary losses, for a given structure located at site D. The performance is computed by evaluating the triple integral described by Equation 1.1 and illustrated in Figure 1.12 by computing the probability of the decision variable DV for a given level of damage (DM). This damage is determined as a function of the demand on the structure defined by its engineering demand parameter (EDP) that can be determined from analysis of a representative model of its behaviour. This structural response is then computed for a given level of ground motion intensity (IM), which is then, in turn, linked back to the MAF of exceedance using the site's hazard curve determined from probabilistic seismic hazard analysis (PSHA). Figure 1.12 outlines this procedure from start to finish, where it can be seen how the user progresses from one step to the next in order to quantify the performance of the building defined in terms of a DV such as the expected repair costs due to the induced damage in the various elements at each intensity.

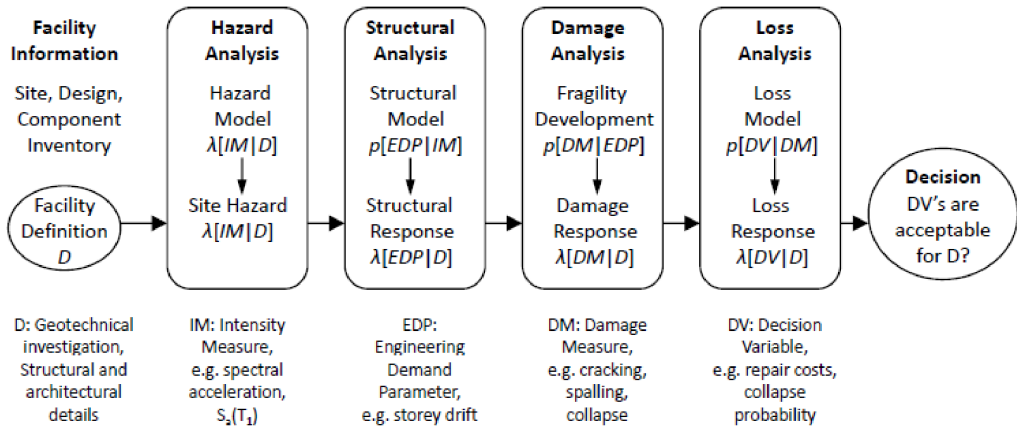

Figure 1.12. Overview of PEER PBEE assessment framework outlined by Porter and Kiremidjian [2001].

If one then considers the expected losses due to the repairs required at each intensity, the expected annual loss (EAL) of a building for a given site location can be computed by integrating the expected losses expressed as a function of intensity over the site hazard curve obtained from PSHA to give:

$$\mathrm{EAL} = \int \mathrm{E}\left[\mathrm{L_T}|\mathrm{IM}\right] \left|\frac{\mathrm{d}\lambda_{\mathrm{IM}}}{\mathrm{dIM}}\right| \mathrm{dIM} \qquad \textbf{Equation 1.2}$$

where $\mathrm{E}[\mathrm{L_T}|\mathrm{IM}]$ represents the total expected losses for a given intensity intensity measure (IM) of shaking and site D, as described above.

The framework outlined above has been the focus of much research in the US since the 2000's leading to the eventual development and publication of a number of FEMA guidelines, including FEMA P58 [FEMA P58-1, 2012], which aims to provide practising engineers with tools and procedures to quantify the performance of buildings in terms of expected loss, downtime and casualties. Numerous PhD theses have been completed in the process of developing such guidelines in order to benchmark the performance and investigate the various aspects of the assessment framework when applied to the different structural typologies typically found in California. Mitrani Reiser [2007], for example, conducted a large benchmark study to quantify the performance in terms of expected losses of newly designed RC frames in California, in addition to highlighting various aspects regarding the implementation of the methodology for such structures, whereas Ramirez and Miranda [2009] examined the incorporation of residual drifts into the framework, among other things. In addition, Haselton and Deierlein [2007] examined the collapse risk

of modern ductile buildings where the various aspects required to model such building typologies was extensively calibrated by Haselton *et al.* [2007], allowing for the modelling uncertainty and various impacts of structural modelling on the different facets of the framework to be investigated. Liel [2008] conducted a similar study to examine the collapse risk associated with older existing RC buildings with no masonry infill in California to outline and quantify the performance of such buildings designed before the introduction of seismic design codes. To summarise, numerous extensive research campaigns have been undertaken during the process of the development of the FEMA guidelines in the US for new and existing buildings in California, where the various aspects of newer and older RC frame construction have been examined both in terms of the loss assessment and collapse risk in addition to structural retrofitting to improve these.

In the context of the assessment of existing Italian buildings the current assessment code in place is the NTC 2008 [NTC, 2008], which for the most part is an adoption of Eurocode 8 [EN 1998-3:2005, 2005]. Pinto and Franchin [2014] describe how the extended use of the NTC 2008 in Italy, especially following the 2009 L'Aquila earthquake, have highlighted its inadequacy and limitations to provide consistent and unequivocal results. This has resulted in the Consiglio Nazionale delle Richerche (CNR) to produce a higher level probabilistic assessment framework in the form of the CNR-DT 212/2013 guidelines [CNR, 2014] that permit the characterisation of the building performance through the computation of the MAF of exceedance of different limit states, where different sources of uncertainty are considered in what can be considered a very broad and comprehensive document. While these guidelines undoubtedly offer a superior means with which to characterise the performance of an existing RC building in Italy with respect to NTC 2008, the framework focuses on limiting the MAF of exceedance of different limit states, which correspond to those listed in the NTC 2008 document and on limiting the annual probabilities of exceedance specified to offer similar levels of protection to those outlined in NTC 2008. However, the performance of the building is still expressed in terms of limit state performance checks whereas the use of a performance metric defined in terms of monetary losses could be argued to a more preferred route. What makes the CNR-DT 212/2013 superior with respect to NTC 2008, however, is the manner in which the MAF of exceedance of these limit states is computed as the process is probabilistic to allow proper treatment of uncertainties. Reflecting on some of the noted benefits of the PEER PBEE methodology from Section 1.1, it was noted how the expression of the performance of buildings in terms of metrics such as monetary losses was also advantageous as it means conveying the building's seismic performance in a manner that may be considered more accessible to building owners and stakeholders. Calvi *et al.* [Calvi, 2013; Calvi *et al.*, 2014] argue that by adopting an assessment framework such as that outlined in FEMA P58 to then quantify and classify the performance of a building in terms of its expected annual loss, building owners would be more motivated and incentivised to carry out retrofitting works on their property. This way, communities as a whole would benefit from the

increased resilience to not only avoid collapse during stronger earthquakes but also limit monetary losses during more frequent events and it was proposed that a mechanism to enourage action would be to consider a "seismic insurance premium" and a tax break system. Both of these recently proposed assessment frameworks for existing Italian structures are very promising in that they highlight the evolution of how building performance is to be quantified in a more probabilistic manner with appropriate consideration of the relevant sources of uncertainty. The following section highlights the scope of this thesis in relation to these in addition to identifying the layout of the following chapters with respect to this.

1.3 SCOPE AND ORGANISATION OF THESIS

In terms of the assessment of gravity load designed (GLD) RC frame buildings with masonry infill using the methodology outlined in FEMA P58, a recent study by Cardone and Perrone [2016] examined the application of these guidelines to an existing structure in southern Italy. They followed the general approach outlined in the FEMA P58 guidelines, whereby any of the empirical values required were adopted as per the guidelines to highlight the applicability to the case study building examined. It should be noted that while studies such as these are encouraging, as it demonstrates the desire among the Italian research community to employ more advanced methods of seismic assessment, it should be recalled that numerous PhD theses work of research went into the development and quantification of different aspects of the methodology to produce the FEMA P58 guidelines in their present form. Considering this, the focus of this thesis is to examine the assessment of existing GLD RC frames in Italy through the extensive characterisation of their performance in addition to exploring various ways with which it can be improved. In addition to the discussion of extensive numerical analysis, more simplified methods of assessment are explored with respect to the structural typologies considered. This is to not only highlight the applicability of such methods within the GLD RC frame context but also to propose novel considerations and required empirical demand dispersion and correlation quantification currently unavailable for such building typologies. As such, this thesis is organised as follows:

- Chapter 2 discusses the numerical modelling of GLD RC frame buildings with masonry infill, where an extensive literature review of existing experimental data is carried out to characterise the behaviour of the various structural elements specific to these frame typologies, such as beam-column frame members with limited ductility capacity, weak beam-column joints and masonry infills. Using this experimental data, a comprehensive calibration of these different structural elements is conducted to characterise not only the general strength and stiffness but also the degradation necessary to properly capture the ultimate limit states of the various member's behaviour required in collapse assessment. This numerical

modelling will not only provide an experimentally calibrated modelling approach with which analyses in future chapters will be conducted, but also valuable information regarding the dispersion in the various modelling parameters such that this uncertainty can be incorporated into the performance-based assessment of the GLD RC frames examined here.

- Chapter 3 explores the development of a software tool developed in MATLAB in order to conduct a full loss estimation of a single case study building. The development of this tool is discussed alongside the various pertaining aspects it considers with regards to the assessment of existing buildings. This tool is used to conduct the loss estimation of the case study buildings examined in later chapters such that the various points regarding the assessment of GLD RC frames can be made. In addition, numerous aspects with regard to the seismic assessment of structures in general are discussed to illustrate some of the implications of more refined considerations of structural response and damage assessment when conducting loss estimation of irregular and torsionally sensitive buildings. This numerical tool discussed here is developed with these in mind to allow for more refined assessment of buildings in the future.
- Chapter 4 discusses the incorporation of modelling uncertainty into the performance-based assessment of GLD RC frames with masonry infill. This chapter utilises the data provided from the numerical calibration in Chapter 2 in order to quantify the effects of modelling uncertainty on not only the various demand parameters used in loss estimation but the collapse performance. This quantification study is then synthesised to produce a set of empirical dispersion coefficients that can be used to account for the effects of modelling uncertainty when assessing the various structural typologies outlined here at the various limit states.
- Chapter 5 examines the response characterisation of a number of case study GLD frames buildings with masonry infill, where a variety of modelling assumptions regarding the incorporation of masonry infill and the potential shear failure in the column members are explored. Extensive incremental dynamic analysis (IDA) is conducted on a variety of case study building to not only characterise the median response with respect to intensity but also the record-to-record variability and demand parameter correlations, which are later used in Chapter 7 to propose empirical values for more simplified assessment approaches. The influence of the various modelling decisions is also highlighted throughout, whereby the relative impacts on the performance of the building defined in terms of limit state exceedance and collapse are outlined. The applicability of a more simplified method of collapse assessment with the SPO2IDA tool available in the literature and incorporated into FEMA P58 is also examined.
- Chapter 6 conducts an extensive loss estimation study of the case study frames examined in Chapter 5, whereby assuming an inventory of damageable elements

the expected loss with respect to intensity is computed to characterise the different trends in direct economic loss for the various modelling variations examined. Considering both the collapse safety and performance of the structure defined in terms of EAL, different retrofitting strategies are conducted to investigate the possibility of using non-structural retrofitting as an effective strategy to improve the overall performance for cases where the collapse safety of the existing building is satisfactory. Finally, a comparison between the expected loss ratio curves with the fragility functions for the NTC 2008 limit states derived in Chapter 5 is conducted where the expected loss ratios and overall damage accumulated at each of the limit states can be computed compared with respect to qualitative descriptions provided in the codes.

- Chapter 7 provides a synthesis of the work presented in the previous chapters, where more simplified methods are investigated using the extensive analysis conducted in the previous chapters. This comparison utilises the results of the extensive IDA conducted in Chapter 5 to validate the use of a more simplified assessment methodology in displacement-based assessment (DBA) to estimate building response. The use of this simplified method of structural assessment is then expanded to loss estimation where the use of DBA to estimate median demands in conjunction with the various empirical values of demand dispersion and correlation quantified in Chapters 4 and 5 can be used along with the assessment tool outlined in Chapter 3 to provide a simpler and more direct way of estimating the EAL computed for the case study buildings examined in Chapter 6. In addition, further consideration is given to the closed form expressions initially proposed by Cornell *et al.* [2002] to estimate the MAF of exceedance of different limit states so as to calibrate and validate some of the assumptions required by this method when applied to GLD RC frames.
- Chapter 8 presents an application of the different aspects of the previous chapters where the assessment framework described in Chapter 7 is applied to evaluate the buildings performance and demonstrate how this may be improved via retrofitting. In addition, the simplified assessment procedure outlined in Chapter 7, along with the empirical values for demand dispersion and correlation are examined with respect to the existing values outlined in FEMA P58, is applied to the school building and compared to the results of the more rigorous analysis procedure to provide a concluding illustration and validation of much of the work carried out in this thesis with regards the assessment of GLD RC frames with masonry infills.

Overall, the work presented here is aimed to give the reader a full understanding of the various aspects involved in the assessment of GLD RC frames with masonry infill, whereby using the numerous quantifications, calibrations and general considerations outlined in this study, the assessment approach outlined in FEMA P58 can be adopted with a degree of

confidence that the numerical modelling approach in addition to the quantification of empirical values to be used in more simplifying methods and assumptions are representative of the structural typologies examined.

2 NUMERICAL MODELLING OF GLD RC FRAME MEMBERS IN ITALY

O'Reilly, G. J., Sullivan, T. J. [2017] "Modelling Techniques for Seismic Assessment of Existing Italian RC Frame Structures," *Journal of Earthquake Engineering* (Under Preparation).

2.1 INTRODUCTION

The behaviour of existing RC structures in Italy and across the Mediterranean area has been the focus of much research over the past number of years. In Italy, prior to the introduction of seismic design provisions in the 1970's, structural design was largely based on the Royal Decree [Regio Decreto, 1939] published in 1939. This document provided a basis for structural design in Italy for the best part of 30 years, during which a large amount of RC frame structures were built during the reconstruction following World War II. Regarding the actual detailing rules prescribed, allowable stress values were used in design and smooth reinforcing bars anchored with end-hooks in the beam-column joints were also quite common, with the beam-column joint region typically being void of transverse reinforcement. In particular, the complete lack of seismic design provisions among the Italian building stock constructed during this period has led to a large amount of existing RC frame structures being quite vulnerable to excessive damage under seismic loading. Subsequent experimental work and observations from past earthquakes in Italy have highlighted these problems in RC frame structures, resulting in the widespread damage discussed in Chapter 1.

Current methods of seismic assessment look toward evaluating the probability of damage among the damageable components with a view to providing means to determine a retrofitting strategy such that the socio-economic losses can be mitigated. To conduct such analyses and determine the various components with a high probability of damage, in addition to the associated repair costs, a number of analysis tools are necessary that best represent the expected behaviour of such structures. The various components of GLD RC frames constructed prior to the 1970's have been experimentally demonstrated to exhibit not only poor behaviour but also undesirable global response mechanisms. Therefore, analysis tools developed and calibrated for modern, seismically-detailed structures are no longer valid for assessment. As such, this chapter aims to bridge this gap in the structural analysis of older RC frames in Italy by collecting available experimental test data to both calibrate and validate numerical models that represent the behaviour of the various

elements, such as beam-column frame elements and joints. In addition to the frame elements, the interaction of masonry infills is also discussed such that the local shear effects on the adjacent columns can be accounted for, which has been discussed in Chapter 1 to be a major cause of structural damage in these types of structures. Existing work in this field is discussed and developed to provide a comprehensive guide to how one would go about constructing a numerical model of an RC frame with masonry infills, such that a more comprehensive seismic performance assessment of existing RC frame structures in Italy can be carried out in later chapters.

2.2 BEAM-COLUMN MEMBERS

To model the behaviour of RC frame members, it is important to accurately represent the behaviour of the beams and columns constructed with older design practices such as the use of smooth bars, low concrete grade and inadequate shear reinforcement. This section describes the modelling of these types of elements, where the existing experimental data available in the literature is discussed to highlight the behaviour typically observed.

2.2.1 Experimental Testing on Beam-Column Members

The behaviour of the beam-column members with smooth reinforcement differs to that of deformed bars due to the poor bond strength between the bar and the concrete paste resulting in a more pinched hysteretic behaviour. A number of experimental test campaigns have been conducted on beam-column members with smooth bars to establish their hysteretic behaviour. For example, Verderame *et al.* [2008a; b] conducted both monotonic and cyclic testing on a number of RC beam-columns with smooth reinforcing bars and bar lapping just above the column base. In general, they were found to give satisfactory behaviour in terms of their deformation capacity, although it was noted that this comes from a concentration in end-rotation along a few cracks resulting in a localised deformation as opposed to a larger spread in plasticity along the member plastic hinge zone that is typical of members with deformed bars. The overall hysteretic dissipation of the specimens is noticeably more pinched due to the presence of smooth bars than is typically expected with deformed bars, with Verderame *et al.* [2008b] noting that as the axial force increases on the members, this pinching effect is less pronounced implying that a higher axial force is beneficial for energy dissipation. Verderame *et al.* [2008b] also compare the ultimate chord rotation capacity observed in the tests and the predicted capacity using the expression in Eurocode 8 [EN 1998-3:2005, 2005] that defines the ultimate chord rotation corresponding to a 20% loss in load carrying capacity. Modifications to the expression given in Eurocode 8 have been proposed with the intention of accounting for the lack of seismic detailing and the use of smooth bars. Comparing the Eurocode 8 values with the observed experimental ones, the expression in Eurocode 8 tends to underestimate the ultimate chord rotations of the members due to additional deformation associated with smooth bars, especially in the case of the columns with a low axial load ratio. Subsequently, Verderame *et al.* [2010]

conducted a review of the various parameters used by the Eurocode 8 expression to evaluate ultimate chord rotation capacity while accounting for old member detailing. Using experimental data provided by Verderame *et al.* [2008a; b] and Di Ludovico *et al.* [2013], Verderame *et al.* [2010] assessed and proposed a modification to the existing expressions provided by the 2009 edition of Eurocode 8 [EN 1998-3:2009, 2009] to account for the use of smooth bars with lapping as a result of more recent experimental test data. In terms of using smooth bars, experimental tests carried out on similar specimens with both smooth and deformed bars by Di Ludovico *et al.* [2013] showed an increase in the ultimate deformation capacity of RC beam-columns with smooth bars by a factor of about 1.4 when compared to the corresponding deformed bar specimens. This was noted as a result of the increased rigid end rotation. This is contrary to the initial proposal within Eurocode 8, which had initially looked to reduce the ultimate rotation capacity of the member due to the presence of smooth bars, whereas experimental evidence has shown the contrary.

Lap splicing has been long recognised to be an undesirable feature within the expected plastic hinge zone with Priestley *et al.* [1996], among others, noting that these are to be avoided in the plastic hinge zones as they tend to break down under cyclic inelastic action when poorly confined. Comparison between specimens both with and without lap splicing in the plastic hinge zone by Verderame *et al.* [2008b] noted how their presence tended to concentrate the damage more so than that of the members with continuous bars. In terms of its effect on the inelastic cyclic behaviour and ductility capacity, Verderame *et al.* [2010] proposed a modification factor for the determination of the ultimate chord rotation capacity to take into account the presence of bar lapping, whereby lap-splices with a lap-length of at least 50 times the bar diameter were implied to be the same as continuous bars. A further study by Melo *et al.* [2015] proposed of a more refined correction factor calibrated from 48 tests specimen results to estimate the ultimate chord rotation capacity. In addition, Melo *et al.* [2015] conducted a number of tests on RC columns with smooth bars and lap-splicing in the plastic hinge zones. Similar to Verderame *et al.* [2008a], Melo *et al.* [2015] concluded that the presence of smooth bars resulted in a reduction of energy dissipation and a more pinched hysteretic behaviour, where columns with large cross-sections tended to suffer more pinching than smaller cross-sections. Observations regarding the spread of plasticity in specimens with smooth bars are also reported to be noticeably more concentrated than the corresponding deformed bar specimens. Lap-splicing in the specimens tested was also noted by Melo *et al.* [2015] to decrease the energy dissipation capacity of the member and result in a concentration of damage in the member ends.

2.2.2 Numerical Modelling of Beam-Column Members

As previously highlighted, these members typically possess smooth reinforcing bars and lap splices that result in a pinched hysteretic response of the member. Figure 2.1 outlines the proposed numerical modelling approach for these members where a lumped plasticity

element is used to represent the flexural behaviour, whereas an uncoupled shear hinge is introduced to capture the shear behaviour of the member. The member essentially functions as a classical lumped plasticity member, but with an additional hinge definition that allows for a shear mechanism to form. This is particularly important in the case of Italian construction as the interaction of RC frames with masonry infills has resulted in many cases of short column shear failures in past earthquakes, as discussed in Chapter 1. Section 2.2.2.1 discusses the determination of the parameters required to determine the flexural behaviour of the member, while Section 2.2.2.2 discusses the incorporation of a shear hinge into this element.

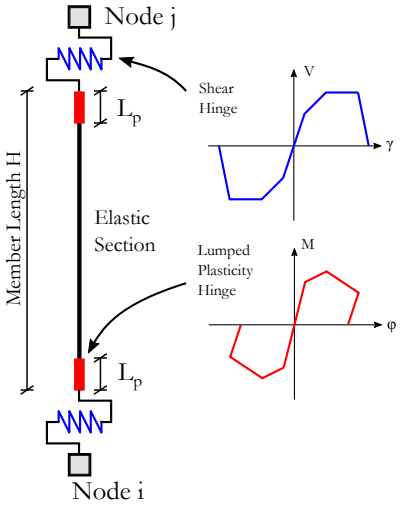

Figure 2.1. Proposed beam-column element modelling that consists of a lumped hinge beam-column element to describe the flexural behaviour of the member together in series with an aggregated shear hinge that allows for the uncoupled shear response of the member to be accounted for.

2.2.2.1 Flexural Behaviour

This section will describe the various parameters required to determine the flexural behaviour of a poorly detailed beam-column member to be used with a lumped plasticity element. The available experimental test data in the literature has been collected and is summarised in Table 2.1. From each of the tests, the results are used to validate the approach described herein to determine the hysteretic backbone associated with older RC members. A lumped plasticity approach to representing the behaviour up to collapse is preferred as a fibre-based approach has been judged by Haselton *et al.* [2008] to unsuitable to capture the effects of bar buckling and fracture. It is intended that this section will provide an adequate description of the various parameters such that a user can construct a numerical model, similar to what has been carried out by Haselton *et al.* [2008] for members

with ductile member detailing. It is noted that Haselton *et al.* [2008] considered a large test database of up to 500 test specimens that allowed for investigation into the effects of different parameters and therefore proposal of the various predictive equations with multiple variables to account for their influence. However, the amount of available test data for specimens with smooth bars and poor confinement typical of older Italian structures is very limited. Therefore, such elaborate predictive equations cannot be reasonably developed until more test data becomes available. The approach of this section is to review existing approaches and provide a series of simple expressions that can predict the backbone behaviour of members with smooth bars reasonably well. By providing simple predictive expressions, assessment of existing structures can be performed even when relatively little information regarding cross-sectional detailing is available. This is typically the case when performing an assessment on buildings constructed over 40 years ago where detailed technical information regarding the buildings structural design details and reinforcement content is often limited and sometimes not available at all.[1]

As highlighted in Figure 2.1, the flexural model consists of a lumped plasticity element with an internal elastic section assigned cracked section stiffness properties. Such an element, therefore, requires the definition of a moment-curvature relationship and a plastic hinge length to represent the lumped hinges. Figure 2.2 shows the basic definition of the hysteretic rule adopted here, which is obtained by using the Pinching4 material model[2] provided in OpenSees [McKenna *et al.*, 2000]. The following text will describe the determination of the various parameters associated with the hysteretic rule illustrated for members with smooth bars, where available test data in Table 2.1 will be used to justify the model definition. To quantify the accuracy of the various expressions discussed, the error will be presented through the use of the logarithmic standard deviation, or dispersion, of the ratio between the experimental and predicted values of the various terms. Following this approach to quantify the variance, a lognormal distribution is inherently assumed similar to Haselton *et al.* [2008] for ductile members with deformed bars. This statistical information then forms the basis of the modelling uncertainty study carried out in Chapter

[1] This was witnessed first-hand by the author when as part of a national project to assess Italian schools across Italy. Detailed structural information for each school structure was seldom available with architectural drawings illustrating position and geometry of members often being the only available information. Any information regarding material strength and reinforcement content of the members was available as a result of more recent in-situ investigations. A similar note was made by Pinto & Franchin [2014] during and illustrative example of an older RC frame building in southern Italy.

[2] http://opensees.berkeley.edu/wiki/index.php/Pinching4_Material

4, which examines the impact of modelling uncertainty on the response parameters of GLD frames.

Table 2.1. Experimental database of 23 test specimens collected from the literature for beam-column members with smooth bars and lapping typical of pre-1970 Italian RC frame construction.

#	Reference	ID	b x h [cm]	ν	ρ_{TOP}	ρ_{BOT}	ρ_{SHR}	Loading	Lapping
1	Verderame et al. [2008]	C-270A1	30x30	0.12	0.43%	0.43%	0.34%	Cyclic	40Ø
2	Verderame et al. [2008]	C-270A2	30x30	0.12	0.43%	0.43%	0.34%	Cyclic	40Ø
3	Verderame et al. [2008]	C-270B1	30x30	0.12	0.43%	0.43%	0.34%	Cyclic	Continuous
4	Verderame et al. [2008]	C-540A1	30x30	0.24	0.43%	0.43%	0.34%	Cyclic	40Ø
5	Verderame et al. [2008]	C-540B1	30x30	0.24	0.43%	0.43%	0.34%	Cyclic	Continuous
6	Verderame et al. [2008]	C-540B2	30x30	0.24	0.43%	0.43%	0.34%	Cyclic	Continuous
7	Melo et al. [2015]	CPA-1	30x30	0.16	0.43%	0.43%	0.17%	Cyclic	Continuous
8	Melo et al. [2015]	CPA-3	30x30	0.19	0.43%	0.43%	0.17%	Cyclic	Continuous
9	Melo et al. [2015]	CPB	30x30	0.17	0.43%	0.43%	0.17%	Cyclic	30Ø
10	Melo et al. [2015]	CPC	30x30	0.20	0.57%	0.57%	0.17%	Cyclic	Continuous
11	Melo et al. [2015]	CPD	30x30	0.19	0.57%	0.57%	0.17%	Cyclic	30Ø
12	Melo et al. [2015]	CPE	30x40	0.14	0.31%	0.31%	0.17%	Cyclic	Continuous
13	Melo et al. [2015]	CPF	30x50	0.11	0.32%	0.32%	0.17%	Cyclic	Continuous
14	Verderame et al. [2008]	M-270A1	30x30	0.12	0.43%	0.43%	0.34%	Monotonic	40Ø
15	Verderame et al. [2008]	M-270A2	30x30	0.12	0.43%	0.43%	0.34%	Monotonic	40Ø
16	Verderame et al. [2008]	M-270B1	30x30	0.12	0.43%	0.43%	0.34%	Monotonic	Continuous
17	Verderame et al. [2008]	M-270B2	30x30	0.12	0.43%	0.43%	0.34%	Monotonic	Continuous
18	Verderame et al. [2008]	M-540A1	30x30	0.24	0.43%	0.43%	0.34%	Monotonic	40Ø
19	Verderame et al. [2008]	M-540B1	30x30	0.24	0.43%	0.43%	0.34%	Monotonic	Continuous
20	Di Ludovico et al. [2012]	S300P-m	30x30	0.20	0.43%	0.43%	0.22%	Monotonic	Continuous
21	Di Ludovico et al. [2012]	S300P-c	30x30	0.20	0.43%	0.43%	0.22%	Cyclic	Continuous
22	Di Ludovico et al. [2012]	R300p-c	50x30	0.10	0.43%	0.43%	0.13%	Cyclic	Continuous
23	Di Ludovico et al. [2012]	R500p-c	30x50	0.10	0.24%	0.24%	0.22%	Cyclic	Continuous

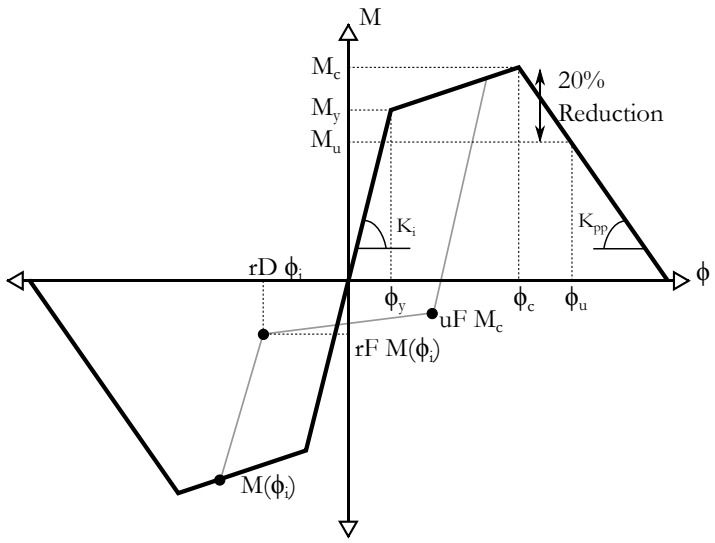

Figure 2.2. Proposed moment-curvature relationship for beam-column plastic hinge zone, where the behaviour is idealised with an initial elastic stiffness to the yield point, followed by plastic deformation to the capping point with a subsequent in-cycle stiffness degradation to represent the loss in strength and stiffness of the member.

The yield curvature of the section can be determined either from moment-curvature analysis or from the simplified expression given in Priestley *et al.* [2007] for RC members as:

$$\phi_y = \frac{2.1\epsilon_y}{h} \qquad \textbf{Equation 2.1}$$

where ε_y is the yield strain of the reinforcement and h is the section height. To find the nominal yield moment, sectional analysis is performed at the yield curvature given above to find the corresponding bending moment. It should be noted that the term yield moment (M_y) is used here to indicate the point at which the bilinear definition of the response enters the plastic region, which is termed nominal moment capacity (M_N) in Priestley *et al.* [2007]. For the section analysis, a parabolic concrete material model is assumed and the reinforcing steel is idealised as elastic perfectly plastic, as described in Collins and Mitchell [1991]. Comparing the computed yield curvatures and corresponding bending moments to those observed in the test specimens listed in Table 2.1, the 1 to 1 plot of the predictions are shown in Figure 2.3 and Figure 2.4. A degree of scatter can be observed in the data in both cases, however, a good match is observed to the point where the above approach is deemed appropriate for use in RC members with smooth bars. This approach neglects any influence of bar-slip on the moment capacity discussed by Calvi *et al.* [2002b] as a lack of experimental

observation of the behaviour is absent to properly quantify its effect in addition to uncertainty regarding appropriate bond condition parameters.

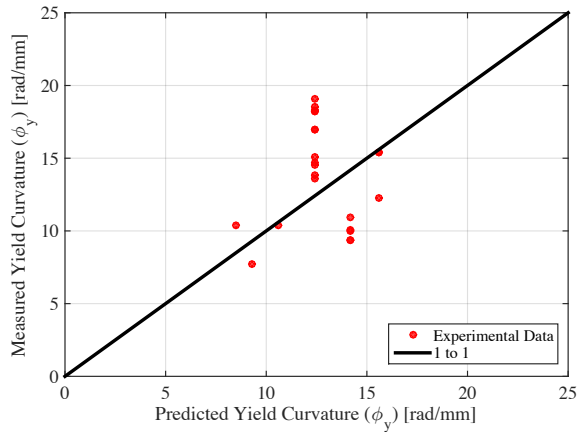

Figure 2.3. Comparison of the measured yield curvature from a total of 23 experimental test specimens to that predicted using Equation 2.1, with a dispersion of 0.287.

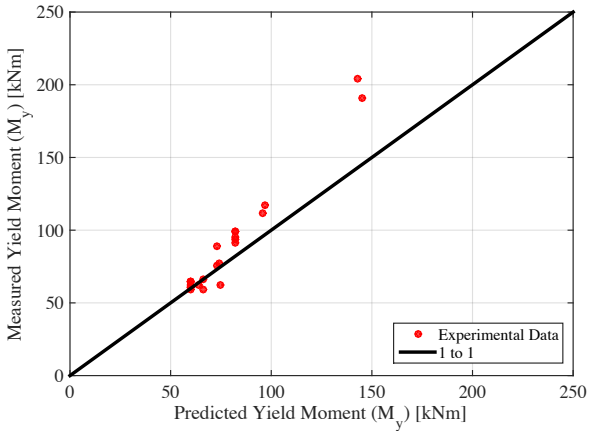

Figure 2.4. Comparison of the measured yield bending moment from a total of 23 experimental test specimens to that predicted using sectional analysis, with a dispersion of 0.122.

Regarding the capping moment (M_c), this term has been discussed in Haselton *et al.* [2008] to be slightly correlated to the axial load ratio of the member, but plotting the ratio of observed capping to yield moment of the available data in Figure 2.5, no such trend is obvious here. In addition, Haselton *et al.* [2008] provide a more simplified form of the

equation, where the ratio is simply set to 1.13. Considering that no real trend with axial load is observed for the members examined here, it is simply proposed to take the median value of all the values to give:

$$\frac{M_c}{M_y} = 1.077 \qquad \textbf{Equation 2.2}$$

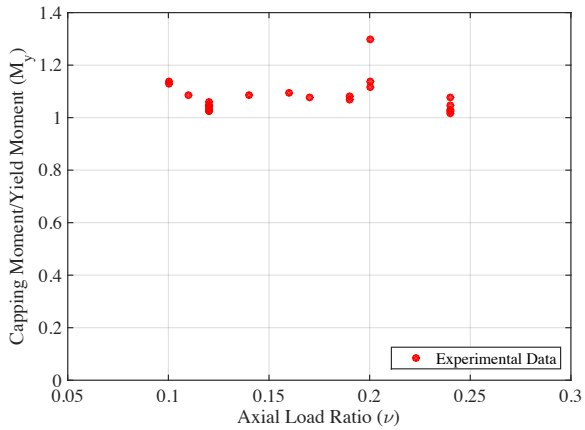

Figure 2.5. Capping to yield moment ratio versus axial load ratio from a total of 23 experimental test specimens, where the ratio remains relatively constant with a median of 1.077 and a dispersion of 0.053.

In addition to knowing the moment-curvature relationship of the RC member, the model is shown in Figure 2.1 requires the definition of a plastic hinge length (L_p). The expression proposed in Paulay and Priestley [1992] is used here and is given by:

$$L_p = 0.08L_s + 0.022f_{yL}d_{bL} \qquad \textbf{Equation 2.3}$$

where L_s is the shear span and d_{bL} is the longitudinal bar diameter. It should be noted that this expression was developed for members with deformed bars and ductile detailing, hence its applicability to members with smooth bars warrants further discussion. Considering some of the general observations from the test specimens used here, it was noted in most cases members with smooth bars tend to form few but large flexural cracks in the plastic hinge zone. This was specifically highlighted by Di Ludovico *et al.* [2013] where a direct comparison between members with deformed and smooth bar specimens showed how deformed bar specimens produced many small cracks in the plastic hinge zone, which allowed the plasticity to spread along the member ends. The corresponding smooth bar specimen, however, was reported to have developed fewer but larger cracks in the member

ends, somewhat restricting the spread of plasticity. This above observation would suggest that the above expression for plastic hinge length is not appropriate for RC members with smooth bars. However, experimental testing on an RC beam member by Melo *et al.* [2011] measured plastic hinge lengths for a beam specimen that gave a good match when compared to the above expression from Paulay and Priestley [1992], which suggests it may actually be valid here also. However, a general lack of reported plastic hinge lengths from other specimens makes it difficult to propose or validate any alternative expression and since no alternative exists, the above expression is adopted, noting that it appeared to give representative values in the specimens tested by Melo *et al.* [2011]. The overall effect of this assumption is not expected to be significant, as the experimentally measured chord rotation is converted to a "pseudo" section curvature via an assumed plastic hinge length and then back to a chord rotation in the numerical model via the same assumed plastic hinge length. This is merely a consequence of the beam formulation requiring a plastic hinge length to be specified.

Since many of the specimens tested in Europe tend to define the ultimate section curvature or chord rotation as the point at which the lateral load capacity has dropped by 20% from its maximum, a third point corresponding to this definition has been highlighted in the descending branch of the backbone curve shown in Figure 2.2. As the point corresponds to a 20% loss from the maximum moment, its value is already known, leaving just the plastic curvature component to that point to be computed. As previously discussed in Section 2.2.1, Verderame *et al.* [2010] considered the use of the Eurocode 8 expressions to compute the ultimate chord rotation capacity of RC members with smooth bars and lap-splices. A modification was proposed by Verderame *et al.* [2010] to account for bar lapping but no adjustment was made to the original expression, despite experimental evidence by Di Ludovico *et al.* [2013] suggesting that the plastic chord rotation capacity of members with smooth bars was slightly larger than that of a member with deformed bars. This was again seen in the test observations presented in Verderame *et al.* [2008b] where by comparing the observed chord rotation at the ultimate moment to that of the Eurocode 8 prediction, it was shown how the code expression gave quite conservative estimates of the actual capacity. This can be seen in the case of the specimens collected here in Figure 2.6, where a plot of the observed ultimate chord rotation to the adjusted expression by Verderame *et al.* [2010] shows that this expression is quite conservative, with a median ratio of measured to predicted of 1.58 and a dispersion of 0.284. This has been subsequently noted by Melo *et al.* [2015], who proposed a further correction to the Eurocode 8 formula to account for the increased ultimate chord rotation of members with smooth bars, and how this correction gives a better estimate of the ultimate chord rotation from Figure 2.6 with a median ratio of measured to predicted of 1.11 and a dispersion of 0.268, which still slightly conservative. This relation is described in Melo *et al.* [2015] to be:

$$\theta_u = 0.016(0.3)^{\nu}\left(\frac{\max\left(0.01,\omega'\right)}{\max(0.01,\omega)}f_c'\right)^{0.225}\left(\min\left(\frac{L_s}{h},9\right)\right)^{0.35}25^{\left(\frac{\alpha\rho_v f_{yv}}{f_c'}\right)}\ldots$$
$$\ldots\times 1.25^{(100\rho_d)}\left(1.72-0.055\nu^{0.5}f_c'L_s^{0.667}\right)$$

Equation 2.4

While the above approaches rely on a more empirical approach to computing the ultimate chord rotation, a more mechanics-based approach is also investigated here where the ultimate chord rotation is computed using strain-based limit states and the corresponding curvatures and chord rotations are thus found. The strain limit states defined in Crowley *et al.* [2006] are adopted here, where the minimum curvature corresponding to the concrete and reinforcing steel strains at the extensive damage limit state are used. These correspond to concrete compressive strain range of ε_c=0.005-0.01 and reinforcing steel tensile strain of ε_s=0.015-0.03, respectively and the plastic hinge length was as before. Figure 2.6 shows the comparison of the ultimate chord rotation predicted using this mechanics-based approach and those observed from testing, where again the prediction is actually quite conservative with a median ratio of measured to predicted of 1.41 and a dispersion of 0.274, which is again quite conservative.

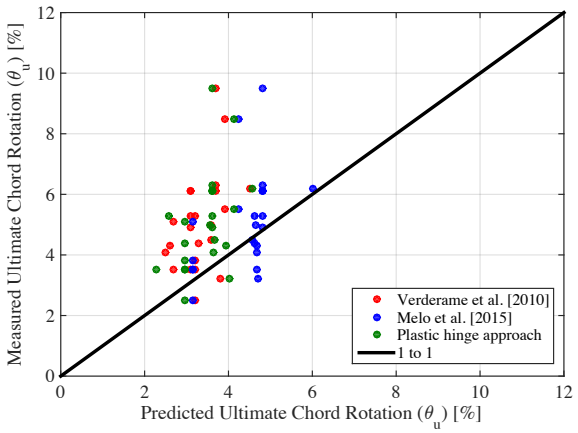

Figure 2.6. Measured ultimate chord rotation capacity versus predictions from a total of 23 experimental test specimens using empirical approaches by Verderame *et al.* [2010], Melo *et al.* [2015] and also a mechanics-based plastic hinge approach. The resulting median ratios of measured-to-predicted are 1.58, 1.11 and 1.41, respectively, while the corresponding dispersions are 0.284, 0.268 and 0.274.

Since the objective of this study is to assess the non-linear behaviour of RC members and not to conduct chord rotation validation checks, an adequate representation of the plastic curvature capacity at the ultimate moment is required; hence the proposal by Melo *et al.* [2015] is adopted since it gives the best estimate of ultimate chord rotation of all of the approaches considered here. In addition, if one considers the curvature ductility, defined as the ultimate curvature (ϕ_u) divided by the yield curvature (ϕ_y), and plots this against the axial load ratio, as shown in Figure 2.7, it is clear that there is a trend of decreasing ductility with increasing axial load ratio in the experimental data shown in black, which was noted in some test campaigns. The curvature ductility predicted by the other approaches has also been plotted in Figure 2.7 along with the median trend line with respect to the axial load ratio. While predictive expressions, such as Equation 2.4, tend to describe the plastic capacity as a function of many terms as large data sets were available for calibration, although such a large data set is not available here to examine the influence of variables such as reinforcement ratios and material strength. In the interest of providing a simple but reasonably accurate values, a simplified relation depending on axial load ratio can be proposed by performing a least-squares regression fit to the data presented in Table 2.2 and plotted in Figure 2.7 to give:

$$\mu_\phi = 22.7 - 47.4\nu \qquad \textbf{Equation 2.5}$$

which is represented by the black line in Figure 2.7. As expected, there is a degree of scatter in the experimental data, although when compared to the predictions provided by the modified expression by Verderame *et al.* [2010] or the mechanics-based plastic hinge approach outlined earlier, the proposed relation in Equation 2.5 gives a better representation of the observed results and is very close to the proposal Melo *et al.* [2015] that was shown to give the best prediction of ultimate chord rotation in Figure 2.6. With a much more simple form, Equation 2.5 may be a useful substitute in situations when very little detail is known about the beam or column member. Since no test data is available for axial load ratios outside the range of 0.1 to 0.25, the proposed expression is to be used within this range and for an axial load ratio outside of this range; the limit values are to be used pending further information from future testing.

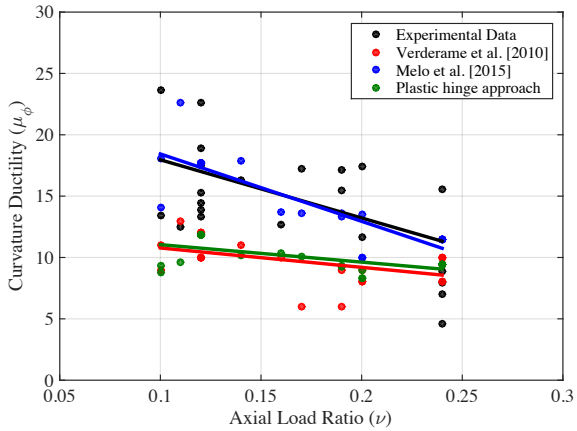

Figure 2.7. Comparison of the different approaches of computed curvature ductility as a function of axial load ratio based on a total of 23 experimental test specimens.

The remaining part of the hysteretic rule shown in Figure 2.2 is the definition of the post-capping stiffness K_{pp}. Haselton *et al.* [2008] proposed a relation for post-capping rotation capacity based as a function of both axial load ratio and shear reinforcement ratio. The dependence on axial load ratio is investigated and plotted in Figure 2.8, where the post-capping stiffness computed from experimental test specimens is expressed as a ratio to the initial stiffness K_i through the term a_{pp}. From Figure 2.8, there is an inverse trend between the post-capping stiffness ratio and the axial load ratio. A linear trend line plotted in Figure 2.8 is proposed for determining the post-capping stiffness as a function of the axial load ratio as:

$$a_{pp} = -0.1437\nu - 0.0034 \qquad \textbf{Equation 2.6}$$

which gives a logarithmic standard deviation of 0.413. Similar to Equation 2.5, since no test data is available for axial load ratios outside the range of 0.1 to 0.25, the proposed expression is to be used within this range and for an axial load ratio outside of this range; the limit value is to be used. To conclude the construction of the backbone hysteresis behaviour of the sections, the section curvature at capping moment can be defined by rearranging the above expressions to give:

$$\phi_c = \phi_y \left(\mu_\phi + \frac{0.2 \frac{M_c}{M_y}}{a_{pp}} \right)$$ **Equation 2.7**

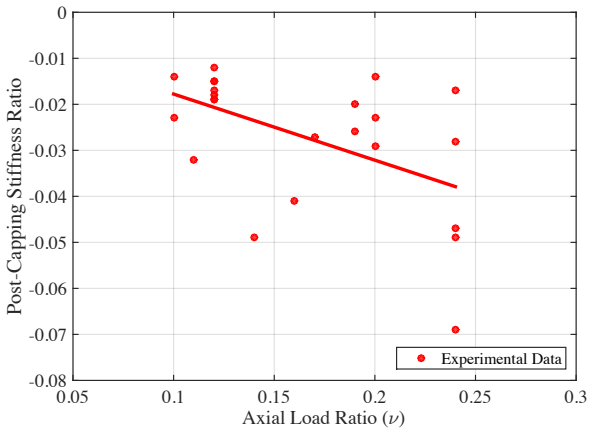

Figure 2.8. Proposal of a simplified relation for post-capping stiffness ratio defined a function of axial load ratio based on a total of 23 experimental test specimens.

It should also be appreciated that while the expressions proposed above are relatively simple and contain some degree of dispersion, this is due to the limited amount of experimental data available to calibrate the expressions. Ideally, a large database of experimental testing would be available to perform regression analysis on the data and determine a number of predictor variables for the terms, such as that performed by Haselton *et al.* [2008]. However, since limited information exists and the proposed expressions have been shown to give reasonable predictions when compared to other more elaborate expressions, they may be used with a degree of confidence in the structural assessment. In addition, these expressions were developed with a desire to reduce the complexity of the expressions such that they can be used when relatively little information about the actual member section properties is known, as is often the case in assessment of older structures. In addition, further studies in later chapters look to quantify and incorporate the impacts of modelling uncertainty associated with each of these terms when performing a complete assessment of case study structures.

Since the model being developed here consists of a tri-linear hysteretic backbone (Figure 2.2) having a descending post-peak branch with no cyclic strength or stiffness degradation included, a clarification must be made. As noted by Ibarra and Krawinkler [2005], three

general sources of structural collapse are collapse due to excessive deformation whereby the vertical gravity loads cause an excessive overturning moment in the building, typically referred to as "P-Δ effects", where the other two sources are as a result of the degradation of the backbone hysteretic response of the members. This degradation is subdivided into degradation caused by the negative post-peak stiffness envelope of the members, known as in-cycle degradation, and the cyclic degradation of the members typically based on the amount of hysteretic energy dissipated, which is known as cyclic degradation. The first of these three effects has been widely adopted in NRHA and is now considered common practice in the field with Ibarra and Krawinkler [2005], for example, demonstrating how it is a critical modelling parameter to simulate structural collapse. The effects of strength degradation, whether in-cycle or cyclic, are parameters which are not so well established in terms of how one should quantify them. In an extensive calibration effort by Haselton *et al.* [2008] for RC beam-column members with ductile detailing, parameters were established for the cyclic degradation of ductile members. Haselton *et al.* [2008] went on to show through a simple example how the use of in-cycle degradation only in place of a cyclically degrading backbone leads to a conservative estimate of the behaviour of the system. Due to the very limited experimental dataset to recomputed a cyclic degradation term for older RC members and an observed incompatibility of the expressions proposed by Haselton *et al.* [2008], the beam-column model developed here does not include a cyclic degradation term. Instead, it relies on the post-peak negative stiffness branch to simulate the loss of strength and stiffness in a structural member. As such, the effects of such a modelling decision and the limitations of its application are discussed here.

In a parametric study aimed at quantifying the effects of different modelling parameters on the collapse of structures, Ibarra *et al.* [2005] state that of the three modelling parameters to simulate collapse, the post-peak strength degradation is the most influential parameter to include. That is of course in contrast to using a bilinear hysteretic model that relies solely on P-Δ effects at large lateral deformations to cause structural collapse, which is undoubtedly an important parameter to simulate. In this sense, the inclusion of the post-peak branch is a step in the right direction and the modelling approach here correctly includes what have been noted by Ibarra and Krawinkler [2005] to be two of the most critical parameters in simulating structural collapse. The third parameter that is not incorporated here is the cyclic degradation term due to a lack of available experimental data to appropriately quantify it since many of the test specimens listed in Table 2.1 were not tested to the point of complete loss of lateral strength. Hence, the discussion moves towards what is the implication of not including a cyclic degradation term. Haselton *et al.* [2008] have previously shown how ignoring this can lead to a conservative estimate of the median collapse intensity through a single illustrative example, but more extensive analysis by Ibarra *et al.* [2005], however, reports that the actual ductility capacity and post-peak stiffness are the most influential parameters in assessing collapse, noting that while cyclic degradation is an important parameter, it tends not to be the most critical when assessing

collapse. This argument that a cyclic degradation parameter is not a critical issue is further supported by a study by Liel *et al.* [2009] on the effects of modelling uncertainty on the collapse fragility of ductile and non-ductile RC frames. Of the numerous modelling parameters considered, strength and ductility capacity of the beam and column members was shown to have the most influence on the collapse fragility, where cyclic degradation was noted not to have a significant effect, supporting the earlier observations by Ibarra *et al.* [2005]. Lastly, Ibarra *et al.* [2005] note how the response of two systems with and without cyclic degradation are essentially the same prior to the achievement of the peak capacity of the system. It is clear that while including a cyclic degradation term in the beam-column member's hysteretic backbone would be a more favourable approach, a lack of usable experimental data on older RC beam-columns does not permit an appropriate calibration of such a term. From the above discussion, however, it is fair to conclude that the omission of such a term is not a critical issue to conduct a reasonable structural response assessment of RC frame buildings using the modelling approach developed here, where many of the key parameters influencing the behaviour have been incorporated. It is stated that this is a key issue to be addressed in future modelling refinements pending the availability of more detailed experimental data.

From the above discussion, the backbone of the hysteretic model outlined in Figure 2.2 can be defined. To complete the definition of the moment-curvature hysteretic relationship the parameters describing the stiffness transitions need to be defined to represent the pinching behaviour associated with members with smooth bars. Using the beam-column element model illustrated in Figure 2.1 and the proposed values listed in Table 2.2 for the Pinching4 material model in OpenSees, a comparison between the proposed element and experimental test results available in the literature can be made. The details of the test specimens have been outlined in Table 2.1 and a comparison between the observed experimental responses and the proposed parameters are outlined in Figure 2.9 to Figure 2.12. The plots show how the backbone of the response is well represented, especially the post-peak degrading branch of response. The stiffness transitions between cycles to represent the pinching behaviour associated with the use of smooth reinforcing bars is also reasonably well represented. A possible future development would be an investigation of the impact of axial load ratio on the proposed terms in Table 2.2, as previous experimental testing noted how the pinching and unloading stiffness ratio tended to be affected by increased axial load ratio.

Table 2.2. Proposed Pinching4 hysteretic parameters for flexural hinge.

	Parameter	Proposed Value
Reloading Disp.	rDispP	0.1
	rDispN	0.1
Reloading Force	fForceP	0.4
	fForceN	0.4
Unloading Force	uForceP	-0.8
	uForceN	-0.8

2.2.2.2 Shear Behaviour

The modelling of the shear deformation in beam-column elements is often omitted as the flexural behaviour and deformation are assumed to be the more dominant response mechanism. However, many Italian RC structures were observed in Chapter 1 to suffer extensive shear damage and failure either as a result of poor detailing or the interaction with the masonry infill. In addition to this, Ozcebe and Saatcioglu [1989] noted that some experimental testing has shown that even in the case of a beam-column member possessing a large shear capacity, this does not necessarily mean that the member will remain elastic in shear throughout large inelastic flexural deformation. Some shear models, such as the UCSD shear model described in Priestley *et al.* [1993], provide a means to check that the shear demand observed in numerical analysis against the member's shear capacity to verify that a shear mechanism has not occurred. Elwood [2004] reported how the evaluation of member's performance in shear ought to be carried out in terms of both strength and deformation, since testing has shown that shear failure is also a function of the shear deformation in the member and not just capacity, as indicated in the model outlined by Priestley *et al.* [1993] where the shear capacity is a function of the flexural curvature ductility. As a result of this, Elwood and Moehle [2003] developed a modelling technique in OpenSees whereby the shear and axial failure of the column member could be modelled through the introduction of a set of nonlinear springs which interact via a predefined limit state surface. This approach gave good predictions in terms of predicting the failure mechanism behaviour when compared to shake table testing. However, some of the drawbacks of the model proposed by Elwood and Moehle [2003] is that the user is confined to a single hysteretic model within OpenSees. In addition, the beam-column element used by Elwood and Moehle [2003] is required to have a positive slope in order to obtain a unique solution, which may lead to difficulties in accounting for strength degradation in the plastic hinge regions simultaneously. It is also noted by Zimos *et al.* [2015] that the approach by Elwood and Moehle [2003] assumes the axial failure of the member occurs when the shear capacity reaches zero is not entirely correct as there is much experimental evidence to suggest that it may occur before the loss of shear capacity.

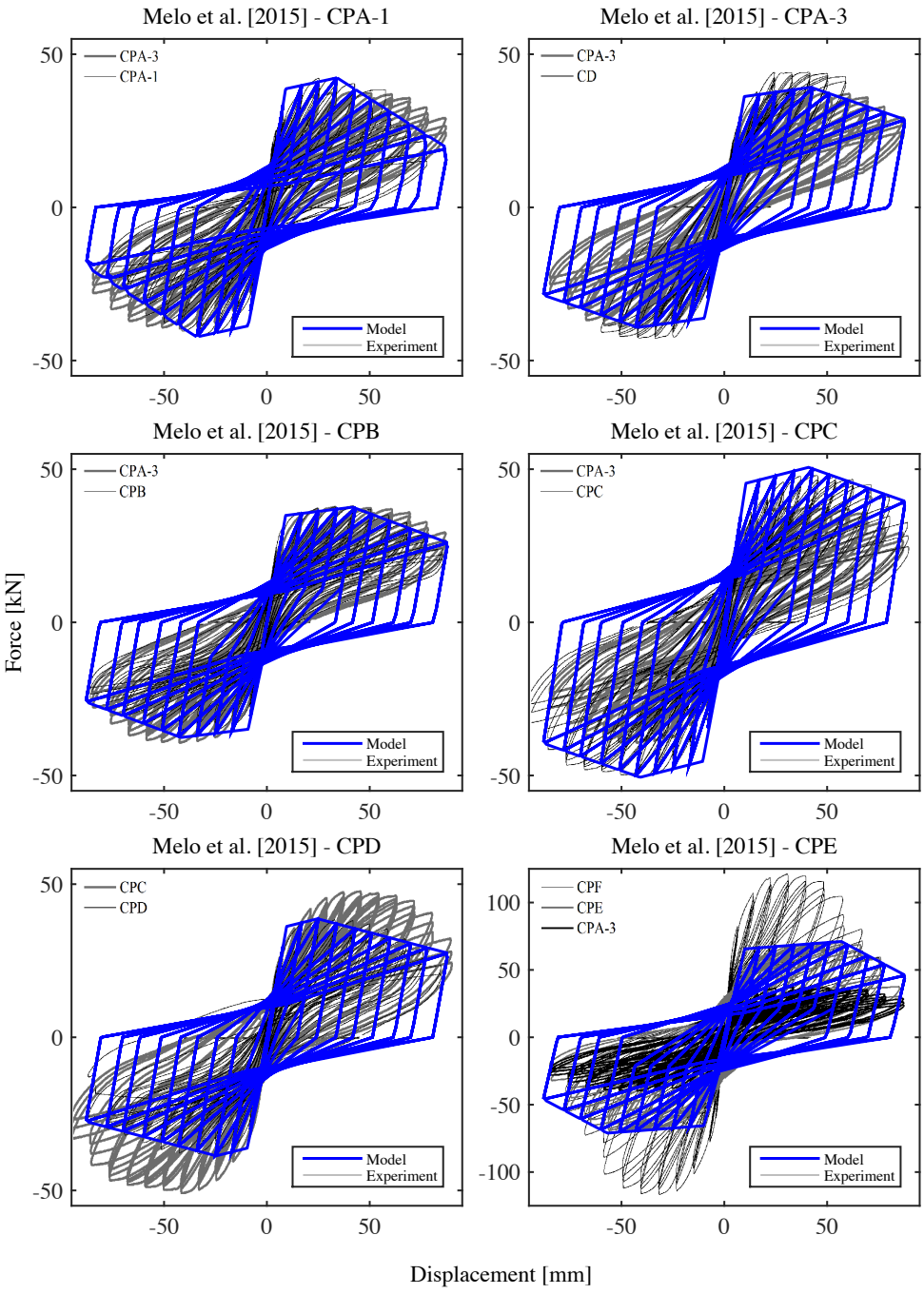

Figure 2.9. Comparison of proposed hysteretic model with experimental test specimens.

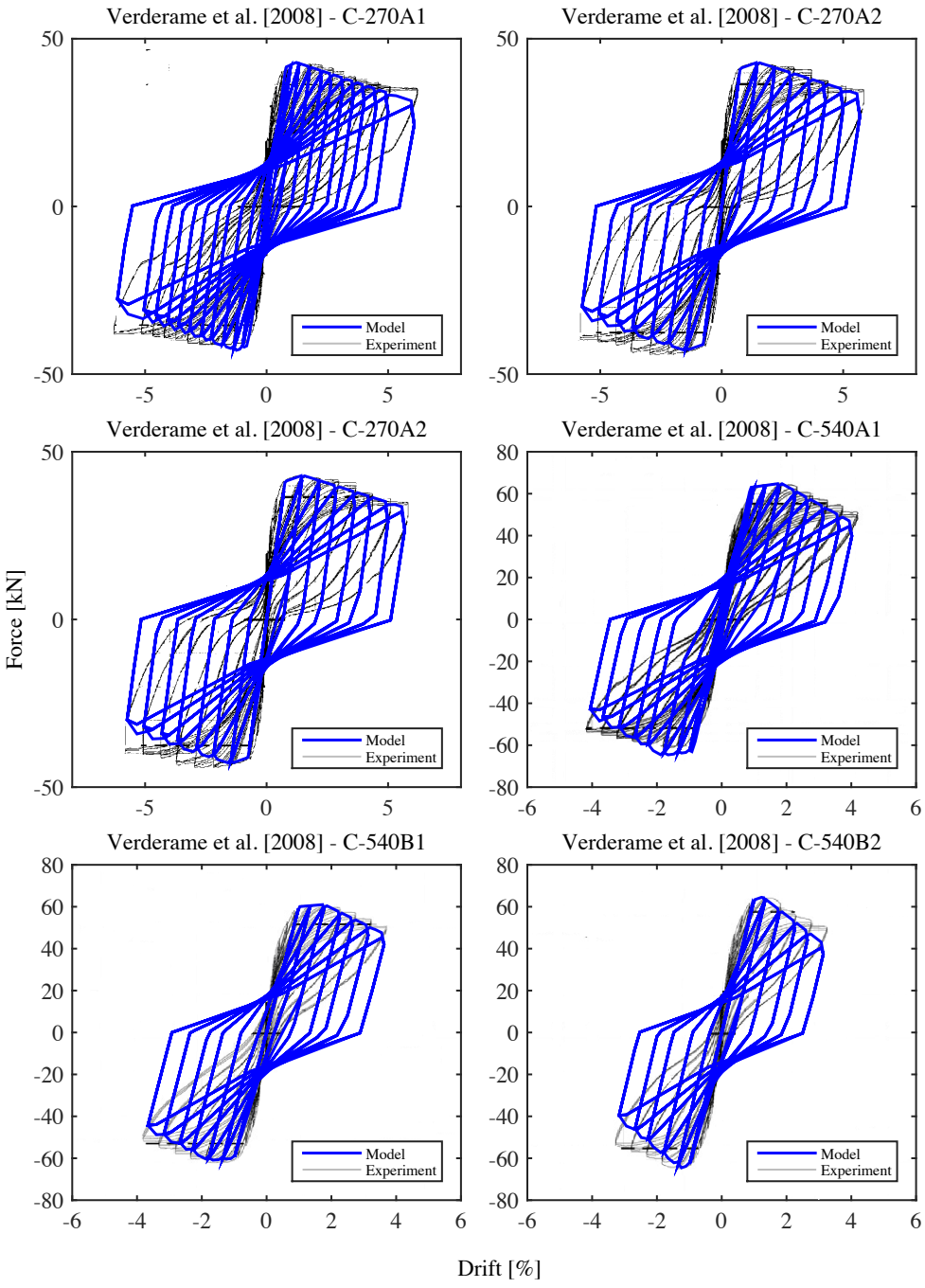

Figure 2.10. Comparison of proposed hysteretic model with experimental test specimens.

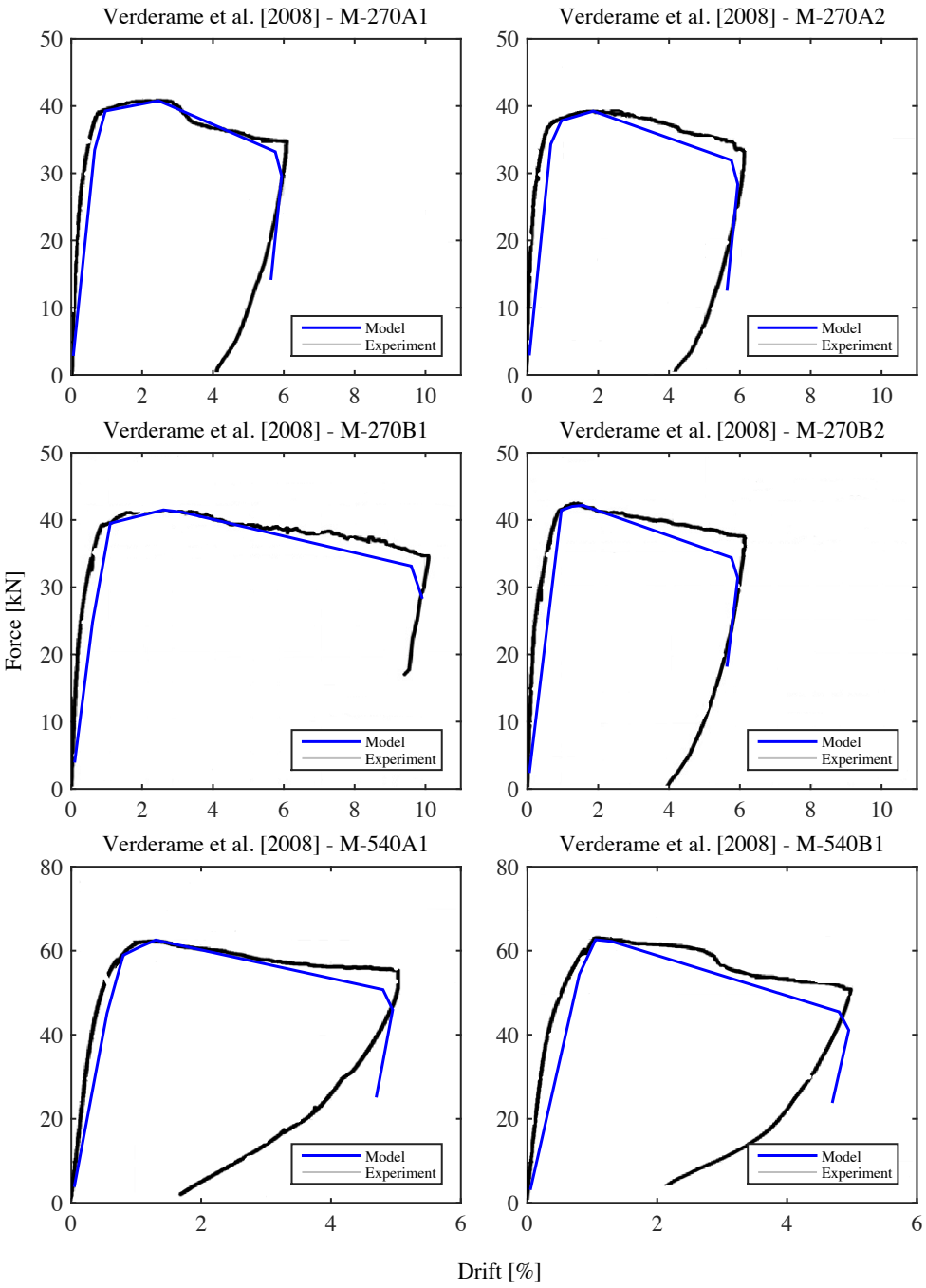

Figure 2.11. Comparison of proposed hysteretic model with experimental test specimens.

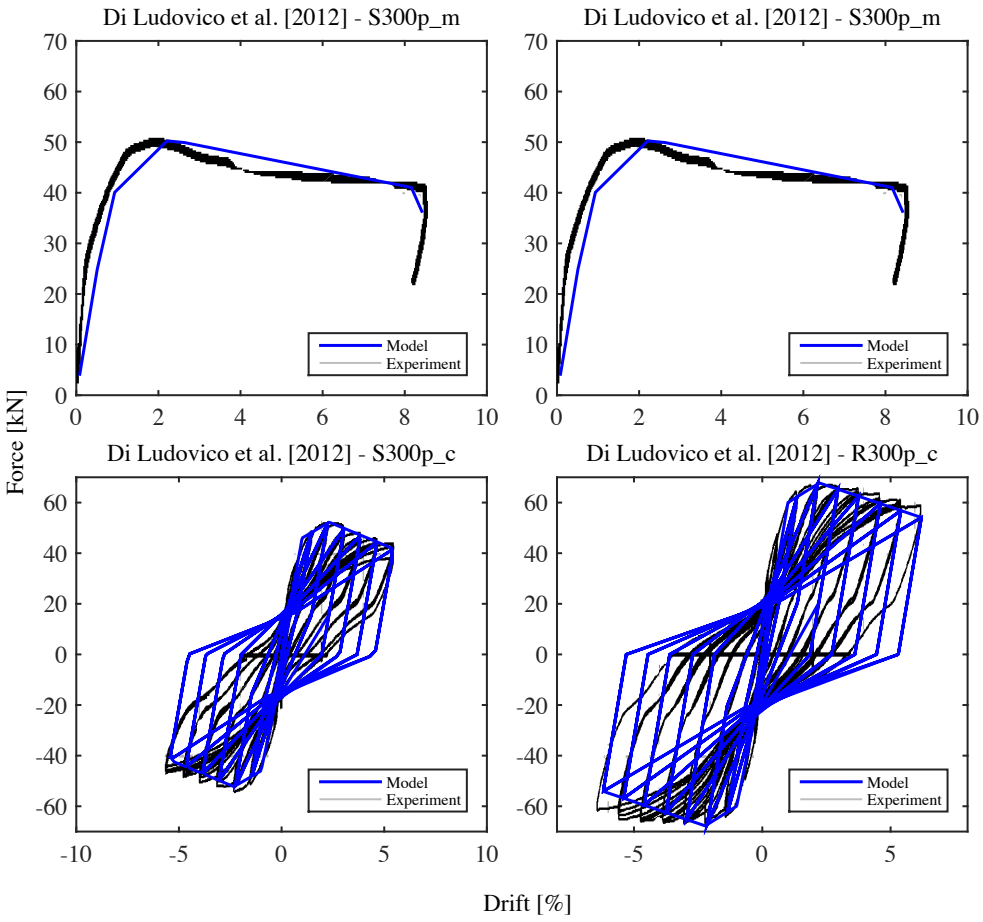

Figure 2.12. Comparison of proposed hysteretic model with experimental test specimens.

Another approach developed by Mergos and Kappos [2008] and subsequently by Mergos and Kappos [2012] and Zimos *et al.* [2015] is a hysteresis model based on regression of a large number of experimental tests to give quite a good match in terms of both mean ratio and coefficient of variation. These tests consist of a wide range of column members that consider both monotonic and cyclically loaded members, although the majority were cyclically loaded, in addition to having a broad range of designs, loading and being tested up until the occurrence of an axial failure of the member. Mergos and Kappos [2008, 2012] proposed a set of expressions to calculate the backbone shear deformation curve of RC members, whilst adopting a modified version of the unloading and reloading hysteretic rules proposed by Ozcebe and Saatcioglu [1989]. This model is matched from a large test data set and does a good job of predicting the member behaviour up until shear failure,

with no post-peak cyclic behaviour modelled. Zimos *et al.* [2015] extended the work of Mergos and Kappos [2008, 2012] by considering a database of 150 tests to calibrate expressions to determine the post-peak shear deformation capacity to axial failure and the steepness of this degradation.

While the use of regression equations is undesirable in some ways as it removes some of the essence of the mechanics of the failure, methods such as the modified compression field theory (MCFT) [Vecchio and Collins, 1986] provide exactly the opposite through a rational mechanics-based reasoning approach to the problem. While the MCFT is an attractive approach to computing the shear response, the majority of the work conducted on MCFT has been for monotonic loading, for which the test to predicted response comparisons are very promising. However, the approach outlined Vecchio and Collins [1986] does not directly translate to computing member backbone response for cyclic loading as the cyclic response force-deformation backbone is typically lower than that of the monotonic response. Lowes *et al.* [2003] utilised the MCFT for computed RC member capacities and used the recommendations of Stevens *et al.* [1991] to account for the discrepancy between monotonic and cyclic response. More recent research by Ruggiero [2015] at the University of Toronto has also identified this difference in monotonic and cyclic response of members subjected to shear, noting that the cyclic response can be as much as 25% lower than the corresponding monotonic test. As a result, Ruggiero [2015] developed the general crack component model (GCCM) which accounts for the strength decay and offsets through a detailed consideration of crack dilation and crack tooth angle decay in members subjected to shear. The GCCM was validated via numerous experimental tests performed by Ruggiero [2015] and others to provide a more comprehensive description of the mechanics of the strength degradation in members subjected to reverse shear cycles. However, the GCCM approach by Ruggiero [2015] is quite detailed and difficult to implement in a simple model intended for NRHA. Hence, the simpler approach of regression to many tests is favoured here until a simpler and practical approach is developed for methods such as the GCCM for members subjected to seismic loading.

Similar to previous work on the modelling of short link eccentrically braced frames (EBFs) by O'Reilly and Sullivan [2015b] where an uncoupled shear spring is aggregated into the lumped plasticity beam-column element to capture the effects of the shear degradation and failure. Through this approach, the failure in shear as a result of short-column effects and masonry infill interaction can be detected during the analysis using a simple and reasonably robust modelling approach, and also does away with the need to post-process shear demands in terms of member capacity only. The backbone response of the proposed shear force-deformation by Zimos *et al.* [2015] is shown in Figure 2.13 and consists of 4 phases; the initial elastic behaviour, post-cracking, peak response and strength degradation.

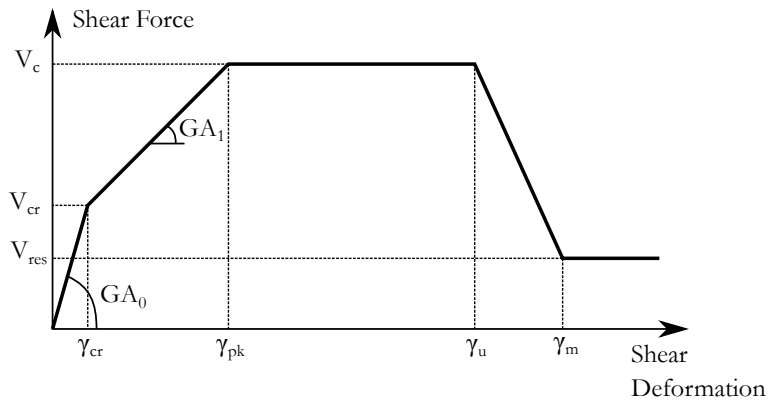

Figure 2.13. Shear force-deformation backbone hysteresis.

For the initial elastic response, the initial shear stiffness of a rectangular section is given as:

$$GA_0 = 0.8A_gG \qquad \textbf{Equation 2.8}$$

where $0.8A_g$ is the approximate shear area expressed as 80% of the gross cross-sectional area and G is the shear modulus of concrete. The cracking shear is then calculated using the approach of Sezen and Moehle [2004] from:

$$V_{cr} = \frac{f_{cr}}{L_s/h}\sqrt{1+\frac{N}{f_{cr}A_g}}0.8A_g \qquad \textbf{Equation 2.9}$$

where f_{cr} is the cracking strength of concrete, taken from Collins and Mitchell [1991] as:

$$f_{cr} = \frac{1}{3}\sqrt{f_c'} \qquad \textbf{Equation 2.10}$$

where f_c' is the compressive cylinder strength of the concrete, L_s is the shear span, h the section height and N is the axial load. Using these expressions outlined in Zimos *et al.* [2015], the first part of the curve is constructed. The post-cracking behaviour is determined via two parameters, the maximum capacity and the deformation at first occurrence of the maximum. The maximum capacity is given by Zimos *et al.* [2015] using the approach of Priestley *et al.* [1993] as:

$$V_c = k\sqrt{f_c'}0.8A_g + N\tan(\alpha) + \frac{A_{sv}f_{yv}}{s}(d - d')\cot(\theta) \qquad \textbf{Equation 2.11}$$

where k is a function of flexural ductility given by Priestley *et al.* [1993] and is illustrated in Figure 2.14, α can be approximated as h/L_s, A_{sv} is the shear reinforcement area, f_{yv} is the yield strength, s is the stirrup spacing, d and d' are the depths to the bottom and top layers of rebar, respectively and θ is the shear crack angle at maximum stress, proposed by Mergos and Kappos [2012] to be taken as 45°, since this is noted by Zimos *et al.* [2015] to provide the best results in terms of regression, despite Priestley *et al.* [1993] having previously noted that 30° is to be used in assessment and 45° in design. Since the shear hinge defined in OpenSees will be uncoupled from the flexural behaviour, the definition of the k factor as a function of the plastic hinge curvature needs to be clarified. One of the principle interests of including a shear hinge in the beam-column element is to be able to simulate the possible shear failure caused by the interaction of the RC frame with masonry infill. However, the peak capacity of a masonry infill typically occurs at quite a low storey drift level, with Sassun *et al.* [2015] noting a median value of 0.46% storey drift at peak force. Comparing this value of storey drift to typical yield drifts of RC frames, it can be concluded that for the range of response of the masonry infills that is of interest for what concerns shear behaviour in columns, the curvature ductility in the column members can be assumed to be quite low, and most likely less than unity at peak response of the infills. Therefore for simplicity, the value of k in Figure 2.14 is taken here as a constant value of 0.29.

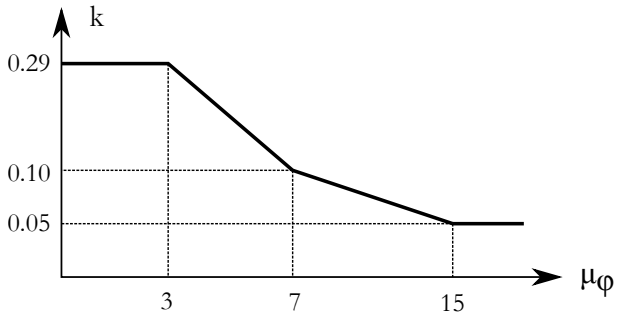

Figure 2.14. k factor given in Priestley *et al.* [1993].

The calculation of the post cracking stiffness GA_1 is found in Mergos and Kappos [2012] by considering the truss analogy given by Park and Paulay [1975] as:

$$GA_1 = \frac{E_s b(d - d')\rho_v \sin^4\theta \cot^2\theta}{\sin^4\theta + \eta\rho_v} \qquad \textbf{Equation 2.12}$$

which if θ is taken as 45° can be reduced to:

$$GA_1 = \frac{E_s b(d - d')\rho_v}{1 + 4\eta\rho_v} \quad \textbf{Equation 2.13}$$

where E_s is the steel elastic modulus, b is the section width, ρ_v is the shear reinforcement ratio given by A_{sv}/bs. The modular ratio η is defined as the ratio of elastic moduli of steel and concrete, given as E_s/E_c. The shear deformation at peak force is derived from the above with two modifications proposed by Mergos and Kappos [2012] to give:

$$\gamma_{pk} = \left(\gamma_{cr} + \frac{(V_c - V_{cr})}{GA_1}\right)(1 - 1.07\nu)\left(5.37 - 1.59\min\left(2.5, \frac{L_s}{h}\right)\right) \quad \textbf{Equation 2.14}$$

The capacity of the shear hinge then remains constant until the onset of shear degradation in the member. The shear deformation at the onset of degradation is given in Mergos and Kappos [2012] as:

$$\gamma_u = (1 - 2.5\min(0.4, \nu))\left(\min\left(2.5, \frac{L_s}{h}\right)\right)^2 \left(0.31 + 17.8\min\left(0.08, \frac{A_{sv}f_{yv}}{bsf_c'}\right)\right)\gamma_{pk} \geq \gamma_{pk}$$

Equation 2.15

The residual strength and post-peak deformation capacity is determined from the expressions developed by Zimos *et al.* [2015], where the post-peak deformation capacity is given by:

$$\gamma_{pp} = 0.65\left(\frac{\rho_l}{A_{conf(\%)}}\right)^{1.2}\sqrt{\frac{\rho_v f_{yv} A_{sl} f_{yl} dbd\sqrt{f_c'}}{NsV_c}} \quad \textbf{Equation 2.16}$$

where $A_{conf(\%)}$ is the confinement ratio of the section and the subsequent shear deformation at which Zimos *et al.* [2015] describe axial failure to occur is given as:

$$\gamma_m = \gamma_u + \gamma_{pp} \quad \textbf{Equation 2.17}$$

The corresponding shear force at this deformation is found from the degrading stiffness expression proposed by Zimos *et al.* [2015] and it is assumed here that the shear force remains constant beyond this point. The residual strength is therefore given by:

$$V_{res} = V_u - S_{pp}\gamma_{pp} \quad \textbf{Equation 2.18}$$

where S_{pp} is the degrading stiffness and is given by:

$$S_{pp} = 7.36 + \frac{0.28\sqrt{\nu + 0.02}}{(\rho_v + 0.0011)\left(\frac{\rho_l f_{yl}}{A_{conf(\%)}}\left(\frac{\phi_{l,ave}}{d}\right) + 0.06\right)} \qquad \textbf{Equation 2.19}$$

where $\phi_{l,ave}$ is the average longitudinal bar diameter.

Since the discussion here has been largely based on the work of Mergos and Kappos [2008] and Zimos *et al.* [2015], where the loading of members with additional axial load resulted in a shear response of the member and a subsequent axial failure of the member following the loss of shear capacity, some limitations of the applicability need to be highlighted. First is for the modelling of beam members; since the same element and hysteretic rules are proposed in the previous sections for both beam and column members, the modelling of the shear hinge in the beam members is not recommended. This is as the testing used to develop the expressions for the shear backbone of the hinge possessed some degree of axial loading, whereas beam members in RC frames are assumed to not have much, if any, axial loading during response due to the presence of the floor slab system, although the presence of a floor slab system can induce varying levels of axial loading during seismic response. In addition, the principal motivation behind the inclusion of such a shear behaviour is to be able to account for the potential shear failure of column members, which was highlighted during past earthquakes and discussed in Chapter 1. Beam members, however, are generally not expected to be subjected to such large shear forces and hence, the inclusion of a shear behaviour is not necessary.

The hysteretic parameters adopted here for the shear hinge model are based on those proposed initially by Ozcebe and Saatcioglu [1989] and subsequently modified by Mergos and Kappos [2008], where the parameters specified for the Pinching4 material model in OpenSees are calibrated in order to give a similar hysteretic rule that compares well with the test specimens used by Ozcebe and Saatcioglu [1989]. These parameters in the Pinching4 material are given in

Table 2.3. Figure 2.15 shows a comparison between the four specimens outlined in Ozcebe and Saatcioglu [1989] and the hysteretic parameters proposed here, where a reasonably good match in terms of the pinching, unloading and reloading stiffnesses of the specimens can be observed. No cyclic degradation parameters are specified for strength, unloading or reloading stiffness and hence, all of the model associated parameters are set to zero.

Table 2.3. Proposed Pinching4 hysteretic parameters for the shear hinge.

	Parameter	Proposed Value
Reloading Disp.	rDispP	0.4
	rDispN	0.4
Reloading Force	fForceP	0.2
	fForceN	0.2
Unloading Force	uForceP	0.0
	uForceN	0.0

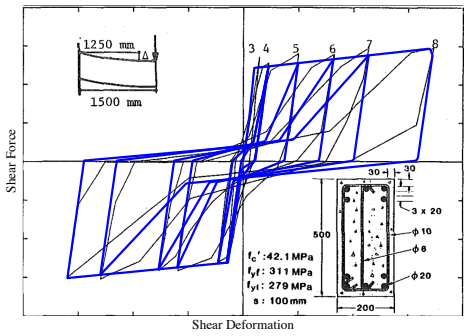

(a) Specimen 1B tested by Tankut *et al.* [1981].

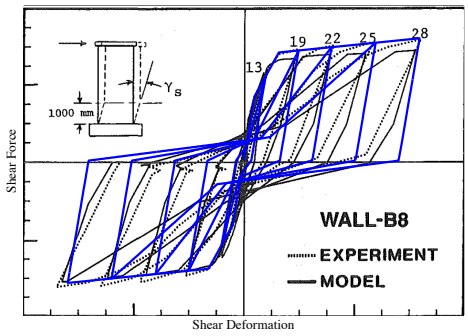

(b) Specimen B8 tested by Oesterle et al. [1979].

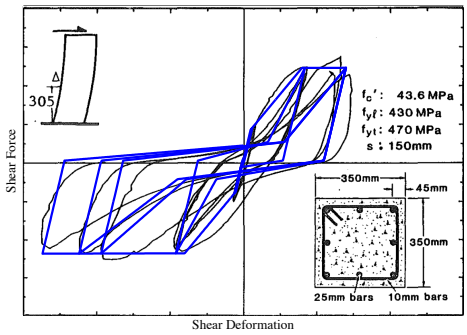

(c) Specimen U1 tested by Saatcioglu & Ozcebe [1988].

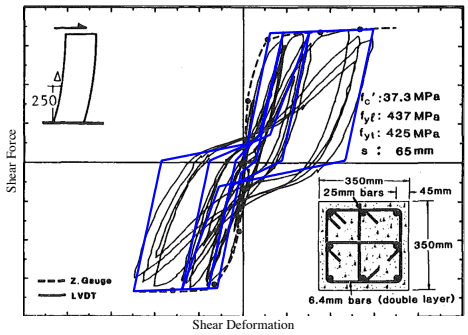

(d) Specimen U6 tested by Saatcioglu & Ozcebe [1988].

Figure 2.15. Comparison of the proposed unloading/reloading hysteretic parameters with test specimens outlined in Saatcioglu and Ozcebe [1989].

2.3 EXTERIOR BEAM-COLUMN JOINTS

Following the modelling of the beam-column members in RC frames, another critical component is the behaviour of the exterior beam-column joints as past observations in Chapter 1 have highlighted them to be a particularly vulnerable component. As such, this section provides a review of experimental testing on older exterior RC beam-column joints. From this, a review of existing numerical modelling approaches to exterior beam-column joints is presented, followed by the recommendations in terms of the modelling of such joints while capturing behaviour such as hysteretic pinching and strength degradation of the response.

2.3.1 Experimental Testing on Exterior Beam-Column Joints

Exterior beam-column joint flexibility and deformation have been noted from experimental testing to greatly influence the performance of the overall structure. Depending on the country, different end-anchorages were adopted for the termination of longitudinal bars in the exterior joint where, for example, bars with 180° end-hooks were common practice in Italian construction [Pampanin *et al.,* 2002], whereas Turkish construction tended to have bars bent into the joint (see Figure 2.16) and sometimes welded to each other [Bedirhanoglu *et al.,* 2010]. All of the aforementioned end-anchorage solutions have been studied to some extent and have been identified to be substandard anchorages when no joint shear reinforcement is present. This comes from the inability of the joint with such detailing to develop a diagonal strut mechanism capable of transferring the shear forces across the joint. Other factors, such as the use of smooth bars and the presence of joint shear reinforcement also greatly affect the performance of the joint. This section reviews the relevant experimental testing carried out on exterior beam-column sub-assemblages designed for gravity loading only. In addition to having no seismic provisions, the specimens are detailed with smooth reinforcing bars, low-strength concrete, no joint reinforcement and end-hook anchors in the exterior joints. However, due to the limited amount of test data conforming to the above criteria, and more specifically the Italian standard of practice pre-1970, some of the experimental test results discussed here do not possess all of the characteristics defined above but are included nonetheless as they often provide a direct comparison between different parameters that contribute to the overall discussion of the behaviour. In addition, these specimens are included in the following discussions but the influence of the "added" feature (e.g. deformed bars) is noted and taken into consideration whilst interpreting the results.

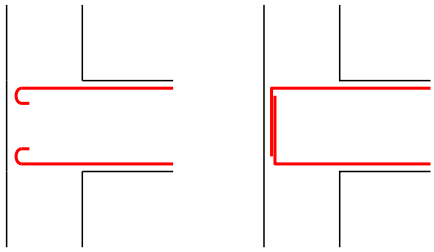

(a) End-hook anchorage. (b) Bars bent into the joint.

Figure 2.16. Different end anchorages in exterior beam-column joints.

As outlined in Pampanin *et al.* [2002], the use of exterior beam-column joints with end-hook anchorages illustrated in Figure 2.16(a) was quite common in Italy up until the introduction of modern seismic detailing codes in the 1970's. Pampanin *et al.* [2002] tested two sub-assemblages of exterior beam-column joints with end-hooks and smooth reinforcing bars. The performance of these joints was shown to be very brittle, where diagonal cracking of the joint along with slippage of longitudinal bars led to concrete being spalled off, in what was termed the "concrete wedge" by Pampanin *et al.* [2002]. This resulted from insufficient joint shear reinforcement leading to cracking of the joint concrete from excess loading, as shown in Figure 2.17. These diagonal cracks in combination with the longitudinal bars slipping due to poor bond conditions with the surrounding concrete resulted in the bars tending to push the outer wedge of the joint concrete out of the joint. In a similar study, Calvi *et al.* [2002a] conducted testing on a 2/3 scale three storey RC frame with detailing typical of pre-1970's construction in Italy, where the damage sustained by the structure was concentrated in the exterior beam-column joints of the bottom two storeys, with the "concrete wedge" behaviour being observed in both cases. This represented an important observation regarding the performance of older RC beam-column joints, as previous testing on joints with bars bent into or out of the joint did not demonstrate such a mechanism. The result of this concrete wedge spalling on either end of the structure meant a shear hinge mechanism formed in the joints, which spread the increased deformation of the joint over the two adjacent storeys, as opposed to a single storey, which would have been the case had a flexural hinge formed in the column members.

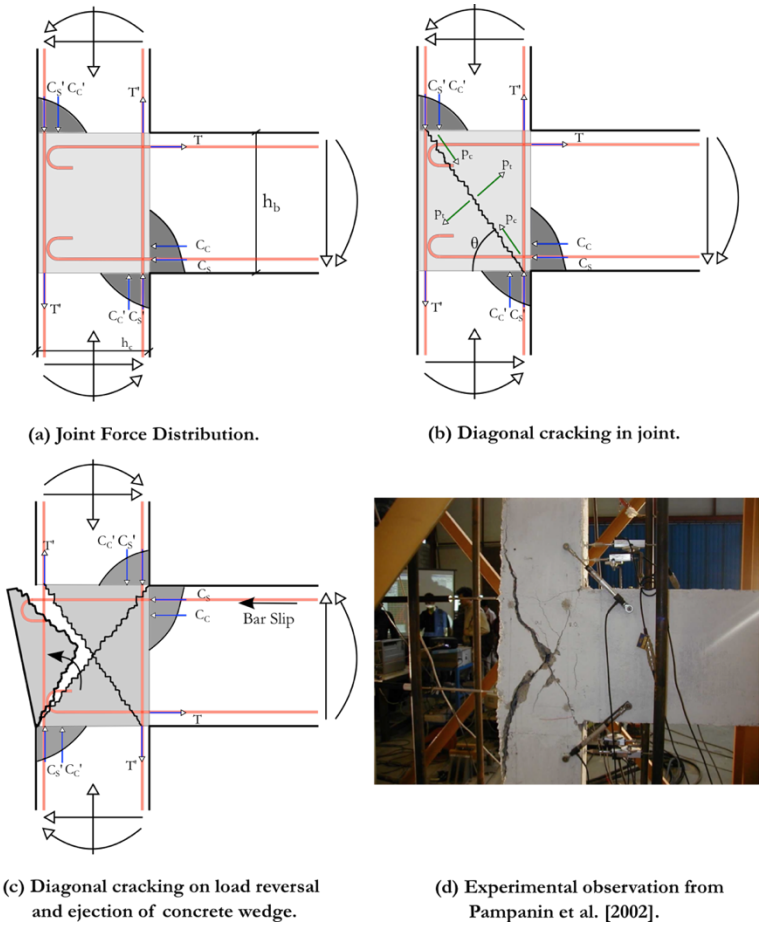

(a) Joint Force Distribution.

(b) Diagonal cracking in joint.

(c) Diagonal cracking on load reversal and ejection of concrete wedge.

(d) Experimental observation from Pampanin et al. [2002].

Figure 2.17. Diagonal cracking of joint and formation of concrete wedge mechanism Pampanin *et al.* [2002].

Braga *et al.* [2009] tested exterior beam-column joint specimens similar to those examined by Pampanin *et al.* [2002], where the smooth longitudinal bars were terminated with 180° hooks in the joint. The general behaviour of the joint is similar as that previously reported, where large diagonal cracking appeared in the joint region, but slight flexural yielding was also reported in the beam element through a single crack appearing in the plastic hinge zone. The concrete wedge mechanism was also observed by Braga *et al.* [2009], although it was noted that the hook anchors did not show any significant slip inwards or outwards, as reported by Pampanin *et al.* [2002]. Instead, the formation of the concrete wedge was attributed by Braga *et al.* [2009] to the opening and closing of the shear hinge gradually squeezing the wedge outwards. This may have contributed to the ejection of the concrete wedge in the case of the specimens tested by Pampanin *et al.* [2002] and Calvi *et al.* [2002a],

but it is concluded that the presence of the bars pushing outwards would more likely contribute to the ejection of the wedge as opposed to the opening and closing mechanism squeezing it out. Again, a lack of experimental data on the subject is a major limitation to identifying the exact failure mechanism of such joints, although the fundamental brittle behaviour remains nonetheless. Akguzel [2011] tested a single exterior joint constructed to pre-1970 Italian detailing standards and the observations were as previously reported in Pampanin *et al.* [2002] with high pinching and low energy dissipation. The concrete wedge failure mechanism formed at around 3% drift in the absence of any slipping of the bars, which was recorded during the test, which therefore supports the previous finding by Braga *et al.* [2009]. This formation of the wedge resulted in the buckling of the column longitudinal bars in the joint, although no axial load readings are provided in Genesio [2012] to establish the level of force required to cause the buckling of the column bars, who reported the same test specimen results. While the above comments reflect largely on the strength capacity of the test specimens, the deformation capacity is not discussed to the same extent since the data reported from test reports was not available in s consistent way to allow for meaningful comparison between different test campaigns, but will be examined further in Section 2.3.2.2.

Bedirhanoglu *et al.* [2010] conducted a number of tests on exterior beam-column joints with beam bars bent into the joints (Figure 2.16(b)), which was typical of Turkish construction practice prior to 1970. Comparisons between the variation of axial load with added joint shear reinforcement were performed, in addition to welding the bars together within the joint. The main difference with this practice of bending bars into the joints instead of using end-hooks means that a more stable diagonal compressive strut can be formed within the joint. This was observed for all specimens, where diagonal cracking was observed for all specimens but the response was typically stable and did not show a concrete wedge failure mechanism similar to that observed for the case of end-hook anchors. As anticipated, the use of some joint reinforcement resulted in thinner cracks occurring in the joint region, larger lateral load carrying capacity and more strain demands in the beam longitudinal reinforcement. This demonstrates the clear benefit of using joint reinforcement as the response becomes more stable and moves damage away from the joint. It was also noted that the increase of axial force on the columns resulted in increased strength capacity, more energy dissipation and less pinching in the hysteretic loops.

2.3.2 Modelling of Exterior Beam-Column Joints

Considering the experimental observations of the behaviour of pre-1970's exterior beam-column joints subjected to cyclic loading, a numerical model is herein proposed to consider this behaviour for future seismic assessments of existing structures. Firstly, methods of evaluating joint shear strength are reviewed and proposed, followed by the description of the numerical model.

2.3.2.1 Shear Strength Modelling in Exterior Beam-Column Joints

In order to assess the shear strength capacity of exterior beam-column joints, an appropriate strength model ought to be adopted to accurately represent the behaviour of the joint. Such a strength model depends on numerous parameters, such as the type of bars used, the level of transverse shear reinforcement in the joints, if any, and the end anchorage conditions of the longitudinal beam reinforcing bars. This section presents a brief review of existing shear strength models available in the literature for exterior beam-column joints. The expressions used here are then subsequently described and derived in detail.

2.3.2.1.1 Review of Existing Shear Strength Models

The strength of beam-column joint is characterised by the joint's ability to transfer the shear, flexure and axial forces across the joint. Many shear capacity models have been proposed in the past, where these vary from empirical approaches to approaches based on strut-and-tie models or principle stress models. Sharma *et al.* [2011] provide a critical review of existing shear strength models for exterior beam-column joints. In this review, Sharma *et al.* [2011] discussed how some empirical approaches have been proposed by authors [Bakir and Boduroğlu, 2002; Hegger *et al.*, 2003], where the models were typically related to parameters such as reinforcement and joint aspect ratios. More advanced approaches which incorporate the use of a strut-and-tie modelling approach have been proposed by Hwang and Lee [1999] and Wong [2005]. More recently, Metelli *et al.* [2015] expanded the work of Hwang and Lee [1999] to develop the Modified Softened Strut-and-Tie Model for exterior beam-column joints with smooth bars and hook-ended anchorage. When comparing the difference between the predicted to observed joint shear capacity in six different experimental test specimens, the approach by Hwang and Lee [1999] showed an average difference of 71.6%, whereas the modified approach proposed by Metelli *et al.* [2015] shows an average difference of 4.4%. The method proposed by Metelli *et al.* [2015] gives very good results in terms of predicting the shear capacity of the joints, although it should be noted that this approach requires numerous steps of iteration to determine the joint's strength capacity.

A more direct approach has been outlined in Priestley [1997] for the case of joints with deformed bars with no transverse shear reinforcement where the use of principle stresses was employed. This is illustrated in Figure 2.17, where the principle stresses in the joint at an angle θ are seen. These principle tensile (p_t) and compressive (p_c) stresses are computed directly from consideration of the forces acting on the joint and also allows for the consideration of the biaxial stress state caused by the presence of the horizontal and vertical stresses due to column axial load. This model has the advantage of being defined by a number of parameters and was then developed further for the case of smooth hook-ended bars by Pampanin *et al.* [2003]. Comparison by Metelli *et al.* [2015] showed this approach was within 3.2% in terms of predicting joint shear capacity. Sharma *et al.* [2011] expanded

this general model by Priestley [1997] of principle tensile stresses to consider the effects of the additional net shear force of exterior joints resulting from the beam shear transfer. This approach by Sharma *et al.* [2011] results in the need to iterate to satisfy equilibrium and introduces a level of complication in what has been shown by Metelli *et al.* [2015] to be quite a simple and effective model. The following section describes the approach adopted and proposed here using principle tensile stresses. In addition, the beam shear force transfer acting on the joint as outlined by Sharma *et al.* [2011] is considered, but with a different approach taken to solve the equations and realise a closed-form expression such that no iterations are required in determining the joint's capacity.

2.3.2.1.2 Adopted Shear Strength Model

The layout of an exterior joint is shown in Figure 2.18. The equilibrium across Section A-A is found to give the horizontal shear force acting across the joint as follows:

$$V_{jh} = T - V_c \qquad \textbf{Equation 2.20}$$

$$= \frac{M}{jd} - V_c \qquad \textbf{Equation 2.21}$$

$$\approx \frac{M_j}{jd} - \frac{M_j}{H} \qquad \textbf{Equation 2.22}$$

$$= M_j \left(\frac{1}{jd} - \frac{1}{H} \right) \qquad \textbf{Equation 2.23}$$

$$\tau_{jh} b_j h_c = M_j \left(\frac{1}{jd} - \frac{1}{H} \right) \qquad \textbf{Equation 2.24}$$

and when rearranged gives the following for the moment in the joint:

$$M_j = \tau_{jh} b_j h_c \left(\frac{Hjd}{H - jd} \right) \qquad \textbf{Equation 2.25}$$

where the term τ_{jh} is found by considering the principle tensile stress in the joint.

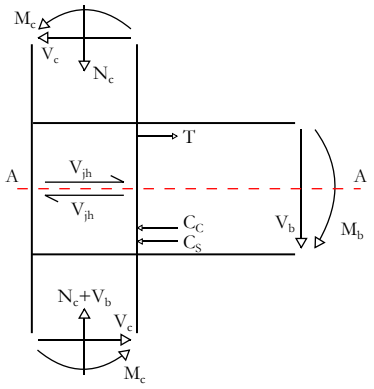

Figure 2.18. Forces acting within an exterior beam-column joint subassembly.

Evaluation of the vertical forces in Figure 2.18 begins with the determination of vertical stress in the joint as the summation of the column axial force (N_c) and the transferred beam shear force (V_b). This additional transfer of the beam shear force had, in fact, been previously considered by Priestley *et al.* [1996] in the context of exterior knee bridge bents. As previously highlighted by Sharma *et al.* [2011] in the context of exterior beam-column frame joints, no equal and opposite beam shear is transferred in exterior joints and therefore the total vertical stress in the joint is given by:

$$\sigma_{jv} = \frac{N_c + V_b}{b_j h_c} \qquad \textbf{Equation 2.26}$$

However as per Sharma *et al.* [2011], the beam shear (V_b) can be related through joint equilibrium to the horizontal shear force by the term α, given by:

$$V_b = \frac{h_b}{h_c} V_{jh} = \alpha V_{jh} \qquad \textbf{Equation 2.27}$$

and the resulting vertical stress in the joint is found to be:

$$\sigma_{jv} = \frac{N_c}{b_j h_c} + \frac{\alpha V_{jh}}{b_j h_c} \qquad \textbf{Equation 2.28}$$

$$= \sigma_a + \alpha \tau_{jh} \qquad \textbf{Equation 2.29}$$

The principle joint stresses are then found via Mohr's circles of stresses to give:

$$p_t = -\frac{\sigma_{jv}}{2} + \sqrt{\left(\frac{\sigma_{jv}}{2}\right)^2 + \tau_{jh}^2} \qquad \textbf{Equation 2.30}$$

giving:

$$p_t = -\frac{\sigma_a + \alpha\tau_{jh}}{2} + \sqrt{\left(\frac{\sigma_a + \alpha\tau_{jh}}{2}\right)^2 + \tau_{jh}^2} \qquad \textbf{Equation 2.31}$$

which represents the closed-form solution of the iterative approach outlined in Sharma *et al.* [2011]. This expression is rearranged in terms of the horizontal shear stress across the joints to give:

$$\tau_{jh} = p_t\frac{\alpha}{2} + p_t\sqrt{\left(\frac{\alpha}{2}\right)^2 + 1 + \frac{\sigma_a}{p_t}} \qquad \textbf{Equation 2.32}$$

and substituting in the terms previously defined for the moment in the joint to give:

$$M_j = p_t b_j h_c \left(\frac{Hjd}{H - jd}\right)\left(\frac{h_b}{2h_c} + \sqrt{\left(\frac{h_b}{2h_c}\right)^2 + 1 + \frac{N_c}{p_t b_j h_c}}\right) \qquad \textbf{Equation 2.33}$$

where the value of p_t for each limit state is determined from comparison with experimental tests by means of a κ coefficient which is related to the tensile strength of the concrete as proposed by Priestley [1997], who proposed a set of coefficients for structures with deformed bars and no joint transverse shear reinforcement. This is represented by:

$$p_t = \kappa\sqrt{f_c'} \qquad \textbf{Equation 2.34}$$

Further experimental work in Pavia, Italy [Calvi *et al.*, 2002b; Pampanin *et al.*, 2003] resulted in a revised set of coefficients for specimens with smooth hook-ended bars compared to those initially outlined by Priestley [1997]. This approach of cracking and peak force are adopted here, in addition to the introduction of an ultimate strength to represent the strength and stiffness degradation in the joints. The κ coefficients derived here will differ slightly from those of Pampanin *et al.* [2003] since the additional shear force transfer provided by the beam section is considered here. The following section will also discuss the determination of the shear deformation at the various limit states mentioned previously. The shear strength of the joint is represented in terms of moment capacity since the

numerical modelling employs the use of a zero-length rotational spring, where the spring rotation is taken to be equal to shear deformation of the joint, as per previous numerical modelling approaches outlined in Section 2.3.2.2.

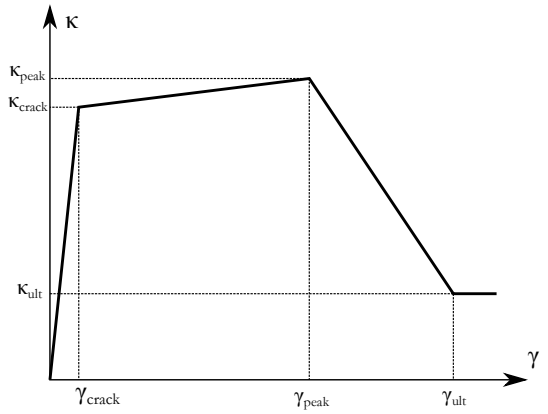

Figure 2.19. Monotonic backbone curve of beam-column principle tensile stress limit states for exterior beam-column joints.

2.3.2.2 Numerical Modelling of Exterior Beam-Column Joints

For this research, the joint strength capacity model described in the previous section needs to be developed into a numerical model to represent both the strength, stiffness and also the hysteretic response of the beam-column joint. This section first presents a discussion of some existing numerical modelling approaches for exterior beam-column joints followed by the numerical model adopted here.

2.3.2.2.1 Review of Existing Numerical Models

Modelling of exterior beam-column joints has received much attention in terms of research throughout the past 30 years, with many different modelling approaches being proposed, varying from single spring model models to more detailed multi-spring models and more advanced finite element models. While a critical review of each of the available models in the literature and how these proposals pertain to the numerical modelling of exterior joints would be a welcome discussion here, numerous literature reviews on the past proposals and the evolution in terms of complexity can be found in the literature [Celik and Ellingwood, 2008; Shafaei *et al.*, 2014; Sharma *et al.*, 2011] and are thus omitted here for brevity. In place of this, a brief discussion on some of these existing models that are of direct relevance to the work presented here is provided.

Many of the more recent models proposed in the literature present two principle differences to the joints considered in this study; many of these models are developed for

specimens with deformed bars and with different end-anchorage conditions. These are important features as the use of smooth bars greatly increases the bar slip due to a poorer bond which results in an increased lateral deformation of the structure and the use of end-hook anchored bars has been shown to cause a rather brittle joint failure mechanism. As a result of the experimental campaign carried out by Pampanin *et al.* [2002], a numerical model was proposed in Pampanin *et al.* [2003] in order to model the behaviour of the shear hinge observed in the specimens and how the influence of this brittle behaviour could be accounted for. Further work by Galli [2006] using this same modelling approach showed how a reasonably good estimate could be obtained when compared to the specimens tested by Pampanin *et al.* [2002] and Calvi *et al.* [2002a]. While this modelling approach for smooth bars with end-hooks worked well in terms of the capacity of the connection, the material model was unable to capture the strength degradation in the joint, which was observed to be significant during testing.

Sharma *et al.* [2011] proposed a model, which considered the shear deformation within the joint and compared it to numerous test specimens with deformed bars and different anchorage conditions showing very promising results in terms of strength and stiffness prediction. However, the calibration by Sharma *et al.* [2011] was a monotonic pushover and did not include any specimens with end-hook anchorage, but did highlight the importance of considering the joint behaviour by showing the response of a model omitting the joint behaviour which was often very different to the measured test specimen terms of strength and ductility capacity.

2.3.2.2.2 Proposed Numerical Model

The proposed numerical model for exterior beam-column joints is composed of various springs and elements to account for the different behaviours and mechanisms discussed previously, which mainly concern the adequate representation of the beam and column member response and the joint behaviour. Section 2.2.2 discussed the modelling of beam-column members consisting of smooth bars. The proposed model shown in Figure 2.1 illustrates how both the flexural and shear behaviour of the members is modelled using a lumped plasticity approach for the flexure and an uncoupled shear spring to account for the shear behaviour of the element, which can capture the element's behaviour in shear. Both the shear and flexural springs are defined using a set of expressions, which have been calibrated to existing experimental data from testing of on members with smooth bars and were outlined in Sections 2.2.2.1 and 2.2.2.2 for flexure and shear, respectively. The shear behaviour of the joint has also been outlined earlier in this section, where the parameters to be used for the modelling are defined later.

Using this combination of beam-column elements and joint springs, the proposed model is illustrated in Figure 2.20, where the layout and connectivity of the various elements and

springs are shown. The joint region is represented by a series of rigid-link offsets with a lumped rotational spring to represent the shear deformation of the joint region.

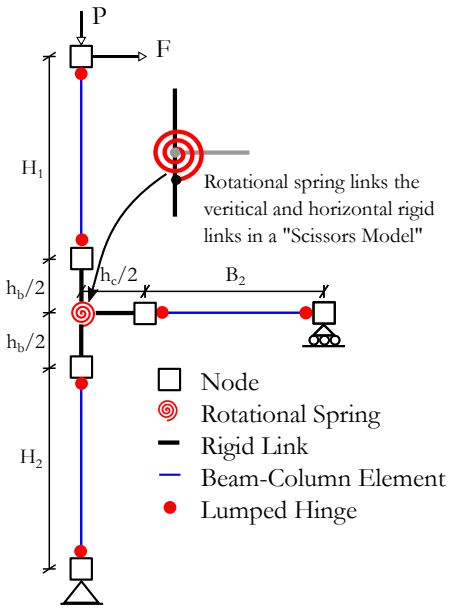

Figure 2.20. Proposed model layout for exterior beam-column joints.

As previously discussed in Section 2.3.2.1, the proposed model adopts the approach of using principle tensile stress limit states for the definition of the joint behaviour. These principle tensile stress limit states are determined through experimental observation and are expressed as a function of the concrete tensile strength, as initially proposed by Priestley [1997]. The recommended coefficients are given in conjunction with to the calibrated model in Section 2.3.2.1, and the set of proposed coefficients is based on comparison with experimental test results. The actual values of κ used here are determined based on the median calibrated values outlined later in Table 2.7. While there have been many proposals for coefficients for exterior beam-column joints, such as 0.2 by Pampanin *et al.* [2003], it must be stated that the values here are slightly lower than these due to the fact that in Section 2.3.2.1, the proposed model accounts for the contribution of the beam shear force transfer when computing the vertical stress acting in the joint, which had previously been considered by Sharma *et al.* [2011] but not in the initial work by Pampanin *et al.* [2003]. From these calibrated values, the median values are proposed here for use in uniaxially loaded exterior beam-column joints and are given in Table 2.4.

Table 2.4. Proposed shear strength coefficient (κ) values for each limit state in exterior joints.

Limit State	κ	Dispersion*
Cracking	0.135	0.166
Peak	0.135	0.166
Ultimate	0.050	0.091

*Based on data from 10 test specimens

Since the capacity of the rotational spring can be computed using the expressions in Section 2.3.2.1, the corresponding shear deformation limit states need to be defined. These are illustrated in the monotonic backbone curve in Figure 2.19 to correspond to first cracking of the concrete, peak load and degradation to a residual strength. Some test campaigns have proposed reasonable ranges for the joint's shear deformation and it's corresponding limit state, such as Pampanin *et al.* [2003], which are based on visual observation during tests in addition to measured values from testing by Akguzel [2011]. The approach here is to calibrate the three limit states shown in Figure 2.19 to the existing experimental information and compare these with the existing proposals of shear deformation to also propose a general set of limit state shear deformations for exterior beam-column joints with smooth end-hook anchorage. Table 2.7 shows the different parameters used in the calibration to 10 different experimental tests. Among these are the values assumed for the shear deformation at the three different limit states, which were calibrated based on the experimental tests in order to give the best representation of the initial stiffness of the rotational spring and also to capture the peak loading and descending branch of the response.

The proposed values are given in Table 2.5 and some comments can be made in relation to existing proposals of joint shear deformation limits states. The shear deformation at cracking has been set at 0.0002 radians as initially proposed by Pampanin *et al.* [2003] since, as will be seen in the following section, this value gives quite good results in terms of matching the initial stiffness of the model and test data. It should be noted, however, that one parameter which may lead to an increase in the value for shear deformation at cracking is the axial load ratio. This trend was highlighted in a numerical parametric study by Genesio [2012] and also in the approach proposed by Metelli *et al.* [2015]. However, since the axial load ratio of the specimens tested here was quite low and relatively constant (ν between 0.06-0.21 with a mean of 0.12), it was rather difficult to confirm this trend from experimental data, so much so as to warrant inclusion in the limit state definition. This trend also applies to the other limit states and is stated here to be an area that needs further work to clarify an appropriate trend. Similarly, Genesio [2012] and Metelli *et al.* [2015] both note a dependence of the shear deformation limit states on beam to column height ratios, but due to the relatively constant ratios in the test data here, a similar conclusion to that of the axial load dependence is drawn.

Comparing the shear deformations at peak, which corresponds to the points at which degradation of strength begins, and ultimate responses to that of the measured experimental value of the "2D1" specimen plotted in Akguzel [2011], the proposed values match well with this specimen's response in that the principle tensile stress capacity begins to degrade at roughly the same shear deformation proposed here. Similarly, the values proposed in Pampanin *et al.* [2003], which are based on test observations suggests that extensive damage and repairability issues arise at deformation levels between 0.01 and 0.015 radians, where deformations exceeding 0.015 rad were noted to lead to incipient collapse. Comparing these values with those of Table 2.5 shows that the proposed median values for the defined limit states match reasonable well, with the proposed value for peak and ultimate response falling within the ranges proposed by Pampanin *et al.* [2003].

Table 2.5. Proposed shear deformation (γ) values for each limit state in exterior joints.

Limit State	γ [rad]	Dispersion*
Cracking	0.0002	-
Peak	0.0127	0.286
Ultimate	0.0261	0.229

*Based on data from 10 test specimens

Since the monotonic behaviour of the joint can now be defined, the last remaining detail to be defined is the hysteretic behaviour of the rotational spring element. The hysteretic model used is the Hysteretic[3] uniaxial material model available in OpenSees and has been calibrated based on the existing experimental data in the literature, as will be shown in the next section. This material model allows for the definition of a set of parameters to control the pinching behaviour and also the degradation of the unloading stiffness. In addition, cyclic strength degradation can be defined in terms of both energy and ductility. Table 2.6 shows the parameters adopted here, where the parameters are illustrated in Figure 2.21.

[3] http://opensees.berkeley.edu/wiki/index.php/Hysteretic_Material

Table 2.6. Calibrated hysteretic parameters for the exterior joint Hysteretic material model.

Parameter	Proposed Value
pinchX	0.6
pinchY	0.2
damage1	0.0
damage2	0.0
beta	0.3

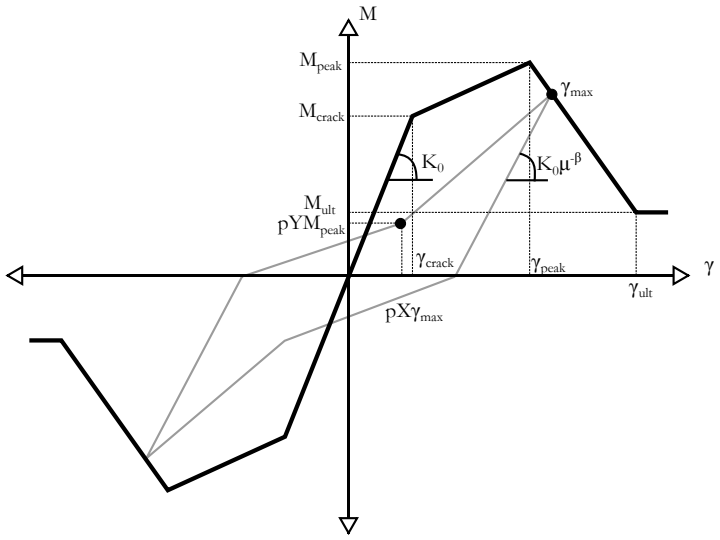

Figure 2.21. Hysteretic material model for exterior beam-column joints.

2.3.2.2.3 Comparison with Experimental Test Results

Using the model previously described, this section collects and presents the available test data on exterior beam-column joints with smooth end-hooked bars and no transverse shear reinforcement in the joint. The results from each of these tests are then compared with that of the model described earlier, where for the case of the joint, a number of parameters outlined in Figure 2.19 are calibrated. Table 2.7 outlines a total of 10 experimental tests on exterior joint specimens constructed with smooth bars with end-hooks. For each of the specimens listed in Table 2.7, a numerical model was constructed according to the layout in Figure 2.20 and a static cyclic pushover analysis was performed. The parameters associated with the strength and deformation capacity of the rotational shear hinge were then calibrated based on comparison with the observed test data. For some of the tests, actual data was not available to be plotted and hence a screenshot of the test plot from the

publication is placed behind the images at the correct scale to give an indication of the model comparison. In some cases, there is more than one set of test data plotted in the original publication, therefore the reader should be aware what comparison is being made here with reference to the background image. The hysteretic parameters used for each of the test specimens are given in Table 2.7 and using these parameters the comparative plots are made in Figure 2.22 and Figure 2.23, where the reference of each test is given above each subplot.

Comparing the results of the experiments of the cyclic pushover analyses of specimens with those of the experiment results the match is quite good. The backbone matches well in terms of initial stiffness and strength envelope including the degradation of the test specimens at large shear deformation. In addition, the hysteretic behaviour is quite good, where the pinching behaviour of the specimens is modelled well, with the stiffness transitions between positive and negative loading well represented. Also, the unloading stiffness of the specimens is well represented by the fact that the β factor used in the Hysteretic material model was set to allow a gradual degradation of the unloading stiffness with increasing ductility. While the κ values outlined in Table 2.7 were calibrated based on the hysteretic behaviour of the specimens, the residual strength values for κ_{ult} were chosen as an appropriate value, since none of the tests pushed the specimens to a complete loss of strength, meaning it was quite difficult to determine a residual strength. This represents an area in which future tests on such specimens could lead to improved understanding, as this capacity could greatly influence structural behaviour at ultimate limit states.

Table 2.7. Calibrated shear hinge parameters for exterior beam-column joint specimens.

#	Reference	ID		κ_{crak}	κ_{peak}	κ_{ult}	γ_{crack} [rad]	γ_{peak} [rad]	γ_{ult} [rad]
1	Pampanin *et al.* [2002]	T1	(-)	0.13	0.13	0.06	0.0002	0.014	0.025
			(+)	0.11	0.11	0.06	0.0002	0.015	0.025
2	Pampanin *et al.* [2002]	T2	(-)	0.13	0.13	0.05	0.0002	0.009	0.020
			(+)	0.11	0.11	0.05	0.0002	0.009	0.020
3	Braga *et al.* [2009]	T23-1	(-)	0.11	0.11	0.05	0.0002	0.018	0.026
			(+)	0.12	0.12	0.05	0.0002	0.015	0.025
4	Melo *et al.* [2012]	TPA-2	(-)	0.14	0.14	0.05	0.0002	0.012	0.025
			(+)	0.14	0.14	0.05	0.0002	0.012	0.025
5	Melo *et al.* [2012]	TPB-2	(-)	0.14	0.14	0.06	0.0002	0.016	0.030
			(+)	0.14	0.14	0.06	0.0002	0.016	0.030
6	Melo *et al.* [2012]	TPC	(-)	0.11	0.11	0.05	0.0002	0.007	0.016
			(+)	0.11	0.11	0.05	0.0002	0.007	0.016
7	Akguzel [2011]	2D1	(-)	0.20	0.20	0.05	0.0002	0.015	0.030
			(+)	0.18	0.18	0.06	0.0002	0.015	0.030
8	Akguzel [2011]	3D1x	(-)	0.16	0.16	0.05	0.0002	0.012	0.03
			(+)	0.14	0.14	0.05	0.0002	0.012	0.03
9	Akguzel [2011]	3D1y	(-)	0.14	0.14	0.05	0.0002	0.012	0.03
			(+)	0.14	0.14	0.05	0.0002	0.012	0.03
10	Beschi *et al.* [2014]	CJ	(-)	0.12	0.12	0.05	0.0002	0.018	0.04
			(+)	0.12	0.12	0.05	0.0002	0.018	0.04

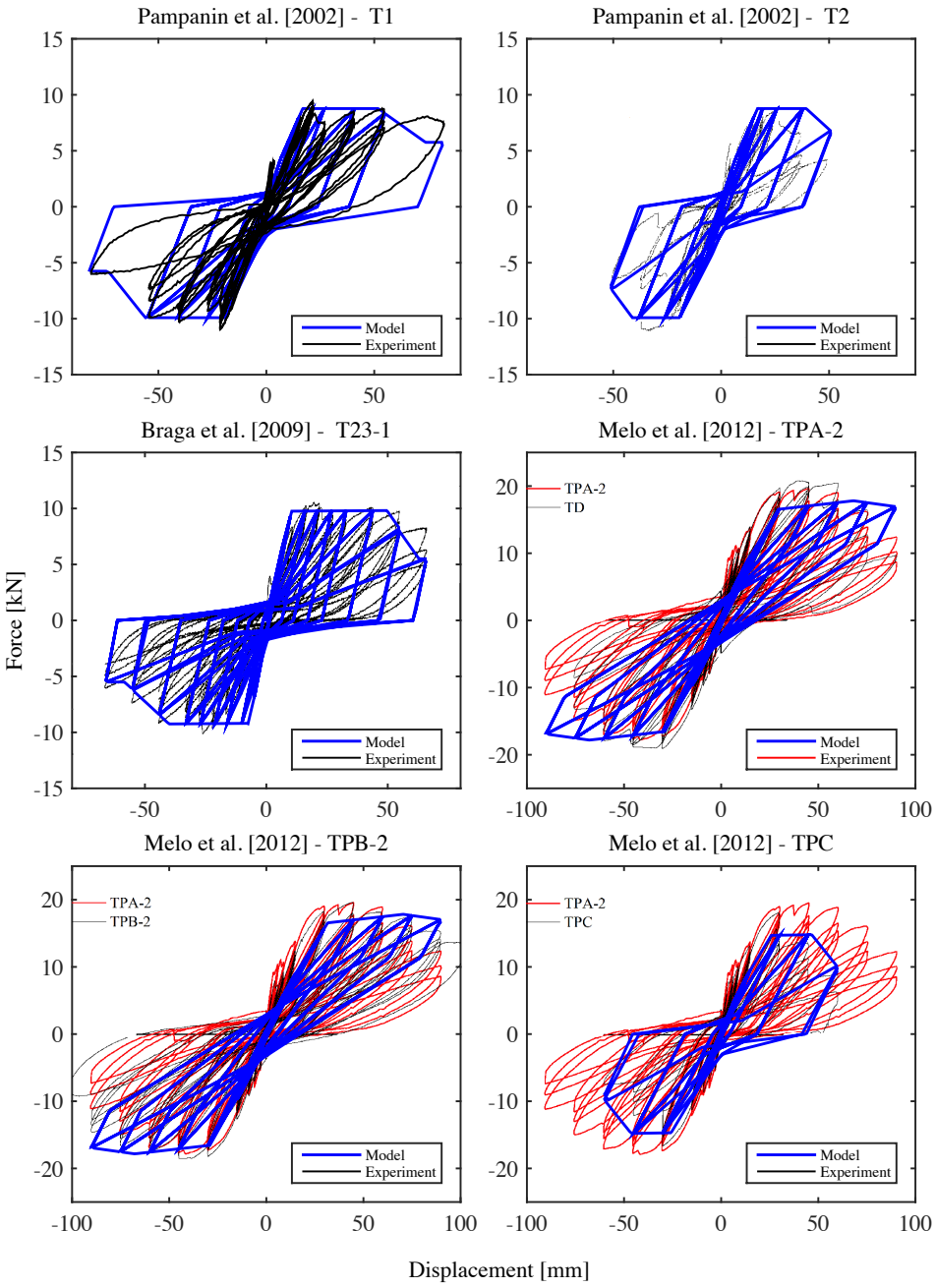

Figure 2.22. Cyclic pushover comparison of experimental and numerical model on exterior joints.

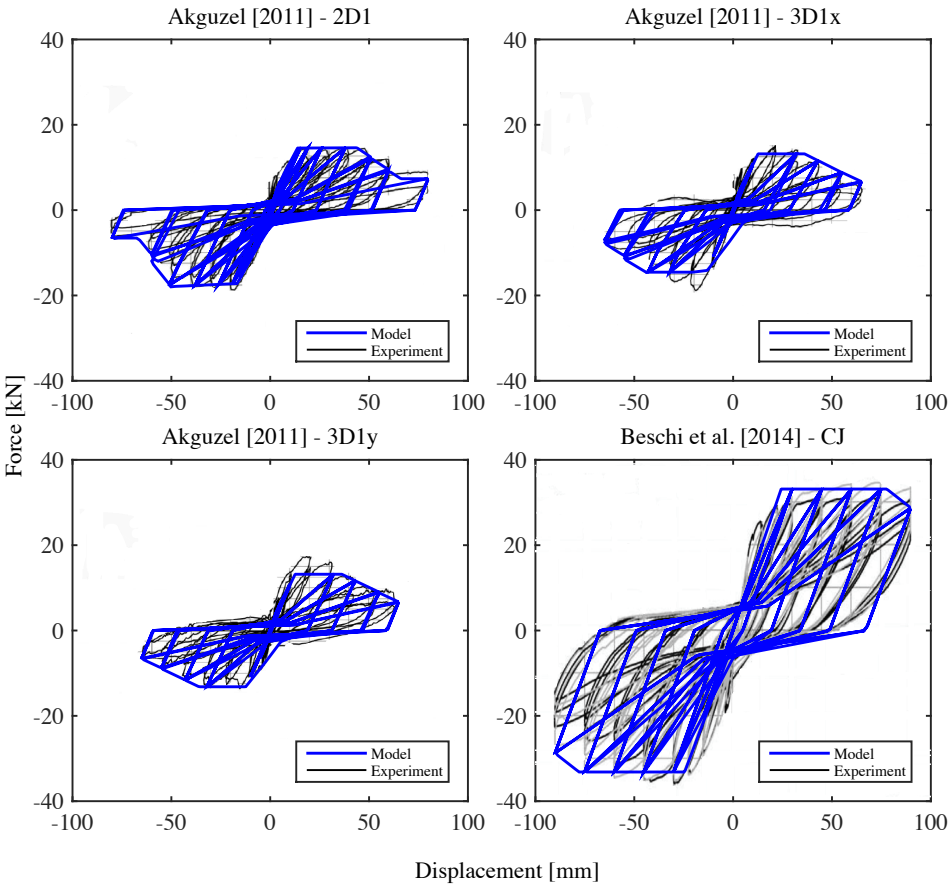

Figure 2.23. Cyclic pushover comparison of experimental and numerical model on exterior joints.

2.4 INTERIOR BEAM-COLUMN JOINTS

In addition to the modelling of exterior joints of older RC structures in Italy, the modelling of the interior joints warrants similar consideration. Although the end anchorage failure mechanisms such as the concrete wedge mechanism are not expected in interior joints, the behaviour needs to be clarified, mainly as a result of the effects of no shear reinforcement in the joint. This section presents a similar piece of work to that of exterior joints, where experimental testing is reviewed to highlight the behaviour of these types of joints. The numerical modelling is then outlined and the proposed model described and compared to available experimental tests.

2.4.1 Experimental Testing on Interior Beam-Column Joints

Pampanin *et al.* [2002] conducted two tests on interior beam-column joints at the University of Pavia, which were representative of a 3-storey RC frame designed to pre-1970 standards in Italy. From the cyclic testing of the specimens, Pampanin *et al.* [2002] noted that the occurrence of a plastic hinge mechanism in the column member relatively early in the tests resulted in a concentration of damage in this region and as a result, very little joint damage was observed. This highlighted the lack of strength hierarchy in the beam-column joint as is the case with modern capacity design considerations, where the strength of the column member is set to be higher than the corresponding beam strength to ensure a more stable beam-sway mechanism develops. As a result of the flexural yielding in the column member, Pampanin *et al.* [2002] reports that the use of smooth reinforcing bars resulted in a large amount of slippage of the longitudinal reinforcing bars in the column members, which enhanced their deformation capacity.

Melo *et al.* [2014] tested a total of 5 interior beam-column joints constructed in accordance with the pre-1970 Portuguese design code. The detailing of the specimens is quite similar to that of the Italian specimens, where smooth reinforcement is used in conjunction with lapping of the column bars above the joints and stirrups closed at 90°. In addition to lapping of longitudinal bars in the column members, Melo *et al.* [2014] conducted testing on a specimen, that had lapping of the beam longitudinal bars also. A sixth specimen was also constructed using deformed bars in order to compare with the smooth bar specimen. Contrary to the testing performed by Pampanin *et al.* [2002] on interior beam-column sub-assemblages, only one of the specimens tested by Melo *et al.* [2014] reported flexural yielding of the beam or column members, with the joint shear deformation the principle mode of failure in the rest of the tested specimens. This flexural yielding occurred in the upper column for the specimen with lapping in both the column and beam plastic hinge zones. As reported by Braga *et al.* [2009], the flexural cracking in the specimens with smooth bars tended to concentrate in the beam and column member ends whereas the specimen with deformed bars spread the cracks much more over the end-zone. Melo *et al.* [2014] also tested a specimen containing a slab cast in with the beam section. The global hysteresis of the specimen was quite similar when compared to the reference specimen, but with a slight increase in the global strength capacity in the negative direction. Testing by Fernandes *et al.* [2012] again showed how the presence of smooth bars significantly affected the response of the interior beam-column test specimens in terms of its pinching behaviour. It was also reported how the loading history did not affect the peak response that much, and it was noted how an increase in axial load resulted in an increase in strength degradation upon reaching peak response of the specimen.

2.4.2 Modelling of Interior Beam-Column Joints

Considering the experimental observations of the behaviour of pre-1970's interior beam-column joints subjected to seismic loading, a numerical model is herein proposed to consider this behaviour for future seismic assessments of existing structures. Firstly, methods of evaluating joint shear strength are reviewed and proposed, followed by the description of the numerical model.

2.4.2.1 Shear Strength Modelling in Interior Beam-Column Joints

Similar to the previous section on exterior beam-column joints, this section examines the analytical approach to quantifying the shear strength of interior beam-column joints. A brief review of existing approaches followed by a description of the adopted model. Since the basis of the model adopted here is fundamentally the same as proposed by others, the discussion is quite brief and is included for clarity.

2.4.2.1.1 Review of Existing Shear Strength Models

Many of the studies examining the behaviour and response of interior beam-column joints tend to also examine the response of exterior beam-column joints to represent the response of an entire RC structure, as does this report. As has been previously noted in Section 2.3, the performance of exterior beam-column joints with sub-standard joint detailing can be quite critical and hence, much research has been devoted to modelling the behaviour of these with the various aspects such as anchorage detailing and bar type being accounted for. As for interior joints, the end anchorage differences observed between different countries does not tend to cause a problem when examining interior joints from different regions.

Previous efforts to model the behaviour of poorly reinforced beam-column joints can be found in studies such as Lowes and Altoontash [2003], where the modified compression field theory was used to predict the joint strength, following some modifications proposed by Stevens *et al.* [1991] to account for cyclic loading of the joint. However, as previously highlighted in Section 2.2.2.2 of this report, a significant discrepancy between the monotonic and cyclic loading of shear panel specimens was noted, to which the GCCM was proposed to account for this behaviour. However, this method is quite complicated and the required level of user input makes it impractical in its current development and considering the aims of this research. Following the test campaign carried out by Calvi *et al.* [2002a], Pampanin *et al.* [2003] developed a simplified approach for characterising the shear strength of interior beam-column joints, which was based on the principle joint stresses initially proposed by Priestley [1997]. This approach compared the observed principle tensile stress limit states for interior joints with smooth bars and no transverse reinforcement and compared them to values initially proposed by Priestley [1997] for well-detailed joints. As a result, a revised set of coefficients were proposed by Pampanin *et al.*

[2003] for joints using plain bars and having no transverse joint reinforcement. This initial proposal by Priestley [1997] and refinement by Pampanin *et al.* [2003] is a direct and accurate approach to assessing the strength of beam-column and is therefore adopted here, as in the case of exterior joints. The following section describes the process to determine the capacity of an interior beam-column joint, which will be later confirmed by the experimental evidence available in the literature.

2.4.2.1.2 Adopted Shear Strength Model

The layout of an interior beam-column joint is shown in Figure 2.24. Taking the equilibrium across the Section A-A, the horizontal shear force acting across the joint is given by:

$$V_{jh} = T_1 + C_{S2} + C_{C2} - V_c \qquad \textbf{Equation 2.35}$$

and by using the balance of cross-section forces in the left-hand side beam, this gives:

$$T_2 = C_{S2} + C_{C2} \qquad \textbf{Equation 2.36}$$

resulting in the following for the horizontal shear forces across Section A-A:

$$V_{jh} = T_1 + T_2 - V_c \qquad \textbf{Equation 2.37}$$

The tension force in beam reinforcement can be related to the bending moment (M_b) as follows:

$$T = \frac{M_b}{jd} \qquad \textbf{Equation 2.38}$$

where jd is the distance between the tensile reinforcement and the centre of compression in the section, typically taken as 0.9d, where d is the depth to the centre of the tensile reinforcement in the section. Using this relation, the horizontal shear across Section A-A can now be written as:

$$V_{jh} = \frac{M_{b1}}{jd_1} + \frac{M_{b2}}{jd_2} - V_c \qquad \textbf{Equation 2.39}$$

The shear in the column is related to the moment in the joint through:

$$V_c = \frac{M_j}{2}\frac{2}{H} = \frac{M_j}{H} \qquad \textbf{Equation 2.40}$$

where H is the interstorey height and M_j is taken as the sum of the beam moments to be:

$$M_j = M_{b1} + M_{b2}$$ **Equation 2.41**

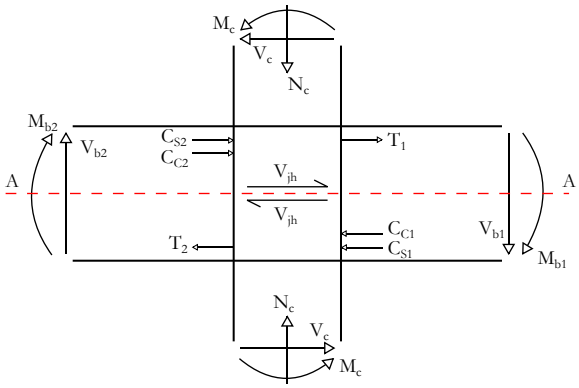

Figure 2.24. Forces within an interior beam-column joint subassembly.

If the beam sections on either side of the joint are taken as equal, this implies:

$$jd = jd_1 = jd_2$$ **Equation 2.42**

which can be substituted in the above expression for V_{jh} as follows:

$$V_{jh} = \frac{M_{b1}}{jd_1} + \frac{M_{b2}}{jd_2} - V_c$$ **Equation 2.43**

$$= \frac{M_{b1}}{jd} + \frac{M_{b2}}{jd} - \frac{M_j}{H}$$ **Equation 2.44**

$$= \frac{M_j}{jd} - \frac{M_j}{H}$$ **Equation 2.45**

$$= M_j \left(\frac{1}{jd} - \frac{1}{H} \right)$$ **Equation 2.46**

The horizontal shear stress across Section A-A in the joint is given as:

$$\tau_{jh} = \frac{V_{jh}}{b_j h_c} \qquad \textbf{Equation 2.47}$$

where h_c is the column section height and b_j is the joint width given by NZS 3101 [2006] as:

$$b_j = \begin{cases} \min(b_c, b_b + 0.5h_c) \text{ if } b_c \geq b_b \\ \min(b_b, b_c + 0.5h_c) \text{ if } b_b \leq b_c \end{cases} \qquad \textbf{Equation 2.48}$$

where b_c and b_b are the column and beam section widths, respectively. Since the beam sections on either side of the joint are assumed to be of the same section, their equal magnitude and opposing directions cancel out and the vertical stress in the joint (σ_{jv}) is given as:

$$\sigma_{jv} = \frac{N_c}{b_j h_c} \qquad \textbf{Equation 2.49}$$

and from Mohr's circles of stresses, the principle stresses (tension and compression) in the joint are determined as:

$$p_{t,c} = -\frac{\sigma_{jv}}{2} \pm \sqrt{\left(\frac{\sigma_{jv}}{2}\right)^2 + \tau_{jh}^2} \qquad \textbf{Equation 2.50}$$

where the principle tensile stress (p_t) is given as:

$$p_t = -\frac{\sigma_{jv}}{2} + \sqrt{\left(\frac{\sigma_{jv}}{2}\right)^2 + \tau_{jh}^2} \qquad \textbf{Equation 2.51}$$

and is then rearranged in terms of τ_{jh} as:

$$\tau_{jh} = p_t \sqrt{1 + \frac{\sigma_a}{p_t}} \qquad \textbf{Equation 2.52}$$

Combining the above terms by relating the horizontal joint shear term, it becomes:

$$\tau_{jh} b_j h_c = M_j \left(\frac{1}{jd} - \frac{1}{H}\right) \qquad \textbf{Equation 2.53}$$

which is then rearranged to:

$$M_j = \tau_{jh} b_j h_c \left(\frac{Hjd}{H - jd} \right) \qquad \textbf{Equation 2.54}$$

and substituting Equation 2.53 into Equation 2.54 gives:

$$M_j = p_t b_j h_c \left(\frac{Hjd}{H - jd} \right) \left(\sqrt{1 + \frac{N_c}{p_t b_j h_c}} \right) \qquad \textbf{Equation 2.55}$$

where the principle tensile stress (p_t) is represented by:

$$p_t = \kappa \sqrt{f_c'} \qquad \textbf{Equation 2.56}$$

where the coefficients κ are illustrated in Figure 2.25 with respect to the different limit states of joint cracking and ultimate force. These coefficients are determined from experimental testing observations at the two limit states considered.

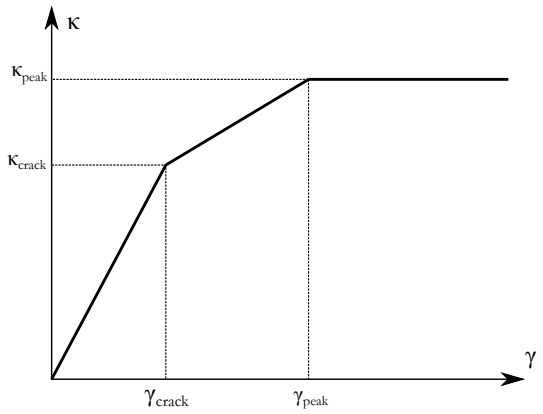

Figure 2.25. Monotonic backbone curve of beam-column principle tensile stress limit states for interior beam-column joints.

2.4.2.2 Numerical Modelling of Interior Beam-Column Joints

This section briefly reviews some of the previous modelling interior beam-column joints, both in terms of the modelling layout and the hysteretic parameter definition of the model. The proposed model is then outlined and described in detail followed by a comparison with existing experimental data available in the literature to calibrate its accuracy.

2.4.2.2.1 Existing Numerical Models

As previously mentioned, many of the existing models previously proposed for the modelling of interior beam-column joints correspond to the variations of the same models proposed for exterior joints. As such, much of the discussion in Section 2.4.2 regarding the developments of different joint layouts for interior joints is valid for the current discussion. That is, the different proposals in terms of joint modelling layout where a number of springs and degrees of freedom (DOF) varied from more detailed models, such as the 12 degree of freedom model developed by Lowes and Altoontash [2003] to the simpler scissors model proposed by Alath and Kunnath [1995]**.** The model adopted here is a development of the scissors model proposed by Alath and Kunnath [1995], where the joint hinge's hysteretic behaviour is calibrated to capture strength degradation.

2.4.2.2.2 Proposed Numerical Model

For the numerical modelling of interior beam-column joints, the proposed model consists of a number of different features to capture the behaviour of the various components of the beam-column joint subassembly. The first of these is the consideration of the beam and column elements previously described in Section 2.2 that were calibrated against numerous experimental test results on beam-column members constructed with smooth reinforcing bars and poor shear reinforcement stirrups. To account for the joint behaviour, the joint shear model previously described in Section 2.4.2.1 to develop a moment-rotation relation is used to define the rotational spring's hysteretic behaviour. Combining these different modelling parameters to account for the different sources of deformation, the final model for an interior joint sub-assembly is illustrated in Figure 2.26.

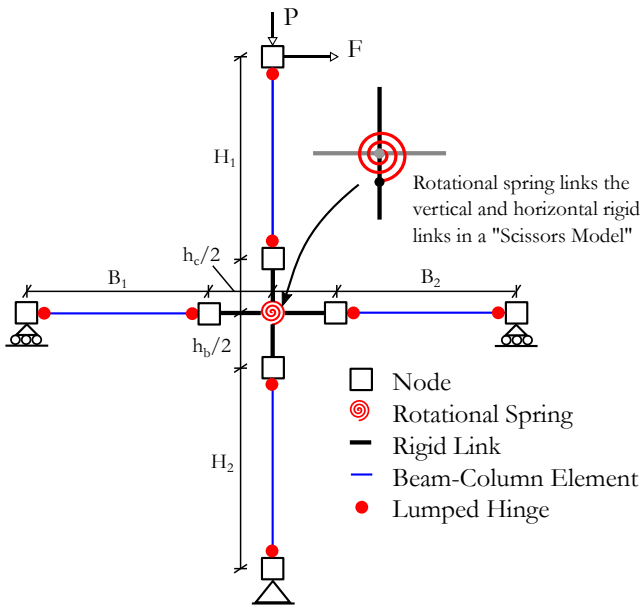

Figure 2.26. Proposed model layout for interior beam-column joints.

As previously mentioned, the rotational spring located at the beam-column intersection is to represent the shear deformation behaviour of the joint region. The general behaviour of this hinge is illustrated in Figure 2.27, where the hysteretic rule adopted is that of the Hysteretic uniaxial material model in OpenSees, as per the exterior beam-column joint case. As described in Section 2.4.2.1, the backbone of the rotational hinge is described using the derived expressions. To determine these, the parameters κ are needed for each limit state considered, which for the interior joint are the joint cracking and reaching of peak response. Since this hinge defined in the numerical model is defined as moment versus rotational deformation to represent joint shear force versus shear deformation, this implies that the joint rotational deformation and shear deformation are considered equal, which is a reasonable assumption as per Pampanin *et al.* [2002], among others. The values of κ and γ for each limit state are determined from the available experimental data, which will be discussed in more detail in the following paragraphs when the comparison of the proposed model with test data is discussed.

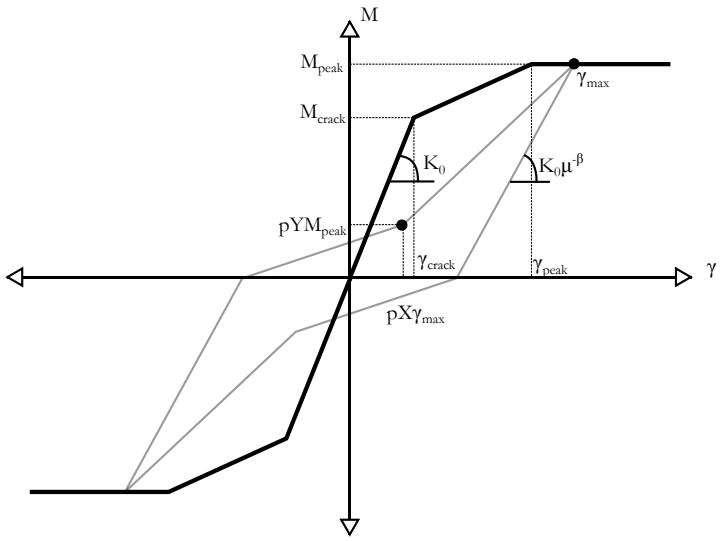

Figure 2.27. Hysteretic material model for interior beam-column joints.

For the two limit states outlined in Figure 2.27, the proposed coefficients are given in Table 2.8 and Table 2.9, which are based on the median calibrated values for 15 different experimental test specimens available in the literature for the shear strength coefficient and shear deformation, respectively. As can be seen from Table 2.8, the proposed values for κ correspond to those previously proposed by Pampanin *et al.* [2003] following the testing of Calvi *et al.* [2002a], although the proposed γ values in Table 2.9 differ slightly. The proposed γ values stem from the calibration of the observed joint damage to the numerical model definition. The level of dispersion, or logarithmic standard deviation, associated with each of the proposed coefficients is also provided in Table 2.8 and Table 2.9.

Table 2.8. Proposed shear strength coefficient (κ) for each limit state in interior joints.

Limit State	κ	Dispersion*
Cracking	0.29	0.237
Peak	0.42	0.163

*Based on data from 15 test specimens

Table 2.9. Proposed shear deformations (γ) values for each limit state in interior joints.

Limit State	γ [rad]	Dispersion*
Cracking	0.0002	-
Peak	0.0085	0.133

*Based on data from 15 test specimens

In contrast to the exterior beam-column joint model, the hysteretic behaviour of the proposed interior joint backbone curve does not possess an in-cycle strength degradation to a residual strength. This is because the in-cycle strength degradation of the interior joints was often reported to be not as detrimental as the degradation of exterior joints, where the shear hinge and concrete wedge mechanisms were reported resulting in a more abrupt and severe loss of strength. It is acknowledged, however, that a certain amount of cyclic strength degradation does exist within interior joints, as will be seen in the following paragraphs and this has been accounted for by introducing an energy-based degradation parameter in the Hysteretic material model used in OpenSees. This way, the gradual degradation of the interior joint shear strength can be accounted for. In addition to the other hysteretic parameters previously outlined in the corresponding exterior joint model, the proposed parameters are given in Table 2.10 for the modelling of interior beam-column joints with smooth bars without any joint shear reinforcement.

Table 2.10. Calibrated hysteretic parameters for the interior joint Hysteretic material model.

Parameter*	Proposed Value
pinchX	0.6
pinchY	0.2
damage1	0.0
damage2	0.010
beta	0.3

*For definition of parameters, see OpenSees command manual.

2.4.2.2.3 Comparison with Experimental Test Results

Existing experimental data available in the literature is compared with the proposed numerical model outlined in the previous section to demonstrate its accuracy. Table 2.11 shows the list of test specimens collected for various different experimental campaigns. Using this test data, a comparison between the computed response and the observed is provided in Figure 2.28 to Figure 2.30 for the 15 specimens listed in Table 2.11. For the hysteretic properties of the shear hinge used in each case, Table 2.11 lists the calibrated parameters, to which the values proposed in Table 2.8 are derived.

Examining the response of the numerical model compared with the test results for all of the specimens shown in Figure 2.28 to Figure 2.30, the backbone response of the specimens is well represented by the numerical model. This is especially prominent through the cyclic degradation of the specimens with increasing energy, where the gradual degradation of the specimens is well represented by the numerical model. In addition, the pinching behaviour characteristic of specimens with smooth bars is also well represented between cycles, although the numerical model tends to overestimate the unloading strength of the specimens, where the tests tend to show more pinching when unloading from peak response.

Table 2.11. Calibrated shear hinge parameters for interior beam-column joint specimens.

#	Reference	ID		κ_{crack}	κ_{peak}	γ_{crack}	γ_{peak}	d_2
1	Pampanin *et al.* [2002]	C2	(-)	0.29	0.5	0.0002	0.011	0.010
			(+)	0.29	0.42	0.0002	0.010	
2	Pampanin *et al.* [2002]	C4	(-)	0.29	0.5	0.0002	0.011	0.010
			(+)	0.29	0.42	0.0002	0.010	
3	Braga *et al.* [2009]	C23-1	(-)	0.29	0.6	0.0002	0.011	0.008
			(+)	0.29	0.6	0.0002	0.010	
4	Braga *et al.* [2009]	C23-2	(-)	0.29	0.52	0.0002	0.011	0.008
			(+)	0.29	0.52	0.0002	0.010	
5	Braga *et al.* [2009]	C11-1	(-)	0.29	0.52	0.0002	0.008	0.010
			(+)	0.29	0.52	0.0002	0.008	
6	Melo *et al.* [2014]	IPA-1	(-)	0.29	0.42	0.0002	0.008	0.015
			(+)	0.29	0.42	0.0002	0.008	
7	Melo *et al.* [2014]	IPA-2	(-)	0.29	0.42	0.0002	0.008	0.016
			(+)	0.29	0.42	0.0002	0.008	
8	Melo *et al.* [2014]	IPB	(-)	0.29	0.42	0.0002	0.008	0.016
			(+)	0.29	0.42	0.0002	0.008	
9	Melo *et al.* [2014]	IPD	(-)	0.29	0.42	0.0002	0.008	0.020
			(+)	0.29	0.42	0.0002	0.008	
10	Melo *et al.* [2014]	IPE	(-)	0.29	0.42	0.0002	0.008	0.016
			(+)	0.29	0.42	0.0002	0.008	
11	Fernandes *et al.* [2012]	JPA-1	(-)	0.29	0.42	0.0002	0.007	0.002
			(+)	0.29	0.42	0.0002	0.007	
12	Fernandes *et al.* [2012]	JPA-2	(-)	0.29	0.42	0.0002	0.007	0.002
			(+)	0.29	0.42	0.0002	0.007	
13	Fernandes *et al.* [2012]	JPA-3	(-)	0.2	0.42	0.0002	0.008	0.008
			(+)	0.2	0.42	0.0002	0.008	
14	Fernandes *et al.* [2012]	JPB	(-)	0.15	0.32	0.0002	0.008	0.002
			(+)	0.15	0.32	0.0002	0.008	
15	Fernandes *et al.* [2012]	JPC	(-)	0.15	0.32	0.0002	0.008	0.002
			(+)	0.15	0.32	0.0002	0.008	

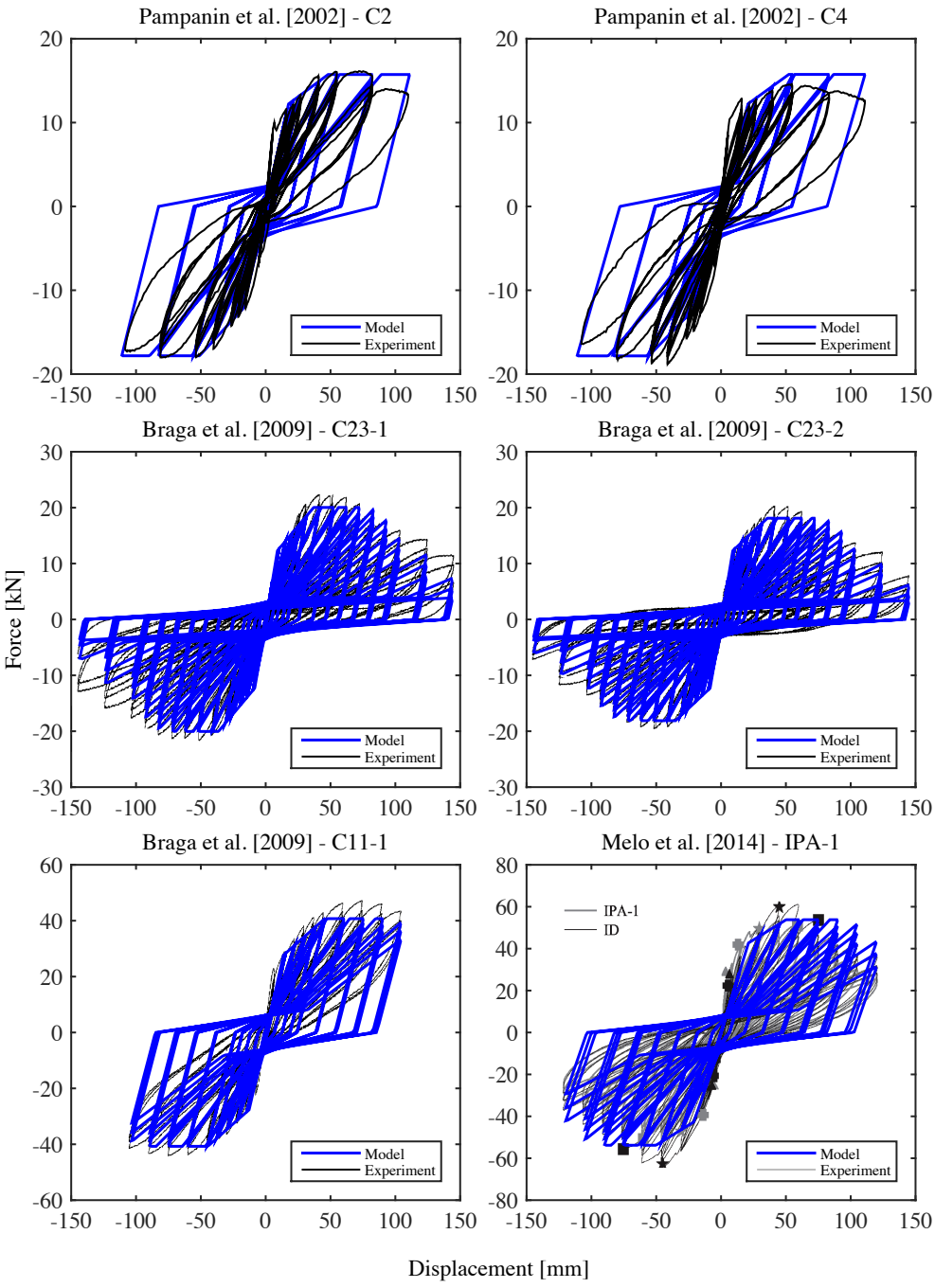

Figure 2.28. Cyclic pushover comparison of experimental and numerical model on interior joints.

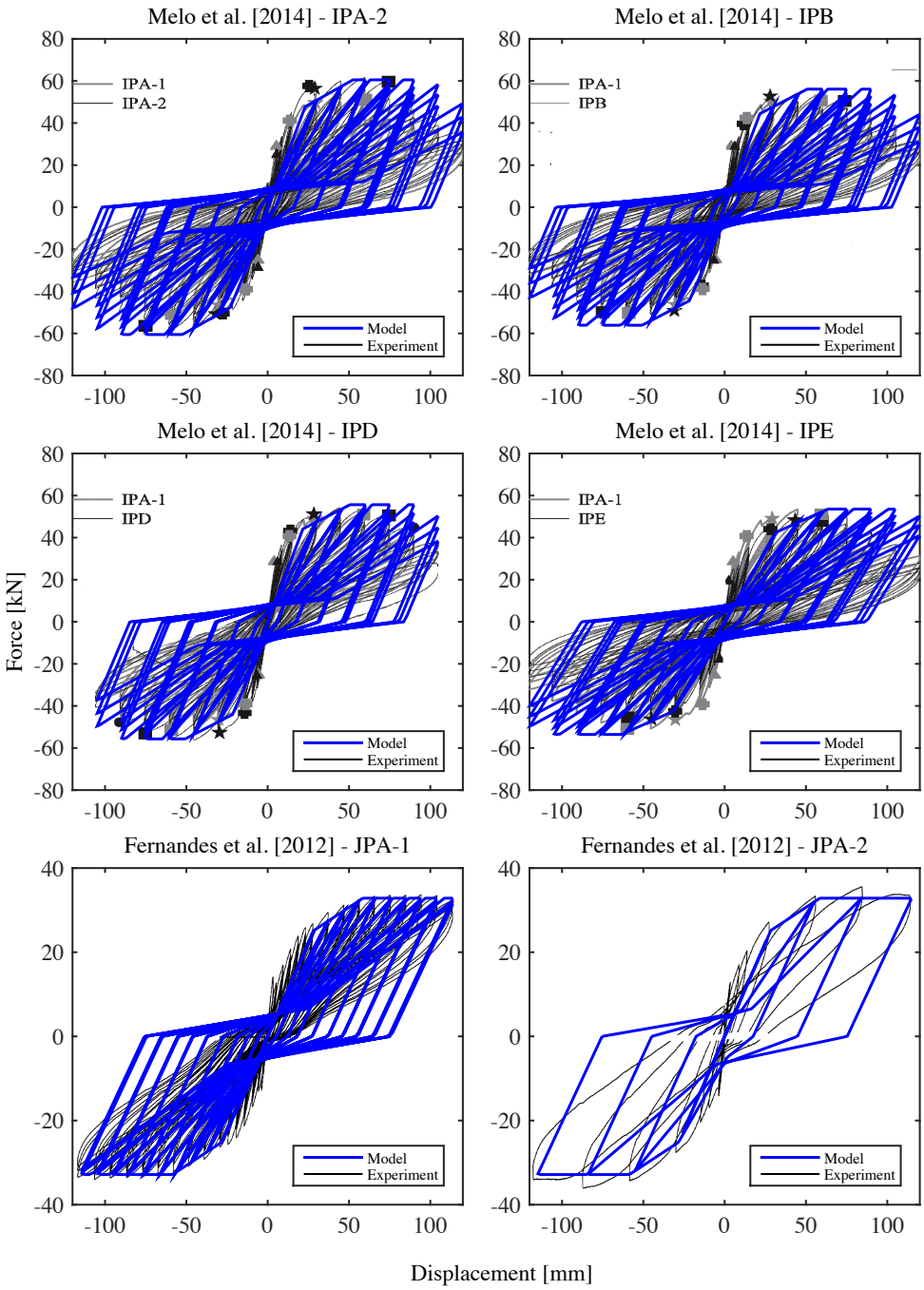

Figure 2.29. Cyclic pushover comparison of experimental and numerical model on interior joints.

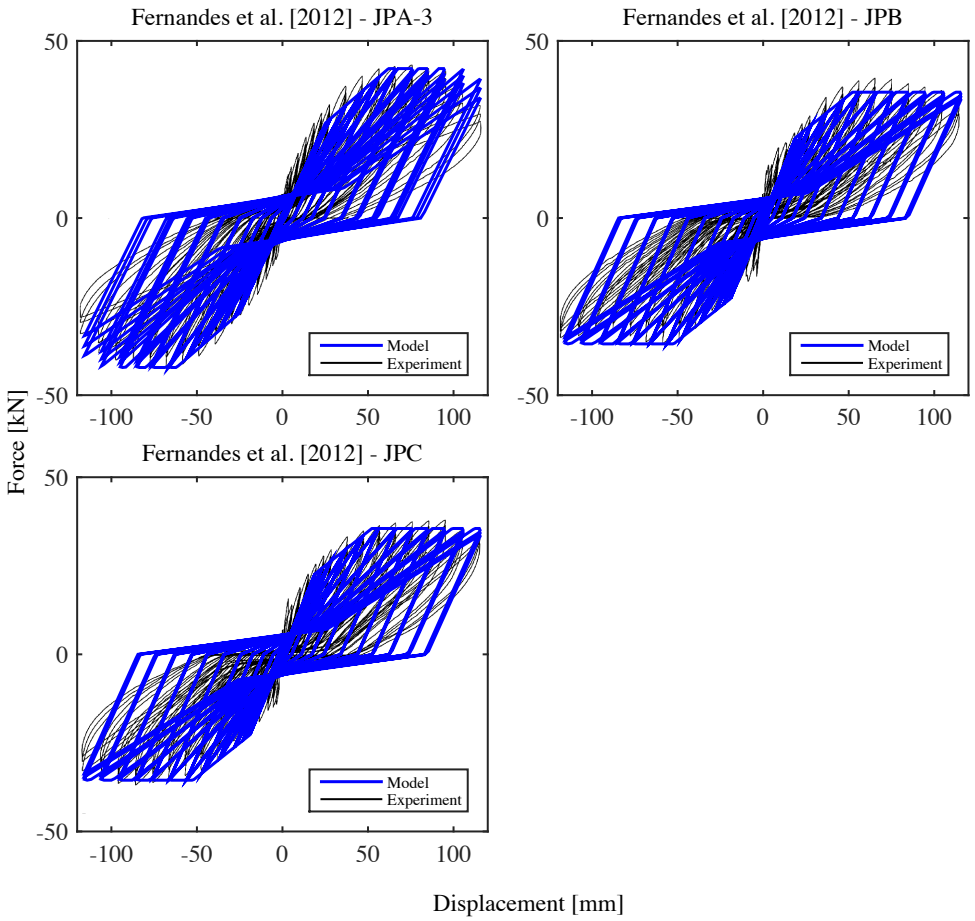

Figure 2.30. Cyclic pushover comparison of experimental and numerical model on interior joints.

Another point worth noting from the experimental observation was the source of damage mechanism. The testing by Pampanin *et al.* [2002] noted that the column members actually showed flexural hinging rather than the actual joint showing much shear behaviour. This was captured by the numerical model presented here, where the majority of the damage was concentrated in the column members above and below the joint. This highlights that while the joint deficiencies are very important in strength assessment, they do not necessarily correspond to the most likely failure mechanism in older RC structures. In this case, a flexural mechanism would have resulted in a more critical mechanism by concentrating damage in just a single floor instead of spreading the deformation over the two adjacent floors as is the case with the so-called shear hinge, as reported by Calvi *et al.* [2002a].

2.5 NUMERICAL MODEL VALIDATION

In order to validate the proposed modelling of older RC frames outlined in the previous sections, a comparison between the response of an entire frame structure as opposed to sub-assembly tests specimens is herein presented. This is done in terms of comparing the global response of the frame via pseudo-static cyclic pushover analysis and also examining the observed local damage pattern. The results presented here show the proposed model is well suited to the modelling and analysis of such RC frames with smooth bars and poor joint detailing.

2.5.1 Overview of Experimental Test

The test campaign carried out by Calvi *et al.* [2002a] looked at the response of a 2/3 scale 3 storey RC frame detailed for gravity loading only, representing a typical RC frame structure constructed in Italy prior to the introduction of seismic codes around the 1970's. The structure, shown in Figure 2.31, was designed using the Regio Decreto [1939] standard and other relevant design manuals [Pagano, 1963; Santarella, 1956], later summarised in Vona and Masi [2004] to be representative of construction practice at the time in Italy. The frame was constructed using smooth reinforcing bars terminated with end-hooks in the exterior beam-column joints and longitudinal column bar lapping just above the joint region, as illustrated in Figure 2.31.

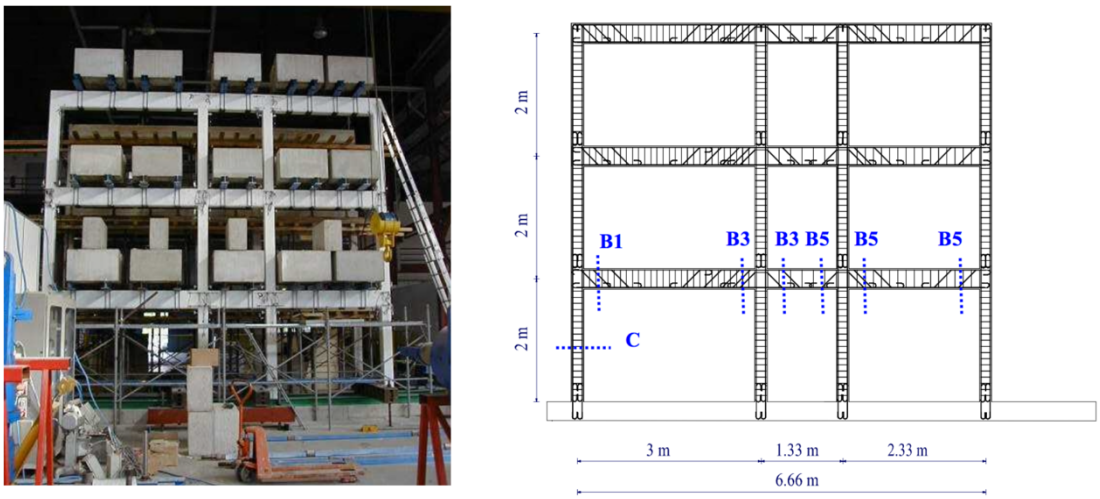

Figure 2.31. Layout of three storey RC frame tested by Calvi *et al.* [2002a].

The layout of reinforcement is shown in Table 2.12 for each of the members, where it is noted that the beam profile is the same at each level since the frame was GLD designed.

In addition, the column member sections are constant throughout the height of the structure, which was quite common practice for the ease of construction in using a constant profile throughout the height of the structure. Further details regarding the test setup frame details can be found in Calvi *et al.* [2002a].

The results of the quasi-static cyclic pushover of the three-storey structure clearly demonstrated the brittle behaviour of the exterior joints and interior column members. This is highlighted by the crack pattern shown in Figure 2.32, where the damage was heavily concentrated in the exterior joints on the first floor of the structure, where the concrete wedge mechanism reported from sub-assembly test specimens tested by Pampanin *et al.* [2002] was also observed for the whole frame. This resulted in the formation of a shear hinge mechanism, which spread the joint deformation over the adjacent floors, as opposed to concentrating the damage in a single storey, as would be the case had a soft storey mechanism formed due to flexural yielding at the column ends.

Table 2.12. Member details for three storey frame tested by Calvi *et al.* [2002a].

Section	b [mm]	h [mm]	Longitudinal Reinforcement	Transverse Reinforcement
Column	200	200	Top: 3Ø8 Bottom: 3Ø8	Ø4@135mm
Beam (B1)	200	330	Top: 2Ø8 + 2Ø12 Bottom: 2Ø8 + 2Ø12	Ø4@115mm
Beam (B3)	200	330	Top: 2Ø8 + 3Ø12 Bottom: 2Ø8	Ø4@115mm
Beam (B5)	200	330	Top: 2Ø8 + 2Ø12 Bottom: 2Ø8+1Ø12	Ø4@115mm

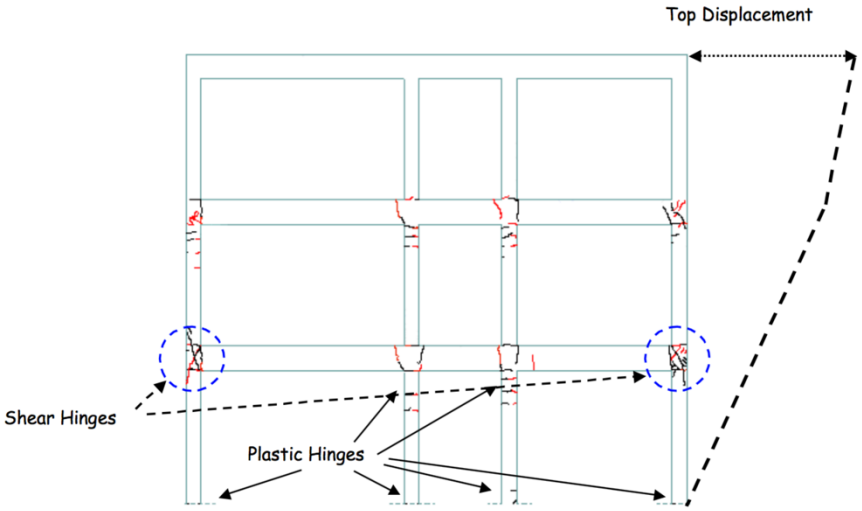

Figure 2.32. Crack damage reported by Calvi *et al.* [2002a] at a roof drift of 1.6%.

2.5.2 Comparison of Numerical Model with Experimental Test Results

The test results on the three-storey GLD RC frame highlighted the need for accurate representation of the failure mechanisms particular to these types of structures built throughout Italy prior to the 1970's. This section looks to take the proposed elements and joint models previously proposed in Sections 2.2 to 2.4 in order to construct a full model of the structure and compare the numerical model prediction with the observed test results. This is conducted both in terms of the global pushover response and displaced shape. Using the frame geometry, reinforcement layout and material properties reported in Calvi *et al.* [2002a] and the proposed parameters for the beams, column and joints proposed here, the model is constructed and subjected to a cyclic pushover analysis that consisted of a series of three cycles at increasing level of roof drift (±0.2%, 0.6% and 1.2%) with one conclusive cycle at ±1.6%. Figure 2.33(a) shows the global response of the structure in terms of base shear and roof drift.

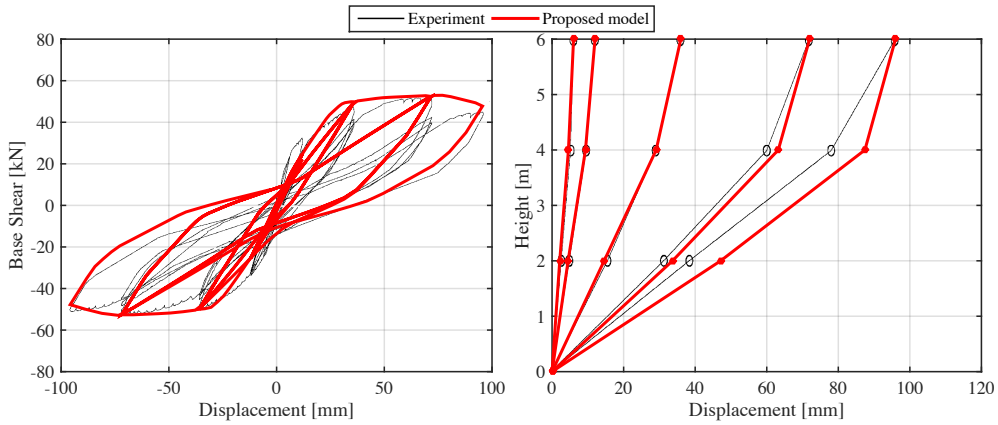

(a) Hysteretic response **(b) Displaced shape**

Figure 2.33. Comparison of predicted pushover response of the three-storey frame to the observed tests results.

First discussing the compared response in terms of the overall strength, that the predicted response is very good, with the yield force of the structure well represented along with the gradual degradation of the frame at higher displacement levels. The hysteretic response of the structure in Figure 2.33(a) is also well represented, both in terms of the unloading stiffness and pinching and also during the reloading phases of the response. This demonstrates the accuracy of this modelling procedure outlined here as these characteristics are typically overestimated by the previous modelling not considering the pinching behaviour of the specimens Galli [2006]. A comparison between the observed displaced shape and the numerical model prediction at a number of different roof displacement levels is outlined in Figure 2.33(b). The overall matching of the displaced shape is excellent, with the evolution of the deformation being tracked well at each cycle. This is particularly evident in the way the shear hinge in the first floor resulting in a spread of deformation over the two adjacent floors. This highlights the model's ability to adequately represent the mechanism typically found in older GLD frames in Italy.

In addition, comparisons between the response of the same numerical model using two other approaches are shown in Figure 2.34. These approaches comprise of the assumption of a rigid joint region with an alternative element formulation. The first of these is using the lumped plasticity model calibrated by Haselton *et al.* [2008] that has been calibrated using numerous experimental test specimens to calibrate the hysteretic backbone of ductile beam-column members with proper detailing. The second approach consists of using a force-based fibre element approach for the beam and column members, where the cross section is discretised into a number of fibres to represent the constitutive material behaviour of both the concrete and reinforcing steel.

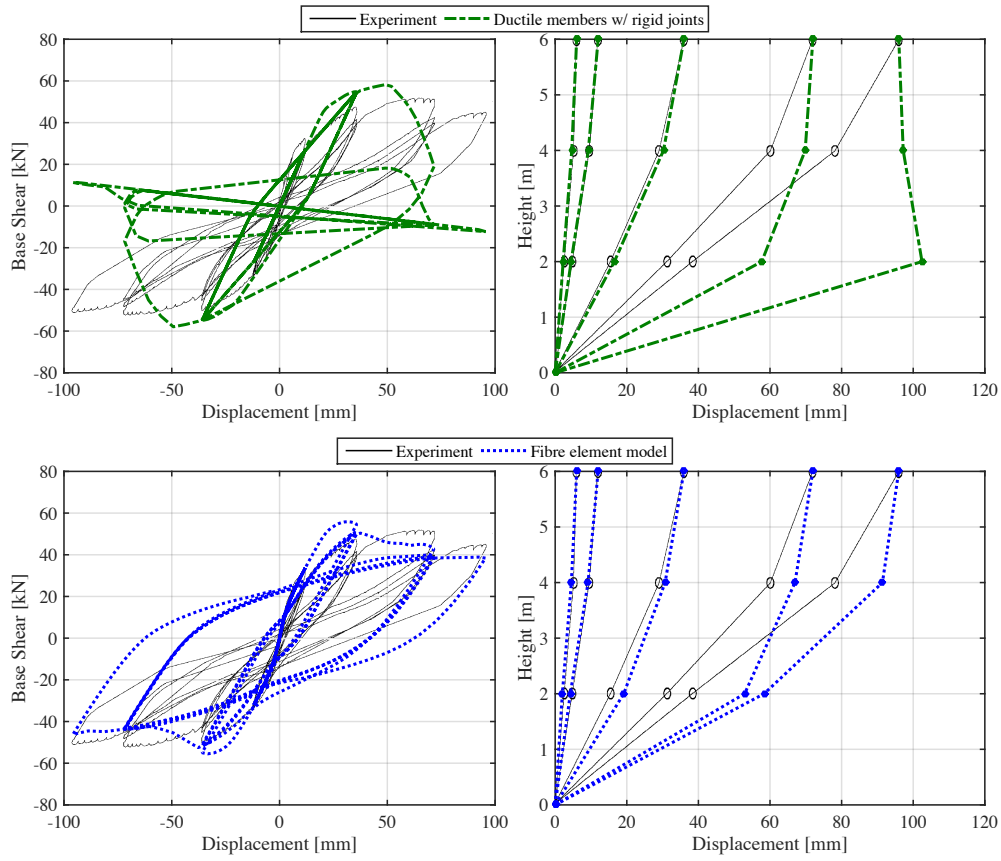

(a) Hysteretic response **(b) Displaced shape**

Figure 2.34. Comparison of response model without any joint modelling and the ductile lumped plasticity calibrated by Haselton *et al.* [2008] and a force-based beam column member.

The difference in response is immediately obvious from the pushover curve, where the use of the lumped plasticity elements actually results in a reduced drift capacity, where the fibre elements modelled shows fatter hysteretic loops without a significant degradation of the strength of stiffness after numerous cycles of loading. Upon closer examination of the displaced shape, the cause of this apparent non-ductile response using the lumped plasticity elements is due to the formation of a soft storey mechanism at the base of the structure, therefore concentrating the damage on the lower column members. Comparing this to the proposed model, where the formation of a shear hinge in the joint resulted in the spread in deformation over the two adjacent storeys resulting in a more stable response of the structure. This highlights that even though the detailing of the members may be insufficient by modern design code standards, the response of the structure may not necessarily be

worse as the joint mechanism alters the global structural response. The fibre element model, on the other hand, shows a reasonable comparison if one were to consider just the envelope of the response. However, the stiffness transitions between cycles are not well represented resulting in a much fatter hysteretic loop and consequently increased hysteretic energy dissipation, than the actual test specimen that shows a much more pinched response. Again, the fibre model does not capture the occurrence of the joint shear mechanism either; and does not exhibit a soft storey response as was the case with the lumped plasticity elements. This can be attributed to the lack of any special attention to incorporate the post-peak strength and stiffness degradation in the fibre member, which is one of the main advantages of the lumped plasticity approach by Haselton *et al.* [2008]. The purpose of these comparisons is not to demonstrate that these two aforementioned approaches are incorrect and the proposed approach is better, but rather to illustrate how they are of limited applicability when assessing GLD RC frames in Italy that possess more particular mechanisms not accounted for by these models. Hence, it is very important that these types of mechanisms observed here can be adequately represented and captured numerically to perform an accurate assessment of older RC structures, as the assumptions made for the design and assessment of modern ductile structures may no longer hold true. This is again highlighted in the comparison of the storey drift profiles of the different models shown in Figure 2.35, where all models represent the drift profile well for the initial cycles until the models without joint modelling and ductile members form a soft storey and concentrate the damage at that level, whereas the proposed model do a much better job of representing the redistribution drift over the first and second levels as a result of the joint damage.

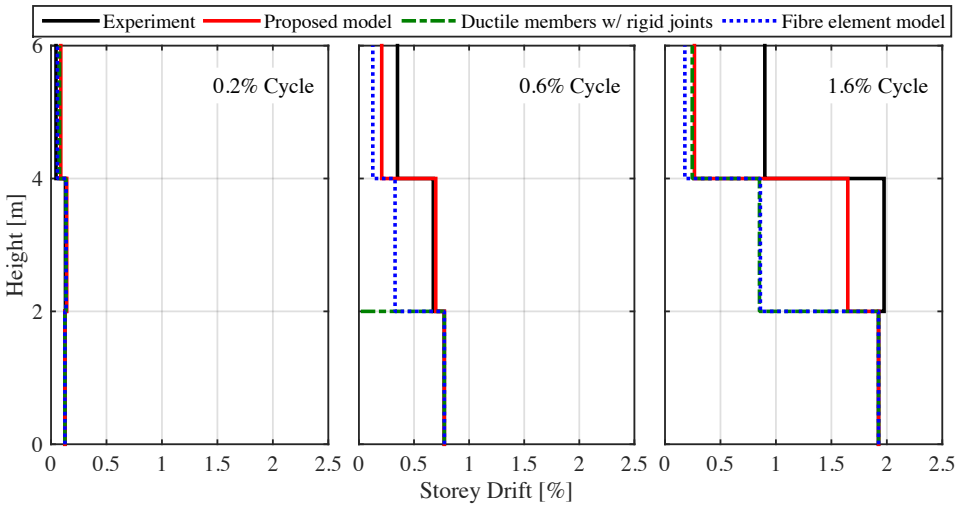

Figure 2.35. Storey drift profile at peak displacement of various cycles normalised to interstorey drift observed on the first floor.

Overall, the comparison between the observed and predicted response using the proposed model is quite good, which suggests the modelling procedures outlined here are suitable for the analysis of older RC frame structures constructed in Italy prior to the introduction of seismic design requirements in the 1970's.

2.6 MASONRY INFILLS

The modelling of masonry infill panels has received much attention over recent years since numerous reconnaissance reports throughout Italy and elsewhere document that the effects of masonry infills on the response of a structure can be quite significant. Masonry infills have been considered non-structural elements not considered in design, and whose addition to the structure was considered beneficial as it offered additional resistance to lateral loads. The detrimental effects of the lack of the consideration of masonry infill interaction has been demonstrated to be a critical factor in the assessment of the behaviour of RC frame structures from past observation of damage in earthquakes [Augenti and Parisi, 2010; Decanini *et al.*, 2004; EERI, 2009; Verderame *et al.*, 2009]. The presence of masonry infills in RC frames has two effects on the global response of the frame. The first of these is that the initial stiffness of the structures increases greatly, with some comparative studies by O'Reilly and Sullivan [2015a], among others, highlighting that the presence of such infills reduces the initial period of the structure significantly. In addition to the increase in initial stiffness, the lateral yield force of the structure is greatly influenced by the presence of infills, as illustrated in Figure 2.36. Further to the global effects of the presence of the masonry infill panels on the response of the structure, additional shear forces can be induced in the column members such that they experience a brittle shear failure mechanism, as observed in past earthquakes. One of the main challenges in the assessment of RC frames with infills is the accurate representation of these effects both on a global level and also on a local response level for a given structure. This section presents a review of such models available in the literature and describes a modelling approach that can be adopted within the OpenSees framework.

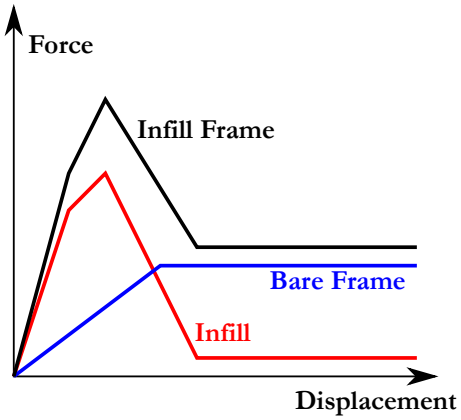

Figure 2.36. Influence of the presence of infill on the global response of an RC frame.

2.6.1 Strut Modelling Approach

While numerical modelling approaches may consist of more refined analyses such as finite element analyses, the use of such analysis may not be feasible in the assessment of entire structural systems, which means that a compromise between accurate representation and numerical efficiency must be found in order to assess large RC frame systems on a large scale. Such a compromise is found through the use of the equivalent diagonal struts, where the strut action of the infill is represented through the introduction of diagonal compression-only struts. Crisafulli *et al.* [2000] present a comprehensive literature review of various layouts of such diagonal struts, where both the global and local effects of adding such a layout of elements are discussed. Generally speaking, most strut models available in the literature [Crisafulli *et al.*, 2000; Decanini *et al.*, 2004; Furtado *et al.*, 2015] amongst others, provide a reasonably good representation of the influence of the infills on the global behaviour. Some models tend to represent the backbone response of a masonry infill with a diagonal cracking mechanism, for example, Panagiotakos and Fardis [1996], while other models distinguish between failure mechanisms such as diagonal cracking, corner crushing or shear sliding, such as Decanini *et al.* [2004]. However, current state-of-the-art equivalent strut models consider the interaction of the masonry infill with the surrounding frame, namely what is typically termed the "short column effect" on the column members where an additional shear force is induced often causing a brittle failure mechanism in the column. In the general review of infill strut modelling by Crisafulli *et al.* [2000], a comparison between various approaches to modelling such an effect were discussed, where two of such approaches are the use of a single strut and a double strut model, illustrated in Figure 2.37.

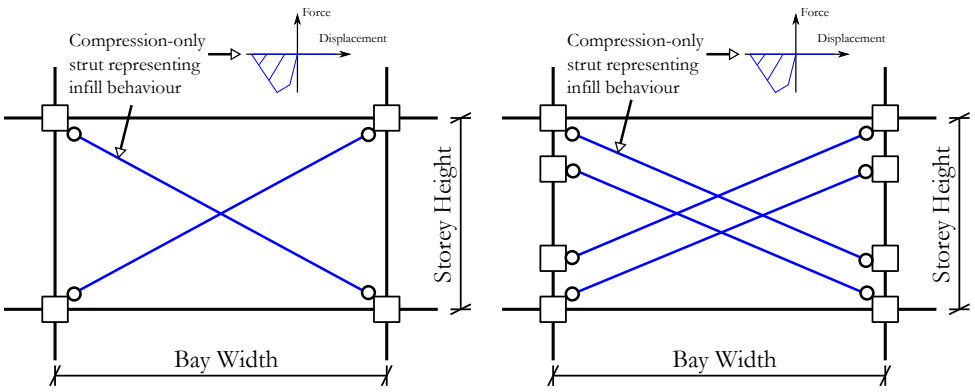

(a) Single strut model. **(b) Double strut model.**

Figure 2.37. Various equivalent diagonal strut modelling approaches.

The influence of various strut modelling approaches shown in Figure 2.37 in terms of both the global and local effects was discussed by Crisafulli *et al.* [2000], where the comparison to a more refined finite element model of the case study structure was used. The effects of different strut modelling approaches on the bending moment and shear force induced in the columns were examined in detail to provide insight into which strut modelling approach provides the most accurate representation of the frame and infill interaction. Crisafulli *et al.* [2000] concluded that each approach gave more or less the same lateral stiffness and that for modelling the global effects of infills, a single diagonal strut is sufficient for such analysis, which has also been noted by other researchers (e.g. Celarec and Dolšek [2013]), but the use of a single strut did not accurately represent the increase in shear force demands in the column members. The double strut model illustrated in Figure 2.37(b) was observed to be a better approach since the global behaviour was well represented, in addition to a more realistic representation of the shear force distribution, albeit the shear force transferred to the column was slightly higher than those observed from more refined analysis.

Such models have been adopted over the past decade in studies that look to analyse the influence of masonry infills on the response of RC frames. Studies such as Dolšek and Fajfar [2008] used a single strut modelling approach, while Celarec and Dolšek [2013] used the double strut and Jeon *et al.* [2015] used a triple strut approach. No consensus has been agreed as to which approach is the most realistic since this depends on what the analyst requires and whether the layout of elements accurately represents the actual conditions of the infills. In addition, the relative ratios of strength of the different struts can also be an important parameter, where for the double strut modelling approach Crisafulli *et al.* [2000] suggested that the capacity of the double struts be split evenly over the two struts, but for

a triple strut approach to assign 50% of the strength to the centre strut and 25% to each of the offset diagonals. Jeon *et al.* [2015] adopted this triple modelling approach, where the strength ratios were defined by a number of unspecified terms to give what was deemed to be the best representation of the interaction. However, while it may seem that the triple strut modelling approach represents the best approach to capturing the complete behaviour of the infills, Celarec and Dolšek [2013] suggests that a double strut approach may suffice since the actual connectivity and contact between the top of a masonry infill wall and the underside of the upper beam may be quite weak. In addition, it may not be critical that the additional forces induced on the surrounding beam elements be modelled with such precision since the majority of problems with infills that have been observed in past earthquakes have resulted from interaction with the surrounding column members.

2.6.2 Backbone Calculation

Following the discussion of the in-plane modelling layout of the masonry infill in the previous section, this section discusses the computation of the backbone hysteresis of the infill to be supplied to the strut models. The various terms of the backbone curve are outlined in Figure 2.38 along with an illustration of the various terms.

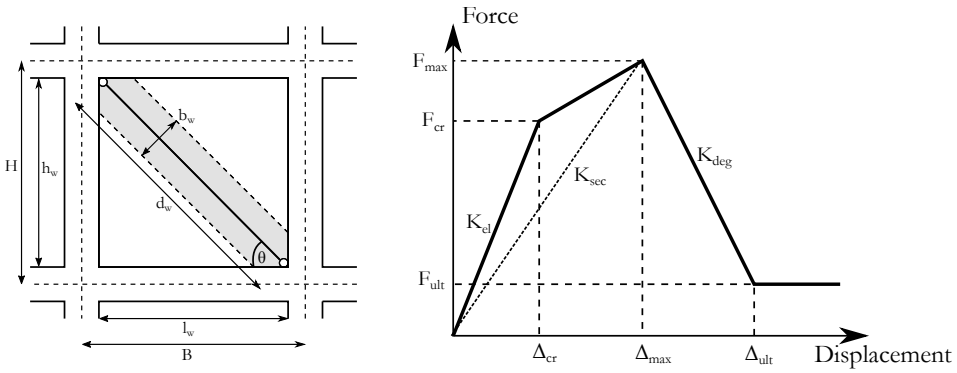

Figure 2.38. Illustration of infill backbone definition.

One of the first terms to be defined from Figure 2.38 is the thickness of the equivalent strut for the infill, which is assumed to have a thickness equal to that of the infill (t_w). One of the more common ways of expressing the strut width is through the use of a width-to-thickness ratio of the infill. One such proposal is by that of Bertoldi *et al.* [1993], which states:

$$b_w = \left(\frac{K_1}{\lambda H} + K_2\right) d_w \qquad \textbf{Equation 2.57}$$

where K_1 and K_2 are constant terms expressed as a function of the parameter λH, which is defined by Stafford Smith [1966] as:

$$\lambda = \sqrt[4]{\frac{E_{w\theta} t_w \sin 2\theta}{4 E_c I_c h_w}} \qquad \textbf{Equation 2.58}$$

and H is the height between the centre lines of the storey. Knowing the value of λH, the coefficients K_1 and K_2 are determined from Table 2.13. The terms E_c, I_c, $E_{w\theta}$ correspond to the elastic modulus of concrete, second moment of area of the column and elastic modulus of the masonry, respectively. The elastic modulus of the masonry, $E_{w\theta}$ in the inclined direction is based on the model for orthotropic materials subject to biaxial stress states and is determined from the following expression:

$$E_{w\theta} = \left[\frac{\cos^4 \theta}{E_{wh}} + \frac{\sin^4 \theta}{E_{wv}} + \sin^2 \theta \cos^2 \theta \left(\frac{1}{G} - \frac{2\nu}{E_{wv}} \right) \right]^{-1} \qquad \textbf{Equation 2.59}$$

Table 2.13. Coefficients proposed by Bertoldi *et al.* [1993].

	$\lambda H<3.14$	$3.14< \lambda H<7.85$	$\lambda H>7.85$
K_1	1.300	0.707	0.470
K_2	-0.178	0.010	0.040

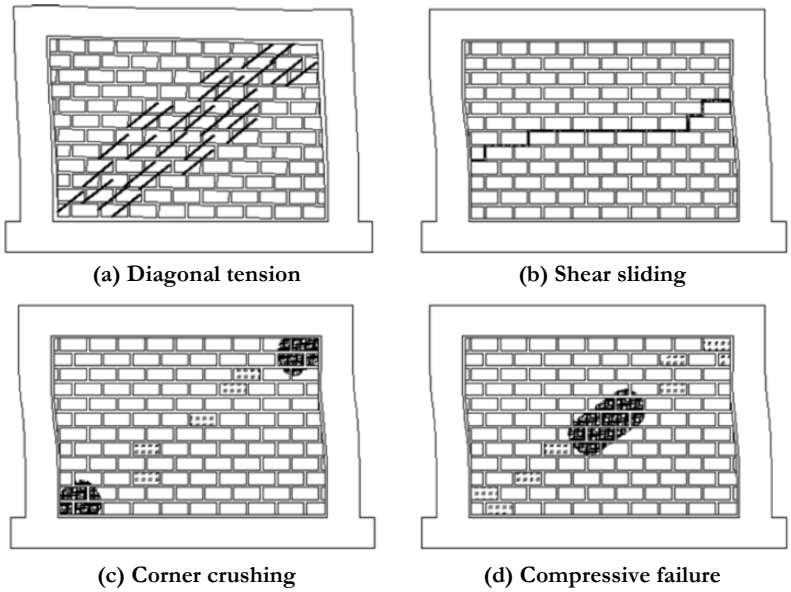

(a) Diagonal tension (b) Shear sliding

(c) Corner crushing (d) Compressive failure

Figure 2.39. Different failure modes of infills proposed by Decanini *et al.* [2004].

A significant advantage of the model outlined by Decanini *et al.* [2004] is its ability to account for different failure mechanisms in the infill. These are; diagonal tension failure of the infill, shear sliding in the mortar joints, corner crushing of the infill and compressive failure at the centre of the infills, which are illustrated in Figure 2.39. The expression described in Decanini *et al.* [2004] for each of these failure modes are listed below.

Diagonal failure of the infill

$$\sigma_w = \frac{0.6f_{ws} + 0.3\sigma_v}{\frac{b_w}{d_w}} \qquad \textbf{Equation 2.60}$$

Shear sliding in the mortar joints

$$\sigma_w = \frac{(1.2\sin\theta + 0.45\cos\theta)f_{wu} + 0.3\sigma_v}{\frac{b_w}{d_w}} \qquad \textbf{Equation 2.61}$$

Corner crushing of the infill

$$\sigma_w = \frac{1.12f_{wv}\sin\theta\cos\theta}{K_1(\lambda H)^{-0.12} + K_2(\lambda H)^{0.88}} \qquad \textbf{Equation 2.62}$$

Compressive failure of infill centre

$$\sigma_w = \frac{1.16f_{wv}\tan\theta}{K_1 + K_2\lambda H} \qquad \textbf{Equation 2.63}$$

where f_{ws}, f_{wu}, f_{wv} are the diagonal shear compression strength, sliding resistance of the mortar joints and the vertical compressive strength measured on the masonry specimens, respectively. The term σ_v represents the vertical stress imposed on the masonry due to gravity loading in the frame. From each of the different values of the maximum stress in the strut associated with each of the different failure modes, the minimum value is chosen and used to compute a strut axial strength from:

$$F_{max} = \min(\sigma_m)\, b_w t_w \qquad \textbf{Equation 2.64}$$

for which the secant stiffness of the strut is computed from:

$$K_{sec} = \frac{E_{w\theta} t_w b_w}{d_w} \qquad \textbf{Equation 2.65}$$

To compute the remaining points on the backbone curve, some reasonable assumptions are made regarding the strength and stiffness ratios of the infill outlined in Sassun *et al.* [2015] who cite experimental support from studies such as Parducci and Mezzi [1980] and Stylianidis [1998]. The cracking and residual forces (F_{cr} and F_{ult}) are determined as:

$$F_{cr} = 0.8F_{max} \qquad \textbf{Equation 2.66}$$

$$F_{ult} = 0.10F_{max} \qquad \textbf{Equation 2.67}$$

The ratios between the different stiffness's are given as:

$$K_{el} = 4K_{sec} \qquad \textbf{Equation 2.68}$$

$$K_{deg} = -0.02K_{sec} \qquad \textbf{Equation 2.69}$$

The values above represent the parameters used in the computation of the axial behaviour of a single strut. To convert this behaviour to a force-displacement response of the storey, the necessary transformation of the components needs to be performed, i.e. forces times $\cos\theta$ and stiffness's times $\cos^2\theta$.

Sassun *et al.* [2015] proposed the adoption of the above approach where the lateral forces are derived using the previously described equations, but the storey drifts for each of the DSs are used, which are listed in Table 2.14. These median values correspond to those derived from the experimental values without segregating in terms of masonry typology as the differentiated values listed in Sassun *et al.* [2015] are quite similar, with the exception of DS4, which is a little higher for the case of solid clay brick infills.

Table 2.14. Storey drift values proposed for masonry infills by Sassun *et al.* [2015].

Damage State	Median [%]	Dispersion
Operational (DS1)	0.18%	0.52
Damage Limitation (DS2)	0.46%	0.54
Life Safety (DS3)	1.05%	0.40
Ultimate (DS4)	1.88%	0.30

A simple example is illustrated through the computation of the backbone of a single storey and single bay frame's infill response using the expressions described in the previous sections in addition to a demonstration of how the shear failure of the column members can be accounted for during the analysis. The frame in question is assumed to have a bay length of 4.5m, storey height of 3.5m, beams of dimension 300x500mm and columns of dimension 300x300mm. The type of infill is assumed to be a weak infill, with the properties taken from those reported in Hak *et al.* [2012]. The beams and column are modelled using lumped plasticity hinges at both ends, where the hysteretic model used is an elastic-perfectly plastic hinge with a capacity of 100kNm in the columns and 50kNm in the beams. These values do not correspond to any particular reinforcement layout but are merely arbitrary values to illustrate the model. The shear behaviour of the beams and columns is done using the same aggregated shear hinge element described in Section 2.2, where the hysteretic behaviour of the shear hinge is also assumed to be bilinear with a capacity of 200kN.

A single pushover to 2.5% storey drift is performed on the three different models and the backbone behaviour is shown in Figure 2.40, where the double strut model is considered with and without shear hinge modelling in the column members. As is immediately apparent, the introduction of the infills to the frame results in a marked change to the global behaviour of the frame. The governing mechanism for the infill failure is diagonal tension in each case. The slight reduction in the global pushover force for the double strut model compared to the single strut model can be explained by the additional end flexibility introduced to the strut model by connecting them to an offset of the column instead of obtaining a concentric strut action that the single strut achieves.

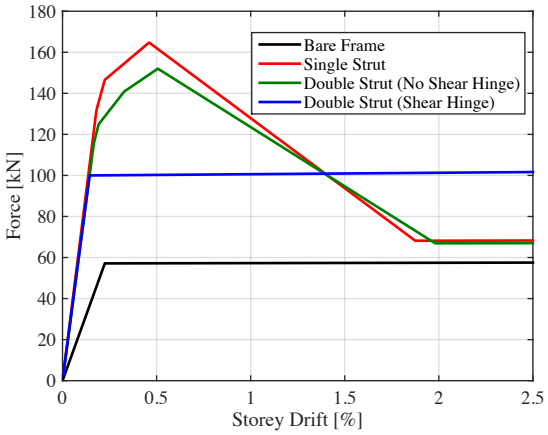

Figure 2.40. Pushover of the frame with different infill arrangements, without considering nonlinear shear behaviour in the columns.

In addition to the global pushover results of the infilled frame, the local response of the short-column created by the addition of the double strut model can be examined. The left uppermost column is considered here, and the shear force versus drift is plotted in Figure 2.41 for each of the three cases. As can be seen, there is no difference in the shear forces observed in the case of the bare frame and the single strut model, since no additional forces are being induced directly into the column. However, a clear increase in the shear force in the column for both double strut models is observed.

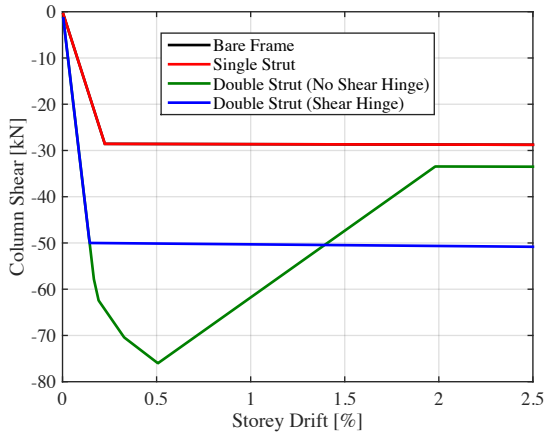

Figure 2.41. Shear force versus drift in the upper left column, without considering nonlinear shear behaviour in the column.

An arbitrary column shear capacity of 50kN is now introduced to the double strut model such that the model without any column shear hinge modelling in Figure 2.41 should result in a shear hinge in the column element. Figure 2.40 and Figure 2.41 show the corresponding pushover curve and column element response plots where the effect of the introduction of the shear hinge is clear as it results in a loss of strength and stiffness of the frame upon shear yielding. Since the shear hinge is a bilinear model here, the frame maintains its capacity until the end of the analysis. However, the shear hinge modelling discussed in Section 2.2 would capture the eventual degradation of the shear behaviour to result in a loss of capacity also.

A final set of parameters for the modelling of the infill struts that requires consideration is the hysteretic behaviour of the struts, or more specifically how to incorporate the pinching of the material model. Previous work by Kumar *et al.* [2015] defined a set of parameters to be used with the Pinching4 material in OpenSees on the basis of test result comparison. However, these parameters were calibrated for a single spring used to model the complete infilled frame, hence these parameters represent the pinching of both the infill frame plus the actual masonry infill together, and therefore are not considered appropriate for the modelling approach discussed here. The values adopted here are based on those originally proposed by Panagiotakos and Fardis [1996] and are adopted into the Pinching4 material model in OpenSees. As such, the parameters adopted into in the model are 0.8 for the rDisp parameter, 0.2 for the rForce parameter and 0.0 for the uForce parameter, where all degradation parameters are set to 0.0 such that no cyclic degradation is included. Values could be calibrated for this, but is deemed beyond the scope of this work, where the values proposed are deemed sufficient for the type of analysis this modelling is intended for. In addition, Landi and Benedetti [2013] propose the use of the same hysteretic behaviour parameters for masonry infills as such parameters gave a good match when compared to experimental test specimens from both Colangelo [2004] and Pires [1990], further justifying the parameters used here for the numerical modelling of masonry infills.

2.6.3 Summary

The previous sections discussed the modelling of the masonry infills in RC frames using macro element models. This was discussed in terms of strut layout and hysteretic backbone computation. The use of a double strut model to consider the shear behaviour in the columns, is adopted where the backbone is computed using the approach of Decanini *et al.* [2004] in conjunction with the modifications proposed by Sassun *et al.* [2015]. This offers the advantage of being a simple model that considers different failure mechanisms, in addition to defining the storey drift values at each limit state in accordance with experimentally measured values of numerous test specimens. However, the consideration of openings such as doors or windows was not considered in addition to the consideration of the out-of-plane failure of the infill.

2.7 SUMMARY AND CONCLUSIONS

This chapter discussed the numerical modelling and calibration of older GLD RC frames in Italy using OpenSees to existing experimental data available in the literature. Some of the main aspects and contributions of the work and discussion of this chapter are discussed below.

The behaviour of beam-column elements with smooth bars and poor detailing typical of older GLD RC frames in Italy was calibrated numerically. A total of 23 experimental test specimens were collected from the literature in order to calibrate the various aspects of the hysteretic backbone behaviour based on the available information. From this, the following is concluded:

- Existing expressions to compute the moment capacity and yield curvature of the members were validated against the experimental data, whereas existing expressions to compute the post-yield ductility capacity were reviewed. It was shown how existing expressions to compute yield curvature and moment capacity work well, whereas existing expressions to compute the ductility capacity tended to underestimate the capacity of the older GLD frame members.
- The more recent proposal by Melo *et al.* [2015] was shown to give the best comparison with the experimental data and is recommended for use in the numerical modelling of such GLD RC frame members. In addition, a simplified expression to estimate the ductility capacity as a function of axial load ratio was also provided. This is based on comparison with the proposal of Melo *et al.* [2015] and experimental data and is intended for use in situations where very little detail is known about member properties, such as material properties or reinforcement ratios.
- Following the work of Ibarra and Krawinkler [2005], three key elements to model structural collapse were shown to be the modelling of P-Delta effects along with in-cycle and cyclic degradation. This chapter looked to consider the post-peak degradation of members and to appropriately simulate the structural collapse of GLD frames due to the exhaustion of the column member's ductility capacity. Based on the limited available experimental data, the in-cycle degradation was calibrated to capture this degradation in post-peak strength and stiffness of the members. The cyclic degradation term was not calibrated due to a lack of available information and is proposed as a future development pending future experimental testing of members. However, the quantification of the post-peak stiffness of members represents a marked improvement on some existing models that rely solely on P-Delta effects to simulate structural collapse. The omission of the cyclic degradation terms results will possibly result in the slight overestimation of the collapse capacity of GLD frames should the eventual effects of cyclic degradation

be found to be significant with respect to the other two, although this difference is not expected to be as significant as if the in-cycle degradation considered here had been omitted.

- The incorporation of the shear hinge element into the beam-column formulation described here allows for the shear response of the frame members to be incorporated. This is particularly important in the analysis of GLD frames as numerous cases of infill interaction causing a brittle shear failure of the member have been noted from past earthquakes in Chapter 1. This definition of shear behaviour has been adopted from a more recent study by Zimos *et al.* [2015] to capture the shear degradation and subsequent failure of RC members. Adopting this approach here allows for the investigation of the effect of such shear failure of RC columns interacting with the masonry infill on the overall performance of the structure in terms of response, collapse capacity and monetary losses, which are to be discussed later in this thesis.

In addition to the model calibration for the beam-column members, this chapter examined the behaviour and numerical modelling of RC beam-column joints. For both interior and exterior joints, a total of 15 and 10 experimental test specimens were utilised, respectively. Following the derivation of the some of the main expressions used to compute the joint shear capacity through consideration of the principle tensile stresses and comparing this to experimental test data, the following points are made:

- The shear failure of the beam-column joints was calibrated using experimental test data specific to the detailing of GLD RC frame beam-column joints in Italy. That is to say, joints with no transverse shear reinforcement and smooth bars with end-hooks anchored in the joints. This calibration resulted in coefficients to capture the degradation of beam-column joints to simulate the loss of joint capacity. Such a simple and robust model to capture this degradation of the joints for Italian GLD frames has not been studied previously in detail, meaning that the work concluded here represents a significant contribution to the assessment of such frames.
- The computation of the exterior joint shear capacity was also derived from considering the additional shear transfer of the beam to the joint, where a close form solution was derived in place of the existing iterative approach outlined in Sharma *et al.* [2011].

The numerical modelling of masonry infill elements was discussed, where the incorporation of the shear hinge model for the RC members to account for the potential shear failures of the column members due to interaction with the masonry was included. It was illustrated via a simple example how the inclusion of such a shear hinge can result in the loss of the

columns strength and stiffness should the shear force induced by the masonry infill on the column exceed the column's shear capacity. This is an important consideration in the study of infilled RC frame members as it means that the shear failure of the columns due to interaction with masonry infill can be captured during numerical analysis and means that other compromises such as post-processing of shear failures or other iterative procedures are not required.

Using the modelling approaches for the various elements of GLD RC frames, a comparison with a three-storey experimental test specimen subjected to pseudo-static cyclic pushover analysis was carried out. This was evaluated in terms of the global response of the frame and the following remarks are made:

- The proposed numerical model tracked the evolution of deformed shape with every increasing cycle of lateral displacement excellently, where the formation of a shear hinge in the first floor resulting in a spread in deformation over the two adjacent floors was captured.
- The initial stiffness, overall lateral strength and pinching of the cyclic loading was also very well represented by the model.
- A comparison of the test specimen with two different models with rigid joints and ductile RC frame members was carried out to illustrate what the predicted response would have been if an analyst were to not consider the joint behaviour or the limited ductility of the frame members through the adoption of models typically used to model modern, ductile structures. This was shown to have a massive effect on the model's response, with the overall response mechanism not being captured in addition to the overall global ductility not being well represented at all.

These above points demonstrate how the numerical modelling approach described in this chapter represents an appropriate way to analyse GLD RC frames in Italy, albeit with some limitations due to lack of suitable experimental data. Despite this, the overall response of test specimens is well represented in addition to incorporating methods with which more particular mechanisms such as the degradation of columns and joints, or more brittle mechanisms such as the shear failure of the columns due to infill interaction, can be accounted for. In addition to this calibration, the statistical information such as dispersions in predictive expressions derived from the comparisons with experimental data can be used as the basis for a study into the effects of modelling uncertainty on the demand parameters of interest in performance-based earthquake engineering. In summary, the numerical modelling developed and described here forms the basis for a broader study into the behaviour of GLD frames in Italy, which will be examined in future chapters of this thesis.

3 DEVELOPMENT AND IMPLICATIONS OF A MORE REFINED DAMAGE AND LOSS ESTIMATION TOOL

A significant portion of the work presented in this chapter is based on a conference paper presented at the 16th World Conference on Earthquake Engineering, available at:

O'Reilly, G. J., Sullivan, T. J., Filiatrault, A. [2017] "Implications of a More Refined Damage Estimation Approach in the Assessment of RC Frames," *16th World Conference on Earthquake Engineering*, Santiago, Chile.

3.1 INTRODUCTION

Since the inception of what is commonly referred to as the PEER PBEE methodology in the early 2000's [Porter, 2003; Porter and Kiremidjian, 2001], many advancements have been made in developing this framework to incorporate various types of structures. One of the main aims of such a methodology is to quantify the performance of buildings in a way that is more helpful to stakeholders when planning a new building's design or deciding on an existing building's retrofit strategy. This framework has been extensively developed and consequently, FEMA has published the P58 guidelines [FEMA P58-1, 2012] to aid practitioners in implementing the method. This document represents a major step forward in the assessment of structures as it provides a clear, yet relatively simple description on how to apply the procedure along with the performance assessment calculation tool (PACT) software [FEMA P58-3, 2012].

One of the limitations of the assessment tools in FEMA P58 is that they have been developed with a number of simplifying assumptions that are suited to regular and symmetric structures. That is, torsionally responding structures or structures with high irregularity in plan and elevation are not covered to any great extent in the guidelines. This represents a limitation to the current state-of-practice, as many existing structures possess some degree of irregularity. The aims of this chapter are to develop a MATLAB based software tool that can better facilitate the assessment of irregular structures and highlight how the use of a more advanced assessment approach compares to that of a more simplified approach, where various assumptions need to be made. The chapter begins by giving a brief overview of the current state-of-practice assessment of buildings followed by a discussion on the limitations and unintended consequences of these methods. A software tool developed to advance the state-of-practice and address the limitations outlined is described in detail, with the assessment process followed and how the user can input

analysis results and obtain loss estimates relatively easily. This is illustrated through an example application to a case study frame both before and after some form of retrofitting approach to illustrate the application of the program and how it can be used to evaluate different retrofitting solutions. An additional application of such a refined assessment approach presented by O'Reilly *et al.* [2017] is then included to highlight the impacts of such a refinement in the damage and loss estimation with respect to the torsional response of RC frames.

3.2 DEVELOPMENT OF A SOFTWARE TOOL TO ALLOW COMPONENT-BASED SEISMIC LOSS ESTIMATION

3.2.1 Overview of the Current Framework

As previously outlined in Section 1.2 the probabilistic assessment framework shown in Figure 1.12 that is commonly referred to as the PEER PBEE assessment methodology consists of a triple integral given in Equation 1.1 to describe the MAF of exceedance (λ) of a certain DV for a given structure D. This DV is typically one of the "3Ds" used within the PEER framework, which refer to deaths, dollars and downtime, but is not limited to these.

This framework has been developed over the past decade to provide guidance in the form of the FEMA P58 guidelines on how one should implement the methodology to assess the performance of structures. By considering the DV that indicates the likely economic impact of a given site's seismic hazard on given building, we begin to refer to economic losses. Then by examining the losses that are incurred due to the damage to the building and it's associated structural and non-structural element components and contents, we begin to refer to the direct economic losses of a given building. We can then define the expected total direct loss $E[L_T|IM]$, which refer to the losses accumulated due to repair and replacement costs, for a given structure at a given value IM as:

$$E\left[L_T|IM\right] = E\left[L_T|NC, IM\right](1 - P[C|IM]) + E\left[L_T|C\right]P[C|IM] \quad \textbf{Equation 3.1}$$

where $E[L_T|NC, IM]$ is the expected loss at given intensity level, conditioned on no collapse (NC) of the structure. $P[C|IM]$ is the probability of collapse given IM and $E[L_T|C]$ is the expected loss given collapse or more simply put, the replacement cost of the building including demolition and removal of debris. This can then be expanded further based on the proposals by Ramirez and Miranda [2009] to considering the probability of requiring demolition given the building did not collapse ($P[D|NC,IM]$) but retains excessive residual drifts to require demolition as follows:

$$E\left[L_T|IM\right] = E\left[L_T|NC \cap R, IM\right](1 - P[D|NC, IM])(1 - P[C|IM]) \quad \textbf{Equation 3.2}$$

$$+E\left[L_T|NC \cap D\right]P[D|NC, IM](1 - P[C|IM])$$

$$+ E\left[L_T|C\right]P[C|IM]$$

where $E[L_T|NC \cap R, IM]$ describes the expected loss at given intensity condition on no collapse and the repairability of the building, $E[L_T|NC \cap D]$ is the expected loss given no collapse and the building not being repairable, which is essentially the cost of demolition. This expression forms the basis as to how expected losses are computed in a structure, where the IMs at which the losses are computed are compared with the site's mean hazard curve to link the different levels of direct economic losses with an MAF of exceedance. These can be then integrated together to result in the EAL of the structure, which can be thought of as the structure's annual loss due to its current seismic hazard exposure and structural vulnerability. This EAL parameter has been the focus of much research in recent years, with some researchers in the US aiming to quantify the typical levels associated with modern ductile construction, while in Italy a recent proposal by Calvi *et al.* [2014] to use EAL as a classification to quantify seismic resilience and encourage retrofitting. In order to compute such annualised losses in a structure, the individual losses associated with each of the individual damageable components need to be quantified. The computation of these losses can be broken down into the sum of its components as follows:

$$E\left[L_T|NC, IM\right] = \sum_{n=1}^{N_c} E\left[L_n|NC, IM\right] \qquad \textbf{Equation 3.3}$$

which describe the summation of the expected loss for the n^{th} component summed together for N_C number of damageable components in the building. The loss associated with an n^{th} component can be further broken down into its different contributions as:

$$E\left[L_n|NC, IM\right] = \sum_{r=1}^{N_{DS}} E\left[L_n|DS_r\right] \times P\left[DS_r|NC, IM\right] \qquad \textbf{Equation 3.4}$$

which describes the summation of the expected repair cost of a component (n) for a damage state (DS) (r) weighted by the probability of such DS, conditioned on no collapse of the structure, where N_{DS} is the number of DSs for a given component (n). The probability of each DS can be determined from the components corresponding fragility function, and the expected loss associated with each DS of the component can be found from its consequence function that describes the repair actions required for a given level of damage, and the corresponding repair cost. Breaking down the expressions in this form gives a clear impression of how the individual component's contribution can be assembled and summed together to give the total expected direct losses in a structure at a given IM.

3.2.2 Unintended Consequences of Current State-of-Practice Application

While the general concept of the previous section should be clear and relatively simple, the actual implementation of such a procedure requires further consideration. Consider the case of a frame structure whose structural response is known at a number of intensity levels. In order to sum the individual components' expected losses together, one must break the problem down further such that each component is correctly assigned to the corresponding EDP that is damaging it in the structure. That is, the damageable components must be separated in terms of their corresponding EDPs and locations within the structure. Such a breakdown does not typically require much extra effort and can be represented as follows:

$$E\left[L_T|NC, IM\right] = \sum_{j=1}^{N_{EDP}} \sum_{n=1}^{N_C} E\left[L_n\middle|NC, IM, EDP_j\right] \qquad \textbf{Equation 3.5}$$

where the distinction between the j^{th} EDP is made. This expression can be broken down even further to be expressed in terms of what level of the building it is located, which if the components are assumed to be the same on each level can be simply given as:

$$E\left[L_T|NC, IM\right] = \sum_{m=1}^{N_{LVL}} \sum_{j=1}^{N_{EDP}} \sum_{n=1}^{N_C} E\left[L_n\middle|NC, IM, EDP_j, LVL_m\right] \qquad \textbf{Equation 3.6}$$

whereby examining the form of the expression given in the equation above, the assemblage of the expected losses in a structure for a given IM and conditioned on no collapse have been broken down in terms of their associated EDP and the level within the structure. This represents the current state-of-practice application, PACT [FEMA P58-3, 2012], and integrates well with the current method in which engineers would conduct and report NRHA results, where for a given structure the response of the structure at a number of intensities would be examined and the NRHA results would be reported in terms of a single value of peak drift and floor acceleration at each level of the structure, for example. Therefore, if we structure our assemblage of expected losses in such a way, we can pass rather easily from the NRHA results to the total expected losses in the structure by defining a number of damageable components at each level of the structure and specifying which EDP they are sensitive to. This is the default approach within PACT where the user is prompted to insert the NRHA results for each GM record at each level of the structure, for each EDP and a corresponding damageable component inventory is assigned based on the level within the structure and damaging EDP. This approach is easy to follow as the NRHA results are typically pasted into the program from a spreadsheet making it quite user-friendly.

One must remember, however, that there are a number of assumptions that have been made by adopting an assessment approach such as that outlined above. If one were to assign the drift and acceleration sensitive components in a structure to a single EDP value on each floor, this would imply we are expecting equal damage in all components at that level regardless of their location in the floor plan. For regular and symmetric structures, this will be shown later not to be an issue as the EDPs at the structure's centre of mass (COM) suffice in estimating damage. Although for torsionally sensitive structures, O'Reilly *et al.* [2017] have shown that this leads to unconservative estimates of damage if the COM demands are used, which will be discussed in more detail in Section 3.4. This is not difficult to imagine conceptually as if a torsionally sensitive structure is excited in two directions, the drift or acceleration will no longer be uniform throughout the structure's floor plan meaning that the COM demands become less meaningful to estimate damage at all locations of the floor plan as some parts of the building are likely to be more damaged than others.

As previously mentioned, O'Reilly *et al.* [2017] highlighted the influence of different approaches in defining EDPs in the damage and loss estimation stages of PBEE assessment of structures. This was highlighted through the examination of a regular RC frame both with and without torsional irregularity, with the results showing that by using simplified EDPs such as the drift at the structure's COM, unconservative estimates of damage and subsequently losses are obtained for a torsionally responding building. This issue is not limited to the torsional response of structures and some further pertaining issues are discussed in the following paragraphs.

Consider the case of estimating damage to RC beams, such as the sub-assembly shown in Figure 3.1. Fragility functions typically used to estimate the damage to the plastic hinges occurring in the beams are defined as a function of drift, whereby a certain level of drift at the storey would return various probabilities of each of the DSs associated with all of the beam plastic hinges located in the frame. However, if one were to consider the case shown in Figure 3.2, where a frame of unequal bay lengths and constant beam depth is being assessed, some inconsistencies in this approach arise. The use of a fragility function defined in terms of a single value of drift implies equal damage at all plastic hinges at that level in the structure, but from mechanics-based reasoning it can be shown that the rotation demands on the plastic hinge regions of the interior bay of shorter length are much larger that those of the longer exterior bays. As such, the interior beam's plastic hinges will be expected to exhibit more extensive damage than those in the exterior bays for a given level of drift in the storey. One can also see this when considering the expression of yield drift of an RC frame sub-assemblage, shown in Figure 3.1, given in Priestley *et al.* [2007] as:

$$\theta_y = 0.5\left(\frac{\epsilon_y L_b}{h_b}\right) \qquad \textbf{Equation 3.7}$$

where ε_y is the yield strain of the rebar, h_b is the beam height and L_b is the bay length.

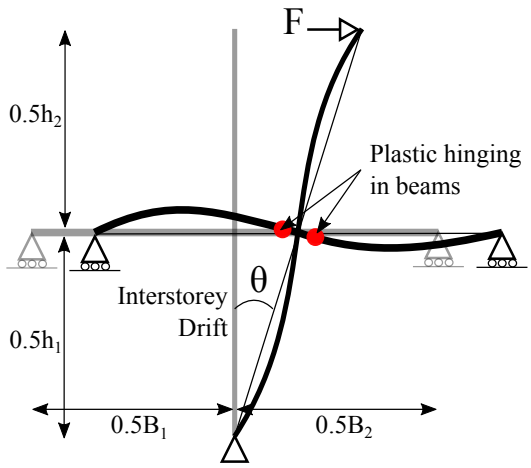

Figure 3.1. Definition of drift typically used in RC beam-column sub-assemblages referred to here as interstorey drift, which is taken as the relevant displacement between column contraflexure points (illustrated here to be at the mid-height of the storey) divided by the distance between them.

To compute the drift at limit states beyond beam yielding, this approach can be extended by assuming that upon yielding, the only contributor to the drift is the plastic deformation in the beam hinges to give:

$$\theta_{ls} = \left(\frac{1.55L_b}{6} + (\mu_{\phi,ls} - 1)(0.04L_b + 0.022f_y d_{bl})\right)\left(\frac{2.1\epsilon_y L_b}{h_b}\right) \qquad \textbf{Equation 3.8}$$

which assumes the plastic hinge length expression given by Paulay and Priestley [1992] and the shear span is given by half the bay length, where $\mu_{\phi,ls}$ is the curvature ductility at a given limit state, f_y is the steel yield strength and d_{bl} is the bar diameter. This clearly shows how the drift at various limit states of the beams is linked to the length of the bays in the frame. As such, the use of a single fragility function expressed in terms of drift without any consideration of bay length introduces additional error to the damage estimates. A solution to this inconsistency would be to define the damage in terms of the member's chord rotation, as this has been widely used in the research community to define the DSs of RC members during experimental testing and subsequent predictive equation development. This would require multiple definitions of a beam or column chord rotation EDPs at each

level of the building, which can become cumbersome to handle during analysis, in addition to new fragility functions required to be defined in terms of local member deformation such as chord rotation or curvature.

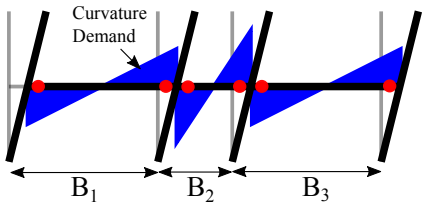

Figure 3.2. Beam curvature demands in frames with different bay lengths.

Another issue highlighted here is the definition of drift in the actual building itself. If one were to examine a series of experimental test reports and articles examining the behaviour of RC frame sub-assemblages, a typical response plot would report the actuator force versus the interstorey drift. Such a test assembly shown Figure 3.1 is quite common and a large amount of existing fragility function sets for RC frames have been based on such a definition of interstorey drift, which is taken as the relative displacement between the contraflexure points divided by the distance between them. However, when conducting numerical analysis of a case study structure, such as that shown in Figure 3.3, the drift is often defined as the relative displacement between two slabs divided by the storey height, whose more appropriate term would be storey drift, since it refers to the drift of an actual storey and not between two adjacent storeys. This introduces another inconsistency in the definition of currently available fragility functions as the definition of drift from which fragility functions were developed (interstorey drift) and the definition with which they are being applied (storey drift) are not the same. They are strongly correlated, but not equal. Furthermore, one may speculate as to how appropriate it is to use the storey drift from the lower storey to predict damage in the beams located between two storeys. The use of interstorey drift appears more appropriate but then a difficulty arises in actually obtaining this since the relative distance between contraflexure points must be recorded during analysis, which can often only be done by introducing more intermediate nodes to the member, which results in an increased model size that may run much more slowly. The same points also hold when evaluating the performance of beam-column joints, whose damage is often defined in terms of interstorey drift, but whose numerical modelling is defined in terms of joint rotation. On the contrary, the use of storey drift is an excellent demand parameter when considering the damage to non-structural elements such as partitions, since the relative displacement of the floor slabs is what is damaging them and not a combined drift of two adjacent floors. As a result, it appears that two separate definitions of drift should be used in assessment, but rarely is such a distinction actually made.

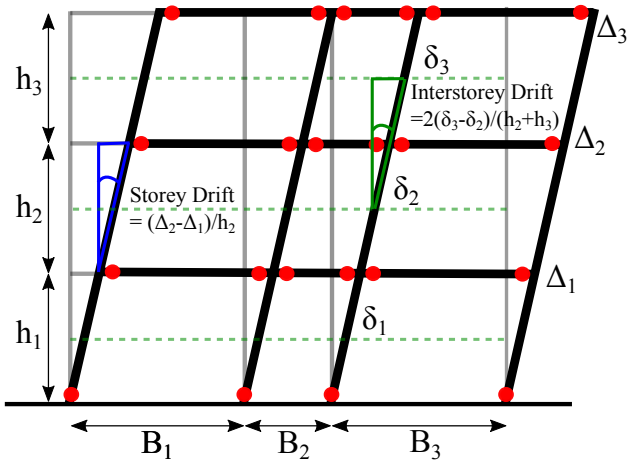

Figure 3.3. Typical definition of drift used in structural analysis, referred to here as storey drift, which is taken as the relevant displacement between floor slabs divided by the storey height.

3.2.3 Potential Improvements to the Current State-of-Practice Application

From the discussion presented in the previous section, it is clear that there are numerous areas in which the current state-of-practice application (i.e. PACT) of the PEER PBEE methodology can be refined or improved. While many of these have been highlighted in the previous section, these are summarised here to provide a basis for which an improved software tool can be developed for the assessment of structures.

- Local EDPs - The first of these is the use of local EDPs, where typical demand parameters such as peak drift and acceleration are usually defined by one global value per floor. In order to allow consideration of local demand parameters, such as joint rotation, where multiple definitions of the same demand parameter exist per floor, the current approach needs to be broken down further to account for this. This would enable a more refined consideration of local demand parameters and torsional response in irregular buildings since the user would not be confined to using COM demands, as highlighted in the previous sections.
- Modelling Uncertainty - The second issue that is addressed here involves the treatment of epistemic or modelling uncertainty in loss estimation. This will be discussed in depth in Chapter 4 where appropriate values for the assessment of older RC frame structures in Italy have been proposed for different structural typologies. During this quantification of modelling uncertainty, the general trends of modelling uncertainty were observed and it was seen how the magnitude of the modelling uncertainty is not only a function of the limit state at which the structure is responding but also the EDP being examined. As such, an improvement on the current handling of epistemic demand uncertainty would be to allow for the

definition of EDP specific values at various intensity levels. This would allow for more refined values of uncertainty to be adopted rather than using generic conservative values that increase the uncertainty in the overall results.

- Script based - A further improvement that is worth consideration is the creating of a computer code-based environment for conducting loss estimation. This is as the most commonly used tool, PACT, is an interface based program that requires users to interact with menus and selectable items. For single assessment cases, this is a great asset as it allows for clear and comprehensive instruction as to how the method is working and how the user can obtain results. However, within a research environment this approach is actually quite constraining as in order to conduct multiple assessments, compare results and identify trends, the research user is required to interact with the interface as opposed to running various assessments in large batches. The use of a code-based tool would potentially allow for more extensive studies to investigate the various aspects of loss estimation and pave the way for sensitivity and parameter studies to provide a better understanding into how some of the decisions made during the assessment procedure can affect the loss estimations and enable the development of simplified methods of assessment. Such an approach is already commonplace in research when conducting structural analysis, where analysis programs such as OpenSees [McKenna *et al.*, 2000] or Ruaumoko [Carr, 2007] allow the user to conduct hundreds upon thousands of analyses with a single command. To further quantify and calibrate typically expected loss values for various structural and non-structural configurations, a code-based environment represents a step forward as it means many analyses can be performed quickly to allow for proper consideration of the actual results. The software tool to be developed herein intends to bridge these current gaps in the current state-of-practice of loss estimation.

With the above points in mind, the following sections will describe the development of a MATLAB [Mathworks, 2014] based software tool to conduct seismic loss estimation and incorporate the improvements described above.

3.3 IMPLEMENTATION OF A TOOL FOR MORE REFINED SEISMIC LOSS ESTIMATION (TOMS)

Following the discussion on the development of a more refined approach to conducting loss estimation, this section will discuss the development of a **TO**ol for **M**ore Refined **S**eismic Loss Estimation (TOMS). The structure and procedure followed in the MATLAB based tool are illustrated in Figure 3.4. The following subsections discuss the various stages of the tool in terms of what is required from the user and how it is handled within the program. The aim of these subsections is to go over the fundamental aspects of what the program does and how it does it without dwelling too much on commands.

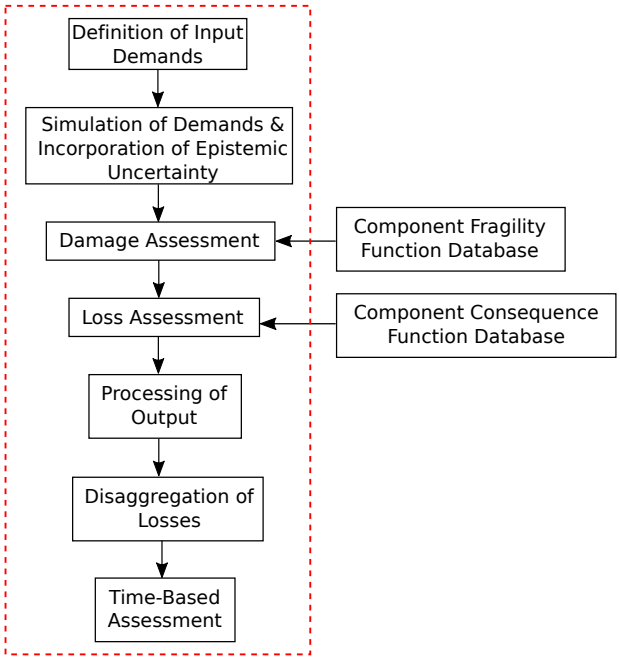

Figure 3.4. Structure of the TOMS software tool.

3.3.1 Refined Assessment

3.3.1.1 Definition of the Inputs Demands

When evaluating the performance of a building, a typical approach is to run a series of NRHA at a number of intensities and track the evolution of damage throughout the structure in what is commonly referred to as incremental dynamic analysis (IDA) or multiple stripe analaysis (MSA). This type of analysis results in a series of "stripes" of results along the same intensity to give a distribution of EDPs such as drift or acceleration for a given IM level. As such, for a given structure we will have a set of EDPs for each IM level examined during the MSA. These EDPs are then to be sorted, into a more orderly fashion such that the assessment can be conducted. That is, the EDPs are to be sorted in terms of the intensity level (i), the GM record number (q), the demand parameter (j), the global direction in which they act in the structure (k), the level of the structure to which they belong (m) and the component number (n) for a given EDP at a given level. This results in the demand parameter being loaded into the **res** structure of the MATLAB tool in the following form:

```
res.(j){i}(q,k,m,n)
```

where (j) represents the demand parameter substructure of the structure res, {i} represents the cell of results from a given intensity and (q,k,m,n) represents the 4-dimensional array of results for that intensity.

3.3.1.2 Simulation of Demand Data and Incorporation of Modelling Uncertainty

Following the completion of the MSA using a single numerical model, the size of the dataset at each IM level depends on the number of GM records ran and these MSA results will possess aleatory randomness due to record-to-record variability. However, the effects of modelling uncertainty have yet to be accounted for. In addition, since the number of data points from MSA tend to be limited by the number of GM records considered, it is of interest to take the actual analysis results and simulate a much larger data set with similar statistical properties such as median, dispersion and correlations between the various EDPs. In order to create a much larger simulated dataset from the actual MSA dataset whilst also taking the modelling uncertainty (β_{DU}) discussed in Chapter 4 into consideration, a Latin Hypercube Sampling procedure [McKay *et al.*, 1979] is followed where the distributions of the EDPs obtained at each stripe of the MSA results are maintained while at the same time incorporating the modelling uncertainty into the sampling procedure by inflating the variability of the samples with respect the original MSA data. This section describes the procedure behind the simulation of the demand parameters used in the loss estimation tool.

The original publication in which this following procedure was first discussed within the seismic loss estimation framework appears to be Yang *et al.* [2009], where the input of a set of demand data of dimensions m by n, where n is the number of EDPs, such as storey drift, and m is the number of observations of this demand, which will be the number of GMs ran. The main goal of simulating the input EDPs is to increase m from a number typically around 20 or 30 (i.e. the number of GMs ran) to a number s that is much higher. This statistical similarity between the simulated demand data and the input demand data can be thought of as follows. Say we obtain 10 values of storey drift from MSA. We would like to take the distribution of these 10 values and generate 200 points that will have the same median and dispersion as the original 10. However, since a multi-storey structure will provide more than one EDP (i.e. a storey drift at each level) the 200 storey drifts at each level can not be simulated independently without considering the correlation between these two EDPs. This has been previously discussed in Section 1.2 as the EDP|IM correlation and is explained here again for clarity. Simply put, if the storey drift at the 2nd floor of a structure is reasonable high then the storey drift at the 3rd floor will more than likely be high also, given a stable mechanism is maintained, since structural dynamics tells us that these are typically related to each other, or in other words, they are correlated. Otherwise, we may end up with the situation where we have sampled a relatively high 2nd storey drift but a very low 3rd storey drift that in a global sense, does not make sense since the

correlation between the EDPs has not been respected. As such, this correlation between the EDPs parameters must be respected such that simulated data will not only have the same median and dispersion as the original demand data but the same correlation between different demand parameters. Bradley and Lee [2010] outline simplified expressions that can be used to estimate these correlations between peak storey drift (PSD) and peak floor acceleration (PFA) in RC frame structures, although these expressions were developed for ductile, capacity designed frames in New Zealand. Similar expressions are proposed for the GLD RC frames in Italy using the results of extensive NRHA in Section 7.3.2.2.

The first step of the process illustrated in Figure 3.5 below is to take the demand array **X** that has dimensions of m rows by n columns (m by n), where the columns contain all the EDPs such as PSD or PFA and the rows contain the value for each GM (m). This matrix **X** is assumed to be lognormally distributed, which leads to the corresponding normally distributed matrix **Y** (m by n) that is found by taking the natural logarithm of **X** using MATLAB as follows:

$$\mathbf{Y} = \log(\mathbf{X}) \qquad \textbf{Equation 3.9}$$

Using this normally distributed matrix **Y**, some additional properties are established. The mean ($\mathbf{M_Y}$) (1 by n), variance ($\boldsymbol{\sigma}_\mathbf{Y}$) (1 by n), covariance ($\boldsymbol{\Sigma}_{\mathbf{YY}}$) (n by n) and correlation coefficients ($\boldsymbol{\rho}_{\mathbf{YY}}$) (n by n) are found using the following commands:

$$\mathbf{M_Y} = \text{mean}(\mathbf{Y}) \qquad \textbf{Equation 3.10}$$

$$\boldsymbol{\sigma}_\mathbf{Y} = \text{var}(\mathbf{Y}) \qquad \textbf{Equation 3.11}$$

$$\boldsymbol{\Sigma}_{\mathbf{YY}} = \text{cov}(\mathbf{Y}) \qquad \textbf{Equation 3.12}$$

$$\boldsymbol{\rho}_{\mathbf{YY}} = \text{corr}(\mathbf{Y}) \qquad \textbf{Equation 3.13}$$

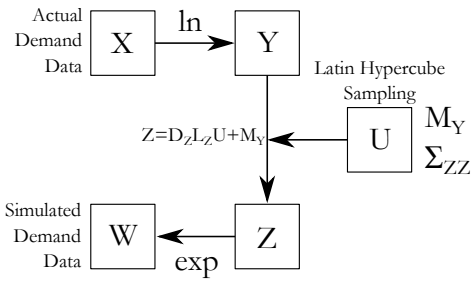

Figure 3.5. Flowchart for simulation of demand data (Adopted from FEMA P58-1 [2012]).

At this point, the variance of the data is increased to account for additional uncertainty in the demand data. This is done by first decomposing the covariance matrix $\boldsymbol{\Sigma}_{\mathbf{YY}}$ into the variance $\boldsymbol{\sigma}_{\mathbf{Y}}$ and correlation coefficients $\boldsymbol{\rho}_{\mathbf{YY}}$. From this, the variance of **Y** is increased to account for these uncertainties due to modelling uncertainty $\boldsymbol{\beta}_{\mathbf{DU}}$ to give a new variance $\boldsymbol{\sigma}_{\mathbf{Z}}$ that will be combined with the original correlation coefficient matrix $\boldsymbol{\rho}_{\mathbf{YY}}$ to give the new covariance matrix $\boldsymbol{\Sigma}_{\mathbf{ZZ}}$ that accounts for the additional uncertainties. As will be seen shortly, the dataset **Y** will be simulated to give a much larger dataset termed **Z** (s by n), where s is the number of simulations, which has the same statistical properties as **Y** in addition to modelling uncertainty consideration. Hence, this new covariance matrix uses the subscript **Z** as opposed to **Y**, since it represents the properties of the simulated data **Z**. Since variance is given by the square of the standard deviation of a normal distribution, it follows that this is equal to the dispersion of the corresponding lognormal distribution **X**. This is given as follows:

$$\boldsymbol{\sigma}_{\mathbf{Y}} = \boldsymbol{\beta}_{\mathbf{X}}^{\mathbf{2}} \qquad \textbf{Equation 3.14}$$

meaning that the individual entries of $\boldsymbol{\sigma}_{\mathbf{Y}}$ correspond to the lognormal dispersion $\boldsymbol{\beta}_{\mathbf{X}}$ squared. When combining the additional uncertainties into a single value, the dispersion is often combined using a square root sum of the squares (SRSS) approach, which when dealing in terms of variance means that the variances are added. These operations are carried out as follows in MATLAB to combine the individual vector entries:

$$\boldsymbol{\sigma}_{\mathbf{Z}} = \boldsymbol{\sigma}_{\mathbf{Y}} + \boldsymbol{\beta}_{\mathbf{DU}}^{\mathbf{2}} \qquad \textbf{Equation 3.15}$$

Combining this adjusted variance with the correlation coefficient matrix to get the new adjusted covariance matrix $\boldsymbol{\Sigma}_{\mathbf{ZZ}}$ gives the following:

$$\boldsymbol{\Sigma}_{\mathbf{ZZ}} = \mathrm{diag}(\sqrt{\boldsymbol{\sigma}_{\mathbf{Z}}})\boldsymbol{\rho}_{\mathbf{YY}}\mathrm{diag}(\sqrt{\boldsymbol{\sigma}_{\mathbf{Z}}}) \qquad \textbf{Equation 3.16}$$

Now that the properties of the original demand data have been determined and adjusted to account for additional sources of uncertainty, the demand data can be simulated. This data is simulated such that in the case of no additional uncertainty, the statistical properties such as mean, variance and correlation will be the same but the dataset will be much larger. Of course, the fact that the variance has been adjusted means that the variance of the simulated data will be slightly higher. The basic form of the expression used to simulate the new demand data **Z** is given in Yang *et al.* [2009] as:

$$\mathbf{Z} = \mathbf{D}_{\mathbf{Z}}\mathbf{L}_{\mathbf{Z}}\mathbf{U} + \mathbf{M}_{\mathbf{Y}} \qquad \textbf{Equation 3.17}$$

where $\mathbf{M_Y}$ are the mean values already computed and $\mathbf{U}$ (1 by s) is a vector of a standard normal random variable with length s. These values can be simulated using either a Monte Carlo Simulation MCS approach, as is typically done in FEMA P58, or by using an Latin Hypercube Sampling (LHS) method which is a form of stratified sampling technique used in statistics which typically requires fewer simulations than that of the MCS method. Both methods are implemented in the tool and can be changed by the user, where the default method is LHS. The other terms $\mathbf{D_Z}$ (p by p) and $\mathbf{L_Z}$ (n by p) listed above are derived from the newly computed covariance matrix $\mathbf{\Sigma_{ZZ}}$, where the value p is the rank of the covariance matrix $\mathbf{\Sigma_{ZZ}}$. The terms $\mathbf{D_Z}$ and $\mathbf{L_Z}$ are then found by partitioning the eigenvalues and eigenvectors of the covariance matrix $\mathbf{\Sigma_{ZZ}}$, respectively.

The rank of the covariance matrix $\mathbf{\Sigma_{ZZ}}$ is found in MATLAB using:

$$p = \text{rank}(\mathbf{\Sigma_{ZZ}}) \qquad \textbf{Equation 3.18}$$

and the value of p is an important parameter since if p is equal to n, then we say that the covariance matrix s of full rank. However, if p<n then the covariance matrix is not of full rank and arises as a result for two reasons:

1. The number of demand variables is greater than or equal to the number of observations (i.e. m<n), which can easily arise when not enough GMs are run.
2. One of the demand parameters is a linear combination of another.

In either case, the fact that the covariance matrix is not full rank tells us that there is insufficient data for generating the covariance matrix. However, the equation outlined above for determining $\mathbf{Z}$ can handle both full and non-full rank covariance matrices. Following the simulation and generation of a new demand data set $\mathbf{Z}$ that is normally distributed, the lognormal distribution is found by taking that exponential of $\mathbf{Z}$ to give the matrix $\mathbf{W}$ (s by n), which is the simulated data to be used in place of the inputted demand data $\mathbf{X}$. Following the simulation procedure above, the simulated data is arranged in the same format as the original MSA data but is added to the **sim** structure as follows:

```
sim.(j){i}(s,k,m,n)
```

where the number of GMs (q) is now replaced by the number of simulations created (s).

3.3.1.3 Damage Assessment

Now that the NRHA data has been imported and simulated to create a larger dataset that accounts for both record-to-record variability and modelling uncertainty, the damage to the structural and non-structural elements can be estimated. This is done through the use of fragility functions, illustrated in Figure 3.6, where for given a demand the probabilities of each DS for the damageable component can be estimated.

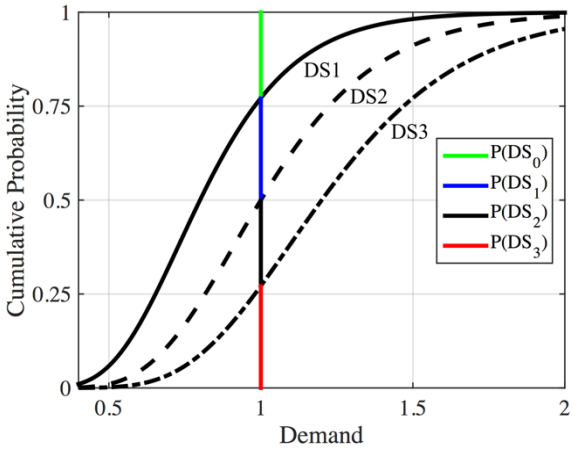

Figure 3.6. Computation of the probability of each DS for a given demand.

Since each of the damageable components within the structure are organised in terms of their level within the structure, direction in which they act and the component of that given level and direction, the fragility functions damaged by that particular EDP can be defined. This is done by creating the **comp** structure that defines the damageable component sensitive to EDP (j), acting in direction (k), at level (m) and component (n) in the structure as follows:

```
comp.(j){k,m,n}={'A101','A102'}
```

where A101 and A102 are the tags of the example fragility functions being damaged by this specific EDP. These fragility functions are defined separately in the component fragility function database illustrated in Figure 3.4.

In situations where the damageable component is non-directional, meaning that it is not sensitive to an EDP in a single direction of the structure's response but all of the directions, extra consideration is required. This type of situation arises in acceleration sensitive components that are damaged by the acceleration they are subjected to regardless of the direction in which it occurs. If one were to simply define this component in both directions separately without any further consideration, this would lead to a double counting of the same damageable component. The approach taken here is to examine the demand in both directions of response and take the maximum of the two demands as the one that will cause the damage in the structure and the consequences in terms of losses will be based on that response with the other being discarded.

Following the above procedure to estimate the probabilities of DS (x) in each damageable component (p) at each intensity level (i), direction (k), level (m), component (n) for a simulation (s), the results of this process are added to the **dam** structure in the following format:

```
dam.(edp).p{i,k,m,n,p}(s,x)
```

which are then used in the next step of the process to estimate the repair costs associated with each of the DS of a given damageable component.

3.3.1.4 Loss Estimation

Using the estimates of the probability of the DSs of each of the damageable components at each intensity level, the expected loss of each component can be estimated through the consequence function associated with the repairs of each of the DSs of the component. The total expected cost of repairs for each damageable component is then estimated by summing the repair costs of each DS weighted by its probability of occurrence. For the damageable components, the cost of repair is defined as a function of both the DS and quantity of that component. This is the approach adopted in PACT, whereby if one were to fix a single quantity of a certain damageable component, there would be a certain cost per unit associated with this but to fix many of the same items, the cost per unit would be expected to reduce. This is illustrated in Figure 3.7, where the cost per unit is constant until a certain minimum quantity is reached, after which the cost per unit is expected to reduce gradually until a minimum cost per unit is reached. The repair cost function illustrated in Figure 3.7 shows the mean cost of a particular DS as a function of the quantity of the respective components.

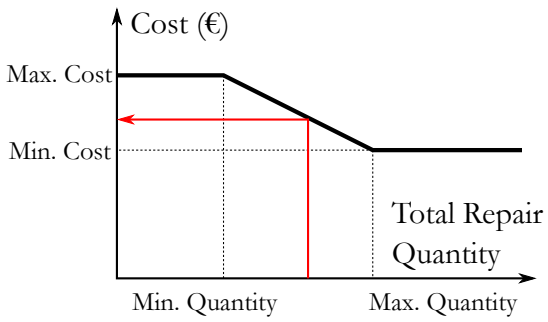

Figure 3.7. Estimation of the mean cost of repair for a given quantity of damageable components.

Following this process for each of the damageable components in the structure, the repair costs for the structure are then computed for a damageable component (p) at each intensity level (i), direction (k), level (m), component (n) for a simulation (s), the results of this process are added to the **repcost** structure in the following format:

```
repcost.(edp).comp{i,k,m,n,p}(s)
```

Since the above process computes the repair costs only, these repair costs are conditioned on no collapse and the repairability of the structure, as defined in Equation 3.1. As such, in order to compute the total expected losses of the structure, the replacement cost and demolition of the structure is also required. This is typically estimated using costing manuals and is input directly as a single value to the program.

Another issue that is considered here is the effect of costing surge. This can occur for many reasons but is mainly concerned with the increase in cost of repairs following an earthquake event due to a shortage of material or labour, where the original costing functions developed for a particular component are no longer be accurate to the actual cost as the shortage of materials and/or labour means that the repair costs are being underestimated. This is handled in the tool by means of a cost multiplier, where the costing functions supplied to the tools are universally amplified up or down to account for the variation in costing. This is also useful in situations where costing has been based on one region and is being applied in another. For example, costing manuals from northern Italy may have been used to develop consequence functions for the different elements, but the repairs need to be carried out in the southern regions of Italy where costing may be less, or even more depending on the location. In addition to the replacement cost of the building, a threshold value must be defined that defines the ratio of expected loss to the replacement cost to for which the stakeholder would elect to demolish the building rather than repair the existing, heavily damaged one. For example, FEMA P58-1 [2012] suggests a value of 40%, although more recent work by Cardone and Perrone [2016] examine actual reconstruction data following earthquakes in Italy. Cardone and Perrone [2016] note how that according to [Dolce and Manfredi, 2015], costs of between 60%-75% of the replacement cost were sustained following the L'Aquila earthquake of 2009. This has been incorporated into the tool, where the user defines a ratio to replacement cost that is checked for each realisation, where realisations that exceed this ratio are substituted with the cost of replacement.

Section 3.2.1 discussed the computation of individual expected losses to each of the damageable components in structure and how these can be summed to give the total expected loss for the whole structure for collapsing and non-collapsing cases. In order to properly compute the variance associated with these losses, the correlation between the various components needs to be addressed. That is, the three sources of correlation outlined in Bradley and Lee [2010] where the correlation of EDP|IM, which has been

previously addressed in Section 3.3.1.2, along with the correlation between DS|EDP and L|IM. As previously discussed, these correlations affect only the estimation of the variance of the losses and do not impact the estimation of expected losses. In addition, Bradley and Lee [2010] note how actually establishing these correlations for the cases of DS|EDP and L|IM is rather difficult and proposed an approximate solution, which when applied to a case study RC frame observed that the inclusion of such correlation resulted in a large increase in computation time. It was reported, however, that incorporating the EDP|IM correlation and assuming no correlation in the other two sources was a reasonable compromise when computing the variance in losses should the computation of partial correlation factors for all sources be deemed excessive. As such, since the EDP|IM correlations have been previously addressed in Section 3.3.1.2 and given the difficulty reported by Bradley and Lee [2010] in establishing and implementing the other two, these are not considered here. This omission will not impact the expected losses but rather the variance associated with these losses and is therefore not deemed a significant limitation. TOMS does output the 16th and 84th percentiles of the loss; although following the discussion above these will be underestimating the "true" variance. These are included to give the user to give an appreciation of what the variance is and are not intended for further use.

3.3.1.5 Time-Based Assessment

Since the expected losses have been computed at each IM for all of the damageable components in the structure, this can be combined with the site's mean hazard curve to perform a time-based assessment. That is, the expected losses in the structure can be related to a certain return period rather than just being expressed as a function of IM. Porter *et al.* [2004] discussed some of the different ways of expressing the economic seismic risk in structures, with one of these being the aforementioned EAL in Section 1.2, where the expected loss is annualised to represent the loss that is to be expected each year due to the building's seismic exposure and it's vulnerability. It is therefore calculated by integration the total expected loss as a function of IM with the site's mean hazard curve as follows:

$$\mathrm{EAL} = \int \mathrm{E}\left[\mathrm{L_T}|\mathrm{IM}\right] \left|\frac{\mathrm{d}\lambda_{\mathrm{IM}}}{\mathrm{dIM}}\right| \mathrm{dIM} \qquad \textbf{Equation 3.19}$$

3.3.2 Simplified Assessment

While Section 3.3.1.1 assumes that the user has conducted extensive NRHA on a representative numerical model of the structure so that NRHA data can be used to generate the simulated demands, TOMS also allows for simplified assessment results from methods such as DBA to be input, where median response parameters are specified in the **res** structure along with a definition of the expected record-to-record variability and the EDP

correlations to be respected when generating the simulated demands as described above. Therefore, the simplified assessment methods are input as follows:

```
res.(j){i}(1,k,m,n)
```

To define the estimated dispersion due to record-to-record variability, an additional variable is required. These are defined in correspondence to each definition of the demand parameters (j). For example, if PFA was defined as a demand parameter estimated from simplified analysis, the specification of both the median values and dispersion from record-to-record variability would be as follows:

```
res.PFA{i}(1,k,m,n)

res.PFA_RTR{i}(1,k,m,n)
```

For the use of simplified analysis results, the specification of the modelling uncertainty remains unchanged between methods, although for simplified analysis an EDP correlation matrix **rho** to be respected during the numerical simulation of demand parameters is required. This is not discussed in detail here, but further discussion on the definition of such EDP correlations can be found in Bradley and Lee [2010].

Chapter 5 discusses the NRHA of a number of structural typologies typical of GLD frames found throughout Italy. Using the results of this extensive analysis, Section 7.2.1 discussed the implementation of a simplified method of estimating the median demand parameters for GLD RC frames and Section 7.3.2 proposes simplified expressions to estimate record-to-record variability and demand parameter correlations required here.

3.3.3 Example Application to a Frame Building

The following sections describe the application of the TOMS tool to a multi-storey steel frame building. The intention of this section is to illustrate the results that can be obtained from the tool and how it can be used to make more informed retrofitting decisions through comparison of the EAL, for example.

3.3.3.1 Overview of Case Study Building

This section presents an example of a six storey steel moment resisting frame, shown in Figure 3.8, described in Tsai and Popov [1988]. The dead load is assumed to be 3.8 kPa at the roof and 4.5 kPa at each floor, whereas the roof live load is taken as 1.0 kPa and the floor live load 3.8 kPa, where an additional loading of 1.7 kPa to account for exterior cladding is considered. The steel grade is assumed to be A36 (nominal f_y=290 MPa) for all

members and the plastic resistance at the hinges is based an expected yield strength of 290 MPa.

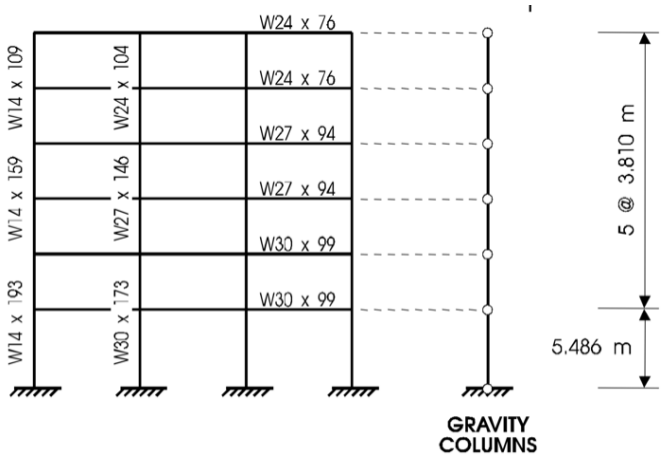

Figure 3.8. Illustration of six storey steel moment resisting frame building described in Tsai and Popov [1988].

The numerical model is developed in OpenSees [McKenna *et al.*, 2000], where only the bare steel frame is included in the analyses, i.e., the slab participation as a composite beam is not included. The inelastic response is concentrated in plastic hinges that could form at both ends of the frame members. Only half of the building is modelled, as the structure is assumed to be symmetrical in both directions. The total gravity loads acting on the interior columns are applied to the gravity column in the model and both the gravity column and the exterior frame are constrained to experience the same lateral deformation on each floor. Rigid-end offsets are specified at the end of the frame members to account for the actual size of the members at the joints. The panel zones of the beam-column connections are assumed to be stiff and strong enough to avoid any panel shear deformation and yielding under strong earthquakes. The columns are fixed at the ground level, except the gravity column that is assumed pinned at the base and at each level. P-Delta effects are accounted for in the analyses by means of an external P-Delta column shown in Figure 3.8. Rayleigh damping of 5% based on the first two elastic modes of vibration of the structure is assigned. It is recognised that this damping may not reflect reality but it is a common modelling approach that is, in any case, an assumption that is not envisaged to affect the relevance of this study. To capture the potential brittle failure of the welded beam-to-column connections, the flexural strength degradation model is introduced at the ends of the beam and column elements. In the plastic hinge model, a maximum curvature of ductility of 11.0

is specified for simplicity by using the MaxMin[d] material wrapping model available in OpenSees. These modelling parameters are not intended to be representative of state-of-the-art steel frame modelling and are merely adopted for illustrative purposes.

3.3.3.2 Structural Analysis Results

The case study structure was subjected to a number of GM intensity levels to evaluate its performance and enable a time-based loss estimation to be conducted. The site hazard information is taken as the LA Bulk Mail Facility from the report by Haselton *et al.* [2007] where the GM records from FEMA P695 [2009] are each scaled to match the spectral acceleration at the first mode period of vibration of the structure, which from modal analysis of the numerical model was found to be 1.3 seconds. Since the aims of this example are to illustrate the functionality of the software tool, no in-depth consideration of GM record selection was considered and the above assumptions were made for simplicity.

As such, the GMs were scaled to the various intensities and the results of the MSA are shown in Figure 3.9. This shows the median response and distribution of the maximum PSDs and maximum PFAs recorded at each intensity along with the associated dispersions. These MSA results are then used to perform the loss estimation in the following sections. Finally, in order to assess both the collapsing and non-collapsing sources of loss, the collapse fragility function is required. This was estimated by performing IDA [Vamvatsikos and Cornell, 2002] on the numerical model using the same GM records described above until a complete global collapse was observed due to excessive lateral drift. The median and dispersion of the lognormal distribution fitted to the collapse fragility were 1.31g and 0.56, respectively, where no modification to account to account for spectral shape or modelling uncertainty was considered for simplicity.

[d] http://opensees.berkeley.edu/wiki/index.php/MinMax_Material

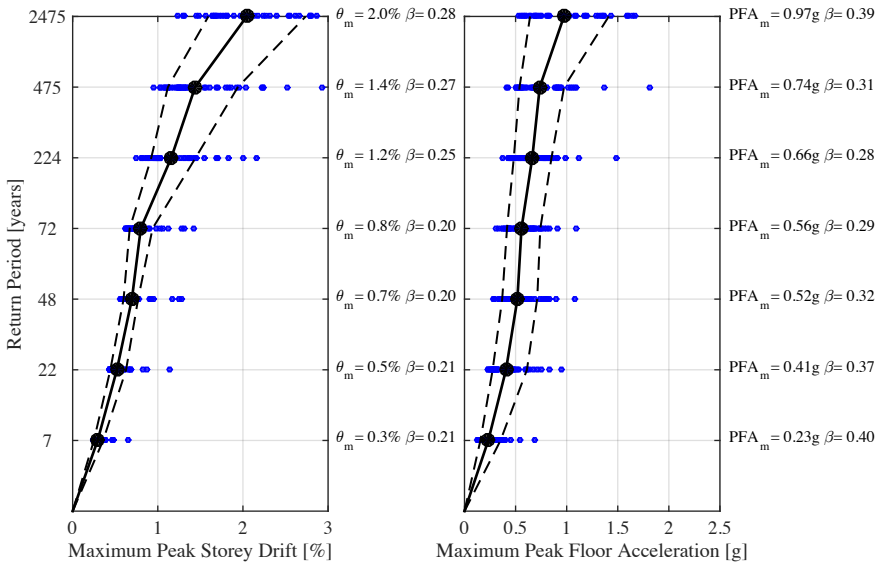

Figure 3.9. MSA results for six storey steel MRF case study structure.

3.3.3.3 Structural and Non-Structural Element Inventory

In order to conduct a full loss estimation on the case study structure, a list of damageable structural and non-structural elements needs to be compiled, along with the associated consequence and fragility functions. Table 3.1 lists an example inventory for the structure where the fragility and consequence functions have been taken from the PACT database for simplicity, where the associated PACT ID number is provided in each case. Another assumption that has been made is that the structure is symmetric in both directions, meaning that the MSA results shown in Figure 3.9 will be used to assess the structure in both principal directions of response. This is again a simplifying assumption made for the purpose of illustration.

Some other assumptions regarding the performance assessment of the case study structure are that the replacement cost has been assumed to be €3M, while the additional modelling uncertainty outlined in Section 3.3.1.2 has been set at a fixed value of 0.30 for both demand parameters used and the number of demand values to be simulated is set at 500. Residual drifts are also not considered as part of this illustration.

Table 3.1. List of damageable components in case study structure.

Component Name	PACT ID	EDP	Quantity*
Post-Northridge RBS	B1035.001	Drift	6
Curtain Walls	B2022.001	Drift	156
Wall Partition 1	C3011.002c	Drift	2
Wall Partition 2	C3011.001b	Drift	2
Wall Partition 3	C1011.001b	Drift	2
Wall Partition 4	C1011.001c	Drift	2
Raised Access Floor	C3027.002	Acceleration	36
Independent Pendant Lighting	C3034.002	Acceleration	8
Suspended Ceiling 1	C3032.003a	Acceleration	26
Suspended Ceiling 2	C3032.003b	Acceleration	4
HVAC Ducting	D3041.011c	Acceleration	2
Control Panel	D3067.013b	Acceleration	2
Fire Sprinkler	D4011.053a	Acceleration	2
Hydraulic Elevator	D1014.021	Acceleration	2 (Ground Floor)
Chiller	D3031.013h	Acceleration	1 (Roof Level)
Air Handling Unit	D3052.013k	Acceleration	1 (Roof Level)

* Actual building quantities are defined in multiples of the unit quantities prescribed for each component in PACT.

3.3.3.4 Application of the TOMS to the Case Study Structure

For the structure and component list described in the previous sections, a full loss estimation using the TOMS tool can be conducted by arranging the MSA results into the required format in MATLAB and defining the fragility function and consequence function libraries, as illustrated in Figure 3.4. The following paragraphs provide commentary to the output from the software and highlights instances where the different presentation of the loss estimation results may be of use when identifying retrofitting strategies for a given structure.

Figure 3.10 illustrates various outputs from the tool that convey the performance of the structure in different ways. Figure 3.10(a) shows the vulnerability function aggregated into the contributions from the collapsing and non-collapsing cases according to Equation 3.1, where the non-collapsing cases contribute to the majority of the losses up until about the 2475 year return period intensity when the contribution for the collapsing cases becomes more significant. Regarding the non-collapsing cases, Figure 3.10(b) shows the contributions to the expected losses from each of the damageable components conditioned

on no collapse of the structure. This figure highlights how the "Wall Partition 1" contributes a significant proportion to the expected loss, with the damage in the "Chiller" component also contributing significantly. This disaggregation of the expected losses is useful as it can show more prominent sources of loss in the building and be used to guide the retrofitting process. In this case, it is clear that a more resilient wall partition system is required to replace the "Wall Partition 1", as it is completely dominating the expected losses at all intensity levels. Again for the non-collapsing cases, Figure 3.11(a) shows the expected loss given no collapse separated in terms of the contributing EDP. This is a useful plot as it distinguishes the more critical demand parameter to which initial retrofit approach can be based on. For example, for cases in that drift is dominating the expected losses (such as this one), one may seek to implement a structural intervention scheme that will mitigate excessive drift of the building, such as diagonal bracing or RC wall elements. In situations where floor accelerations contribute significantly to the losses, one may try to reduce the floor accelerations in the building through the use of base isolation or viscous dampers and avoid the use of diagonal bracing, which would stiffen the building to potentially lead to even higher floor acceleration or overload elements that fall within the brace load path to further exacerbate the problem. In addition, Figure 3.11(b) shows the time-based assessment of the structure where the total expected loss is plotted versus MAF of exceedance and from Equation 3.1 the EAL ratio can be computed. The dashed lines in the plots of Figure 3.10 represent the 16^{th} and 84^{th} percentiles of the expected loss being described. It should be noted that this dispersion relates to the record-to-record and modelling uncertainty in the input EDP data and does not incorporate the effects of the DS|EDP and L|DS correlations discussed in Section 7.3.2.2, therefore underestimating the true variance. However, these dispersions are included as a guide to the user to give a feel for the magnitude of variance involved in the results.

To examine the contribution of losses from each floor of the structure in either direction, Figure 3.12 shows a profile plot of the building where the contribution to the expected loss given no collapse can be seen. In this case, the building shows relatively regular contribution to the expected losses at each level, with the exception of the non-directional equipment placed at the roof level. This highlights how by improving the resilience of these components placed at the roof through the use of component isolators, for example, the associated expected losses can be reduced in a more targeted fashion. In addition, such a plot can be useful to illustrate cases where the structure is particularly vulnerable in a specific direction or at a specific floor level. These situations may arise due to the lateral load resisting system being particularly vulnerable in one direction or in situations where a soft storey mechanism is likely to occur, therefore providing further guidance to the engineer as to the exact locations that are particularly vulnerable in the structure and contributing significantly to the expected loss.

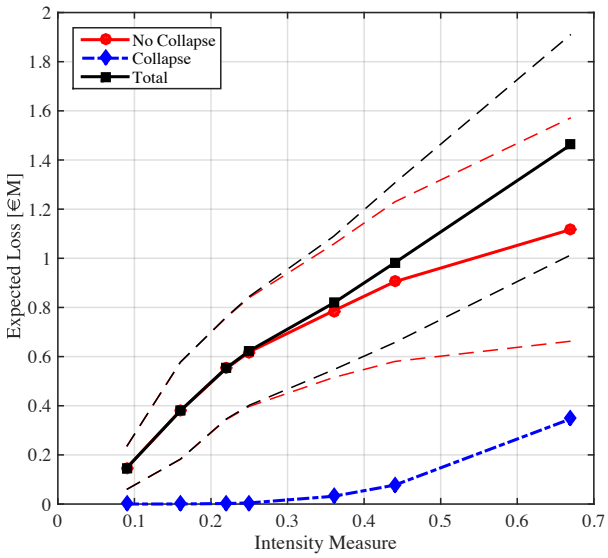

(a) Total expected loss as a function of IM.

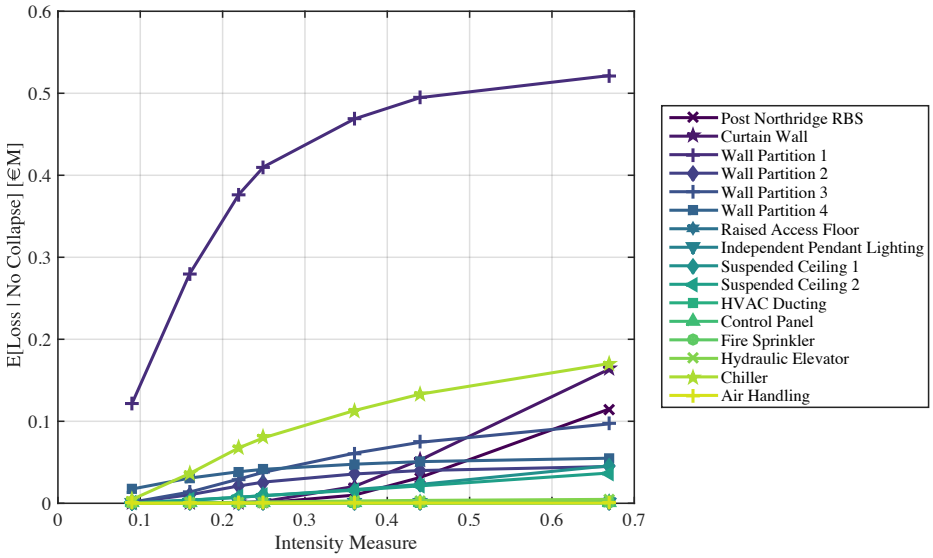

(b) Expected loss given no collapse of the various damageable components expressed as a function of IM.

Figure 3.10. Various output from the TOMS tool for the case study MRF building.

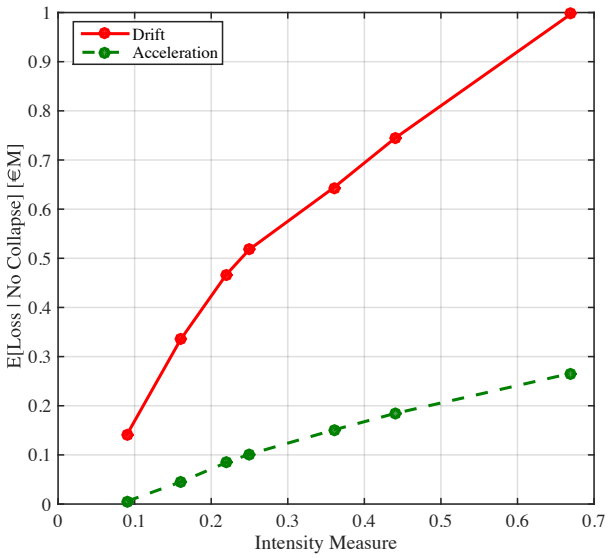

(a) Expected loss given no collapse separated in terms of the damaging EDP.

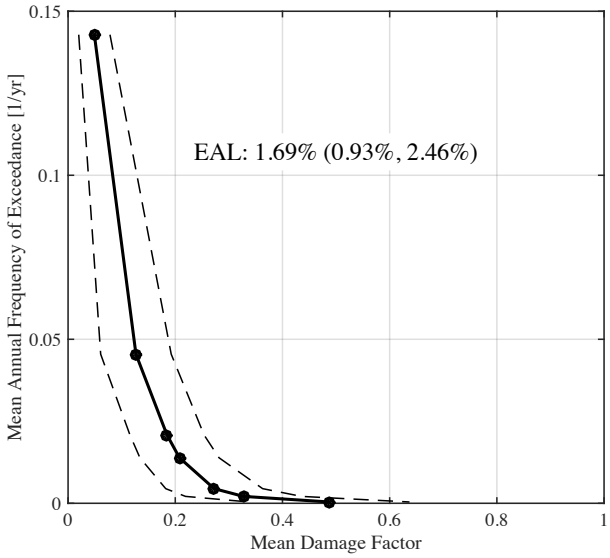

(b) Time-based assessment of the structure to compute the EAL ratio.

Figure 3.11. Various output from the TOMS tool for the case study MRF building.

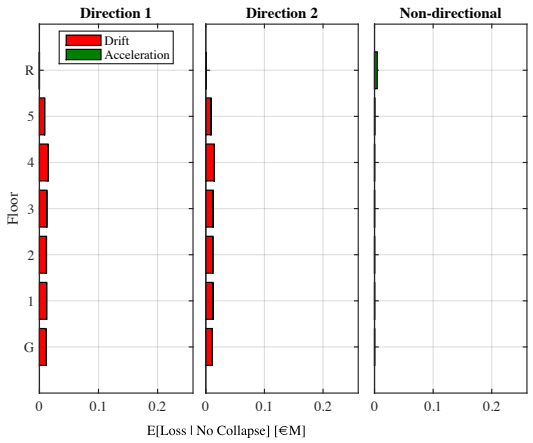

(a) Expected loss given no collapse at each floor level (T_R=7 years).

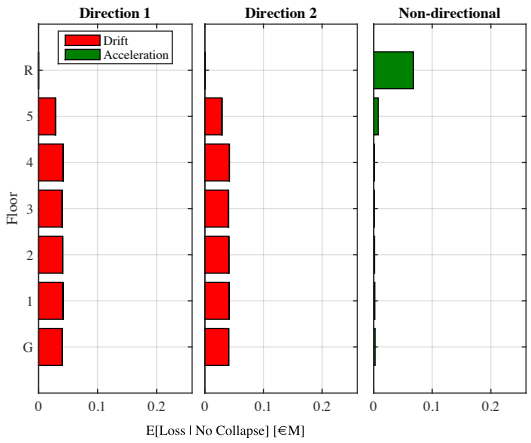

(b) Expected loss given no collapse at each floor level (T_R=48 years).

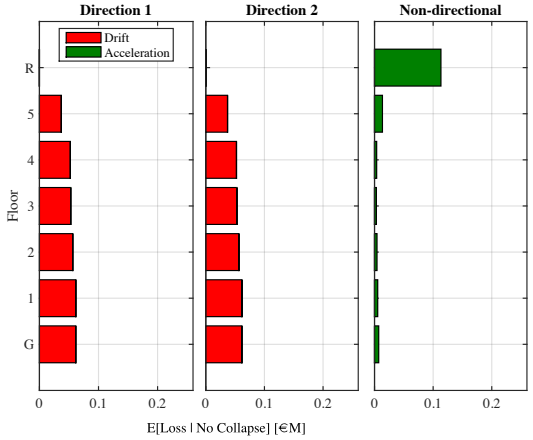

(c) Expected loss given no collapse at each floor level (T_R=224 years).

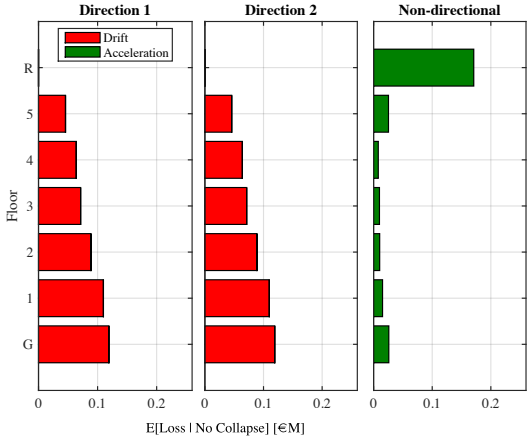

(d) Expected loss given no collapse at each floor level (T_R=2475 years).

Figure 3.12. Loss contribution profile of the case study structure at various return periods.

Since the above information can be used to assess and guide different retrofitting approaches, this can be illustrated here through the application of two different retrofits and using the TOMS tool to plot and compare the results of each case. For simplicity, two retrofits have been chosen to target the structural and non-structural elements, respectively. These two retrofit solutions are:

1. Structural Retrofit – This is a hypothetical retrofit carried out by adding some diagonal bracing to the structure. This has been idealised by taking the MSA results of the original case study building and uniformly reducing the PSDs by 20% since the increased stiffness provided by diagonal bracing will be expected to provide an overall reduction in the lateral response of the structure. In addition, the increased stiffness of the structure is expected to increase the PFAs in the structure and as such, these have been amplified by 10%. Furthermore, the median collapse intensity has been amplified to 1.6g with the dispersion remaining constant. No changes to the non-structural elements have been made. It is also assumed for simplicity that the initial period will not change significantly, meaning that the same condition period and hazard curve are used. This is elaborated on further in Section 6.4.3.
2. Non-Structural Retrofit – This has been implemented by taking the original case study structure and modifying the behaviour of the non-structural elements through the uniform amplification of the median value of each for each damageable components fragility function to represent an improvement in the non-structural performance. The dispersion and the repair costs have not been modified. Again, this is a hypothetical retrofit used here merely for illustration.

The outcome of both of these retrofitting strategies have been recomputed using the TOMS tools and the comparison between the results is illustrated in Figure 3.13. This shows how the two different solutions provide an improved performance of the structure when considering the vulnerability functions of the two retrofit solutions shown in Figure 3.13(a). The two approaches to either improving the structural performance or the non-structural performance result in a reduced vulnerability for the case study structure. This is also reflected more or less the same way in Figure 3.13(b) where the contribution to the losses due to collapses is reduced due to the increased collapse capacity in the case of the structural retrofit solution. The plotting of the various EDPs can be used to guide the retrofitting of the structure. In Figure 3.14(a) the insertion of the diagonal bracing to help reduce the losses associated with the PSD sensitive damageable components as expected, but with the adverse effects on the PFA sensitive losses due to the increase in stiffness in the structure. This type of trade-off ought to be considered carefully when deciding on retrofit strategies and plots such as Figure 3.14(a) clearly illustrate this. On the contrary, Figure 3.14(a) shows how the non-structural retrofitting provides a uniform reduction in the expected losses for both EDPs. Finally, the overall performance of the retrofitting solutions can be compared using time-based assessment shown in Figure 3.14(b) when the effect of the different solutions can be assessed in terms of the EAL, where the structural retrofit solution is seen to have an 18% reduction in the EAL, while the non-structural a 22%. These numbers are not meant to be representative of actual retrofitting targets but are an illustrative example of an approach that may be followed.

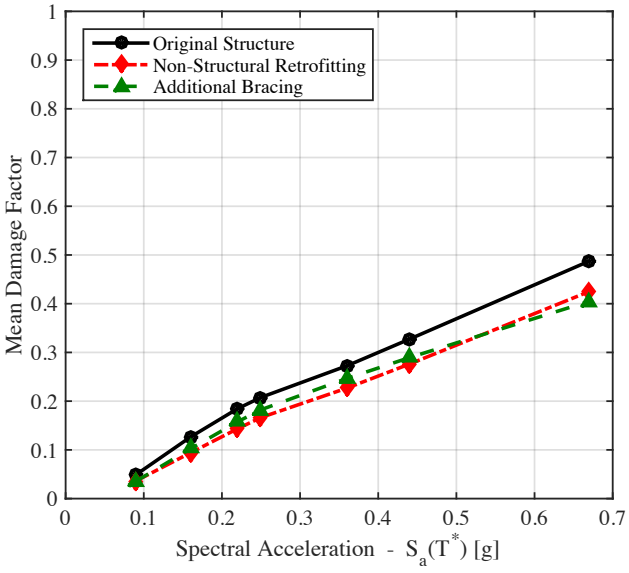

(a) Total expected loss as a function of IM

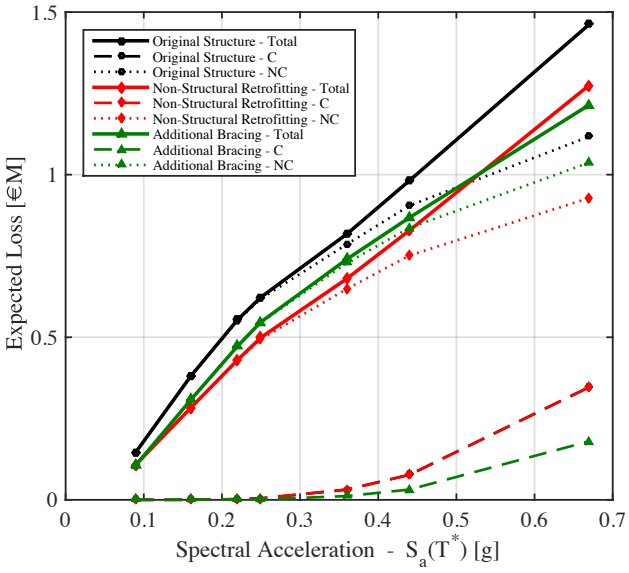

(b) Total expected loss for both collapse and no collapse as a function of IM

Figure 3.13. Illustration of different retrofit solutions using the TOMS tool for the case study 6 storey MRF structure.

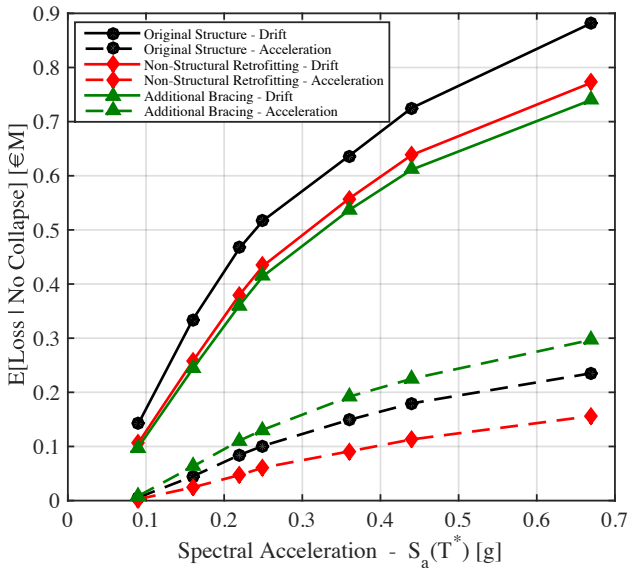

(a) Expected loss given no collapse separated in terms of the damaging EDP

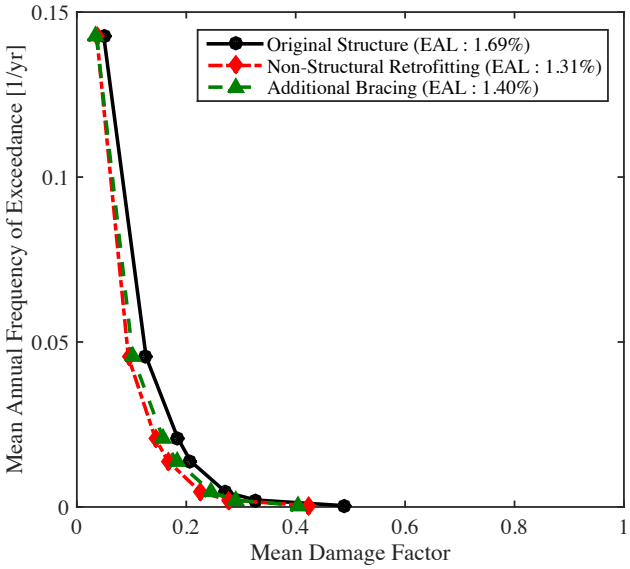

(b) Time-based assessment of the structure to compute the EAL ratio

Figure 3.14. Illustration of different retrofit solutions using the TOMS tool for the case study 6 storey MRF structure.

3.3.4 Limitations of the Assessment Tool and Future Developments

As seen in the previous sections, the TOMS tool developed here provides a simple but yet advanced consideration of expected losses for a given structure, where it was shown how the tool can also be used to compare and contrast different retrofitting options to enable the examination of their impact on the various DVs such as structural and non-structural performance in addition to damage and loss estimates. While this illustrated the capabilities of the tool, the user must also be aware of some of the current limitations that arise as a result of continuing development of the tool. This section discusses some of these limitations and the anticipated future developments.

Section 3.3.1.4 examined the various sources of correlations discussed in Bradley and Lee [2010] where it was noted how the process implemented here considers the correlation between different EDP|IM but omits the correlations of DS|EDP and L|DS due to a lack of data and difficulty in the actual implementation of such correlations without compromising on computation time. Since the inclusion of these correlations will only affect the variance of the results and not the expected values, it is not deemed a critical issue. Although the user should note that this additional source of variance has been omitted in the bounding percentile presented in Figure 3.10 which have been included to give an idea of the magnitude of the variance in the loss estimates.

Different collapse modes have not been accounted for different collapse modes and consider only the complete collapse, leading to possibly conservative estimates of the expected number of casualties, but this is not expected to have any impact on the findings of this study. This could be implemented by including an additional option to define different modes, but such a feature is not deemed critical for now. Finally, it is recognised that TOMS is a novel computational tool developed as part of this study to address some of the issues previously listed. To validate the usage of this tool and proceed with a degree of confidence for the future studies discussed this thesis, comparisons were made using reference building models between the existing PACT software and TOMS.

3.4 IMPLICATIONS OF SUCH A REFINEMENT IN THE SEISMIC ASSESSMENT OF STRUCTURES

The previous sections discussed some of the limitations with the current state of practice implementation of seismic loss estimation. A more refined approach has been thus developed to account for such limitations and provide a simple and efficient tool to conduct loss estimation within a research environment. As such, this section investigates the impact of using more generalised methods, where the damage in deformation sensitive elements in a structure can be estimated using a single demand parameter at each level of the structure. This is compared with a more refined approach to estimate the damage where multiple definitions of deformation demand are defined at each level of the structure to

better represent the actual demand the various damageable elements are experiencing at different parts of the building. By investigating the response of a case study RC frame building, both with and without torsional response, the impact of using a general approach to assessing damage at various intensity levels is compared to that of a more refined method. The effects of these two approaches are also quantified in terms of direct economic loss in order illustrate how such simplifications in the structural analysis and damage assessment of irregular structures can impact the salient parameters the PBEE framework aims to provide.

3.4.1 Design and Numerical Modelling of Case Study Buildings

3.4.1.1 Design of Case Study Buildings

To illustrate the differences between assessment approaches, a series of case study structures have been designed. These consist of a three and six storey regular ductile RC frame with five unequal bays in the principal X direction and three unequal bays in the Y direction, as shown in Figure 3.15. Some of the typical details of the frame are outlined in Figure 3.15, where the total seismic weight of each floor is taken as 8kPa, the expected yield strength of the reinforcing steel bars is taken as 500MPa and an expected concrete compressive strength of 30MPa. In addition, Figure 3.15(b) shows the same structure but with two RC walls each with a nominal moment capacity of 12,000 kNm added to one end of the structure after the seismic design of the structure has been completed. This will induce a stiffness eccentricity in the structure and result in a torsional response, whose effects will be investigated and used as an example of how torsional response affects the estimation of damage in the various frame components. The dimensions of the columns were kept constant along the height of the building for simplicity during design, whereas in practice these would typically be expected to reduce with height, but it is expected that this assumption is not likely to impact the findings of this study. The structures with a plan layout shown in Figure 3.15(a) will be referred to herein as Frame A, while the corresponding ones shown in Figure 3.15(b) will be referred to as Frame B.

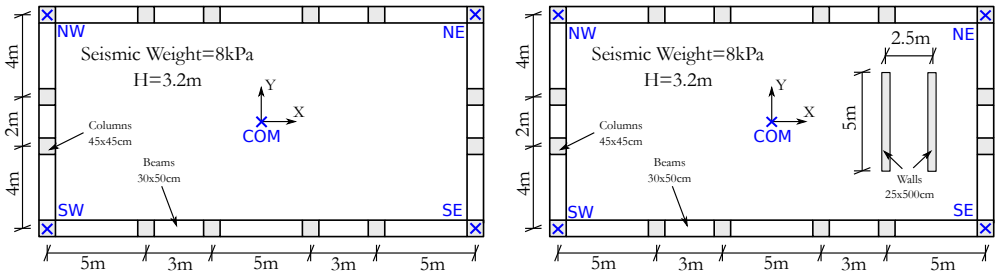

(a) Frame A – Symmetric in plan. **(b) Frame B – Asymmetric in plan.**

Figure 3.15. Layout of case study RC frames.

For the purpose of assigning reasonable levels of strength and stiffness, the structures are designed using the direct displacement-based design (DDBD) method outlined in Priestley *et al.* [2007], where the most recent developments described in the model design code (DBD12) [Sullivan *et al.*, 2012] are adopted here. The buildings are presumed to be located at a site characterised by seismic hazard at the damage control limit state corresponding to Eurocode 8 [EN 1998-1:2004, 2004] Type 1 spectrum with PGA = 0.4g, soil type C and T_D >4s. The target design drift θ_c is taken as 2.5%, while section sizes are as illustrated in Figure 3.15. For brevity, a summary of the salient design parameters for each frame in both X and Y directions are listed in Table 3.2 to arrive at the final design base shear which is then distributed along the height of the building to arrive at the final design solution. In order to ensure a strong column-weak beam strength hierarchy in the frame, the column design moments are amplified such that the strength ratio at each joint satisfies a strong column-weak beam ratio of 1.3. This capacity design requirement is also in line with the requirements of Eurocode 8 to ensure a ductile beam-sway mechanism in the frames. The presence of the RC walls in Frame B are not accounted for during the design process and are introduced in the numerical modelling to induce a torsional behaviour on Frame B, which will be investigated further in later sections. Hence, the two frames are designed with the same sections sizes and member capacities. The frames will be labelled using the system of number of storeys followed by design variation, such that the three storey building with no RC walls is referred to as 3A, for example.

Table 3.2. Summary of the salient DDBD design parameters.

		X direction		Y direction			
		3 Storey	6 Storey	3 Storey	6 Storey		Reference
Design Displacement	Δ_d	0.157	0.282	0.157	0.282	m	DBD12 Eqn 5.2
Effective Height	H_e	7.3	13.5	7.3	13.5	m	DBD12 Eqn 5.10
Effective Mass	m_e	461	872	461	872	T	DBD12 Eqn 5.7
Yield Displacement	Δ_y	0.076	0.141	0.060	0.110	m	DBD12 Eqn C7.1
Ductility	μ	2.1	2.0	2.6	2.6		DBD12 Eqn 7.1
Equivalent Viscous Damping	ξ	14.3%	14.0%	16.1%	15.9%		DBD12 Eqn 7.4
Spectral Reduction Factor	R_ξ	0.66	0.66	0.62	0.62		DBD12 Eqn 1.2
Effective Period	T_e	1.40	2.49	1.47	2.64	s	DBD12 Eqn 5.6
Effective Stiffness	K_e	9349	5535	8385	4941.3	kN/m	DBD12 Eqn 5.4
Design Base Shear	$V_{b,total}$	1515	1654	1364	1486	kN	

3.4.1.2 Numerical Modelling of Case Study Buildings

The numerical modelling is carried out using OpenSees [McKenna *et al.*, 2000], where lumped plasticity models are adopted for the frame members. The moment-curvature relation used to describe the plastic hinge behaviour is determined based on the provided member capacities determined from design and the assumed section size. The yield curvature is determined using the equations provided in Priestley *et al.* [2007], which allows the computation of the cracked stiffness of the member, where the internal elastic portion of the element is also modelled using this cracked section stiffness. The post-yield hysteretic backbone parameters are determined as per the expressions given in Haselton *et al.* [2008], which describe the behaviour of ductile RC frame members. The parameters are then implemented into the model using the modified Ibarra-Medina-Krawinkler [Ibarra *et al.*, 2005] hysteretic model to adequately capture the post-yield behaviour of the RC members to account for concrete spalling, core crushing and rebar buckling through the strength and stiffness degradation of the members. The plastic hinge length is determined using the expression given in Priestley *et al.* [1993]. The floor diaphragms are assumed to be rigid in-

plane and the gravity loads are modelled using a single P-Delta column placed at the COM of the structure. The foundations of the structure are considered to be rigid. Table 3.3 shows the first mode periods of the frames in both directions, where the periods of the frames are seen to be the same in the X direction for Frames A and B, but the presence of the RC walls is seen to reduce the initial period of the Frame B structures in the Y direction. For simplicity, no out-of-plane modelling of RC walls was considered. Had this been considered, one would see a slight shortening in the T_X values of 3B and 6B.

Table 3.3. First mode periods of vibrations in the two principal directions of the structures.

	3 Storey		6 Storey	
Layout	T_X	T_Y	T_X	T_Y
Frame A	0.94s	0.93s	1.64s	1.64s
Frame B	0.94s	0.49s	1.64s	1.08s

3.4.2 IDA of the Case Study Frames

Numerical models of the frames described in the previous section have been subjected to a set of accelerograms at a number of intensities to investigate the progression of damage with increasing intensity. The set of 22 GMs pairs available from FEMA P695 [FEMA P695, 2009] are used and scaled to a number of intensities to perform what is commonly referred to as IDA [Vamvatsikos and Cornell, 2002], where the IM is taken here as the spectral acceleration at conditioning period T^*, where T^* is defined as the average between the first periods of the structure in the X and Y direction, as suggested by FEMA P58 [FEMA P58-1, 2012]. Figure 3.16 and Figure 3.17 shows some of the structural analysis results for the frames, where it is clear that for both 3A and 6A, the COM response is the same as the response at different locations throughout the floor plan since the median and percentiles plot of the maximum of all the PSDs throughout the height of the building at the different locations are the same, whereas the response of 3B is seen to be markedly different at different locations due to the influence of the torsional behaviour in the Y direction, which is seen through the increased demand on the west side of the building and a reduced demand on the east side, where the RC walls are located. This is, of course, an expected observation, but important to investigate further in terms of implications for damage assessment since if the COM storey drift is used to estimate drift at all locations in the floor plan, one would expect that each of the drift sensitive components are equally damaged, whereas in actual fact the components on the west side of the building floor plan are much more damaged than those on the east, as illustrated in Figure 3.16(b) and Figure 3.17(b).

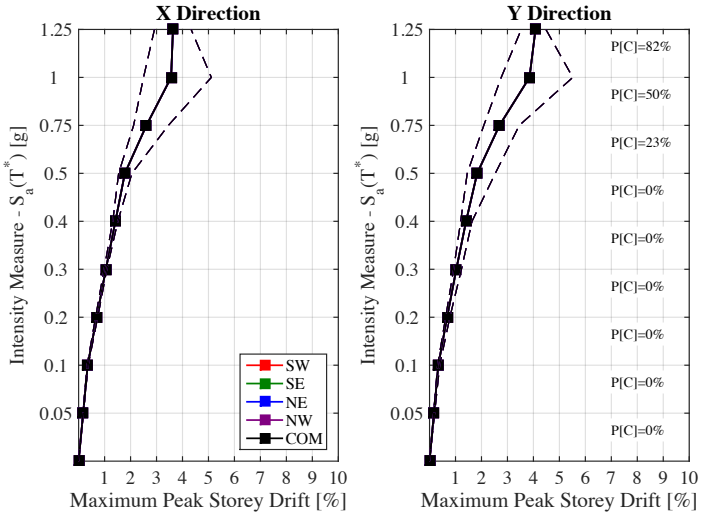

(a) 3 Storey Frame A - 3A

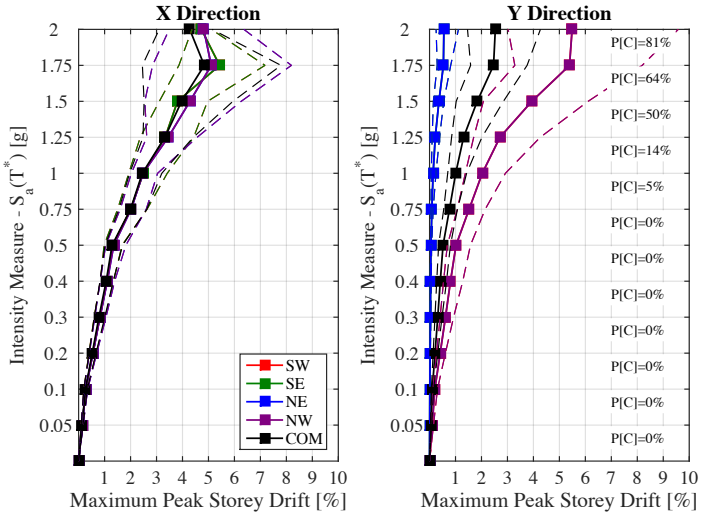

(b) 3 Storey Frame B - 3B

Figure 3.16. Median, 16th and 84th percentiles of the maximum PSD of the case study frames.

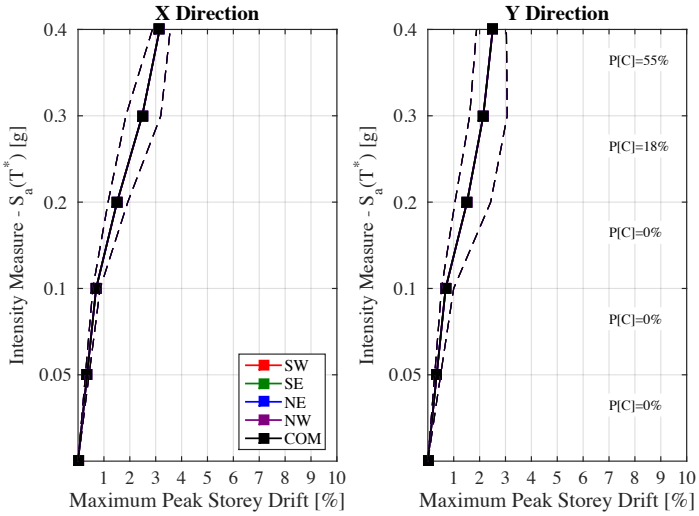

(a) 6 Storey Frame A - 6A

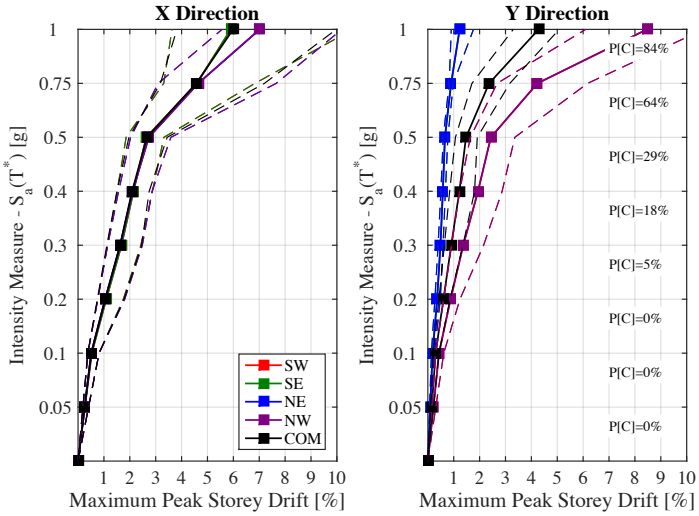

(b) 6 Storey Frame B - 6B

Figure 3.17. Median, 16th and 84th percentiles of the maximum PSD of the case study frames.

3.4.3 Damage Assessment of Case Study Frames

Using the results of the analyses conducted in the previous section for each of the frames, a damage assessment of the structural members is conducted using two different methods:

- Method 1: For each of the frames, the damage to RC frame members is computed by using the structural analysis results recorded at the COM at each level of the structure. This means that despite the frame elements being located on the north/south and east/west faces of the structure, the drift at the COM is used as a representative demand parameter for the damage induced in the drift sensitive components at all locations in the floor plan. This is the default approach used in the software PACT [FEMA P58-3, 2012] which requests a single drift in both principal directions of the structure, to which the various drift sensitive components are assigned. This is a common approach that works well, albeit with some other limitations discussed further in Section 3.2.2, in situations where the structure is regular in plan and elevation with a rigid diaphragm.
- Method 2: The local demand parameters associated with each of the various damageable components located throughout the structure are used with the TOMS tools described in Section 3.2. For example, the drift demand recorded on the west side of the structure during the numerical analysis is used to compute the damage in the corresponding elements. This is essentially using a better demand parameter to estimate actual damage since the drifts that that particular side of the building has experienced are being used to compute the damage in the elements. This implies that even in the case of an irregular plan building, a demand parameter that is representative of the damage that the frame is experiencing at that location on the floor plan is still being used.

The approach advocated by Method 2 may seem like a simple and logical process, but one must consider that current software tools to conduct such an assessment, whereby multiple definitions of demand parameters exist per floor of the structure, are not widely available and as such, more simple definitions of demand parameters are typically adopted to conduct damage assessments and subsequent economic loss estimations. This does not imply that current methods are wrong, but rather that they rely on certain simplifications to the idealised structure, which if the actual structure being assessed does not fit, leads to greater uncertainty being introduced to the performance results due to a lack of alternatives. This paper argues the case for such an alternative with the TOMS software tool described in Section 3.2 enabling this more refined assessment. The fragility functions used to evaluate the probability of various DSs are those available within PACT for ductile RC beams with interior and exterior beam-column joints (ID's B1041.002a and B1041.002b in PACT). These consider three DSs corresponding to member cracking (DS_1), spalling (DS_2) and crushing of core concrete and/or rebar buckling (DS_3). The following sections describe the damage assessment of the various frames using the aforementioned fragility functions and two methods of assessment.

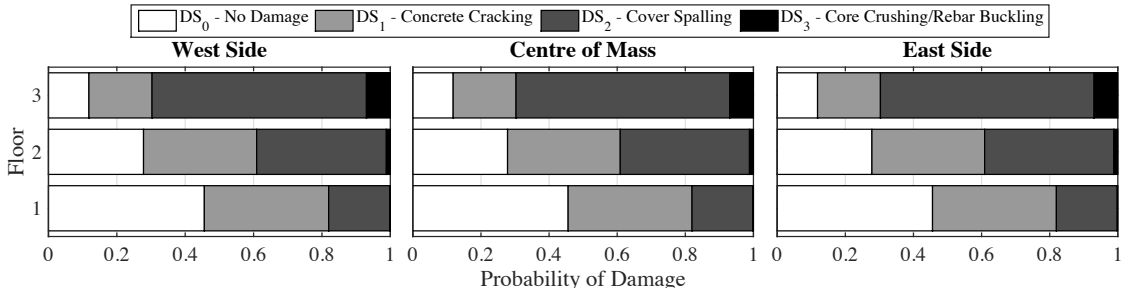

(a) Frame A – 3 storey (3A) at $S_a(T^*)$ = 1.0g

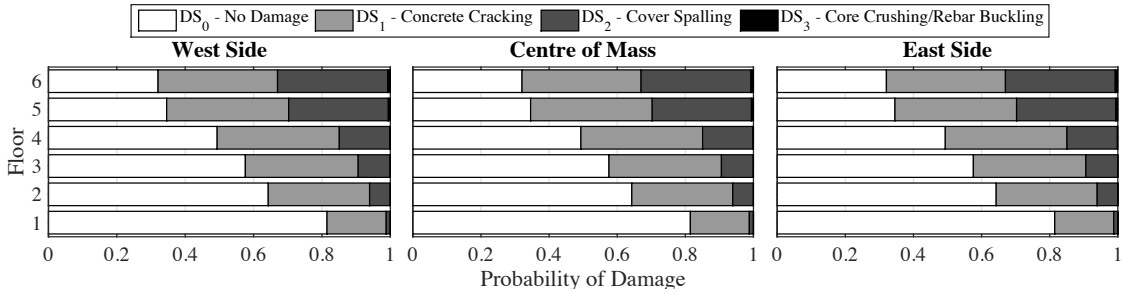

(b) Frame A – 6 storey (6A) at $S_a(T^*)$ = 0.4g

Figure 3.18. Damage probabilities in the Y direction at each floor of the Frame A type buildings where the median response was used to compute the probabilities of each DS.

3.4.3.1 Frame A

For simplicity, the damage to the perimeter frames located on the east and west ends of the structure are presented here for Frame A, which is the regular plan frame shown in Figure 3.15(a). Figure 3.18 shows the probabilities of each of the DSs for the three and six storey frames using both damage assessment methods. The central subplot shows the probabilities of damage for all frame elements if just the drifts at the COM are used (Method 1), whereas the plots on either side show the probabilities of damage for the respective perimeter frame elements using the actual drift demands recorded at that end of the building (Method 2). It is clear from Figure 3.18 that the damage distribution at each floor for both frames is the same regardless of whether Method 1 or Method 2 is used. This is obviously because the frame in symmetric and a rigid floor slab has been assumed. As such, the use of Method 1 would suffice to estimate the damage to the frame members at all locations of the building. This is in line with current assessment approaches for structures as it fits the typical assumption of a regular floor plans that does not possess any torsional response.

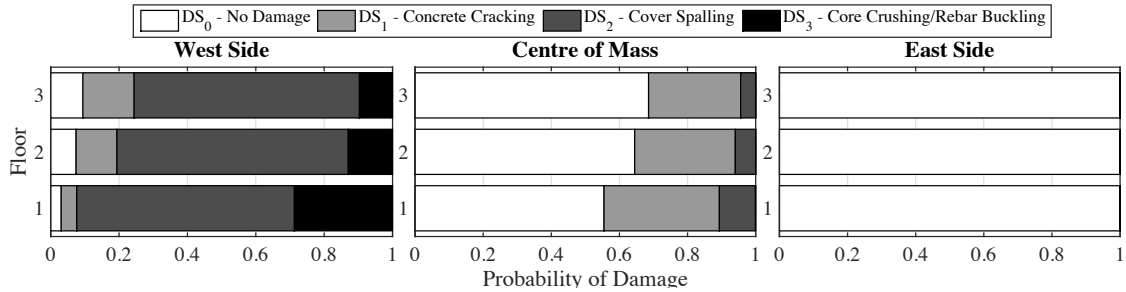

(a) Frame B – 3 storey (3B) at $S_a(T^*)$ = 1.5g

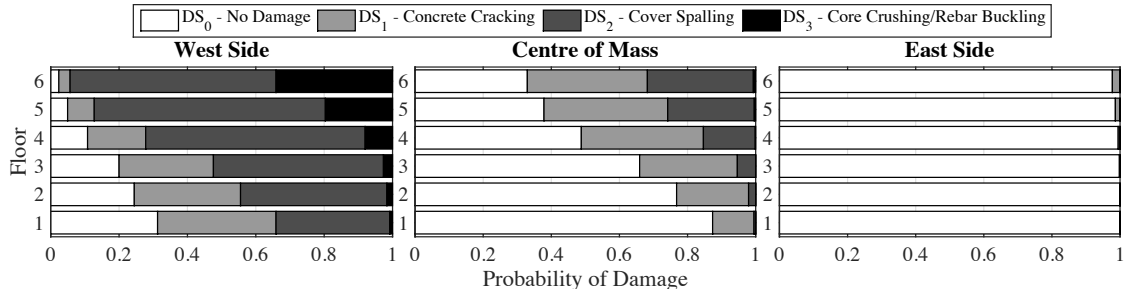

(b) Frame B – 6 storey (6B) at $S_a(T^*)$ = 0.75g

Figure 3.19. Damage probabilities in the Y direction at each floor of the Frame B type buildings where the median response was used to compute the probabilities of each DS.

3.4.3.2 Frame B

Now let us consider the case of the Frame B type structures, which are essentially the Frame A type structures just with additional RC walls added to the east side in order to induce a torsional response of the structure. Again, only the response in the Y direction is discussed here and Figure 3.19 shows the estimation of damage using both Methods 1 and 2 as before. As can be seen from the central column of both figures, using the drift demand at the COM of the structure gives a moderate level of damage at each level for both frames, which by definition of Method 1 means that all of the RC frame members across the floor plan in the Y direction will possess such damage. However, by examining the estimated damage in the outer columns that used the local drift demand at the respective ends of the frame (Method 2), it is clear that there is some degree of discrepancy. The torsional response of the frames due to the presence of the RC walls on the east side of the building means that the west end will move much more due to the east end being relatively stiffer. As a result, the west end will experience much more damage that the east end, which is clearly illustrated in Figure 3.19 as the east end shows essentially no damage, whilst the west end is experiencing heavy damage. While this is an expected outcome, it is important to note that if one had used the COM drifts to estimate damage, a much lower level of damage would have been estimated. This highlights the need for tools to conduct damage and loss

estimation on irregular structures, such as Frame B, since the assumption of using a single demand parameter at each level leads to unconservative and erroneous estimates of damage across the building floor plan, which in turn will affect the final DVs that performance-based assessment aims to provide.

3.4.4 Loss Estimation of Case Study Frames

The previous sections have shown how the estimation of damage in RC frame members using two different demand parameter approaches leads to the same results in the case of Frame Types A, which were regular and symmetric frames, and unconservative estimations of damage by using Method 1 for Frame Types B, which were irregular due to the presence of additional RC walls on the east side of the structure. This section takes these damage estimates for both Method 1 and 2 to compute the resulting direct economic loss associated with repairing the RC frame elements using TOMS. This will illustrate how such discrepancies in the damage assessment of the structure impact the direct economic losses at the various intensities investigated in the MSA of the buildings. The consequence functions used to estimate the repair costs for each DS are taken from the same source as the fragility functions for ductile RC frames in PACT.

Figure 3.20 shows the trend of the mean direct economic losses in the buildings versus IM, also commonly known as a vulnerability function, which consists of the direct losses associated with repairing the RC frame elements only. No other structural or non-structural elements are considered since the purpose of this figure is to illustrate the economic impact of the different damage assessment methods discussed in the previous section. The same concept is applicable to many other types of damageable components, both drift and acceleration sensitive, therefore the conclusions drawn here are not limited to RC frame elements. In the case of Frame type A, Figure 3.20(a) shows the two methods of damage assessment provide the same mean vulnerability function, as the two lines are exactly the same. This is to be expected when one considers that in Figure 3.18, the estimates of damage were the same regardless of which damage assessment method was adopted. As such, the direct losses associated with the repair of these elements should also return the same answer. However, in the case of Frame B, there is a clear discrepancy between the two approaches where Method 2 results in higher direct losses versus intensity compared to that of the Method 1 results. This discrepancy is in line with the observations of Figure 3.19, whereby using Method 1 to assess damage in the structure, a lower pattern of damage was observed in the overall structure. However, Method 2 showed that, in fact, the west side of the building had experienced extensive damage and the east side relatively little. The overall discrepancy between the two methods in terms of direct losses is quantified as approximately 30% for the three storey frame, and about 15% for the six storey frame. The largest discrepancy can be seen in the intermediate intensities since at lower intensities, the torsional response has not become pronounced enough to result in a significant difference

between the two methods. In addition, as the intensity increases the difference also reduces the direct losses due to the collapse of the building become more probable, whose economic consequence is the same for both building types. As such, the intermediate intensities are seen to exhibit the biggest differences, which is interesting to note since these would correspond to, depending on the site's mean hazard curve, the more frequent seismic events where most of the annualised losses are saturated, further highlighting the importance of properly establishing the losses at such intensities. The conclusions made here in terms of losses have been in reference to the repair costs associated with the RC frame elements of a bare frame, although the same conclusions may be drawn for an entire building with a full inventory of damageable structural and non-structural components. Such a study was not conducted here in order to clearly demonstrate the point being made regarding the differences in damage and loss for a single component.

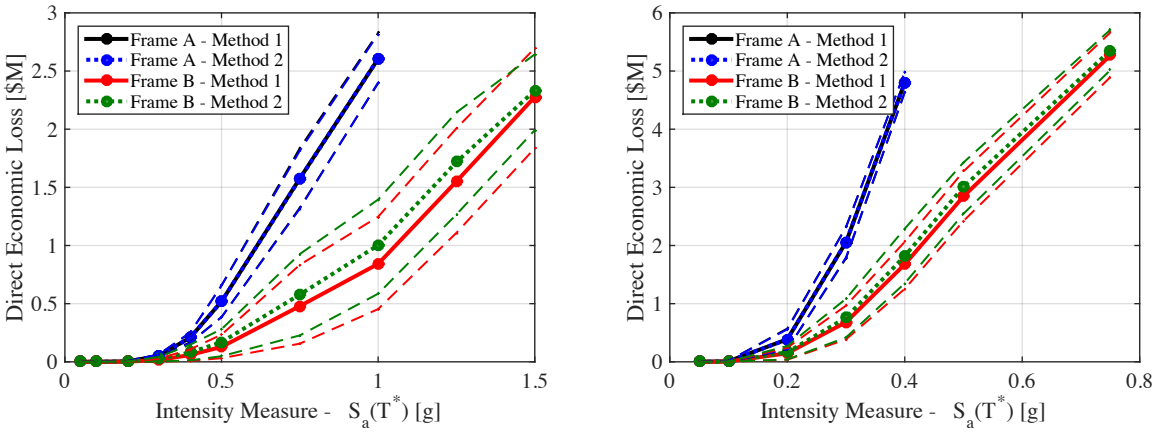

(a) 3 Storey **(b) 6 Storey**

Figure 3.20. Expected and 16th/84th percentile of direct economic loss versus intensity for both frame types A and B using both Methods 1 and 2 to estimate the damage to the RC frame members.

3.5 SUMMARY AND CONCLUSIONS

This chapter discussed some of the current limitations with the current state of practice when implementing the PEER PBEE methodology in the assessment of structure. Issues such as torsional response, generalised handling of modelling uncertainty, unequal bay lengths and inconsistent definitions of drift demand parameters were highlighted to make the case for the development of tools that allow for more complex and irregular structures to be assessed with more confidence. A tool to address these issues was developed (TOMS) that addresses these limitations and also provides a relatively quick process to conducting loss estimation by facilitating the consideration of many loss estimation studies through

batch mode analysis, which can be very useful in research to conduct parametric studies and identify trends in the performance of various buildings. This tool was described in depth and its application to a case study structure was covered, where it was shown that by using the TOMS output for a case study building, more informed retrofitting decisions can be made. This was illustrated for the case study building where an example retrofit was conducted and a comparison with the original assessment was shown to illustrate how such informed decisions can be made during the retrofit process to effectively reduce the building's vulnerability.

The latter part of this chapter examined the aforementioned case of torsionally responding structures. A series of case study buildings were designed and assessed by using different approaches to demand parameter definition. The results of IDA show that for regular and symmetric structures, the use of a single drift at the COM suffices in estimating the damage to the frame members at any location across the building's floor plan. However, in cases where the structure is no longer regular and possesses some torsional irregularity, the use of drift at the COM was seen to be no longer accurate and not only underestimates the damage to the frames members but also provides unconservative estimates of direct loss in the range of 15-30% for the case study buildings examined. These finding illustrates the need for more advanced tools for seismic assessment, such as TOMS, that incorporate many definitions of demand per floor to provide a more representative estimate of damage and losses for structures where the simplifying assumptions required for current methods no longer hold true.

4 QUANTIFICATION OF THE MODELLING UNCERTAINTY IN GLD RC FRAMES IN ITALY

O'Reilly, G. J., Sullivan, T. J. [2017] "Quantification of the Modelling Uncertainty in Existing Italian RC Frames with Masonry Infill," *Earthquake Engineering & Structural Dynamics* (Under Preparation).

4.1 INTRODUCTION

Following the structural analysis of a case study structure using either simplified methods or more advanced NRHA, the dispersion in the demand parameters of interest need to be accounted for. In the case of NRHA using a single deterministic model, such as what is typically carried out using the PEER PBEE methodology [FEMA P58-1, 2012; FEMA P58-2, 2012; FEMA P58-3, 2012], the epistemic uncertainty associated with modelling uncertainty is incorporated into the results alongside the aleatory randomness that is already present due to record-to-record variability of the various GM records used in analysis. The incorporation of modelling uncertainty is of utmost importance, with Gokkaya *et al.* [2016] noting how the inclusion of modelling uncertainty amplified the MAF of collapse by around 1.8 times. More simplified approaches, such as displacement-based assessment (DBA) (see Priestley *et al.* [2007], for example) and the N2 method (see Fajfar and Dolšek [2012], for example) involve using simplifying assumptions to estimate the response of the structure with a subsequent approximation of dispersion in the response due to modelling uncertainty and record-to-record variability. Both of these aforementioned methods require some form of dispersion estimate for the modelling uncertainty, which ought to come from appropriate quantification studies. As highlighted on multiple occasions during the description of using the N2 method to estimate failure probability of a structure, Fajfar and Dolšek [2012] note: *"For practical applications, predetermined default values for the dispersion measures, based on statistical studies of typical structural systems, are needed."* and *"In a practice-oriented approach, default values for the dispersion measures have to be used. Reliable data for large populations of buildings are not yet available."* before concluding the manuscript with *"Default values for dispersion measures are needed."* While Fajfar and Dolšek [2012] were referring to the dispersion measures that fit directly into the SAC/FEMA approach described by Cornell *et al.* [2002], the issue remains the same that default values for the various types of dispersion are necessary, whether they be for the estimation of the annual probability of exceedance of a given limit state as per Fajfar and Dolšek [2012], or the annualised losses using the PEER PBEE methodology. It is the aim of this chapter to estimate such default values of

modelling dispersion to be used when conducting a seismic assessment of GLD RC frames in Italy.

Previous research on the topic is first examined and some of the principal observations of the effects of modelling uncertainty are summarised to provide further insight into the different aspects to consider here. The methodology used to quantify the modelling uncertainty is then described and a study on various structural typologies is conducted such that modelling uncertainty values for the collapse fragility and demand parameters used in loss estimation are proposed. This is done using the statistical information regarding the uncertainty in the various modelling parameters established during the numerical model calibration in Chapter 2. These default values for modelling uncertainty are defined in terms of structural typology, demand parameter and limit state under consideration to provide a set of default values for the modelling uncertainty in structural typologies found throughout Italy.

4.2 PAST RESEARCH ON QUANTIFYING MODELLING UNCERTAINTY

In the following sections, a brief overview into some of past research into quantifying modelling uncertainty as presented. Some of the general themes of these various publications have been grouped together below to highlight past observations which are then summarised with a view to providing a basis for the results and observations discussed in the following sections.

4.2.1 Random Variables to Consider

Of the numerous studies regarding modelling uncertainty available in the literature, one of the more critical aspects is the initial identification of appropriate and relevant RVs to employ. The methods used and subsequent assumptions can require very computationally expensive procedures involving simulation to generate a sufficient number of realisations followed by NRHA that somewhat limit comprehensive studies on the topic. Hence, past research on the topic is first used discussed here to get an insight into the relative impact on the structural response of different RVs.

Some studies [Celarec *et al.*, 2012; Celik and Ellingwood, 2010; Dolšek, 2009; Yu *et al.*, 2016] have considered characteristic material properties from the concrete and reinforcing steel in RC frames and also the mass distribution as part of their studies, as information on such material properties can be characterised relatively easily. In general, such studies have reported that these have limited effect on the dispersion when compared to other RVs. Dolšek [2009] demonstrates this quantitatively through the use of a Spearman Rank coefficient to show that, in addition, the elastic damping, the ultimate rotation capacity of the beam and column members were the most influential RVs. Such findings are further reflected in the comments by Liel *et al.* [2009] that, referring to work by Haselton and

Deierlein [2007] among others, concrete and steel material strengths have been shown in the past to have limited influence on the collapse limit state (LS) compared to the deformation capacity and post-peak stiffness which are shown to have a major role, as observed in the extensive parametric studies by Ibarra and Krawinkler [2005]. Haselton and Deierlein [2007] have also shown that the effects of mass, elastic damping, hysteretic pinching and residual strength are not so influential for the collapse LS. Liel *et al.* [2009] then demonstrate through a sensitivity study that column strength and ductility are the most influential RVs. These findings regarding the influence of strength and ductility of frame members are also echoed in Vamvatsikos and Fragiadakis [2010].

With regard to elastic damping, some studies [Haselton and Deierlein, 2007; Liel *et al.*, 2009] have indicated that its effect is relatively minimal while others [Celik and Ellingwood, 2010; Dolšek, 2009] have noted its importance. In terms of the relative influence of the parameters at the collapse LS, this may be the case where the uncertainty in the peak and post-peak deformation capacity dominate the response. Since this study will consider LSs other than collapse and also from past sensitivity studies (O'Reilly and Sullivan [2015], among others), the elastic damping is an uncertain parameter that merits consideration. In addition to the RC frame elements, some other modelling parameters pertaining to this study are the relative importance of the beam-column joint and masonry infill properties. Celik and Ellingwood [2010] conducted a sensitivity study on a number of parameters for non-ductile RC frames, where in addition to the elastic damping, the shear strain at cracking in the beam-column joints was shown to be a key parameter. Similarly, Celarec *et al.* [2012] performed a sensitivity study on older RC frames with masonry infills where it was shown that for lower LS, the uncertainty in the masonry infill properties had the largest impact, whereas, at LSs closer to the collapse of the structure, the ultimate chord rotation capacity of the beam and column members played a more significant role.

Another very noteworthy comment was made by Jalayer *et al.* [2010] regarding random variable (RV) choice in such modelling uncertainty studies concerning older RC structures where quite often, very little structural details are available. Jalayer *et al.* [2010] suggested that in addition to characteristic properties of the reinforcing steel and concrete in the beam and column members, the actual quantity of reinforcement should be considered an RV. This was noted to perhaps arise due to human error in the placing an incorrect bar diameter size during construction, but it can also be argued that this is particularly important in any case. When performing an assessment of an older RC frame, the section details are often not available and the engineer is faced with either conducted a simulated design to estimate what the structural engineer at the time would have computed using allowable stress design, or similar, or assume a reasonable percentage of reinforcement based on engineering judgement, or conduct in-situ testing to determine the actual reinforcement present. The latter approach is much costlier and invasive and may not be possible for various reasons, while the former two approaches introduce a significant uncertainty to models when one

considers how the reinforcement impacts the member strength, which has been previously shown to be a key parameter.

As such, the critical RVs pertaining to this study ought to be in terms of frame member strength, deformation capacity and reinforcement content, joint deformation, masonry infill strength and deformation capacity, elastic damping. While not shown to be a significant parameter by Celik and Ellingwood [2010], the consideration of the joint strength should be investigated given the impact in terms of global mechanism observed by Pampanin *et al.* [2003], whereby forming a shear hinge in the joint, the deformation was spread over the two adjacent storeys rather than concentrating in a single storey, thus increasing the lateral capacity of the frame. This was also observed numerically in Section 2.5, whereby comparing the response of a model with poor joints and non-ductile members to that of a model with rigid joints and ductile members, the ductile frame actually exhibited less global capacity than the non-ductile frame due to the concentration of damage in a single storey rather than distributed deformation over two adjacent floors as a result of the joint mechanism. This observation can be expanded into a broader consideration that the modelling uncertainty would also be expected to be a function of the failure mechanism developed in the structure. As such, a number of different GLD frames are to be considered that exhibit different global failure mechanisms highlighted during past earthquakes.

4.2.2 Overall Effects of Modelling Uncertainty

One of the goals of examining the modelling uncertainty is to examine its overall influence with respect to the randomness associated with record-to-record variability. Research to date generally agrees that the inclusion of modelling uncertainty increases the overall uncertainty of the system (e.g. [Dolšek, 2009; Liel *et al.*, 2009], among others), but to what extent with respect to record-to-record variability has not been consistent. Early studies by Ellingwood *et al.* [2007] elected to neglect the effects of modelling uncertainty since previous research by Kwon and Elnashai [2006] suggested that compared to the record-to-record variability the modelling uncertainty does not appear to be significant, a finding further echoed in the work by Jeon *et al.* [2015]. This aspect is considered in Vamvatsikos and Fragiadakis [2010] and Figure 4.1 is adopted from that publication to illustrate the different contributions. For low levels of drift demand, the contribution of the modelling uncertainty (β_U) is seen to be rather low with respect to the record-to-record variability (β_R), although at high levels of demand the modelling uncertainty is seen to become more prominent. Dolšek [2012] discusses the influence of modelling uncertainty with respect to risk since the discussion thus far has referred to different LSs and not considered the combination with a given hazard curve to discuss the actual implications on risk. Dolšek [2012] concludes that the effects of modelling uncertainties, in addition to record-to-record variability, increase with the severity of the LS such that, for the near collapse LS, the risk

considering both sources of uncertainty is more than double if compared with the risk determined solely from record-to-record variability. Porter *et al.* [2002] also considered the effects of modelling uncertainty on loss estimation, where they conclude that modelling uncertainty has a modest effect but represents a relatively minor contributor to the overall uncertainty when compared to a contractors unit repair costing.

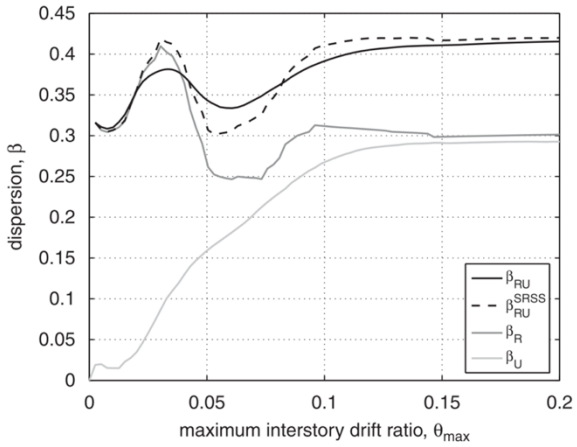

Figure 4.1. Contribution of record-to-record- variability (β_R) and modelling uncertainty (β_U) to the overall uncertainty (β_{RU}) with increasing demand illustrated by Vamvatsikos and Fragiadakis [2010], where for lower levels of drift demand the overall uncertainty is dominated by the record-to-record- variability.

In an opinion paper by Bradley [2013], a discussion into the current state-of-the-art in terms of quantifying modelling uncertainties is presented. Bradley [2013] notes that studies to date have typically focused on variability in constitutive model parameters, with no consideration of more modelling approaches on a higher, more conceptual level. This is typically referred to as model type uncertainty [Kazantzi *et al.*, 2014], whereas the discussion so far has considered model parameter uncertainty. This is a valid argument when one considers, for example, the dispersion in results observed in blind-prediction test results of a single bridge pier Terzic *et al.* [2015]. In order to examine these considerations in modelling, a large coordinated parametric study would be required to adequately reflect this source of uncertainty. Bradley [2013] further remarks that in their opinion, these uncertainties are likely to be more significant than those associated with constitutive model parameters and concludes by saying this should be a key research area in the coming years. They note that with respect to record-to-record variability, the current sentiment that modelling uncertainty is negligible to be a fallacy and suggests that the modelling uncertainty may, in fact, be more significant than that of the record-to-record variability. While the sentiments of Bradley [2013] are certainly valid, such a study into model type

uncertainty is beyond the available time and resources available to this study and are hence not considered further, as the state-of-the-art methodologies already require very computational expensive approaches.

4.2.3 Effects of Modelling Uncertainty on Median Response

While the effects of modelling uncertainty on the overall dispersion have been recognised and adapted well into the SAC/FEMA methodology, the effects on the median response provide some extra food for thought. This is as one of the underlying assumptions in the framework outlined in Cornell *et al.* [2002] was that modelling uncertainty affects the overall dispersion but the median response remains unchanged. This has been shown by numerous studies [Dolšek, 2009; Gokkaya *et al.*, 2016; Liel *et al.*, 2009; Vamvatsikos and Fragiadakis, 2010] not to be the case. Results show that the inclusion of modelling uncertainty in the analysis tends to reduce the median IM when approaching the collapse LS, as shown in Figure 4.2. This makes sense intuitively as if one imagines a structural system as a chain, where the earthquake identifies the weakest link of that chain and the resulting mechanism ensues, and one begins to sample more and more RVs, it is more likely to have sampled a weaker component which could then reduce the intensity required to achieve a given LS. The reverse is also true, where a stronger component may be sampled, but earthquakes punish the weakest link in structures and a reduction in the intensity required to achieve that LS is seen through the shift in median response with increasing number of RVs in Figure 4.2.

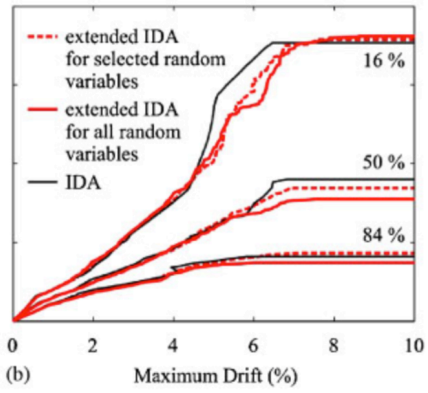

Figure 4.2. This shows the median and dispersion are not greatly affected by RVs far from collapse, but at collapse, the median is gradually reduced for increasing number of RVs. This is the weak link concept, whereby sampling more and more RVs, we are more likely to find another weaker link in the chain (Adopted from Dolšek [2009]).

4.2.4 Modelling Uncertainty vs. Limit States

Some of the earlier work on modelling uncertainty typically considered the collapse LS of the structure. However, if one considers the response of a structure at collapse versus the response at lower LSs, for example, the relative contribution to the overall uncertainty shown in Figure 4.1, there is a marked difference in the modelling uncertainty with increasing ductility. Liel *et al.* [2009] reported that comparing the two LSs, 1% storey drift and collapse, the modelling uncertainty is not so significant when compared with that at the collapse. Similar findings were reported in Yu *et al.* [2016] who proposed different values of modelling uncertainty based on the LS being considered based on static pushover analysis (SPO) results with the modelling uncertainty increasing with the severity of the LS, a similar observation to that of Dolšek [2012] and Vamvatsikos and Fragiadakis [2010], among others.

4.2.5 Summary and Main Conclusions

From the discussions provided in the previous sections, some observations can be made. These are highlighted here as they will become important points of reference during the discussion of the analysis results in the following sections. The main conclusions to be drawn from past research on the quantification of modelling uncertainty are:

- In terms of RVs, material properties have been seen to be not so influential when compared to other RVs such as chord rotation capacity. Other RVs such as joint strength, elastic damping ratio and longitudinal reinforcement ratio have been noted to be pertinent RVs that ought to be considered.
- The effects of modelling uncertainty in relation to their contribution to the overall uncertainty have been observed to be a function of increasing demand and not a necessarily a constant value over all limit states.
- The numerical model with median values does not necessarily correspond to the median response, where the median IDA curve was shown to decrease with increasing number of RVs being sampled. This is a reflection of the weakest link concept, whereby sampling more and more RVs, the chance of sampling a weaker component increase, which will result in a decreased intensity whereas sampling a stronger component will not have the opposite effect.

4.3 QUANTIFYING THE MODELLING UNCERTAINTY

4.3.1 Overview of Methodology Employed

As discussed previously, the variability in the different modelling parameters is propagated through the structures response to result in a variability in the demand parameters of interest. This is in conjunction with the inherent variability due to record-to-record variability when performing NRHA. While the record-to-record variability is typically accounted for with large sets of suitable GMs, the modelling uncertainty is somewhat more

difficult to quantify. This is as the individual distributions of the various RVs to be considered in the structure are required along with an appropriate method in which a number of different numerical model realisations can be generated. As discussed previously, the typical approach is to quantify the effects of this modelling uncertainty on the various demand parameters of interest and incorporate the effects of this post analyses alongside the record-to-record variability. This section, therefore, aims to conduct such a study to quantify the modelling uncertainty that can be anticipated for different demand parameters such as PSD and PFA in various RC frame structural typologies found in Italy.

The approach adopted here is illustrated in Figure 4.3, where a number of model realisations are to be generated to take into account the variability in the different RVs considered. These model realisations are then analysed using IDA at a number of intensity levels such that the modelling uncertainty can be examined as a function of intensity and demand parameter. That is, for a given GM and intensity level, the dispersion in the demand parameter due to modelling uncertainty can be quantified. Likewise, for a given model realisation and intensity level, the record-to-record variability can also be computed. In addition to examining the effects of the modelling uncertainty on the demand parameters with respect to intensity, the influence on the collapse fragility median and dispersion are also investigated. The following subsections describe the various steps involved in the study with the following section presenting the results and proposed values for older RC frame structure typologies typically found in Italy.

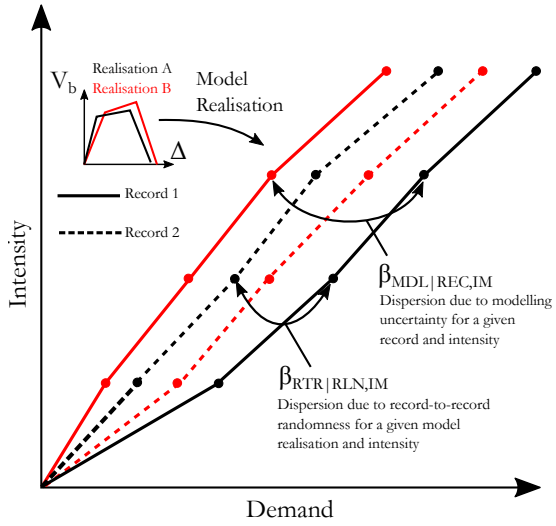

Figure 4.3. Illustration of the procedure used to identify the modelling uncertainty in various structural typologies with increasing intensity. The use of numerous model realisations and GMs means that the variance with respect to either of the two source of uncertainty (i.e. record-to-record variability or modelling uncertainty) can be quantified.

4.3.2 Random Variables and Associated Probabilistic Distribution

Based on the discussions of Section 4.2.1, the RVs to be selected as part of this modelling uncertainty quantification study for GLD RC frames typically found in Italy are established along with a brief description of the source of such information and the relevant justification for their consideration. Table 4.1 lists the initial list of RVs selected for each of the beam and column members, interior and exterior beam-column joints, masonry infill and other global modelling parameters.

Regarding the adopted distributions for each of the structural elements, these are justified as follows. The beam and column member distributions are adopted directly from the information presented in Section 2.2, where the calibration information regarding the member capacity, stiffness and ductility capacity are adopted as they come from the calibrations to actual test data available in the literature. The noted source of "computed" for these members in Table 4.1 refers to how the median value is not a fixed value, but a computed value from the expressions described in Section 2.2 (e.g. the yield moment (M_y) is not a fixed value for every member, but depends on section dimensions and reinforcing content), where the associated dispersion was computed from the comparison of the relevant expression to the actual test data. On the other hand, the values used for the interior and exterior beam-column joints come from the calibrated values in Section 2.3 and 2.4, respectively. Other information regarding masonry infill median drifts and dispersions are adapted from the study by Sassun *et al.* [2015], whereas other information regarding appropriate dispersions for elastic damping and structural mass are adopted from a similar study concerning modelling uncertainty in RC frames conducted by Haselton *et al.* [2007].

4.3.3 Structural Typologies

Using the list of RVs identified in Table 4.1, a number of different structural typologies typical of pre-1970s construction in Italy can be examined. These consist of both RC frames both with and without masonry infill, also with two different typologies referred to herein as "weak" and "strong" infill and also RC frames with ground floor opening, also known as Pilotis frames. These structures correspond to the two and three storey 2D frames originally described by Galli [2006]. The various assumptions regarding their design and member properties are discussed later in further detail in Section 5.1, thus these details are omitted here for brevity.

Table 4.1. List of preliminary random variables to be considered for quantification of modelling uncertainty in GLD RC frames (Notation as per model definitions in Chapter 2).

	#	RV	Source	Median	Dispersion	Distribution	Reference
Beams	1	M_y	Computed	-	0.122	Lognormal	Section 2.2
	2	ϕ_y			0.287		
	3	μ_ϕ			0.326		
	4	a_{pp}			0.413		
	5	ρ_L			0.25		
Columns	6	M_y	Computed	-	0.122	Lognormal	Section 2.2
	7	ϕ_y			0.287		
	8	μ_ϕ			0.326		
	9	a_{pp}			0.413		
	10	ρ_L			0.25		
Exterior Joints	11	γ_{cr}	Test Data	0.0002	0.3	Lognormal	Estimate
	12	γ_{pk}		0.0127	0.286		Section 2.3
	13	γ_{ult}		0.0261	0.229		
	14	κ_{cr}		0.135	0.166		
	15	κ_{ult}		0.05	0.091		
Interior Joints	16	γ_{cr}	Test Data	0.0002	0.3	Lognormal	Estimate
	17	γ_{pk}		0.0085	0.133		Section 2.4
	18	κ_{cr}		0.29	0.237		
	19	κ_{pk}		0.42	0.163		
Masonry Infills	20	F_{max}	Equation	-	0.3	Lognormal	Estimate
	21	θ_{DS1}	Test Data	0.18%	0.52		Sassun *et al.* [2016]
	22	θ_{DS2}		0.46%	0.54		
	23	θ_{DS4}		1.88%	0.38		
Global	24	ξ	Assumed Value	0.05	0.6	Lognormal	Haselton [2007] - Miranda [2005], Porter *et al.* [2002], Hart *et al.* [1975]
	25	M	Given	-	0.1	Lognormal	Haselton [2007]

These different typologies are examined so as to provide representative values of modelling uncertainty for the various structural frame typologies typically found in Italy. To date, most existing research on the quantification of the modelling uncertainty in RC frames has focused on bare frames with no masonry infill. Given that a large portion of the Italian building stock consists of infilled RC frames and RC frames with ground floor openings, the results of this study will provide a novel contribution to the assessment of existing RC frame structures in Italy. While it would be of interest to examine structural typologies with different numbers of storeys, the sheer amount of numerical analysis required to conduct a study such as that discussed herein means that the analysis time begins to become unreasonable when considering the number of GMs, intensity levels and infill model variations, even when operating on multi-core servers. As such, the present study is limited to a two and three storey case study structure of different typologies described further in Section 5.1.

4.4 GENERATION OF MODEL REALISATIONS

4.4.1 Background Theory

In order to examine the modelling uncertainty in the response of a structural system due to a set number of RVs whose distribution are known or can be estimated, a number of realisations need to be generated. That is, for each RV considered a random sample from its distribution is obtained and input to the structural model to create what is termed a single model realisation. For completeness, a model in which all of the median values are input for the RVs is referred to here as the deterministic or reference model.

To generate such random samples for each RV, the Latin Hypercube Sampling (LHS) technique [McKay *et al.*, 1979] is employed along with some modifications outlined in Olsson *et al.* [2003] to reduce spurious and unintentional correlations. The process is as follows; consider k number of RVs for which n number of realisations are to be generated. A random permutations matrix **P** of size n by k is first generated, such that each column that corresponds to a different RV and consists of a random permutation of the integers 1 through n. This operation can be performed in MATLAB [Mathworks, 2014] using the command **randperm**. The next step is to generate a random matrix **R** of size n by k, such that each entry is sampled from the uniform distribution and is between 0 and 1, performed using the **rand** function in MATLAB. Combining these two matrices **P** and **R** the basic sample of the RVs as indicated in Olsson *et al.* [2003] is obtained by performing:

$$\boldsymbol{S}(i,j) = 1/N\ (\boldsymbol{P}(i,j)\ -\ \boldsymbol{R}(i,j)) \qquad \textbf{Equation 4.1}$$

where **S** is the basic LHS sample matrix whose elements are in the range of 0 to 1. Using these samples in **S** and the known distribution of each of the RVs, a sample can be obtained using the RV's distribution to generate the RV sample matrix **X**, as illustrated in Figure 4.4. As such, each entry in the matrix **X** corresponds to the sample value to be used in the

structural system, where each column of **X** corresponds to an RV j, and each row of **X** corresponds to a single realisation i.

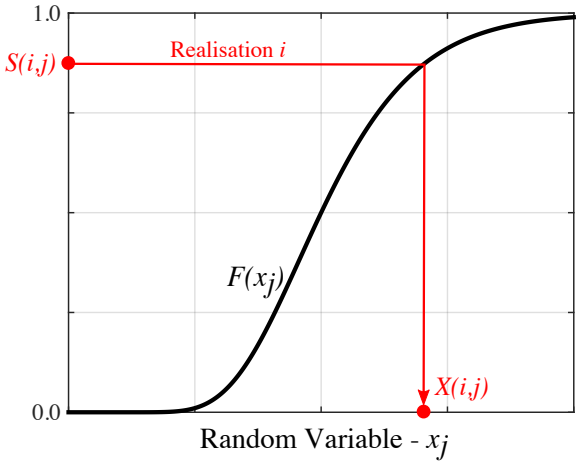

Figure 4.4. Generation of random samples X from the basic LHS sample S.

Using this approach, the required number of realisations can be sampled for any number of RVs. However, it can introduce unintended correlations between different RVs as a result of them having been sampled independently, which is reflected in the correlation matrix for **S**, $\boldsymbol{\rho}_{\mathbf{S}}$. For example, if one examines the correlation between two RVs such as steel yield strength and masonry infill strength in a structural model, one may find that a strong positive correlation exists between these RVs in the generated sample matrix **S**. Such a correlation obviously has no basis and is not intentional but arises due to the way the samples were generated. As described in Olsson *et al.* [2003], the random permutations matrix **P** is modified to address the aforementioned spurious correlations that arise in LHS using what is termed by Olsson *et al.* [2003] as Correlation-Reduced Latin Hypercube Sampling (CLHS), and is summarised below.

A matrix **Y** of size n by k is first identified by taking the random permutations matrix **P** and mapping it onto a Gaussian distribution with mean 0 and standard deviation of 1. The covariance matrix of **Y** is then computed and its Cholesky decomposition found to give:

$$\mathrm{LL}^{\mathrm{T}} = \mathrm{cov}(\mathrm{Y}) \qquad \textbf{Equation 4.2}$$

where **L** is the lower triangle Cholesky decomposition. This can be conducted in MATLAB using the command **chol**. The process requires that the covariance matrix of **Y** be positive definitive, which essentially means that the number of required realisations should exceed the number of RVs (i.e. n>k), although a more recent proposal by Vamvatsikos [2014]

introduces an alternative sampling approach that removes such a constraint. The next step is compute a new matrix **Y*** with a sample covariance given by:

$$\mathbf{Y}^* = \mathbf{Y}\left(\mathbf{L}^{-1}\right)^{\mathrm{T}} \qquad \textbf{Equation 4.3}$$

and from **Y*** a sample matrix **S*** is generated by following the previous operation mapping **Y** to **P** and subsequently finding **S** as per Equation 4.1 in reverse.

However, if a target correlation (**ρ**) between the RVs is required, then the above operation is modified such that:

$$\mathbf{Y}^* = \mathbf{Y}\left(\mathbf{L}^{-1}\right)^{\mathrm{T}}\mathbf{W}^{\mathrm{T}} \qquad \textbf{Equation 4.4}$$

where **W** is the lower triangle Cholesky decomposition of the target correlation matrix **ρ**. As mentioned, this **Y*** matrix is then converted back to a new random permutations matrix **P***, which is in turn used to generate a new sample matrix **S***, which is used in conjunction with the RV's known distributions to generate the samples **X*** for the structural system. If one computes the original correlation matrix $\boldsymbol{\rho}_{\mathbf{S}}$, the spurious correlations between the different RVs will be obvious from the off-diagonal terms of $\boldsymbol{\rho}_{\mathbf{S}}$. Recomputing the correlation matrix for the correlation reduced sample **S***, $\boldsymbol{\rho}_{\mathbf{S}*}$, it will be seen how such spurious correlations have been reduced. This approach is adopted here for the generation of the various RVs, such that n number of realisations for k number of RVs can be generated while proper consideration is also given to the correlation between these samples. This CLHS process has been utilised in a previous study by Yu *et al.* [2016] that looked at the modelling uncertainty in Chinese RC frames via SPO analysis. A different method, but with a similar end goal of reducing spurious correlations in random samples, known as simulated annealing [Vorechovsky and Novak, 2003] is employed by Dolšek [2009] where the method looks to minimise the difference between the prescribed correlation matrix, **ρ**, and the generated sample correlation matrix $\boldsymbol{\rho}_{\mathbf{S}}$, through the use of a norm E defined in Vorechovsky and Novak [2003] as:

$$\mathrm{E} = \sqrt{\sum_{i=1}^{k-1}\sum_{j=i+1}^{k}(\rho(i,j) - \rho_S(i,j))^2} \qquad \textbf{Equation 4.5}$$

where the smaller the value of E, the closer we are to sampling an RV set with correlation closer to the desired one. This norm E may also be used as a check during the CLHS process to quantify the improvement the new **S*** sample generated has over the initial sample S.

4.4.2 Adopted Approach

The previous section showed how realisations of a structural model for a given number of RVs can be generated. Using this CLHS approach, a number of realisations of each

structural model are developed. Each of the 25 RVs listed in Table 4.1 are sampled a number of times to generate n number of model realisations. As mentioned previously, the number of model realisations needs to be greater than the number of RVs k in order for the CLHS method to function. As such, the number of realisations was chosen here to be 40. This number was selected based on the parametric study by Dolšek [2009] who noted that 20 appeared to be a reasonable value for the number of model realisations. Obviously, this would too low in the present study since a number greater than 25 is required, hence, 40 appears to be a reasonable value. Also of note are the correlations assumed between different RVs, which were assumed to be independent and uncorrelated for simplicity of analysis. Each of the various elements in the structures were sampled together and not considered individually (e.g. the sample value of column yield curvature was assumed to be equal in each column member) as this would have resulted in a very large number of RVs to be considered and would have drastically increased the number of model realisations required, meaning that the study would have been unfeasible from a numerical computation perspective, although incorporating the recent work by Vamvatsikos [2014] that has also been applied in Kazantzi *et al.* [2014] can overcome this in future studies. This assumption was also adopted in Gokkaya *et al.* [2016], who justify this assumption due to the beam and column members being part of the same building and built by the same contractors. Physical relations between different RVs were maintained through the model definition, such as the yield moment and the percentage of reinforcement since the yield moment is computed using the sampled value of reinforcement through sectional analysis. Similarly, with the floor mass and the design axial loading on columns, which influences the member ductility and post-peak ductility capacity of the members.

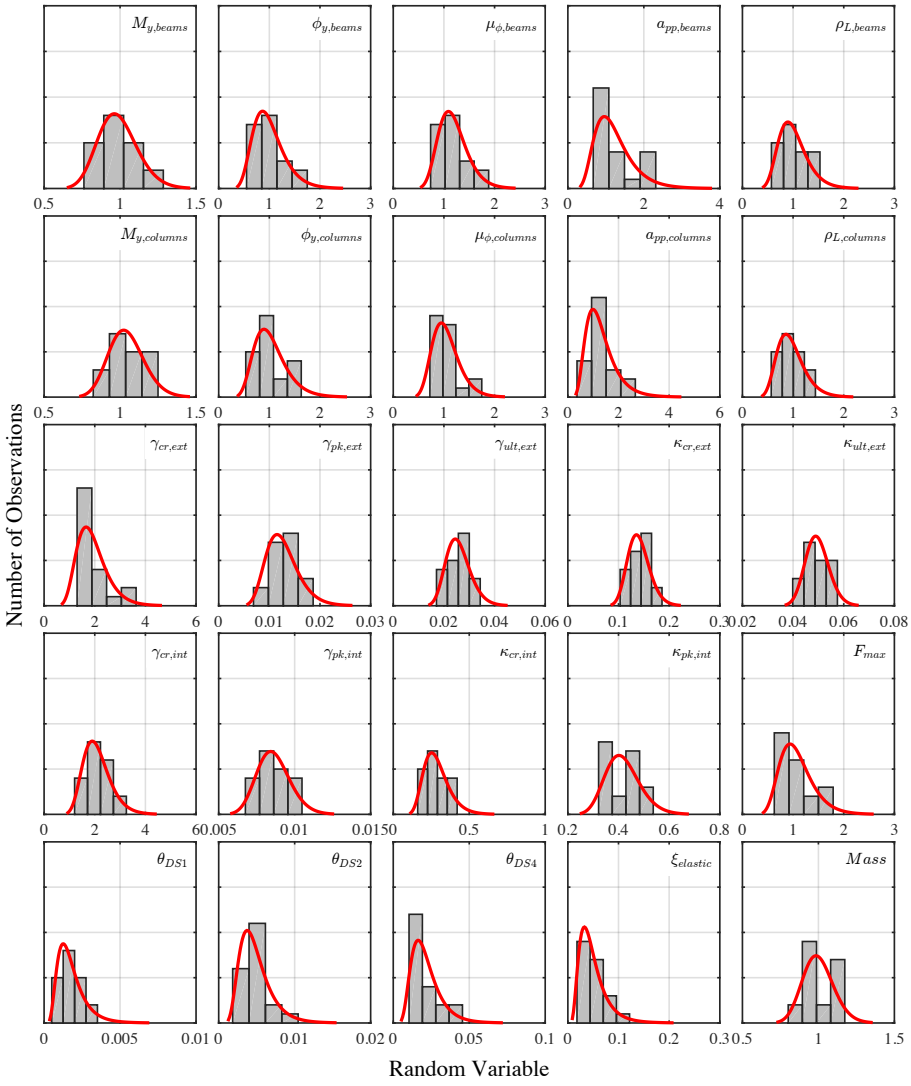

Figure 4.5. Histograms of the sampled random variable values for each of the generated model realisations.

While each of the RVs are sampled according to the aforementioned distributions, care was taken to ensure that no instances of unrealistic model realisations arise. For instance, the sampled value of θ_{DS2} was checked to be always greater than that of the lower drift θ_{DS1}. Other checks on the beam-column joint rotation samples were also applied in addition to the joint shear strength coefficients. For each of the model realisations sampled here and

illustrated in Figure 4.5, the structural typologies discussed previously were analysed using ten GMs taken from the FEMA P695 [FEMA P695, 2009] set. These ten GMs were selected in order to maintain a good match in terms of median and dispersion with the original set. While ten records may be considered a small ground motion set, these records are not used to compute record-to-record variability but only the modelling uncertainty. Each of these GMs were scaled to a number of intensities for the seismic IM employed using IDA, which in this case was the spectral acceleration at the first mode period of vibration of the structure, $S_a(T_1)$. The adjustment of the fragility functions to account for the effects of spectral shape prescribed by FEMA P695 were not considered. The reasons for this were twofold. First, the use of the same GMs in IDA for all modelling realisations aims to examine the progression of damage versus intensity until eventual collapse. This is a relative comparison between different model variations, hence it could be argued that the influence of such spectral shape effects to the "true" collapse is likely to likely to be the same for the different modelling variations. Second, the adjustment factors prescribed by FEMA P695 as a function of the epsilon [Baker and Cornell, 2006] are developed for ductile construction in the US and whose application to the structural typologies has not been investigated. This quantification represents a supplementary quantification study by itself. In addition, more recent work by Eads *et al.* [2016] shows that this approach adopted by FEMA P695 to account for spectral shape using epsilon may not actually be the best predictor of collapse since, by definition, it is an indirect measure of spectral shape. Eads *et al.* [2016] explored the use of other measures of spectral shape and demonstrated that other definitions that considered the range over a certain period range to be better. As such, further work to incorporate the influence of spectral shape as result of IDA on collapse ought to consider this recent proposal by Eads *et al.* [2016] rather as opposed to the approach outlined in FEMA P695.

4.5 ANALYSIS RESULTS

Using the methodology and model realisations described in the previous section, the results of the modelling uncertainty study are presented here. First, the influence on the collapse fragility of the various structures is investigated and proposals are made on how to account for the effects of modelling uncertainty on the collapse fragility curve. The results are then presented in terms of the two demand parameters of interest; PSD and PFA, such that similar proposals can be made on how one can simply account for the effects of modelling uncertainty when performing risk or loss estimations on GLD RC frame structures in Italy.

4.5.1 Collapse Fragility

By analysing the different structural typologies at different intensity levels via a truncated IDA [Vamvatsikos and Cornell, 2002] for computational economy, the number of collapses with respect to intensity, GM and model realisation can be computed. For a given combination of the above, the probability of collapse can be computed by dividing the

number of collapsed analyses (# of collapses) by the number of analyses (# converging runs (collapsed and non-collapsed)). Using the maximum likelihood method proposed by Baker [2015], the collapse fragility of the different structural typologies can be computed with respect to each GM record or model realisation. Collapse is typically defined as when the IDA trace "flatlines" or becomes sufficiently large to cause dynamic instability. This point is defined quantitatively as when the maximum PSD exceeds 10%, which is deemed sufficiently large to have caused collapse. These collapse fragilities are plotted in Figure 4.6 for each of the structural typologies and number of storeys considered, where the plots labelled RTR, MDL and TOT represent the mean collapse fragilities considering record-to-record variability only, modelling uncertainty only and both record-to-record variability and modelling uncertainty, respectively. The TOT fragility functions are considered the most accurate of the three as these consider the both of the aforementioned sources of uncertainty. By performing an IDA using a given set of GMs on a deterministic model of a case study structure, the resulting collapse fragility function would correspond to that of the RTR lines plotted in Figure 4.6. Comparing this to the more representative TOT fragility functions, the ratios of median collapse intensity and dispersion differ somewhat. The mean ratio of TOT to RTR for the median collapse intensity is 0.95 and the 1.27 for the associated dispersions. That is, the RTR fragility functions tend to overestimate the median collapse intensity and underestimate the dispersion when compared to the collapse fragilities that account for both aforementioned sources of uncertainty. The difference in the dispersion is an expected result and is typically accounted for by inflating the collapse dispersion by a prescribed value to account for the effects of modelling uncertainty. This is the approach of the FEMA P695 guidelines [FEMA P695, 2009] that prescribe values to which the RTR collapse fragility is to be increased using an SRSS combination, among others. However, guidelines such as FEMA P695 only propose a modification to the dispersion when accounting for modelling uncertainty despite Figure 4.6 illustrating that this tends to overestimate the median collapse intensity and the actual median tends to be somewhat lower. This observation was also noted in numerous studies discussed in Section 4.2.3, where the slight reduction in median collapse intensity was noted to be as a result of weakest link concept, whereby continuing to sample more and more values of the RVs, the likelihood of sampling an unusually weak structural components increases and is then reflected in the median collapse intensity. Gokkaya *et al.* [2016], for example, noted this reduction in the median collapse intensity to be up to 20%, with this reduction being more pronounced for non-ductile frames compared to modern ductile frames. However, further investigation by Gokkaya *et al.* [2016] showed that by modifying just the dispersion by a slightly higher value of modelling dispersion such that the tails of the collapse function match well with the TOT collapse fragility may suffice. This was justified by Gokkaya *et al.* [2016] by computing the MAF of collapse of the various adjustment procedures where the adjustment to match in the tail region of the collapse fragility at the intensity where MAF of collapse was found to saturate. While this approach of providing a single modification factor to account for modelling uncertainty, further work is required to examine the full

extent of the limitations of this approach with the authors concluding that the findings were subject to the limitations of RC frames assessed for a high seismicity site in LA.

Considering the above remarks regarding the comparisons between RTR type collapse fragility functions and bearing in mind the need to provide simple ways to account for modelling uncertainty in collapse assessment of older GLD RC frames in Italy, some simplified adjustments are thus proposed. These consist of providing an adjustment to both the median collapse intensity and dispersion to account for the effects of modelling uncertainty. This is done through a prescribed reduction factor for the median collapse intensity (R_c) and a dispersion due to modelling uncertainty ($\beta_{UC,IM}$) to be combined with the existing dispersion due to record-to-record variability ($\beta_{RC,IM}$) using an SRSS combination as follows:

$$\beta_{TOT,IM} = \sqrt{\beta_{RC,IM}^2 + \beta_{UC,IM}^2} \qquad \textbf{Equation 4.6}$$

which assumes the two sources of uncertainty to be independent of each another. Another approach would be that of Gokkaya *et al.* [2016], who in addition to providing modification values to the median and dispersion, described a method where just the dispersion could be modified. This was done by examining the saturation intensity for the MAF of exceedance of collapse and focusing on matching the two fragility curves in that intensity range. This approach involves a number of iterations and also requires the definition of a site hazard curve in addition to representatively selected and scaled GMs and as such, the initial approach of modifying the median and dispersion is followed here. The above notation follows that of Cornell *et al.* [2002] in order to maintain consistency with the notation used throughout the thesis to distinguish different types and sources of dispersion. These prescribed modifications are proposed in terms of structural typology and are listed in Table 4.2, where the coefficients of variation for each modification term is included in parenthesis. This proposal is labelled as ADJ2 in Figure 4.6, where examining the ratios between this and the TOT collapse fragility functions, it is seen to work well with overall mean ratios of 1.00 and 0.98 between the median collapse intensity and dispersion of the TOT and ADJ2 collapse fragilities, respectively. Comparing these to some existing values in the literature from both FEMA P695 [2009] and Dolšek [2009], the values appear reasonable and of the same order of magnitude, with FEMA P695 [2009] proposing values of $\beta_{UC,IM}$ between 0.10 and 0.50 depending on how well the model represents the actual structural behaviour and how robust that model is. Dolšek [2009] on the other hand proposed a $\beta_{UC,IM}$ of 0.52, which at first appear a little higher than those listed in Table 4.2. However, two differences that ought to be considered in the case of the values proposed by Dolšek [2009] are that this value applies to frames modelled without infill only and also that PGA is used as the IM, as opposed to $S_a(T_1)$ used here. This difference could explain the increase in modelling uncertainty with respect to the values proposed here. In any case,

the quantification of the effects of modelling uncertainty in infilled RC frames has not been exclusively addressed in either of the two aforementioned studies and as such, the values in Table 4.2 represent a novel contribution in this regard. In addition, the modification to the median and increase in overall dispersion proposed by Gokkaya *et al.* [2016] for bare non-ductile bare frames with no masonry infill in the US are somewhat similar to the corresponding case here. An average reduction of 0.95 in the median collapse intensity and an additional dispersion to account for modelling uncertainty of 0.33 noted, which are quite similar to corresponding values in Table 4.2, where Gokkaya *et al.* [2016] employed the same IM as that used in this study.

Table 4.2. Proposed collapse fragility modification factors to account for the effects of modelling uncertainty on the median collapse intensity and dispersion, where the coefficients of variation for each term are provided in parenthesis.

Structural Typology	R_c	$\beta_{UC,IM}$
w/o Infill	0.89 (0.04)	0.30 (0.06)
Pilotis Frame	0.95 (0.04)	0.30 (0.02)
Infill Frame	0.99 (0.01)	0.15 (0.07)

Table 4.2 shows how the influence of the modelling uncertainty on the collapse fragility is somewhat higher for the frames without infill modelled and pilotis frame typologies than for the infill frames since the median collapse intensity remains unchanged and the increase in dispersion is lower. One possible reason for such a difference could be that the infill frame response tends to be dominated by the presence of the infill, and less so by the actual surrounding RC frame. Therefore, there are fewer RVs that are influencing the response of the frames as the variability mainly comes from the infill and not the frame elements such as beam, columns and joints that possess many more RVs. This above comment, however, would require further confirmation through more detailed sensitivity studies.

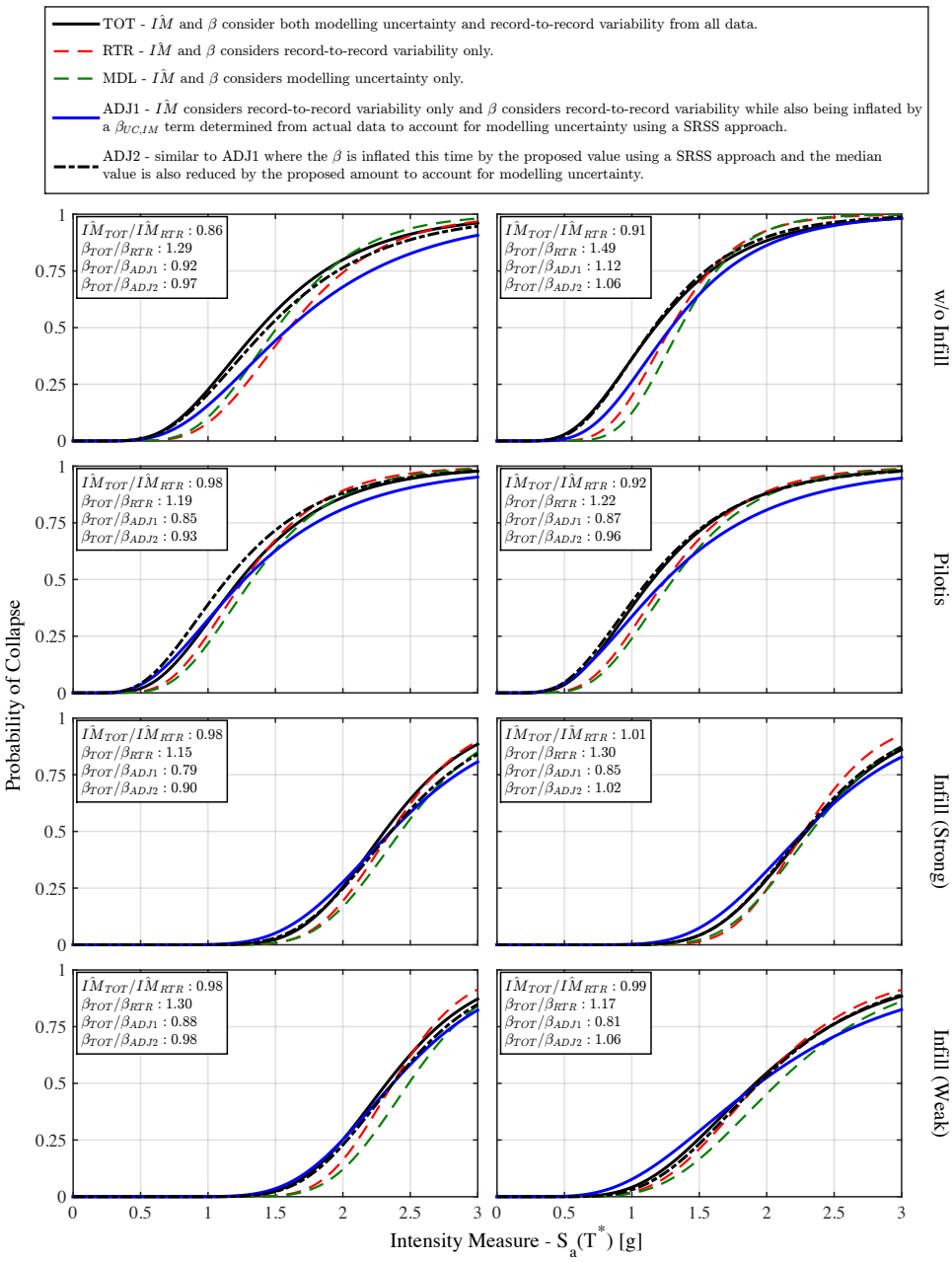

Figure 4.6. Comparison of the collapse fragility functions considering different sources of uncertainty compared with the two methods of adjusting the collapse fragility function to account for modelling uncertainty in GLD RC frames. Left and right-hand plots correspond to the 2 and 3 storey frames, respectively.

4.5.2 Demand Parameters with Respect to Intensity

While the previous section looked at the influence of modelling uncertainty on the collapse fragility of the structural typologies investigated here, this section discusses the effects of the modelling uncertainty on the demand parameters that are typically used for the seismic assessment of structures, namely the PSD and the PFA. Similar to the approach adopted for the collapse fragility functions, the effects of modelling uncertainty are incorporated by using an SRSS combination with the record-to-record variability to represent the overall dispersion in the demand parameters, described by the following expressions if the two sources are assumed to be uncorrelated:

$$\beta_{D,\theta} = \sqrt{\beta_{DR,\theta}^2 + \beta_{DU,\theta}^2} \qquad \textbf{Equation 4.7}$$

$$\beta_{D,a} = \sqrt{\beta_{DR,a}^2 + \beta_{DU,a}^2} \qquad \textbf{Equation 4.8}$$

Figure 4.7 and Figure 4.8 show the plots of PSD and PFA in the various structural typologies to show how the use of an SRSS combination of the record-to-record variability with the modelling uncertainty compares with the actual overall dispersion in the data. From these figures, it is seen how the use of an SRSS combination of the two sources of uncertainty gives a good representation, albeit slightly conservative, of the overall dispersion in the two demand parameters. The conservatism is owed to slight correlations that exists between the two sources of uncertainty [Cornell *et al.*, 2002], where the above expressions would read $\beta^2 = \beta_D^2 + \beta_C^2 - 2\rho\beta_D\beta_C$ implying that for a slight correlation between the demand (D) and the capacity (C), the overall dispersion will be reduced, as is the case here. This correlation could equally be positive also, resulting in an increase in overall dispersion [Kazantzi *et al.*, 2014]. As such, this slightly conservative approach is deemed appropriate and trends in the actual modelling uncertainty are therefore identified with respect to the various limit states of the buildings, which are then to be used as per Equation 4.7 and Equation 4.8 to compute the total dispersion for each demand parameter.

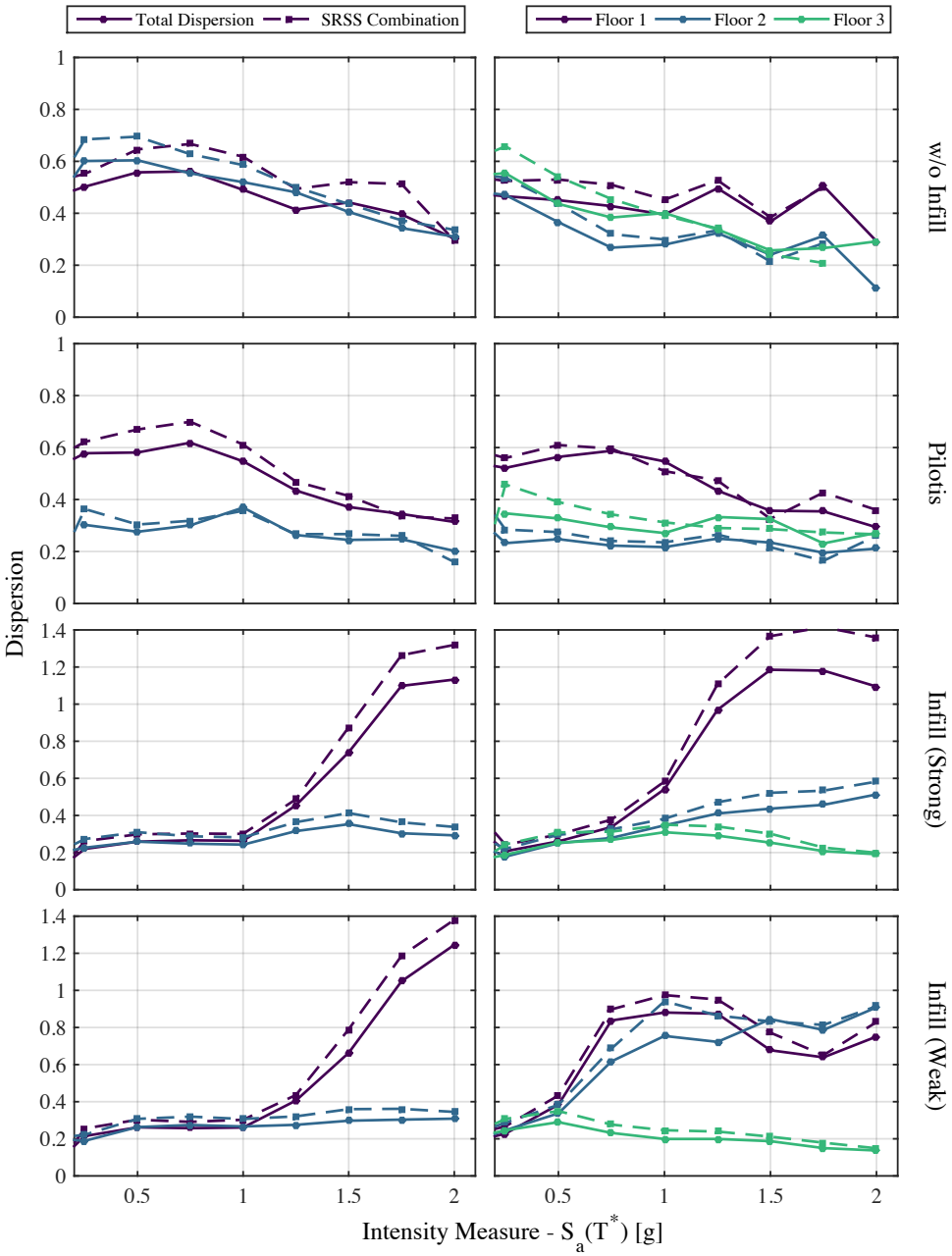

Figure 4.7. Comparison of SRSS combination of record-to-record variability ($\beta_{DR,\theta}$) with modelling uncertainty ($\beta_{DU,\theta}$) to overall uncertainty for the PSD of the various structural typologies.

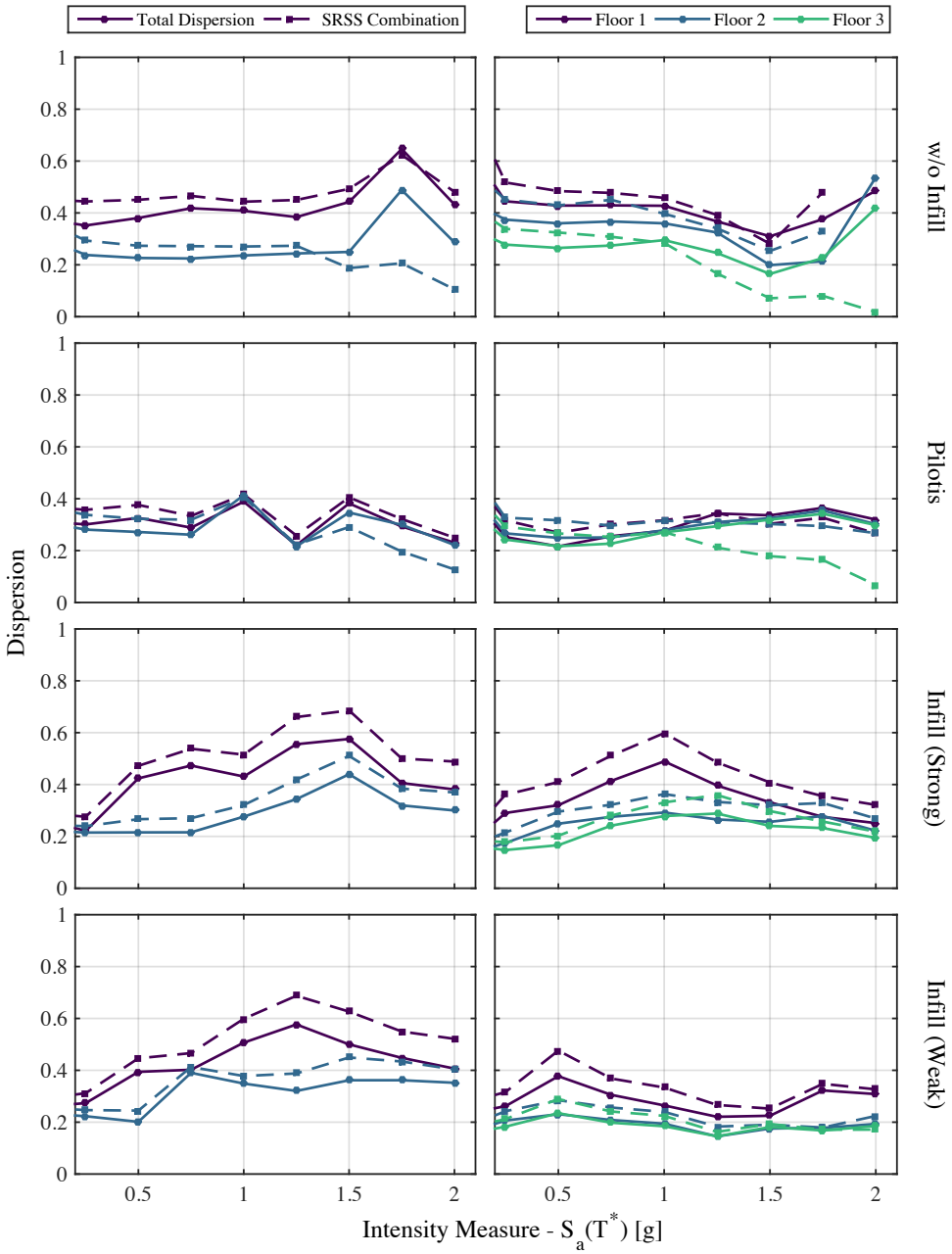

Figure 4.8. Comparison of SRSS combination of record-to-record variability ($\beta_{DR,a}$) with modelling uncertainty ($\beta_{DU,a}$) to overall uncertainty for the PFA of the various structural typologies.

In order to compute the dispersion in the two demand parameters due to modelling uncertainty, the results of the analysis are analysed with respect to both a given GM record and model realisation, as illustrated in Figure 4.3. Therefore, the modelling uncertainty versus intensity will be investigated for both demand parameters at each floor for the case study structures investigated. As concluded in Section 4.2.5, previous research suggests that the modelling uncertainty is not only a function of the demand parameter of interest but also to the limit state being considered, where the limit states described here are as per the definitions discussed later in Section 5.2. As such, the median intensities of the four limit states discussed later in Section 5.2 are used here. The estimation of these median limit state intensities will be discussed in detail later in Section 5.5. Figure 4.9 and Figure 4.10 present the modelling uncertainty versus IM for both demand parameters, where the median intensity for the four limit states considered are shown also. These proposed values plotted in the following are also listed in Table 4.3 in terms of the structural typology and demand parameter of interest. They are intended to provide an upper bound on the expected modelling uncertainty. It should be noted that these values have been developed using low-rise RC frames with two and three floors and as such, trends with respect to the number of floors etc. have not yet been identified. Future work may be carried out to identify sets of coefficients that are a function of this, or indeed the first mode period of a structure as is done in FEMA P58-1 [2012], but for now a single set has been proposed.

Table 4.3. Proposed modelling uncertainty values (β_{DU}) for both PSD and PFA as a function of structural typology and anticipated limit state.

Structural Typology	Modelling Uncertainty					
	<SLO	SLO	SLD	SLV	SLC	>SLC
Peak Storey Drift ($\beta_{DU,\theta}$)						
w/o Infill	0.40	0.50	0.50	0.50	0.45	0.20
Pilotis Frame	0.40	0.50	0.50	0.50	0.40	0.20
Infill Frame (Strong)	0.15	0.50	0.80	0.90	0.90	0.90
Infill Frame (Weak)	0.15	0.30	0.50	0.60	0.60	0.80
Peak Floor Acceleration ($\beta_{DU,a}$)						
w/o Infill	0.30	0.30	0.30	0.30	0.30	0.20
Pilotis Frame	0.25	0.25	0.25	0.25	0.25	0.20
Infill Frame (Strong)	0.15	0.40	0.30	0.30	0.30	0.30
Infill Frame (Weak)	0.15	0.30	0.30	0.30	0.30	0.30

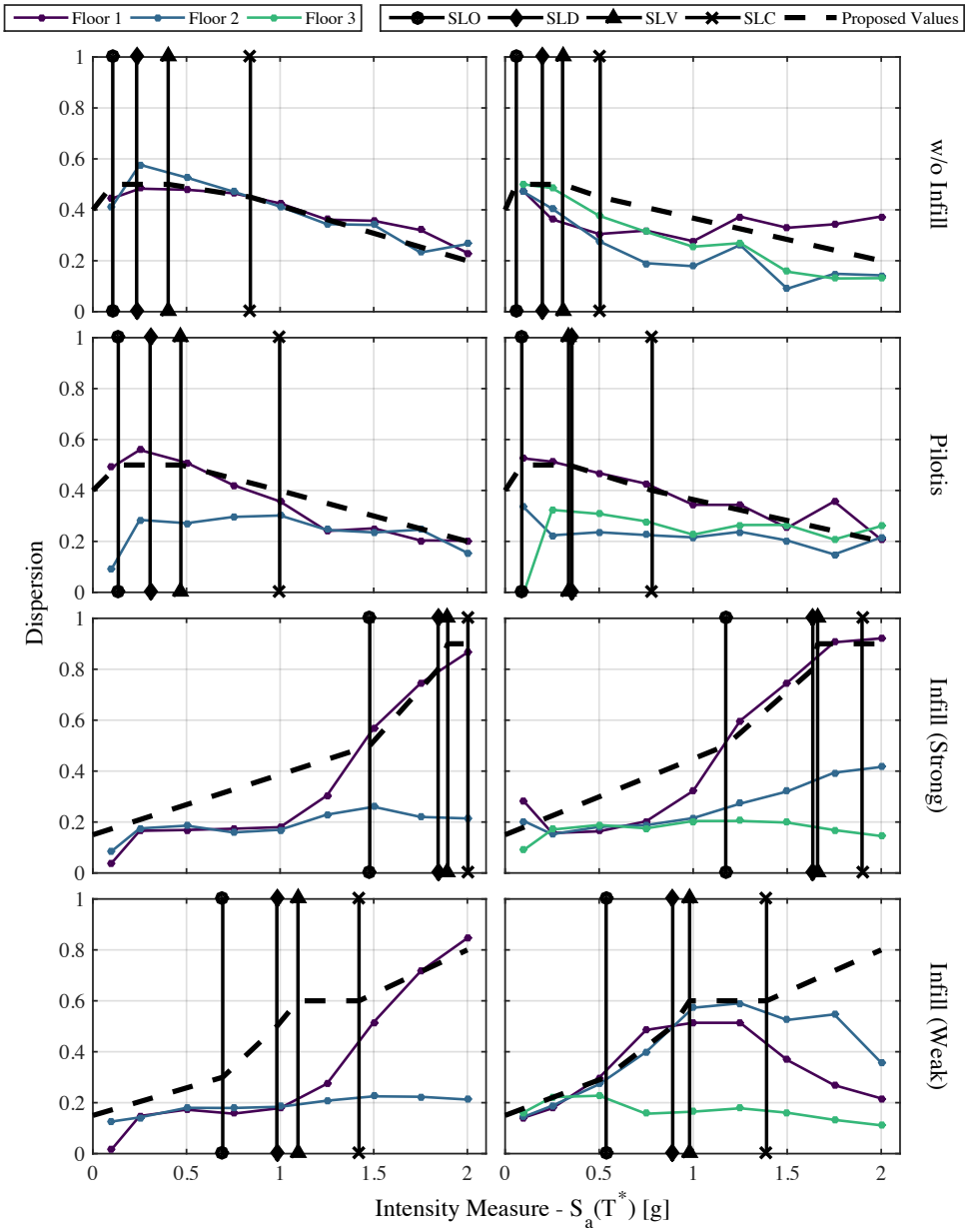

Figure 4.9. **Modelling uncertainty associated with the PSD ($\beta_{DU,\theta}$) versus intensity for the different structural typologies, where the median intensities for the four limit states of interest are plotted alongside the proposed values.**

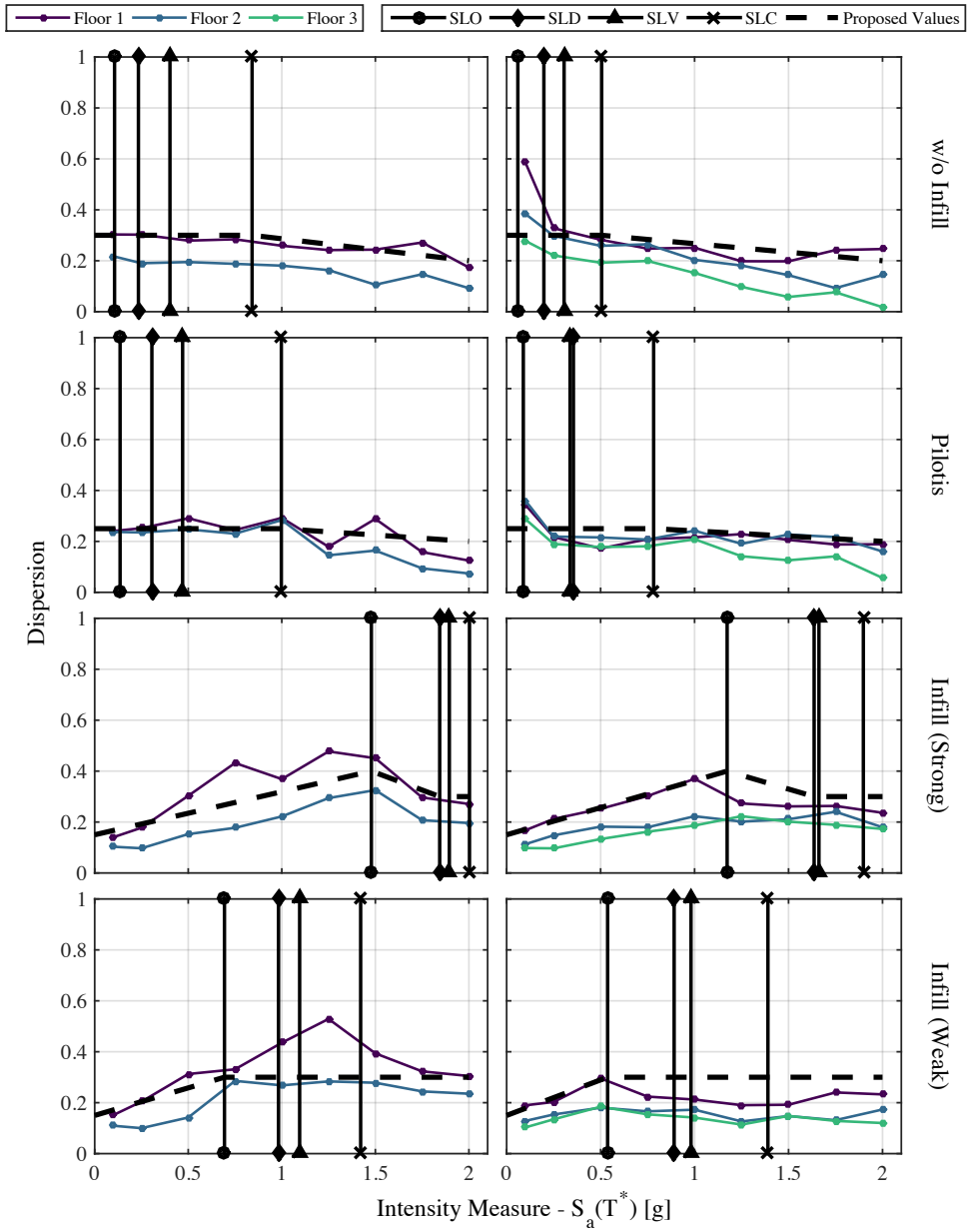

Figure 4.10. Modelling uncertainty associated with the PFA ($\beta_{DU,a}$) versus intensity for the different structural typologies, where the median intensities for the four limit states of interest are plotted alongside the proposed values.

Some initial comments that can be made regarding the values are that the PFA values tend to be much lower than those of PSD; a trend that is also present in the proposed values of FEMA P58-1 [2012]. In addition, the modelling uncertainty tends to increase with more severe limit states for the PSD but tends to plateau for the PFA. One reason for this may be due to the structure becoming more non-linear with increasing intensity and thus being influenced by the dispersion in more RVs for the backbone behaviour, whereas the PFAs tend to be capped by the first mode lateral yield strength of the structure. For instance, consider the modelling uncertainty values associated with the PFA in the pilotis frames. The behaviour of these frames is almost always governed by the soft-storey forming in the bottom storey, and dispersion due to modelling uncertainty for PFA will come from the lateral capacity of that floor only meaning that the influential RVs are greatly reduced compared to other frames. This could explain the slightly lower dispersion of the PFA for the pilotis frame with respect to the other frame typologies. In addition, the dispersion in PSD in the upper floors for pilotis frames does not reduce significantly with respect to the ground floor in the same way the median demands do. In fact, the median demands do decrease but the relative dispersion in these values still remain significant.

The PSD dispersion tends to reduce for intensities beyond the SLC limit state in the cases of the frames without infill modelling and the pilotis frames. This can be explained conceptually as being due to the structure being highly non-linear and as a result, the mechanism formed acts a fuse to which all of the median PSD demand is concentrated. This increase in PSD demand and formation of a mechanism reduces the amount of RVs that are directly influencing the overall response of the frame and as a result, the dispersion would be expected to reduce with respect to the lower limit states, as is illustrated in Figure 4.9. This reduction is not evident for the infilled frames since the intensities up to which this study was conducted do not surpass the SLC limit state intensity of the infilled frames very much to observe such a trend, although is it somewhat apparent in the case of the three storey weak infill frame.

Another observation worth commenting on is the relative magnitude of the PSD dispersion in the infill frames with respect to the frames modelled without infill and the pilotis frames. These values are of a much higher order of magnitude with respect to these other typologies and also with respect to the other levels in the same structures. This was observed to have occurred due to the large peak resistance of the infill that needs to be overcome in order to enter the range of relatively large drift demands. Following this peak, however, the rapid degradation of the infill strength means that the drift demand tends to increase rather significantly. This results in the situation where many records have not been able to surpass the infill strength and therefore the maximum PSD remains a relatively low value or records that have surpassed this infill capacity and resulted in a relatively large PSD demand. This has been identified to be the culprit of such large dispersion in the case of the infill frames, and is more pronounced in the case of the strong infill with respect to the weak infill.

Examining the PSD dispersion in at lower intensities in such frames shows how a relatively low demand, the dispersion remains within an expected range when compared with other frames typologies, but the progression of response into the higher limit states results in this kick out in dispersion for the drift.

4.5.3 Limitations of the Current Study

While the study conducted here has provided a set of default values to quantify the modelling uncertainty in various RC frame typologies, some limitations of this work and possible future directions are noted. Firstly, the number of storeys is a parameter that ought to be investigated further, since the above study considered the modelling uncertainty in just two and three storey frames due to limitations in terms of computing power. As such, the modelling uncertainty values proposed in Table 4.3 are to be applied to low-rise buildings and preliminary application to buildings with a larger number of storeys, pending future work. Another issue that has not been considered is the effect of double strut modelling of the masonry infill on the modelling uncertainty. This was not included here due to numerical convergence issues, as when trying to achieve a robust model for each realisation proved rather problematic. This is of particular interest as considering the shear behaviour in the columns could be expected to increase the overall dispersion in the demand parameters, although this remains to be investigated further. This consideration would allow for the further investigation of the modelling uncertainty on the expected failure mechanism in the structures, where one would expect that depending on the expected failure mechanism the modelling may be refined. Lastly, model type uncertainty has not been considered here and could be a very interesting topic for future work so as to consider the impact of different modelling techniques in addition to model parameters on overall modelling uncertainty.

4.6 SUMMARY AND CONCLUSIONS

This chapter discussed the quantification of the modelling uncertainty associated with the various demand parameters typically used in the assessment of GLD RC frames Italy. Existing research on the general topic of quantifying modelling uncertainty was first reviewed to provide insight into various aspects to be considered. This was then followed by the description of the CLHS methodology used to generate the modelling realisations using the various RVs established for the structural members such that their effects on the collapse fragility and the PSD and PFA demand could be quantified. From this quantification study, the following notes can be made:

- The effects of modelling uncertainty on the collapse capacity of the structures showed that the median collapse intensity tends to reduce and the dispersion tends to increase. This finding is also in line with previous research on various structural typologies reviewed in this chapter. From this, empirical values for the reduction

of the median collapse intensity and the increase in the dispersion for the collapse fragility were provided with respect to structural typology.

- Similarly, the effects of modelling uncertainty on the dispersion of the PSD and PFA of the different structural typologies were investigated, where the uncorrelated SRSS combination of the dispersion due to record-to-record variability and modelling uncertainty was shown to give a reasonable estimate of the overall dispersion, implying that the effects of modelling uncertainty on these demand parameters can be aggregated into the record-to-record dispersion via SRSS combination. Using this, a set of empirical dispersion values to account for modelling uncertainty were proposed as a function of the different limit states, structural typology and the demand parameter of interest.

These values represent a novel contribution to the field as such values to directly quantify the effects of modelling uncertainty with respect to GLD RC frames in Italy do not yet exist, especially for infilled frames and frames with pilotis infill configuration. The proposals outlined here will serve as the basis for the extensive assessment studies to be conducted for numerous case study frames in the following chapters, as it provides direct values for GLD RC frames as a function of limit state and demand parameter, values which have not yet been quantified in the literature for the structures examined here. In addition, this study has directly addressed the comments made by Fajfar and Dolšek [2012] that highlighted the need for these default values for modelling dispersion to be quantified for assessment of such structural typologies.

5 RESPONSE ASSESSMENT OF GLD RC FRAMES IN ITALY

This chapter presents and analyses a number of GLD case study structures to enable a comprehensive assessment of their characteristics and behaviour through various types of numerical analyses. The buildings are first presented and a brief description of the philosophy used to design them is provided, followed by a description of the different variations of the structures to be examined. The buildings are then modelled using the techniques discussed in Chapter 2 to conduct both SPO and IDA of the buildings from low levels of intensity up to higher intensities. As such, the performance of the buildings is evaluated over various limit states and a comparison and discussion of the results is provided to characterise their behaviour.

5.1 DESCRIPTION OF CASE STUDY FRAMES

The case study frames to be examined consist of 2D and 3D RC frames of various number of storeys, which are shown in Figure 5.1 and Figure 5.2, respectively. The 2D designs are adopted from a previous study by Galli [2006] and the corresponding 3D ones are adopted from another study by Piazza [2013]. Both sets of case study frames have been designed for gravity load only using allowable stress and other such design provisions specified in Regio Decreto 2229/39 [Regio Decreto, 1939], along with other common construction conventions prior to the introduction of seismic design provisions in Italy in the 1970's [Pagano, 1963; Santarella, 1956], which are reviewed by Vona and Masi [2004] and listed in Table 5.1.

Table 5.1. Overview of the typical design criteria given in Regio Decreto 2229/39 and other design conventions [Vona and Masi, 2004].

Structural Elements	Design Objective	Building Code	Manuals*
Columns	N (axial force)	Structural mechanics methods	Normal centered compression stress
	Concrete section		$A_c=N/\sigma_{c,allowable}$
	Longitudinal reinforcement	>0.8%A_c for A_c < 2000 cm^2 >0.5%A_c for A_c > 8000 cm^2	>0.8%A_c, at least Ø12
	Transverse reinforcement	s < min(1/2b, 10Ø) 50% stirrups, 50% bent bars	
Beams	M (bending moment)	Structural mechanics methods	Structural mechanics methods, simplified equations
	Concrete section		$h = r\sqrt{M/b} \times b$
	Longitudinal reinforcement		$A_{rebar} = t\sqrt{M \times b}$ for most stressed side, 2Ø12 for other side
	Transverse reinforcement	50% stirrups, 50% bent bars	Bent bars calculated with shear stress, stirrups with constant spacing

*Refers to available design manuals at the time [Santarella, 1956; Pagano, 1963]

Some typical details of these gravity-load only designs are the complete lack of capacity design considerations in the beam and column members as the columns were sized principally for axial loading and the beam members were typically designed by considering the hogging and sagging moments of a continuously loaded multi-support beam. This approach was quite common during the construction boom that followed the second world war across southern Europe and resulted in many RC structures vulnerable to undesirable seismic response, as has been observed in past earthquakes in Section 1.1. In addition to the out-of-date seismic provisions (or in many cases, no seismic provisions at all) adopted during past construction, another detail regarding the construction of these buildings that leaves them quite vulnerable to seismic loading is the use of smooth reinforcing bars in the beam and column members, which affects the bonding of the reinforcement to the concrete paste resulting in a modified ductility and moment capacity compared to newer

ductile detailing, as outlined in Calvi *et al.* [2002b]. The shear reinforcement requirements listed in Table 5.1 that were implemented at the time also resulted in a very small percentage of shear reinforcement stirrups in the beam and column members and no reinforcement in the beam-column joints, which combined with the use of smooth end-hooked bars was shown to be particular vulnerable during experimental testing by Pampanin *et al.* [2002] and also past earthquakes, as highlighted in Section 1.1. Many of these aspects of design were observed during the post-earthquake reconnaissance conducted by EERI [2009], where all of the above features were noted from inspection of the damaged buildings.

The layout and various details regarding the member cross-sections of the case study structures are shown in Figure 5.1 and Figure 5.2, where the column section sizes remain constant for the two and three storey frames and the lower levels have slightly larger sections in the four and six storey frames. It is immediately apparent that the reinforcing ratios for the column sections are rather low (<1.3%) since these were sized for axial loading rather than capacity designed with respect to the strength hierarchy of the beams, as described in Table 5.1. The strength of the reinforcing steel and concrete were 3800kg/cm^2 (372MPa) and 200kg/cm^2 (19.6MPa), respectively, whereas the floor loadings were taken as 500kg/m^2 for the roof levels and 600kg/m^2 for each floor, as per typical design manuals in use at the time of construction.

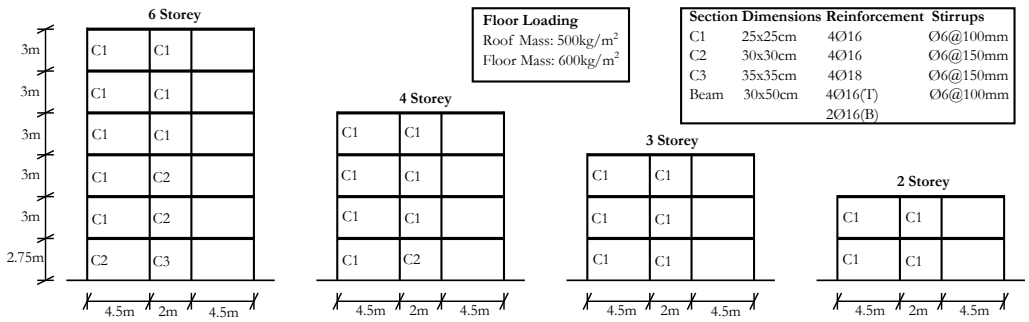

Figure 5.1. Layout of 2D case study structures adopted from Galli [2006].

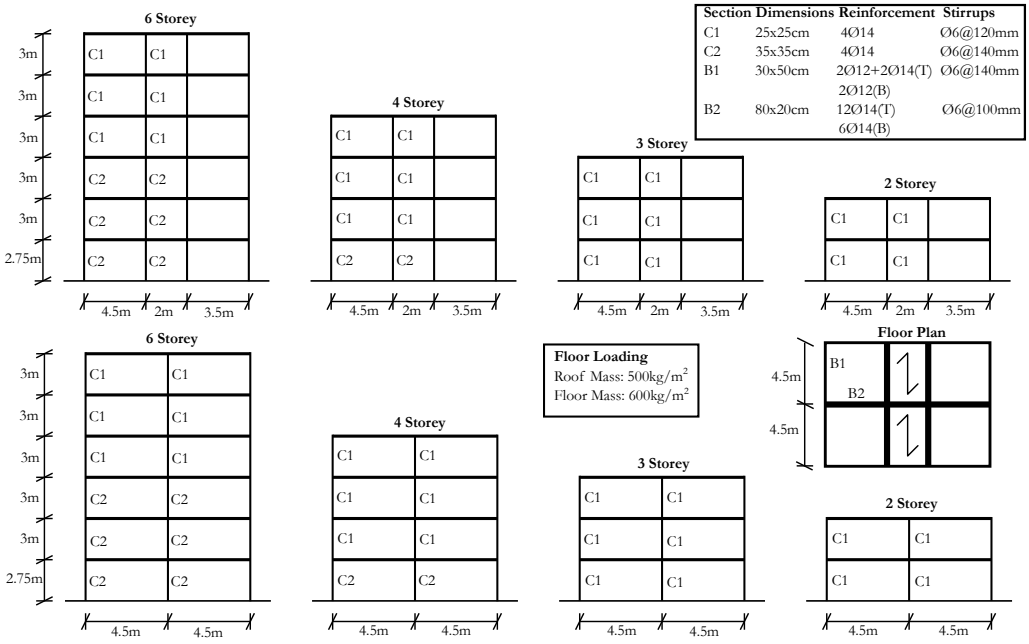

Figure 5.2. Layout of 3D case study structures adopted from Piazza [2013].

In terms of modelling the case study frames, the developments of Chapter 2 are adopted herein for the structures. For the case of the 2D frames shown in Figure 5.1, a tributary width of 4.5m was adopted and the associated mass used in the numerical model with the remaining mass related with the structure assigned to a leaning P-Delta column during the analysis to capture second-order geometry effects. The floor system is modelled using a rigid diaphragm, which is deemed a reasonable assumption for the "laterizio" floor systems that were quite common in Italy at the time of construction.

While the case study frames have been designed as bare frames, common practice throughout southern Italy was to insert masonry infills in the structures without considering their effects on the surrounding frame during the design process. As such, a number of different infill case study frames are also investigated here to illustrate their effects on the structural behaviour and overall performance of GLD RC frames. Two different infill layouts were considered; a uniform infill throughout the height of the building and a uniform infill layout with an open ground floor, commonly referred to as a "pilotis" frame. These pilotis frames were, and still are, quite popular throughout Italy as they offer large open areas very suitable for retail space at the ground floor, while the upper storeys tend to be used for other purposes. These architectural advantages are of course now well known in the earthquake engineering community to be of detriment to the buildings

seismic behaviour unless properly considered, as they encourage the classic case of a soft-storey response on the ground floor. In addition to the uniform infill and pilotis frames, two types of masonry infill have been used and are termed "weak" and "strong" infill, as per Hak *et al.* [2012] and illustrated in Figure 5.3*,* where weak infill corresponds to the 8cm thick single leaf infill and 30cm thick block, respectively. These are adopted in order to illustrate the effects of different infill typology on the seismic behaviour and overall performance of the structure. Lastly, both the single and double infill strut models outlined in Section 2.6 are adopted to investigate the influence of modelling the shear behaviour of the columns due to the forces induced by the infill on the column members, as was seen to be a prominent failure mechanism during past earthquakes in Italy (Section 1.1). The effects of modelling openings such as windows or doors were not considered as part of this study.

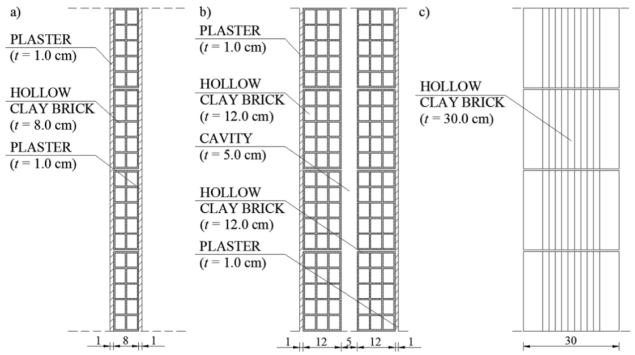

Figure 5.3. Illustration of the different masonry infill typologies adopted in this study (Adapted from Hak *et al.* [2012]).

In short, the case study structures investigated here allow for the consideration of the influence of many parameters on the performance and also the demand parameters to be used in future chapters. Some of these parameters that will be investigated are:

- The influence of the number of storeys to investigate how certain parameters such as median collapse intensity and base shear coefficient are influenced.
- 2D and 3D modelling to examine any fundamental differences in behaviour and to validate whether it is reasonable to study a 2D frame representation of a 3D structure for the parametric studies examined here.
- Frames both with and without masonry infill modelled to highlight the fundamental difference in response and to examine the impact of ignoring the

presence of masonry infill at various stages of the seismic assessment, both in terms of response and monetary losses.

- Shear modelling in columns to highlight the impact of considering the failure in the columns, as this has been a prevalent damage mechanism during past earthquakes in Italy.
- Strong and weak masonry infill typologies to examine the influence of the relative strength of masonry infills on different aspects of the assessment.

For each of the case study structures described above, a numerical model has been built in OpenSees [McKenna *et al.*, 2000] using the modelling parameters described in Chapter 2. The following sections describe the results of an extensive set of numerical analyses to characterise the behaviour and performance of the case study frames. These range from SPO analyses to characterise the progression in damage throughout the structures and identify the occurrence of various limit states, followed by IDA [Vamvatsikos and Cornell, 2002], where a set of GMs are scaled and applied to the structures at numerous intensities to characterise the response with increasing GM intensity. The application of IDA here is somewhat similar to that of MSA, where the GMs are scaled to certain stripes of IM. This has been done for the computational economy of using truncated IDA in addition to using the same set of GMs for the different structural typologies. While actual MSA ought to select hazard compatible GMs at each stripe, which is described in Chapter 8, this simplification has been done here as these results are intended to be illustrative and not representative of the exact values of GLD frames in Italy, although they will not be too far of depending on various seismic hazard-related issues. The outcome of this extensive analysis on GLD frames is that the general performance of the various case study variations can be investigated and compared, in addition to these results being used as the basis for loss estimation studies to be discussed in the following chapters.

5.2 STATIC PUSHOVER ANALYSIS

The first set of analysis conducted on the case study frames are SPO analysis, where a set of lateral forces are applied to the numerical models in proportion to the product of the mass at each level and the first mode shape, which is then scaled incrementally until the control node of the numerical model reaches a specified target displacement. This approach is commonly referred to a displacement-controlled pushover analysis.

In the case of the 2D frames, Figure 5.4 shows the plot of the SPO curves where the base shear coefficient is plotted versus the roof displacement and Figure 5.5 shows a similar plot for the 3D case study frames. As is immediately evident from Figure 5.4 and Figure 5.5, the presence of masonry infill significantly modifies the lateral behaviour of the frames, which is seen through the increased initial stiffness and peak base shear capacity of the

frames. In terms of the number of storeys, the peak base shear coefficient tends to reduce with increasing storey number. This can be expected when one considers that the base shear coefficient is defined as the total base shear normalised by the total building weight. As such, the normalising term obviously gets larger for increasing storey number whereas the maximum base shear tends to remain relatively constant for all buildings as the lack of capacity design in the GLD frames tends to result in a column-sway mechanism in the frames (see Figure 5.7 and Figure 5.8) as opposed to a fully ductile mechanism throughout the height of the building involving plastic hinging in the beam-ends at multiple levels. As such, the peak base shear capacity tends to be limited by the capacity of a single storey and remains somewhat constant, meaning that when normalised by the total building weight it will decrease for the taller buildings. This can be seen in the case of the 2D and both principal directions of the 3D frames without infill.

Comparing the response of the frames without infill modelled and pilotis infill frames, in each case the presence of the masonry infill in the upper storeys of the floor tends to increase the initial stiffness of the structures but provide a similar maximum base shear capacity since the governing mechanism is a column-sway mechanism on the open ground floor. What is important to note that since the GLD frames are designed without capacity design, a non-ductile mechanism such a column-sway can be expected to form in the case of the frames without infill modelled, which is confirmed in Figure 5.7 and Figure 5.8. The presence of masonry infill in the upper levels of the pilotis frames then, as anticipated, forces this soft-storey to form on the open ground floor. The slight difference in capacity noted in Figure 5.5 for the 3D frames stems from the different frame arrangement in the two directions, as illustrated in Figure 5.2.

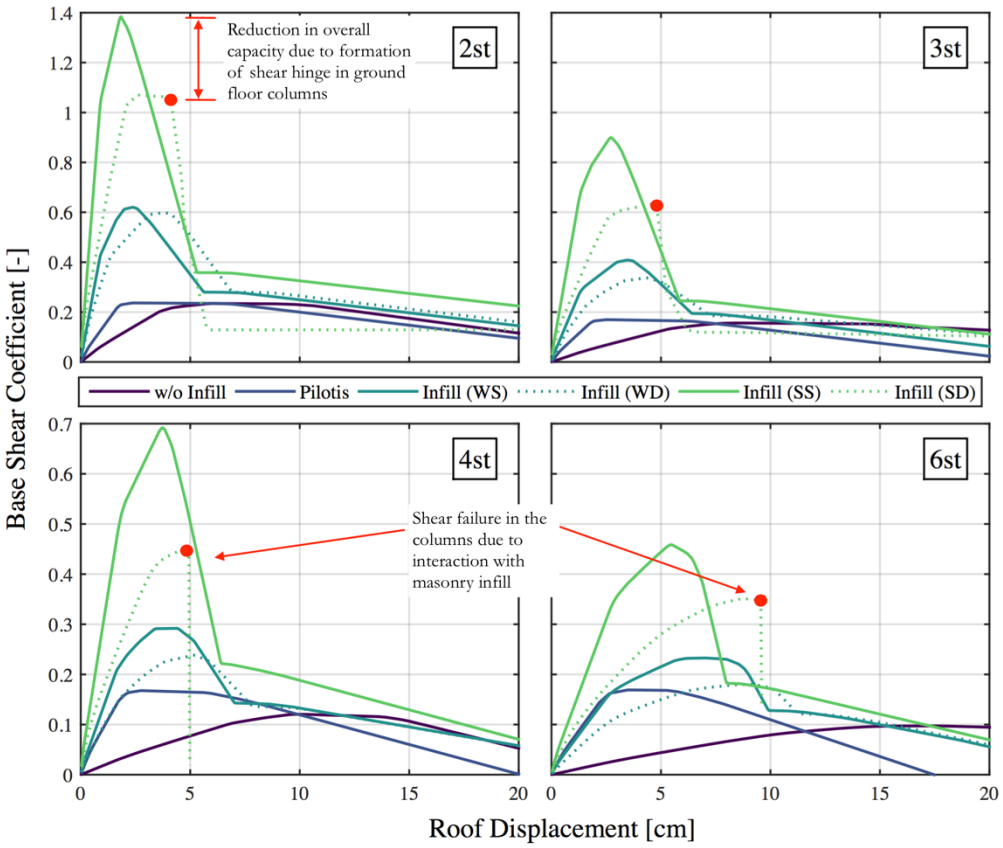

Figure 5.4. SPO curves showing base shear coefficient versus roof displacement of the structure for each modelling variation of the 2D frames.

In the case of the 2D frames, a comparison between the modelling of the shear behaviour of the column members has been conducted by using a double-strut approach to modelling the masonry infill followed by the insertion of shear hinge springs at both ends of the column members as outlined in Section 2.2.2.2. This comparison was conducted for the 2D frames only, as numerical convergence issues in the 3D frames resulted in some difficulties in achieving a robust, converging numerical model even in the case of SPO analysis. The models required special attention and were convergable, but were not robust enough to be included in the large parametric studies being conducted as part of this study and were therefore omitted as the effects of shear hinge modelling could be examined from the 2D frames in any case. From Figure 5.4, the initial stiffness of the single and double-strut infill models for both weak and strong infill typologies can be seen to be quite comparable, although the double-strut models tend to be slightly more flexible due to an

additional shear flexibility in the columns where the diagonal struts are connected to the surrounding frame. This additional flexibility is also reflected in the eigenvalue analyses, where considering the double-strut infill model and shear deformation in the columns results in an increase of up to 15% in the first mode period of vibration for the frames with respect to corresponding single-strut cases. The overall peak capacity of the double-strut frames is noted to be slightly reduced compared to that of the single-strut ones also.

One of the main advantages of incorporating the shear behaviour and failure of the columns due to the interaction with the masonry infill is that this damage mode can be directly simulated during analysis to incorporate its influence on the actual peak response and not require post-processing checks to determine whether the shear in the column is critical or not. One such approach is the iterative pushover procedure outlined in Celarec and Dolšek [2013] who looked to analyse Italian GLD RC frames with masonry infills using SPO analysis. To account for the effects of shear failure in the column due to infill interaction, a demand/capacity check was performed by post-processing the SPO results and for cases where the shear capacity was exceeded, the flexural capacity and behaviour of the plastic hinges was reduced to account for this shear issue using a series of model iterations. While such a procedure can be considered approximate at best, it fails to account for the additional deformation offered by the shear damage to the columns, where the discussion in Section 2.2.2.2 highlighted that the shear failure can be a function of deformation in addition to strength. As such, the approach adopted here represents a marked improvement in terms of capturing the effects of shear failure, since it directly accounts for its impact in the model using the shear strength and deformation capacity expressions discussed by Zimos *et al.* [2015].

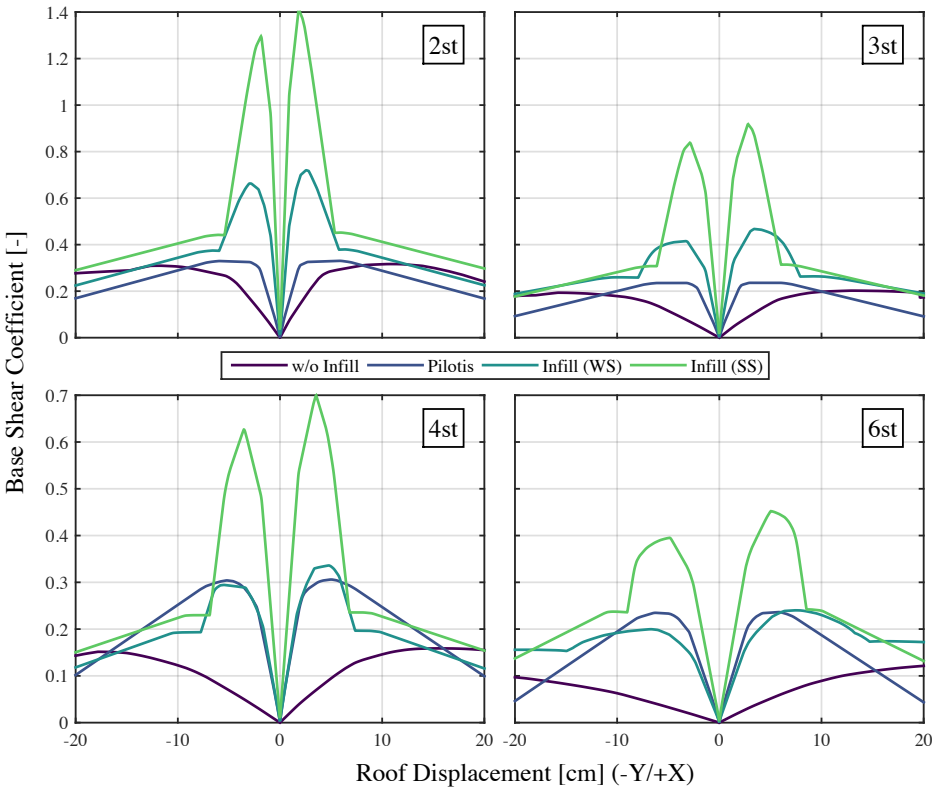

Figure 5.5. SPO curves for each modelling variation of the 3D frames, where the positive and negative value SPO curves represent the pushovers in the principal X and Y directions, respectively.

In addition to using the SPO analyses to characterise the general behaviour of the frames, these can also be used to define the performance criteria for various limit states to describe the overall performance of the building. This refers to the various performance levels often cited in PBEE documents such as the Vision 2000 document [SEAOC, 1995] or the Italian National Code (NTC 2008) [NTC, 2008], among others. These limit states are defined by the NTC 2008 as follows:

- **Stato Limite di Operatività – "*Operational*" (SLO):** following the earthquake the building's structural and non-structural components maintain their function and do not suffer any damage or significant interruption of their usage.

- **Stato Limite di Danno – "*Damage Control*" (SLD):** following the earthquake the buildings structural and non-structural elements suffer damage that does not put the occupants at risk and do not significantly compromise the overall capacity and stiffness of the structure to maintain the vertical and horizontal actions.
- **Stato Limite di salvaguardia della Vita – "*Life Safety*" (SLV):** following the earthquake the building suffers damage and collapse to the non-structural elements and damage to the structural elements that results in a significant loss of lateral stiffness, but still maintains gravity load carrying capacity and a margin of safety against collapse.
- **Stato Limite di prevenzione del Collasso – "*Collapse Prevention*" (SLC):** following the earthquake the structure suffers heavy damage to both structural and non-structural elements; the structure maintains gravity load carrying capacity and has a slender margin of safety against collapse.

Using the above descriptions of the different limit states, these need to be actually defined quantitatively. For the first two limit states, these are defined arbitrarily in a 2009 addendum to the NTC 2008 guidelines in Italy as fixed values, while the last two limit states are defined based on the occurrence of the ultimate chord rotation in the frame members using the expression given in Equation A.3 of Eurocode 8 – Part 3. It has been previously discussed in Section 2.2.2.1 that such an expression may not be appropriate for members using smooth reinforcing bars and low levels of shear reinforcement and therefore for simplicity, the limit states to be used here will be defined as a function of the SPO curves as:

- SLO – 0.25% PSD based on the median values of the first for typical gypsum partitions and other drift sensitive non-structural elements.
- SLD – the minimum value between 0.5% and the structural yield point on the SPO curve, which is in keeping both with the non-structural drift requirements of NTC 2008 and also so as not to significantly compromise the overall capacity and stiffness of the structure.
- SLV –the point of maximum lateral capacity of the structure, as this corresponds to a significant loss of lateral stiffness, but still maintains gravity load carrying capacity and a margin of safety against collapse.

- SLC – this is defined as the point of a 20% drop in lateral capacity of the structure, as this maintains gravity load carrying capacity and has a slender margin of safety against collapse.

It is noted that these definitions are in terms of the SPO curves for the frames with no infill but are used to assess the performance of each of the modelling variations. This approach is adopted since if the above definitions of each limit state were to be applied to the infilled frames, the definition of collapse prevention (SLC) would correspond to the drop in capacity following the exhaustion of the masonry infills contribution to the lateral capacity, despite the actual RC frame still offering some lateral capacity and the masonry infill being in many ways a non-structural element as opposed to a structural one. In order to maintain consistency in the definition of each limit state between the different structures, their occurrence for the frames with no infill modelled are adopted.

The actual procedure followed to identify the limit state of each structure is illustrated in Figure 5.6, whereby performing the SPO analysis and plotting the backbone response of the structure, the various limit states can be identified. Using these points identified on the SPO backbone, the displaced shape profile at that point along the SPO can be used to identify the critical storey drift in the structure for that particular limit state. These storey drifts identified for each limit state are then used during the IDA discussed in the following sections to assess to the exceedance of each limit state with respect to seismic intensity and to develop limit state fragility curves.

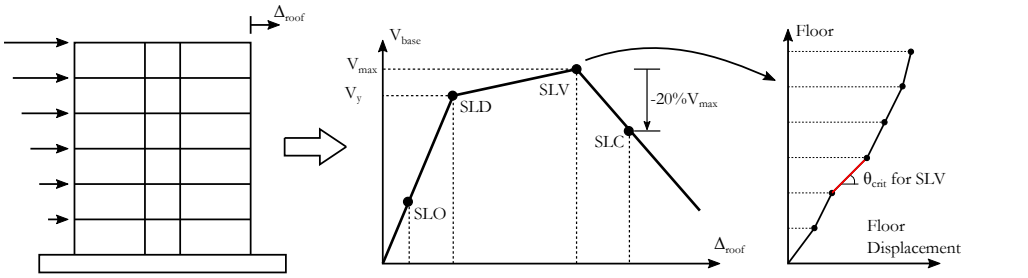

Figure 5.6. Illustration of establishing performance criteria for each limit state using the SPO analysis results.

Figure 5.7 and Figure 5.8 then show the displaced shape of the case study frames at the different limit states normalised to the roof displacement of the SLC limit state. For most of the structures, a soft-storey mechanism is anticipated due to column-sway at the upper limit states, although in the case of the three storey frames, a joint mechanism appears more

likely due to the apparent spread in deformation across two adjacent storeys in the lower levels, as was observed in experimental testing by Calvi *et al.* [2002] and noted during the discussion of Section 2.5.

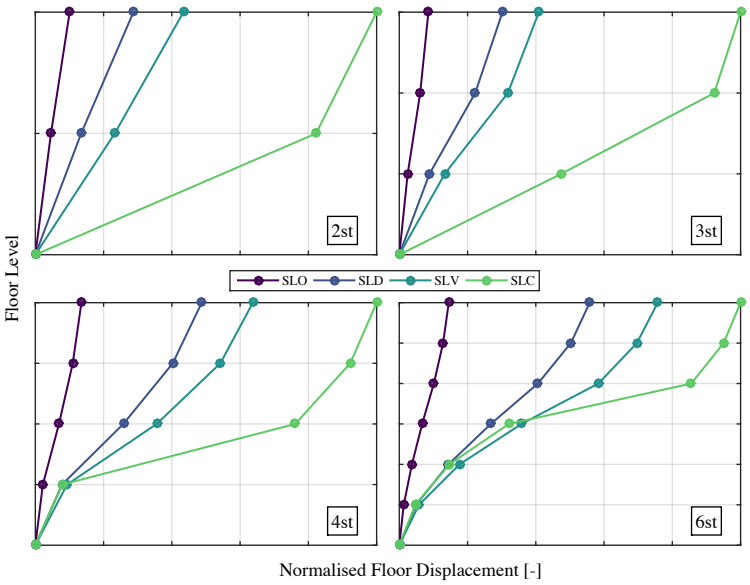

Figure 5.7. Displacement profile (normalised to the SLC roof displacement) of the 2D frames at each limit state determined during SPO analysis.

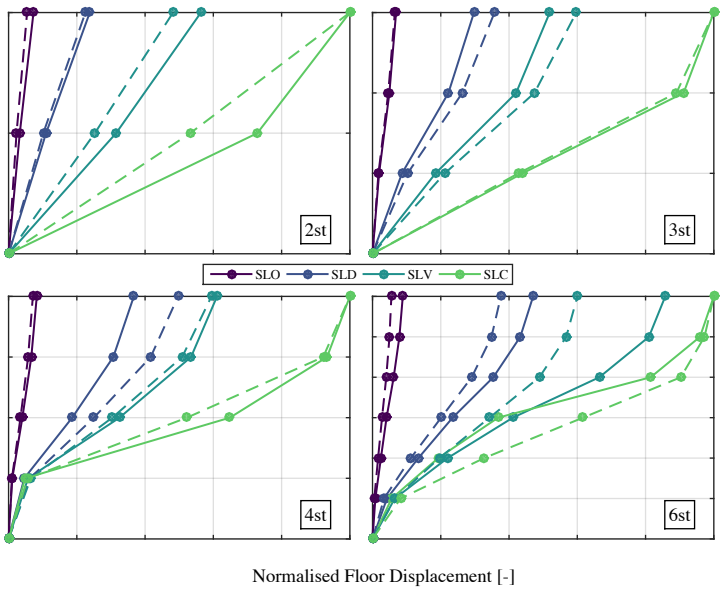

Figure 5.8. Displacement profile (normalised to the SLC roof displacement) of the 3D frames at each limit state determined during SPO analysis, where the solid and dashed lines represent the displacement in the principal X and Y directions, respectively.

5.3 INCREMENTAL DYNAMIC ANALYSIS

The next set of analyses that are conducted on the case study frames is IDA, where a set of GM records are scaled to a particular intensity and applied to the structure to examine its response parameters. This process is repeated for increasing levels of intensity to enable a description of damage with respect to seismic intensity to be developed, commonly referred to as IDA and is outlined in Vamvatsikos and Cornell [2002]. The seismic IM used is the spectral acceleration at a conditioning period T^* ($S_a(T^*)$) where for the 2D structures T^* corresponds to the first mode period of vibration of the structure (T_1) and in the case of the 3D case study structures, T^* is taken as the average of the first mode periods of vibration in the two principal directions of the building, which is as per the recommendations of the FEMA P58 guidelines [FEMA P58-1, 2012]. A Rayleigh damping model is adopted by applying 5% of equivalent critical damping to the first and third modes of vibration. The GM record set used to track the evolution of damage and response in the structure is that given in FEMA P695 [FEMA P695, 2009]. It is acknowledged that the use of a single set of GMs scaled using IDA raises some issues regarding hazard consistency. Referring to the original publication by Vamvatsikos and Cornell [2002], this issue is addressed and justified by the authors through use of an appropriately defined IM, where the example discussed Vamvatsikos and Cornell [2002] states how the use of $S_a(T_1)$

(adopted here) as the IM for scaled record is expected to be representative of a similar response using unscaled records, whereas using PGA as an intensity measure would not due to the inherent issues with using this as the IM. As such, it can be argued that the approach of scaling records here through IDA to examine the progression of damage in the case study structures is justifiable due to the selection of appropriate IM in $S_a(T_1)$. Future work, however, could look to incorporate more recent findings of Kohrangi *et al.* [2016a; b], where more advanced IMs were shown to have additional benefits with respect to that of $S_a(T_1)$.

In terms of actual results, each frame and modelling variation is analysed and the pertaining demand parameters examined with respect to model typology and seismic intensity. This results in quite a lot of numerical analysis output that, in the interests of being brief, are largely omitted here and are included in Appendix A, whereas the results are summarised in terms of their medians for general comparison. The complete set of NRHA results is used in the loss estimation in the following chapters and an example of these results is first shown in Figure 5.9 for the maximum PSD of the 2D frames without infill and the maximum PFAs in Figure 5.10 for the 2D single-strut models with strong masonry infill, where the term "maximum peak" refers to the maximum value across each storey, and the peak refers to the maximum recorded at each floor over the duration of the record.

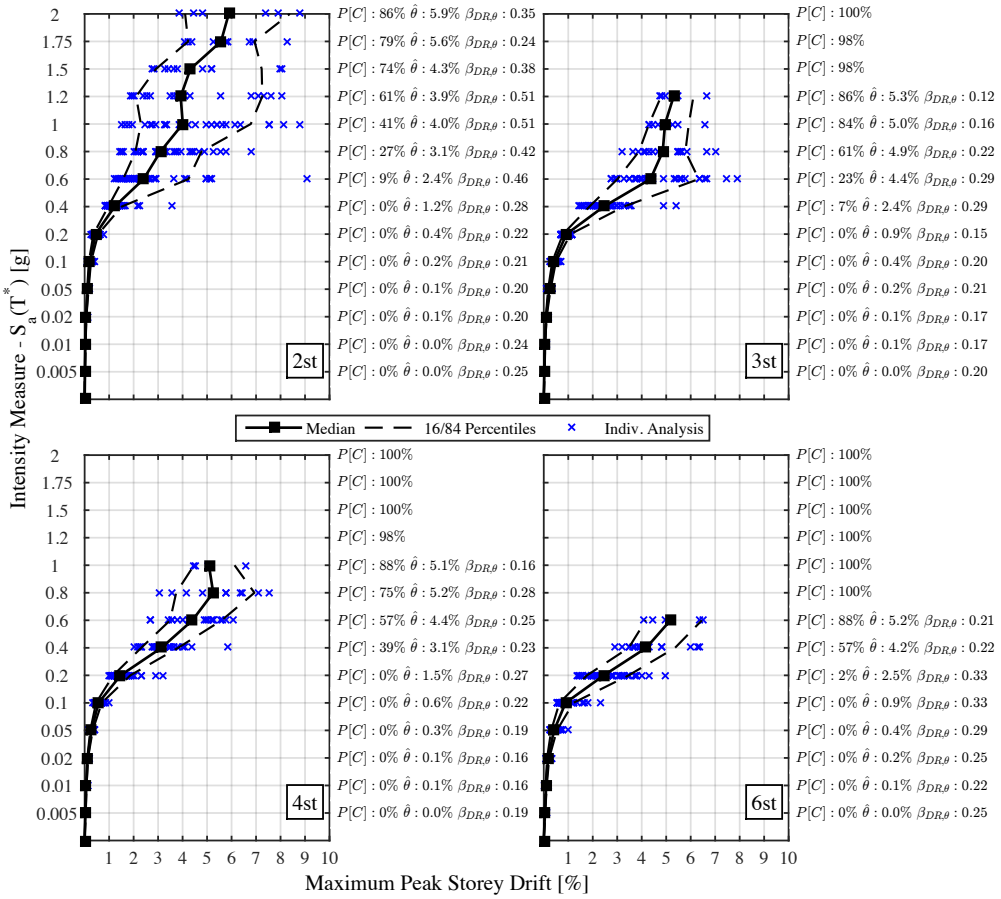

Figure 5.9. Illustration of the progression of maximum PSD with increasing intensity in the case of the 2D case study frames without infill.

In the case of the results plotted in Figure 5.9 and Figure 5.10, the drift demand increases with intensity in addition to the probability of collapse at each stripe of the IDA, to be discussed further in Section 5.4, where for cases when all but a few GMs cause a global collapse, the IDA results are not plotted. The median response is reported along with the lognormal dispersion in the data for each stripe, which provides the basis for the medians and dispersions required for loss estimation studies examined in later chapters, in addition to valuable data that can be used to develop and validate more simplified procedures to estimate the median response of such structures and also more refined estimates of the expected level of record-to-record dispersion. These comparisons between the refined

analysis results presented here and more simplified procedures are presented and discussed in depth in Section 7.2.

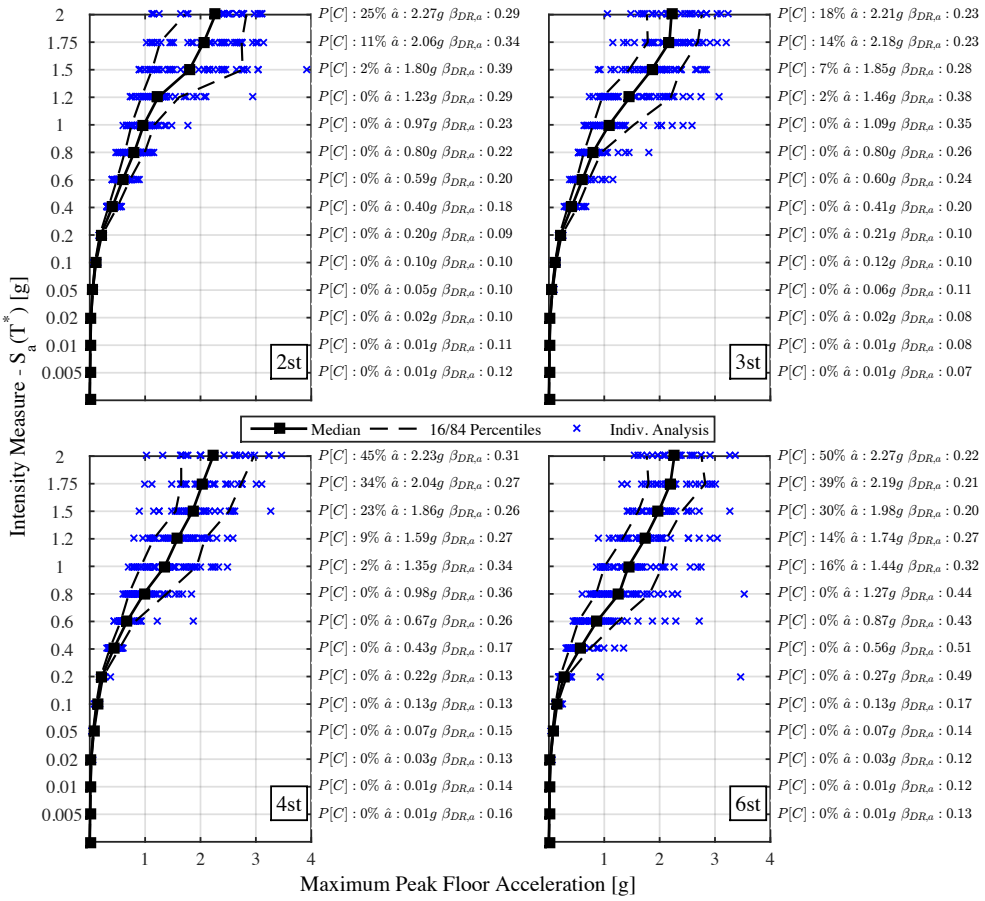

Figure 5.10. Illustration of the progression of maximum PFA with increasing intensity in the case of the 2D case study frames infilled with strong masonry infill.

While the above plots present the behaviour of two case study structure types, Figure 5.11 and Figure 5.12 plot the median values of maximum PSD for the 2D and 3D frames, respectively, while Figure 5.13 and Figure 5.14 plot the corresponding median values of maximum PFAs. Since the T^* is different for each building, the IMs are not directly comparable by themselves. These are therefore normalised by the intensity at the 2500 year return period ($S_{a,2500yrs}$) for a given site. This site chosen is the L'Aquila site described further in Section 6.2.5, where the $S_a(T)$ at the period closest to T^*. This normalisation allows the

median values from the different structural typologies to be compared. Regarding the notation used in these figures, the term WS in relation to infills refers to the weak infill with single-strut modelling, while WD corresponds to the same infill typology with double-strut modelling and so on for the case of the strong infill. These plots illustrate how the demand evolves in each of the case study structures with respect to IM. Some of the plots are cut short at the higher intensities as this correspond to cases where the probability of collapse exceeded 90%.

First comparing the differences in the responses of the structures with respect to number of storeys, the maximum PSD demand tends to increase with increasing number of storeys, which is a somewhat expected result, whereas the maximum PFAs appear to be less influenced. In addition, similar overall observations can be made when comparing the response of the 2D and 3D frames. The drift response of the frames with no infill modelled and pilotis frames is anticipated to be much higher than that of the fully infilled frames although floor accelerations appear to be quite similar at lower intensities before the infill frames tend to generate much higher PFAs at the larger intensities.

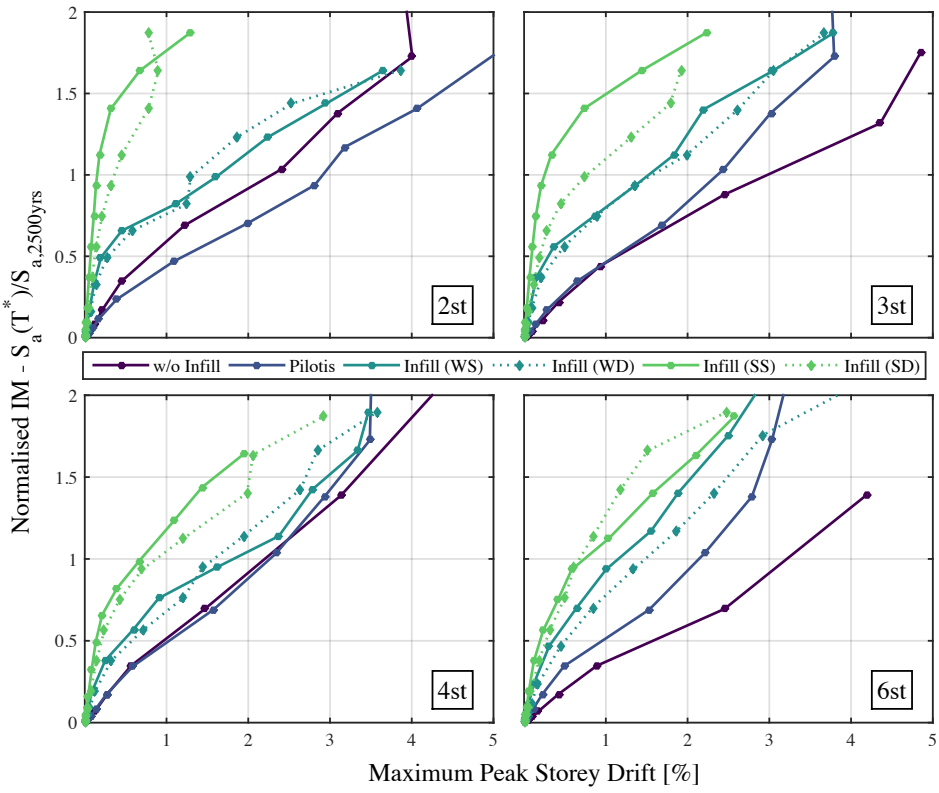

Figure 5.11. Median value of the maximum PSD at each normalised intensity of the IDA for each of the 2D frames.

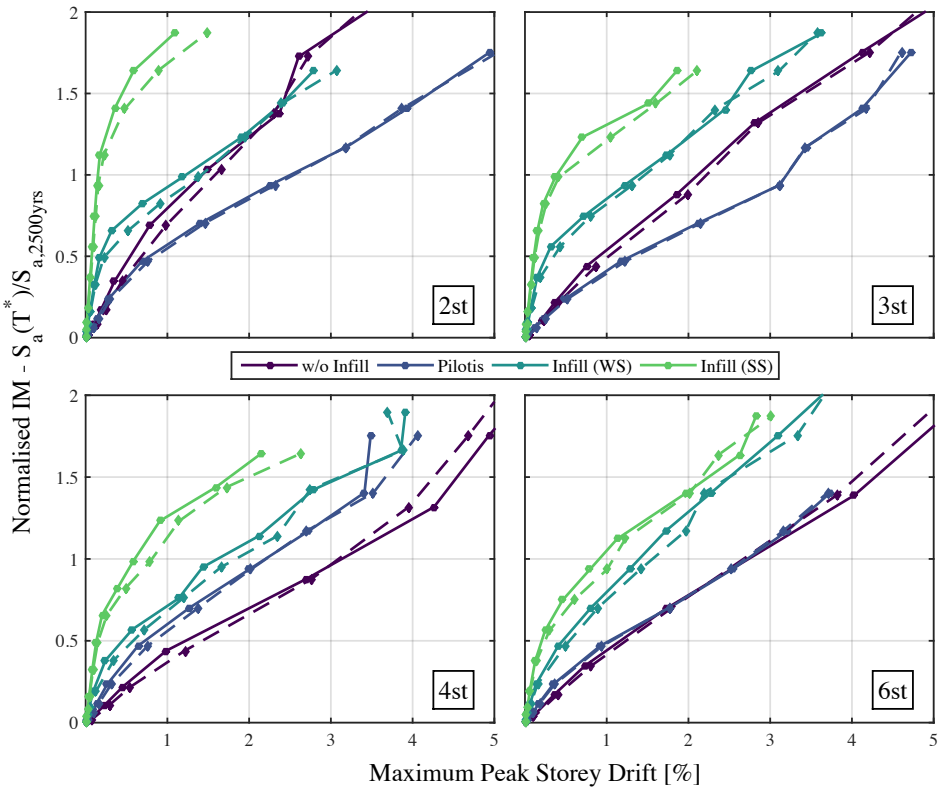

Figure 5.12. Median value of the maximum PSD at each normalised intensity of the IDA for the 3D frames, where the solid and dashed lines represent the responses in the principal X and Y directions, respectively.

Comparing the general response of the frames in terms of bare and infill frame typology, the anticipated results in terms of drift and acceleration demand are observed with the bare frame displaying much higher drift demand than that of the infilled frame and the influence of the masonry infill strength can also be observed. In terms of floor acceleration demand, the infill frames show a much higher demand than the corresponding frames without infill modelling, which is to be expected as the stiffer infill frames would be expected to generate higher floor accelerations compared to a more flexible structure such as a frame without masonry infill modelling. Again, it is seen how the strength of the masonry infill influences these floor accelerations with the stronger infill resulting in a higher acceleration demand than that of the weaker infill.

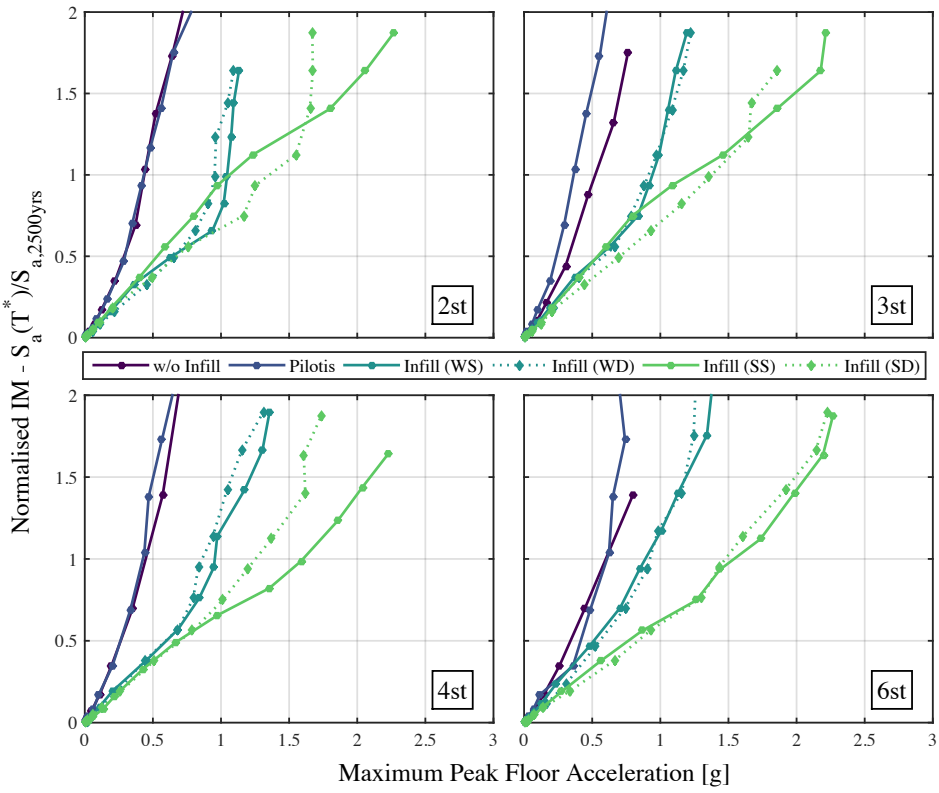

Figure 5.13. Median value of the maximum PFA at each normalised intensity of the IDA for the 2D frames.

Finally, comparing the response of the single-strut and double-strut masonry infill frames, it is evident that in terms of maximum PSD demand, the double-strut models show a general increase with respect to the single-strut models, which an observation consistent with the findings of the SPO analysis where the double-strut models tended to be slightly more flexible than the corresponding single-strut ones. In terms of floor accelerations, there is no obvious difference between the two models, although it could be argued that the use of double-strut models leads to a slight decrease in the maximum PFAs.

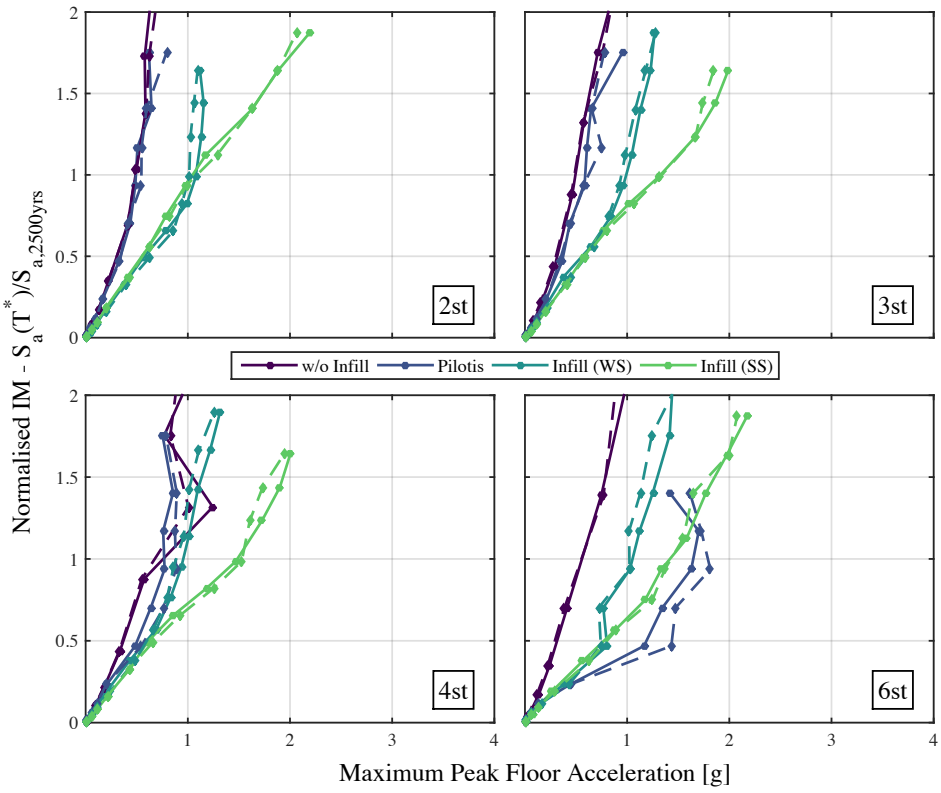

Figure 5.14. Median value of the maximum PFA at each normalised intensity of the IDA for the 3D frames, where the solid and dashed lines represent the responses in the principal X and Y directions, respectively.

5.4 COLLAPSE ASSESSMENT

This section discusses the collapse fragility of the case study frames. The first part of this section looks at estimating the collapse fragility via the advanced numerical analysis methods discussed in the preceding section that involves the use of numerous NRHA results to quantify the building response with respect to increasing intensity. The second half of this section then examines the computation of the collapse fragility using a more simplified in the SPO2IDA tool described by Vamvatsikos and Cornell [2005] that uses the SPO curve along with empirical relationships to estimate the IDA trace by exploiting the relationships between the two curves identified by Vamvatsikos [2002]. The applicability of such a simplified tool, which has been developed into a simple spreadsheet-based tool and subsequently adopted in the FEMA P58 guidelines [FEMA P58-1, 2012], is therefore

examined in the case of Italian GLD frames with masonry infill and commented on with respect to the collapse fragilities estimated using NRHA.

5.4.1 Estimating the Collapse Fragility from Analysis

In order to assess the collapse behaviour of the frames, the IDA results described in the previous sections are utilised here. During each GM of the IDA, analyses were subjected to a constant check on the current maximum PSD in the structure at each moment in time during the analysis. If the current maximum PSD exceeded a prescribed maximum storey drift capacity, the GM was terminated at that point and marked as a collapsed case. This avoids cases where a structural model has accumulated excessive drift and has essentially collapsed, but the software continues to run the GM record until the end of its duration regardless. This can lead to situations where the numerical model is still being subjected to deformation demands that would, in reality, be deemed a collapse due to excessive permanent deformations following visual inspections, but it continues nevertheless to execute successive steps of the analysis and runs into great difficulty to achieve numerical convergence. By imposing such a storey drift capacity check during the analyses, which is in this case 10% storey drift, the aforementioned situation where a structure has essentially collapsed but the program attempts to finish the GM record and spends a long time trying to achieve convergence without much prospect, or even need, of achieving it is avoided. This limited of 10% maximum PSD has also been used in past studies by Gokkaya *et al.* [2016], for example. However, it must be stated that this storey drift capacity check is only applied to structures with fully converged response and is not applied to situations where, for various reasons, a numerical model is unable to achieve convergence for a particular GM without having entered into the predefined collapse storey drift range. These situations are removed from the analysis results and are not used any further, since the fact that a model is unable to converge does not necessarily mean that the structure has actually collapsed, unless the drift demand is already quite high.

Using the above definition of collapse, the IDA returns a certain number of collapses (# of collapses) and a certain number of fully converged and completed analyses (# converging runs (collapsed and non-collapsed)) for each intensity. This means that the ratio between these two can be used to describe the probability of collapse for a given intensity, which is the values plotted as P[C] at each stripe of the IDA in Figure 5.9 and Figure 5.10. This information can be used to construct the actual collapse fragility of the structure using the maximum likelihood method, whose application to fitting fragility functions to truncated data sets from truncated IDA has been described in Baker [2015]. This method works by assuming a lognormal distribution for the collapse fragility and by trialling a value for median collapse intensity and dispersion, compares the likelihood of the actual data retrieved from IDA to the trialled combination of median and dispersion to fit the distribution, and iterating until the best match is found.

Figure 5.15 shows these fitted collapse fragilities for each of the 2D case study structures. Again, the IM for each frame is normalised so as to enable a relative comparison between the different structural typologies. It is important to note that the median and dispersion in the collapse fragility functions described here account for record-to-record variability only and do not incorporate the adjustments proposed in Chapter 4 to account for modelling uncertainty, which are assumed to be incorporated by the user when used to compute the expected loss of MAF of exceedances. This adjustment prescribed in FEMA P695 for spectral shape is also omitted as considering the discussion in Section 4.5.1, the factors provided in FEMA P695 are developed for ductile structures in the US not necessarily applicable here, in addition to the approach of FEMA P695 having been recently shown to possess its limitations by Eads *et al.* [2016]. Finally, the purpose of this section is to illustrate the progression of damage via IDA and not propose recommended values of characteristic values of existing GLD RC frames in Italy. In order to properly consider the effects of spectral shape and maintain hazard consistency, numerous sets of GMs should be properly selected according with the chosen sites hazard characteristics at each intensity, such as the procedure outlined by Jayaram *et al.* [2011], for example. Alternatively, a different IM may be adopted as a compromise in considering spectral shape, such as that outlined by [Kazantzi and Vamvatsikos, 2015]. Using this approach for selecting GMs along with the analysis approach outlined, which would be termed MSA, these above issues regarding spectral shape and hazard consistency would be resolved. This will be illustrated in Chapter 8 through an example application of the analysis described herein to an existing school structure in Italy.

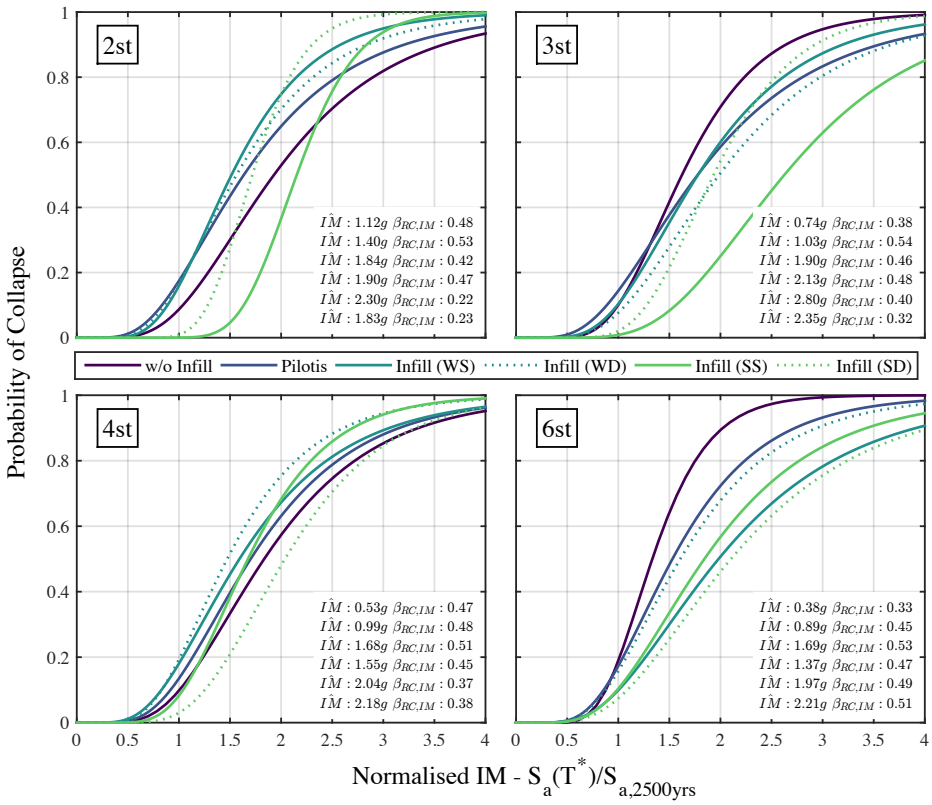

Figure 5.15. Collapse fragility curves for each of the 2D structures. Note: These collapse fragility functions account for record-to-record variability in the collapse fragility ($\beta_{RC,IM}$) and do not contain the proposed adjustments to the median and dispersion (R_c and $\beta_{UC,IM}$).

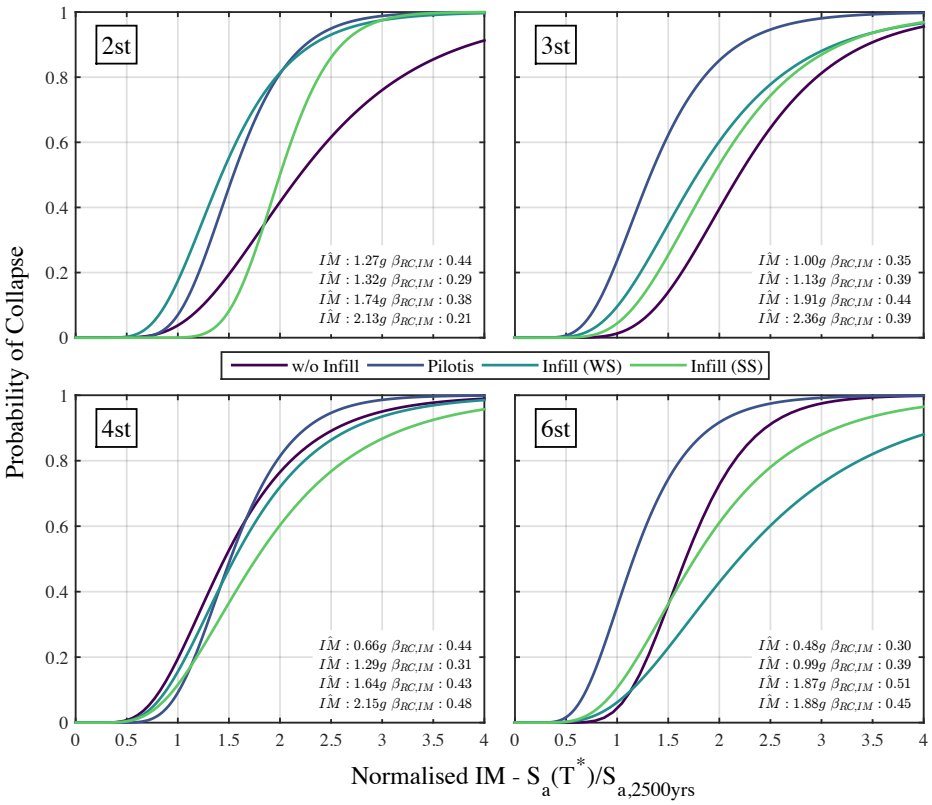

Figure 5.16. Collapse fragility curves for each of the 3D structures. Note: These collapse fragility functions account for record-to-record variability in the collapse fragility ($\beta_{RC,IM}$) and do not contain the proposed adjustments to the median and dispersion (R_c and $\beta_{UC,IM}$).

As can be seen in Figure 5.15, the trends in collapse fragilities tend to follow the observations in the IDA results presented in Section 5.3, where the structures with the masonry infill tend to have a much higher median collapse intensity than that of the frames without infills modelled and pilotis frames, but when examining the normalised intensity are seen to be similar if not worse than the bare frames cases. Similar observations for the case of the 2D and 3D case study structures (Figure 5.15 and Figure 5.16, respectively) in terms of how the frames without masonry infill modelled appear more fragile (i.e. have a lower median collapse intensity) than those of the infill frames, as shown in Figure 5.17. While these median collapse intensities may appear somewhat large, comparison with values from previous studies by Dolšek [2009] and Landi *et al.* [2016] showed that these values are quite similar to the case studies considered in those studies, where the IM used was PGA in both cases and when considering an approximate ratio of ~2.5 between the PGA and the constant acceleration period range of a design spectra where these frames

would be expected to lie, the median collapse intensities are noted to be of similar magnitude to those reported here for both frames with and without infill modelling.

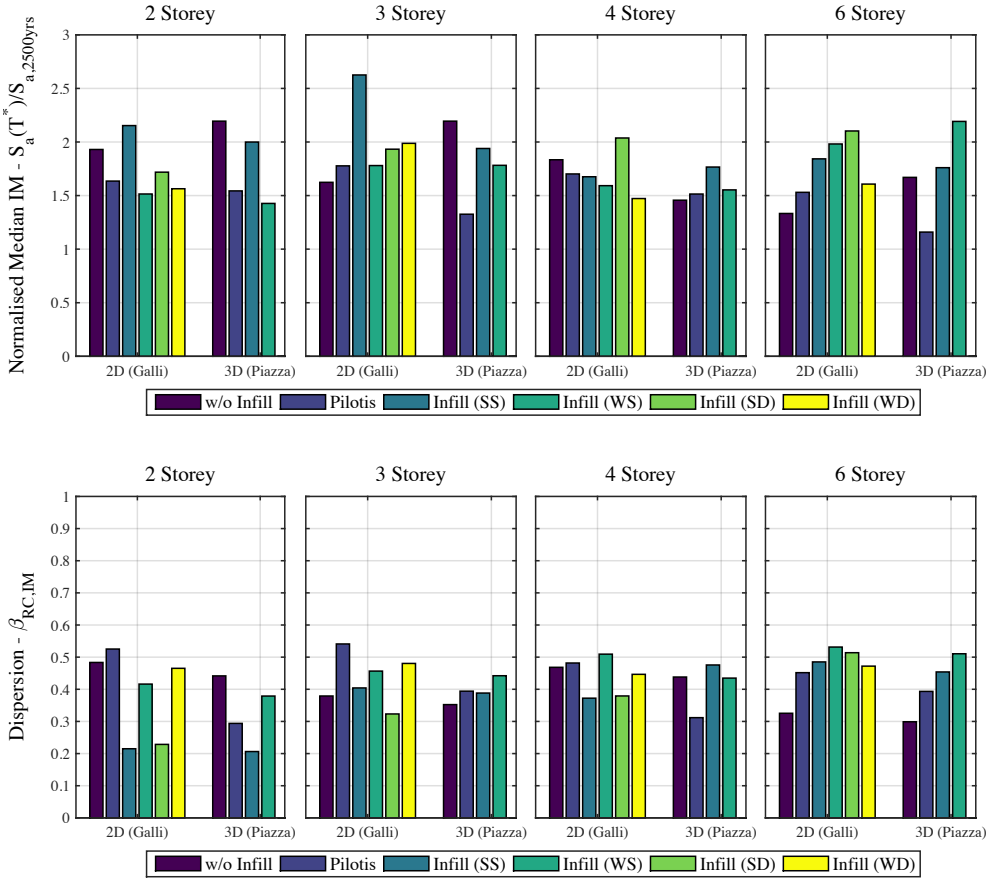

Figure 5.17. Normalised median collapse intensity and dispersion of both the 2D and 3D case study frames from Galli [2006] and Piazza [2013], respectively. Note: These collapse fragility functions account for record-to-record variability in the collapse fragility ($\beta_{RC,IM}$) and do not contain the proposed adjustments to the median and dispersion (R_c and $\beta_{UC,IM}$).

Comparing the collapse fragility of the 2D frames without infill modelled and pilotis frames, the pilotis frames tend to have a lower normalised median collapse intensity. This agrees well with past earthquakes where the presence of an opening ground floor tends to result in many instances of collapse. Another important point of observation is the comparison between the response of the single and double-strut models of the masonry infill structures. This is because the use of the double strut infill model allows the

consideration of the shear flexibility and possible failure of the columns during the analysis, where the inclusion of such a double strut model in SPO analysis revealed the shear failure in the column members for the strong infill, whereas for the weak infill an increased flexibility of the frames was observed. Therefore the impact of this on the collapse fragility is of particular interest given the prevalence of this failure mode in past earthquakes in Italy (see Section 1.1). The IDA results discussed in Section 5.3 showed that the double-strut models tended to report a higher maximum PSD than their single-strut model counterparts, which was noted to be an expected result due to the additional flexibility of the double-strut frames.

However, comparing the median collapse intensities illustrated in Figure 5.18, for both weak and strong masonry infill typology, the median collapse intensity of the double-strut is not always lower that the corresponding single strut model (i.e. more vulnerable to collapse) and in some cases slightly higher than the corresponding single-strut model (i.e. three story weak infill and four and six storey strong infill). This is a peculiar observation at first that somewhat contradicts the overall observations of the IDA results, where the double-strut models were actually more vulnerable in the sense that they showed higher deformation for a given intensity when compared in terms of the maximum of the peak profiles. To investigate this observation further, the displaced shape at a number of intensities have been plotted in Figure 5.19 and Figure 5.20 for the weak and strong infill typologies, respectively. For the noted cases above where the double-strut infill was shown to have a lower median intensity vulnerable than the corresponding single-strut model, Figure 5.19 shows that the two models have two differing deformed shapes at the various intensities plotted. That is, for the three storey frame with weak infill, the single-strut model shows a parabolic median displaced shape whereas the double-strut model seems to be concentrating the damage in the bottom two storeys. Similarly, for the strong infill, the four and six storey infill cases show two differing deformed shapes. Again consulting the median collapse intensities in Figure 5.18, for cases where the single and double strut models maintain the same deformed shape, the median collapse intensity of the double strut model reduces by up to 20%. However, in cases where the deformed shape is not the same between the two models, the consideration of the deformation and damage due to shear in the columns can sometimes lead to an increased median collapse intensity in some cases due to the modification of the damage mechanism of the structure. This observation highlights the importance of appropriate numerical modelling of all of the anticipated mechanisms in the structures rather than simply relying on post-processing checks to determine whether the effects of column shear behaviour are relevant or not, since this approach inherently assumes that the deformed shape of a structure will be the same regardless of whether the shear behaviour is incorporated or not, which these cases highlighted here show to be not always the case. However, as was previously stated that for the case of the 3D case study frames, actually implementing such shear behaviour can become problematic and lead to difficulties in achieving numerical convergence.

Nevertheless, the impact of considering such a failure mechanism in the columns in cases where the deformed shape was the same between models showed how the median collapse intensity can be significantly affected, as has been demonstrated on numerous occasions during past earthquakes in Italy.

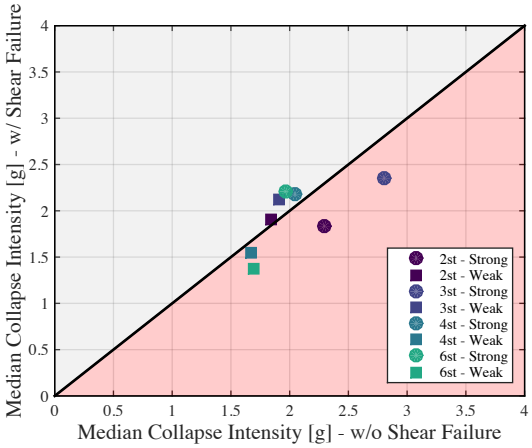

Figure 5.18. Comparison of the median collapse intensities for the single and double strut models for both weak and strong infill typologies.

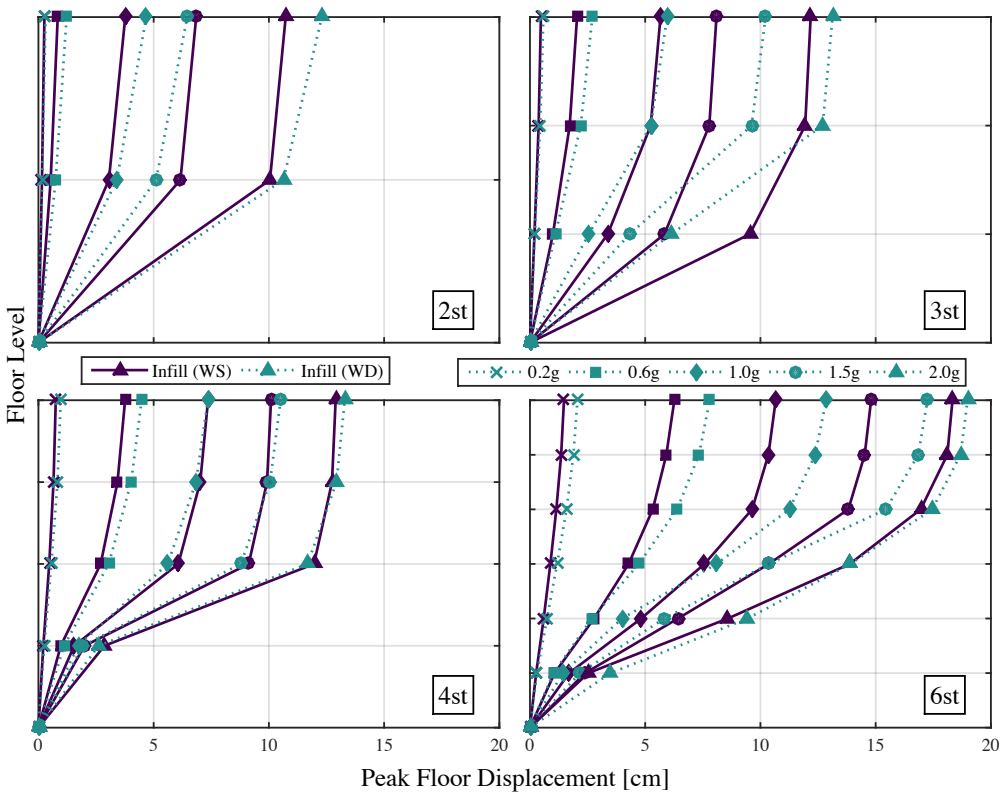

Figure 5.19. Comparison between the median peak displaced shape profiles of the non-collapsing cases for the 2D single-strut and double-strut infill models for the weak infill typologies at intensities of $S_a(T^*)$ of 0.2g, 0.6g, 1.0g, 1.5g and 2.0g, respectively.

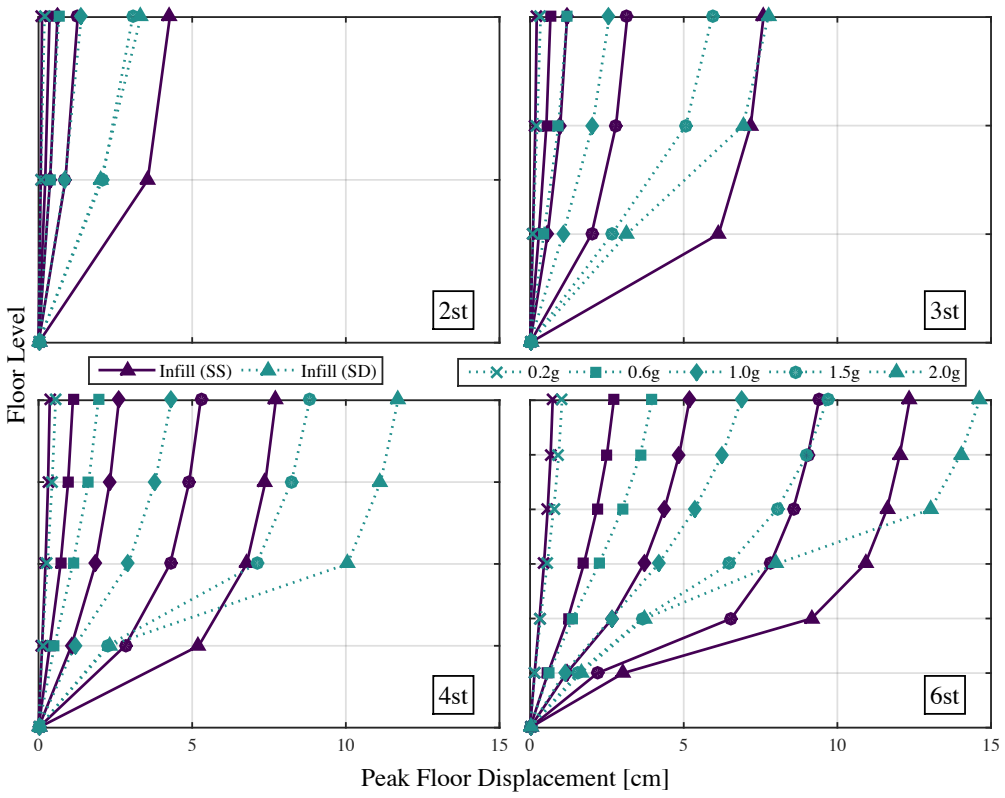

Figure 5.20. Comparison between the median peak displaced shape profiles of the non-collapsing cases for the 2D single-strut and double-strut infill models for the strong infill typologies at intensities of $S_a(T^*)$ of 0.2g, 0.6g, 1.0g, 1.5g and 2.0g, respectively.

5.4.2 Estimating the Collapse Fragility using the SPO2IDA Tool

While the previous section outlines how the collapse can be estimated using the data obtained from IDA followed by a fitting of the collapse fragility with respect to intensity using a maximum likelihood fit, a simpler way of estimating the collapse fragility is examined here in the SPO2IDA tool outlined by Vamvatsikos and Cornell [2005]. This tool, illustrated in Figure 5.21, takes the SPO curve and by defining a multi-linear backbone, determines an IDA trace using a series of empirical expressions related to the definition of the input multi-linear backbone. This approach worked remarkably well for a tool of its simplicity in the illustrative examples discussed in Vamvatsikos and Cornell [2005], with the 16th and 84th fractile traces also being well represented. As such, it would be of great interest to be able to estimate the collapse fragility function (defined as the flat line of the IDA trace) using such a simplified method, where in combination with more simplified

methods to be outlined in Section 7.2.1 both the performance conditioned on collapse and non-collapse of a structure can be estimated with reasonable accuracy without the necessity of advanced numerical models and extensive NRHA.

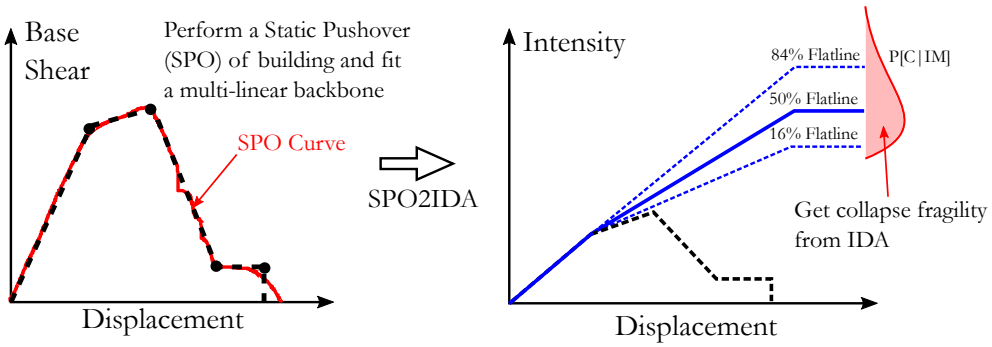

Figure 5.21. Estimation of the collapse fragility function from the IDA curves generated using the SPO2IDA tool described by Vamvatsikos and Cornell [2005].

Following the above approach, the SPO2IDA tool is applied to each of the 2D case study frames to examine the applicability of such a simplified tool to GLD frames with masonry infills. These are compared in terms of the median collapse intensity and the dispersion, which is computed from the 16% and 84% flatlines using:

$$\beta_{RC,IM} \approx \frac{\log(IM_{84\%}) - \log(IM_{16\%})}{2} \qquad \textbf{Equation 5.1}$$

where this term corresponds to the anticipated dispersion due to record-to-record variability. The median collapse intensity is computed by reading off the 50% flatline in Figure 5.21 and is compared with the median intensities described in the previous section for the various structural typologies. It should be noted that the median collapse intensities and dispersion discussed here are compared to those illustrated in Figure 5.15, where the modelling uncertainty adjustments outlined in Chapter 4 for collapse are not considered as the IDA and SPO analysis were both conducted using deterministic models.

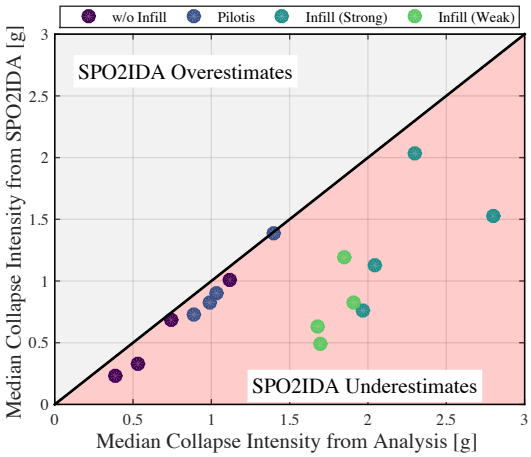

Figure 5.22. Comparison of the median collapse intensity computed from NRHA with that estimated using the simplified SPO2IDA tool for the various structural typologies.

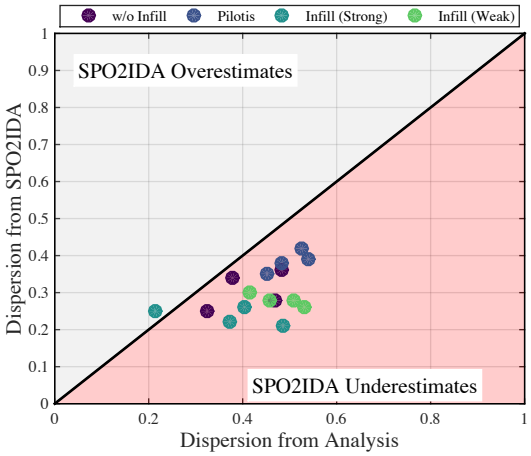

Figure 5.23. Comparison of the dispersion computed from NRHA with that estimated using the simplified SPO2IDA tool for the various structural typologies.

Figure 5.22 and Figure 5.23 illustrate the comparison between the two approaches for the median intensity and dispersion, respectively. Regarding the dispersion, the SPO2IDA tends to underestimate the dispersion in most cases - especially for the infilled frames. In the case of the median collapse intensities, the frames modelled without infills and the pilotis frames tend to be estimated well by SPO2IDA, albeit a little conservative, whereas the infill frames are not well represented at all. This difference arises due to the fundamental difference in behaviour of the frames, where for the frames modelled without masonry

infill and the pilotis frames, the first mode dominates the response and a first mode SPO is representative of the dynamic response of the building as per the requirements of SPO2IDA outlined in Vamvatsikos and Cornell [2005]. In the case of the infilled frames, however, the first mode response is not necessarily representative at all ductilities as the exhaustion of the masonry infill capacity at one or more storeys results in a fundamental change in response to cause a period shift in addition to a modification of the first mode behaviour. The presence of the infill alongside the RC frame results in the presence of two "yield" displacements of the frame corresponding to the yielding of the infill and the yielding of the frame. In fitting the SPO2IDA curve to the SPO backbone, the first yield point to be matched in the case of the infilled frames will be the peak capacity, which in the original definition of the hysteretic behaviour by Vamvatsikos and Cornell [2005] represents the point to which ductility will be measured. This means that the frame ductility is being expressed as a function of the infill peak force displacement rather than the actual yield displacement. This represents a confusion in definitions for which the SPO2IDA was not initially developed. As a consequence, the error in estimating the median collapse intensity should be a somewhat expected result.

Such an error in estimating the collapse fragility for GLD frames with masonry infill using SPO2IDA was also recently observed by Cardone and Perrone [2016], where the median collapse intensity was noted to be much lower when compared to the number of actual collapses noted from NRHA, which agrees with the findings of Figure 5.22. Cardone and Perrone [2016] noted this discrepancy between the estimated collapse fragilities and the actual percentage of collapses in the NRHA but refrained from investigating the cause of this inconsistency further. Instead, the authors conducted a sensitivity study whereby the influence of median collapse intensity on the EAL of the case study structure was compared. It was shown that the EAL for the specific building examined was relatively insensitive to an increase in median collapse intensity, but this insensitivity actually arose due to the median collapse intensities falling within the range where the structure had already reached a total expected loss ratio of unity. As a result of this apparent insensitivity, Cardone and Perrone [2016] go on to suggest, but not explicitly state, that SPO2IDA may be used in estimating the collapse fragility for GLD frame structures with masonry infill. This has been shown to be not the case in Figure 5.22 for numerous buildings and is noted as an area in which further development is required for simplified tools in the assessment of GLD frames with masonry infill.

5.5 Assessment of Limit States

Similar to the way the collapse fragilities were established in the previous section, the limit state drifts from SPO analysis defined in Section 5.2 can be used with the IDA results to determine the number of exceedances per intensity and generate a corresponding fragility function set using the maximum likelihood method described in Baker [2015]. These drift

limits are noted here to be deterministic values and do not consider the possible dispersion in the drift capacity of a limit state or the potential correlation between demand and capacity, as discussed in Cornell *et al.* [2002]. This was done for simplicity and aims to replicate prescriptive drift limits specified in guidelines to assess the performance of a building.

Applying this to each of the case study frames results in numerous plots and therefore the results will be condensed down for comparison and commentary, where the complete set of data is included in Appendix A. First, however, an example of the application and resulting plots for 2D frame with weak infill typology and the 3D frames without the infill modelled are shown in Figure 5.24 and Figure 5.25. Similar to the collapse fragilities presented in Section 5.4, the number of exceedances of the limit state are plotted using the markers at each intensity and the fitted lognormal cumulative distribution plotted around it. The clear progression between limit states with respect to the seismic intensity can also be observed, where for the case of the 3D frames with no infill the first operational limit state (SLO) is exceeded very early in each case, whereas the 2D weak infill cases show a slightly higher level of resilience to this limit state. In addition, the definition of the collapse prevention limit state (SLC) as the point corresponding to the 20% drop in maximum base shear shear seems to be an adequate definition here since comparing the fragilities of the SLC limit state and the actual collapse fragility function computed from IDA it can be seen that in each case, this SLC limit state provides a margin of safety against actual collapse of the structure, since the median collapse intensity is a degree higher than the SLC's one in each case, although the quantitative impact of such a difference will be highlighted in later sections though time-based assessment.

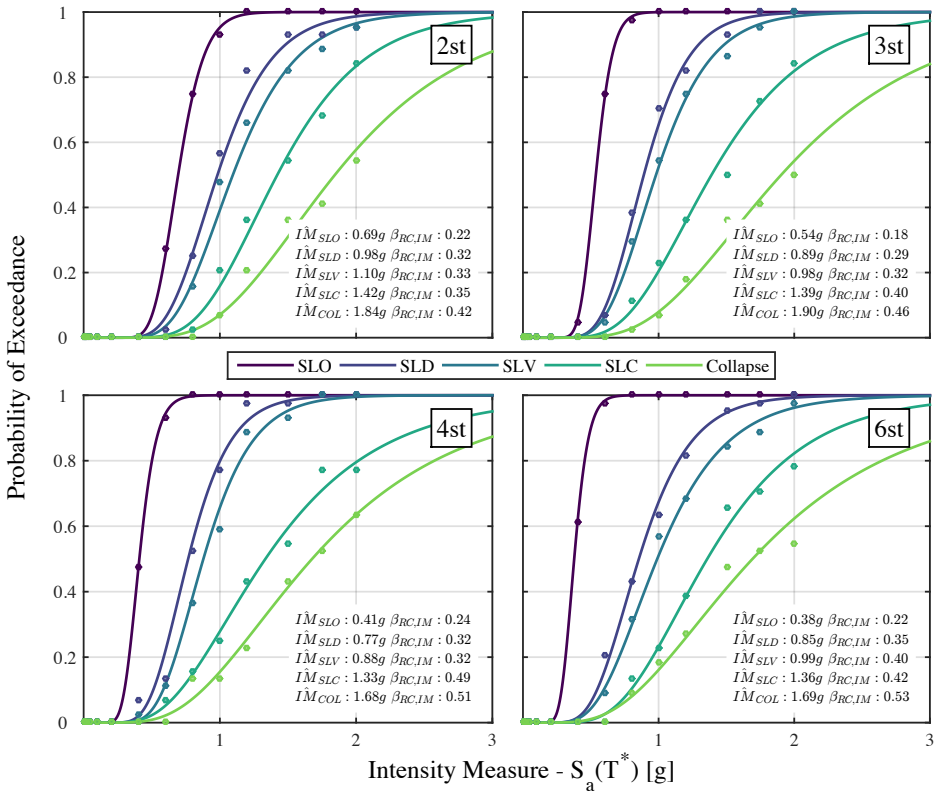

Figure 5.24. Limit state fragility curves for the 2D structures with a single-strut model for weak masonry infill typology. The fragility functions are fitted using the maximum likelihood method and are shown along with the actual data (dots) obtained from each stripe of the IDA. Note: These limit state fragility functions account for record-to-record variability in the demand ($\beta_{RC,IM}$) and do not include the modelling uncertainty ($\beta_{UC,IM}$).

Following a similar procedure for each of the case study frames, the median and dispersions of the fitted lognormal distributions will be examined to observe some overall trends in the results. Figure 5.26 shows a number of subplots of the normalised median intensities for each building of a various number of storeys in each column and each limit state along the rows, where the individual subplots compare the actual model variations. Again, these are normalised by the intensity 2500 year return period in order to make the median values comparable between buildings. Figure 5.27 shows a similar plot for the corresponding dispersions.

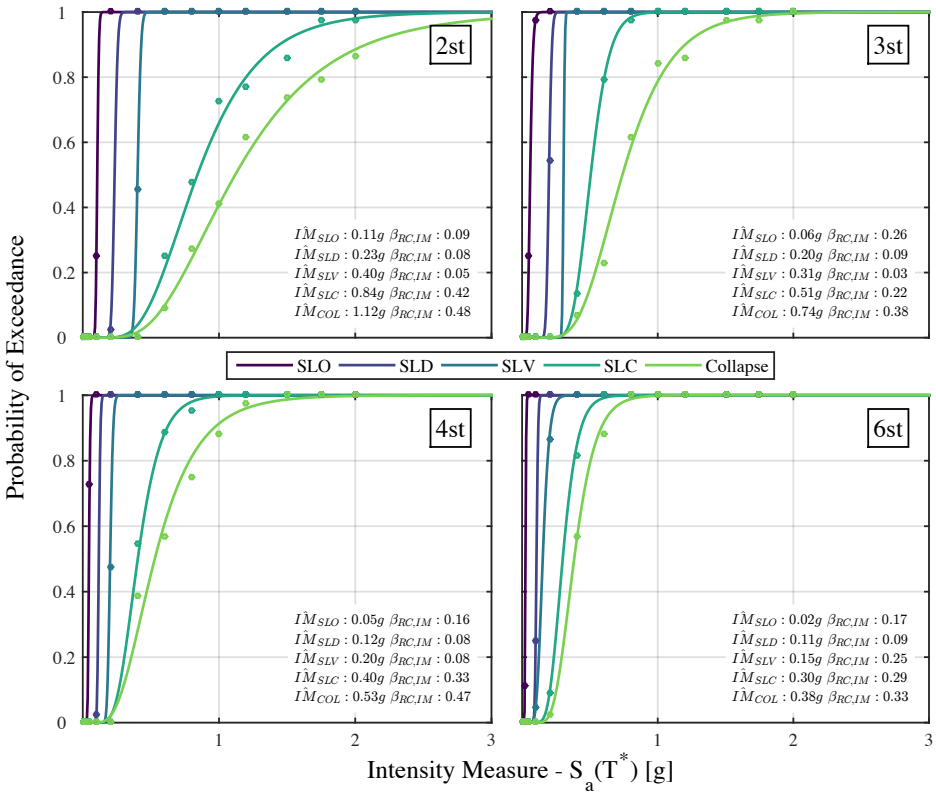

Figure 5.25. Limit state fragility curves for the 2D frame structures with no infill modelling. The fragility functions are fitted using the maximum likelihood method and are shown along with the actual data (dots) obtained from each stripe of the IDA. Note: These limit state fragility functions account for record-to-record variability in the demand ($\beta_{RC,IM}$) and do not include the modelling uncertainty ($\beta_{UC,IM}$).

By examining the influence of number of storeys on the various limit state medians in Figure 5.26, it can be seen that for SLO, SLD and SLV in particular, the median intensity tends to decrease with increasing number of storeys, possibly indicating the increased impact of P-Delta effects on the collapse capacity of the buildings. In addition, the relative progression of limit state median intensity for the frames without infill or pilotis frames is much larger than that of the infilled. In short, once the infilled frames reach the first limit state, it does not require much more intensity to achieve the next few whereas, for the pilotis frame this increment between limit states is much larger. This is a consequence of the initial intensity required to damage the infills followed by the sharp post-peak drop in strength and stiffness observed in SPO analysis.

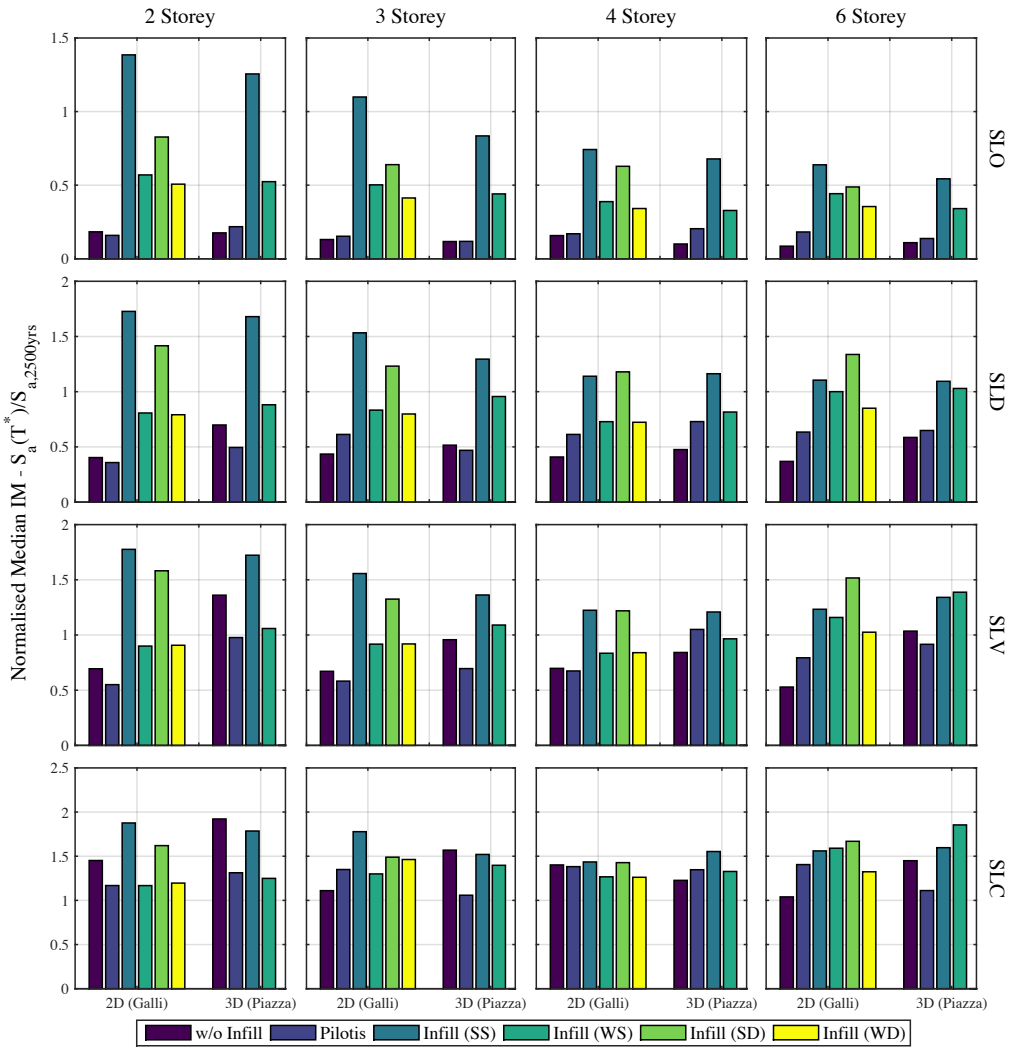

Figure 5.26. Normalised median intensity for the identified limit states of the case study structures. Note: These limit state fragility functions account for record-to-record variability in the demand ($\beta_{RC,IM}$) and do not include the modelling uncertainty ($\beta_{UC,IM}$).

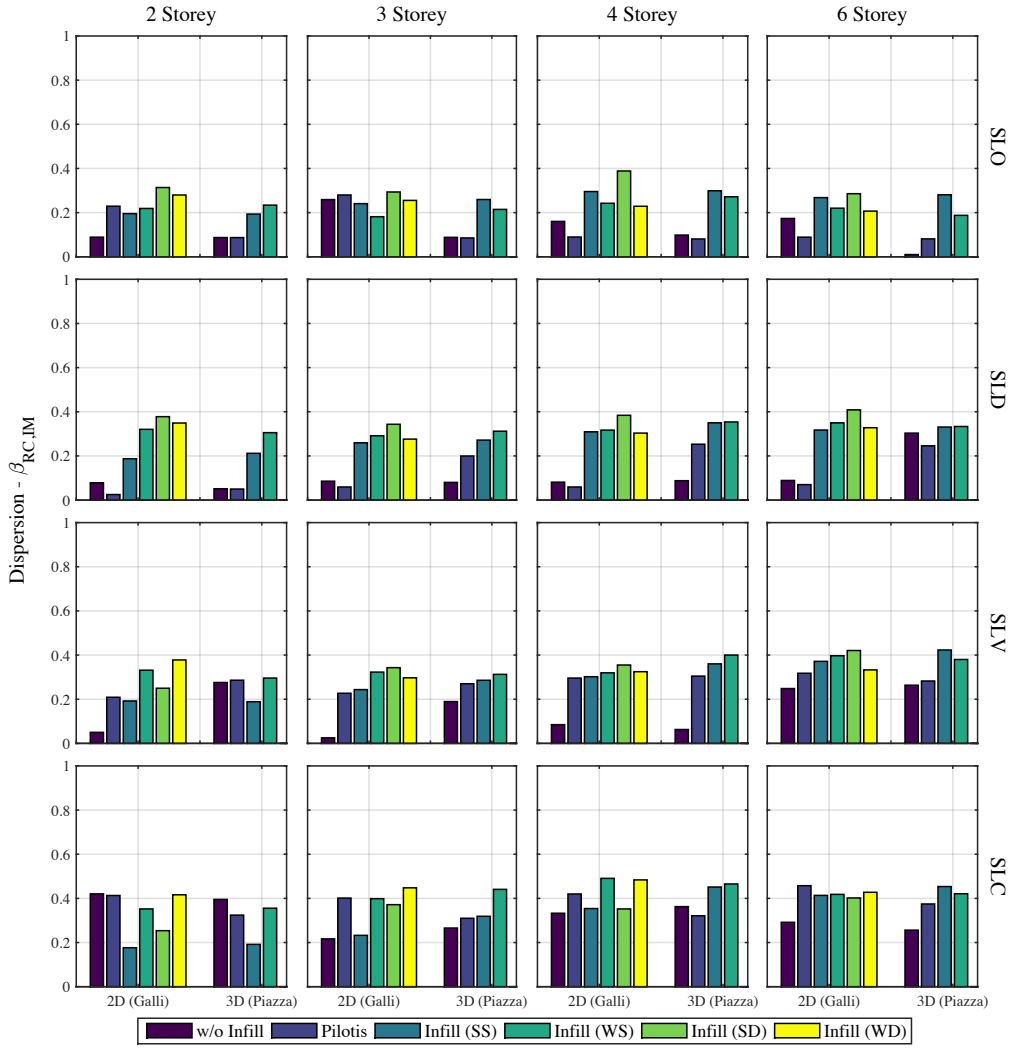

Figure 5.27. Dispersions for the identified limit states of the case study structures. Note: These limit state fragility functions account for record-to-record variability in the demand ($\beta_{RC,IM}$) and do not include the modelling uncertainty ($\beta_{UC,IM}$).

In general, it can be noted that many of the trends identified in the previous section for collapses are also valid here. For example, the same trends in median intensities are seen when comparing the single and double-strut infill models, with the double-strut models being on average more vulnerable than their single-strut counterparts, where some

exceptions are noted. These exceptions correspond to the same cases investigated further in Section 5.4 where it was seen how the change in deformed shape between strut modelling approaches resulted in the double-strut models forming a mechanism at a different location in the building. Regarding the dispersions presented in Figure 5.27, the values presented here are what would typically be expected with the lower limit states such as SLO and SLD showing relatively low dispersion due to the structures responding predominantly in the elastic range; whereas the higher limit states such as SLC and collapse show a higher degree of dispersion since the structure is behaving in the highly nonlinear response region and possibly leads to an increase in uncertainty.

These results presented here permit the identification of different limit states with respect to seismic intensity, although such intensity levels will be somewhat limited to the case study frames examined in this study. This identification permits the validation of more simplified methods to identify the intensity (and subsequently probability of exceedance) of various limit states using more simplified methods to be discussed in Section 7.2. Secondly, the results presented here can also be tentatively used with mean hazard curve to compute the MAF of exceedance to both compare and validate other simplified methods, which will be discussed in Chapter 7.

5.6 SUMMARY AND CONCLUSIONS

This chapter examined the response of a number of different structural typologies typical to GLD RC frames in Italy. A number of case study buildings were analysed using various analytical methods to quantify the performance for further examination in the next chapters and also to study the influence of various parameters on the response of such buildings. Regarding the performance of older GLD RC frames with masonry infill, the following comments can be made regarding their overall behaviour:

- Overall, the structural typologies examined exhibited rather non-ductile modes of response such as column-sway mechanisms, column shear failure and beam-column joint mechanism, as was highlighted in Section 1.1. Each of these mechanisms are characteristic to GLD RC frames with masonry infill and differ from modern construction where proper detailing rules and design considerations result in structures with more stable damage mechanisms. As such, assessment of such older structures should properly account for this behaviour and recognise that approaches developed for new construction is not necessarily applicable to existing buildings.
- The response of frames modelled with masonry infill was completely modified with respect to models void of masonry infill. This was shown to be not only in terms of lateral capacity but also in the damage mechanism formed, where the presence of strong masonry infill along with double strut infill modelling clearly

illustrated the issue of shear failure in the columns, which has been observed on numerous occasions during past earthquakes. This confirms what is now widely known that frames with masonry infill cannot be conservatively assessed by ignoring the effects of infill on the response.

- The response of the 2D and 3D structures were shown to be quite similar in terms of their overall deformation demands and collapse capacity. As such, it is concluded that for more detailed parametric studies conducted throughout this thesis, the use of the 2D frames will suffice in illustrating the various arguments examined.
- The modelling of the aforementioned shear behaviour of the column members to capture the effects of shear damage due to interaction with the masonry infill on the response was discussed. It was shown how the overall flexibility of the frames tended to increase slightly - increasing the first mode period by up to 15%. In terms of damage mechanism, it was shown via SPO how the failure of the columns in shear for the strong infills resulted in a reduced base shear capacity of the frame along with a reduced overall lateral capacity. This impact of the direct shear hinge modelling was also noted during the collapse assessment where, generally speaking, the inclusion of a double strut infill model with shear hinges in the columns resulted in a decrease of up to 20% in the median collapse intensity. The impact of this on the MAF of collapse will be examined in later chapters. In some cases, however, the shear deformation in the columns resulted in a change in the collapse mechanism in the structures resulting sometimes in an increased collapse median.
- The limit states outlined in the Italian code NTC 2008 were also applied to the case study buildings to identify the exceedance of each limit state with respect to intensity and therefore generate fragility functions for the various structural typologies. These limit states, in addition to the overall collapse of the structure, have been quantified and can be used in combination with appropriate modelling uncertainty considerations and representation of hazard to assess the further implications of such definitions of performance on MAF of exceedance and expected monetary losses in future chapters.
- It was shown how the use of the simplified SPO2IDA tool to compute the collapse fragility does not work for all of the structural typologies discussed here. For pilotis frames and frames without infill, the tool worked very well in terms of predicting the median collapse intensity when compared to actual collapse data obtained from NRHA and is therefore deemed fit for purpose. However, the presence of the masonry infill modifies the backbone such that the SPO2IDA significantly underestimated the collapse capacity of the structure. For a given hazard curve, this would translate as an increased MAF of collapse, which would be conservative. But using such a conservative collapse fragility in loss estimation studies can lead to situations where losses due to collapse can begin to dominate and inflate the

expected loss when the actual loss may be much less. Further work to expand this tool to frames with masonry infill needs to be conducted in the future.

6 ASSESSMENT AND RETROFITTING OF GLD RC FRAMES IN ITALY

O'Reilly, G. J., Sullivan, T. J. [2017] "On the Assessment and Retrofit of Existing Italian RC Frames with Masonry Infill," *Journal of Earthquake Engineering* (Under Preparation).

6.1 INTRODUCTION

This chapter builds on the analysis conducted in Chapter 5 to carry out a loss estimation study and present the impacts of different modelling decisions for GLD frames in terms of direct losses. By first taking each of the structural typologies and assuming a structural and non-structural element inventory, the expected loss with respect to intensity can be established to illustrate the relative vulnerability of each case study frame. These results are also used to conduct a time-based assessment of each of the structural typologies for various locations throughout Italy to examine the impacts of different modelling decisions on performance measures such as EAL.

In addition to the assessment of the existing vulnerability of the case study structures defined in terms of direct losses, a study is also carried out to examine the relative impact of different retrofitting measures. These retrofitting measures target the improved performance of both the structural and non-structural elements to illustrate how shrewd retrofitting of non-structural elements that are contributing most to the expected loss can result in better overall performance. This is highlighted in terms of the EAL and probability of collapse of the various retrofitting strategies to demonstrate how their overall effectiveness could be evaluated in terms of expected loss rather that relying on code defined storey drift limits to ensure satisfactory performance of the building at the damage limitation and life-safety limit states. Finally, an examination of the expected losses at each of the limit states outlined in the current assessment guidelines in Italy is discussed to illustrate how for the case of GLD RC frames with masonry infills, significant economic losses can be induced at the serviceability limit states so as to leave the building in a state of damage much worse than the descriptive performance the codes aim to provide.

6.2 ASSESSMENT OF EXISTING CASE STUDY BUILDINGS

This section carries out an assessment of the different case study frames previously examined. This is done both in terms of the life safety requirements outlined in current codes such as NTC 2008, in addition to examining the direct monetary losses in the

buildings through the detailed consideration of the damageable elements in the buildings to compute the expected levels of damage and subsequently direct losses due to repair costs. The following sections examine how the collapse safety of the case study buildings is first verified for three different hypothetical site locations in Italy, followed by the loss assessment of the buildings to quantify their performance in terms of direct monetary losses should the life safety requirements be met.

6.2.1 Collapse Assessment

In order to evaluate the collapse performance of each of the buildings examined here, the collapse requirements outlined in FEMA P695 [2009] are adopted to check that the probability of collapse does not exceed a prescribed level of 10% at the MCE intensity. This is done by taking the collapse fragility functions for each of the case study buildings developed in Section 5.4 along with the proposed adjustments to median and dispersion to account for modelling uncertainty proposed in Section 4.5.1, to compute the probability of collapse at the MCE intensity level.

As the GLD RC frames analysed here have no seismic provisions incorporated into the design process, these are anticipated to be representative of RC frame buildings throughout Italy constructed prior to 1970, as prior to then structures such as these were sized to resist gravity loads only. Therefore, three different hypothetical site locations are chosen here to examine the relative performance of the case study structures at different levels of seismic hazard. These three sites are listed in Table 6.1 along with the INGV ID numbers[5]. The INGV database [Montaldo and Meletti, 2007] provides seismic hazard data for a number of periods of vibration and return periods.

Table 6.1. Location and ID number of each of the different hypothetical site locations according to the INGV online database.

Site	Region	INGV ID
L'Aquila	Abruzzo	26306
Napoli	Campania	32979
Reggio Calabria	Calabria	45211

The NTC 2008 collapse prevention requirements are specified as 5% probability of exceedance in the specified reference period, which can be taken to be 50 years assuming

[5] http://esse1-gis.mi.ingv.it/

a Class II usage. The gives a return period of 975 years for the collapse prevention requirements of NTC 2008 assuming a Poisson distribution. Contrasting this value to that typically adopted in FEMA P695, which utilises a return period of 2475 years, the intensity is somewhat lower. This difference may be due to the disparities in expected seismicity between Italy and California, although this is not the focus of the study described herein. In order to maintain consistency with the collapse prevention return periods prescribed in NTC 2008 for Italy, a return period of 975 years is adopted here and the probability of collapse at this intensity is determined for each frame and checked against the prescribed limit of 10%. Figure 6.1 shows this comparison for each of the hypothetical site locations investigated, where the general trend is that the buildings meet the collapse criteria, with the exception of a few pilotis frames and frames without masonry infill modelled slightly exceeding. This compliance is noted for the two sites of relatively high seismicity in L'Aquila and Reggio Calabria, whereas for the relatively lower seismicity at Napoli the criteria are easily met. It should be noted, however, that these probabilities of collapse may be considered slightly conservative as the effects of spectral shape on the collapse fragility were not accounted for. Accounting for this effect tends to increase the median collapse intensity, which if applied here would be seen not to change the overall conclusions. It is noted, however, that if the 2475 year return period intensity had been used, it is likely that the criteria would not be met, but this is beyond the scope of this work. The principal conclusion drawn here is that for the three sites examined, the majority of the case study buildings tend to satisfy the NTC 2008 collapse prevention criteria defined in terms of collapse risk, although those violating tend to just slightly exceed the limits for the 2D frames, which will be examined in the next sections. As such, the performance of the 2D structures is considered reasonably satisfactory to the point where structural invention does not appear necessary in order to meet the collapse prevention criteria and the structures can now be examined in terms of the expected losses, which is the focus of the subsequent sections.

6.2.2 Overview of Loss Estimation of Case Study Frames

As previously mentioned, this section builds on the case study structures examined in Chapter 5, where in combination with an assumed inventory of damageable structural and non-structural elements, the expected loss versus intensity of each structure examined can be computed and discussed as part of a general vulnerability assessment of the different structural typologies. This loss estimation is conducted using the TOMS software tool discussed in Chapter 3 that utilises the PEER PBEE methodology described in Chapter 1. These loss estimation results are discussed here in terms of the influence of the various numerical modelling aspects, in addition to highlighting how by identifying the prominent sources of direct economic losses in the different structures, more informed decisions regarding the retrofitting of these structures can be made, which is discussed further in Section 6.3. From the vulnerability functions established for each structural typology, a

time-based assessment is conducted by the hypothetical site hazard at the three site locations listed in Table 6.1 in order to illustrate some of the impacts of the different retrofitting measures on EAL of the structures.

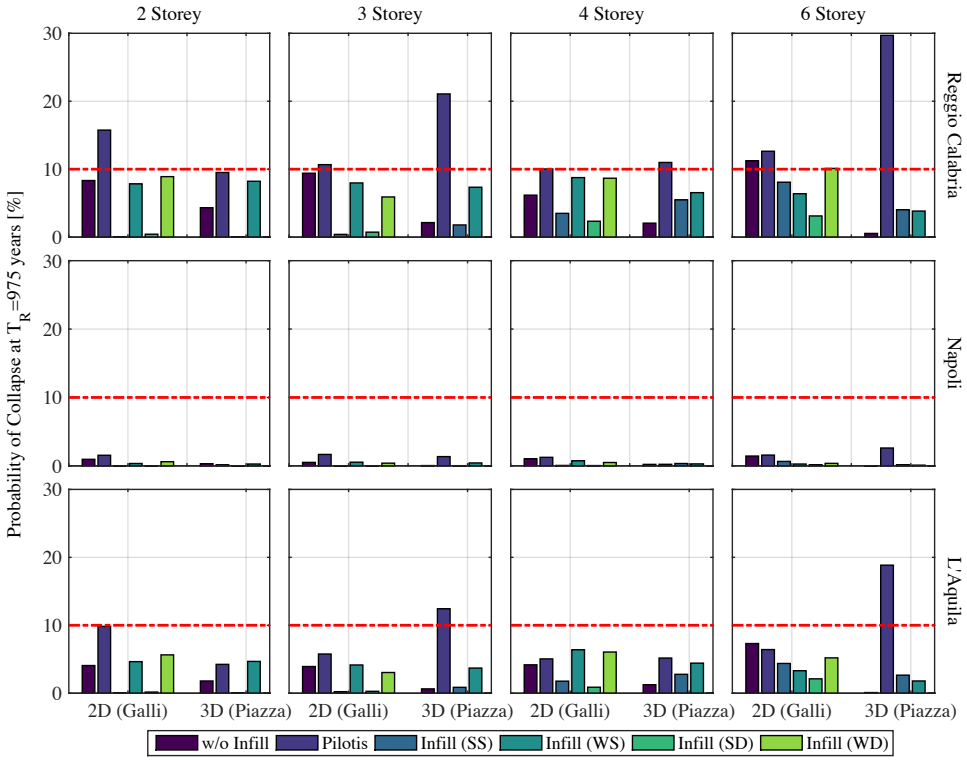

Figure 6.1. Probability of collapse for the different case study buildings that is checked at T_R=975 years to not exceed a value of 10% marked in red, as per the FEMA P695 [2009] guidelines.

The following subsections discuss some of the assumptions made regarding the building damageable inventories used for the loss estimation, such as the types of damageable elements, assumed fragility functions and associated repair cost functions. It should be noted here that this study focuses on direct economic losses that arise from repair and replacement of damaged components, where other aspects such as indirect losses and downtime are not discussed and deemed beyond the scope of this thesis. The inclusion of these aspects are not anticipated the general conclusions outlined here as this chapter focuses on the relative performance of the structural system and it's associated damage using different retrofitting techniques and additional considerations within the context of GLD RC frames in Italy.

6.2.3 Structural and Non-Structural Element Inventory

For each of the case study structures described in Section 5.1, a standard inventory of damageable structural and non-structural elements has been assumed. Table 6.2 provides a typical list of damageable elements considered and in each instance, the demand parameter to which they are assumed to be sensitive. It is noted that the masonry infill is listed in Table 6.2 as being sensitive to PSD only, although it has been shown by Morandi *et al.* [2013], among others, to be a function of the interaction of both in-plane (IP) PSD deformation and out-of-plane (OOP) acceleration of the wall whereby the infill can be expected to collapse (i.e. DS4 as per Sassun *et al.* [2016]) in the OOP direction if the OOP acceleration required to eject the infill is attained. In order to incorporate this combined effect of the fragility function being linked to two different demand parameters, detailed considerations are required. For example, Barrera *et al.* [2016] implemented a scheme whereby a rainflow cycle counting method of tracking the PSD in the frame with respect to time during the earthquake and reducing the OOP collapse resistance defined in terms of acceleration based on the magnitude of the current maximum of the rainflow cycle count of the IP PSD. While such a consideration is very useful and advantageous in terms of its comprehensive attention to the potential OOP failure of the infill, its implementation into assessment software, such as TOMS or PACT, is not currently available due to the specific data which would be required to be input and processed individually on a wall by wall basis such that in order to incorporate this type of approach in the process illustrated in Figure 3.4, further developments are required. Should these results be considered manually outside of the software used to implement the loss estimation with a view to incorporating the damage estimates at a later state, difficulties would arise in accounting for the additional dispersion due to modelling uncertainty that is aggregated into the simulated demands shown in Figure 3.5, which can be very influential when considering the magnitude of the typical values of dispersion for infilled frames observed in Chapter 4. More recently, however, Kohrangi *et al.* [2016] considered the combined effect of the PSD and OOP acceleration on infill collapse by determining the probability of damage as a function of the as-recorded peaks of both PSD and PFA without considering the time-history response individually. Kohrangi *et al.* [2016] investigated the influence of considering the impact the OOP failure on the EAL of three case study GLD RC frame structures versus the case where the infill collapse is considered sensitive to IP deformation only, which is assumed here. Kohrangi *et al.* [2016] concluded that the consideration of the OOP collapse of the masonry infill during the damage assessment had a relatively small effect on the EAL of the buildings examined, with no significant or obvious trend noted. This may be due to the different contributions to the EAL of a structure tending to saturate at the lower intensities of response where the annual probability of exceedance is much higher. If the OOP collapse of the infill is not very prominent at these lower intensities where the EAL tends to saturate, then the impact of the OOP collapse of the infill would not be expected to be significant, as noted by Kohrangi *et al.* [2016]. This observation, of course, applies to the

direct losses associated with repairing the building damage and does not consider the additional impact of the OOP collapse of the infill on the indirect losses due to loss of functionality or potentially fatal consequences of masonry infill falling from the building onto the street level below. In this respect, it is clearly an important issue but considering that the focus of this study is the relevant differences of direct losses associated with repair cost only, in addition to the observation by Kohrangi *et al.* [2016] with respect to its observed influence on EAL, the additional consideration of the OOP failure of masonry infill is not expected to have an impact on the conclusions of the study presented herein.

Table 6.2. List of damageable structural and non-structural elements for assessment of case study buildings.

Damageable Elements	Demand Parameter
Structural Elements	
Non-Ductile Columns	Peak Storey Drift
Exterior Beam-Column Joints	Peak Storey Drift
Interior Beam-Column Joints	Peak Storey Drift
Non-Structural Elements	
Exterior Masonry Infill (No Windows)	Peak Storey Drift
Exterior Masonry Infill (with Windows)	Peak Storey Drift
Interior Masonry Partitions (Doors)	Peak Storey Drift
Internal Partitions & Finishes	Peak Storey Drift
Ceilings and Lighting	Peak Floor Acceleration
Hot & Cold Water Piping	Peak Floor Acceleration
Windows	Peak Storey Drift
Elevators	Peak Floor Acceleration
HVAC & Air Handling	Peak Floor Acceleration

Once the list of damageable elements in the structures has been established, three further pieces of information are required - the quantity of each particular damageable element; an appropriate set of fragility functions to assess the probability of each damage state for a given demand; and an appropriate set of repair cost functions that can be used to estimate the expected repair costs associated with each damage state. Table 6.3 lists this information for both 2D and 3D case study buildings, along with the quantity of each damageable element in addition to the sources for both the fragility functions and repair cost functions. It is noted that in the case of the 2D case study structures, the entire damageable element inventory is assessed using the structural analysis results from the single direction analysed. This is a simplifying assumption that assumes that similar structural response is to be

expected in both directions of the structure and that reasonable estimates of economic loss can be obtained for such regular buildings.

In Table 6.3, each of components quantity, corresponding fragility and repair cost functions are listed along with the actual ID of each element in the original source publication. For the 2D and 3D case study buildings, quantities of each element were estimated based on the size of buildings where the usage could be considered that of a commercial office or a public school building. The types and typical quantities of each of the elements were based on judgement following building surveys conducted on a number of school buildings in Italy, to be discussed further in Chapter 8. One important note to make regarding some of the elements is for the case of the PFA sensitive elements such as the suspended ceilings, the same total quantity is assumed in both directions of the building as these are classed as non-directional elements, meaning that they can be damaged by the demands from either direction and are not sensitive to demand in a unique direction of response. As such, the total quantity of each non-directional element is defined in both orthogonal directions and the associated repair costs to be used in the final loss estimation will be taken as the maximum of the two directions of response. It is noted, however, that a consistent treatment of directionality effects such as that discussed in Nievas and Sullivan [2016] is not within the scope of this research, but a relevant issue nonetheless.

Another more general note regarding the non-structural elements in the structure is that these elements have been intentionally selected as having no seismic design provisions, such as bracing of the ceiling or piping systems, or protection of acceleration sensitive equipment via special snubbers etc. This was done so as to be more representative of the observed non-structural detailing of older structures in Italy, where seismic design considerations were not even adopted for the actual structure not to mention the non-structural elements. Hence, the assumption of such poorly detailed non-structural elements. Section 6.3 looks to investigate the relative impact of improving these non-structural element details on the overall performance of the structure.

It is further noted that many of the assumed fragility and repair cost functions are taken from the PACT fragility library [FEMA P58-3, 2012], which has been largely developed for use in the US. In order to make the repair cost functions applicable to older Italian buildings examined here, an equivalent conversion between average construction costs in the US and Italy for 2013 was utilised in such cases. This conversion was carried out with the assistance of a consulting engineering firm in Italy, where the costing manuals from both countries were used to give the best estimation of the repair cost conversions. The resulting average ratio between the two construction costs in 2013 was found to be 1.22 times the US cost, which also takes into account the currency conversion from the same year. While it would be ideal to derive such costing functions from scratch using Italian costing manuals, such an approach was deemed beyond the scope of this thesis due to the vast amount of

information and experience required. As such, the equivalent conversion utilised here may be thought of as a suitable compromise for the comparative studies presented herein and is not envisaged to have an effect on the overall conclusions of this work.

Table 6.3. Inventory list of the damageable structural and non-structural elements with the corresponding assumed quantities, fragility and repair cost functions for the case study buildings.

Damageable Elements	Quantities			Fragility and Repair Cost Functions
Structural Elements	2D	3D-X	3D-Y	
Non-Ductile Columns	12	12	12	Cardone [2016] - DWC (continuous)
Exterior Beam-Column Joints	14	6	8	Cardone [2016] - EWJs (end hooks)
Interior Beam Column Joints	10	6	4	Cardone [2016] - IWC
Exterior Masonry Infill (No Windows)	60m^2	33m^2	27m^2	Cardone and Perrone [2015] - EIW
Exterior Masonry Infill (Windows)	60m^2	33m^2	27m^2	Cardone and Perrone [2015]- EIW_w
Interior Masonry Partitions (Doors)	24m^2	12m^2	12m^2	Cardone and Perrone [2015]- IP_d
Non-Structural Elements				
Internal Gypsum Partitions	100ft	50ft	50ft	FEMA P58-3 [2012] - C1011.001a
Internal Gypsum Partition Wallpaper Finish	100ft	50ft	50ft	FEMA P58-3 [2012] - C3011.001a
Internal Gypsum Partition Ceramic Tile Finish	100ft	50ft	50ft	FEMA P58-3 [2012] - C3011.002a
Suspended Ceilings	1065ft^2	1065ft^2	1065ft^2	FEMA P58-3 [2012] - C3032.001b
Cold Water Piping	1000ft	1000ft	1000ft	FEMA P58-3 [2012] - D2021.011a
Cold Water Piping Bracing	1000ft	1000ft	1000ft	FEMA P58-3 [2012] - D2021.013b
Hot Water Piping	1000ft	1000ft	1000ft	FEMA P58-3 [2012] - D2022.011a
Hot Water Piping Bracing	1000ft	1000ft	1000ft	FEMA P58-3 [2012] - D2022.011b
Glazed Windows	10	6	4	Sassun [2014] - Glazing Panels 1.0x2.5m
Lighting	15	15	15	FEMA P58-3 [2012] - C3034.001
Elevator	1*	1*	1*	FEMA P58-3 [2012] - D1014.012
HVAC In-Line Fan	2	2	2	FEMA P58-3 [2012] - D3041.002a
HVAC Ducting	2	2	2	FEMA P58-3 [2012] - D3041.011a
HVAC Diffusers	2	2	2	FEMA P58-3 [2012] - D3041.031a
HVAC Fan	1**	1**	1**	FEMA P58-3 [2012] - D3041.101a
Chiller	1*	1*	1*	FEMA P58-3 [2012] - D3031.011a
Air Handling Unit	2**	2**	2**	FEMA P58-3 [2012] - D3031.021a

*At ground level only

** At roof level only

In addition to the repair costs, an appropriate estimate of the replacement cost of each structure is required so that the contribution to the expected losses from the collapsing cases can be estimated, as per Equation 3.2. To estimate these replacement costs, available information in Italy following the 2012 Emilia-Romagna earthquake was used to find the typical cost of replacing a building per unit area in addition to the costs of demolition and removal of debris. Again with the aid of an Italian consulting engineering firm, the average replacement costs using the data obtained were found to be €1,805.75 per m^2 and an additional €95.50 per m^2 for demolition and removal of the existing structure, which are both inclusive of VAT, administrative and technical costs and the average discounts offered by construction companies. In addition to the replacement cost of the building, a threshold value must be defined that defines the ratio of expected direct loss to the replacement cost, for which the stakeholder would elect to demolish the building rather than repair the existing, heavily damaged one. FEMA P58-1 [2012] suggests a value of 40%, although more recent work by Cardone and Perrone [2016] examines actual reconstruction data following earthquakes in Italy. Cardone and Perrone [2016] note how that according to Dolce and Manfredi [2015], slightly higher cost ratios of between 60%-75% of the replacement cost were sustained following the L'Aquila earthquake of 2009. Using this information, a threshold value of 60% was adopted for all analysis discussed herein. This value considers the ratio of the direct losses to the overall replacement cost, where if the indirect losses were to be considered this value could be expected to somewhat lower. However, since this study focuses on direct losses, the adopted value of 60% is considered reasonable. Residual drifts are also incorporated by adopting a residual drift fragility curve with a median value of 1.5% maximum residual story drift with a dispersion of 0.3, as per Ramirez and Miranda [2009], to determine the situations where demolition is also likely due to excessive residual drifts in the structure.

For the actual loss estimation using TOMS, some further parameters need to be defined. The first of these is the number of demand simulations to be generated per intensity of the actual input demand data. Since TOMS employs a Latin Hypercube Sampling scheme, fewer demand simulations are required than what would be typically required from a Monte Carlo Simulation approach. Therefore, a total of 200 demand simulations are generated here per intensity. Another aspect of loss estimation in TOMS is the incorporation of modelling uncertainty in the demand simulations, which from the discussion presented in Chapter 4 are defined as per the proposed values given in Table 4.3 for the PSD and PFA demand parameters, respectively. In addition, the median and dispersion for the collapse fragilities presented in Section 5.4 for each structure were adjusted to account for modelling uncertainty using the proposed values given in Table 4.2.

Using the above information regarding the damageable inventory, fragility and repair cost functions, the above assumptions for the loss estimation in addition to the IDA results

presented in Chapter 5, the full loss estimation can now be conducted for each case study building. The following section presents and discusses the different aspects of the results.

6.2.4 Loss Estimation

Similar to the presentation of the IDA results, the loss estimation of each case study buildings results in a vast amount of information. As such, summary plots of the expected losses versus normalised intensity (referred to herein as vulnerability functions) are presented together and more specific plots of individual cases related to the discussion are presented to provide further details on the different comments and observations being made. As in the previous chapter, the intensity measure is normalised here by spectral acceleration corresponding to the 2500 year return period at the period of vibration closest to T^* available from the hazard information at the L'Aquila site in order to make the different buildings somewhat comparable. Figure 6.2 presents the vulnerability functions for each of the 2D case study structures in addition to a breakdown of the expected losses conditioned on no collapse for the two demand parameters examined here, while Figure 6.3 presents the same data for the 3D structures.

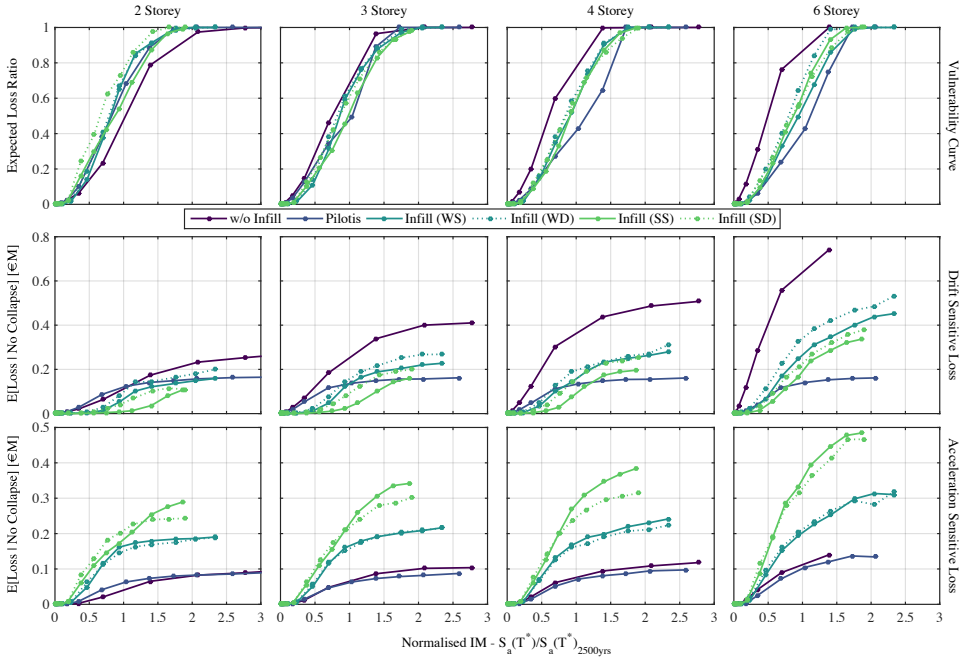

Figure 6.2. Expected loss versus normalised intensity and disaggregation of expected losses in terms of demand parameter for 2D case study structures.

By first comparing the vulnerability functions in Figure 6.2 and Figure 6.3, which plot the total expected loss from both collapsing and non-collapsing cases normalised by the replacement cost of the structure versus the normalised IM, the expected losses from both the 2D and 3D cases show similar trends. In the case of the pilotis frames, the contributions of the drift sensitive elements to the expected losses are capped by the same amount for each building. This is due to the formation of a soft-storey in the ground floor in each case meaning that the expected loss due to PSD tends to be capped by the repair cost associated with that floor. For the PFA sensitive losses, however, a similar trend can be observed where the expected losses tend to be capped for each of the buildings, although a slight increase in the case of the six storey frame can be noted. This could be due to the possible increased contribution of higher mode effects on the structure resulting in a slightly increased PFA profile to induce more damage to the components in the upper storeys. In addition, the increased column size at the ground floor of the six storey pilotis frames means that the storey yield acceleration has slightly increased, meaning that the soft-storey will allow the transmission of a slightly higher PFA to the upper floors.

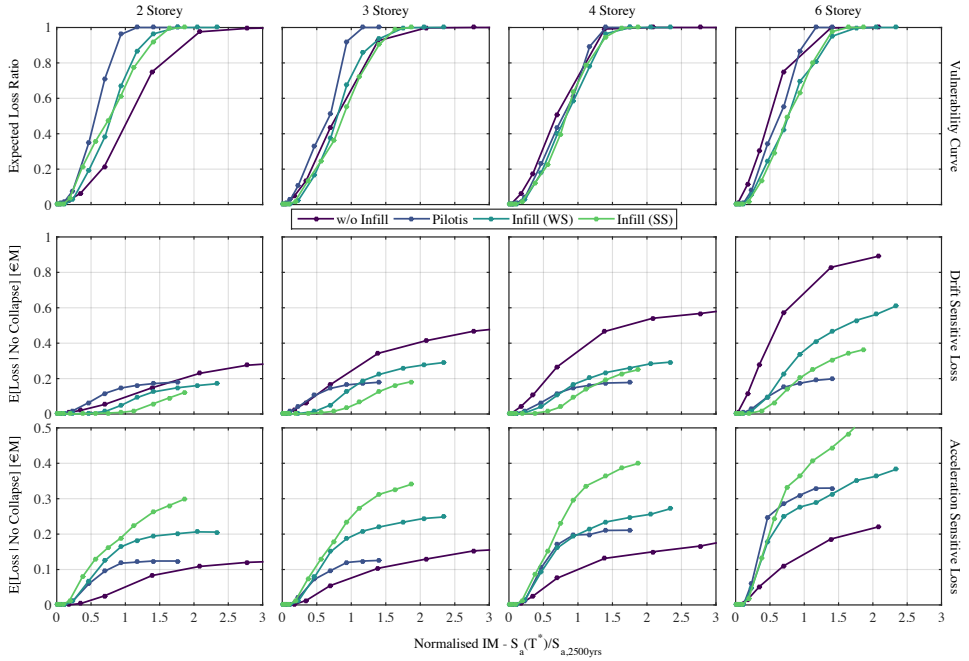

Figure 6.3. Expected loss versus normalised intensity and disaggregation of expected losses in terms of demand parameter for 3D case study structures.

In addition, the demand parameter plots show how the frames without masonry infill modelling tend to accumulate more losses from the drift sensitive elements compared to the infilled frames that accumulate a substantial portion from the acceleration sensitive elements. This can be further examined from the TOMS output that illustrates the disaggregation of losses both in terms of location within the building in addition to the contributing damageable element. In the case of the 3D three storey frame with no infill modelled, Figure 6.4 shows the disaggregation of expected losses for the non-collapsing cases at the different levels of the building, where the expected loss is similar in both directions of response of the structure. Further to the above comments, the general magnitude of the losses associated with the PSD is much larger than that of the PFA. Furthermore, the disaggregation of expected loss in terms of damageable element is illustrated for the same structure in Figure 6.5, where the most prominent sources of expected loss come from drift sensitive elements (e.g. wall partition finishes, columns and exterior and interior beam-column joints). While this is a somewhat expected result, it is highlighted here that such a disaggregation of expected losses is very useful for deciding how to improve the overall performance of the building, as it points out the biggest culprits in terms of expected loss and their corresponding location within the structure such that

effective retrofitting could be carried out with more accuracy and efficiency by targeting these elements.

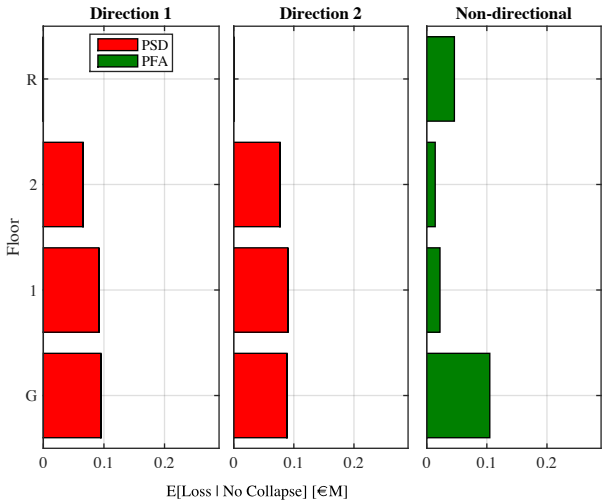

Figure 6.4. Disaggregation of expected loss given no collapse in terms of the location within the structure for the 3D three-storey frame structure modelled without masonry infill at an intensity of $S_a(T^*)=1.0g$.

Comparing the above observations with those of the infilled frames, Figure 6.2 and Figure 6.3 show that in the case of all infilled structures the PFA sensitive elements begin to dominate the expected losses of the structures, which makes sense intuitively as the addition of masonry infill tends to result in a stiffer building leading to higher floor acceleration than a corresponding frame modelled without masonry infill that tends to be more flexible. Again, this is examined through the disaggregation of the expected losses for the case of the 3D six storey strong infill frame in Figure 6.7. In contrast to the frame modelled without masonry infill presented in Figure 6.4, the PFA sensitive elements appear far more prominent with Figure 6.8 showing that these are mainly coming from the air handling units at the roof level, the suspended ceilings at each level and the chiller located at the ground floor. The slight increase in the contribution of the roof components at the top storey and roof level is also a reflection of the large roof amplification due to second mode contribution, where the contribution of higher modes means a "kick-out" in PFA results that is reflected in the loss contribution in Figure 6.8. This again highlights the principal differences in the behaviour of the frames with no infill modelling and fully infilled frames not just in terms of dynamic response to GMs, but also the difference in the most vulnerable components in the respective structures. These observations regarding the dominance of the acceleration sensitive elements to the overall damage has been observed

during past events in Italy, where EERI [2009] reported that while many older RC buildings with infills performed well from a structural and life safety standpoint, extensive damage to the interior elements such as infills, interior partitions, ceilings and piping were observed following the L'Aquila event in 2009, for example. One case highlighted in EERI [2009] was for the City Planning Offices in L'Aquila, which exhibited very little exterior building damage, but is seen from Figure 6.6 to have significant damage to these aforementioned non-structural elements.

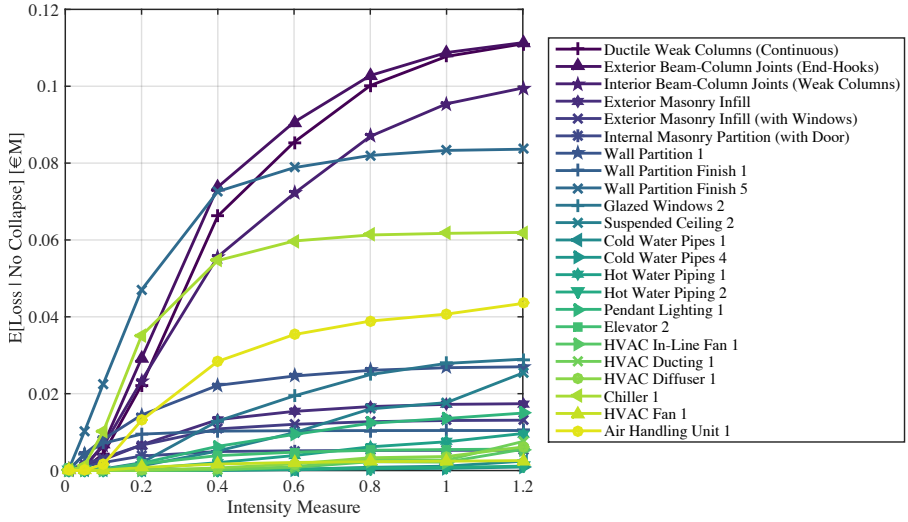

Figure 6.5. Disaggregation of expected loss given no collapse in terms of damageable element for the 3D three-storey frame modelled without masonry infills.

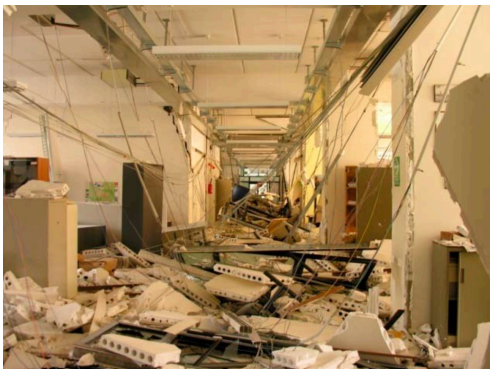

Figure 6.6. Illustration of the observed non-structural element damage to the City Planning Offices in L'Aquila, whose building was noted by EERI [2009] to have sustained very little detectable damage to the exterior.

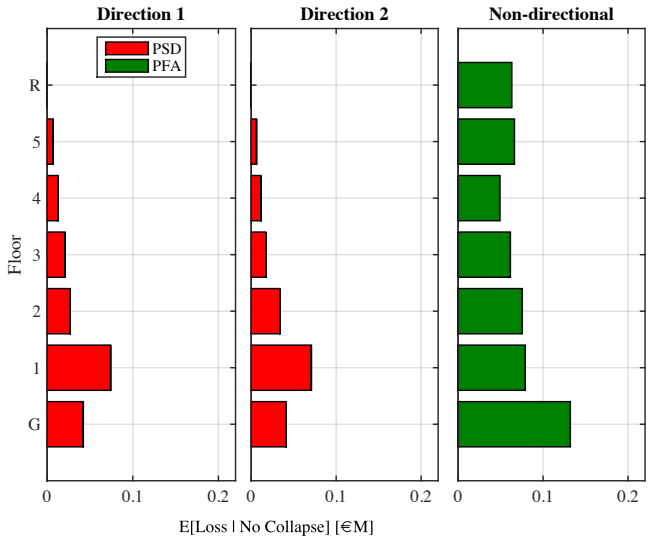

Figure 6.7. Disaggregation of expected loss given no collapse in terms of the location within the structure for the 3D six-storey strong infill frame structure ($S_a(T^*)$=1.2g).

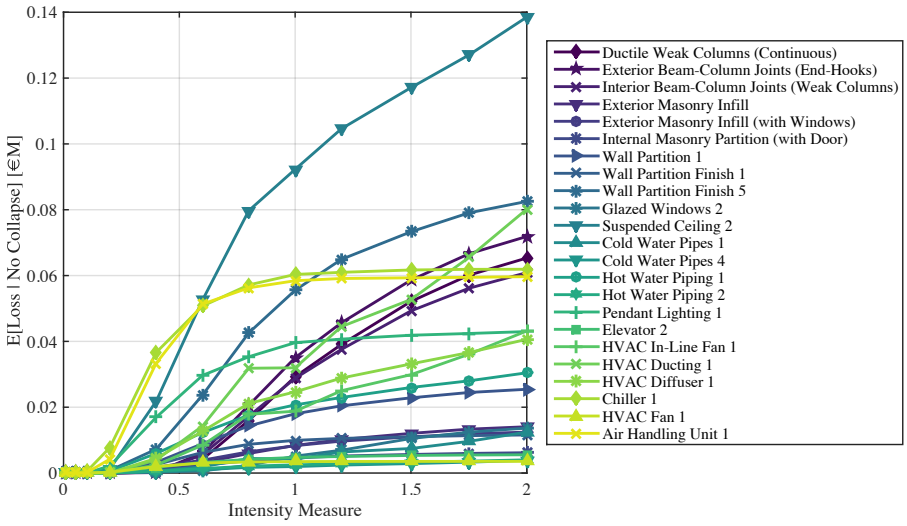

Figure 6.8. Disaggregation of expected loss given no collapse in terms of damageable element for the 3D six-storey strong infill frame structure.

Some other observations regarding the influence of the infill typology and modelling techniques can be drawn from the plots of Figure 6.2 and Figure 6.3, where the use of a double strut model for both infill typologies results in a similar trend in overall expected loss accumulation, but the double strut models being slightly more vulnerable in each case. However, the breakdown of expected losses in terms of demand parameter is shown in Figure 6.9 shows how the single strut models accumulate more acceleration sensitive losses while the double strut models tend to accumulate more in the drift sensitive elements. This conclusion agrees with the overall findings of the SPO and IDA results that previously showed how the structures with double strut models tended to be slightly more flexible than their single strut counterparts. Again, this highlights the importance of proper modelling of the anticipated shear behaviour in the columns.

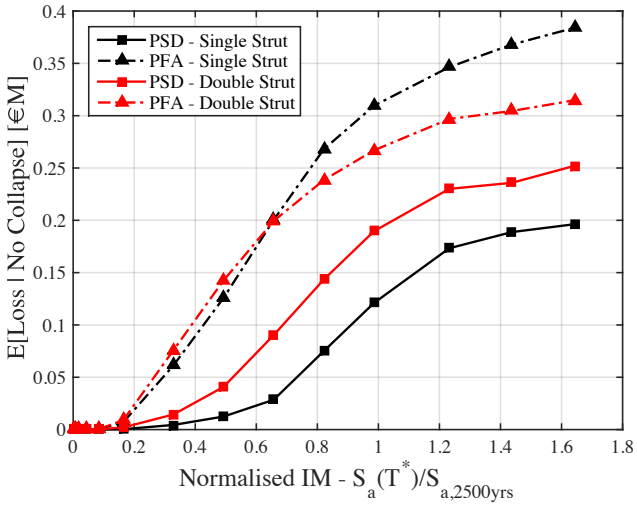

Figure 6.9. Comparison of the expected loss as a function of demand parameter for the three storey frame with strong infill modelled using both single and double strut infill approaches.

This section has presented the initial loss estimation of each of the case study buildings and discussed some of the main observation between the relative performances of the different models with respect to the observations from structural analysis. It was shown how depending on the structural typology in question, the source of expected loss differed both in terms of location within the building in addition to the actual damageable component source, which corresponded well with damage observations following the 2009 earthquake event in L'Aquila. This was highlighted through the various expected loss disaggregation plots produced by TOMS and noted how such information may be used to guide engineers and stakeholders on more effective and economical solution to improving the performance of the structure when considering expected losses as the DV to be reduced, as discussed

previously in Section 3.3.3.4. The results presented here will serve as the basis for a number of structural and non-structural retrofitting solutions for the case study structures to be examined in Section 6.3.

6.2.5 Time-Based Loss Assessment

In order to conduct a time-based assessment of the case study buildings using the vulnerability functions presented in the previous section, a site hazard is required in order to integrate the expected losses with a mean hazard curve to obtain the EAL. By doing this the overall performance of each building typology can be evaluated and compared more directly as the vulnerability function is combined with the hazard associated with each building's intensity measure. Using the hazard for the three hypothetical site locations outlined in Table 6.1, the expected loss can be integrated with the respective mean hazard curve according to Equation 1.2 to give the EAL of the structure. As for the actual implementation of Equation 1.2, the numerical expansion of this expression described as "Method 1" in Porter *et al.* [2004] is followed to compute the EAL ratio, which is the EAL normalised by the replacement cost of the building including demolition and removal of debris. The resulting EAL for each of the case study frames are presented in Figure 6.10. While the magnitude of the EAL of the different structural typologies is a very useful decision making metric in PBEE, the values in Figure 6.10 should be treated with care since these are case study buildings with an estimated damageable inventory and an assumed seismicity. As such, the relative differences and trends in the EAL of the different structural typologies are of more interest here than the specific EAL values for GLD frames in Italy. Given this, comparisons with EAL for non-ductile RC frame structures from studies such as Liel [2008] are not possible for a number of reasons, including differences in the actual definition of "non-ductile" between countries, but also because the seismicity is typically expected to be higher for California in addition to the assumptions regarding the replacement costing and the buildings damageable inventory will undoubtedly differ. Nevertheless, the values presented here are of particular use to examine the relative trends and comparative differences in EAL for some of the different modelling assumptions outlined in Chapter 5, in addition to how one could identify the prominent sources of expected losses from disaggregation plots.

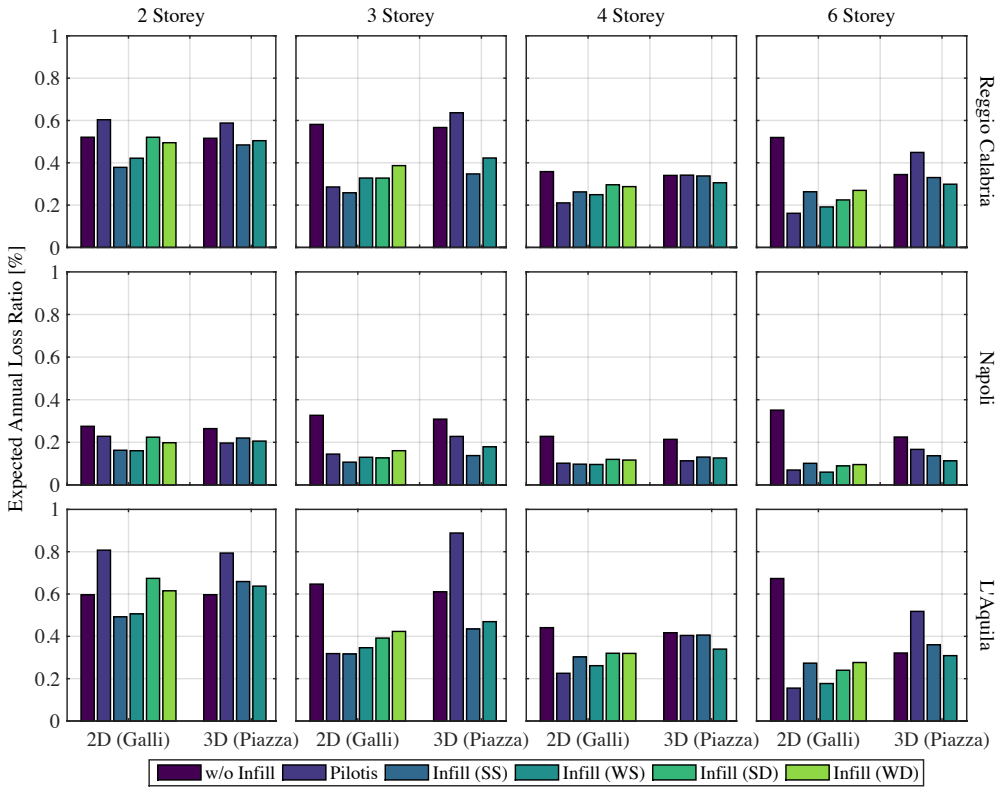

Figure 6.10. EAL for each of the case study buildings examined for the hypothetical site locations considered.

Examining some of the trends for the different buildings, the EAL with respect to the number of storeys is plotted in Figure 6.11, where a similar trend to that identified in Calvi *et al.* [2014] is seen where the EAL tends to decrease with respect to the number of storeys. This is a somewhat expected result, especially in GLD frames examined, as a concentration in damage at a single or a confined number of storeys results in a relatively small estimated loss when compared to the replacement cost that is normalising it.

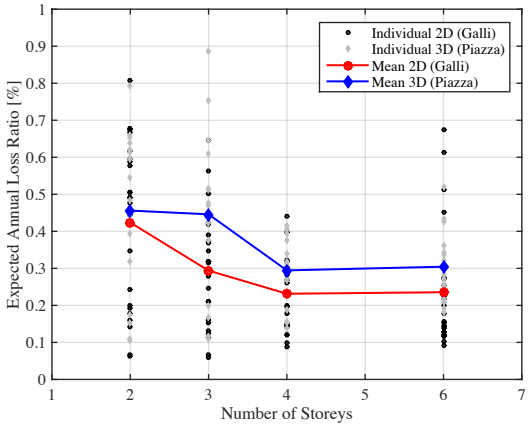

Figure 6.11. Illustration of the trend of EAL with respect to the number of storeys for each of the case study frames, where the mean ratio of all typologies considered shows the decrease of EAL with increasing number of storeys.

Another interesting observation is presented in Figure 6.12 where a comparison of the EAL ratio between the frames with no infill modelled and the corresponding infilled ones is shown. This is of interest, as it shows no specific trend between the expected losses in frames both with and without infill modelling such that the loss estimation from a bare frame can not be applied even in the presence of masonry infills, therefore highlighting the importance of infill modelling. This is obviously due to the differing sources of direct losses discussed in Section 5.3, where frames with no infill modelled tended to accumulate loss from drift sensitive components whereas the infilled frames were more sensitive the floor acceleration induced damage. This is a somewhat expected remark, but important to highlight. Figure 6.13 compares the EAL for the infilled frames both with and without shear hinge modelling in the columns. This was previously shown in Chapter 5 to have a noticeable impact on both the response of the structure during SPO analysis, where the premature failure of the columns resulted in a reduced overall deformation capacity and also the collapse performance. By incorporating the shear behaviour of the column members, the EAL increases on average by over 30% with respect to the numerical models that omitted it. This is a significant increase that highlights the need for proper consideration of the shear failure of column members due to interaction with the masonry infill in GLD frames.

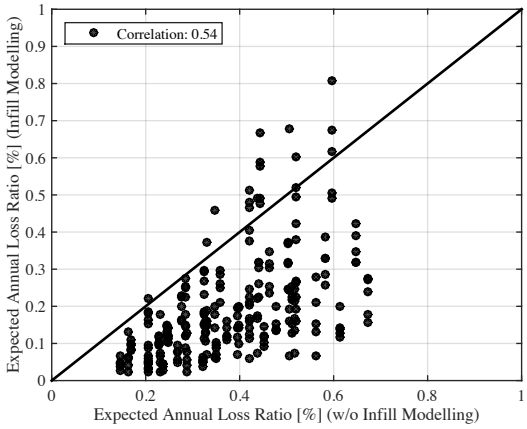

Figure 6.12. Illustration of the lack of a clear trend between the effects of modelling masonry infill on the EAL of the case study buildings.

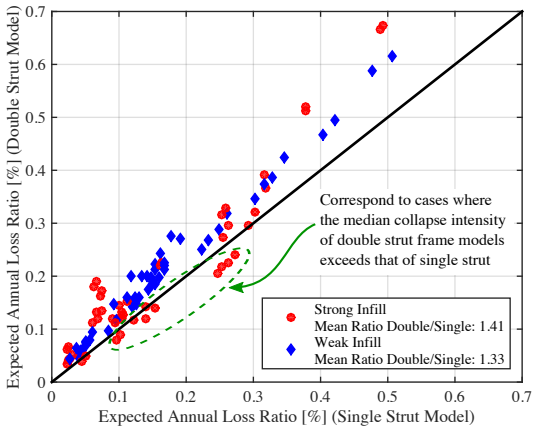

Figure 6.13. Illustration of the influence on the EAL of modelling the shear failure in column members of GLD RC frames with masonry infill.

6.3 RETROFITTING OF CASE STUDY BUILDINGS

Following the assessment of the various building typologies discussed in the previous section, retrofitting of the structure may be required in order to comply with code or building owner's requirements in terms of expected performance, which could be either in terms of ensuring life safety during more rare earthquake events or to mitigate potential monetary losses from excessive damage during more frequent events. Examining the

collapse assessment of the buildings outlined in Section 6.2.1, it was shown how most buildings considered here met, or were quite close, the collapse criteria for the return period specified such that collapse was not established to be a significant issue that needed to be addressed via intervention. On the other hand, Section 6.2.5 examined the time-based loss assessment and highlighted the EAL for the different building typologies examined. Since no requirements regarding acceptable levels of EAL are currently available in design codes or guidelines, the evaluation of this level of expected loss rests with the client; who when considering the annualised losses induced in their structure may elect to retrofit their building to achieve a better performance. Retrofitting has traditionally implied that the structural elements are to be modified or upgraded to improve strength, stiffness or ductility capacity. Elnashai and Pinho [1998], among others, discuss different selective techniques to which the three aforementioned capacities of RC walls can be improved. Such retrofitting is intended to improve the performance of the structure, which is defined in Eurocode 8 [EN 1998-1:2004, 2004] in terms of the storey drift at the "damage limitation" limit state and the strength and ductility requirements and the "no-collapse" limit state. By controlling these two limit states, Eurocode 8 aims to provide adequate overall performance of the structure by both preventing structural collapse during rarer events and excessive damage during more frequent events. Similarily, NTC 2008 [NTC, 2008] specifies the satisfaction of both the SLU and SLE limit states, which refer to the ultimate limit states (SLV and SLC) and the serviceability limit states (SLO and SLD), respectively. The qualitative descriptions and compliance criteria for each of the limit states listed in NTC 2008 are discussed further in Section 6.5.

In light of the assessment results presented in Section 6.2, this section examines the impacts of using a retrofitting philosophy such as that outlined in NTC 2008 on the overall performance of the structure defined in terms of expected losses in addition to life safety of the building. This is carried out only for the 2D frames discussed in Section 6.2 for simplicity, as it is deemed based on the presented in the previous section that the loss estimates for the 2D case study frames are also representative of the 3D frames and can be used as an illustrative example. Section 6.3.1 first describes the different structural retrofitting solutions explored for the structures, where the sizing of such retrofits is in order to meet the requirements of NTC 2008 for both the serviceability and life safety limit states. The loss estimation procedure described in the previous section is then repeated and a comparison of the expected losses between the original frames and the structurally retrofitted frames is presented. Following this, non-structural element retrofit solutions are explored in Section 6.3.2 to examine the potential benefits of targeting selected non-structural elements in order to achieve the maximum impact in terms of reducing the expected loss. That is, the original structures are retrofitted solely in terms of the non-structural elements and a comparison of the expected losses is then carried out. It is envisaged that this approach of non-structural element retrofitting could be less invasive

on the actual structure usage, meaning that implementation would require a shorter timeframe with less interruption.

6.3.1 Structural Retrofitting

6.3.1.1 Overview of Structural Retrofitting

In order to meet the requirements of Eurocode 8, both the damage limitation and no-collapse limit states need to be satisfied. The no-collapse limit state requirements are defined in terms of maintaining a stable, ductile mechanism that avoids soft-storey failure and promotes a ductile mechanism with the appropriate strength hierarchy requirements. The damage limitation limit state, on the other hand, defines the performance requirements in terms of the PSD to avoid excessive damage to the non-structural elements. This section describes the implementation of two retrofitting solutions to the case study frames that consist of using RC jacketing of the column and beam-column joints or the insertion of an RC wall. In addition, it is assumed that case study frames with masonry infills will be retrofitted by means of a perimeter gap between the infill and the surrounding RC frame in order to isolate the infill from the frame and prevent it from impeding the response of the RC frame, as illustrated in Figure 6.14. As noted by Charleson [2008], however, cutting a perimeter gap around the masonry infill will reduce the OOP stability of the infill as the infill becomes free on three edges and restrained on only one. This problem can be rectified by the provision of OOP restraints such as perimeter clips shown in Figure 6.14 so that the overall OOP vulnerability of the frame can be assumed to be unchanged with respect to the original. Using this retrofitting approach for the masonry infills, it can be argued that this results in the situation where each of the case study frames will be responding as if it were a bare frame. Therefore, for simplicity in analysis, the frames previously modelled without infills are retrofitted using the two aforementioned approaches, where the RC jacketing of the columns and joints is intended to induce a beam-sway mechanism and avoid a soft-storey. This is done by ensuring the strength hierarchy at each joint satisfies the strong column-weak beam requirements of NTC 2008. The provision of an RC wall also means that a soft storey mechanism can avoided and a more stable mechanism will be ensured.

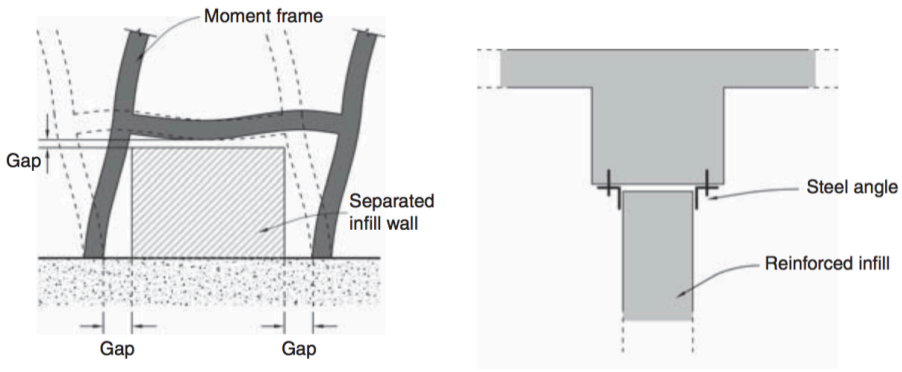

Figure 6.14. Provision of perimeter gap to isolate the masonry infill from the surrounding frame (left) and provision of steel angle to maintain adequate OOP restraint (right) (Adapted from Charleson [2008]).

In terms of sizing the actual retrofitting solutions, the RC jacketing, illustrated in Figure 6.15, is sized such that the strength hierarchy is maintained in accordance with the ultimate limit state requirements of NTC 2008. As such, no direct design calculations with respect to a design seismic hazard are required in the sense that the required moment capacities for the column and joints are determined from the comparison of the beam moment capacities and the strength hierarchy requirements. From this, it is assumed that an RC jacketing solution to achieve this capacity of each member is provided. This is then represented numerically by increasing all of the member moment capacities to the required values to assign the initially cracked member stiffness and assuming an elastic response, as illustrated in Figure 6.17. For the RC wall retrofitting, for which an example application is shown in Figure 6.16, in order to maintain some level of consistency with the RC jacketing solution, a single RC wall of length 5m, with thickness 250mm is provided to each frame, where the moment capacity of the wall is set such that the total base shear capacity of the structure is approximately equal to that of the RC jacketing solution. This is then represented numerically by adding a cantilever wall element with the required base moment capacity within each frame, as illustrated in Figure 6.17, where the hysteretic backbone parameters in terms of strength and stiffness degradation are estimated using the expressions provided in Haselton *et al.* [2008] for ductile, well-detailed members.

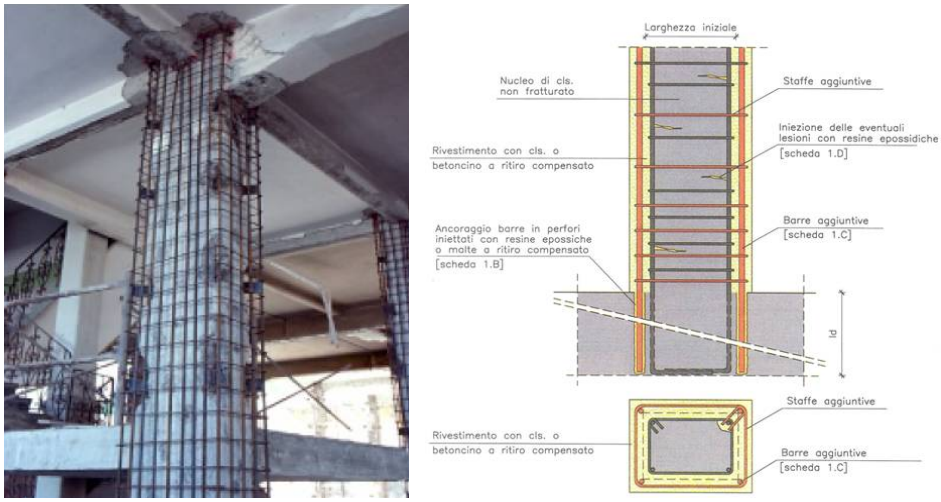

Figure 6.15. Illustration of the retrofitting RC columns and beam-column joints using an RC jacketing retrofitting strategy (Images from Prof. A. Masi and Dr. M. Vona of Università di Basilicata).

Figure 6.16. Illustration of the retrofitting strategy of inserting additional RC wall elements (Image from Prof. A. Masi and Dr. M. Vona of Università di Basilicata).

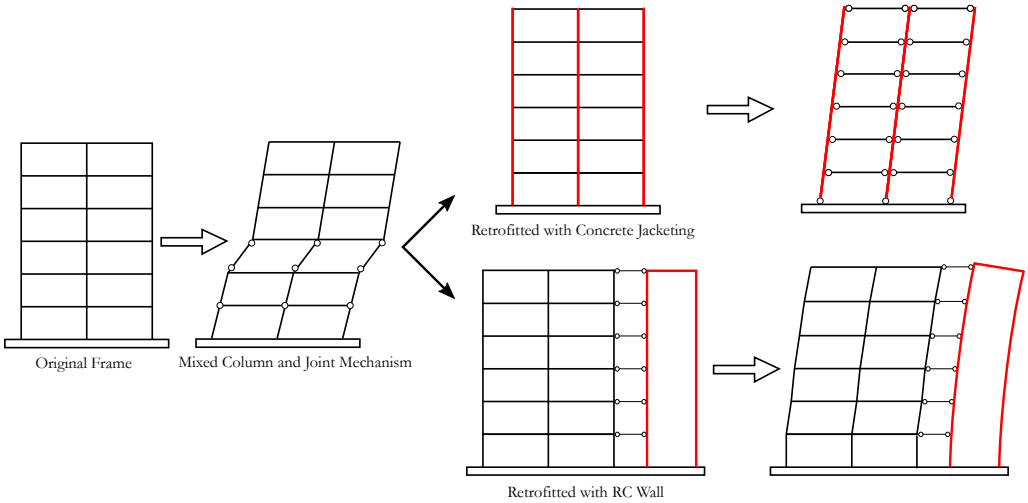

Figure 6.17. Illustration of two different structural retrofitting strategies, which involve either the RC jacketing of the columns and joints or the insertion of an RC wall.

Using this preliminary sizing of both the RC jacketing and RC wall retrofits, these were checked against the aforementioned code requirements at the serviceability and ultimate limit states. To do this, a design spectrum is required for the two limit states to check the respective requirements that are assumed to correspond to design return periods of 50 and 475 years for the serviceability and ultimate limit states corresponding to the prescriptions for SLD and SLV outlined in NTC 2008, respectively. The design spectra are constructed using the recommendation of the NTC 2008 and the PGA values required to construct the spectra are taken from the 2007 INGV hazard data available online [Montaldo and Meletti, 2007]. The site is taken to be located in L'Aquila as in Section 6.2, which has a PGA corresponding to 0.10g and 0.25g for the two limit states considered. The retrofitted structures are assessed using the N2 non-linear static procedure [Fajfar, 2000] outlined in Appendix B of Eurocode 8, which uses SPO analyses of each frame to determine the performance point with respect to the assumed design spectra. The structures are then checked at the performance points for both limit states to ensure the performance requirements are met. These performance requirements are taken to be that the maximum storey drift does not exceed 0.5% for damage limitation and that a stable mechanism results for no-collapse such that no soft storey mechanism is expected to develop. This is done by verifying that the chord rotation demands do not exceed the ultimate chord rotation capacities computed for the members of both structural typologies. For the RC wall, this was done by adopting the expression provided in NTC 2008 for the ultimate chord rotation of the expected hinge location at the base of the wall. For the RC jacketing retrofit, the ultimate chord rotation capacity of the beam members is computed using a similar expression but with the modifications proposed by Melo *et al.* [2015] described in Equation

2.4 to account for the effects of the non-ductile detailing and use of smooth reinforcing bars on the ultimate chord rotation of the beam members. Carrying out the various steps of the procedure, the expected drift profiles at the performance points are plotted in Figure 6.18 for both intensities considered, where the maximum storey drift has been successfully reduced below the 0.5% threshold specified for the damage limitation limit state for both retrofitting solutions. For the life safety limit state, the drift profiles have again been reduced, which when combined with a beam-sway mechanism in the concrete jacketing retrofit and the RC wall ensuring that a soft storey mechanism is to be avoided, results in the performance criteria being deemed to have been satisfied. It is noted, however, that the RC wall retrofitting for the two and three storey frames are slightly conservative. This is a consequence of the simplistic assumptions to sizing the retrofit solutions adopted, whereas in practice one would expect to further refine such a retrofit. This could potentially have the impact of increasing the floor accelerations due to this additional overstrength of the building.

For both of these structural retrofitting schemes outlined here, the complete set of NRHA analysis is performed once more as per Section 5.3 using the improved structural models to obtain the retrofitted structures response ordinates with respect to intensity that will be used to repeat the loss estimation.

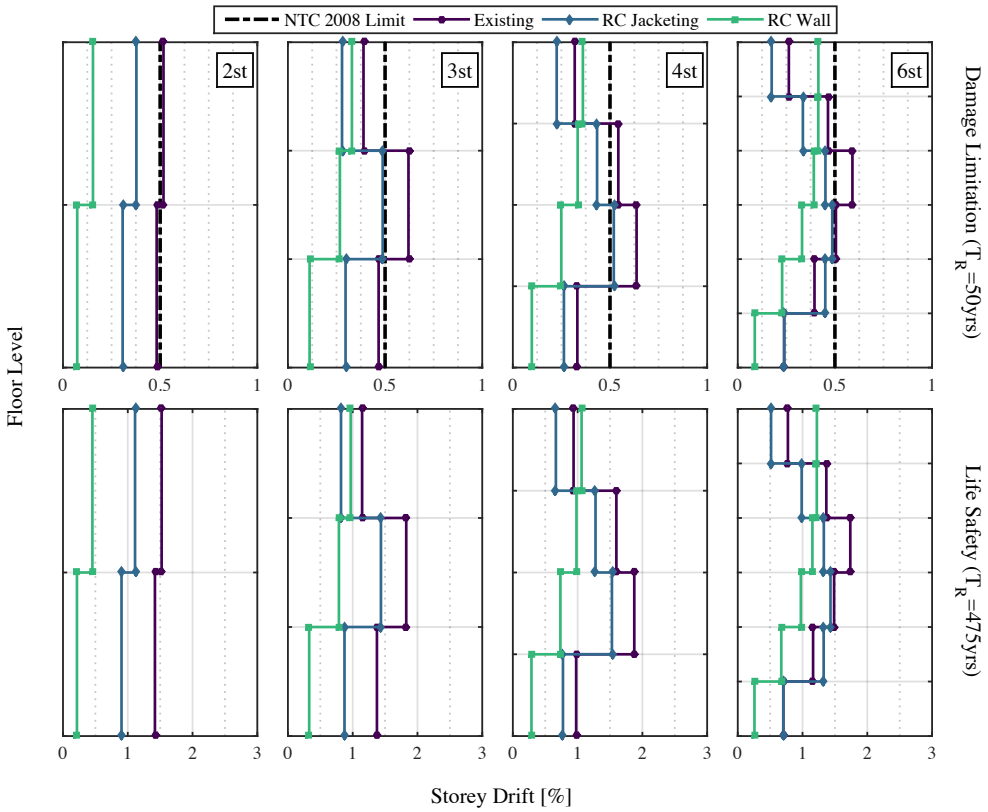

Figure 6.18. Evaluation of the two structural retrofitting solutions with respect to the performance requirements at the two limit states considered.

6.3.1.2 Structural Element Inventory

Using these two retrofitting solutions for the 2D case study frames, the loss estimation procedure outlined in Section 6.2.4 is repeated to examine the improvements in building performance defined in terms of expected losses. However, the list of damageable structural and non-structural elements needs to be updated since the performance of some elements and therefore also the fragility functions and associated repair functions has been improved. The retrofitting carried out in each case consists of either RC jacketing or insertion of an RC wall in addition to the perimeter gap-cutting of any masonry infills. Table 6.4 shows the fragility functions that will, therefore, be used to assess the RC jacketing retrofit cases, and Table 6.5 lists the corresponding RC wall retrofit inventory.

Table 6.4. Inventory list of the damageable structural elements with the corresponding assumed quantities, fragility and repair cost functions for the case of RC jacketing retrofitting.

Damageable Elements	Quantities	Fragility and Repair Cost Functions
Weak Exterior Beams	14	FEMA P58-3 [2012] – B1041.102a
Weak Interior Beams	10	FEMA P58-3 [2012] – B1041.102b

Since the structural elements in the existing frame have been upgraded for the case of the RC jacketing, a fragility function set is required to reflect the concrete jacketing of the column and beam-column joints to ensure a beam-sway mechanism in the frames. Therefore, the "Weak Exterior Beams" and "Weak Interior Beam" fragility functions have been adopted from FEMA P58-3 [2012] as they represent weak beams with strong joints and a strong column-weak beam strength hierarchy. In the case of the RC wall retrofitting scheme, the existing vulnerable elements such as weak columns and beam-column joints still remain but the addition of the RC wall needs to be considered. Similarly, the fragility function listed in Table 6.5 has been adapted from FEMA P58-3 [2012] to represent the additional RC wall element added to the structure. This fragility function defines the damage to the RC wall as a function of storey drift, which is acknowledged to be not without its limitations. More refined methods of assessment using the base hinge curvature in the wall, for example, would be anticipated to be a better demand parameter to estimate damage but is not the focus of the current study and the adopted fragility functions deemed appropriate for the comparative study discussed herein. In addition, adopting this fragility function assumes an RC wall section detailed to modern seismic detailing provisions, where adequate core confinement is provided through proper stirrup spacing in addition to ribbed reinforcing bars.

Table 6.5. Inventory list of the damageable structural elements with the corresponding assumed quantities, fragility and repair cost functions for the case of RC wall retrofitting.

Damageable Elements	Quantities	Fragility and Repair Cost Functions
RC Wall	32m^2	FEMA P58-3 [2012] – B1044.003
Non-Ductile Columns	12	Cardone [2016] - DWC (continuous)
Exterior Beam-Column Joints	14	Cardone [2016] - EWJs (end hooks)
Interior Beam Column Joints	10	Cardone [2016] - IWC

6.3.2 Non-Structural Retrofitting

6.3.2.1 Overview of Non-Structural Retrofitting

While the previous section looked to improve the overall performance by strengthening and stiffening the structures, this section looks to propose a set of non-structural retrofit solutions. This comes from the fact that a large percentage of the direct losses in a structure arise from damage to the non-structural elements, as highlighted in Taghavi and Miranda [2003]. Therefore, the most prudent solution when trying to mitigate expected loss in a structure is to reduce the vulnerability of such elements contributing most to its vulnerability. Compared to the case of structural retrofitting, non-structural retrofitting offers some benefits aside from those to be discussed in Section 6.4. Among these is the ease at which non-structural retrofits can be implemented with respect to structural retrofits. For example, to retrofit using RC jacketing previously discussed, one needs to uncover each element in the structure which can often times be buried behind partition walls or other fixtures and fittings. Following this, extensive work to prepare the existing structural element and insert the additional reinforcement and concrete needs to take place such that continued occupancy of the structure during retrofitting is unlikely to be possible. On the contrary, take the retrofitting of an air-handling unit placed at the roof level for example. A simple retrofitting solution such as insertion of isolators under the units could be conducted with relative ease. In addition, the insertion of additional piping bracing or ceiling system restraints can also be carried out relatively easily compared to a solution that requires a building remain unused while retrofitting is underway.

In addition to the relative ease of some non-structural retrofitting solutions with respect to structural ones, Section 6.4.3 will describe how in some cases, the EAL of a building retrofitted by strengthening and stiffening measures can actually result in situations where the reduction in PSD losses can be countered by an increase in PFA induced losses to result in an increased vulnerability and EAL. The concept of retrofitting the non-structural elements in a structure as a retrofitting option to reduce the expected losses in a structure has been previously trialled in Calvi *et al.* [2014], where the option of improving internal partition details to reduce their vulnerability to drift demand in a ductile RC bare frames was outlined conceptually. It should be noted, however, that retrofit of non-structural elements will mainly target the expected losses and in cases where the probability of collapse is unacceptably high, will not suffice. As such, this idea of retrofitting non-structural elements inherently assumes that the collapse requirements are met, which have been checked for the case study buildings examined here in Section 6.2.1. This section expands on this concept, whereby the expected losses in different structural typologies typical to GLD RC frames in Italy are to be examined, proposing ways in which the overall performance of these buildings can be improved by considering alternative retrofitting strategies that target both the drift and acceleration sensitive losses.

6.3.2.2 Non-Structural Element Inventory

Similar to structural element retrofitting, an appropriate set of fragility functions to be representative of the improved non-structural elements is required. This is essentially done by considering the seismically deficient non-structural elements, initially assumed as part of the building's damageable inventory in Section 6.2.3, have been retrofitted to bring them in line with the current design code requirements. Unlike the structural retrofitting, no actual re-running of NRHA is required as the response of the structures is taken as independent of the non-structural components, meaning that the improved fragility functions can be inserted in place of the older ones and the loss estimation analysis repeated. These improved fragility functions are taken from the FEMA P58-3 [2012] database and are listed in Table 6.6. Such an approach can be justified when considering that non-structural elements in existing buildings constructed in Italy prior to the 1970's are not likely to have any provisions for adequate protection of non-structural elements, seeing as the first consideration of assessing forces on non-structural elements appeared in 1964 Uniform Building Code in the US [Filiatrault and Sullivan, 2014]. That is, the minimum requirements in terms of fixtures and fittings for the various non-structural elements would be anticipated to have been installed such that the element remains in place, but no proper consideration given to its protection under seismic excitation. This was observed during the site visits to the school buildings such as that discussed in Chapter 8 where, for example, the suspended ceiling system consisted of just vertical hangers to fix the ceiling to the underside of the upper slab, whereas no consideration was given to inserting diagonal splay wires to prevent excessive movement horizontally, such as those illustrated in Figure 6.19. As such, existing fragility functions for non-structural elements with no seismic design provisions can be considered adequate to estimating the damage of these elements examined here. The retrofitted non-structural elements, on the other hand, are evaluated with fragility functions designated for elements with seismic design provisions as the retrofitting scheme implemented is intended to bring the element's seismic performance in line with the current design code requirements, such as ASCE 7-10 [ASCE 7-10, 2010].

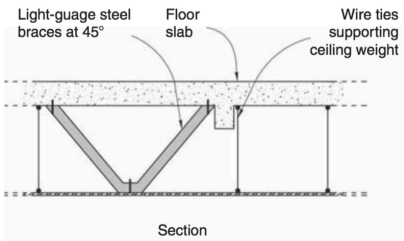

Figure 6.19. Illustration of modern non-structural element provisions for suspended ceilings, where in addition to the vertical wire ties to support vertical loading, additional bracing to provide lateral support is inserted.

Table 6.6. Inventory list of the improved non-structural elements with the corresponding quantities, fragility and repair cost functions for the case of non-structural element retrofitting.

Damageable Elements	Quantities	Fragility and Repair Cost Functions
Internal Gypsum Partitions (w/ Slip Tracks)	100ft	FEMA P58-3 [2012] - C1011.001d
Internal Gypsum Partition Wallpaper Finish (w/ Slip Tracks)	100ft	FEMA P58-3 [2012] - C3011.001d
Internal Gypsum Partition Ceramic Tile Finish (w/ Slip Tracks)	100ft	FEMA P58-3 [2012] - C3011.002d
Suspended Ceilings (Additional lateral bracing)	1065ft^2	FEMA P58-3 [2012] - C3032.003b
Cold Water Piping (Additional Bracing)	1000ft	FEMA P58-3 [2012] - D2021.013a
Cold Water Piping Bracing	1000ft	FEMA P58-3 [2012] - D2021.013b
Hot Water Piping (Additional Bracing)	1000ft	FEMA P58-3 [2012] - D2022.013a
Hot Water Piping Bracing	1000ft	FEMA P58-3 [2012] - D2022.013b
Glazed Windows***	10	Sassun [2014] - Glazing Panels 1.0 x 2.5m
Lighting (Additional lateral bracing)	15	FEMA P58-3 [2012] - C3034.002
Elevator***	1*	FEMA P58-3 [2012] - D1014.012
HVAC In-Line Fan (Additional lateral bracing)	2	FEMA P58-3 [2012] - D3041.002c
HVAC Ducting (Additional lateral bracing)	2	FEMA P58-3 [2012] - D3041.011c
HVAC Diffusers (Additional lateral bracing)	2	FEMA P58-3 [2012] - D3041.031c
HVAC Fan	1**	FEMA P58-3 [2012] - D3041.101a
Chiller (Vibration Isolated)	1*	FEMA P58-3 [2012] - D3031.013a
Air Handing Unit (Vibration Isolated)	2**	FEMA P58-3 [2012] - D3031.023a

*At ground level only

** At roof level only

***No retrofitting

6.4 ASSESSMENT OF RETROFITTED BUILDINGS

This section looks to take the case study buildings retrofitted in the previous section using both structural and non-structural approaches to examine the overall impact on the performance of the buildings. Again, this is done both in terms of examining the collapse safety of the retrofitted buildings, which had already been deemed to be satisfactory, in addition to the direct monetary losses associated with repair of the building seen through the EAL. The following section briefly acknowledges the collapse performance of the buildings followed by a more detailed consideration of the relative impacts of the different retrofitting strategies on the EAL and its implications within a PBEE framework for GLD RC frames.

6.4.1 Collapse Assessment

Recalling how the initial collapse assessment of the case study buildings outlined in Section 6.2.1, the collapse safety of the structures was seen to be satisfactory when compared to limits proposed in current guidelines. However, in order to acknowledge the effects that the structural retrofitting has on the collapse performance of the structurally retrofitted frames, the probability of collapse at the MCE level previously outlined in Section 6.2.1 is computed and shown in Figure 6.20.

Comparing the probabilities of collapse at the MCE intensity, it can be seen from Figure 6.20 that the retrofitting of the non-structural elements does not have any impact on the collapse fragility of the buildings, which is to be expected since the non-structural elements were not explicitly modelled in neither the existing nor the retrofitted buildings, meaning that the collapse fragility remains unchanged. This has the implication that in order for the non-structural retrofitting to become an option to deliberate when improving the performance at the serviceability limit states, it must be shown that the same structure meets the requirements in terms of collapse safety. For most cases shown in Figure 6.20, the collapse probability of the existing buildings is below the specified threshold, which satisfied the above condition. Examining the structural retrofits, however, it is seen that retrofitting the structure via RC jacketing of the columns and joints or insertion of an RC wall have a notable effect on the collapse performance. This is an anticipated result for strengthening to reduce collapse risk, but it is noted here that in many cases such a reduction in the probability of collapse was not deemed necessary when considering the life safety criteria prescribed and evaluated in Section 6.2.1. In summary, the non-structural retrofitting has no effect on the collapse fragility whereas the structural retrofitting is seen to have a notable effect. These points are noted for the discussion of impacts on EAL in the following section.

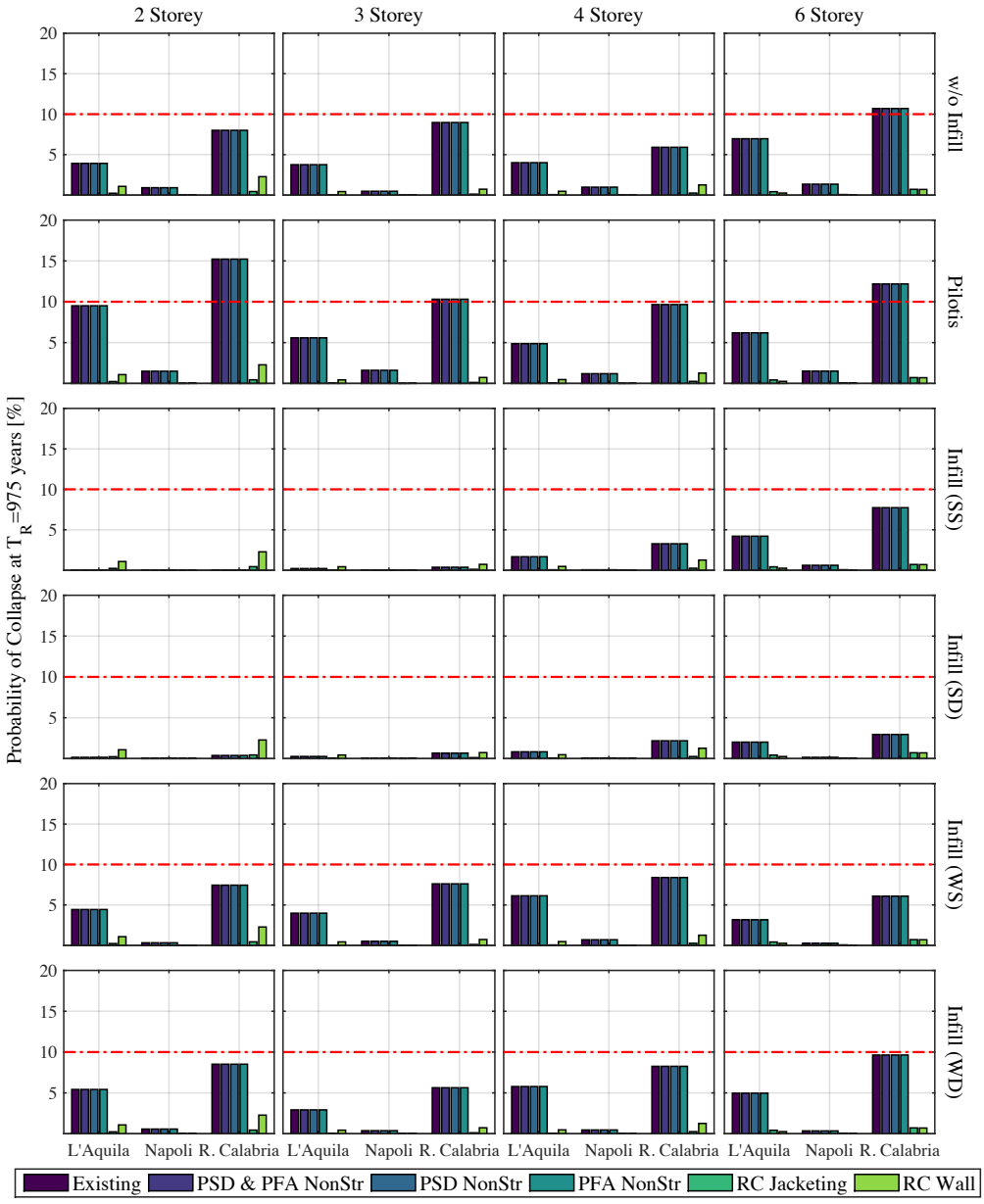

Figure 6.20. Probability of collapse for the different retrofitted case study buildings that is checked at T_R=975 years to not exceed a value of 10% marked in red, as per the FEMA P695 [2009] guidelines.

6.4.2 Loss Estimation

Using each of the retrofitting solutions for the various structural typologies, the loss estimation procedure is repeated using TOMS and the relative improvements in performance in terms of direct losses can be examined. This section discusses the different impacts each solution has on the EAL of each building, in addition to comparing the relative improvement in EAL to the actual cost of implementing that retrofit.

By performing loss estimation of each of the case study structures with the improved structural and non-structural damageable element inventories for each of the site hazards considered, the vulnerability functions and EAL can be computed as before. The retrofitting solutions to be examined are listed here once more for clarity:

1. "PSD & PFA NonStr" – The improved detailing for both the PSD and PFA sensitive non-structural elements is implemented.
2. "PSD NonStr" – The improved detailing for the PSD sensitive non-structural elements is implemented.
3. "PFA NonStr" – The improved detailing for the PFA sensitive non-structural elements is implemented.
4. "RC Jacketing" – The structures have ben retrofitted by RC jacketing the column and beam-column joints.
5. "RC Wall" – The structures have ben retrofitted by inserting an RC wall.

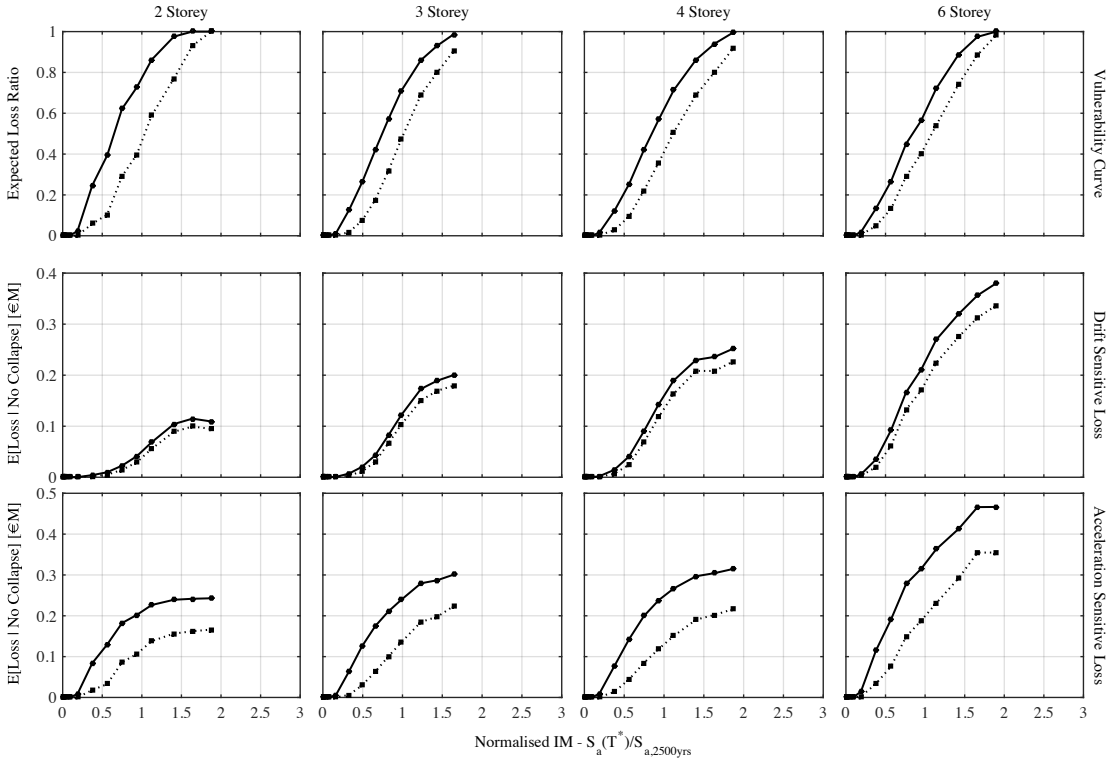

Figure 6.21. Vulnerability function and disaggregation of expected losses in terms of demand parameter for the case study buildings with strong masonry infill modelled using double struts. Dotted and solid lines represent the vulnerability functions of the retrofitted with improved non-structural elements and original building, respectively.

Each of these retrofitting schemes is implemented and the vulnerability functions computed. As noted previously, in order to make meaningful comparisons between the various retrofits then the vulnerability curves need to be incorporated to consider the time-base results of the different solutions compared to one another. As an illustrative example of the modification to the vulnerability function, however, Figure 6.21 plots the vulnerability function for the case study frames with strong masonry infill modelled with double struts, where retrofitting of both the PSD and PFA sensitive non-structural elements is employed. The overall vulnerability of the buildings is reduced by the shifting of each curve slightly to the right, meaning that the intensity required to induce a given level of expected loss in the structure has increased.

6.4.3 Time-Based Loss Assessment

By integrating these individual vulnerability functions previously discussed with the assumed mean hazard curves for the three example sites in Italy, discussed in Section 6.2.5, a time-based assessment can be carried out to examine the impact of the different retrofitting strategies on the EAL. Figure 6.22 plots the EAL for each of the original structural typologies along with the EAL for each of the five retrofitting schemes investigated here. These are separated in terms of storey number, structural typology and site hazard to illustrate the respective influence of the retrofitting in each case.

From the information presented in Figure 6.22, a number of general observations can be made regarding the effectiveness of the various retrofitting strategies. The first observation is that the retrofitting of the non-structural elements is a beneficial solution in every case whereas depending on whether the structural typology is a frame modelled with or without infill, the PSD or PFA-based schemes have the maximum impact. For the case of the frames modelled without infills, a mean reduction in EAL of approximately 24% was noted for PSD-based retrofitting whereas only a 12% reduction was observed for the PFA retrofitting. Compare this to the case of the infilled frames, where PSD-based retrofitting reduced the EAL by approximately 10% whereas PFA based returned up to a 60% reduction, highlighting the importance of PFA sensitive elements in the overall performance of infilled frames. This is noteworthy as some traditional approaches to retrofit, such as those prescribed for the SLE limit states of NTC 2008, aim to mitigate excessive damage and maintain the structures operational function by limiting the PSD in the structure.

Figure 6.22. EAL for each of the structural typologies along with the retrofitting schemes described to show the relative impact of each with respect to the existing building.

Examining the performance in terms of EAL of the structural retrofits with respect to the existing buildings, some rather peculiar results are observed at first. While some results may show how both RC jacketing and inserting an RC wall reduces the EAL, some instances where this EAL is actually worsened arise. For example, the two storey frame modelled without infill retrofitted with RC jacketing examined further in Figure 6.23 shows a clear increase with respect to the original building. In short, strengthening the building to ensure a more stable mechanism via RC jacketing of the columns and beam-column joints results in an increased EAL. Comparing this to the performance of the RC wall retrofitting, where only a slight reduction in EAL results, begs some questions as to why such an observation can occur if both were intended to improve performance by satisfying the prescribed drift limits. It is highlighted that in both cases, Figure 6.20 illustrates how the probability of collapse of the retrofitted frames decreases significantly. Figure 6.23, however, illustrates that despite this improvement with respect to the collapse performance, the subsequent change in expected loss due to increased floor acceleration or more distributed damage throughout the height of the building may have worsened the performance. This raises the issue that when initially assessing the building in Section 6.2, the collapse assessment of this particular building was shown to meet the prescribed criteria. The EAL of this building was evaluated to have not been satisfactory and the code prescriptions to retrofit the structure to meet the prescribed drift limits at the damage limitation were implemented in Section 6.3.1 with a view to improving the EAL through this verification of damage limitation drift criteria. Figure 6.23 illustrates that this initial objective of improving the performance of the building in terms of EAL has, in fact, been worsened meaning that the result is a building more resilient to collapse but more susceptible to monetary losses, despite collapse not being the issue at hand. It should be noted, however, that some instances, such as the three storey strong infilled frame modelled with double struts shown in Figure 6.24, exhibit decrease in the EAL for the case of RC jacketing, albeit rather small, which is more in line with the initial objective of retrofitting the building.

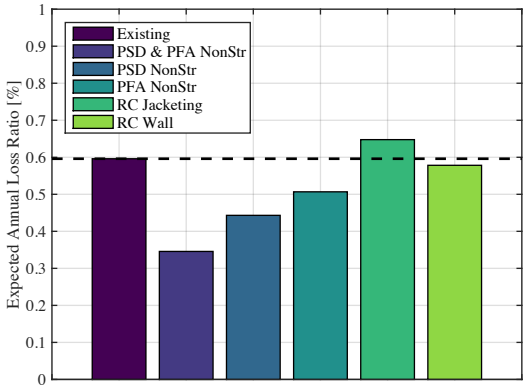

Figure 6.23. Illustration of the effectiveness of the different retrofitting strategies defined in terms of EAL for the case of the two storey frame modelled without masonry infill at the L'Aquila site.

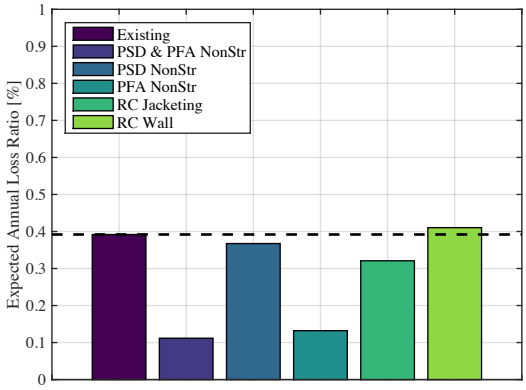

Figure 6.24. Illustration of the effectiveness of the different retrofitting strategies defined in terms of EAL for the case of the three-storey strong infill frame modelled with double struts at the L'Aquila site.

These cases where the structural retrofitting of the buildings actually worsens the performance are illustrated in Figure 6.25 where a plot of the EAL before retrofitting versus after retrofitting using different techniques is shown. The points in the shaded red zone correspond to these cases where the retrofitting measure has actually resulted in a worsening of the buildings performance defined in terms of EAL.

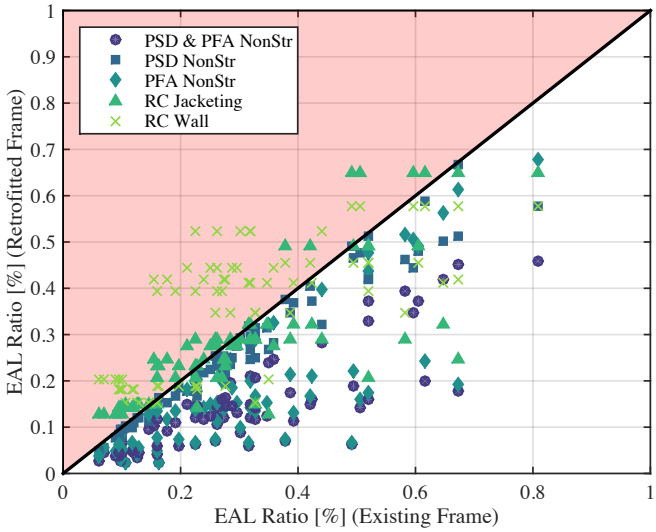

Figure 6.25. Illustration of the relative improvement in performance defined in terms of EAL with respect to the existing building. Points in the zone shaded in red correspond to cases where the EAL of the building actually increased following the retrofitting measure.

This is a rather strange observation at first, as one would expect the performance of the building to be improved following structural intervention, so the question remains as to why this occurs? As previously mentioned, the EAL is the integration of the vulnerability function with the mean hazard curve so a reduction in vulnerability (i.e. shifting to the right) ought to correspond to a reduction in EAL? This is only true if the hazard curve remains constant, in addition to the relative changes of the vulnerability function. Figure 6.26 illustrates this remark more clearly, to which there are actually two observations to make. For the structural retrofitting, a combined effect on the different structural typologies is observed where for the frames without infill modelling, the PSD sensitive losses decreased and the PFA losses increased, whereas for the infilled frames the opposite occurred. Structural retrofitting, therefore, appears to become a trade-off where the expected demand decreases in one source possibly resulting in an increase in the other, as illustrated in Figure 6.26(c). This is also combined with the fact that the new prominent source of losses may actually be occurring at a lower, more frequent intensity level to further increase the weighting during the hazard integration, which is shown Figure 6.26(b) through the decrease in the intensity required to begin accumulating expected losses. This aspect was observed during the recent 2016 earthquake in Ecuador for hospital buildings, where Morales *et al.* [2017] note how following the 1998 earthquake in Ecuador, the Ecuadorian Ministry of Public Health embarked on a program to retrofit existing hospital structures by strengthening through RC jacketing and RC walls to a level beyond the

building code requirements and achieve an almost elastic building response. Morales *et al.* [2017] note how this approach would be expected to lead to higher PFA in the structures and subsequently increase PFA sensitive non-structural damage. Following the 2016 earthquake, post-earthquake reconnaissance of the hospital buildings by O'Connor and Morales [2016] noted that although none of the hospital facilities collapsed, 22 were left inoperative due to excessive non-structural damage. This resulted in aid being provided from temporary shelters, which was noted to have resulted in overcrowding and unsanitary conditions. This observation of these counterproductive strengthening measures carried out in Ecuador echo the above comments regarding the potential worsening of performance due to structural retrofitting.

The second aspect of the structural retrofitting highlighted here and illustrated in Figure 6.26(d) is the modification of the fundamental period of vibration of the building as result of the strengthening and stiffening. This results in a change in T_1, which when combined with the IM employed here of $S_a(T_1)$ means that the definition of the mean hazard curve must also be updated to maintain consistency in the definition of IM. In cases such as that illustrated in Figure 6.26(d), this will result in an increase in the MAF of exceedance for a given level of intensity, resulting in an increased EAL. These two observations regarding structural retrofitting help explain the cases shown in Figure 6.22 in which the strengthening of the structure actually worsens the performance when defined in terms of EAL.

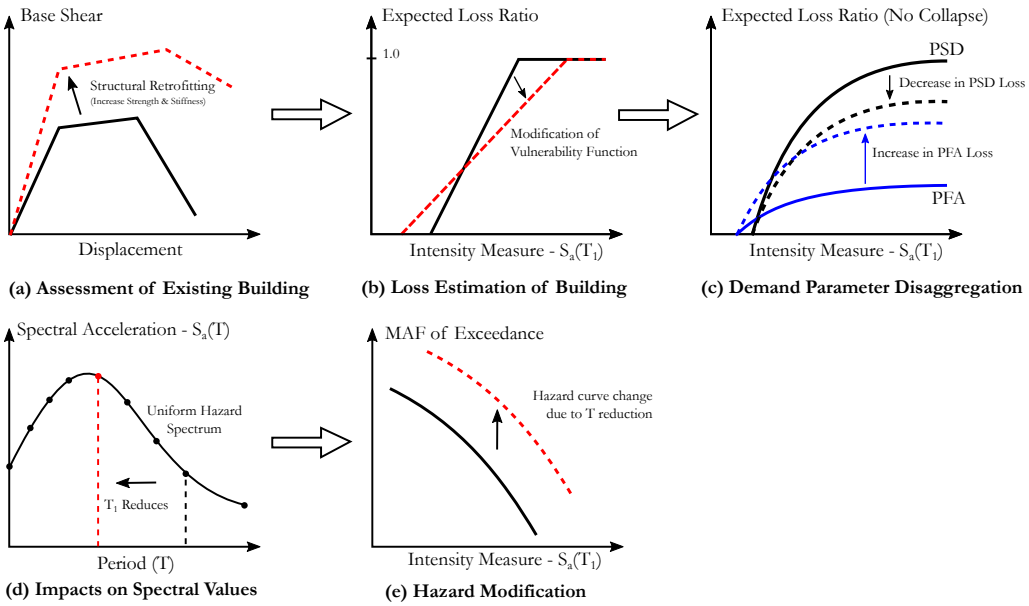

Figure 6.26. Illustration of the potential impact of structural retrofitting where strengthening and stiffening of the structure can actually worsen the EAL performance due to the combined effect of an increase in loss from higher PFA and a shift in the mean hazard curve due to period shortening.

It should be noted that while the general theme of the discussion presented above indicates that engineers should instead focus on non-structural elements when retrofitting a building, it is still maintained that the fundamental requirement of ensuring life safety still needs to be satisfied. This aspect implies that, should the MAF of collapse of a building be sufficiently low but the overall performance of the structure in terms of monetary losses be unacceptably high, it may be more beneficial to consider the retrofitting of the main culprits contributing to the expected loss that are in this case the non-structural elements, rather than applying strengthening and stiffening measures that may actually worsen the situation when speaking in terms of EAL.

Regarding the actual use of EAL as a performance metric with which to classify structures, some further comments are made. First of all, the values presented in Figure 6.22 are used within the scope of relative comparison since an exhaustive study of the different non-structural elements specific to different types of Italian occupancy was not considered in detail, although every effort was made to ensure the information was reasonably representative. In order to quantify representative values of EAL to be used within a classification framework, an extensive study is required that applies the above loss estimation procedure to structures where exhaustive lists of damageable components are

compiled and can be considered representative in different types of buildings, such as residential, commercial office space, schools, hospitals etc. In addition to this, some additional aspects to be considered for the use of EAL as a standardised performance measure, as proposed by Calvi *et al.* [2014], are illustrated in Figure 6.27.

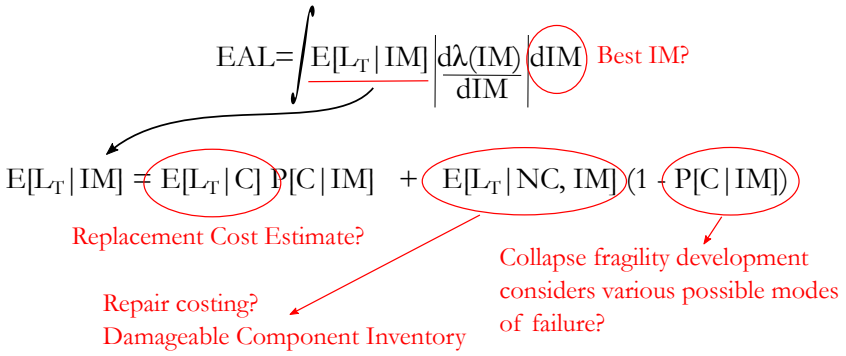

Figure 6.27. Various consideration when using EAL as a seismic performance classification metric.

One of the first issues illustrated in Figure 6.27 for the computation of EAL is the collapse probability, P[C | IM]. In order to have a suitable assessment of collapse fragility, all of the failure modes contributing to the collapse of the structure should be accounted for. For example, Chapter 2 discussed how previous research by Ibarra *et al.* [2005] highlighted the need to consider the post-peak strength degradation in addition to the inclusion of P-Delta effects for collapse. In addition to this, Section 5.4 has shown the importance of considering the shear failure in the column members due to the interaction with the masonry infills, where a reduction of up to 20% in the median collapse intensity was observed. As such, the inclusion of all of the potential failure modes is vital to the appropriate representation of the collapse vulnerability in loss estimation. Whilst discussing the collapse and replacement of a building, the appropriate computation of a replacement cost value is also important in computing EAL since the EAL ratios plotted in Figure 6.25 are expressed as a percentage of the replacement cost. As such, if a building owner were to assess their building in terms of the seismic performance classification framework outlined in Calvi *et al.* [2014] and discover that their building fell just outside of the acceptable range, meaning intervention was required to improve its performance. The temptation would exist on the building owner's behalf to slightly overestimate the buildings replacement cost to artificially reduce the EAL ratio and fall within the acceptable range to result in no required intervention. As such, proper guidance on replacement cost estimation would be required to avoid such situations but still take into account the variation in replacement costs with respect to structural typology and differences in regional pricing throughout Italy. Similarly, the compilation of a representative list of damageable elements and appropriate repair costs should be prescribed in order to achieve the same answer regardless of who applies the

process, thus avoiding situations such as that highlighted in Calvi *et al.* [2014] where for the same case study RC frame structure examined in the US, two independent studies [Krawinkler, 2005; Porter *et al.*, 2004] to quantify the EAL resulted in a difference of over three times when different assumptions regarding replacement costs and damageable inventory were made. Last is the usage of an appropriate IM, where $S_a(T_1)$ is the IM employed in this study as it is used in numerous studies and guidelines, such as FEMA P58-1 [2012]. However, more recent research by Kohrangi *et al.* [2016] suggest that more advanced IMs may actually provide a better way with which to represent the intensity, as opposed to $S_a(T_1)$.

The above discussion is intended to give the reader the sense that while the work presented here intends to provide further guidance on the various aspects to consider and illustrate more astute ways in which improved performance can be achieved, it is still a comparative study for the case of GLD RC frames in Italy. This is as Figure 6.27 illustrates how some of the more important procedural aspects required for the proper quantification of EAL in these types in buildings still require future research. Nevertheless, as discussed in Calvi *et al.* [2014] and also addressed in Porter *et al.* [2004], framing the discussion of assessment and retrofitting of buildings in terms of not only life-safety but also monetary loss metrics such as EAL not only results in more resilient communities that can can cope with the induced damage of an earthquake but also serve as a means with which a building's seismic resilience can be incorporated into a cash-flow analysis.

6.5 COMPARISON OF CODE PRESCRIBED LIMIT STATE PERFORMANCE WITH OVERALL PERFORMANCE

Previous sections have examined the performance of a series of case study Italian GLD RC frame structures with masonry infill from extensive NRHA discussed in Chapter 5 right through to full time-based assessment in this chapter. These structures were evaluated in Chapter 5 with reference to the NTC 2008 guidelines, where the exceedance of the four limit states in the building was evaluated with respect to intensity. This resulted in a set of fragility functions describing the exceedance of each limit state with respect to intensity being developed for each building typology. This section aims to examine the actual performance of the buildings at each of these limit states, where their exceedance is combined with the expected loss information from Section 6.2 to examine the performance of the building defined in terms of the expected loss ratio at each of the limit states. By doing this, the level of damage induced at each limit state can be evaluated to examine whether the descriptive requirements of NTC 2008 are actually being met through the compliance criteria specified in terms of storey drift.

6.5.1 NTC 2008 Compliance Criteria

As previously highlighted, the current seismic design and assessment code in Italy is the Norme Tecniche per le Costruzioni (NTC 2008) document [NTC, 2008], which is a document based in many ways on the requirements of Eurocode 8 [EN 1998-1:2004, 2004; EN 1998-3:2005, 2005] whose use became a mandatory requirement in Italy from July 2009, shortly after the L'Aquila earthquake in April of the same year. Within Part 3 of Eurocode 8, which deals with the assessment and retrofitting of existing structures, a number of limit states are outlined descriptively and listed in Table 6.7 here, followed by the actual compliance criteria for each limit state.

These limit state requirements for Eurocode 8 are echoed in the corresponding descriptive requirements of NTC 2008, which have previously been discussed in Section 5.2 and are listed again in Table 6.8, for convenience. While many of the requirements of NTC 2008 are largely based on those of Eurocode 8, there is a slight modification in that the serviceability limit states (SLE) defined in NTC 2008 appear to a subdivision of the damage limitation requirements of Eurocode 8. The significant damage and near collapse limit states roughly correspond to the SLV and SLC limit states of NTC 2008 when examined in terms of the descriptive performance criteria outlined in the tables below.

Table 6.7. Performance criteria for the various limit states outlined in Eurocode 8: Part 3 [EN 1998-3:2005, 2005].

Limit State	Description
Damage Limitation	The structure is only lightly damaged, with structural elements prevented from significant yielding and retaining their strength and stiffness properties. Non-structural components, such as partitions and infills, may show distributed cracking, but the damage could be economically repaired. Permanent drifts are negligible. The structure does not need any repair measures.
Significant Damage	The structure is significantly damaged, with some residual lateral strength and stiffness, and vertical elements are capable of sustaining vertical loads. Non-structural components are damaged, although partitions and infills have not failed out-of-plane. Moderate permanent drifts are present. The structure can sustain after-shocks of moderate intensity. The structure is likely to be uneconomic to repair.
Near Collapse	The structure is heavily damaged, with low residual lateral strength and stiffness, although vertical elements are still capable of sustaining vertical loads. Most non-structural components have collapsed. Large permanent drifts are present. The structure is near collapse and would probably not survive another earthquake, even of moderate intensity.

Table 6.8. Performance criteria for the various limit states outlined in NTC 2008 [NTC, 2008].

	Limit State	Description
Serviceability Limit States (SLE)	SLO – "Operational"	Following the earthquake the building's structural and non-structural components maintain their function and do not suffer any damage or significant interruption of their usage.
	SLD – "Damage Limitation"	Following the earthquake the buildings structural and non-structural elements suffer damage that does not put the occupants at risk and do not significantly compromise the overall capacity and stiffness of the structure to maintain the vertical and horizontal actions.
Ultimate Limit States (SLU)	SLV – "Life Safety"	Following the earthquake the building suffers damage and collapse to the non-structural elements and damage to the structural elements that results in a significant loss of lateral stiffness, but still maintains gravity load carrying capacity and a margin of safety against collapse.
	SLC – "Collapse Prevention"	Following the earthquake the structure suffers heavy damage to both structural and non-structural elements; the structure maintains gravity load carrying capacity and has a slender margin of safety against collapse.

Examining the description of the performance for the SLE limit states, one sees that buildings are generally expected to maintain their functionality and not suffer an interruption of use; in addition to experiencing little to no structural damage, whereas slight damage can be expected in the non-structural elements. Eurocode 8 notes that for this limit state, the damage to the non-structural elements can be economically repaired while the structural elements do not need repair. While these descriptive requirements of building performance are reasonable expectations for more frequent earthquakes with lower return periods, the actual realisation of such overall performance in terms of expected loss are examined. This stems from the fact that the compliance criteria for these serviceability limit states are implemented in NTC 2008 in terms of PSD limits to protect the drift sensitive components, which are listed in Table 6.9. In relation to the performance of acceleration sensitive equipment, NTC 2008 requires that their functionality is verified by considering the expected seismic demand at the relevant floor although the actual guidance on this is not very extensive.

Table 6.9. Compliance criteria defined in NTC 2008 for the protection of drift sensitive non-structural elements.

Non-Structural Element Typology	Drift Limit
Internal partitions connected rigidly to the structure	0.5%
Internal partitions detailed to not suffer damage due to interstorey displacements	1.0%

While these requirements outlined for the design of new buildings, the assessment of existing buildings is covered in a later section of NTC 2008, where the objective of this sections guidelines is stated as being the evaluation of life safety in the building. It goes on to state how the verification of the SLU limit states is a requirement that must be fulfilled by retrofitting so as to satisfy the requirements outlined for new design in terms of strength and ductility capacity of the structure. For the SLE limit states, however, Section 8.3 of NTC 2008 states that the evaluation of safety and design of retrofitting can be executed with reference to the SLU limit states only, with the SLE limit states being satisfied at the discretion of the designer in consultation with the client. This implies that in order to minimally retrofit a building to be code compliant, the SLE limit states need not be met as the main objective is to maintain life safety, which is, of course, a fundamental requirement that should be met.

The discussion here, however, focuses on the serviceability limit state requirements for both design and assessment, and to how well these drift limits imposed by NTC 208 actually meet the descriptive performance that they are supposedly ensuring. This refers to the descriptions such as "immediate functionality" and "no significant damage" outlined in NTC 2008, whereas Eurocode 8 goes as far as to suggest that non-structural damage could be economically repaired for the damage limitation limit states. The following section will examine whether these definitions of damage outlined in NTC 2008 for the SLE limit states are actually being realistically met from an economic loss standpoint, keeping in mind that for existing structures such as those examined in this thesis, these SLE limit state requirements are not necessarily a requirement to be met in assessment and their satisfaction at the discretion of the designer and client. This discrepancy between the imposed drift limits for the protection of drift sensitive non-structural partitions has been previously examined by Welch and Sullivan [2013] for steel moment frames designed according to the different drift limit requirements of Eurocode 8, where it was shown how for a series of case structures designed and illustrated via NRHA to having met these requirements, significant damage was noted in the internal partitions nevertheless. Also analogous to the current predicament of disparity between drift limitations imposed to

achieve a certain level of performance has also been recently pointed out by Gokkaya *et al.* [2016] where the current drift limits imposed by the new version of the ASCE guidelines in the US [ASCE 7-16, 2016] in order to provide a certain margin of safety against structural collapse have been shown to not always provide adequate protection. While this aspect of collapse is not the focus here, the parallels between disagreement of expected performance and the criteria applied to achieve this are noted.

6.5.2 Limit State Expected Loss Ratios

The previous section described the current Italian code design requirements for the SLE limit states and the expected level of performance that they ensure. The disparity between the drift limits outlined for new design and actual damage observed in the non-structural elements at these drift limits outlined in Eurocode 8 (which are adopted with minor modification by NTC 2008) has been discussed in Welch and Sullivan [2013] for steel moment frames, which concluded that such drift limits do not appear to be sufficient to limiting damage in drift sensitive internal partitions. Further discussion relating to the requirements for the assessment of existing structures in Italy using the NTC 2008 guidelines has been discussed where it was noted that the primary goal of retrofitting existing structures is to ensure the compliance with the SLU limit states which aim to ensure life safety, where the SLE limit states are left as optional and to be decided in consultation with the client. This section aims to expand on this for the existing GLD RC frames with masonry infill in Italy, where the case study buildings are examined in terms of the expected loss at these different limit states to examine whether the qualitative descriptions that these limit states are linked with are actually being met. This is done by using the extensive analysis conducted in Chapter 5 where the fragility functions describing each limit state were established in conjunction with the expected loss information computed in Section 6.2 to examine the actual damage defined in terms of expected loss ratio at these SLE limit states for the case study structures. This, therefore, examines whether the actual compliance criteria specified in terms of drift are actually capable of meeting the performances they aim to provide. The process followed below envisages that when carrying out an assessment of an existing structure, a practising engineer will utilise more simplified methods of analysis such as SPO analysis and subsequently verify the strength and ductility capacity of the structure at the SLU limit states to ensure life safety of the structure. In addition, if the SLE limit states are to be checked, the same SPO analysis results will be used to determine whether the requirements in terms of drift are being met, with no detailed consideration given to acceleration sensitive equipment, unless required to by the client. This is not an unreasonable situation to envisage given the current predicament regarding the proper consideration of non-structural elements in performance-based earthquake engineering, which has been extensively discussed in Welch [2016].

In order to carry out this comparison, the expected loss ratio at each of the four limit states needs to be evaluated such that actual building performance can be described. Figure 6.28 outlines the method with which this is performed, where the same steps outlined previously to identify the limit states in terms of global performance, in correspondence with the descriptive provisions outlined in NTC 2008, and identifying the fragility functions for each of these limit states through IDA, as conducted in Chapter 5. The next step is to integrate the fragility function for each limit state with the expected loss ratio curve determined in Section 6.2 to obtained an estimated expected loss ratio at each of these limit states in the different building typologies. This integration is in many ways analogous to the integration of the collapse fragility function with the mean hazard curve to estimate the MAF of collapse for a building. This integration of the limit state fragility function with the expected loss ratio curve results in the expected loss ratio for each of the limit states being computed, as illustrated in Figure 6.28. By computing the expected loss ratio at each intensity, a better idea of the anticipated impact of the different limit state performance will be obtained as this computed the direct economic impact due to the damage to both the drift and acceleration sensitive components in the structure. This procedure is carried out for each of the case study buildings previously examined, where the expected loss ratio curves are taken as those identified as part of the loss estimation study conducted in Section 6.2for the original building inventory prior to any retrofitting measures. These results are presented for both the SLE and SLU limit states in Figure 6.29.

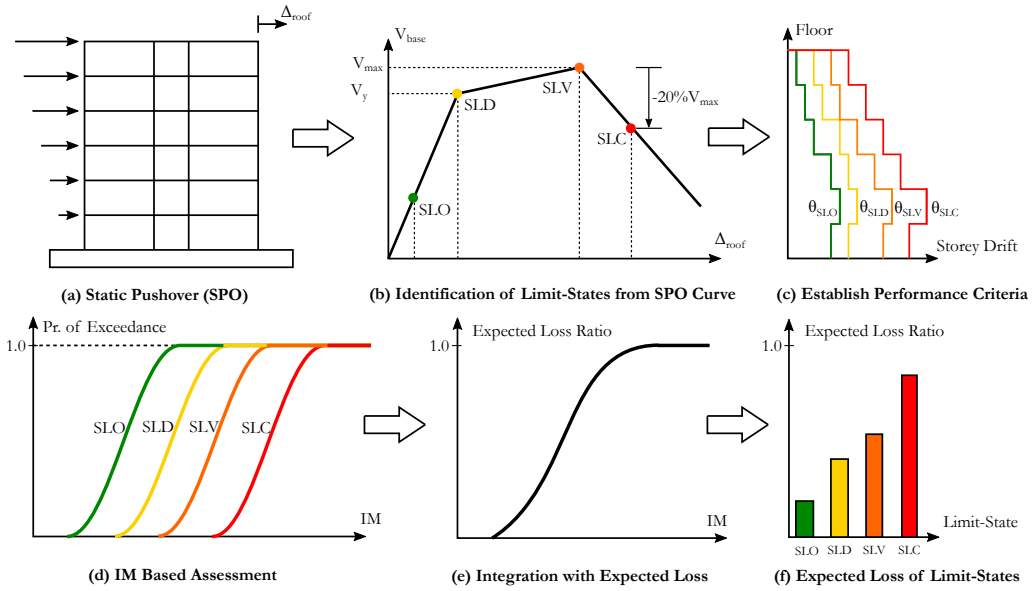

Figure 6.28. Illustration of the computation of the expected loss ratio of the case study building at each limit state obtained by integrating the limit state fragility functions with the vulnerability curve defined as expected loss ratio versus IM. This returns the expected loss ratio in terms of direct economic loss at each of the prescribed limit states.

From Figure 6.29, it is immediately obvious that the case study buildings examined previously can accumulate a significant portion of the buildings replacement cost in terms of expected loss at the SLE limit states outlined in NTC 2008. This is somewhat contrary to what one may expect when examining the description definitions of both of these SLE limit states, where full functionality in addition to minimal economic loss and downtime are not unreasonable to expect based on the qualitative descriptions provided. Figure 6.29 paints a different picture, however. Despite imposing drift limits at the two limit states, whose contribution to the expected losses is hatched in red in Figure 6.29, there is a notable contribution from the acceleration sensitive elements. This is especially pronounced for the infilled frames that appear to be dominated by losses due to damage to the acceleration sensitive elements, whereas the frames without masonry infill modelled or the pilotis frames tend to be less influenced by damage to acceleration sensitive elements. Such an observation makes sense when considering the impacts that the masonry infills tend to have on such structures by increasing the strength and stiffness. This stiffening of the building shortens the period of the structure and tends to move the first mode period into the constant acceleration range of the design spectra. This would be expected to increase the overall PFA profile along the height of the building and was observed in Chapter 5. This increase in the PFA profile of the building for the infilled frames with respect to the frames modelled without infills is then reflected in the jump in losses due to damage in

acceleration sensitive elements, where elements such as ceiling systems, mechanical equipment and water piping begin to become heavily damaged, as illustrated in Figure 6.6.

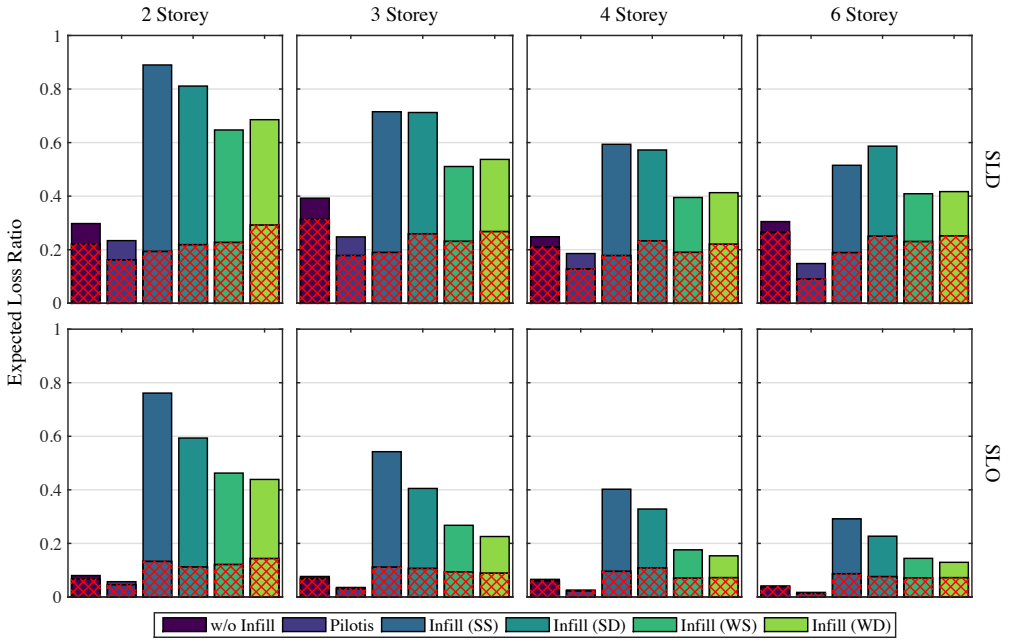

Figure 6.29. Expected loss ratio for each of the original case study buildings at the SLE limit states, where the expected loss is computed for each demand parameter by integrating the expected loss ratio curve determined from loss estimation to give the total expected loss. The hatched area in red represents the contribution to the expected losses from drift sensitive components.

While it is acknowledged that the impacts of the findings above are subject to the assumptions made during this study regarding the damageable inventories of the different buildings, it does highlight some important points. The first of these is that imposing checks on the drift limits alone for the SLE limit states does not ensure the adequate protection of the non-structural elements. The second aspect is that the induced acceleration demands in the buildings due to the presence of the infill can cause significant damage to the acceleration sensitive non-structural elements, which can contribute significantly to the expected losses at the SLE limit states. Overall it has been shown how there is a disparity between the qualitative description of performance of buildings provided by the design codes and the actual performance observed through loss estimation studies. This highlights that the prescriptive requirements in terms of drift limits to ensure such levels of performance at SLE limit states outlined in the code may not be adequate in

ensuring satisfactory performance and how better acceleration-based verification checks are required, although this is an area that requires further work.

6.6 SUMMARY AND CONCLUSIONS

This chapter conducted an extensive loss estimation study for the various structural typologies examined in the previous chapters to highlight the importance and impact of various modelling assumptions on the expected losses of the buildings. Retrofitting measures in terms of both the structural and non-structural elements were investigated to examine the relative impact of the different solutions on the EAL, provided the collapse prevention criteria have been satisfied. It was shown how not only can retrofitting of the non-structural elements be equally if not more effective than some structural retrofits but also how in some cases the insertion of additional structural elements can actually worsen the EAL. This highlights how for situations when the functionality of a building following an earthquake is the main priority, retrofitting of the non-structural elements may be the preferred route. This study was conducted for numerous case study buildings, whereby repair costing functions were estimated for Italy with the assistance of a consulting engineering firm to provide a meaningful comparison of results. For the general loss estimation of the different existing buildings, the following conclusions can be made:

- Frames modelled without masonry infill tend to accumulate losses from drift sensitive elements in the building whereas frames modelled with infill tend to be dominated by acceleration sensitive losses, which was observed in the case of the L'Aquila City Planning Offices in 2009. Modelling without the inclusion of masonry infills has the implication that for a practitioner looking to reduce the overall vulnerability of a structure defined in terms of expected loss, analysing a model that ignores the effects of the masonry infill results in increased drift for a given return period. The exceedance of drift limits due to the model's increased flexibility as a result of this modelling assumption could result in the engineer adopting some form of stiffening or strengthening measure, such as those examined here. It was later shown how such strengthening measures can actually worsen the performance when defined in terms of expected losses.
- Furthermore, the overall loss estimation for the frames modelled without masonry infill to those with shown a very poor correlation such that it cannot be implied that analysis results from a bare frame model could be interpreted as representative of the actual infilled frames results.
- The inclusion of a shear hinge in the modelling of the structures was shown to increase the vulnerability of the structures through an increased level of damage as a result of the amplified drift and overall flexibility. Despite this increased flexibility, the modelling of the infilled frames with column shear behaviour resulted in around a 30% increase in EAL, highlighting the importance that such a behaviour be included in the assessment of GLD RC frames with masonry infill.

- Finally, the comparison of the expected loss ratio at each of the SLE limit states of NTC 2008 has been shown to be quite substantial when compared to the qualitative description of damage outlined by the codes. This was also noted to be as a result of the significant contribution of acceleration-sensitive losses in the structure.

The retrofitting study conducted in this chapter aimed to examine the relative impacts of structural and non-structural retrofitting on the performance of the structure defined in terms of EAL. Following this comparative study, the following conclusions can be drawn:

- The retrofitting of the non-structural elements can have a comparative, if not better impact on the EAL than that of structural retrofitting provided that the collapse prevention requirements are met. If not, then structural retrofitting ought to be considered; although should the collapse of the building be linked to the shear-induced damage of the masonry infill, appropriate isolation of the infill from the surrounding frame to mitigate interaction may prove to be beneficial also.
- In some cases, the strengthening and stiffening of the building by inserting additional structural elements were seen to worsen the performance of the building when defined in terms of EAL. This resulted as a combination of the trade-off in the reduction of drift-induced damage with the increase in acceleration-induced damage; in addition to the change of the definition of hazard due to the periods shortening of the building that is as a result of the IM employed. This is a very important conclusion that should be noted as it clearly illustrated that strengthening and stiffening are not necessarily a good thing when speaking in terms of economical functionality of the building and mitigation of losses. It should be noted, however, that the overall collapse performance of these buildings was markedly improved with respect to the existing ones, although improvement of the collapse performance was not actually needed since the collapse prevention criteria had already been satisfied. This observation was also exemplified in the recent earthquake in Ecuador, where excessive strengthening measures prior to the 2016 event resulted in extensive non-structural damage to hospital structures resulting in widespread loss of functionality of these essential services following the earthquake.

7 TOWARDS A MORE SIMPLIFIED ASSESSMENT FRAMEWORK FOR GLD RC FRAMES IN ITALY

O'Reilly, G. J., Welch, D. P., Sullivan, T. J. [2018] "Displacement Based Assessment of Existing Italian RC Frames with Masonry Infill," *Journal of Earthquake Engineering* (Under Preparation).

7.1 INTRODUCTION

Previous chapters have extensively examined the behaviour and response of Italian GLD RC frames with masonry infill through the use of advanced numerical modelling techniques to capture the different aspects of the behaviour, followed by extensive loss estimation studies to quantify the overall performance of such buildings. In this chapter, the results of these detailed analyses are then taken to explore more simplified methods to estimate the response of the buildings. This entails an extensive comparison with the existing DBA methodology and examines its applicability to GLD RC frames. Some of the various aspects of this methodology, which has primarily been developed for design and assessment of modern RC frames without masonry infill, is examined for the building typologies examined here. This aims to compare and validate the various assumptions required to implement such a methodology in addition to highlighting additional considerations for GLD RC frames with infills in addition to specific areas that require further work to complete the applicability of the methodology.

In addition, this chapter investigates the use of such simplified assessment methodologies to conduct simplified loss estimation of the case study buildings considered here. A comparison of some of the case study buildings examined in Chapter 6 is highlighted in addition to how one would go about utilising a simplified method of assessment to estimate the expected losses in a structure. This examines the use of median values estimated from the aforementioned DBA methodology in conjunction with appropriate dispersion values to account for record-to-record variability and modelling uncertainty in addition to the correlation between the different demand parameters, quantified as part of this study. It is investigated how the use of these medians and empirical values of dispersion compare with the expected losses using extensive NRHA to highlight how more simplified tools for loss estimation of GLD RC frames in Italy can be implemented.

In addition, the validation of another simplified method of assessment to estimate the MAF of exceedance of various limit states using a closed form expression is presented. This

methodology is commonly referred to as the "SAC/FEMA" methodology and provides users with a simplified method with which to assess performance defined in terms of demand parameters such as storey drift or acceleration. The application of this methodology to GLD RC frames with masonry is validated through the calibration of various parameters required in the method currently unavailable for structural typologies such those considered in this thesis. The validation of such a methodology allows practising engineers to quickly assess the exceedance of various limit states defined in terms of drift or acceleration, as is typically the case in code requirements, such that a more probabilistic approach to assessing the performance of existing structures at different limits states can be implemented.

Lastly, a general framework is outlined whereby both an extensive numerical modelling approach to the assessment of frames in addition to the simplified approach outlined here are discussed and compared to that outlined in FEMA P58. Comparisons with the existing procedure outlined in FEMA P58 are made to examine its applicability to the GLD frames considered here. Discussion of the various aspects to consider when assessing such frames is outlined, whereby the various particularities of such frames is highlighted in each case to provide guidance on the assessment of such structures in the future.

7.2 SIMPLIFIED ASSESSMENT OF CASE STUDY FRAMES

Chapter 5 section presented the results of IDA on a number of GLD frame typologies with variations in number of storeys, infill typology. Using the results of these detailed analyses, more simplified procedures can be tested and validated to enable practising engineers to assess the performance of older GLD frames with relatively simple methods, without the need for computationally expensive analysis, if need be. This chapter examines the DBA methodology outlined in Priestley *et al.* [2007] and aims to provide validation for the method to be applied to GLD frames by using the IDA results as a calibration, in addition to highlighting areas that require future work via illustration. Using these results, it will be shown how the DBA method is a relatively simple and effective approach for assessing the behaviour of the frames at various limit states. To date, much of the work on DBA has focused on modern ductile structures that possess some degree of seismic design considerations, with more recent attempts by Sullivan and Calvi [2011] and Saborio Romano [2016], among others, aiming to expand the methodology to older GLD frames by considering different behaviour mechanisms other than a traditional beam-sway mechanism. These studies, however, have been somewhat limited to single case study buildings and therefore cannot be considered a thorough validation of the DBA method for older GLD frames. The work presented in this chapter aims to provide such a validation and illustrate how it is possible to conduct a detailed assessment without the use of advanced modelling techniques, such as those discussed in previous chapters. In addition, it is discussed how the results of DBA could then be used, along with appropriate values

of record-to-record and modelling uncertainty in addition to some demand parameter correlation, to enable full loss estimation to be conducted using the TOMS software tool discussed in Chapter 3. This will be discussed with respect to the broader framework of assessment in Section 7.5.

7.2.1 Displacement-Based Assessment of RC Frames

Since the early 1990's, displacement-based design (DBD) procedures have emerged in the seismic design community in an effort to address the so-called "myths and fallacies" of force-based design (FBD) procedures, with Priestley [1993, 2003] discussing many of these conceptual limitations and shortcomings of the FBD procedures that DBD approaches aim to overcome. Sullivan *et al.* [2003] provide a critical review into many different DBD approaches, with the most notable and developed of these methodologies being the DDBD method developed over many years of research and comprehensively explained in the 2007 text by Priestley *et al.* [2007]. These developments in DBD approaches have undoubtedly improved the appreciation and understanding of how ductile structures behave under seismic loading. However, the same advancements are still being made in the field of seismic assessment, or more specifically the DBA methodology. The basic formulation of the DBA procedure, which is in some ways the DDBD procedure applied in reverse, appears in earlier publications such as Priestley [1997] with a more updated outline of the procedure given in Priestley *et al.* [2007]. The following sections will describe the DBA methodology briefly, with the main focus being on its application to GLD frames examined earlier in this chapter. The various aspects of the method, when applied to older GLD frames, are described and justified here to give the reader a clear impression of how to implement such a method for such structures. As mentioned previously, the ultimate aim of this section is to justify and validate the various steps in the DBA approach by continual comparison with the GLD frames examined in detail in previous sections using refined modelling techniques and extensive dynamic analyses, in addition to highlighting areas that require further work.

7.2.1.1 Overview of the DBA Methodology

Figure 7.1 shows a basic overview of the DBA methodology where one uses the substitute structure concept [Gulkan and Sozen, 1974; Shibata and Sozen, 1976] to characterise the structure as an equivalent SDOF system with effective properties to the displacement capacity Δ_{cap} that may represent the capacity of any given limit state to be considered. In order to convert the multi degree of freedom (MDOF) structure to its equivalent single degree of freedom (SDOF) system, one must be able to assess the likely mechanism to be formed in the structure and determine the displaced shape and internal forces developed to perform the substitute structure transformation. By knowing the mass (m_i) and expected displacement (Δ_i) for floor level *i* for a given limit state to be considered, the equivalent SDOF properties are found from the following expressions:

$$\Delta_{cap} = \frac{\sum m_i \Delta_i^2}{\sum m_i \Delta_i} \qquad \textbf{Equation 7.1}$$

$$m_e = \frac{(\sum m_i \Delta_i)^2}{\sum m_i \Delta_i^2} \qquad \textbf{Equation 7.2}$$

$$H_e = \frac{\Sigma m_i \Delta_i H_i}{\Sigma m_i \Delta_i} \qquad \textbf{Equation 7.3}$$

$$K_e = \frac{V_b}{\Delta_{cap}} \qquad \textbf{Equation 7.4}$$

$$T_e = 2\pi\sqrt{\frac{m_e}{K_e}} \qquad \textbf{Equation 7.5}$$

where V_b is the expected base shear to be developed by the structure for the given limit state, K_e and T_e are the effective stiffness and period of the equivalent system shown in Figure 7.1(d), respectively.

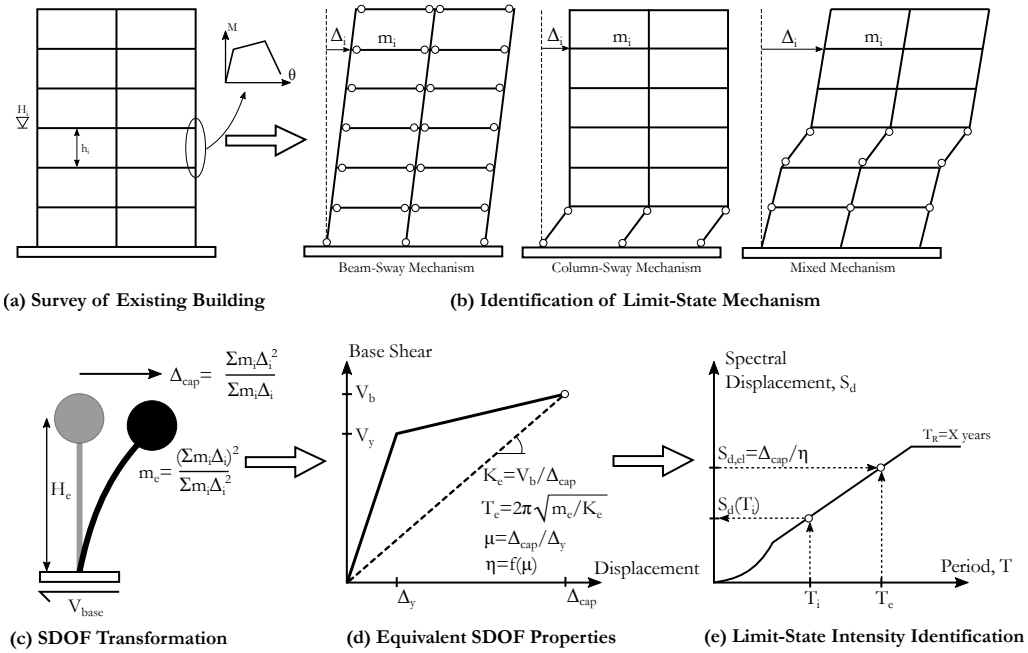

(a) Survey of Existing Building **(b) Identification of Limit-State Mechanism**

(c) SDOF Transformation **(d) Equivalent SDOF Properties** **(e) Limit-State Intensity Identification**

Figure 7.1. Overview of the DBA methodology (After Priestley *et al.* [2007]).

The effects of the inelastic behaviour of the structure are typically accounted for using an equivalent viscous damping (EVD) approach, which is determined as a function of ductility and structural system and is to be discussed in more detail in Section 7.2.1.4. Using an appropriate spectral reduction factor (η), determined from the EVD as a function of the ductility and structural typology, the elastic spectral displacement that the equivalent system resists can be determined from the following relationship:

$$S_{d,el} = \frac{\Delta_{cap}}{\eta} \qquad \textbf{Equation 7.6}$$

which corresponds to the elastic spectral displacement of the system at the effective period ($S_{d,el}(T_e)$), as shown in Figure 7.1(e). Recently, Pennucci *et al.* [2011] advocated the use of displacement dependent reduction factors in place of EVD. From the overall system ductility demand, the initial period (T_i) can be estimated and the corresponding spectral demands at the initial period can also be found. It is noted that $S_a(T_i)$ is an IM commonly used in PSHA and can thus be related to a given return period using an appropriate mean hazard curve for a given site. This will be expanded on further in Section 7.2.3 but is noted here for completeness.

This section has provided a basic overview of the DBA procedure and how it can be applied. The following sections will describe the procedure to determine many of the ingredients required at each step of the method for the case of older GLD frames in Italy, with the relevant justifications and validations with respect to the case study structures outlined in previous sections being provided where relevant, in addition to where future research is required.

7.2.1.2 Establishing the Expected Mechanism and Internal Forces

As previously outlined and illustrated in Figure 7.1(a) and (b), the first step of the DBA process is to identify the likely mechanism in the structure. In order to do this, Priestley *et al.* [2007] describe the sway potential index (S_i) as:

$$S_i = \frac{\sum_j \left(M_{b,left} + M_{b,right}\right)}{\sum_j \left(M_{c,upper} + M_{c,lower}\right)} \qquad \textbf{Equation 7.7}$$

where $M_{b,left}$ and $M_{b,right}$ represent the expected flexural strengths of the left and right-hand side beams at a joint j extrapolated to the beam-column joint centreline. Similarly, $M_{c,upper}$ and $M_{c,lower}$ represent the expected flexural strengths of the upper and lower columns at a joint j extrapolated to the beam-column joint centreline. This index is used to assess the relative strengths of the beams and columns and determine what type of inelastic mechanism can be expected. For S_i greater than 1.0, a column-sway mechanism can be expected and for S_i less than 0.85 a beam-sway mechanism is expected. For intermediate

values of S_i, Priestley *et al.* [2007] suggest it would be wise to conservatively assume a column-sway mechanism develops.

As discussed in Section 5.1, the columns in older GLD frames were typically sized based on the axial load requirements and no capacity design requirements were implemented to ensure a ductile beam-sway mechanism. As such, the sway potential index check in such frames (and will be evident in later sections) will typically result in a column sway or soft-storey mechanism being predicted at many levels due to the relative flexural strength of the beams being much higher than that of the columns. Clearly, however, a soft storey mechanism cannot be expected simultaneously at multiple levels in the same structure. To identify which storey the mechanism will most likely occur, Sullivan and Calvi [2011] introduced the sway demand index (SD_i) that determines the location of the soft-storey based on the most critical ratio between expected storey shear capacity and storey shear demand. It is given by:

$$SD_i = \frac{V_{i,D}}{V_{i,R}} \frac{V_{b,R}}{V_{b,D}} \qquad \textbf{Equation 7.8}$$

where $V_{i,D}$ and $V_{i,R}$ are the demand and resistance shear forces at storey i and $V_{b,D}$ and $V_{b,R}$ are the base shear demand and resistance shear forces. The demand terms above refer to the expected shear demand by assuming a unit base shear, distributing it along the height of the structure and summing the resulting force distribution at each level as follows:

$$V_{i,D} = \sum_{j=i}^{n} F_j \qquad \textbf{Equation 7.9}$$

where:

$$F_i = \frac{m_i H_i}{\sum m_i H_i} V_{b,D} \qquad \textbf{Equation 7.10}$$

where H_i is the elevation of floor i. Since the sway demand index is relative, the actual magnitude of $V_{b,D}$ is irrelevant as it is the relative shear demand on each floor that is of interest and not the actual magnitude. Therefore, a value of 1.0 may be assumed.

The storey shear resistances do not refer to the actual shear capacities of the column members, but rather the storey shear that is expected to develop during the formation of a mechanism at that storey. Sullivan and Calvi [2011] describe the $V_{i,R}$ and $V_{b,R}$ terms as:

$$V_{i,R} = \frac{0.5 \sum M_{jt,i} + 0.5 \sum M_{jt,i-1}}{h_i} \qquad \textbf{Equation 7.11}$$

$$V_{b,R} = \frac{0.5 \sum M_{jt,1} + \sum M_{col,b}}{h_1} \qquad \text{Equation 7.12}$$

where h_i is the storey height of floor i and $M_{col,b}$ are the expected flexural strengths of the base columns. The term $M_{jt,i}$ refers to the total moment resistance at the beam-column joint centreline, which is found for each joint by taking the minimum value between the extrapolated beam moments, extrapolated column moments and actual beam-column joint moment capacities, which are computed using the expressions outlined in Sections 2.3 and 2.4. Sullivan and Calvi [2011] also note that at the roof level, the full value of the first term of the numerator in Equation 7.11 should be taken and not reduced by 0.5 since the full moment of the joint is transferred to the column below and not split between two adjacent storeys. Following the determination of the sway demand index at each storey, the storey that has the maximum value among those that were shown to result in a soft-storey mechanism using the sway potential index will be the expected location of the soft storey in the structure.

While the above steps offer a direct and straightforward procedure to identify the expected plastic mechanism in a structure, one refinement may be suggested based on the results to be discussed in Section 7.2.1.3. When determining the shear demand profile in the structure, Sullivan and Calvi [2011] propose that a lateral force distribution determined in Equation 7.10 be proportioned to the product of the elevation (as opposed to lateral displacement) and mass of each floor and that suffices when determining the approximate storey demand demand, which is then justified from a comparison of pushover results of a single case study building from Galli [2006]. While it is acknowledged that this approach of using floor elevations in place of the floor displacements is preferred since the actual floor displacements are not yet known, initial comparisons to be presented in Section 7.2.1.3 demonstrate that the use of floor elevations actually result in a slightly different prediction in the location of the soft storey mechanism for more than one case study structure, where the use of the actual lateral displacement determined from the displacement profile to be discussed in the next section resulted in the soft-storey location being predicted correctly in each case. As such, it is suggested here that the lateral floor displacements be initially used in place of floor elevations, followed by an iteration of the procedure using the estimated displaced shape.

7.2.1.3 Establishing the Displacement Profile

As previously noted, the expected displaced shape at the given limit state is a crucial step in DBA to establish the equivalent linear SDOF system for a given structure. For more modern structures with capacity design, the expected beam-sway mechanism means that the displaced shape expressions given in Priestley *et al.* [2007] and more recently refined in Sullivan *et al.* [2012] can be used, provided a beam-sway mechanism has been confirmed via the sway potential index. For older structures where capacity design principles were not

enforced and soft-storey mechanisms are prevalent, the use of beam-sway displaced shape expressions is no longer valid. This was noted by Sullivan and Calvi [2011] and a compromising solution was adopted by assuming the yield drift at each storey and scaling it by the ratio of the sway demand index at each floor to the maximum (SD_i/SD_{max}). This approach worked reasonably well when compared to a single case study building, but room for improvement was noted. More recently, Saborio Romano [2016] trialled a more refined approach to determine the displaced shape of a frame structure with expected soft-storey mechanisms based on mechanics-based reasoning of the member strengths, where comparisons to first mode shape of the six storey case study building examined by Saborio Romano [2016] showed good matching. This approach will be described below and compared to the SPO results of the various GLD frames discussed in Section 5.2 to validate its applicability to such frames at various limit states aside from the first elastic mode shape.

The first steps of the procedure outlined in Saborio Romano [2016] are the determination of the sway potential indices at each floor to confirm the presence of multiple soft storeys in the structure, followed by the computation of the sway demand index of each floor to locate the storey in which the soft-storey is expected to form. Following the confirmation of a soft-storey mechanism at one of the levels, the yield drift at each level is computed based on the expected mechanism, where for a beam-sway mechanism ($S_i<0.85$), the following expression from Priestley *et al.* [2007] is recommended:

$$\theta_y = \frac{0.5\epsilon_y L_b}{h_b} \qquad \textbf{Equation 7.13}$$

where ε_y is the yield strain of the rebar, L_b is the bay length and h_b is the beam section height. For cases where a column-sway mechanism is expected, the following expression outlined Glaister and Pinho [2003] is recommended:

$$\theta_{y,i} = \frac{0.43\epsilon_y h_i}{h_c} \qquad \textbf{Equation 7.14}$$

where h_i is the storey height and h_c is the column section height.

For the case of the yield drift of the ground floor, Saborio Romano [2016] trialled and proposed the use of an alternate expression based on the expected contraflexure height in the ground floor columns, which is given as:

$$\theta_{y,0} = \frac{0.7\epsilon_y h_{cf}}{h_c} \qquad \textbf{Equation 7.15}$$

where h_{cf} is the contraflexure height determined from the expected flexural strengths using the following relationship:

$$h_{cf} = \frac{h_1}{\left(\frac{0.5\sum M_{jt,i}}{\sum M_{col,b}} + 1\right)}$$ **Equation 7.16**

Saborio Romano [2016] note how the expression given by Glaister and Pinho [2003] to compute the yield drift does not consider the contribution from the lower floors and therefore trialled an adjustment to account for it by computing a weighted sum of the yield drift of a given floor and the floor below it based on the storey moment capacities as follows:

$$\theta_{y,sys,i} = \frac{\sum M_{jt,i}\theta_{y,i} + \sum M_{jt,i-1}\theta_{y,i-1}}{\sum M_{jt,i} + \sum M_{jt,i-1}}$$ **Equation 7.17**

As in the case of the sway demand index, a shear demand profile is needed to compute the displacement profile. Saborio Romano [2016] suggests the use of floor elevations (more specifically, assume a linear displaced shape) to find a shear profile and calculate the individual inter-storey displacements (δ_i) using the following relation:

$$\delta_i \approx \frac{V_i}{K_i} \approx \frac{V_i\theta_{y,sys,i}h_i}{V_{y,i}}$$ **Equation 7.18**

where the terms $V_{y,i}$ represents the storey yield shear determined from the expected storey mechanism determined the same way as the $V_{i,R}$ term used in the computation of the sway demand in Equation 7.11. Again, it is noted here that the use of floor elevations to compute the shear demand profile is a good first estimate, but it is recommended here to iterate this assumption with the resulting displaced shape profile into Equation 7.10 in place of the floor elevations to get a more representative storey shear demand profile.

In cases of more than one frame acting in a single direction, Saborio Romano [2016] note how these above computations are computed individually for each frame and the average inter-storey displacements ($\delta_{av,i}$) are then found by computing the weighted sum of the storey yield shears as follows:

$$\delta_{av,i} = \frac{\sum \delta_i V_{y,i}}{\sum V_{y,i}}$$ **Equation 7.19**

and using these average inter-storey displacements, the final displaced shape (Δ_i) is then found by summing the individual contributions as follows:

$$\Delta_i = \sum_{j=1}^{i} \delta_{av,j}$$ **Equation 7.20**

which is then to be normalised to its maximum value. Saborio Romano [2016] applied this method to a six storey case study structure where the computed displaced shape compared very well with the first mode shape of the actual numerical model, although comparison with other limit states was not discussed.

Since this approach was developed considering the initial behaviour of the building, it means that for a target limit state drift at the critical storey, the displaced shape cannot simply be scaled uniformly until the drift in the critical storey has been reached. The presence of a soft-storey due to a column sway mechanism means that the deformation will tend to concentrate in a single storey as opposed to a number of storeys and therefore the inelastic displaced shape must be considered properly. The approach suggested here is as follows when dealing with inelastic limit states for structures expected to have a soft storey mechanism:

1. Define a target limit state storey drift θ_{ls}.
2. Identify the critical storey in the structure from the sway demand index i.e. where $SD/SD_{max}=1$.
3. For this storey, check if θ_{ls} is greater than the $\theta_{y,sys}$ of the critical storey. If it is less than $\theta_{y,sys}$, and all other storeys then the structure is still elastically responding and the normalised displaced shape can be uniformly scaled to the required target limit state storey drift.
4. If the θ_{ls} is greater than the $\theta_{y,sys}$ of the critical storey, the building is in the inelastic zone and has formed a soft-storey. In this case, the normalised displaced shape is scaled uniformly to a level that will result in the yield drift in critical storey occurring, after which the remaining drift to reach θ_{ls} is concentrated only in the critical storey.

The above approach essentially means that for linear elastic response of structures expected to form a soft storey the displaced shape can be uniformly scaled, but if the critical storey begins to yield then the deformation is concentrated solely in that storey since it is a soft storey mechanism. It should be noted that this approach ignores the fact that the governing mechanism at the critical floor may, in fact, be a beam-column joint sway rather than a pure column sway that is assumed here. The difference being that a beam-column joint sway will result in the inelastic deformation being "spread" over the two adjacent floors rather than concentrating in a single floor, as illustrated during experimental testing by Calvi *et al.* [2002] and numerical analyses by Pampanin *et al.* [2003]. This is a limitation of the developments of Saborio Romano [2016] and is noted here as a required future development for the DBA of GLD frames in Italy.

7.2.1.4 Accounting for Inelastic Behaviour

Section 7.2.1.1 described how for a given limit state, the properties of the equivalent SDOF system can be established. In order to determine the spectral values at which a given limit state is expected to occur, the inelastic behaviour of the system must be accounted for. The DBA procedure outlined in Priestley *et al.* [2007] describes the use of EVD to be computed as a function of the equivalent systems ductility demand and then computing a spectral DRF (η) as a function of the estimated EVD. In the case of RC frames, the EVD is described in Priestley *et al.* [2007] as:

$$\xi = 0.05 + 0.444\left(\frac{\mu - 1}{\mu\pi}\right) \qquad \textbf{Equation 7.21}$$

with the corresponding spectral reduction factor computed using:

$$\eta = \sqrt{\frac{0.10}{0.05 + \xi}} \qquad \textbf{Equation 7.22}$$

which is then used to compute the elastic spectral displacement as per Equation 7.6. However, more recent work by Pennucci *et al.* [2011] shows that the spectral DRF ought to be computed directly as a function of the ductility, as opposed to computing an intermediate value of EVD as this reduced the sensitivity of the terms to the GMs. While these developments have worked well for ductile RC frames, no such expressions have been calibrated to account for the particular behaviour of GLD frames. This is namely the increased pinching behaviour in the RC frame elements due to poor confinement and usage of smooth bars, the additional energy dissipation capacity of the beam-column joint mechanism and the damage sustained masonry infill elements which all collectively contribute to the overall EVD of the system. In terms of the inelastic behaviour of the beam-column joints , no EVD expressions have yet been quantified to date per se, although expressions to account for the pinched hysteretic response of degrading RC frame members have been recently Landi *et al.* [2016] using fibre-based element, although considering the discussion in Section 2.5.2 with regard to numerical modelling of GLD RC frames with fibre-based elements, such expressions may need to be validated further. To account for the effects of masonry infills, more recent work has been conducted by Landi *et al.* [2016] in an effort to quantify the contribution to EVD to the equivalent SDOF system. Despite these efforts, the expression developed by Landi *et al.* [2016] for infilled frames (Equation 7 in the original publication) tends to compute very large values of EVD when compared to experimental findings reported in Morandi *et al.* [2014] at low ductility levels, although working well for more ductile levels of response. It is acknowledged that this study carried out by Landi *et al.* [2016] represents an initial step in the quantification of EVD for infilled frames, where a limited ground motion set was used and further work is

noted to be required by Landi *et al.* [2016] in order to develop a more generalised formulation such as that proposed in Priestley *et al.* [2007] for ductile RC frames, for example. This will be illustrated further in Section 7.2.2.3 and represents one of the required future developments of the methodology for application to infilled RC frames.

7.2.1.5 Computation of the Governing Mechanism Base-Shear

Of the terms listed in Figure 7.1, one of the more important terms in estimating the characteristics of the equivalent SDOF system is the computation of the base shear (V_b). This term is principally composed of the base shear required to develop the governing mechanism (V_0) along with an adjustment to account for P-Delta effects to be discussed in the next section. For cases where a beam-sway mechanism involving the members throughout the height of the structure has been verified, the base shear can be determined from the expressions described in Priestley *et al.* [2007] for DDBD as:

$$V_0 = \frac{OTM}{H_e} \qquad \textbf{Equation 7.23}$$

where OTM is the sum of overturning moment contributions down the height of the building. However, should a beam-sway not be verified and a column sway mechanism be predicted, particular care needs to be taken in computing the governing mechanism base shear. Previous work by Landi and Benedetti [2013] suggested that in the case of a column-sway mechanism for a mechanism on the ground floor, the base shear term could be taken as the shear capacity of the critical storey via the expressions in Equation 7.11 and Equation 7.12. This approach of assuming the base shear to be the shear capacity of the critical storey works well in the case of a soft-storey at the ground floor since the shear capacity at that level corresponds to the actual shear transmitted to the foundation, but in cases of a column-sway mechanism forming on levels other than the ground floor, underestimation of the base shear can arise. Consider the two diagrams illustrated in Figure 7.2, where one structure is shown to form a soft-storey at the base and the other forms a mechanism at the third floor. In the first case, the shear demand profile increases gradually until the demand reaches the storey shear capacity at the ground floor and the mechanism develops. The actual base shear will correspond to the capacity developed at that floor as the mechanism provides a type of "building plastic hinge" per se, whereby it caps the amount of base shear transmitted to the foundations. In this case, it is correct to assume the base shear corresponds to that of the critical storey (V_{crit}). However, consider the second case where the mechanism forms on the third floor. This storey develops its storey shear capacity as illustrated, but the actual base shear in the structure for this type of mechanism is no longer equal to V_{crit}. This is seen from Figure 7.2 to be as a result of the remaining contributions from the lower floors to the actual base shear. This contribution may be relatively small but in certain situations can be significant and ought to be considered properly. As such, it is recommended here that the mechanism base shear be taken as the

shear force developed at the base of the structure as opposed to taking just the shear developed at the critical storey. In addition, it is noted that this approach applies to situations where the mechanism has actually developed (i.e. $\mu>1$). For situations where a structure expected to form a column-sway mechanism is still responding elastically, the base shear may be computed using the overturning moment approach given in Equation 7.23. This distinction will be particularly relevant in estimating the base shear at lower limit states examined as part of PBEE. The impacts of these different assumptions will be discussed via application to case study frames in Section 7.2.2.2.

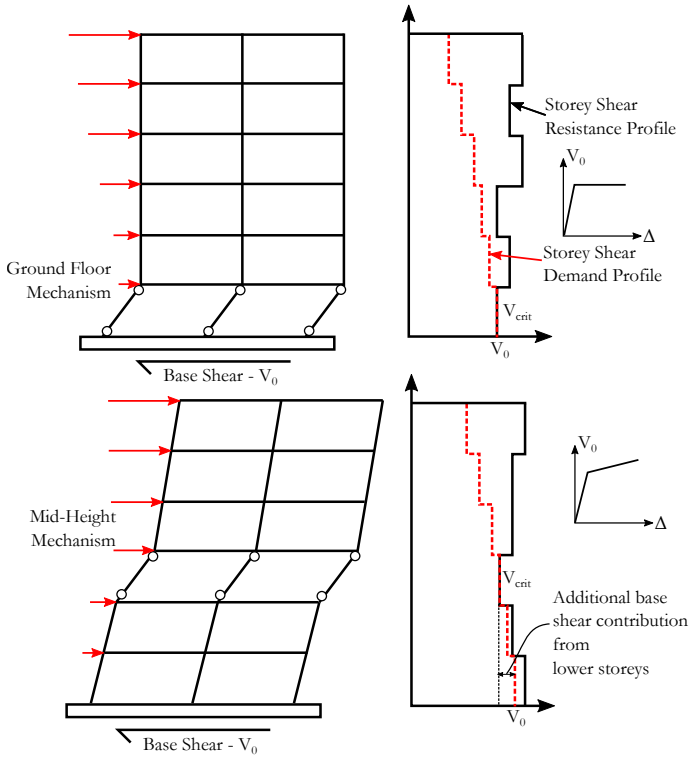

Figure 7.2. Illustration of the estimation of the mechanism base shear demand for column-sway mechanisms occurring at storeys other than the ground floor.

For the case of infilled frames, the storey shear force needs to be modified to account for the additional contribution of the diagonal compression strut action of the masonry infill. This is done by converting the expected diagonal strut force into the corresponding shear force and adding this to the shear capacity of the surrounding RC frames members. Using the masonry infill model described in Section 2.6.2, the masonry infill contribution can be

computed for a given level of storey drift and added to the frame capacity. This allows also for a reduction in the shear resistance of the infill with increasing storey drift.

7.2.1.6 Accounting for P-Delta and Higher Mode Effects

Another issue relating to the DBA of structures relates to the handling of P-Delta effects, which refers to the additional overturning moment present in the structure due to the second-order geometry effects of the gravity loading acting at each level of the building. To account for this, Priestley *et al.* [2007] describe how the total base shear (V_b) can be adjusted to consider P-Delta effects by reducing the base shear computed from the governing mechanism (V_0) by the following term:

$$V_b = V_0 - V_{P\Delta} = V_0 - C\frac{m_e g \Delta_{cap}}{H_e} \qquad \textbf{Equation 7.24}$$

where the coefficient C is a term relating to the structural system being considered. For RC frames, Priestley *et al.* [2007] proposed the use of 0.5 and for steel frame structures C=1.0, for example. It should be noted that this C term has been determined from numerical studies on ductile frame systems that do not consider post-capping strength and stiffness degradation and therefore, should be treated as placeholder values with a view to a more elaborate consideration of second-order geometry effects in addition to strength and stiffness degradation on structures such as those examined previously, where the effects of such strength and stiffness degradation has been noted in studies such as Ibarra *et al.* [2005] to be of crucial importance when considering structural collapse.

In addition to P-Delta effects on the structural response, another issue is the presence of higher mode response and their influence on the structural behaviour. The influence of higher mode effects is mainly a function of the number of storeys and structural system, where Priestley *et al.* [2007], and more recently Sullivan *et al.* [2012], recommend its consideration through the use of a ω_θ reduction term to be applied to the displaced shape expression that is a function of the number of storeys and whether structure is expected to form plastic mechanisms throughout the height of the structure or solely at the base of the structure. Again, it is noted how these recommendations are difficult to apply to a structure such as a GLD frame that is neither a ductile beam-sway frame or an RC wall structure with a hinge at the base, for which these recommendations were developed. Since this term generally comes into play for structures with number of storeys greater than five to ten (using the recommendations of Sullivan *et al.* [2012]), it is not considered further for the structures examined in this study, but is noted as a pertaining issue for tall structures nevertheless and is a topic worth future consideration in the context of GLD frames. In addition, the effects of torsional response are not discussed here as the case study structures are regular and symmetric in plan.

7.2.2 Application to Case Study Frames

The DBA procedure outlined in Section 7.2.1 is now applied to the 2D case study frames discussed in Section 5.1, where the accuracy of DBA in correctly identifying the critical mechanism in the structure, backbone response and GM intensity to achieve a given limit state are compared in the following ways:

1. The displaced shape is at each limit state is computed for each of the four limit states and compared to the displaced shapes of the SPO curves computed in Section 5.2.
2. For each of these four points on the SPO curves, the developed base shear in the system is computed from the mechanical properties of the structure to predict the backbone curve at each of the limit state points discussed in Section 5.2. Comparison is again made with the SPO analysis backbone curves to highlight some critical issues in correctly estimating the backbone for non-ductile column sway mechanisms.
3. Assess its ability to predict the IM at each limit state, meaning that for each $S_d(T_1)$ computed for each limit state, as per Figure 7.1(e), the corresponding $S_a(T_1)$ is computed and this predicted intensity from DBA is then compared to the median intensity for each limit state computed from IDA in Section 5.5

7.2.2.1 Comparison of Displaced Shape

Following the establishment of a procedure to estimate the expected displaced shape at various limit states, the results of the SPO analyses conducted on the 2D GLD frames in Section 5.2 are used for comparison and validation. This comparison is conducted here for the case study frames modelled without infill since the recently developed procedure by Saborio Romano [2016] does not yet account for the presence of masonry infill. The displaced shapes for both of these typologies were shown to be dissimilar via SPO and IDA. As such, the assumption of the displaced shape using the approach proposed by Saborio Romano [2016] to the case of infilled frames cannot be performed without further investigation. This represents another critical area in which the DBA of GLD frames in Italy needs to be developed. In any case, the frames without infill are discussed to highlight how the approach developed by Saborio Romano [2016] provides very promising results in terms of dealing with GLD frames that are expected to form sway mechanisms that are notably different to the traditional beam-sway displaced shape used in DDBD for ductile frames.

As previously discussed, the SPO were conducted at four different limit states that are defined at various levels of ductility in the structure. Figure 7.3 shows the comparison between each of the four case study frames without infill at the four limit states. As is evident, the displaced shape procedure outlined here provides an excellent match across all limit states in nearly every instance. This is especially evident in the case of the six storey

building in how the stiffness of the lower floors is captured well in the elastic range of response and how the displaced shape moves gradually from the elastic first mode pattern to the concentration of damage on the fourth floor for the SLC limit state. One instance where it is clear that more research is required, in terms of considering the beam-column joint mechanism's influence on the distribution in drift between adjacent storeys, is evident in the case of the three storey frame at the SLC limit state. The procedure highlighted above determines that a soft storey mechanism forms at the second storey of the building and when considering the comparison at the lower limit state SLV, it appears the method captures this well. However, at the final limit state SLC, the SPO has formed a joint mechanism between the first and second floors resulting is a spread in drift demand between these two floors.

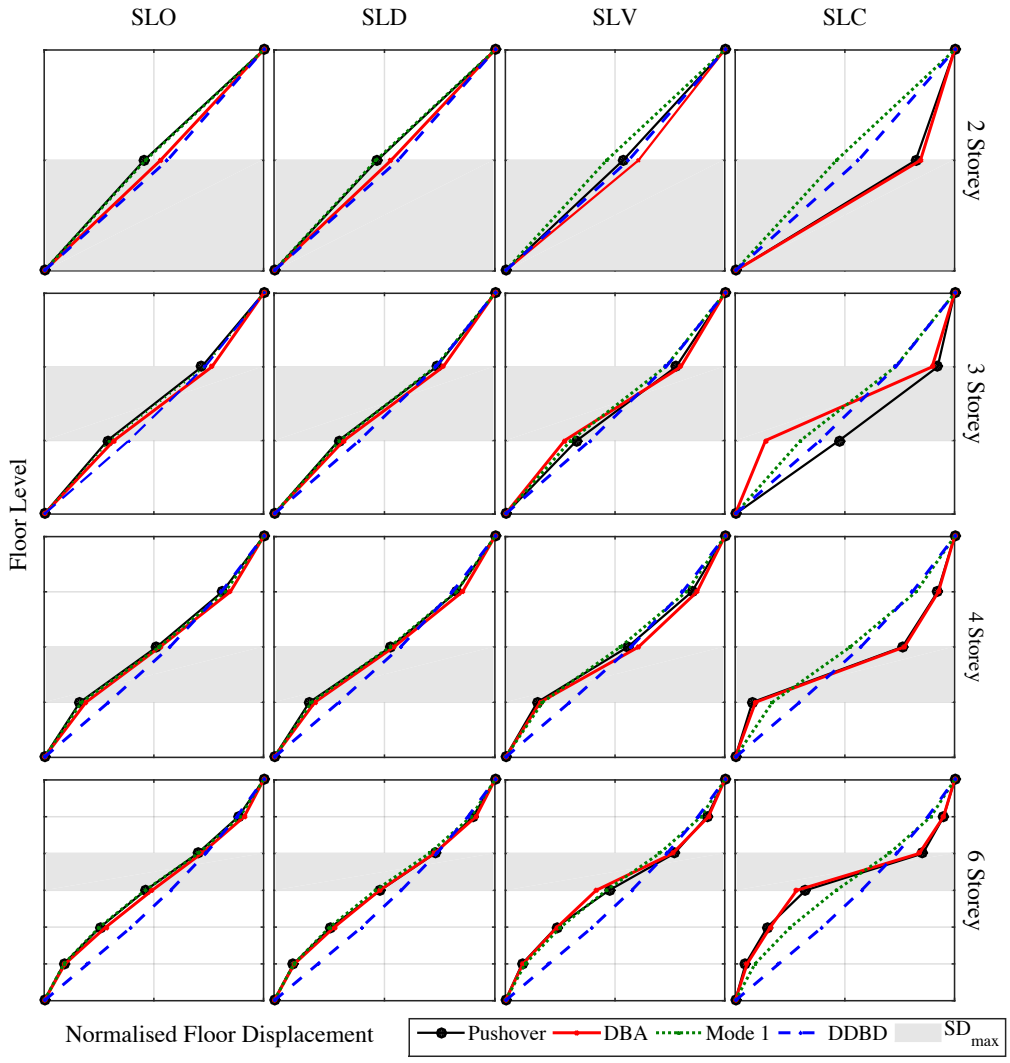

Figure 7.3. Comparison of the normalised displaced shape expression with the SPO analyses at various limit states.

Also noted in blue in each of the plots is the displaced shape that would be expected if a beam-sway mechanism had been assumed and no consideration of the sway potential indices was given, resulting in a blind implementation of the method proposed for ductile frames in Priestley *et al.* [2007] and more recently refined in Sullivan *et al.* [2012]. It is clear that such a definition of displaced shape is inappropriate for the GLD frames considered

here. Lastly, the critical storey predicted using the sway demand index is also hatched in grey for each case study building in Figure 7.3, where it can be seen that the critical storey was predicted correctly in each case. This correct prediction of the storey mechanism in each case provides further validation to the use of the sway demand index as it has not been extensively verified using numerical analyses in the context of GLD frames.

7.2.2.2 Comparison of Backbone Response

Having determined the likely mechanism using the sway potential and demand indices previously discussed, the base shear associated with the anticipated mechanism at different levels of response can be computed to construct the DBA backbone curve. That is, knowing that a column sway mechanism will form, for example, the total base shear can be computed by estimating the storey shear from the critical storey along with the other relevant contributions to the total base shear from the other storeys. For the case of the infilled frames, the contribution of the masonry infill is also incorporated. The contributions from the other floors that are expected to remain elastic are determined as ratio of the expected ductility, whereby using the yield drift approximation formula given in Equation 7.13 or Equation 7.14 for a beam or column sway, respectively, the expected ductility can be computed from the ratio of the limit state demand drift profile. For storeys where the response is expected to remain elastic, the shear contribution is computed as the product of the ductility times the storey shear capacity.

Following this approach, the DBA backbone curves are computed for each of the case study frames and compared to the results of SPO analysis at each of the four limit states previously outlined in Section 5.5. This is done by using the displaced shape along with member properties to compute the relevant mechanism forces. Section 7.2.1.5 highlighted how the use of Equation 7.23 is to be used in cases where a full stable response throughout the height of the building can be expected. For cases where a column mechanism is anticipated, the use of the storey shear at the critical storey as the total base shear has been previously discussed in addition to the use of this shear in combination with any other base shear contribution, as outlined in Figure 7.2. Each of these approaches will be investigated here to illustrate the relative impacts on the backbone estimation. In the case of the SLC limit state, the base shear was calculated by computing the mechanism base shear and reducing it by 20% to account for the reduction in global capacity, as per the limit state definition outlined in Section 5.5.

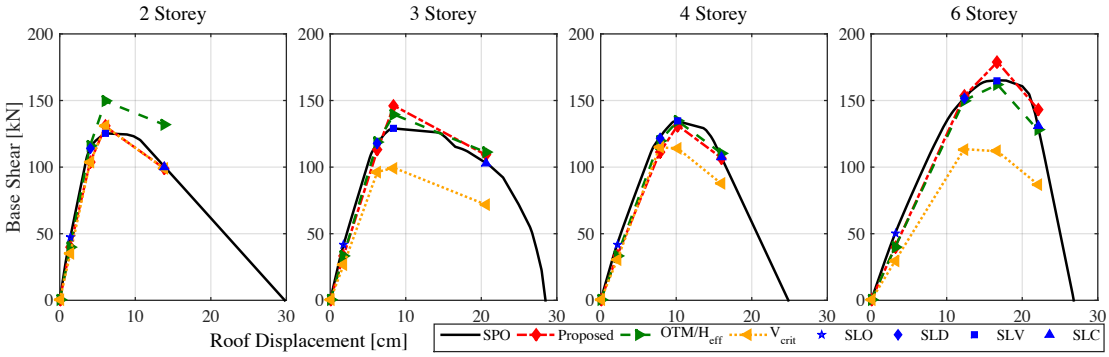

Figure 7.4. Comparison of the backbone response computed via DBA to that of SPO analysis for the case study frames modelled without masonry infill.

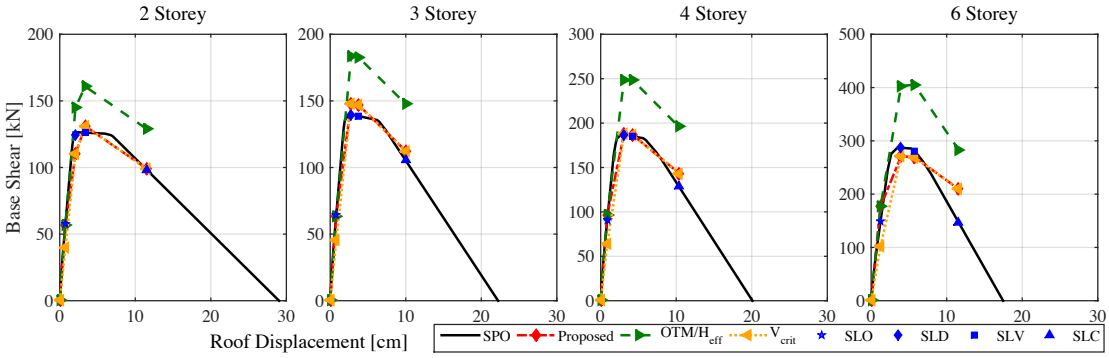

Figure 7.5. Comparison of the backbone response computed via DBA to that of SPO analysis for the case study pilotis frames.

Figure 7.4 and Figure 7.5 show the comparisons of the model without infill and pilotis frame, respectively, whereas Figure 7.6 and Figure 7.7 show the same plots for the infilled frames with strong and weak infills. First comparing the predictions of the four points of the backbone using Equation 7.23, which inherently assumes that a stable beam-sway mechanism has formed up the height of the structure. This approach tends to overestimate the backbone curve since in none of these cases has a beam-sway mechanism formed, leading to the base shear being computed with storey shears at levels above the critical storey that are, in fact, not contributing to the overall base shear since the critical storey acts as a type of structural fuse. This is particularly the case for the infill frames, where examining the pilotis frames in Figure 7.5 the backbone is clearly overestimated since the base shear has been capped by the critical ground floor storey shear capacity.

In addition, the calculation of the backbone curve points using the assumption that the base shear is the critical storey shear capacity is examined. For the case of the pilotis frames, this approach works very well with the SPO curve being very well represented. This is an expected result since the pilotis frames all form their mechanisms at the ground floor. However, in the case of the frames modelled without infill, where Figure 7.3 has shown the critical storey to be at storeys other than the ground floor, this approach of using the critical storey shear capacity for the base shear no longer works very well, as illustrated in Figure 7.4 for the three, four and six storey buildings. The cause of this underestimation was demonstrated in Figure 7.2 and is clearly illustrated here through comparison with the SPO curves. The infilled frames did not form mechanisms at levels above the ground floor, hence, this remark could not be observed in these cases also.

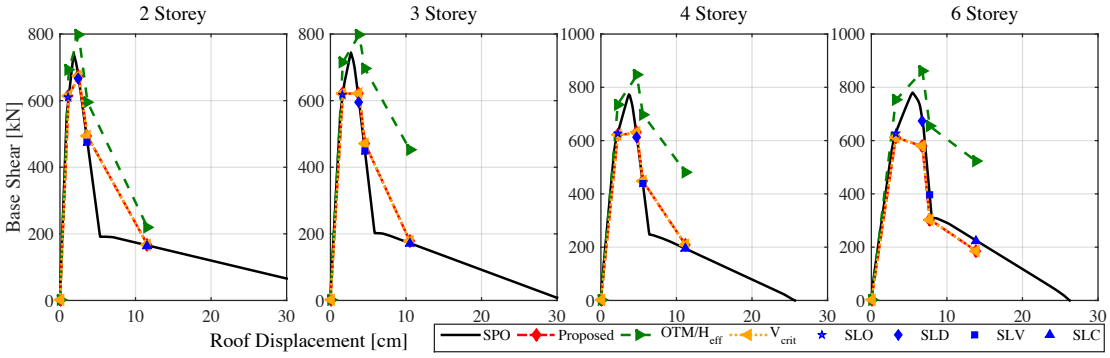

Figure 7.6. Comparison of the backbone response computed via DBA to that of SPO analysis for the case study frames with strong masonry infill.

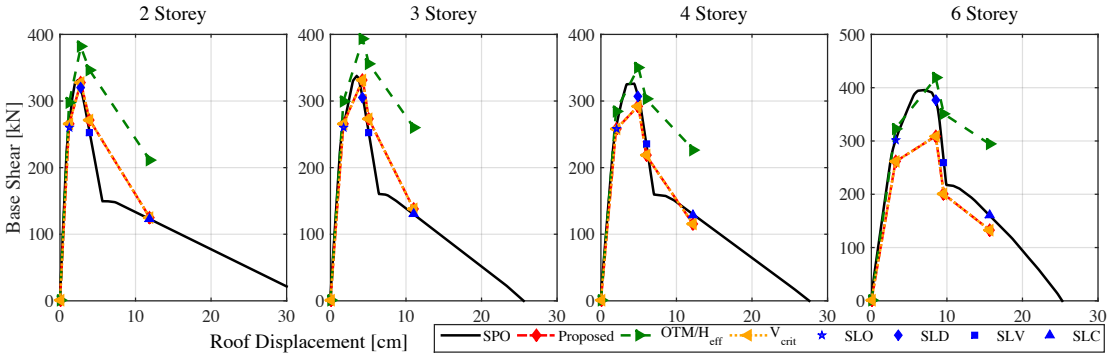

Figure 7.7. Comparison of the backbone response computed via DBA to that of SPO analysis for the case study frames with weak masonry infill.

The final comparison shown in red in each figure corresponds to the recommended approach to computing base shear backbone for each of the frame typologies. This approach is quite simple and works as follows. For the limit states where the structure is expected to be responding elastically (i.e. SLO), the base shear can be computed using Equation 7.23 as the structure is still maintaining a stable mechanism throughout the height of the building. For limit states beyond this, the base shear is computed using the approach highlighted in the lower part of Figure 7.2, where the base shear is computed by taking the base shear on the ground floor of the structure and not solely as the capacity of the critical storey. This approach is shown to work very well in each of the structural typologies, with the elastic base shear being computed quite well along with the peak force and the degrading total base shear due to loss of capacity and P-Delta effects. In addition, the loss of capacity of the masonry infills was also well captured for the frames shown in Figure 7.6 and Figure 7.7, confirming that the approach described in this section worked very well in estimating the backbone response of GLD frames to be assessed using DBA when compared to the results of SPO analysis.

7.2.2.3 Comparison of Median Limit State Intensity

In addition to comparing the SPO displaced shape and backbone curve to that predicted by the DBA method outlined above, the intensity required to induce each limit states can also be computed using the process illustrated in Figure 7.1(e), whereby the estimated displaced capacity of the structure is used in combination with the spectral displacement reduction factor to estimate the elastic spectral displacement demand. This elastic spectral demand at the effective period can then be converted into a spectral acceleration at the first mode period, which is the IM adopted for the IDA discussed earlier in this chapter. The intensity computed for each limit state can then be compared to the median intensity estimated in Section 5.5, where fragility functions were fitted to the IDA data using the maximum likelihood method described in Baker [2015]. Comparing these two intensities will show the DBA methodology's ability to not only correctly predict the expected mechanism but also the median intensity at which it will occur. The ability to estimate this intensity represents a significant benefit of the DBA method as it allows the user to then compute a corresponding MAF of exceedance via an appropriate site hazard curve and thus permit further risk analyses in relation to the current building to be carried out without the need for detailed numerical analyses.

As previously discussed in Section 7.2.1.4 and highlighted in Figure 7.1(e), an estimate of the EVD in the system is required to compute the elastic spectral displacement using Equation 7.6. In the case of the frames modelled without infill, the EVD expression described in Priestley *et al.* [2007] for RC frames is tentatively adopted, whereas for the case of the infill frames the expressions described in Landi *et al.* [2016] as Method B using a secant stiffness that incorporates the strength contribution of the infill is adopted. Figure

7.8 shows the comparison of the median intensities for each of the case study frames modelled without infills, where DBA corresponds to that estimated here and IDA corresponds to the median intensity measure and percentiles representing the record-to-record variability in intensity previously computed in Section 5.5. The percentile values are included to give an idea of the dispersion to be expected with such median values since the maximum likelihood method is a fit to the IDA data and not an exact value. For the case of the frames modelled without infills and the pilotis frames, the comparison between the medians predicted from both methods is very good, with the DBA prediction being very close to that of the IDA fragility function medians or within the percentile range plotted.

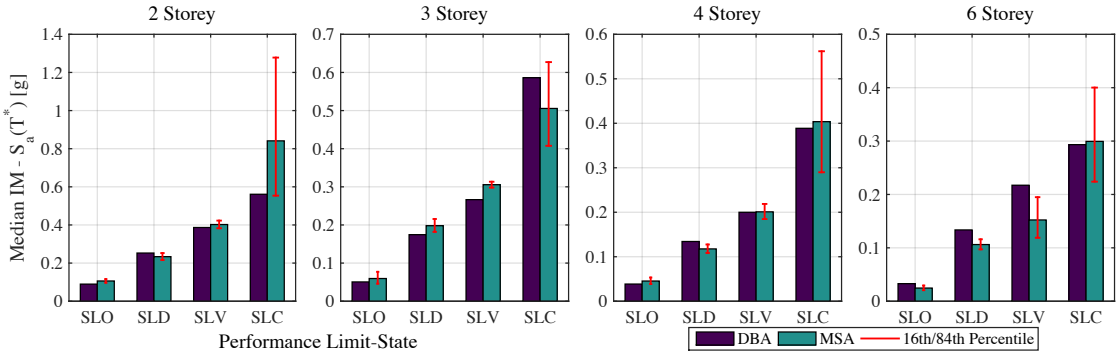

Figure 7.8. Comparison of the median limit state IM computed via DBA to that of IDA for the case study infill frames modelled without masonry infill.

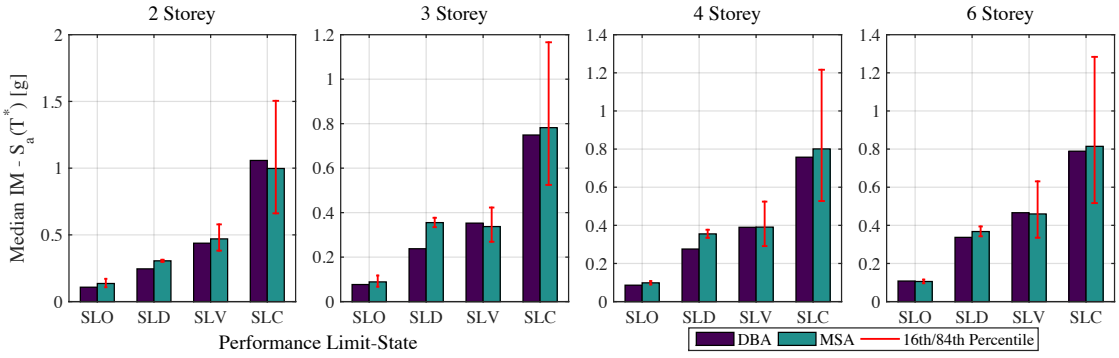

Figure 7.9. Comparison of the median limit state IM computed via DBA to that of IDA for the case study pilotis frames.

For the infilled frames plotted in Figure 7.10 and Figure 7.11, the overall magnitude of the median IM is similar but a few observations can be noted. The first is that the DBA prediction tends to overestimate the median intensity for the SLO and SLD limit states,

where in some cases the intensity is higher than that of the more severe limit states. The two storey frame in Figure 7.10, for example, where SLO and SLD intensities are higher than those of SLV and SLC, which doesn't make sense conceptually. This can be attributed to an overestimation in the EVD as a result of the expressions provided by Landi *et al.* [2016], since the base shear capacity was estimated well using DBA, leaving the EVD expression as the only other source of notable uncertainty when completing the last steps of DBA outlined in Figure 7.1. Examining the EVD computed at these limit states, it is noted how the expressions provided by Landi *et al.* [2016] compute EVD of over 25%, which is rather large when compared to experimental values reported in Morandi *et al.* [2014] that were more of the order of 10%. For the higher limit states, however, the comparisons are much better with the median value general falling within the 16th and 84th percentile valmues. Examining the median values of the weak infill in Figure 7.11, the medians from DBA tend to overestimate those from IDA, whereas the corresponding strong infill ones tended to overestimate the median intensity. This suggests that the expected EVD contribution from the energy dissipation due to damage in the masonry infill is also a function of infill typology, with stronger infill having a higher EVD contribution than the weak infill. This agrees with what one would expect if the steady cycle energy contribution is considered, as the overall higher strength of the stronger infill means that a greater amount of hysteretic energy is dissipated leading to a higher EVD. These observations highlight the urgent need for a large parametric study into the quantification and calibration of appropriate EVD models for various masonry infill typologies.

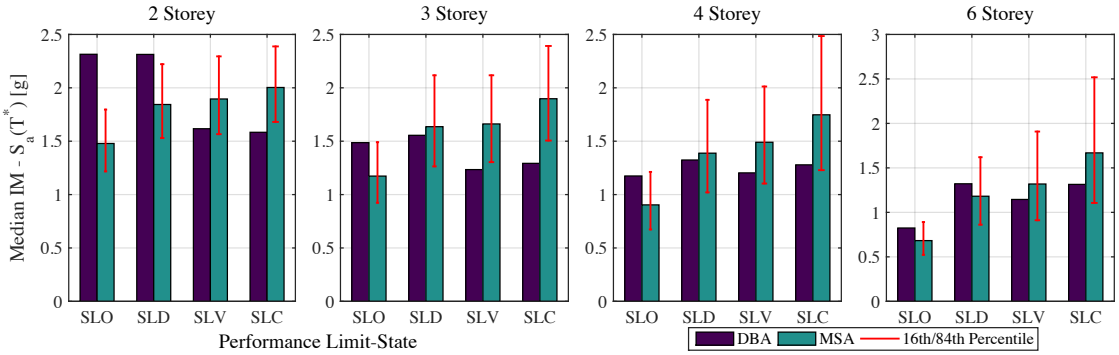

Figure 7.10. Comparison of the median limit state IM computed via DBA to that of IDA for the case study frames with strong masonry infill.

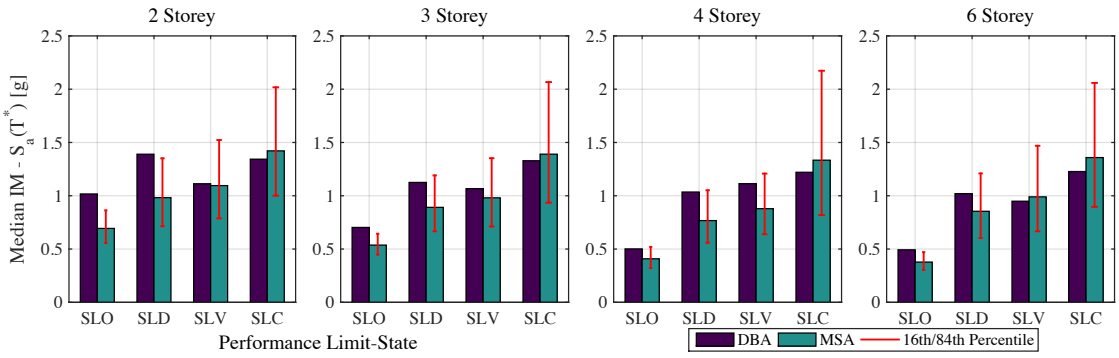

Figure 7.11. Comparison of the median limit state IM computed via DBA to that of IDA for the case study frames with weak masonry infill.

7.2.3 Extension of DBA for Loss Estimation of GLD Frames

Section 7.2.2 has shown how a simple and direct method such as DBA can be used to estimate the median response parameters at various limit states of a building with little seismic design considerations and also the presence of masonry infills. Using this procedure, two distinct parameters can be determined; the intensity at which each limit state is expected to occur and the median demand parameter of interest at that intensity, such as the storey drifts and the floor accelerations. Using these two pieces of information, one can perform what is termed displacement-based loss estimation (DBLE) on these structures to estimate the monetary losses with respect to intensity and other performance metrics such as the EAL, as discussed previously in Sullivan and Calvi [2011]. Figure 7.12 illustrates the basics of the approach described by Welch *et al.* [2014], where the MAF of exceedance of each limit state is estimated from the site mean hazard curve using the computed IM from DBA along with appropriate considerations of dispersion, as per Cornell *et al.* [2002]. This will provide the values on the vertical axis in Figure 7.12. To compute the values of mean damage factor on the horizontal axis in Figure 7.12, which is defined as the expected loss normalised by the replacement cost of the structure, Welch *et al.* [2014] employed the EDP-DV functions developed by Ramirez and Miranda [2009].

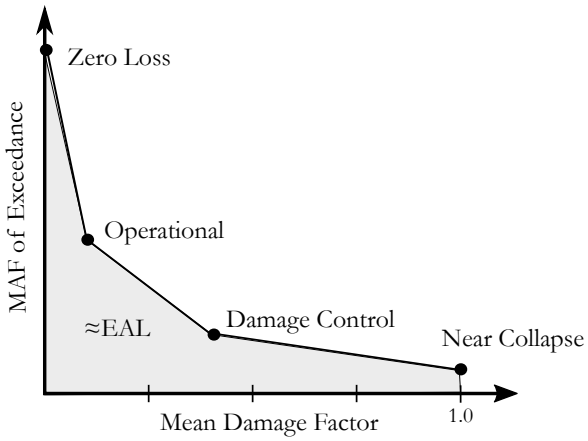

Figure 7.12. Illustration of the fundamental aspects of displacement-based loss estimation (DBLE) (After Welch *et al.* [2014]).

More recently, Sullivan *et al.* [2014] expanded this concept to employ the use of the PACT software [FEMA P58-3, 2012], whereby the DBA methodology is applied at a number of intensities to estimate the median response and intensity at a number of return periods. Using these median response ordinates in combination with estimates of the various dispersions associated with the drift, acceleration and modelling uncertainty, Sullivan *et al.* [2014] outline a simple approach with which the structure can be assessed without the need for advanced numerical analyses. Previous work using DBA and DBLE has tended to focus on more ductile construction (see Welch *et al.* [2014] and Sullivan *et al.* [2014], for example), and what the illustrations and discussions above have indicated is that such a methodology is applicable to older structures (e.g. Cardone and Flora [2014]), albeit with some required developments in different areas.

7.3 IMPLEMENTATION OF A MORE SIMPLIFIED APPROACH TO LOSS ESTIMATION

Section 7.2 discussed the use of more simplified methods for assessing older GLD frames in Italy without the need of computationally expensive NRHA. It was shown how the various behavioural aspects of GLD RC frame typologies can be estimated using more simplified approaches to develop tools that practising engineers can use to estimate the median value of response in practical applications. Section 7.2 discussed the DBA framework as a whole and compared the different ingredients required for the method to the available information for the different structural typologies as a result of extensive NRHA via IDA. This highlighted a number of key areas that need to be developed further in order for DBA to be confidently applied to GLD RC frames in Italy knowing that the various particularities associated with these frames can be adequately captured by the method. However, assuming that one can estimate the median response parameters at

different intensity levels of the case study building using DBA, these median intensities can be used in conjunction with some estimation of the dispersion and correlations in place of more extensive NRHA to conduct a loss estimation of the building. This section looks to outline how one may follow such a procedure in terms of how the median values, dispersions and correlations are to be accounted for and compares them to the results of the loss estimation study carried out in Section 6.2 to examine it's applicability to GLD RC frames. The determination of the median demand parameters is first discussed, followed by the selection of dispersion values to account for record-to-record variability and modelling dispersion for the different demand parameters and in addition to the corresponding correlations between them. This process described here is illustrated in Figure 7.13 and is contrasted to that followed previously in Section 6.2. These are then compared with the extensive NRHA results to examine how simplified method of analysis can be implemented to compute the expected loss curve, followed by a time-based assessment to examine the prediction of the annualised losses through the comparison of the EAL for the different buildings.

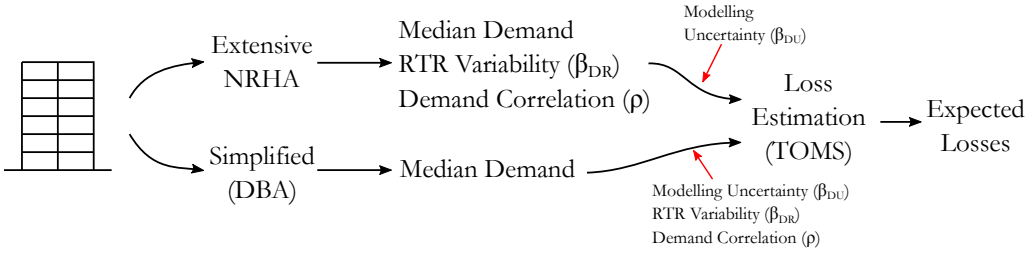

Figure 7.13. Illustration of the process used to conduct a loss estimation using median values obtained from simplified analysis along with some representation of the dispersion and demand parameter correlation.

7.3.1 Estimation of Median Demands

The first step is to compute an estimate of the median demand parameters of interest. In the case study structures examined here, these correspond to the PSD and PFA at each level of the building. This was discussed at length in Section 7.2, where the various aspects of the anticipated behaviour of the frames that need to be considered in order to correctly predict the drift demand at different limit states were discussed. However, when currently available methods were compared with the extensive IDA conducted in Chapter 5, this aspect was noted to be an area in which the DBA methodology is still lacking for application to GLD RC frames with masonry infills. The initial applications to the frames modelled without infill showed very promising results in terms of how the elastic mode shape is captured, in addition to the correct estimate of the expected location of the inelastic mechanism. Contrasting this approach previously discussed with that outlined in FEMA P58-1 [2012] for simplified analysis of structures, no numerical modelling of the structure

was required in order to estimate the response at the different limit states. In addition, the simplified procedure outlined in FEMA P58-1 [2012] relies on elastic analysis and subsequent empirical correction factors to account for the nonlinear behaviour of the structure. The reliance on elastic analysis to examine the inelastic response of a structure at different limit states is somewhat notorious in terms of its limitations and applicability in general (see Priestley [1993, 2003], for example), but the use of such elastic analysis methods inherently assumes that the initial elastic mode shape to be representative of the building's damage distribution with increasing intensity; a point which Figure 7.3 clearly illustrates not to hold true in the case of GLD RC frames. The DBA methodology, on the other hand, has demonstrated its superiority and potential in this regard.

In addition to the estimation of the median PSD at a number of intensities for the different case study structures, the median PFA is a parameter also required in loss estimation. This was not discussed at length in Section 7.2 as initial comparisons with available PFA estimation methods for frames structures were found to be wholly inadequate in their application to GLD RC frames with masonry infill. The reasons for this are two-fold, where existing methods such as that outlined in FEMA P58-1 [2012] or the more recently developed methods [Calvi and Sullivan, 2014; Sullivan *et al.*, 2013], among others, rely on certain assumptions regarding building characteristics and performance. First, these aforementioned methods have been primarily developed for ductile structures that are expected to form a stable and ductile mechanism (e.g. FEMA P58-1 [2012]), whereas others have been developed with more refined considerations of dynamic response but are currently limited to elastically responding structures. This is particularly relevant in the case of GLD frames as the presence of a soft-storey mechanism greatly influences the PFA profile along the building height. Consider the case of the pilotis frames, the presence of the soft storey at the ground storey means that with increasing intensity, the amount of accelerations that can be transmitted up along the height of the structure will be capped by the "yield acceleration" of the ground floor. This results in a sort of upper bound for the PFA profile that depends on the ground storey's strength capacity, but will depend on higher mode contributions also, and will not be greatly influenced by an increasing PGA. Contrasting this with the FEMA P58-1 [2012] that essentially determines a PFA profile and scales this up with increasing PGA, meaning that the filtering of accelerations from a column-sway mechanism storey and up will not be captured. Second, the presence of the masonry infill has yet to be accounted for explicitly with methods such as that provided in FEMA P58-1 [2012] specifying empirical coefficients for wall structures, bare frames and braced frames, but not infilled frames. The influence of the presence of masonry infills will play a significant role in the PFA profile along the height of the building. This was noted in a recent comparison study on RC frames with masonry infill by Lucchini *et al.* [2014], where the impact of masonry infill on floor spectra with respect to a frame without masonry infill was seen to be significant. As such, this aspect should be considered in detail as part of future work.

The above paragraph along with the concluding remarks of Section 7.2 have highlighted how DBA represents a simplified methodology that possesses numerous advantages with respect to existing methodologies developed for modern, seismically designed structures. This was shown in Section 7.2 in how the displaced shape, limit state and column-sway mechanism was captured well when trialled against GLD RC frames modelled without infills. However, a number of remaining developments are required in order to be fully applied without the aid of the advanced numerical modelling for the structures outlined in this thesis. These remaining developments have been identified and noted for future research. The focus of this section, however, is to demonstrate how the eventual DBA methodology for GLD RC frames with infill can be used in conjunction with other information presented in this thesis to perform a simplified loss estimation and determine some of the salient parameters discussed in Section 6.2. To this end and for the purposes of illustration of the procedure, it will be assumed that accurate values of the median response can be obtained. In order to illustrate the application, however, the median values for each demand parameter will be taken from IDA analysis under the assumption that the user will be able to compute these median values using the finalised DBA methodology.

7.3.2 Estimation of Demand Dispersions and Correlations

Chapter 5 presented the results of the IDA and SPO analysis for the various case study frames, which were analysed at various intensities and their performance established in terms of the peak storey drift and floor acceleration demands. While these results provide valuable information regarding the relative performance of the buildings that form the basis of a loss estimation study in Chapter 6, an opportunity to establish some other parameters that are required for more simplified method of analysis arises. The first of these is the dispersion due to record-to-record variability in the demand parameters, where the results in Section 5.3 presented the response in terms of a median and dispersion of the various parameters. This dispersion arises from the record-to-record variability in the response of structures and is classified as an aleatory source of uncertainty, whereas the modelling uncertainty associated with such frames was discussed and quantified in Chapter 4. Given that extensive NRHA has been conducted for various structures with different modelling approaches, this record-to-record variability can be quantified for these frames and simplified empirical values proposed for usage in the absence of more refined analysis. It is acknowledged that there are certain limitations associated with using empirical dispersion values to incorporate record-to-record variability, as highlighted by Fox and Sullivan [2015] who described a more refined approach to quantifying such variability in RC wall structures. However, as a number of the required ingredients to adopt the approach outlined by Fox and Sullivan [2015] are not always available for GLD RC frames (e.g. appropriate equivalent viscous damping and displacement reduction factor models, for example), the use of empirical values is adopted here.

In addition to the record-to-record variability of the individual demand parameters, the actual correlation between each of these parameters needs to be considered such that when the median and dispersion values are supplied to the TOMS software tool presented in Chapter 3, for example, the tool takes these medians and dispersions of the demand parameters to create a larger set of sampled realisations using Latin Hypercube Sampling before proceeding to conduct a damage and subsequently a loss estimation analysis for the given structure and its damageable inventory. During this random sampling, however, it is crucial that the correlations between various demand parameters be respected such that when for a single realisation, a set of demand parameters that are compatible with each other are sampled. This aspect is also discussed in more detail in Section 3.3.1.2, but can be simply stated as follows - if a high value of first storey drift is sampled, modal analysis and mechanics-based reasoning suggest that the second storey's drift is also likely to be high and therefore are correlated, which must be considered during the random sampling.

7.3.2.1 Record-to-Record Dispersion

As previously discussed, following the determination of the median response using DBA some estimate of the dispersion due to both record-to-record variability and modelling uncertainty are required to conduct simplified loss estimation. Chapter 4 discussed the quantification of the modelling uncertainty in older GLD type frames examined here, where the proposed values were specified in terms of demand parameter, structural typology and limit state. This section conducts a similar quantification for the record-to-record variability to propose a similar set of simplified dispersion values for the various structural typologies considered here. The results of the IDA of the 2D case study frames are used as the basis for this quantification to which a simple table of proposed values are given for use in simplified assessment of GLD frame structures. obviously, such a simplification of the demand dispersion is not without its drawbacks in terms of accuracy, but it is deemed to be an improvement on the current default values for record-to-record dispersion available for GLD RC frames in Italy.

As in the case of quantifying simplified values for modelling uncertainty in GLD frames, the dispersion due to record-to-record variability of both PSD and PFA at each storey is separated in terms of structural typology and intensity, which are plotted in Figure 7.14 to Figure 7.19. By separating the dispersions also in terms of number of storeys and limit state and then taking the envelopes of the dispersion with respect to intensity, the proposed values are listed in Table 7.1.

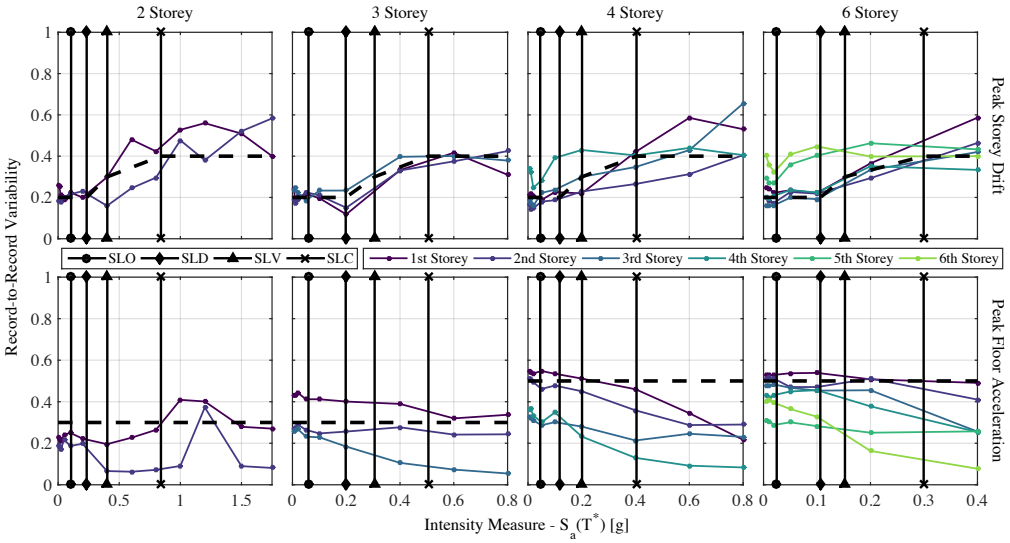

Figure 7.14. Observed record-to-record variability in PSD and PFA for 2D frames without masonry infill modelled along with proposed values.

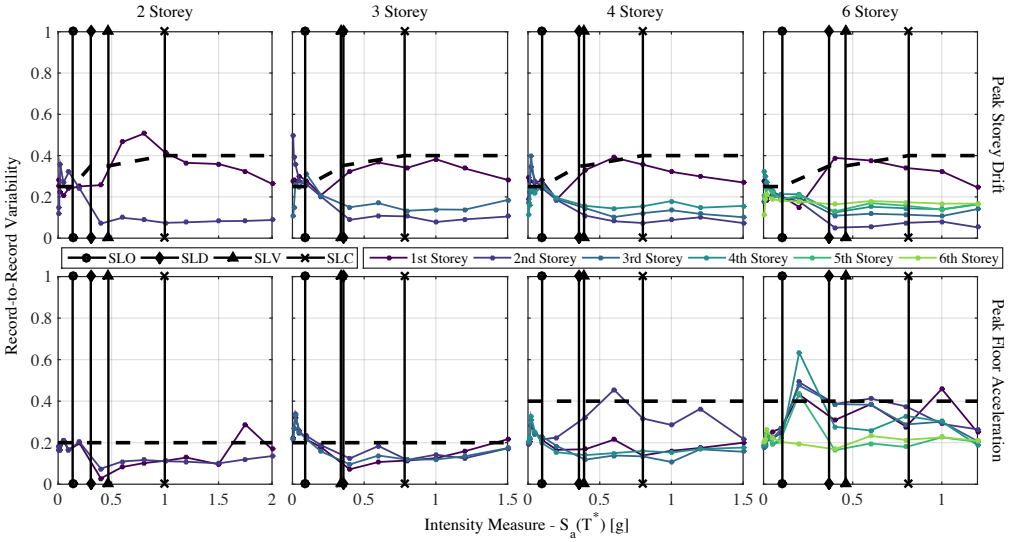

Figure 7.15. Observed record-to-record variability in PSD and PFA for 2D pilotis frames along with proposed values.

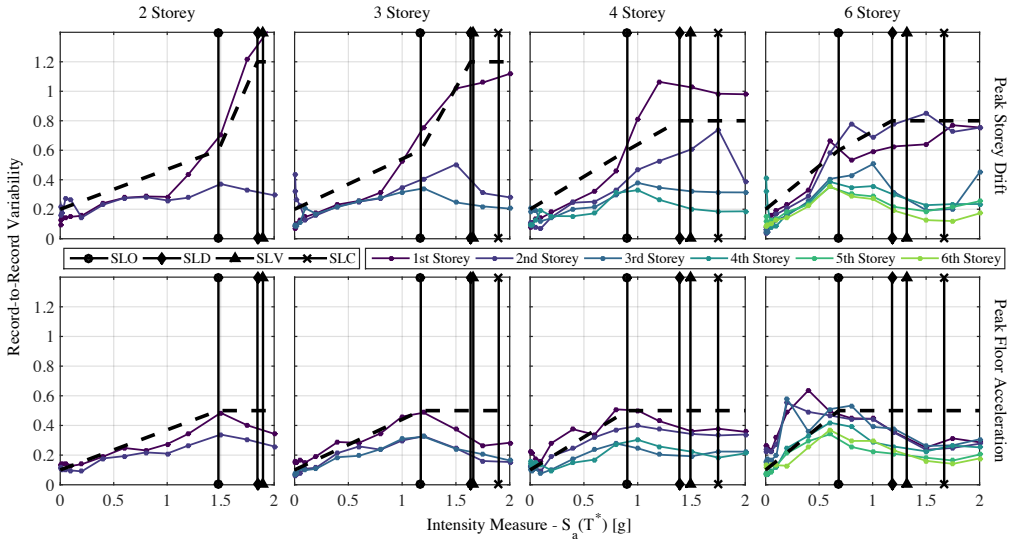

Figure 7.16. Observed record-to-record variability in PSD and PFA for 2D strong infill frames modelled using a single diagonal strut approach along with proposed values.

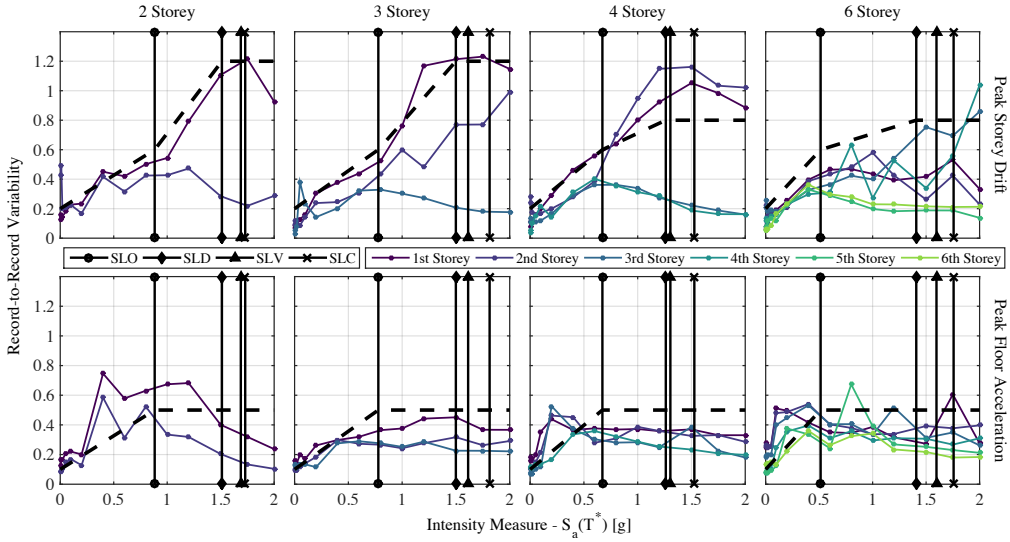

Figure 7.17. Observed record-to-record variability in PSD and PFA for 2D strong infill frames modelled using a double diagonal strut approach along with proposed values.

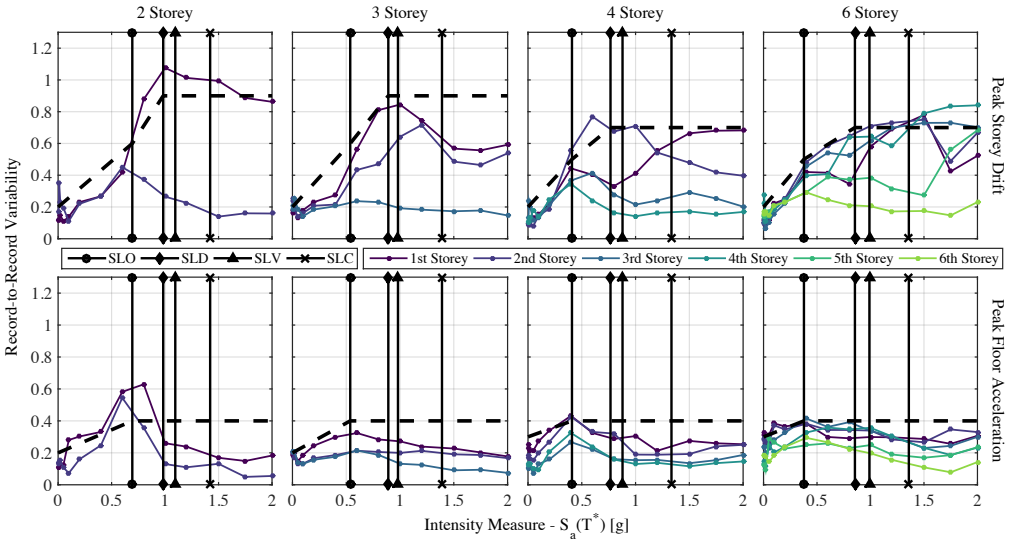

Figure 7.18. Observed record-to-record variability in PSD and PFA for 2D weak infill frames modelled using a single diagonal strut approach along with proposed values.

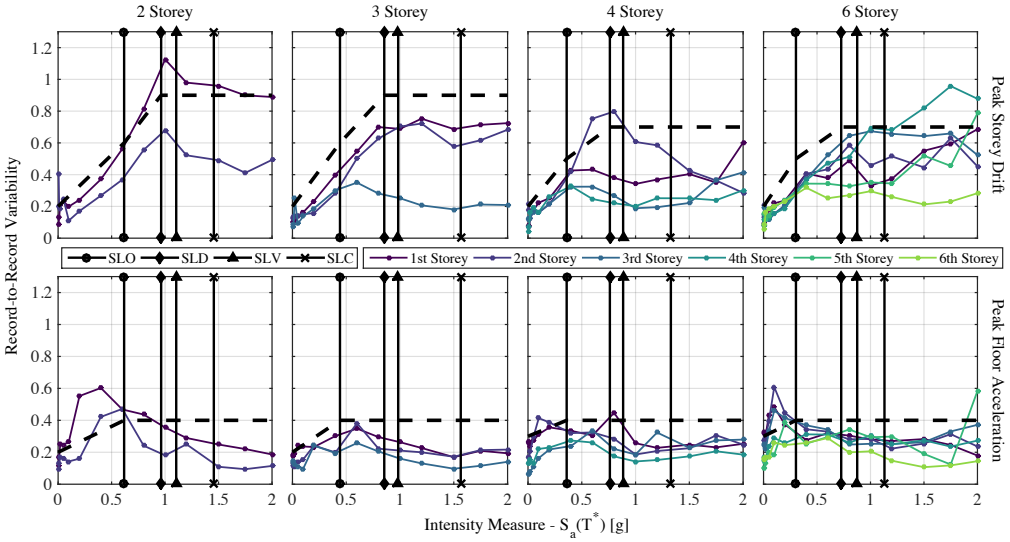

Figure 7.19. Observed record-to-record variability in PSD and PFA for 2D weak infill frames modelled using a double diagonal strut approach along with proposed values.

Some general observations regarding the various trends can be observed from the above figures and the proposed values in Table 7.1. One of the first observations that holds in each case is the relative magnitude of the dispersion for both PSD and PFA, where the dispersion associated with PFA is lower than that of PSD, in addition to being relatively insensitive to the increasing intensity when compared to PSD. This observation also agrees well with the proposed values given in Table 5-6 of FEMA P58-1 [2012] since the formation of a mechanism in a structure with increasing intensity is expected to saturate the accelerations transferred up the building which can lead to a capping effect with increasing intensity. In addition, the dispersion tends to increase with intensity for the PSD, again agreeing with the general trends of the values given in Table 5-6 of FEMA P58-1 [2012].

In relation to the trends between the structural typologies, limit states and number of storeys, some comparisons can be made with an initial pilot study conducted as part of ReLUIS by Fox *et al.* [2015] into quantifying record-to-record variability in RC structures. This study looked at the record-to-record variability in PSD and PFA for numerous frames consisting of GLD frames, modern ductile frames design to the current Italian code and GLD frames with pilotis infill layout. Overall, Fox *et al.* [2015] noted how when compared to the modern ductile design, the dispersion in the older GLD frames with no infill modelled tended to be larger, which highlights the importance of quantification studies such as that discussed here as opposed to relying of existing values such as those proposed in FEMA P58-1 [2012] for modern ductile design, for example. In general, Fox *et al.* [2015] showed an increase in dispersion for both the PSD and PFA of frames with no infill modelled and pilotis frames with respect to the number of storeys, which agrees with the findings reported here in Table 7.1. In addition, Fox *et al.* [2015] report that the PSD dispersion tends to increase with number of storeys citing the possible increased influence of higher mode effects which is accounted for tentatively here by separating the low rise frames of less than four storeys from the higher ones, although further work on higher buildings would be required to confirm this trend fully. In terms of orders of magnitude of the dispersion associated with the frames without infill modelled and pilotis frames, the values reported here in Table 7.1 agree with those described in Fox *et al.* [2015]. However, it should be noted that Fox *et al.* [2015] did not consider fully infilled frames but did note that the insertion of infill for the pilotis frames resulted in a significant jump in the PSD dispersion also observed here for the fully infilled frames typologies. In addition, no significant difference between the dispersion values observed in the case of single strut and double strut modelling of the infills was observed here such that for simplicity, the proposed values for infilled frames do not make a distinction between the two modelling approaches.

For the case of the infilled frames, the record-to-record variability associated with the PSD is rather high for the higher limit states, with the values quantified here much larger than those prescribed in FEMA P58-1 [2012] for ductile moment frames. This is as a result of the particular behaviour of the infilled RC frames, where a high initial stiffness is followed by a quick drop in capacity after overcoming the peak force. This results in many cases where the GMs are not able to overcome the initial peak force and the maximum PSD corresponds to a drift within the narrow elastic drift range of response. However, as the intensity increases some of the records begin to overcome the peak force and immediately descending into the post-peak range where a large value of PSD can be achieved relatively easily due to the drop in capacity and negative stiffness. Therefore, prior to the exceedance of the peak force the maximum PSD values are confined to a narrow band of deformation due to the high initial stiffness of infill frames. Following the exceedance of this peak force, the maximum values of the maximum PSD begin to increase rapidly for the records that overcome the peak. Therefore, a situation arises where for a given intensity many maximum PSD values are still within the narrow band of elastic response whereas the others have overcome this peak and rapidly descended into the post-peak branch to report a relatively large maximum PSD. This large spacing in the demand data then translates into a large dispersion and is illustrated in Figure 7.20 for the IDA of the single strut buildings with strong infill. The rapid increase in demand with increasing intensity illustrated the above point and the large resulting dispersion values are observed in each case.

Table 7.1. Proposed values of dispersion due to record-to-record variability (β_{DR}) for both PSD and PFA as a function of structural typology, number of storeys and anticipated limit state.

Structural Typology	# of Storeys	Record-to-Record Variability					
		>SLO	SLO	SLD	SLV	SLC	>SLC
Peak Storey Drift ($\beta_{DR,\theta}$)							
w/o Infill	< 4	0.20	0.20	0.20	0.30	0.40	0.40
	≥ 4	0.20	0.20	0.20	0.30	0.40	0.40
Pilotis Frame	< 4	0.25	0.25	0.35	0.35	0.40	0.40
	≥ 4	0.25	0.25	0.35	0.35	0.40	0.40
Infill Frame (Strong)	< 4	0.20	0.60	1.20	1.20	1.20	1.20
	≥ 4	0.20	0.60	0.80	0.80	0.80	0.80
Infill Frame (Weak)	< 4	0.20	0.60	0.90	0.90	0.90	0.90
	≥ 4	0.20	0.50	0.70	0.70	0.70	0.70
Peak Floor Acceleration ($\beta_{DR,a}$)							
w/o Infill	< 4	0.30	0.30	0.30	0.30	0.30	0.30
	≥ 4	0.50	0.50	0.50	0.50	0.50	0.50
Pilotis Frame	< 4	0.20	0.20	0.20	0.20	0.20	0.20
	≥ 4	0.40	0.40	0.40	0.40	0.40	0.40
Infill Frame (Strong)	< 4	0.10	0.50	0.50	0.50	0.50	0.50
	≥ 4	0.10	0.50	0.50	0.50	0.50	0.50
Infill Frame (Weak)	< 4	0.20	0.40	0.40	0.40	0.40	0.40
	≥ 4	0.30	0.40	0.40	0.40	0.40	0.40

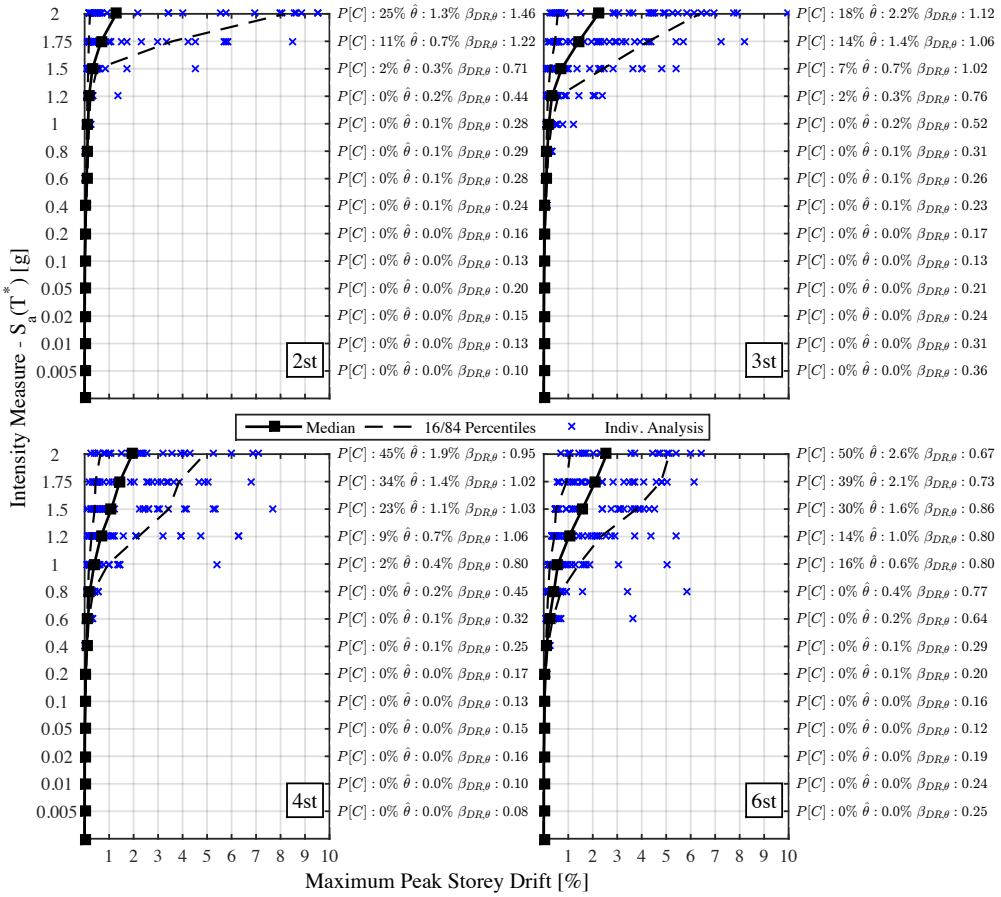

Figure 7.20. Illustration of the progression of maximum PSD with increasing intensity in the case of the 2D case study frames with strong infill modelled with a single strut approach.

7.3.2.2 Demand Parameter Correlation

As previously mentioned and discussed in Section 3.3, the correlation between demand parameters is of crucial importance when conducting extensive loss estimation studies that simulate demands based on the provided input data. Since the DBA methodology discussed above aims to offer a simple method of computing a median response for a given seismic intensity, along with a reasonable estimate of the expected record-to-record dispersion that can be estimated from Section 7.2.1.1 and a modelling uncertainty value that can be obtained from the findings of Chapter 4, some estimate of an appropriate correlation coefficient between the various demand parameters needs to be provided in order to avoid incompatible demands being sampled for loss estimation in TOMS. In order to provide a

means of estimating such demand correlations, the results of the IDA results of Section 5.3 are used and the trends between the various terms are identified.

Bradley and Lee [2010] discussed the influence of the various types of correlations that exist between drift and acceleration demands in structures, where simple relations were proposed based on previous dynamic analysis by the same authors. Bradley and Lee [2010] identified relations between the correlation coefficients of PSD vs. PSD, PFA vs. PFA and PSD vs. PFA, which were established as a function of the number of floors of separation (i.e. the PSDs at the 2nd and 6th floor has four floors of separation between them). These relations proposed by Bradley and Lee [2010] were based on a single ten-storey ductile bare RC frame and work quite well with the data presented. However, for the case of the GLD frames, such coefficients may not be entirely appropriate due to the fundamental difference in behaviour between the structural systems, as illustrated in the comparison shown in Figure 7.21. As such, a similar approach to that of Bradley and Lee [2010] is adopted here, where the demand parameters observed in each of the 2D frames are plotted versus number of floors of separation to identify trends and propose simplified expressions that may be used to identify correlations for use in simplified loss estimation. One principal difference between the results presented here and that of Bradley and Lee [2010] is that here, the correlations are defined between the natural logarithm of the demand parameter as opposed to the actual demand value used in Bradley and Lee [2010]. The reason for this is that during the TOMS process for creating demand simulations, which is illustrated in Figure 3.5, the actual input demand data is converted to its natural logarithm and then the data sampling is performed with its correlation matrix before taking the exponential of this simulated data to give the actual simulated data. As such, it is the estimates of correlation coefficients between the natural logarithms of the demand that are input to TOMS in place of actual data as this is the correlation coefficient matrix that is to be used during the demand simulation. Referring to Figure 3.5 once more, the correlations presented here correspond to the corr(Y), whereas those proposed by Bradley and Lee [2010] corresponds to corr(X). Given that the process followed in TOMS uses the natural logarithms, these are therefore presented here.

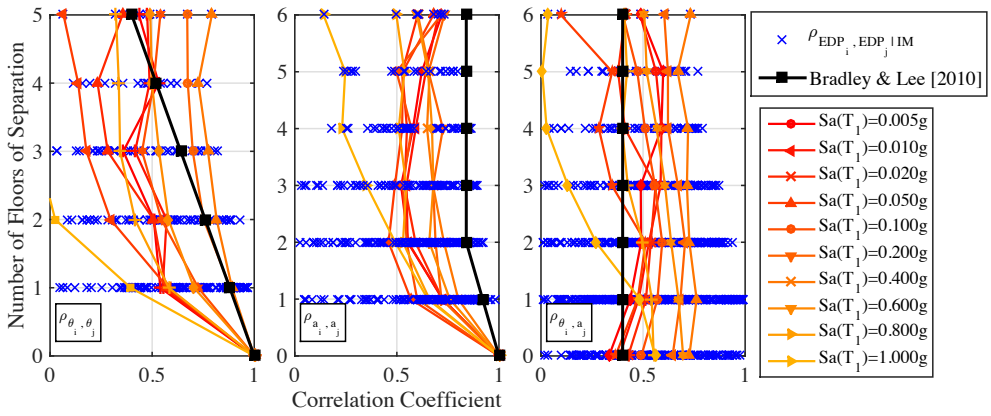

Figure 7.21. Comparison between the demand correlation observed for the frames with weak infill with the empirical correlation expression proposed by Braley and Lee [2010], which illustrates that the empirical relationships proposed in that study are not necessarily applicable in the case of Italian GLD RC frames with masonry infills.

For the various 2D case study frames, Figure 7.22 to Figure 7.27 present the actual demand from the IDA in terms of the PSD and PFA demands. One of the first observations of Bradley and Lee [2010] was that the correlations between individual demand parameters tended to decrease with increasing number of floors of separation, which makes sense when considered from a mechanics-based point of view and is also true for each of the case study frames examined here. The second was that the correlations between the accelerations tended to be higher than those of the storey drift parameters, also observed here. One assumption that was made by Bradley and Lee [2010] based on the results presented in that study was that the correlation coefficients were independent of intensity, which when examining the results presented below does not appear to be the case. This change in correlation with increasing intensity was noted in an earlier study by Aslani and Miranda [2005] who stated that the correlation between demand parameters was, in fact, a function of intensity and is especially relevant for when the structure moves from the elastic range to inelastic range of response. This is particularly obvious in the case of the pilotis and single-strut string masonry infill models, where a clear shift in correlations is observed in each case. In general, it can be seen that as the structures move to higher intensities the correlations tend to reduce with the exception of the strong infill frames, which actually show a clear increase in correlation with increasing intensity. For the weak infill, however, neither a significant increase nor decrease can be seen which suggests that the presence of the infills in the frame has a noticeable effect on the correlations.

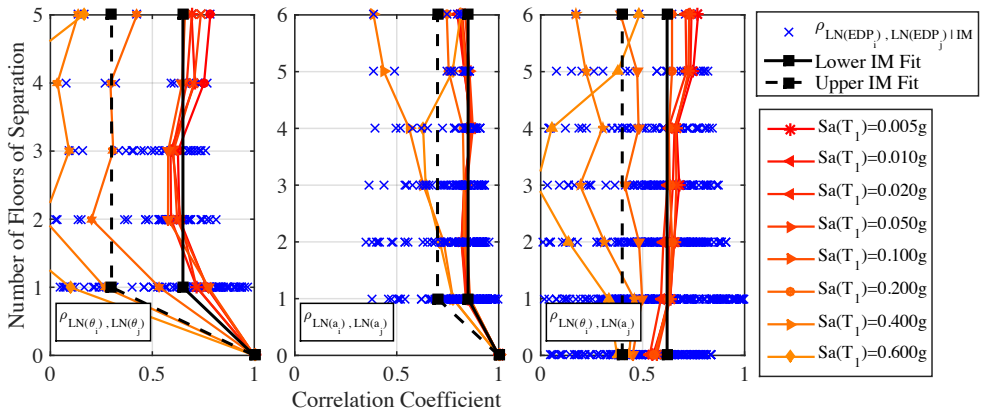

Figure 7.22. Demand parameter correlations for the 2D case study frames without infill modelling.

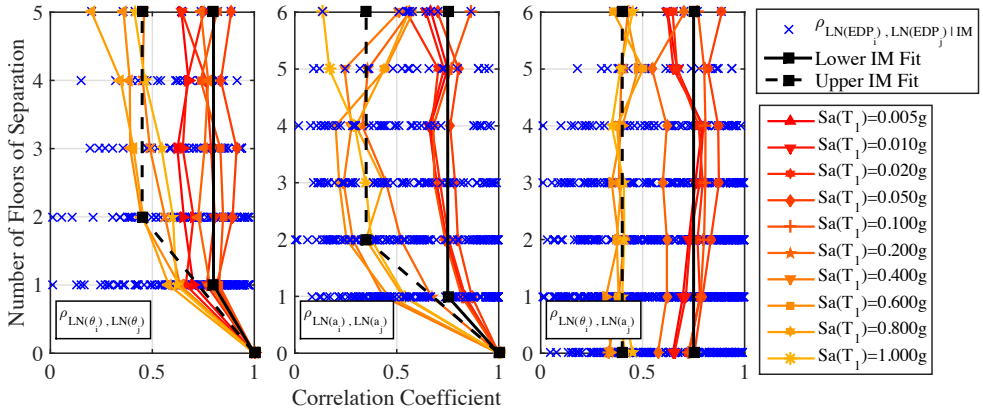

Figure 7.23. Demand parameter correlations for the 2D case study pilotis frames.

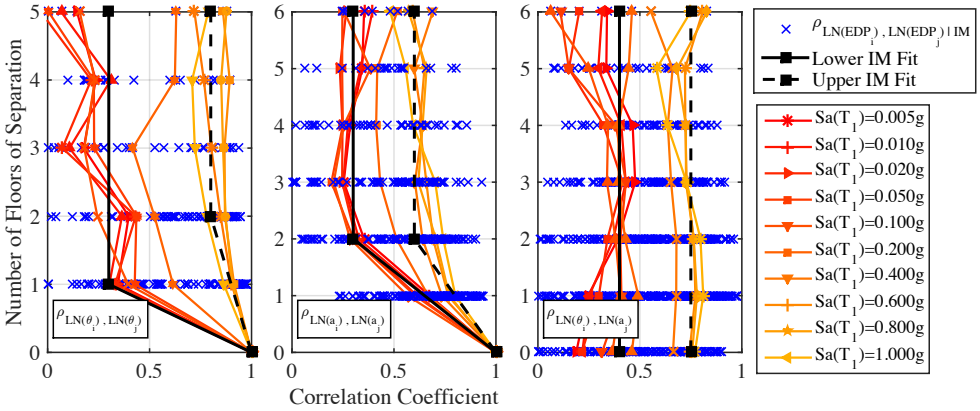

Figure 7.24. Demand parameter correlations for the 2D case study frames with single-strut modelling of strong masonry infill.

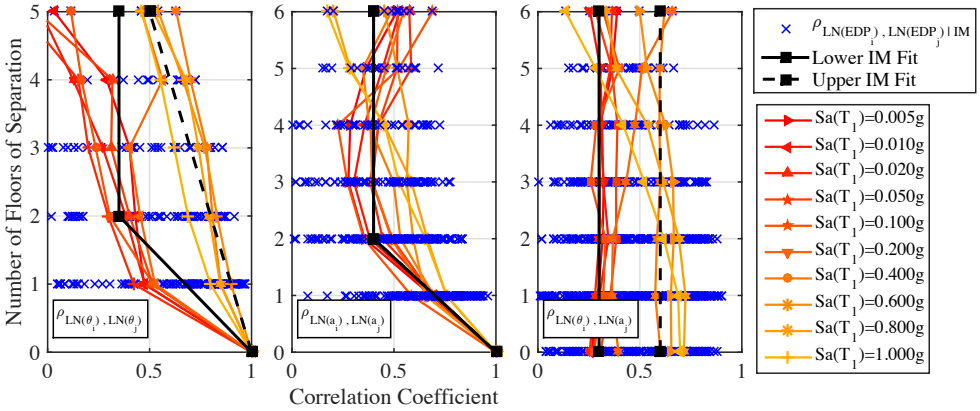

Figure 7.25. Demand parameter correlations for the 2D case study frames with double-strut modelling of strong masonry infill.

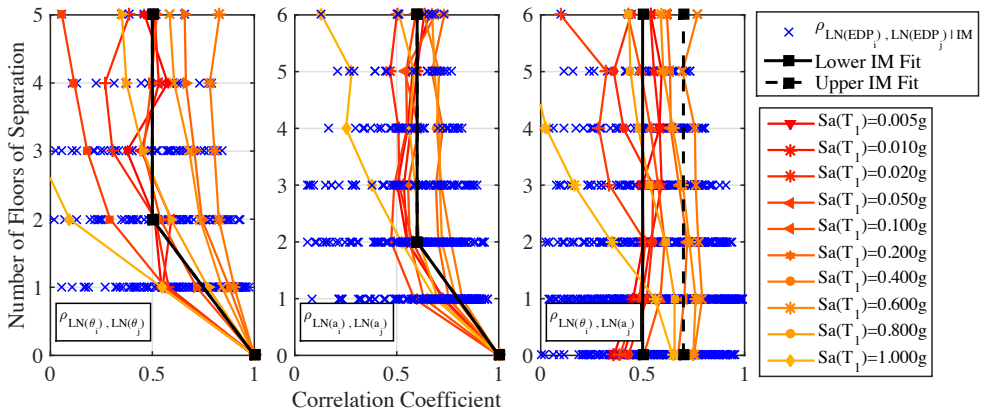

Figure 7.26. Demand parameter correlations for the 2D case study frames with single-strut modelling of weak masonry infill.

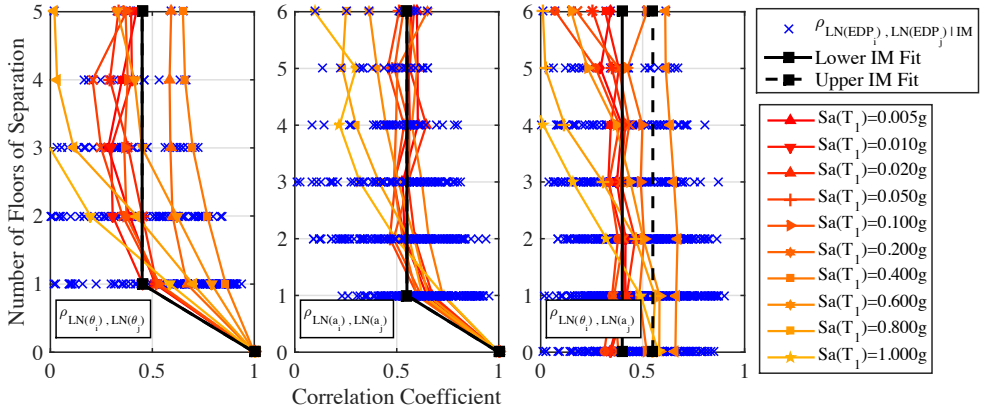

Figure 7.27. Demand parameter correlations for the 2D case study frames with double-strut modelling of weak masonry infill.

Using this data presented above for each of the case study frames, relatively simple fits similar to those of Bradley and Lee [2010] are developed. In addition, a distinction between correlations is maintained here for lower and higher intensities, where the lower intensities noted in the fits for figures correspond to cases where the structure is expected to be in the range corresponding to the SLO and SLD limit states and the higher fits correspond to cases where the structure is anticipated to be in the range of response corresponding to the SLV and SLC limit states. These are plotted in each of the above figures and the actual relations are given in Table 7.2 for each of the demand parameter correlations, where the term n_{fs} represents the number of floors of separation. It is also noted that for the

correlations between the storey drift and floor accelerations, these correlations do not appear to be influenced by n_{fs} and are taken as a constant value in each case, similar to Bradley and Lee [2010]. From the proposed values in Table 7.2, the correlations in the frames without infill modelling and the pilotis frame tend to slightly decrease with respect to intensity. This is an expected result since at low intensity where elastic response is prevalent, the correlations would be expected to be quite high since a stable response along the height is present. However, upon the development of a column-sway mechanism with increasing intensity this correlation between the different storeys reduces as the building is concentrating damage in one storey and no longer possess a stable response. For the infill frames, such a trend is not so obvious and for the case of the strong infill frames without shear modelling in the columns, the correlations slightly increase with increasing intensity. This may be due to the change in behaviour of the building following the damage to the infills where initial response would be dominated by the elastic response due to the strength and stiffness contributions of the infill. With increasing intensity and subsequent damage to these infills, however, the frame may begin to behave more like a bare frame which has a comparatively higher correlation coefficient.

Table 7.2. Simplified expressions to estimate demand parameter correlations in GLD RC frames.

Typology		PSD vs. PSD	PFA vs. PFA	PSD vs. PFA
		$\rho_{(\ln(\theta i),\ \ln(\theta j))}$	$\rho_{(\ln(ai),\ \ln(aj))}$	$\rho_{(\ln(\theta i),\ \ln(aj))}$
w/o Infill	Lower IM	$\max(0.65,1-0.35n_{fs})$	$\max(0.85,1-0.15n_{fs})$	0.62
	Higher IM	$\max(0.3,1-0.7n_{fs})$	$\max(0.7,1-0.3n_{fs})$	0.40
Pilotis	Lower IM	$\max(0.8,1-0.2n_{fs})$	$\max(0.75,1-0.25n_{fs})$	0.75
	Higher IM	$\max(0.45,1-0.275n_{fs})$	$\max(0.35,1-0.325n_{fs})$	0.40
Strong Infill (Single-strut)	Lower IM	$\max(0.3,1-0.7n_{fs})$	$\max(0.3,1-0.35n_{fs})$	0.40
	Higher IM	$\max(0.8,1-0.1n_{fs})$	$\max(0.6,1-0.2n_{fs})$	0.75
Strong Infill (Double-strut)	Lower IM	$\max(0.35,1-0.325n_{fs})$	$\max(0.4,1-0.3n_{fs})$	0.30
	Higher IM	$\max(0.5,1-0.1n_{fs})$	$\max(0.4,1-0.4n_{fs})$	0.60
Weak Infill (Single-strut)	Lower IM	$\max(0.5,1-0.25n_{fs})$	$\max(0.6,1-0.2n_{fs})$	0.50
	Higher IM	$\max(0.5,1-0.25n_{fs})$	$\max(0.6,1-0.2n_{fs})$	0.70
Weak infill (Double-strut)	Lower IM	$\max(0.45,1-0.55n_{fs})$	$\max(0.55,1-0.45n_{fs})$	0.40
	Higher IM	$\max(0.45,1-0.55n_{fs})$	$\max(0.55,1-0.45n_{fs})$	0.55

From the values given in the above table, the demand parameter correlations can be estimated such that in conjunction with the median values of response and an estimation of value of dispersion due to record-to-record variability and modelling uncertainty, a complete loss estimation study can be carried out on the GLD frames presented here without the need of conducting extensive NRHA at numerous intensities and facing the challenges of selecting and scaling a number of GM records to obtain performance assessment results such as expected losses or MAFs of exceedance for older RC frames in Italy.

7.3.3 Comparison of Detailed and Simplified Expected Losses

Using the median profiles along with the associated dispersions and correlations between the demand parameters for each of the structural typologies, a loss estimation using TOMS can be performed by assuming the same damageable component inventory as the original buildings examined in Section 6.2. This comparison is done in terms of the expected loss to highlight the importance of selecting a representative level of demand parameter dispersion and correlation on the vulnerability curve represented by the total expected loss as a ratio of the replacement cost. As mentioned previously, these dispersions for the different structural typologies are taken from the empirical values proposed as a part of this thesis, whereas the median values are taken from the actual IDA curves under the assumption that the future developments of DBA will enable these to be accurately computed. It should be noted how the correlation between the different parameters is considered here as when simulating the data in TOMS, this correlation needs to be respected in order to have meaningful distributions of demand over the building with respect to the input data. Specification of such correlations is not available, for example, during the simplified analysis options in the PACT software [FEMA P58-3, 2012], where a perfect correlation is assumed between the different demands, an approach which is somewhat questionable given the findings of Section 7.3.2.2. The previous section discusses the impact of such correlation and is therefore included here using the simplified expressions provided in that section. In order to investigate the impact of assuming a very low dispersion for each of the demand parameter record-to-record variability and modelling uncertainty, an additional loss estimation was conducted by setting each dispersion to a value of 0.05, which was selected in place of 0.0 in order to maintain stability during the demand simulation in TOMS. Figure 7.28 to Figure 7.31 presents the expected loss curves for each of the structural typologies, where the actual expected loss ratio using extensive IDA is shown along with the simplified approaches that used the median demand along with empirical values for dispersion. It is acknowledged that this comparison presented here does not represent a true verification of the use of empirical dispersion values per se, as these values of dispersion and correlation have been quantified from the same analysis to which they are compared with here, although some important points can be drawn nevertheless. However, application of these empirical dispersion values in the

same manner to an existing Italian school building in Chapter 8 will examine a more appropriate validation of these values when applied to existing buildings evaluated using the same approach to numerical modelling the various potential mechanisms in addition to being analysed with a different GM record set selected specifically to be consistent with the site hazard at the location of the school structure examined.

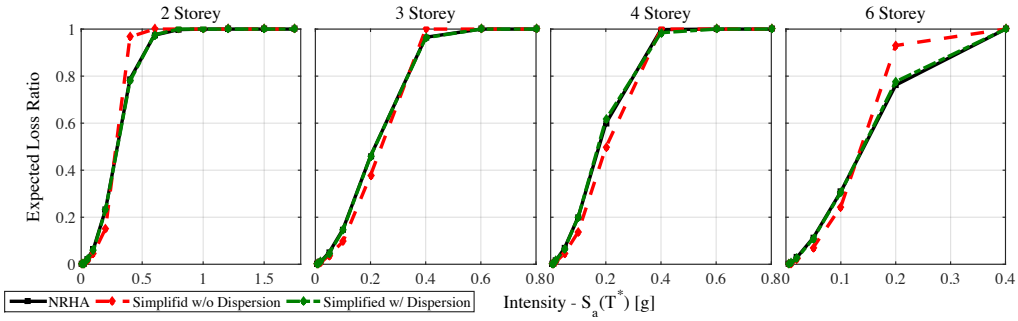

Figure 7.28. Comparison of the expected loss ratio versus intensity using the extensive analysis approach, simplified with no dispersion and simplified with dispersion for the frames modelled without masonry infill.

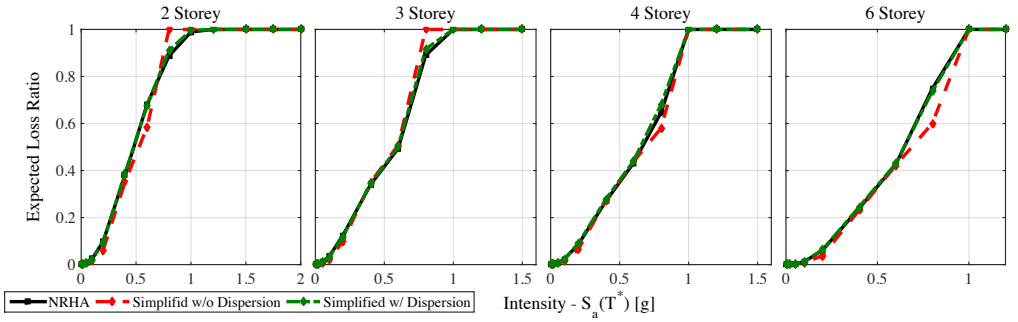

Figure 7.29. Comparison of the expected loss ratio versus intensity using the extensive analysis approach, simplified with no dispersion and simplified with dispersion for the pilotis frames.

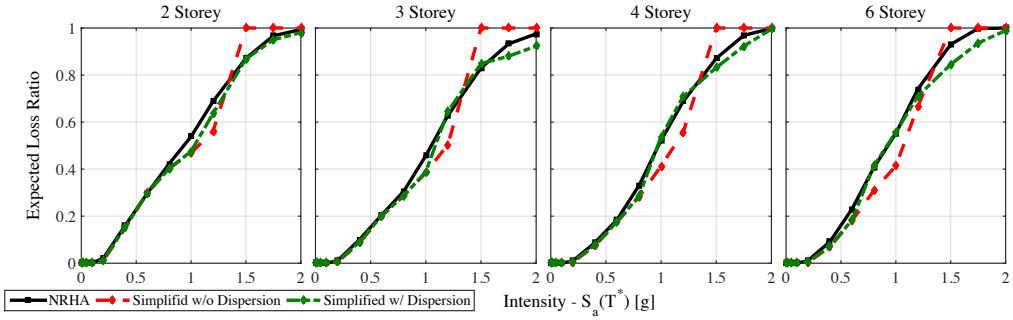

Figure 7.30. Comparison of the expected loss ratio versus intensity using the extensive analysis approach, simplified with no dispersion and simplified with dispersion for the frames with strong masonry infill.

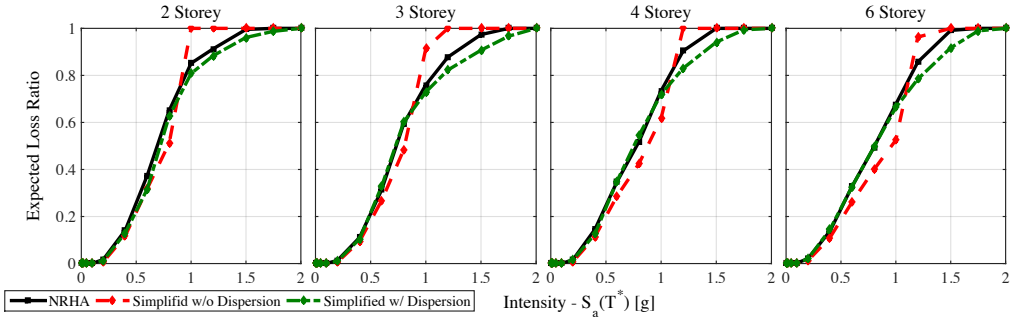

Figure 7.31. Comparison of the expected loss ratio versus intensity using the extensive analysis approach, simplified with no dispersion and simplified with dispersion for the frames with weak masonry infill.

By first comparing the expected loss curve using the extensive analysis, which is considered the most representative curve here, with that of the simplified approach using the prescribed dispersion values, the matching is generally very good. This is seen through the excellent matching to the extensive approach with increasing intensity for each of the structural typologies considered. While it is acknowledged that the median demand parameters, in this case, come from the actual extensive analysis, meaning that a good match should be expected, the implication of this matching is that should a user be able to get a good estimate of the median response at various intensity levels using a methodology such as DBA, combining these with the empirical values for dispersions should give a good match to the expected loss curve.

Some interesting points can also be noted from Figure 7.30 and Figure 7.31 for the infilled frames, where for the higher intensities the matching is slightly off with the simplified

approach using the proposed dispersions tending to underestimate the expected loss. Further examination of the extensive analysis versus the simplified method shows that the empirical dispersion values tend to slightly overestimate the actual dispersion at the upper intensity levels meaning that for a given intensity, there is broader band of demand parameters being assessed resulting in the central tendency to shift downward as the upper loss threshold is reached. This is a consequence of using empirical dispersions, such as those Section 7.3.2.1, where the envelope of the observed record-to-record variability was proposed for simplicity. This results in the maximum dispersion being captured well for the critical storey but also an overestimation in the dispersion at the other floors, which can result in scenarios such as those observed here. The consequence of this underestimation of the expected losses at the higher intensities may not be a critical issue in terms of EAL since the MAF of exceedance at these higher intensities will be quite low and thus, the weighting terms will reduce the impact.

Another comparison is also shown in all of the above figures, whereby the impact of not adopting any dispersion for the record-to-record variability or modelling uncertainty was computed. In each case, the matching is reasonable but not exact. This highlights the significance of the incorporation of appropriate values of dispersion when conducting loss estimation. It is noted here that contrary to the observations above regarding the underestimation of expected losses for the infilled losses at the higher intensities, the simplified approach with no dispersion tends to overestimate this. This again is a consequence of the lack of dispersion in the demand parameters, since this means that the tightly bound demands will tend to reach the loss threshold value of 60% at more or less the same intensity and subsequently be set to 1.0, as the structure will be demolished rather than repaired. This results in the sharp jump between the intensities around the 0.6 expected loss ratio seen for the different buildings. Also of note is the slight underestimation of the expected loss for the lower intensities when ignoring the demand parameter dispersion. This arises due to similar reasons, since the tightly bound demands mean that as the individual loss ratio from each simulation approaches the loss threshold value of 60%, there are no extreme tail values of the demands that would induce slightly higher loss for that simulation, subsequently reaching the loss threshold and subsequently be set to 1.0 meaning that the expected value would tend to shift upward. As a result, the tightly bound demands leads to a slightly underestimated expected loss curve.

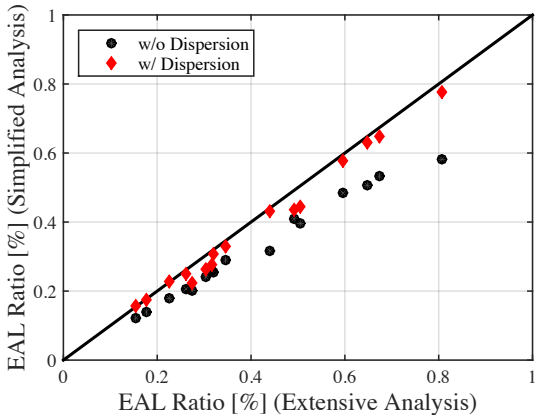

Figure 7.32. Comparison of the EAL estimated from the simplified approach using an appropriate estimation of empirical dispersion for both the record-to-record variability in addition to modelling uncertainty compared to that of the estimations via extensive NRHA.

Furthermore, a comparison of the time-based assessment of all three cases is also presented in terms of the EAL of the various structural typologies in Figure 7.32, where a very good match can be seen between the EAL of the extensive approach and the simplified approach with dispersion. A comparison of the simplified approach that ignored the dispersion shows a worse matching, with the simplified method tending to underestimate the EAL. This highlights again how the simplified approach with an appropriate value of dispersion can be confidently used to compute the EAL for the different case study buildings.

7.4 Assessment of GLD RC Frame Structures using the SAC/FEMA Probabilistic Methodology

The previous sections looked at simplified ways assess a structure's performance in terms of identifying the critical mechanism for a given limit state such that the various consequences in terms of expected losses in the building can be estimated using the median demand estimated along with empirical values of dispersion. While this approach has its own benefits and scope of application, additional methodologies that can simply state the MAF of exceedance of a given limit state in a structure are also of great value as it allows practitioners to quickly assess the exceedance of different limit states in the building in a more code orientated format. The SAC/FEMA methodology offers such a methodology whereby the distributions for demand and capacity of a given limit state are integrated with a specified hazard curve in a closed form solution to return the MAF of exceedance of the defined limit state. This section provides an overview of this methodology in addition to validating its application to GLD RC frames with infills. This is done by calibrating new

coefficients to consider the behaviour of such frames followed by validation with the extensive NRHA on the different structural typologies examined in Chapter 5.

7.4.1 Overview of the Methodology

Around the turn of the millennium, performance-based earthquake engineering began to look to more probabilistic approaches to quantify the seismic performance of structures. What is now a rather infamous paper in world of probabilistic seismic assessment, Cornell *et al.* [2002] described a probabilistic framework for the new SAC/FEMA steel moment frame guidelines, where a closed-form solution that computed the annual probability, or MAF, of exceeding a given limit state with an x confidence level was derived. Although this framework was developed for steel moment frames in the US, the general framework can be adopted for other structural typologies also. The general expression outlined by Cornell *et al.* [2002] for the annual probability of failure with x confidence level (herein referred to as MAF of exceedance) is described by:

$$\lambda_{LS,x} = \lambda(IM) C_H C_f C_x \qquad \textbf{Equation 7.25}$$

where $\lambda(IM)$ describes mean hazard function and the terms C_H, C_f and C_x represent adjustment coefficients to account for hazard, response and confidence interval, respectively. For a full definition of these terms, see Cornell *et al.* [2002]. Of note, however, is the C_x term which is typically taken as 1.0, as Fajfar and Dolšek [2010] suggest that a 50% confidence level is sufficient for practical application purposes meaning that the C_x term becomes 1.0 and is omitted herein for brevity.

While the original proposal by Cornell *et al.* [2002] represented the mean hazard curve using a linear regression fit in log space, Vamvatsikos [2013] has expanded this SAC/FEMA framework to incorporate a quadratic polynomial to provide a much better fit to the curvature of the hazard curve with increasing intensity. This quadratic fit proposed by Vamvatsikos [2013] is described by:

$$\lambda(IM) = k_0 \exp\left[-k_1 \ln(IM) - k_2 \ln(IM)^2\right] \qquad \textbf{Equation 7.26}$$

where k_0, k_1 and k_2 are the parameters to be fitted to the mean hazard curve at the site of interest. While the site hazard curve obtained from PSHA is typically expressed by the MAF of exceedance, the SAC/FEMA methodology described in Cornell *et al.* [2002] defines a C_H term to account for the difference in mean and median. Both Cornell *et al.* [2002] and Vamvatsikos [2013] discuss the adjustment for this through the additional epistemic uncertainty term C_H but suggest that in most cases the mean and median can be assumed to be approximately equal. Vamvatsikos [2013] outlines this by describing that the two are approximately equal when the k_2 term is approximately zero, meaning the curvature of the hazard curve is low. Nevertheless, the discussion in this thesis will be limited to the assumption that this adjustment term is approximately unity and the mean hazard curve

can be used, meaning that the C_H term in Equation 7.25 is taken as unity and is omitted in the expressions described herein.

For intensity-based assessment, Vamvatsikos [2013] defines the MAF of exceedance of a limit state at the 50% confidence level as:

$$\lambda_{LS} = \sqrt{p'}\, k_0^{1-p'} \left(\lambda\left(\widehat{IM}\right)\right)^{p'} \exp\left[\frac{k_1^2 p'}{2}\left(\beta_{RC,IM}^2 + \beta_{UC,IM}^2\right)\right] \qquad \textbf{Equation 7.27}$$

where $\beta_{RC,IM}$ and $\beta_{UC,IM}$ represent the randomness and uncertainty in the capacity of the limit state of interest with respect to IM. The term p' is given as:

$$p' = \frac{1}{1 + 2k_2\left(\beta_{RC,IM}^2 + \beta_{UC,IM}^2\right)} \qquad \textbf{Equation 7.28}$$

In situations where the median intensity associated with a given limit state is not known, but is defined by a demand parameter, an intermediate relation between the two is defined by Cornell *et al.* [2002], using the maximum PSD θ here for example, as:

$$\hat{\theta}(IM) \approx aIM^b \qquad \textbf{Equation 7.29}$$

where a linear relationship is assumed between the demand and intensity in log space to define the terms a and b. Therefore, for a given value of demand, the corresponding intensity can be estimated by rearranging the above relation and inserting it into the following expression to determine the MAF of exceedance of the limit state at the 50% confidence level defined in terms of the demand parameter:

$$\lambda_{LS} = \sqrt{\phi'}\, k_0^{1-\phi'} \left(\lambda\left(IM(\hat{\theta})\right)\right)^{\phi'} \exp\left[\frac{k_1^2 \phi'}{2b^2}\left(\beta_{DR,\theta}^2 + \beta_{DU,\theta}^2 + \beta_{CR,\theta}^2 + \beta_{CU,\theta}^2\right)\right]$$

Equation 7.30

where $\beta_{DR,\theta}$ and $\beta_{DU,\theta}$ represent the demand randomness and uncertainty associated with record-to-record variability and modelling uncertainty with respect to the demand parameter θ in this case. The terms $\beta_{CR,\theta}$ and $\beta_{CU,\theta}$ represent the corresponding capacity randomness and uncertainty associated with record-to-record variability and modelling uncertainty. In situations where a deterministic limit state capacity is defined, these two terms are set to zero. The term ϕ' is defined as:

$$\phi' = \frac{1}{1 + \frac{2k_2}{b^2}\left(\beta_{DR,\theta}^2 + \beta_{DU,\theta}^2 + \beta_{CR,\theta}^2 + \beta_{CU,\theta}^2\right)} \qquad \textbf{Equation 7.31}$$

In order to implement the above approach to the probabilistic assessment of GLD RC frames in Italy, a number of pieces of information are required. Firstly, appropriate values of the various dispersion terms are required for the relevant demand parameter at the limit state of interest. Chapter 4 looked at the quantification of such modelling uncertainty values for the various structural typologies examined here in terms of both limit state and demand parameter. In addition to an appropriately fitted quadratic hazard model, the final piece of information required is the median intensity for the limit state of interest. Often times, it is more convenient to define such limit states in terms of a demand parameter such as storey drift rather than intensity and hence, an intermediate relationship such as that described in Equation 7.29 is employed. However, in order to use such a relationship, these predefined coefficients must be chosen for the relevant structural typology and demand parameter of interest similar to the way that default values of dispersion exist as a result of larger parametric studies. The following section describes the quantification of such coefficients for use in limit state assessment of GLD RC frame typologies.

7.4.2 Quantification of Demand-Intensity Relationships

In the original closed form derivation by Cornell *et al.* [2002], the demand-intensity relationship was assumed to be represented by a linear relationship in log space. For the structures examined in that study, the power term b was suggested to be approximately unity, which was noted by the authors to imply the "equal-displacements" rule. While this equal-displacements approximation of the demand worked well for the steel moment frame structures examined by Cornell *et al.* [2002], they remarked how this worked well for structures with moderate periods and without major strength degradations. Further analysis on mid-rise steel moment frames by the example application presented in Vamvatsikos [2013], for example, showed that this assumption of unity tended to hold well. Other applications of this methodology [Fajfar and Dolšek, 2010, 2012; Welch *et al.*, 2014], among others, have also adopted this value of unity for the b term. However, while the use of unity may be a reasonable approximation in each of these respective studies, its usage in the case of GLD RC frames with infill is questionable. This is highlighted in Priestley [2003], among others, where the assumption of equal displacements does not always hold true, especially in the case of short-period structures such as infilled RC frames. In addition, the limited ductility and presence of masonry infill in GLD frames means that the condition of no major strength degradation outlined in Cornell *et al.* [2002] is no longer satisfied. As such, the validation of appropriate terms for use in the probabilistic assessment methodology outlined above for older GLD RC frames in Italy is needed. This is conducted using the IDA results of the various structural typologies presented in Section 5.3. This is conducted for both the maximum PSD and PFA in the various frame typologies.

In order to conduct the aforementioned quantification, the median maximum PSD is plotted versus IM, which is, in this case, the spectral acceleration at the first mode period.

For illustration, this is plotted in Figure 7.33 for the case of the 2D six storey frame modelled without masonry infill, where the assumption of b equal to 1 appears to work very well.

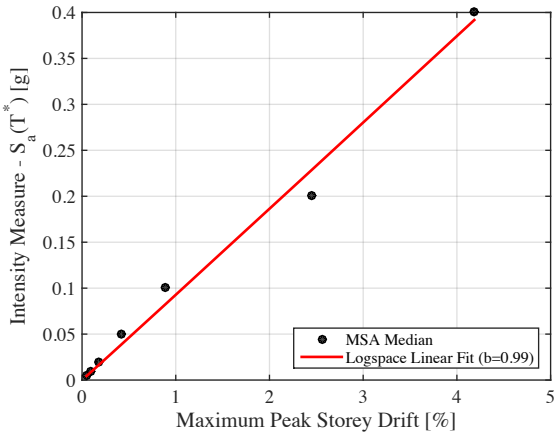

Figure 7.33. Fitting of demand-intensity in log space for the maximum PSD in the 2D six storey case study frame modelled without infills.

Proceeding with the same approach for different frame typologies, a similar plot for the infilled frames with strong infill modelled with single struts is shown in Figure 7.34. From this power fit to the median PSD from IDA, the representation of the demand-intensity using this approach does not work very well for lower intensities. In addition, the fitted curve returns a b value much greater than unity, which is of particular interest here. First, however, the overall fitting must be improved. This is done by first dividing the demand-intensity results from IDA into two regions, termed lower and upper here to refer to lower and upper intensity response, respectively. This approach was described in Ramamoorthy *et al.* [2006] in relation to GLD RC frames without masonry infills in Memphis, USA, where the authors noted that a single expression did not represent the response overall intensity levels and elected to divide the response into two regions and fit two separate relations. In order to define a dividing point in the response of the GLD RC frames examined here, the median storey drift of 0.18% at the first damage limit state of the masonry infill described in Sassun *et al.* [2015] has been investigated. Plotting this with the data presented in Figure 7.34, Figure 7.35 shows how this proposal of a division in the two regions of infill frame response corresponds to where the demand-intensity data appears to change slope, suggesting that the exceedance of the masonry infill capacity causes an overall change in behaviour of the infilled frames. This observation agrees well with the observations in Section 7.3.2.1, where the exceedance of the masonry infill capacity was seen to be a fundamental point in the overall behaviour of the frames.

Using this definition of the two regions of response defined in terms of the median storey drift of masonry infill damage, the bilinear demand-intensity fit outlined in Ramamoorthy *et al.* [2006] in can be applied, where Figure 7.35 shows it to be a much better representation of the response of the case study frame. It is noted how the lower region's fit returns a b value of almost 1, suggesting that the equal displacement rule holds true, which is an expected result since the structure is still responding more or less elastically. However, the upper region of response shows a much higher value of b, which is of particular interest here. It was previously suggested that a value of unity represents a reasonable value in absence of other data, but here it appears to be not true in the case for GLD RC frames with infill. It can be shown through simple calculation that an increase in b greater than unity for the expressions described in Section 7.4.1 results in a decrease in the MAF of exceedance of a given limit state, implying that the default assumption of unity to be conservative. Taking the example outlined in Section 5 of Vamvatsikos [2013], increasing the value of b from 1 to 2, for example, results in the MAF of exceedance reducing by a factor of around 8. Hence, it is of paramount interest that a parameter with such impact on the overall assessment results defined in terms of MAF of exceedance be quantified as accurately as possible when using this demand parameter approach.

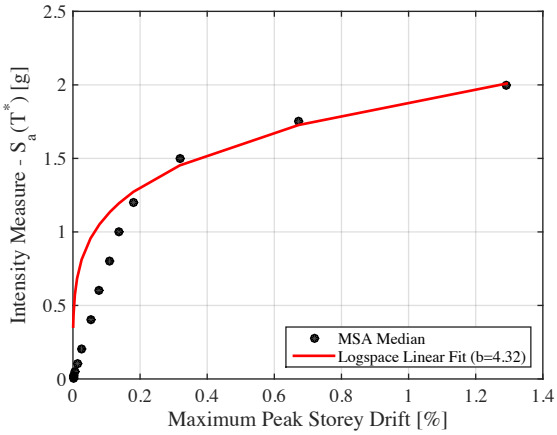

Figure 7.34. Fitting of demand-intensity in log space for the maximum PSD in the 2D two storey case study frame modelled with single strut strong infills.

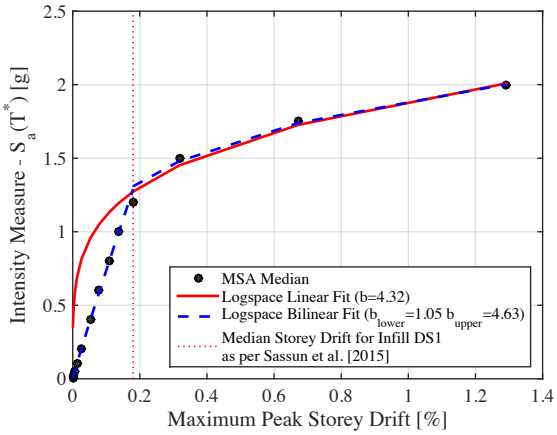

Figure 7.35. Fitting of demand-intensity in log space for the maximum PSD in the 2D two storey case study frame modelled with single strut strong infills, where the demand-intensity is subdivided into two regions of response depending on the masonry infill median damage drift.

Performing the same procedure as that illustrated in Figure 7.35 for each of the 2D case study frames examined in Section 5.3, the bilinear demand-intensity relations can be fitted and are illustrated in Figure 7.36. Of particular interest are the fitted relationships for the frames modelled without masonry infill compared to those with infill. The lack of infill modelling returns a b of essentially 1.0 in each case, whereas the infilled frames return values much larger than unity for the upper region of response. Again, the lower region fits for the infilled frames are all very close to unity since the frames are responding elastically, whereas the surpassing of the infill peak strength results in a sharp increase in this coefficient.

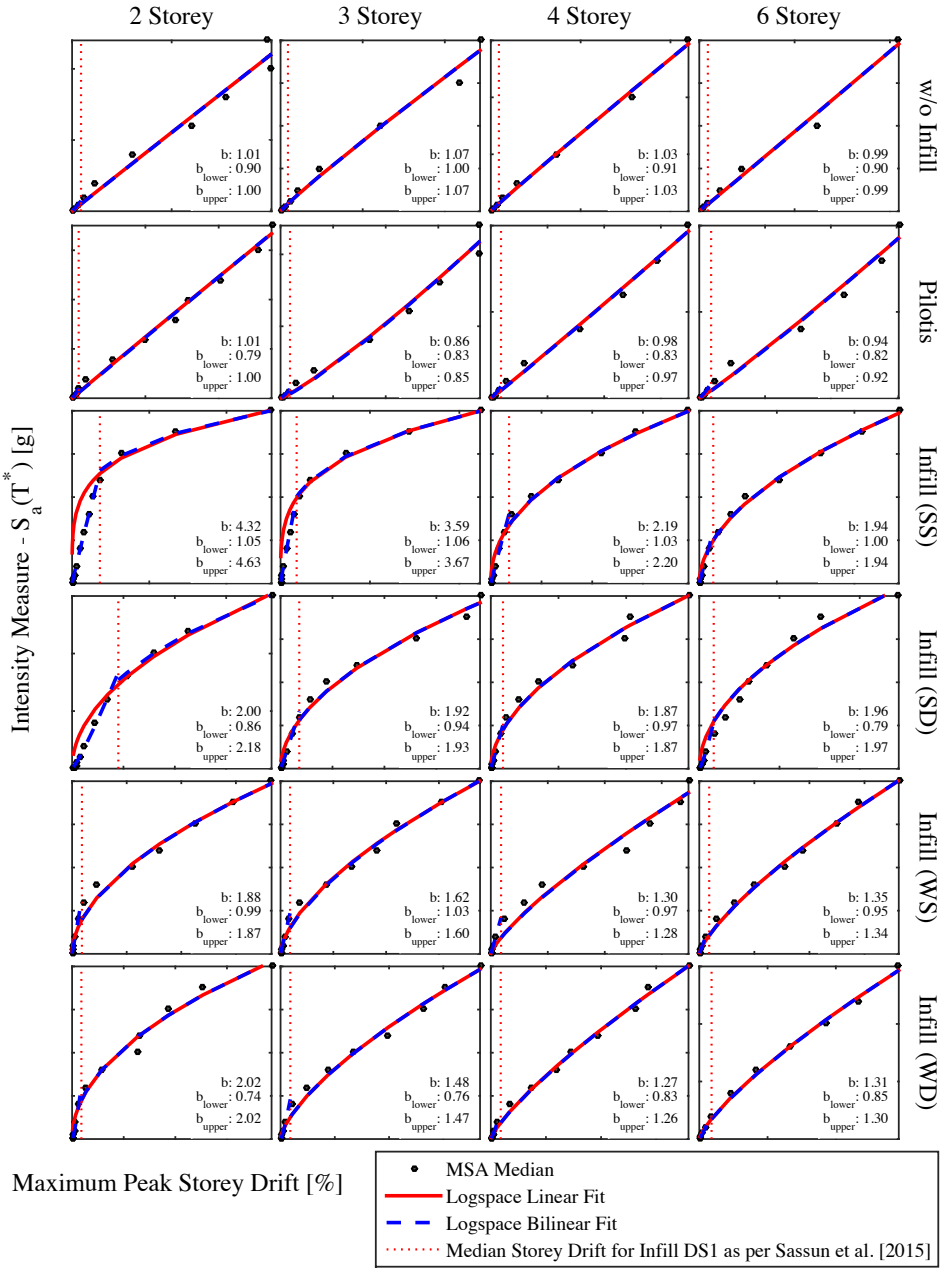

Figure 7.36. Fitting of demand-intensity in log space for the maximum PSD in the 2D two storey case study frames.

Using these values fitted to the median response of each of the frames plotted in Figure 7.36, a comparison of the different typologies' fitted parameters for the upper region versus initial period is illustrated further in Figure 7.37; in addition to the fitted trendlines and their respective parameters to provide some guidance on more refined quantification of the different terms. For the corresponding lower region values, these relate to the region of response where the structure is expected to be responding in the elastic region, therefore a value of unity may be reasonably adopted when consulting the values observed in Figure 7.36. By first examining the b parameter, it can be seen how the value of 1.0 typically assumed in the literature works very well for the frames modelled without masonry infill and the pilotis frame, with the trend line plotted between the different frame typologies showing how the term is essentially unity in each case. It is also worth noting that in each of the aforementioned cases for the bare and pilotis frames, these frames each have a first mode period greater than 0.5s, which would correspond roughly to the beginning of the constant velocity period range of the GM set where the equal displacement rule is traditionally known to work quite well for bilinear systems with initial stiffness proportional viscous damping. Contrast this to the infilled frames that are first noted to fall within a shorter period range of the GMs, where the equal displacements rule no longer hold true (e.g. Vidic *et al.* [1994]). This increased value of the exponent b for the infilled frames implies that for a given intensity, the median drift will be expected to be much higher. The reverse is also true where for a given drift, the corresponding estimate of intensity will be lower, meaning that a lower more frequent intensity will be identified leading to an overestimation of the MAF of exceedance of the limit state.

Comparing the single and double strut models in Figure 7.37, a reduction in the b term is observed for the double strut models with strong infills, implying that for a given intensity the maximum PSD is expected to increase due to the shear modelling of the frames. This agrees with the results presented in Section 5.3. Comparing the fitted b terms for the weak infill frames, a similar trend is observed with the values being slightly above 1.0 and inversely proportional to the initial period. However, when examining the same trend in the strong infill frames, a large discrepancy between the two curves is noted. Further investigation illustrated in Figure 7.37 shows that this discrepancy is largest for the two and three storeys frames. This arises due to the influence of the shear failure of the columns when interacting with the masonry infill, where recalling the collapse fragility functions for the strong infill frames in Section 5.4, the median collapse intensity was notable lower for the double strut model than the single strut model for the two and three storey cases. This failure mechanism is therefore propagated through the results in terms of a reduction in the b term, which for a fixed value of a means that the MAF of exceedance for a given limit state increases. The lack of observed shear failures in the case of the weak infill masonry means that such a differentiation between the single and double strut models is not prominent. Celarec and Dolšek [2013] also indirectly considered the impacts of shear failure of the columns in older RC frames due to interaction with the masonry infill using an

iterative approach. They assumed that the flexural plastic hinge definition in the columns and the masonry infill strut could be modified to approximately account for the shear failure in the column members. Investigating the impact of shear failure in the columns resulted in an MAF of exceedance being between 3 and 8 times larger depending on the limit state considered, which resonates with the above comments. This again highlights the importance of modelling the shear behaviour of column members when susceptible to shear failure due to masonry infill interaction.

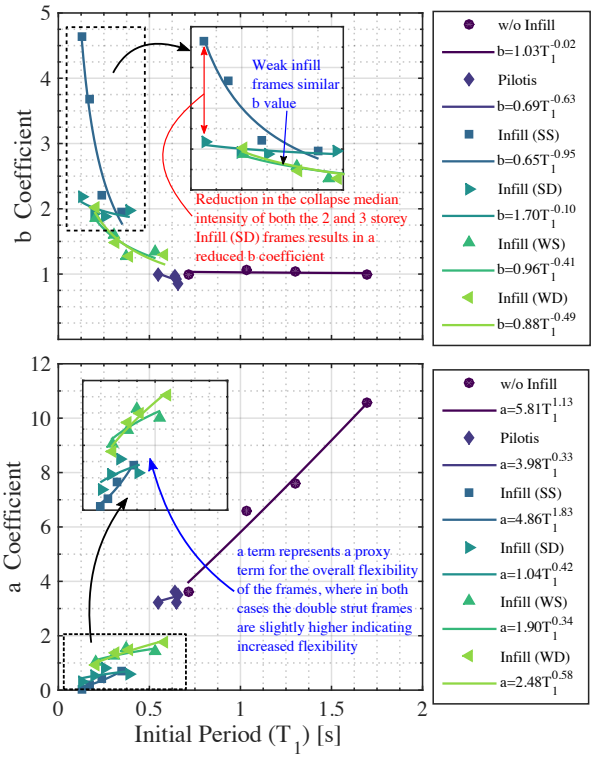

Figure 7.37. Comparison of the coefficients for the upper range fitted for each structural typology plotted versus initial period. The actual data is plotted with the markers whereas the fitted expressions as a function of the initial period are also plotted. The difference in the b coefficient between the strong infill models is further illustrated and accounted for by the reduced collapse capacity for the double strut models, whereas the increased flexibility of the double strut models is also noted through the slight increase in the coefficient a.

In addition to the quantification of the b term, the coefficient a in Equation 7.29 also needs to be quantified. This is a proxy term for the stiffness of the structure, where more flexible frames would be expected to have a higher value. This is particularly obvious in the case of

the frames modelled without infill where the a term is seen almost linearly increase with initial period, whereas a similar but less pronounced trend is seen for the infilled frames. A further comparison between the single and double strut infill frame models, where those models considering the shear behaviour have a slightly higher value of a, meaning that they are slightly more flexible, which is an observation that concurs with that of the IDA results presented in Section 5.

7.4.3 Comparison of the SAC/FEMA Methodology for Limit State MAF Calculation in GLD RC Frames in Italy

The above sections have discussed a simplified closed-form solution to estimate the MAF of various limit states within different structural typologies. This section aims to validate this framework outlined by Cornell *et al.* [2002] through the comparison of the approach described in the previous two subsections with the values obtained from the full integration of the actual response analysis obtained from IDA in Chapter 5. This comparison, therefore, provides a validation for which future analyses on GLD RC frames in Italy can be carried out with a degree of confidence using approaches, such as DBLE outlined in Section 7.2.3. This validation is done by taking the prescribed maximum PSD defined for each limit state in Section 5.5 along with the dispersion due to record-to-record variability in Chapter 5 to compute the MAF of exceedance from Equation 7.30 and compare it with the full integration of the limit state fragility curves derived from extensive IDA in Section 5.5 with the assumed site hazard curve. The drift capacity at each limit state is taken as a deterministic value, which results in the $\beta_{CR,\theta}$ and $\beta_{CU,\theta}$ terms in Equation 7.30 becoming zero.

Following this approach, the ability of the demand-intensity models quantified in the previous sections to predict the median intensity versus that computed from fitting of a fragility function via the maximum likelihood method outlined by Baker [2015] is first examined. While the median limit state intensity computed by fitting a lognormal distribution to the IDA results using the maximum likelihood method is treated as the "correct" value, in this case, it should be noted that this approach is also not without its inherent fitting error from the "true" value. However, of the two approaches here it is considered the more accurate as it involves extensive NRHA of detailed numerical models. A comparison between these two median intensities predicted by Equation 7.29 and computed from IDA is shown in Figure 7.38. In addition, the median intensity prediction using a linear demand-intensity model with the b parameter set as 1.0 previously adopted in the literature is illustrated. By examining the comparison of this model first, it is clear that the use of b equal to 1.0 is not appropriate for the assessment of GLD RC frames with masonry infill, as the comparison clearly demonstrates that the median intensity begins to become drastically overestimated in the case of the infilled frames. The use of the proposed coefficients, however, is seen to work very well for each limit state considered, as indicated

by the strong correlation (ρ) between the predicted and computed values. Overall, the calibrated parameters provide a good match when estimating the median limit state intensity as the increased nonlinearity of the relationship due to the exponent term b being typically greater than one for the infilled frames is well represented. This is perceived in how the comparison is very good in each case for the lower limit states, although a slight degree of overestimation is present for the SLC limit state.

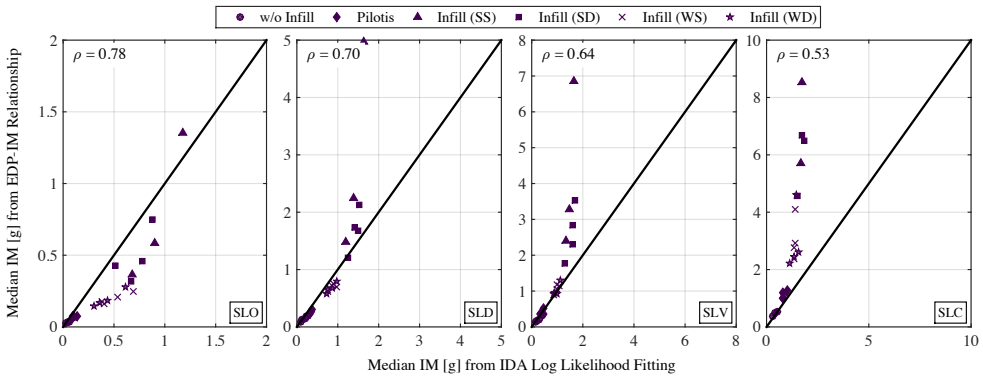

(a) Comparison with the parameter b set to 1.0

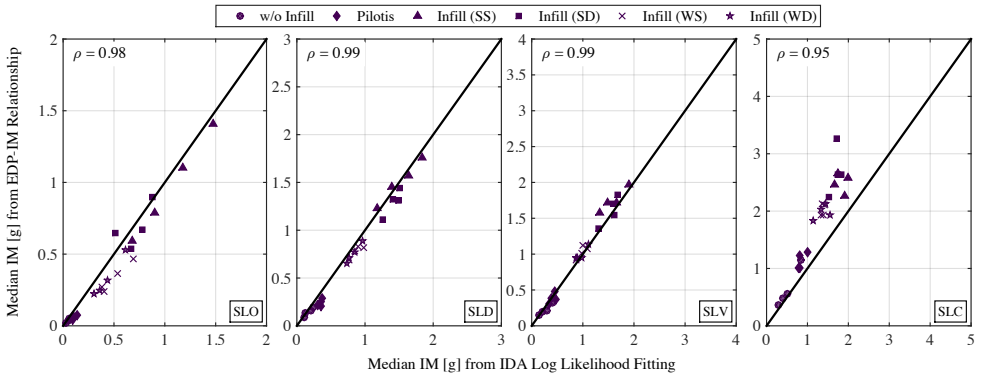

(b) Comparison with the calibrated parameters

Figure 7.38. Comparison of the median limit state intensity computed the demand-intensity models versus the median value computed from maximum likelihood fitting to IDA results.

In addition to the computation of the median intensity of each limit state of the structures, the comparison between the MAF of exceedance for the different limit states is examined. This is done by using the closed-form solution outlined in Equation 7.30, whereby the PSD

at each limit state is employed alongside the various values for dispersion. These are then compared to the result of integrating the limit state fragility functions discussed in Section 5.5 with the assumed site hazard curve for the three different sites examined previously in Chapter 6 to obtain the MAF of exceedance of the different limit states by numerically integrating the results of extensive NRHA. This process is illustrated in Figure 7.39 and aims to give some degree of confidence to the values of MAF of exceedance computed using the closed-form solutions previously discussed.

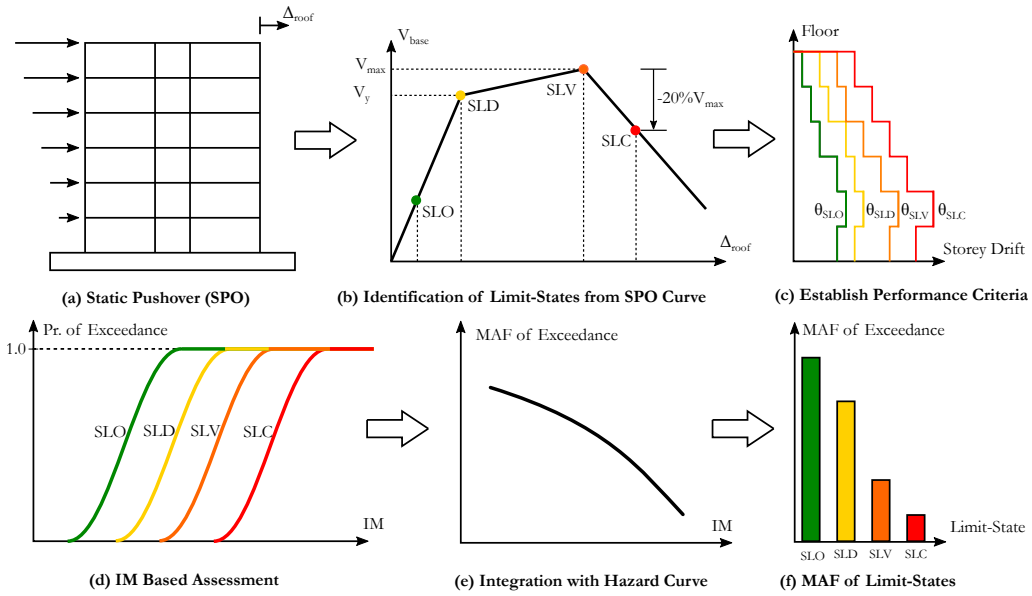

Figure 7.39. Illustration of the process with which the MAF of exceedance of the different limit states are computed using the IDA results from integration with the relevant hazard curves.

As in the case of the median intensity comparison presented in Figure 7.38, a comparison between the MAF estimated from the integration of the IDA results with the closed form solution using both the assumption of the parameter b being equal to 1.0 and the calibrated parameters is presented here. Figure 7.40 presents the two plots where again, the correlations between the two approaches are quite low for the case of the parameter b being equal to 1.0. Examining the comparison between the values computed using the calibrated parameters in Figure 7.37 with those of the IDA integration, the correlation is again quite high, although a degree of scatter is still present. A slight overall underestimation of the MAF of exceeding the SLC limit state is observed also in Figure 7.40. This is a consequence of the demand-intensity relation becoming unconservative by slightly overestimating of the median intensity at this limit state. This slight overestimation in the median intensity is then propagated through the expressions to result in a slight underestimation of the MAF of exceeding this limit state.

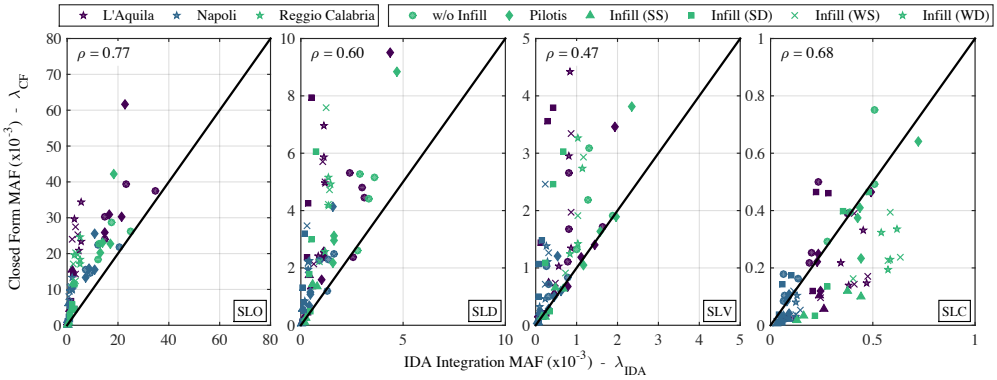

(a) Comparison with the parameter b set to 1.0

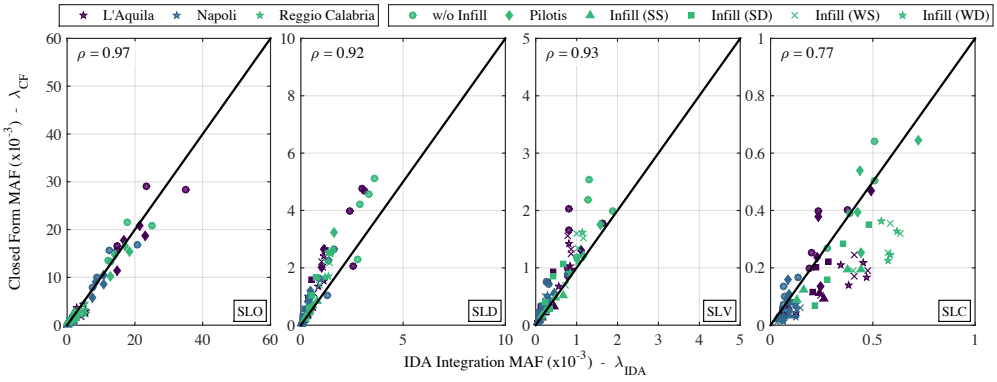

(b) Comparison with the calibrated parameters

Figure 7.40. Comparison of the MAF of exceedance of the different limit states computed the demand-intensity models versus the median value computed from maximum likelihood fitting to IDA results.

The above plots have illustrated how the computation of the MAF of different limit states of interest using the closed-form solutions described in the previous sections compare to those computed using the results of extensive analysis presented in Chapter 5. This comparison has not only shown how these equations work quite well for the different structural typologies examined, but also proposed coefficients can be used in such computations, also highlighting the impacts of the use of default values suggested previously in the literature when applied to GLD RC frames in Italy.

7.5 OVERVIEW OF FRAMEWORK FOR SEISMIC ASSESSMENT OF ITALIAN GLD RC FRAMES

So far, this chapter and chapters previous to this have outlined detailed methods of analysing and assessing the performance of GLD RC frames with masonry infill, typical to older construction in Italy. The development of advanced methods of modelling were highlighted in addition to discussion of more simplified methods of analysis. This section aims to bring this process full circle by outlining a framework that practitioners wishing to assessing such structures, by means of either advanced numerical or simplified methods, can be followed. Figure 7.41 shows this process in the form of a flow chart whereby starting with the structure to be assessed, either approach can be followed to arrive at the estimation of losses in the structure. In many ways, this resembles the assessment framework outlined in FEMA P58, whereby guidance is given on how one should go about conducting a loss assessment for a given structure, where the various aspects are discussed and more simplified methods are given. While a very useful resource, FEMA P58 was developed within a US building typology context and many of the various aspects are not necessarily applicable to GLD RC frames with masonry infills. The following subsections will compare and contrast the procedure outlined in Figure 7.41 with that of FEMA P58 within the context of its applicability to GLD RC frames with masonry infills, providing commentary on the different aspects that require additional consideration to highlight how many of the aspects covered in this thesis should be adopted within such an assessment framework as they have been developed specifically for these structural typologies.

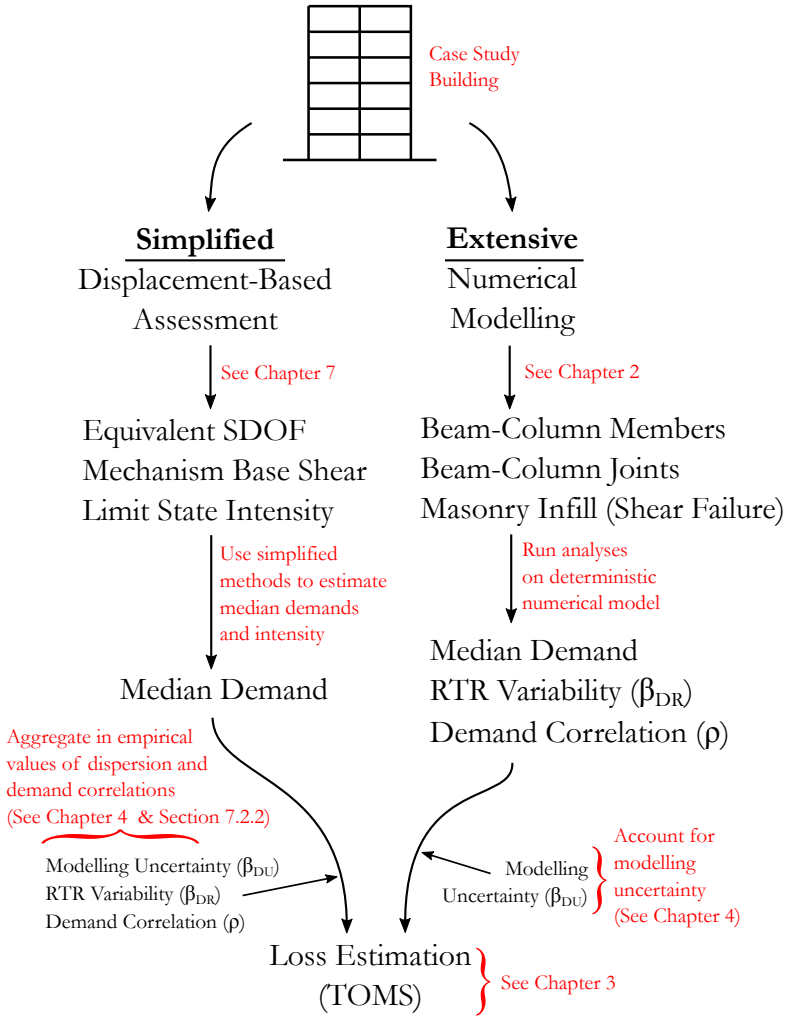

Figure 7.41. Overview of the framework for the assessment of GLD RC frames with masonry infill, where advanced numerical methods to capture the different failure mechanisms are considered in addition to more simplified approaches when establishing the overall response of the building. Further considerations for the proper treatment of randomness due to record-to-record variability and modelling uncertainty in addition proper consideration of the correlations in demand to be respected during loss estimation.

7.5.1 Assessment of Structural Behaviour using Numerical Models

Considering the numerical modelling of GLD RC frames as part of the more extensive approach to establishing the overall response of the building, some of the more pertaining aspects with respect to the modelling of structures outlined in FEMA P58 are noted. This

refers to much of the discussion in Chapter 2, whereby the investigation into the experimental behaviour and numerical modelling of the various elements of GLD frames highlighted numerous inconsistencies with conventional methods of numerical modelling of RC frames. The first of these related to the overall ductility and pinching behaviour of the beam-column members, whereby the use of smooth bars and poor confinement in GLD frame members was demonstrated to exhibit a notably different behaviour to that of more ductile and well-detailed members. As a result, Section 2.2 proposed a numerical modelling approach to better represent the actual behaviour of such members when compared to actual experimental data. In addition, the behaviour of the beam-column joints was considered and a numerical representation developed for both interior and exterior joints such that the strength and stiffness degradation associated with these joint typologies, which typically used no transverse joint reinforcement and smooth bars terminated with end hooks in the joints, can be properly considered. The numerical calibration for these joint models presented in Sections 2.3 and 2.4 illustrated how the modelling approach utilised here effectively captures the failure mechanisms associated with these types of joints. Furthermore, the consideration of shear failure in column members due to interaction with masonry infill so often observed after numerous earthquakes in Italy has also been considered by incorporating a shear spring element into the column member ends such that the short column effect can be adequately represented. Chapter 5 demonstrated the impact of such a consideration, whereby shear failure in the columns resulted in limited global ductility, modified global mechanisms and reduced overall collapse capacity.

The above remarks note the various aspects that require specific consideration in the assessment of GLD RC frames in Italy, which are illustrated in Figure 7.42. Comparing these types of structures that are prone to more particular type of mechanisms to more modern well-detailed ductile designs, it is clear there are some issues that need to be addressed. This is the argument raised here, where if one were to follow conventional approaches to the numerical modelling of GLD frame structures, many aspects of the building behaviour would be missed. This was highlighted in Section 2.5, whereby in comparison with a test of a three-storey RC frame with GLD design and detailing provisions, conventional approaches such as using fibre-based element modelling and the lumped plasticity approach calibrated by Haselton *et al.* [2008] were shown to misrepresent the actual performance of the test specimen. This was seen in how the lumped plasticity approach proposed by Haselton *et al.* [2008] was unable to capture the exterior beam-column joint mechanism forming in the structure and actually resulted in a less ductile response due to the prediction of a soft storey mechanism. Fibre-based element modelling, on the other hand, showed good ability to capture the overall backbone behaviour of the test specimens but failed to properly capture the pinched behaviour of the test specimen and showed much fatter hysteretic loops. Compare this with the numerical modelling approach proposed in this thesis, the overall backbone capacity, hysteretic pinching and

observed joint mechanism were all well represented. This is not to say that the modelling approach proposed by Haselton *et al.* [2008] or fibre-based element modelling are incorrect, but merely to state that their applicability to GLD RC frames with smooth bars and weak beam-column joints is limited. This is because these models were developed with certain assumptions in mind that these members with smooth bars and inadequate reinforcement no longer satisfy. As such, the numerical modelling outlined in Chapter 2 for GLD RC frames with masonry infills is viewed as an improved modelling approach that is recommended for use within the assessment framework outlined in Figure 7.41.

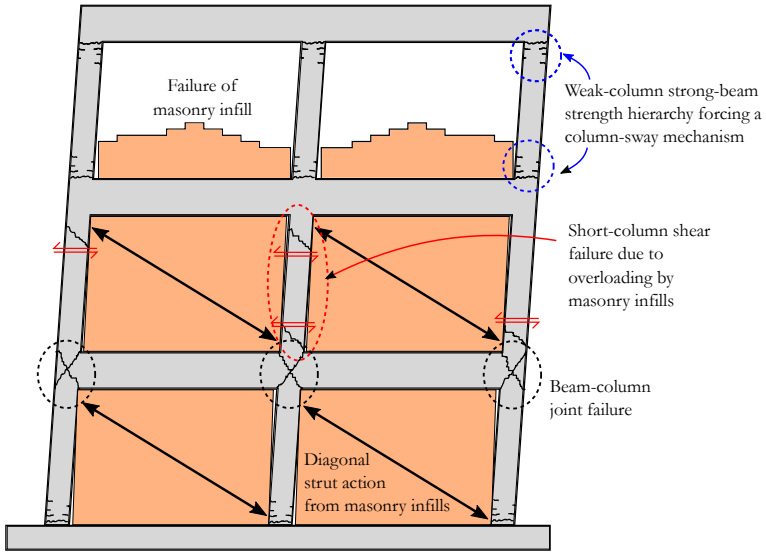

Figure 7.42. Illustration of various aspects to consider when modelling GLD RC frames with masonry infill, where a conventional beam-sway mechanism is replaced with more non-ductile modes of failure such as beam-column joint failure, short column failure due to overloading of columns by masonry infills and column sway mechanism due to a strong beam-weak column strength hierarchy (Note: the locations/combinations of the illustrated mechanisms are illustrative and are not intended to be representative of actual mechanism combinations in real structures).

7.5.2 Assessment of Structural Behaviour using Simplified Approaches

The previous section discussed the numerical modelling of GLD RC frames with masonry infills within the context of the extensive modelling approach to characterising the behaviour, illustrated in Figure 7.41. On the other hand, it is often more convenient to use simpler methods of assessment that do not require advanced modelling techniques such as those outlined previously, but a comprehensive consideration of the likely response mechanism of the building given the mechanical properties of its members. Section 7.2 extensively discussed the application of the DBA methodology to GLD RC frames with

masonry infill, where the various aspects as to how one could consider the behaviour of the structure at different limit states, determine median demands and the corresponding intensity. This approach of using simplified methods as a substitute for extensive analysis resembles the simplified methods outlined in FEMA P58, which aims to provide the user with median values of demand for a given intensity without the use of numerical modelling. However, considering the lengthy discussion in Section 7.2.1 and also in the previous section as to the various particularities of the structural typologies considered here, the commentary below will argue that the simplified approach outlined in FEMA P58 is no longer applicable. This is argued from the point of view of the limitations of the existing approach to capture the particular mechanisms of the GLD frames, much the same way that conventional numerical modelling approaches were seen to be no longer applicable in Section 7.5.1. In addition, the philosophical advantages of adopting a displacement-based rather than a force-based approach are not discussed in depth here, but the interested reader is referred to Chapter 13 Priestley *et al.* [2007] for further discussion.

One of the first items required when conducting a simplified assessment using the approach outlined in FEMA P58 is that the mode shape used to compute the elastic displacement demand for a given intensity must be obtained from a linear elastic structural model of the building so that all distributions of mass and stiffness throughout the building are characterised. For GLD RC frames with infills, this already highlights a number of issues when considering some of the point highlighted in Figure 7.42. Nevertheless, assuming that such a model can be constructed relatively easily, the elastic displacement demand is computed based on the initial elastic behaviour of the building. The actual median demands are then computed by applying an adjustment factor depending on the structural typology, where RC walls, RC frames and braced frames are listed. In these initial steps alone to determine the median drift demands, a number of issues arise when one attempts to apply this to the structural typologies considered here. The first of these is that of the structural typologies listed above, with which one would determine the six empirical coefficients necessary, non-ductile RC frames with masonry infills are not included as this type of construction is not very common most parts of the US with high seismic risk. As such, one is left with no options when applying this method. The second is that such an approach is noted to be limited to structures without significant strength degradation and is anticipated to be applied to structures exhibiting a stable response, such as a beam-sway mechanism. This is implied through the use of elastic analysis to identify the distribution in drift demand through the building, as these are determined for each intensity by applying a set of lateral forces to the elastic model to obtain an elastic drift profile followed by modification to account for other aspects such as nonlinearity and structural typology. By using such an approach, it is inherently assumed that the initial elastic behaviour of the building can be deemed representative of the distribution of demand at all limit states. Recalling the comparisons of the elastic first mode shape with the actual non-linear SPO demand in Figure 7.3, it was noted that the formation of column and joint sway soft storeys

meant that the drift demand distribution changes significantly with increasing intensity for GLD RC frames. This contributes to the reasons why the FEMA P58 simplified approach is no longer applicable to the buildings outlined here. It is noted, however, that the prediction of the displaced shape for these frames using DBA is a required future development, although Section 7.2.2.1 noted how recent progress by Saborio Romano [2016] for frames without masonry infill modelled illustrated how the particularities of GLD frames can be captured excellently using mechanics-based approaches. Therefore, this is noted as future development to be completed rather than a limitation of the actual methodology.

In addition to the limitations outlined above for the use of the elastic analysis to predict the inelastic response of the system, another limitation in the simplified approach outlined in FEMA P58 when applied to GLD frames stems from the assumption that the system being analysed does not contain any significant strength degradation and can be reasonably represented as an elastic-perfectly plastic system. This assumption obviously does not hold here, even in the case of the pilotis frames or the frames without infill modelled since there is a degree of strength and stiffness degradation due to the element's limited ductility capacity. Not to mention the added difficulties that arise when trying to incorporate the effects of the masonry infill on the backbone response. Section 7.2.2.2, however, highlighted how these details regarding increased strength due to infill and strength degradation due to limited ductility can be accounted for in DBA, with Figure 7.4 to Figure 7.7 showing how the backbone response can be estimated excellently for each of the structural systems examined. In addition, more refined considerations were proposed in Section 7.2.2.2 to account for the effects on the mechanism base shear should a column sway mechanism for at storeys other than the ground floor. This development showed improved results when compared to the SPO analysis.

The final step in the analysis of the frames using the DBA methodology previously outlined involves the establishment of the intensity associated with the established displaced shape of the structure. This step differs to that outlined in FEMA P58 due to the fundamental differences in the philosophy behind force-based and displacement-based approaches. The FEMA P58 approaches works on the basis of knowing an intensity level and then estimating the median demands in the structure at that intensity, whereas DBA starts with a demand and works backwards to find the intensity required to develop it. Section 7.2.2.3 demonstrated how the DBA approach works very well in establishing the median intensity required to develop a given mechanism, demonstrating its applicability to the structural typologies considered here, although some issues regarding the equivalent viscous damping contributions in the infilled frames still need to be resolved.

Overall, it can be said that the simplified approach to assessment outlined in FEMA P58 is not applicable to GLD RC frames with masonry infill for a variety of reasons, each of

which stem from the fact that this methodology was not developed with such structures in mind. The DBA methodology, however, represents a very promising approach that, with some future developments in different areas highlighted in Section 7.2, can be adopted as a robust assessment approach in the future to form the simplified method of characterising the response illustrated in Figure 7.41.

7.5.3 Incorporation of Demand Uncertainty and Correlations in Loss Estimation

As illustrated in Figure 7.41, the final step for both the simplified and the extensive approaches to characterising the behaviour of the building is the incorporation of demand uncertainty and correlations into the procedure. This is so that the eventual data supplied to the loss estimation step of the framework contains appropriate representations of these two aspects in addition to the median values.

First considering the extensive analysis option, where a detailed numerical model has been developed and analysed with an appropriate number of GMs to provide a distribution of the demand parameters of interest with respect to intensity. Using this approach, the uncertainty due to record-to-record variability has been inherently considered in the process due to the use of an appropriately large GM ensemble. In addition, the correlations between the demand parameters are also determined since the response of the numerical model to each GM will automatically quantify this correlation. Demand correlation is not such an issue in the extensive analysis approach from the analyst's point of view, as the numerical modelling accounts for this, but it is eventually required when generating simulations needed for loss estimation such that the proper relationships between the various demands is maintained. The randomness due to modelling uncertainty is required when using the extensive analysis as a single deterministic numerical model is used to represent the behaviour. As discussed in Chapter 4, to account for the fact that there is some inherent degree of uncertainty in the actual representation of the true behaviour of the structure via numerical modelling, an additional modelling uncertainty term is incorporated into the procedure. These are typically empirical values that reflect the structural typology and demand parameter, among others, that are often specified as default values for an analyst to adopt in order to give some form of consideration to this source of uncertainty. Within the FEMA P58 guidelines, these values are specified in terms of construction quality and completeness of the numerical model with increasing values of dispersion for lower levels of knowledge in either, with the final value to be combined using and SRSS combination. Chapter 4 examined the modelling uncertainty in GLD RC frames with infills in detail and concluded that not only is the modelling uncertainty a function of the structural typology, it is also a function of the demand parameter under scrutiny, the response limit state characteristics and the floor level within the building. As such, Chapter 4 proposed sets of default values of modelling uncertainty to be incorporated into the loss estimation to properly account for the dispersion in the loss estimates. This approach

defines these empirical values for GLD RC frames in Italy in terms of the structural typology, demand parameter and limit state to give, to the author's knowledge, the only existing set of modelling uncertainty values for the structural typologies considered as part of this study. These values represent a novel contribution as they incorporate the specific aspects of the GLD RC frame response, such as the large uncertainty associated with infilled frames in the post-peak region of response, discussed previously in Chapter 5.

For the more simplified approach illustrated in Figure 7.41, not only does the modelling uncertainty need to be incorporated as before, but the additional uncertainty due to record-to-record variability and the demand correlations need to be amalgamated. Regarding the record-to-record variability, default empirical values have been suggested in Chapter 7 based off of the extensive analysis conducted in Chapter 5 to provide the user with default values in terms of structural typology, demand parameter and limit state. This approach results in a dispersion value to account for modelling uncertainty being selected in addition to another dispersion value to account for the record-to-record variability being selected. Again, these default empirical values presented as part of this thesis represent values that have been specifically developed and quantified for GLD RC frame systems. FEMA P58, on the other hand, specifies a number of dispersion values for record-to-record variability as a function of demand parameter, in addition to limit state response, as proposed in this study. Comparing the values proposed in FEMA P58 with those proposed here shows that these default values may be actually underestimation the dispersion in response for GLD RC frames when compared to the values observed in Section 7.3.2.1. This is especially true in the case of the infilled frames, where the presence of the infills results in a large dispersion in response, as previously discussed. These empirical values proposed here to account for the record-to-record variability in the different demand parameters represents a novel contribution in the context of simplified assessment of GLD RC frames with masonry infill.

The last item to be considered in simplified assessment within the context of the structural typologies considered here is the appropriate attention to the correlation between the different demand parameters. This aspect is very important in the simplified approach, as it is recalled how the simplified approach to loss estimation works on the basis of providing a median and dispersion for each demand parameter such that the simulations sampled during loss estimation can be generated to this distribution. However, of critical importance is the correlation between each of the demand for each simulation generated. If no correlation between the demand parameters is considered, then there is a possibility that a situation where, for example, a high percentile value of drift demand is sampled for the first floor of a frame building and a low percentile of drift demand is sampled on the second floor. As no correlation is defined between these two demand parameters, this situation can arise, which doesn't make a lot of sense as for such a situation one would expect a high percentile of the drift demand of the second floor to be sample also since a correlation

between the two is intuitively expected, although this is a generalised case and exceptions can arise such as in the case of a soft storey, for example. This aspect was discussed at length in Section 7.3.2.2 for the GLD frames where simplified expressions to describe the correlations between the different demand parameters were outlined in terms of the structural typology considered and number of floors separating these correlations. These values can be therefore adopted within this framework for the different structural typologies considered here. Future research may look into further disaggregating such empirical values of demand parameter correlation based on expected damage mechanism, but this aspect is deemed beyond the scope of this work.

Comparing this approach proposed here with that of FEMA P58, where full correlation between the demand parameters is assumed; some discrepancies arise. Firstly, the assumption of full correlation between the different demand parameters (i.e. a correlation coefficient of 1) has been shown to not hold true in Section 7.3.2.2, where the values were much less than 1.0 and varied depending on the demand parameters in question. This means that the assumption adopted in FEMA P58 is overestimating the correlation coefficients. This overestimation translates as an increase in the overall variance of the losses for a given intensity. The expected value does not change due to this overestimation of the correlations and subsequent increase in variance, so the impact of the correlations appears to minimal if the expected losses are of interest. This would hold true only in the situation where a loss threshold not in place, whereby should a particular simulations loss ratio to the building's replacement cost versus intensity curve reach this threshold value less than 1.0 (e.g. 0.60), the loss would be deemed too high to warrant repair and the building would be demolished, meaning that the loss for this simulation has now actual become 1.0. This implication means that an increase in variance of the simulations will actually mean that more and more of the simulations will be running into this threshold value and subsequently becoming set to 1.0 compared to if the overall variance in losses were quite tightly bound. A similar discussion was presented in Section 7.3.3. Therefore, while the increase in variance due to the assumption of full correlations does not theoretically result in a change in expected value, the implementation of threshold losses means that it does with an overestimation in the variance translating as an overestimation in the expected loss. Comparing this with an assumption of no correlation that would have the opposite effect, whereby the overall variance of the losses would be reduced with respect to the actual variance obtained if extensive analysis were to be used. As such, the approach to better account for the correlations in demand parameters is properly considered here for GLD RC frames and should be adopted when performing simplified assessment of such structural typologies as opposed to simply assuming a full correlation, which has been demonstrated to not hold true.

7.6 SUMMARY AND CONCLUSIONS

This chapter explored the use of more simplified methods of assessing GLD RC frames with masonry infill in Italy. First, the DBA methodology was compared and critiqued alongside the results of the extensive analyses to examine the applicability of current state-of-the-art simplified assessment methods for the structures examined here. Following this, a more simplified approach to loss estimation was outlined where the DBA methodology was highlighted as a method with which practitioners can use simplified methods of analysis in conjunction with empirical values of dispersion and demand parameter correlation to conduct loss estimation using the TOMS tool presented in Chapter 3. This approach was compared to the extensive loss estimation study conducted in Section 6.1 to highlight the applicability of such an approach. In addition, the use of a more probabilistic methodology to estimate the annual probability of exceeding a given limit state was discussed within the scope of the structures examined here. The various aspects were discussed and some modifications to the probabilistic methodology were proposed in order to apply this to GLD frames. Finally, the assessment of GLD RC frames with masonry infills within a broader framework was highlighted with respect to the FEMA P58 methodology where the various aspects of the approach highlighted were discussed in relation to the structural typologies considered here to provide a framework with which practitioners in Italy can use.

In terms of the DBA methodology, the applicability in the assessment of GLD RC frames was evaluated with respect to the extensive numerical analysis conducted on the various structural typologies to highlight what implications work well, what requires future work and also how these eventual developments can be used in combination with appropriate estimates of demand parameter dispersion and correlation. In light of this, the following conclusions can be drawn:

- In its current state of development, simplified methods such as DBA cannot be applied to existing GLD RC frame buildings with masonry infill in Italy without assuming approximate values of some key parameters. Although, this is due to the absence of some of the vital ingredients required by the method rather than a fundamental limitation of the approach. This was highlighted through the numerous comparison with the extensive analysis and potential improvements to the various aspects were discussed.
- In terms of the ability to predict the correct displaced shape required at the various limit states for DBA, it was shown how traditional beam-sway mechanism typically used in new design does not work well for frames with other modes such as column-sway. A recent approach trialled by Saborio Romano [2016] to predict the displaced shape of GLD frames without masonry infill was evaluated, where the approach, with some minor modification proposed here, worked excellently in

predicting the displaced shape at each limit state considered. While this approach worked well for the frames without masonry infill vulnerable to a column-sway mechanism, further work is required to include the effects of beam-column joint behaviour, masonry infills and the shear behaviour of weak columns. These three issues were shown to have different adverse effects on the performance of the buildings and should be investigated further.

- The prediction of a given damage mechanism backbone response at different limit states was also compared for each of the case study frames, where compared to the SPO curves showed excellent agreement at each of the limit states considered. Further guidance on the correct estimation of the base shear of the governing mechanism was also discussed. It was shown that using the assumption of the storey shear at the critical storey, the total base shear can be underestimated. This is as when the column sway forms at a storey other than the ground floor, as the additional shear contribution of other elastically responding storeys can provide significant increase in the base shear. Using this proposed base shear consideration, excellent matching with SPO analysis was observed when compared to other approaches suggested in the literature, such as that outlined in FEMA P58 that relies on elastic analysis methods and does not capture the post-peak base shear reduction in the frames. The effect of the shear damage to column members also ought to be investigated further as SPO analysis showed a significant modification in the backbone when shear failures on the columns occurred.
- In the final step of DBA, the seismic intensity required to generate a given limit state is computed, which can then be used in methods such as DBLE. Comparisons of the intensities required for each of the limit states considered were compared to those estimated during the extensive NRHA. This comparison showed that the DBA methodology works quite well in estimating the various intensities for the different structures apart from the frames with masonry infill. This was shown to be a consequence of the absence of an adequate EVD relation to account for the additional hysteretic damping provided by the masonry infill. The recently proposed expression by Landi *et al.* [2016] worked reasonably well but was observed to significantly overestimate the damping at lower levels of ductility. In addition, no distinction between different masonry infill typologies were made in this proposal, which as also highlighted here to be another parameter to consider since the relative energy dissipation capacity of the masonry infill for a given deformation demand and RC frames will be a function of the infill typology and consequently influence the amount of hysteretic damping provided to the equivalent SDOF system. In order to address such a shortcoming, large parametric studies are required in order to better quantify this contribution of masonry infills to the equivalent SDOF systems properties.

As a final remark regarding the above comments, this chapter provides extensive quantification of the response and performance of GLD RC frames with masonry infills. To build on this and explore more simplified methods to which structural analysis can be computed, existing methods are scrutinised with respect to the NRHA data. The areas in which the simplified methods work well are highlighted within the general framework in addition to the areas that require further work such that the missing ingredients of the methods are clear. This is in order to give the reader a full appreciation of the current state-of-the-art limitations in simplified assessment and provide motivation for future research in this area. In any case, the numerical modelling tools defined in previous chapters allow the reader to account for some of these limitations via more advanced methods.

In the second part of this chapter, a more simplified method to conduct loss estimation was then examined whereby the user inputs the median demands from the aforementioned DBA at various intensities in conjunction with an appropriate value of dispersion due to record-to-record variability and demand parameter correlation to conduct a loss estimation study without the need of extensive NRHA. Following this comparison between the extensive approach, simplified approach with empirical dispersion values and simplified approach without dispersion, the following conclusions are drawn:

- Firstly, in order to use the median values of response determined from simplified analysis in loss estimation studies, appropriate values of demand parameter dispersion need to be assumed. This chapter showed how these values of dispersion for the different frame typologies examined here differ somewhat to typical values available in the literature. As a result, the extensive NRHA was exploited and more refined default values for record-to-record variability with respect to limit state, demand parameter and frame typology were quantified. In addition, demand parameter correlations were also identified such that the proper correlations between the different demand parameters can be considered when generating simulated demand using the median and dispersion values. Such as consideration of correlations in simplified methods of assessment is not widely considered in loss estimation studies, with the FEMA P58 guidelines, for example, assuming the full correlation of the demands that have been illustrated by Bradley and Lee [2010] and also here to not be the case.
- In terms of actual loss estimation, if the user is able to accurately estimate the median response of the structure, a reasonable estimate of the expected loss curve and EAL can be obtained using the empirical values of dispersion and correlations proposed in this study. This aspect is further illustrated in Chapter 8 through an application to an existing school building.
- The use of median demand only without the consideration of demand dispersion does not result in the same expected loss curve as the dispersion in demand translates to a dispersion in the expected loss for the different realisations. This

dispersion in expected loss along with the implementation of a threshold value of expected loss ratio, whereby ignoring the dispersion in demand under predicts the expected loss at lower intensities and over predicts it at the higher intensities. This is also shown through example application in Chapter 8.

- Comparing the predictions in EAL from the simplified approach to those both considering an omitting demand dispersion demonstrates how such a simplified approach provides accurate estimates of EAL, whereas the omission of dispersion tends to underestimate the EAL when compared with the results of extensive analysis. Again, this point will be further verified in Chapter 8, where the proposed values from FEMA P58 are also shown to be unsuitable for application to the case study structures examined here.

The exploration of the use of a more probabilistic methodology to estimate the MAF of exceedance of a given limit state was examined using the so-called SAC/FEMA approach. This was evaluated with respect to the extensive analysis conducted previously for the different case-study buildings and from this, the following comments are made:

- The demand-intensity model that is crucial in linking the median demand parameter of interest to a median intensity has been seen to be fundamentally different in its overall trends for GLD RC frames; such that typically values previously adopted in the literature stemming from work carried out on modern RC frames without masonry infills cannot be adopted.
- The was first apparent in the overall trend of the demand-intensity relationship for the maximum PSD of the case study frames, where two separate regions of response became apparent depending on the response of the masonry infill. This corresponded to whether the masonry infill was responding in the elastic range prior to reaching its peak force or in the post-peak region of response. The trend in overall response of the structure was observed to fundamentally change with respect to this limit state of the masonry infill such that two regions of overall response were defined based on this. It was subsequently shown how a bilinear fit in log space could achieve a much better fit to the data for GLD RC frames with infills such that a set of empirical coefficients for such a demand-intensity model for the maximum PSD were outlined using this approach.
- Regarding such coefficients, an assumption of 1.0 for the exponent term b in maximum PSD demand-intensity models was shown to be a good assumption for frames without masonry infill and pilotis frames. This agrees with the value suggested in the initial publication of the methodology by Cornell *et al.* [2002] and subsequently adopted in many other studies. However, when applied to infilled frames it was seen how this assumption of 1.0 no longer holds true and can have a significant impact on the overall annual probabilities computed, with an example

showing an overestimation of the annual probability of exceedance by a factor of 8.

- Further investigation into these coefficients exhibited how the shear failure of the strong infill frames with double strut infills modelled affected the b parameter by imposing a sort of cap on the value, whereas the single strut infill models showed much higher values of b. The impact of this is that by ignoring the shear failure in the columns, this can lead to a substantially higher estimate of b that will affect the estimated annual probabilities of exceedance.
- Comparing this closed form approach to estimating the MAF of exceedance of the different limit states for the case study structures with the actual results from extensive NRHA conducted in Chapter 5 showed how the general approach works very well; in addition to illustrating the errors induced by assuming the b parameter is equal to unity for such frames.

Finally, examining the assessment of the structural typologies considered here with respect to the procedure highlighted in FEMA P58, a number of conclusions can be drawn:

- In its current form, the various details of the FEMA P58 guidelines can not be applied to GLD RC frames with masonry infills in Italy.
- Issues such as the fundamental difference in the actual behaviour of the elements during numerical modelling were discussed, where it was concluded that traditional methods of analysing frames are not necessarily applicable to GLD frames unless special attention has been given to the different aspects of GLD frame response mechanisms.
- The simplified approach to estimating median demands outlined in FEMA P58 can not be applied to GLD frames. Numerous reasons were cited for this where; suffice to say that the method outlined in FEMA P58 was developed for ductile structures in mind that do not contain masonry infills; meaning that it is no longer applicable to the frames described in this thesis.
- The DBA methodology outlined previously was proposed as a suitable substitute as initial comparisons with the extensive analysis carried out here show it to be a promising method in assessing the particular mechanism as associated with these frame typologies.
- The empirical values of dispersion due to modelling uncertainty and record-to-record variability quantified in this thesis were highlighted to significantly differ to those outlined in FEMA P58 for more ductile frames such that the values quantified here are recommended for GLD RC frames with masonry infill.
- The proper consideration of demand parameter correlation was considered where it was highlighted that assuming full correlations between demands will not only overestimate the variance in the loss but also result in an increase in the expected

losses. As such, the simplified expressions proposed here are recommended and their use is further verified through an example application in Chapter 8.

8 CASE STUDY APPLICATION TO AN EXISTING ITALIAN SCHOOL BUILDING

A significant portion of the work presented in this chapter is based on the following article:

O'Reilly, G. J., Perrone, D., Fox, M. J., Moratti, M., Monteiro, R., Filiatrault, A. [2017] "Seismic Assessment of Italian School Buildings Considering Direct Economic Losses," *Bulletin of Earthquake Engineering*, (Under Preparation).

8.1 INTRODUCTION

The work described in previous chapters of this thesis has extensively examined the various aspects of the behaviour and response of GLD RC frames with masonry infills in Italy. Many different aspects were considered in terms of numerical modelling approach and performance-based assessment in terms of both loss estimation and different approaches to retrofitting when aiming to reduce the overall vulnerability of the buildings. This was carried out using a series of case study buildings to clearly illustrate the various points being investigated. This chapter aims to build on much of the work carried out in this thesis by applying some of the same assessment methods and considerations to an existing school building located in central Italy. This structure represents a worthy conclusion and application of the work carried out in this thesis, as it represents an actual structure for which in-situ data was collected and site visits were carried out to determine damageable structural and non-structural elements. The subsequent analysis was then carried using much of the numerical modelling approaches developed here and analysed using an ensemble of hazard consistent GM records, both in keeping with the current state-of-the-art. The following sections follow a similar structure to before, with the various analysis methods being described and carried out before the overall performance of the school building being evaluated.

8.2 OVERVIEW OF CASE STUDY SCHOOL BUILDING

The case study school examined here represents one of many Italian schools selected as part of a national research project in Italy entitled "Progetto Scuole" which looks to examine the vulnerability of the existing school structures throughout Italy. As part of this research project, surveys of the school buildings were conducted and a detailed inventory of the damageable elements recorded so as to enable comprehensive assessment both in terms of life-safety, which was highlighted through the collapse of a school during the 2002 Molise earthquake in Italy killing the young students and a teacher inside [Augenti *et al.*,

2004], and economic losses during more frequent events. The exemplary school building outlined here is shown in Figure 8.1 and consists of a three-storey reinforced concrete frame building constructed in the 1960's, which from the time of construction and examination of the building's structural information indicates that it has not been designed with any seismic design specifications and was designed principally for gravity loading. This is clear upon examination of the strength hierarchy, where a strong-beam weak-column strength hierarchy is present at each floor level. In addition, low levels of longitudinal reinforcement (<1%) and poor grades of concrete were confirmed from in-situ testing of a number of structural elements. As such, this case study school structure corresponds well with the structures investigated as part of this thesis. The following sections describe the initial analysis of the structure to identify the fundamental aspects of its behaviour followed by a more detailed analysis.

Figure 8.1. Front and rear elevation of case study school building.

8.3 NUMERICAL MODELLING AND STATIC ANALYSIS

As previously mentioned, the characteristics of the case study school building correspond well with the general characteristics of GLD RC frames examined in detail in this thesis. As such, the modelling approach outlined in Chapter 2 will be followed herein to model the response of the beam and column members, the beam column joints and the masonry infill. The typical floor layout of the beam and column members in the school is shown in Figure 8.2 in addition to the span direction of the floor slab system, which was confirmed during the site visit.

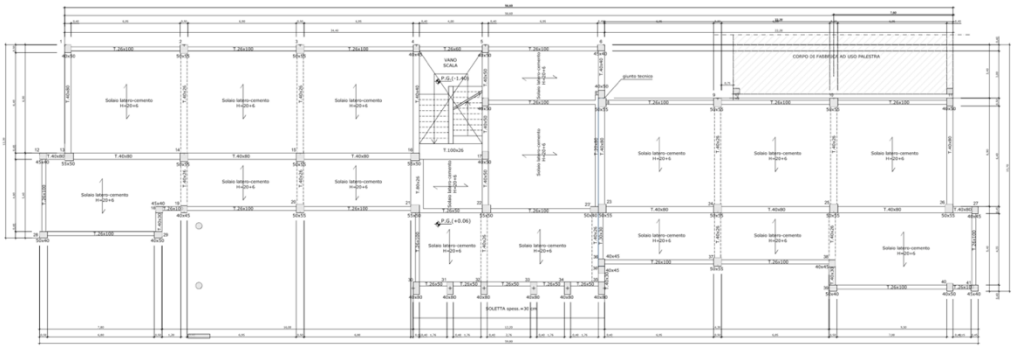

Figure 8.2. Typical floor layout of school, where the beam and columns are dimensioned along with the spanning of the slabs.

Using the layout of the structural members shown in Figure 8.2 along with additional information regarding the member properties, such as material strength and reinforcement ratios, the numerical model of the school is constructed in OpenSees and is shown in Figure 8.3. The information required to model the beam and column members was taken from the available survey reports, where details regarding material properties and reinforcement content were provided for a number of members. For members that had no in-situ test data, a reasonable value was estimated. The beam and column members were modelled using the lumped plasticity element calibrated in Section 2.2 for older RC members with smooth bars and poor confinement. Both the exterior and interior beam-column joints were modelled using the rigid link offset coupled with a rotational hinge at the joint centreline to capture the nonlinear behaviour, which was discussed in Chapter 2 and illustrated in Figure 8.3. The exterior masonry infill was determined to consist of double leaf hollow clay brick masonry and was therefore modelled using the same strut modelled approach adopted previously and illustrated above, but with the "Medium" strength material properties provided in Hak *et al.* [2012] for this type of infill.

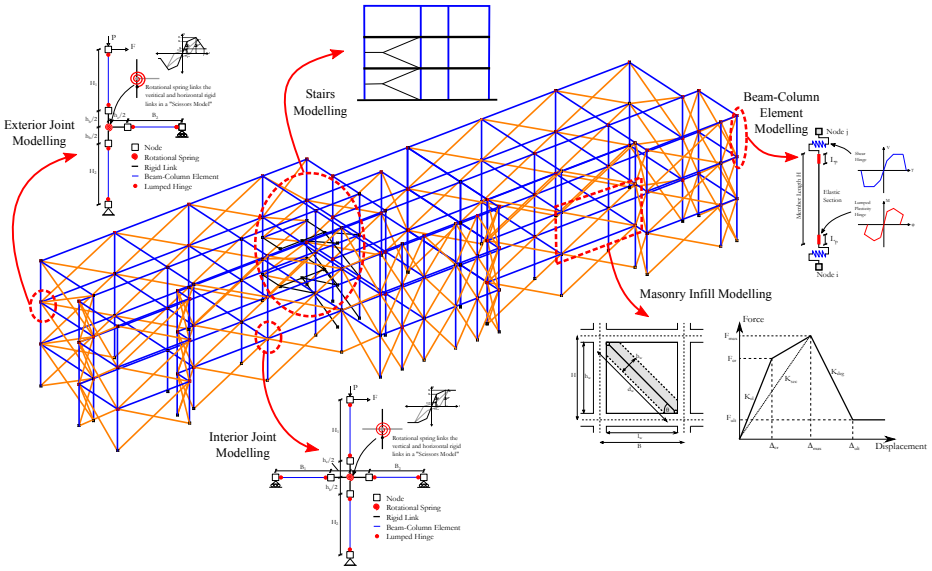

Figure 8.3. Numerical modelling of school building where the various details regarding the modelling of GLD RC frame behaviour are highlighted.

Some other important decisions regarding the modelling of the school also need to be defined. The first of these is regarding the floor slab system, which has been assumed to be rigid in the numerical model. This decision was taken in light of examination of the actual "laterizio" floor system in place. Based on engineering judgement, it was decided that such a system does not represent a floor system flexible enough to have a great impact on the response, and was therefore assumed to be rigid for simplicity during analysis. Another aspect is the incorporation of the second order geometry effects of the gravity loading, which are more commonly known as P-Delta effects. These have been incorporated in the model by applying the tributary loading collected from each floor slab and beam onto the corresponding column. These loads were then applied as a constant load and kept constant throughout the analysis to incorporate the P-Delta effects on the collapse capacity of the structure. The elastic damping in the structure was defined as 5% tangent stiffness proportional Rayleigh damping at the first and third modes periods. Such a value is deemed reasonable when one considers that the building is an RC frame structure where the non-structural elements have not been explicitly modelled. The stairs system has been modelled using a series of elastic elements, with the main purpose of capturing the increased stiffness in that location of the building and potential shear failure of the surrounding columns, as illustrated in Figure 8.3 and previously observed during the L'Aquila earthquake shown in Figure 1.5.

Using this numerical representation of the school building, some initial analysis such as modal and SPO analysis can be conducted to examine the fundamental aspects of the behaviour. The first two fundamental periods of the buildings are listed in Table 8.1, and the corresponding mode shapes shown in Figure 8.4. The analysis in Chapter 5 adopted the IM as the spectral acceleration at the conditioning period T^*, where T^* was set as the first mode period in the case of the 2D frames and the mean value of the two principal direction in the building for the 3D frames. Following the latter approach of the mean value of the two periods in the principal directions, the average of the first and second mode of vibration is found to be 0.494s. This conditioning period is subsequently taken as 0.50s since the hazard disaggregation information required for GM selection tends to be available at a fixed number of periods, of which 0.50s is one. This can be thought of a representative period for the range of periods in which the building has modes of response and is a reasonable assumption to make as it corresponds to a 1.2% difference compared to the mean value period from both directions.

Table 8.1. Periods of vibration for the first two principal modes of response.

Mode	Period [s]
1	0.623
2	0.365

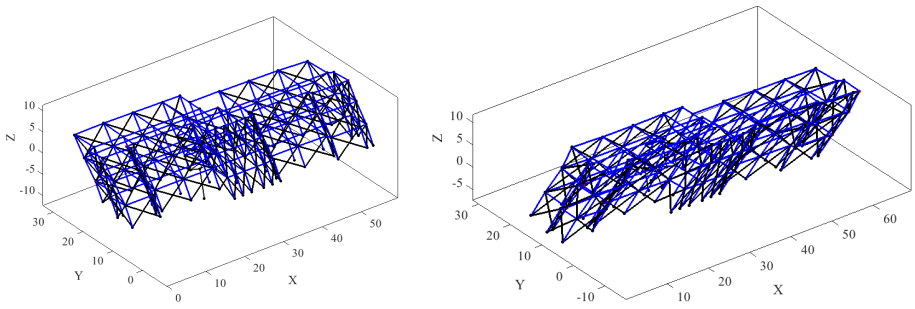

Figure 8.4. Mode shapes of the first two modes.

Using this modal shape information for the two principal directions, a SPO analysis was performed on the school building. This was performed by applying a lateral force pattern to the structure in proportion to the mode shape of the building in both directions and is incremented gradually until the displacement of the control node, which in this case is the roof at the centre of mass, reaches a target value of displacement. The plots of the pushovers in the two principal directions are shown in Figure 8.5, where the displaced shape of the structure at the end of the analysis is also shown. Examining the overall

behaviour of the structures from the pushover curves first, the response of the structure is initially quite stiff due to the presence of the masonry infills, which is then followed by a loss in capacity and a gradual negative slope due to the exhaustion of the masonry infill strength and the yield of the frame members. As highlighted in Chapter 5, this is quite a typical behaviour in older RC frames where the masonry infill provides a significant increase in capacity initially but loses its significance in the higher levels of deformation, where the capacity of the actual frame members and joints govern the behaviour. In terms of the actual capacity, the base shear coefficient of the structure is relatively low when one considers the values typically present in new designs, accounting for the fact that the presence of the masonry infill increases the base shear coefficient significantly. These also correspond well with the value observed in Section 5.2 for the case study buildings previously examined.

The deformed shape of the structure at the end of the pushover is also worth commenting on since the mechanism is slightly different in either direction. In the response of Direction 1, which corresponds to the direction along the longer side of the structure, a soft-storey forms in the middle of the structure, whereas the soft-storey forms at the roof level in Direction 2. This is somewhat strange at first as soft-storey mechanisms at the ground floor are generally the anticipated mechanism in structures without any seismic provisions. Upon further inspection, however, the relative strength of the column members in the upper floors with respect to the beams shows how the columns in the upper floors are relatively weak with respect to the beams (possess a strong beam, weak column strength hierarchy) since these were designed for gravity loading only. This results in the situation encountered previously in Chapter 5, where the beam members are of constant section properties at each floor, whereas the column sections gradually reduce along the building to account for the decrease in design axial load. Therefore, at some point along the height the building the strength ratio between beams and columns changes meaning a soft storey mechanism can be expected, which was also observed for the structures examined in Section 5.2.

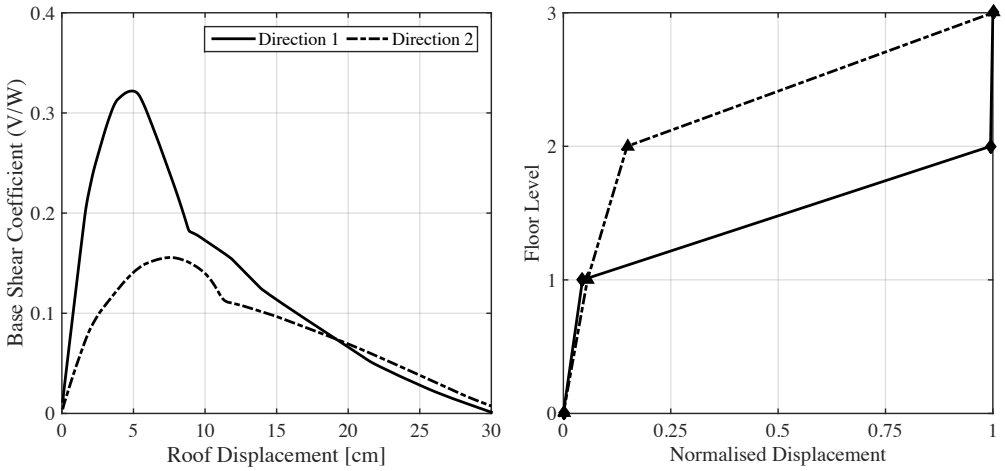

Figure 8.5. SPO curve for both directions of the school in addition to the displaced shape at the end of each SPO analysis.

As in Section 5.2, the four limit states of the structure are determined in accordance with the criteria defined and illustrated in Figure 5.6, which will be used in subsequent sections to assess the performance of the structure at these different limit states.

8.4 MULTIPLE STRIPE ANALYSIS

Following the static analysis of the structure and identification of some of the fundamental aspects of the structural response, a series of NRHA are conducted using MSA where a set of GMs are selected in correspondence with the available hazard disaggregation at the conditioning period to evaluate the response of the structure at increasing levels of intensity. This approach is similar to that adopted in Section 5.3 with the fundamental difference here being that the same GM set is not scaled to different levels of intensity to perform IDA, but are individually selected at each intensity to maintain consistency with the actual seismic hazard of the given site location. This approach of performing MSA is noted to be the more suitable approach for individual assessment of buildings as issues with hazard consistency and spectral shape [Baker and Cornell, 2006; Eads *et al.*, 2015, 2016] are better accounted for than in the case of IDA, although other factors such as the choice of IM [Kohrangi *et al.*, 2016], for example, come into play but are not discussed here in detail. MSA was not previously adopted during the analysis in Chapter 5 as the sheer amount of analysis conducted would have required a very extensive GM ensemble at multiple intensities and multiple periods of vibration, whereas the focus of the study carried out was to characterise the performance of GLD RC frames with masonry infills in general and not to conduct an assessment for a specific location; hence, the single set was adopted for simplicity.

For the case study school building examined here which is located in central Italy, the seismic hazard information illustrated in Figure 8.6 is used for the selection of GMs to match the conditional mean spectrum for different return periods. A total of 20 pairs of GMs were selected[f] at 11 return periods for a site with Soil Type C, as per Eurocode 8 [EN 1998-1:2004, 2004] definition. The GMs were taken from the PEER NGA-West database[g], where a hazard-consistent record selection based on the spectral compatibility with the geometric mean spectrum using the methodology outlined in Jayaram *et al.* [2011], which also considers the conditional variance of the spectral acceleration at the conditioning period. The selection criteria consider the spectral acceleration as the maximum between the two as-recorded component pairs, which is consistent with the GM prediction equation by Ambraseys *et al.* [1996] employed here for the hazard calculations. The seismic hazard calculations and the derivation of the conditional mean spectra were performed using the REASSESS software tool [Iervolino *et al.*, 2015], with the correlation model among spectral acceleration ordinates suggested by Baker and Jayaram [2008] being incorporated. A maximum scaling factor of four was imposed to achieve spectral compatibility, with the exception of the 4975 and 9975 year return periods where scale factors up to a value of eight were considered. Ground motions at such high return periods were required in order to assess the collapse fragility of the building in a hazard consistent manner that would require no adjustment to the median collapse intensity or dispersion in order to account for the effects of spectral shape.

[f] Ground motions selected by Prof. Iunio Iervolino of Università degli Studi di Napoli Federico II as part of a project deliverable for *Progetto Scuole*, a national reserach project regarding Italian school for which the case study school building examined here is a part of.

[g] http://peer.berkeley.edu/ngawest/

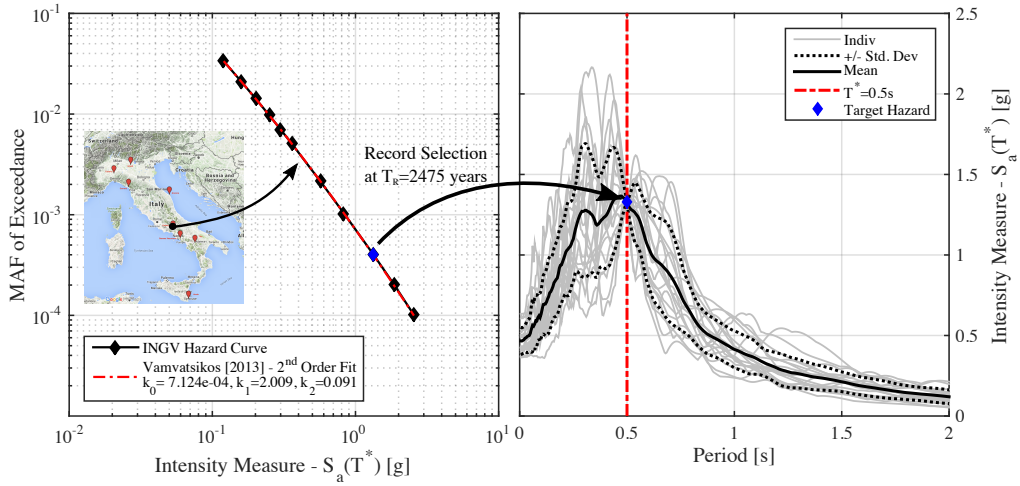

(a) Hazard Curve **(b) Conditional Mean Spectrum**

Figure 8.6. Illustration of the hazard curve for the chosen site in addition to the corresponding GMs selected for each of the conditional mean spectra at each return period.

Following the selection of the GMs at the conditioning period for multiple intensity levels illustrated in Figure 8.6, the NRHA can be conducted using the numerical model previously described. Figure 8.7 shows the plots of the salient demand parameters of interest in this study, defined in terms of the maximum PSD and PFA at any location in the building. These are plotted for each return period along with the median value and the corresponding lognormal dispersion in addition to the probability of collapse at each intensity. This was computed as in Section 5.4 where the total number of collapsing records was taken as a fraction of the total number, where collapse was again defined as when the PSD at any location in the building exceeds 10%. For the last intensity at 9975 years in Figure 8.7, the median values of response are not plotted as for this intensity the probability of collapse is quite and therefore the plotting of the non-collapsing cases in truncated. Comparing the behaviour of the case study school structure's behaviour to that of the case study structures examined previously, the general behaviour is seen to be quite similar in the way that the drift demand is quite low and the more frequent intensities as the building is behaving elastically, after which the response becomes much more non-linear upon overcoming the initial strength provided by the masonry infill.

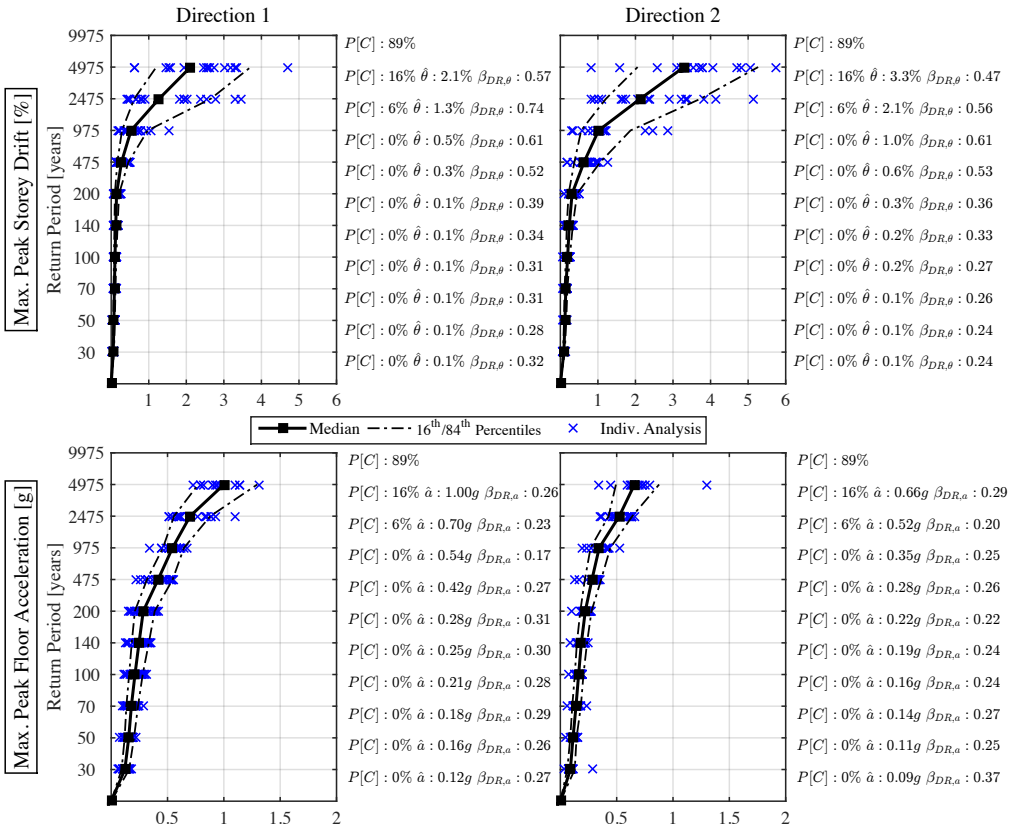

Figure 8.7. Summary plot of the pertaining demand parameters for the case study school building at the chosen site. The median demand, corresponding dispersion and probability of collapse at each stripe of the MSA are illustrated.

In addition to examining the behaviour of the school building's response with respect to increasing intensity, the exceedance of the four different limit states of the structure can be assessed. The exceedance of these limit states was determined using the criteria outlined Section 5.5 for both directions of response of the building. The exceedance of a given limit state is defined as the first exceedance of the PSD criteria for either direction of response. As before, the fragility function associated with each of these limits states can then be determined as a function of IM by fitting a lognormal distribution to the data using the maximum likelihood method outlined by Baker [2015]. Figure 8.8 plots these fragility functions along with listing the median intensities and the corresponding dispersion, which is noted to be related to the record-to-record-variability only and the influence of modelling uncertainty has not yet been incorporated into these values. These values of median and dispersion due to record-to-record variability are seen to be of a similar order of magnitude

when compared with the corresponding values for the case study structures in Section 5.5, bearing in mind that the school building examined here possesses a masonry infill typology that is somewhere in between the two typologies examined in Chapter 5 in terms of its overall strength (i.e. these infills corresponds to the "medium" strength infills defined in Hal *et al.* [2012], whereas the previous analysis examined "weak" and "strong"). These limit state fragility functions will be used in future sections to evaluate the MAF of exceedance of each limit state when integrated with the hazard curve along with the incorporation of the modelling uncertainty.

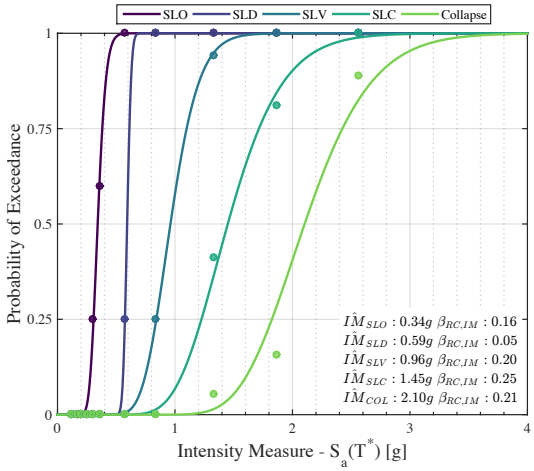

Figure 8.8. Fitted fragility functions corresponding to each limit state in addition to the collapse fragility, where the lognormal distributions are fitted using the maximum likelihood method. Note: the dispersion noted for each fragility corresponds to that arising from record-to-record variability and does not account for the effects of modelling uncertainty.

8.5 Performance Assessment of Case Study School Building

Using the results presented in the previous section, further assessment can be conducted to examine the actual performance of the school building. This will be discussed in the following subsection both in terms of the NTC 2008 limit state requirements and an overall loss assessment of the building is conducted to examine not just the life safety performance of the building, but also its economic vulnerability.

8.5.1 Assessment of the NTC 2008 Limit State and Collapse Safety

By first assessing the limit state requirements of NTC 2008 for the assessment of existing structures, the actual performance of the building with respect to the current guidelines in Italy can be checked. Recalling the discussion in Section 6.5.1 where the four limits states were outlined for assessment of existing structures, although the first two SLE limit states

were not deemed a requirement. These four limit states are listed below in Table 8.2 alongside the specified return periods they are supposed to be verified against. As per NTC 2008, each limit is assigned a probability of exceedance, given in Table 3.2.I of the document, for a reference time period that can then be converted to a return period assuming a Poissonian distribution. The probabilities of exceedance are specified in the code, whereas the reference time period depends on the nominal life of the building and taking the usage class into account. For a school structure, the nominal life of the building can be assumed to be 50 years, as per Table 2.2.I of NTC 2008. As the case study building is a school, its usage class is deemed Class III, meaning that the reference time period is amplified by a factor of 1.5 taken from Table 2.4.II of NTC 2008 to give a reference time period of 75 years. This has the impact of increasing the reference time period which in turn increases the intensity to be verified against for a given limit state. Assuming a Poisson distribution, the return periods and corresponding MAF of exceedances are computed and listed in Table 8.2. In order to determine the intensity corresponding to each of these return periods, the hazard information outlined in Figure 8.6 will be used where to compute the intensity at the intermediate return periods required here, the second-order polynomial fit to the mean hazard curve outlined by Vamvatsikos [2013] is utilised for which the fitted model and associated coefficients are illustrated and listed in Figure 8.6.

Table 8.2. NTC 2008 return period requirements for each of the limit states considered, where the probabilities of exceedance are used in conjunction with the reference period for a Class III usage school building of 50-year nominal life to give the computed return periods, MAF of exceedances and intensities.

Limit State		Probability of Exceedance	Return Period [years]	MAF of Exceedance [x10^{-3}]	$S_a(T^*)$ [g]
SLE	SLO	83%	45	22.14	0.15
	SLD	63%	75	13.26	0.21
SLU	SLV	10%	712	1.40	0.71
	SLC	5%	1463	0.68	1.02

Using these intensities for each limit state, a check on whether the school building satisfies the criteria outlined in NTC 2008 can be performed. This is done by comparing the intensities listed in Table 8.2 to the median values of each of the limit state fragility functions illustrated in Figure 8.8. This comparison is illustrated in Figure 8.9 below, where for each limit state the demand intensity at the prescribed limit state outlined in NTC 2008 is less than the median intensity determined from MSA. While this approach is rather crude as it treats the limit state median intensity in a deterministic way as opposed to considering the dispersion associated with it, it provides a reasonably good indicator of the exceedance

of the limit states. In addition Figure 8.9 plots the 16th and 84th percentile intensities to further illustrate how the limit state criteria are met. These percentiles reflect the overall dispersion of the limit states, where the dispersion due to record-to-record variability ($\beta_{RC,IM}$) outlined in Figure 8.8 is combined via SRSS with an appropriate value of modelling uncertainty ($\beta_{UC,IM}$), as outlined in Chapter 4.

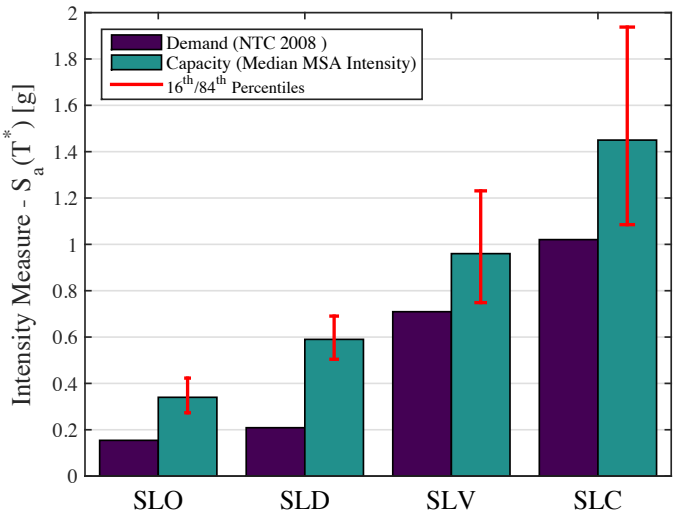

Figure 8.9. Evaluation of the exceedance of the four limit states outlined in NTC 2008 for the case study school building, where the median limit state fragility function value is compared along with its percentile values to the actual demand for each of the return periods specified for this building class in NTC 2008.

In addition to meeting the limit state requirements outlined by NTC 2008, another check is done to assess the collapse safety of the building. The compliance criteria outlined in FEMA P695 [2009] is checked here by verifying probability of collapse at the MCE level is less than 10%. The MCE level is defined as the 2475-year return period event in FEMA P695 guidelines typically, but given that the NTC 2008 specifies an alternative of 1463 years for the life safety limit state, listed in Table 8.2, this value is adopted here. It is acknowledged that these FEMA P695 guidelines have also been developed with US building stock in mind. However, these requirements are deemed applicable as the collapse of the building studied here as the consequences of collapse are the same regardless. Figure 8.10 illustrated this approach whereby the intensity ratio is seen to be greater than unity, implying that the school building satisfies the collapse safety criteria given in FEMA P695. It is noted how the collapse fragility function utilised in Figure 8.10 does not contain any modifications to the median or dispersion to account for the effects of spectral shape

[Baker and Cornell, 2006], as described in FEMA P695 as the GMs used to derive the collapse fragility were selected to be consistent with the site hazard at each intensity stripe, therefore inherently including these effects. In addition, the dispersion of the collapse fragility outlined below considers dispersion associated with the record-to-record variability and modelling uncertainty only and does not incorporate the additional terms for test data quality and design requirements outlined in FEMA P695. This is as the test data amplification term is anticipated to be incorporated in the modelling uncertainty term outlined here, where the design requirements are not deemed applicable in this case as the advanced modelling considered is deemed sufficient to capture the different modes of failure in such frames.

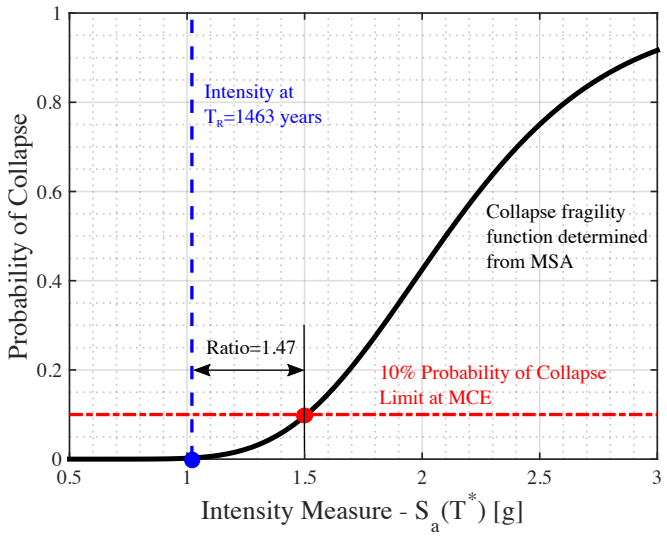

Figure 8.10. Evaluation of the collapse criteria outlined in FEMA P695 for the case study school building, where the ratio at P[C]=10% to MCE (T_R=1463 years) is greater than unity implying that the building passes the collapse safety criteria of FEMA P695.

As the actual structural performance of the school building has been verified against the FEMA P695 requirements adopted for the requirements of NTC 2008 to ensure life safety, further loss estimation studies can be conducted to examine the actual performance of the building during more frequent events to highlight the economic vulnerability of the structure due to expected direct losses.

8.5.2 Loss Estimation of Existing Building

Following the assessment of the case study school building using MSA to quantify its response with respect to increasing intensity and collapse capacity, the actual structural performance with respect to the NTC 2008 code requirements were verified in the previous section in addition to verifying the collapse safety of the building with the FEMA P695 guidelines. However, while the actual structural performance of the building may be deemed satisfactory, the overall performance of building may be investigated further to examine the economic vulnerability of the structure defined in terms of direct economic losses due to the cost of repairs require following an event. This is especially warranted considering the observation in Section 6.5, where for each of the limit states of the case study structures examined, the actual expected loss associated with that limits are were seen to be quite significant. This was especially prominent in the case of infilled frames that highlighted the importance of considering the damage to acceleration sensitive elements. As such, this section aims to evaluate the performance of the school building by conducting a full loss estimation whereby detailed information regarding the damageable structural elements is utilised.

Table 8.3. List of damageable elements considered in loss estimation of case study school building.

Damageable Elements	Fragility and Repair Cost Functions
Structural Elements	
Non-Ductile Columns	Cardone [2016] - DWC (lapped)
Exterior Beam-Column Joints	Cardone [2016] - EWJs (end hooks)
Interior Beam-Column Joint	Cardone [2016] - IWC
Exterior Masonry Infill	Cardone & Perrone [2015] - EIW
Internal Masonry Infill	Cardone & Perrone [2015] - IP
Stairs	FEMA P58-3 [2012] - C2011.011b
Non-Structural Elements	
Internal Partition	Sassun et al. [2016]
Lights	FEMA P58-3 [2012] - C3034.001
Doors	Cardone & Perrone [2015] - IP_d
Windows	Cardone & Perrone [2015] - EIW_w
Piping Systems	FEMA P58-3 [2012] - D2022.011a
Furniture (Desks & Chairs)	Sassun et al. [2016]
Bookcases	FEMA P58-3 [2012] - E2022.104a
Electronic Equipment (PC, Printer, Projector, Electronic Blackboard)	FEMA P58-3 [2012] - E2022.020
Switchboards	FEMA P58-3 [2012] - D3067.011
Chiller & Air Handling Units	FEMA P58-3 [2012] - D3031.011a

The loss estimation of the school can be conducted in the same fashion as that outlined in Chapter 6. As before, conducting loss estimation requires an inventory of the damageable elements along with associated damage and repair cost functions. This inventory was compiled here from the available structural information in addition to an actual visit to the school building to examine the various non-structural element details. A list of the damageable components is given in Table 8.3 alongside the fragility functions used to assess the damage to the various components. The repair cost functions adopted here were as per Section 6.2.3, where with the aid of an Italian engineering firm, the costing was ensured to be representative of the actual costing for the different required repair measures in Italy. The replacement costing was computed as mentioned previously by considering the mean price of reconstruction following the Emilia Romagna earthquake in central Italy in 2012. The loss threshold was again taken to be 60% of the replacement cost during the loss estimation analysis. Using this information, the loss estimation is conducted using TOMS described in Chapter 3 and the pertaining loss assessment information is presented below.

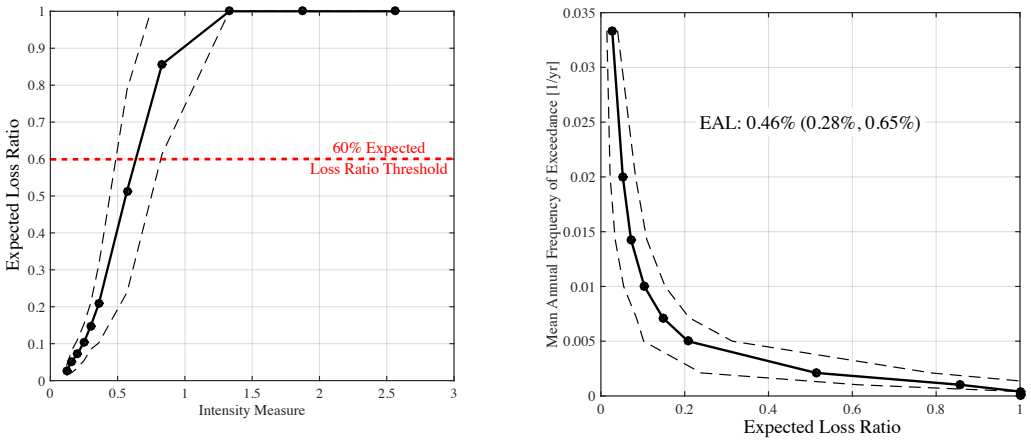

(a) Vulnerability function **(b) Time-based assessment**

Figure 8.11. Plot of the vulnerability function and time-base assessment of the case study school building, where the dashed lines around the expected value represent the approximate variance in loss.

Examining the expected losses from Figure 8.11 above, some general comments regarding the performance of the building can be made. First, the expected loss versus intensity plot show how for the four highest intensity levels examined, the expected loss ratio falls above the loss threshold value meaning that GMs at these return period intensities would be expected to result in a demolition of the school building due to excessive damage. Among these intensities is the SLC intensity previously checked to verify the structural performance of the building in Section 8.5.1. This check in Section 8.5.1 showed how for the life safety limit safety limit states, the structure meets the requirements of the code and the probability of collapse is sufficiently low. However, examining the expected losses of the buildings at these intensities highlights that despite providing adequate safety to prevent collapse and loss of life, the building is expected to suffer extensive damage to the extent that it would most likely be demolished for an event of such intensity.

Examining the time-based assessment of the school structure in Figure 8.11(b), the EAL of the school is noted as 0.46% of the replacement cost. Comparing this value with those values typically observed in Section 6.2 for the case study frames previously examined, this value fits in with the overall trends in those case structure's values illustrated in Figure 6.10. Also shown in Figure 8.11 with the dashed lined is the variance in the losses around the expected value. These are included to give the reader a feel for the typical variance in the results presented here. Examining the variance in the losses with respect to intensity shows how for lower intensities, the variance is relatively low and tends to increase in magnitude with intensity. For the time-based assessment shown in Figure 8.12(b), the impact of this

variance in the loss on the EAL is noted through the values provided in parentheses. Although, strictly speaking, these values are not expected annual loss since the expected values are those marked with the solid line and the dashed lines the 16th and 84th percentile lines. These bound would be better referred to as the "annualised loss percentiles", which indicate the variance in the annualised loss due to the variance in the actual losses with respect to intensity. As these values suggest, the actual variance in the annualised losses can be significant with the percentile values corresponding approximately both a 40% increase and decrease in the annualised loss. This resonates with the commentary provided in Section 6.4.3 regarding the sensitivity of the EAL to different aspects of the assessment procedure, as should the dispersion or correlations in the demand parameters be misrepresented (see Section 7.5.3), the estimated EAL could be adversely affected.

Analysing the expected losses of the school building further by disaggregating in terms of both the demand parameter to which they are sensitive and the location within the building from which they arise, Figure 8.12 can provide further insight into the vulnerability of the school building. Examining the demand parameter disaggregation in Figure 8.12(a), the prominent source of expected loss is due to the PSD sensitive elements such as the masonry infills and the internal partitions. In addition, Figure 8.12(a) shows how the PFA sensitive losses accumulate a considerable amount of expected loss, but upon further examination in Figure 8.12(b), where the disaggregation is presented in terms of location and direction within the building, the PFA induced losses are seen to arise from the damage to the lower floors. This corresponds to the location of some of the heavy mechanical equipment within the school and also the maximum PFA in the building as in the upper levels, the PFA tends to be limited by the soft storey forming on the upper floors. Further examination of Figure 8.12(b) shows how in "Direction 1" of the building, the PSD sensitive losses tends to be higher on the first floor whereas they tend to be higher on the second floor in "Direction 2". This observation corresponds well with the observations of the SPO analysis illustrated in Figure 8.5 that highlighted the likely formation of a soft storey mechanism is both of these floors in the respective directions noted. In addition, Figure 8.13 separates the expected loss ratio for the non-collapsing cases into the structural and non-structural elements, where its is clear that the non-structural elements play a significant role in the loss accumulation for lower intensities, whereas the prominence of the losses due to structural elements damage begins to rise with increasing intensity.

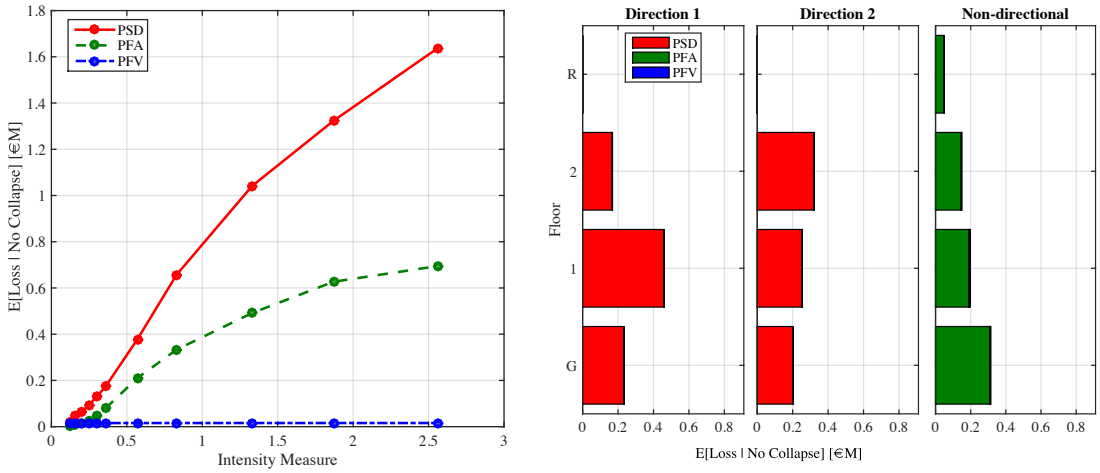

(a) **Expected loss given no collapse disaggregated in terms of contributing demand parameter.**

(b) **Expected loss given no collapse disaggregated in terms of location with the building.**

Figure 8.12. Plot of the expected loss given no collapse disaggregated in terms of both contributing demand parameter and location and direction within the building.

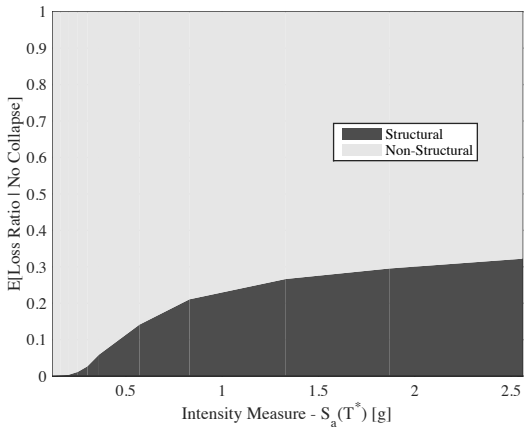

Figure 8.13. Disaggregation of the expected losses given no collapse versus intensity separated in terms of structural and non-structural elements.

8.5.3 Non-Structural Retrofitting of Existing Building

The previous section highlights how despite the case study school building complying with the code requirements in terms of the life safety limit states and collapse resilience, the

performance of the building at weaker and more frequent earthquake events may be deemed unsatisfactory. This was seen through the examination of the expected losses with respect to intensity where a significant portion of losses was seen to arise due to both drift and acceleration sensitive elements. As such, this section will build on some of the discussion in Section 6.4 whereby the non-structural elements will be retrofitted to illustrate how the performance of the school building in terms of monetary losses can be improved without structural intervention since the safety of the structure against collapse has already been verified via code imposed limits.

Examining the disaggregation of the expected loss, it can be seen how a significant portion of the loss arises from the drift sensitive elements on each floor in addition to the acceleration sensitive element on the lower floors. Given this, a non-structural retrofitting scheme is employed where, similar to Section 6.4, the internal partitions are retrofitted to isolate them from the surrounding structure and improve their overall resilience to in-plane damage whereas the OOP resistance by means of restraining clips illustrated in Figure 6.14. In addition, the chiller and air handling equipment are retrofitted by means of providing adequate snubber bearings to protect them from excessive damage due to floor accelerations. Performing this modification to the damageable inventory and rerunning the improved non-structural inventory, the results of the retrofitted building can be obtained. These are plotted in Figure 8.14 along with the original building to illustrate the improvement in expected loss with intensity and subsequently the EAL. The costs of each of these retrofits are estimated using the costing information provided in Chapter 6, and considering the improvement in the EAL the break even time can be computed. Considering the cost of the retrofit is computed to be approximately €40,413 the break-even time is computed to be 16.5 years, which means after 16.5 years the structure will have recovered the initial cost of the retrofitting through overall improvement in performance.

Overall, the effectiveness of retrofitting the non-structural elements alone to improve the overall building performance in terms of monetary losses can be deemed quite effective. This is of special interest to situations such as the case study school building, where structural analysis demonstrated the life safety limit state requirements to be met, although the EAL was still at 0.46% of the replacement cost. By implementing some rather practical non-structural retrofits, however, the EAL is seen to reduce to 0.28% with a break-even time of 16.5 years. However, it must be stated how the primary goal of ensuring life safety must always be met and this example is to illustrate the benefits the improved performance of non-structural elements can have on the overall performance of the building defined in terms of monetary losses.

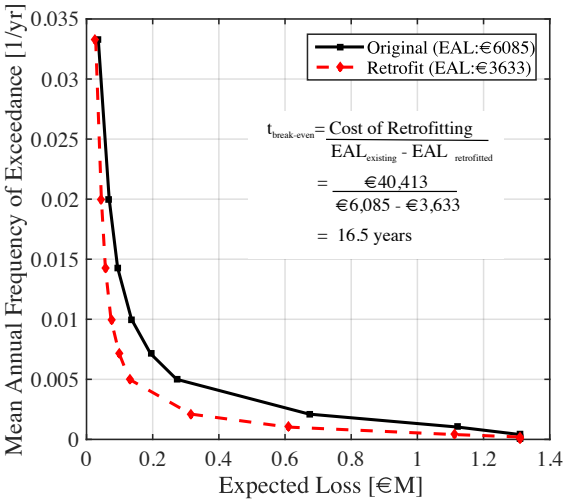

Figure 8.14. Comparison of the existing case study school building compared with the retrofitting of selected non-structural elements.

8.5.4 Application of Simplified Approaches to Loss Estimation

Chapter 7 discussed the use of more simplified methods of analysis to assess existing buildings in Italy, whereby the use of more rational mechanics-based approaches was discussed within a framework applicable to GLD RC frames. It was shown how various aspects such as estimating the median response and proper consideration of the different sources of dispersion in loss estimation need to be properly accounted for; in addition to proper consideration of the different parameter correlations. Section 7.3.3 illustrated the implementation of such a methodology, whereby the empirical values of dispersion due to modelling uncertainty and record-to-record variability proposed in Chapter 4 and Section 7.3.2.1 of this thesis, respectively, were utilised in conjunction with consideration of the demand parameter correlation expressions proposed in Section 7.3.2.2. This comparison highlighted the importance of proper consideration of each of these through example application to the case study structures examined in Chapters 5 and 6. This section conducts such a comparison for the school building analysed as part of this chapter to illustrate the applicability of the proposed empirical coefficients to an existing building other than those analysed in Chapter 5 in addition to using a different set of hazard consistent GMs. A comparison with the empirical dispersion values and correlation assumptions outlined in FEMA P58 for simplified analysis will also be compared to illustrate their impact and highlight the value of the dispersion and correlation quantification studies presented in this thesis within the context of the assessment of Italian GLD RC frames with masonry infill. As highlighted in Chapter 7, the current development of the DBA methodology outlined does not yet allow for accurate implementation within

the context of Italian GLD RC frames with masonry infill although its potential benefits and specific areas that need to be resolved have been highlighted. As such, this section will work on the basis that the median values supplied by DBA are obtainable and are taken from the median values of the MSA conducted in Section 8.4.

For the case of simplified loss estimation, the median and dispersion are determined and appropriate values of demand dispersion and correlations are required in order to conduct a full loss estimation study. This is performed here for the case study school building where the median values are taken from the MSA results and the empirical values of dispersion are taken from the values proposed here in addition to those proposed in FEMA P58. Using this information, Figure 8.15 illustrates the comparison of the expected loss versus intensity for each of the cases analysed, which consist of the full MSA previously outlined; using the proposed dispersions and correlations; and using the values outlined in FEMA P58. By first examining the comparison in the trend of expected loss ratio versus intensity in Figure 8.15(a), the results using the proposed values of dispersion show an excellent match to the extensive analysis using MSA, whereas the same approach using the dispersion values and assumptions regarding the correlations in demand parameters from FEMA P58 are shown to significantly underestimate the expected loss. This is further demonstrated in Figure 8.15(b), where the EAL computed using the proposed values of dispersion and correlation are very close to the extensive analysis approach, whereas using the FEMA P58 values tends to underestimate the EAL.

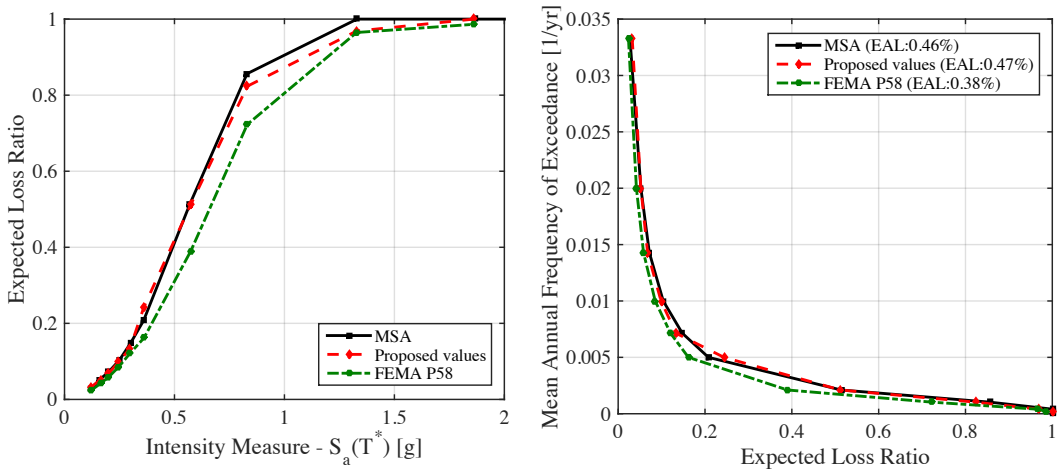

(a) Expected loss ratio versus intensity. **(b) Time-based assessment.**

Figure 8.15. Comparison of the expected loss ratio of the case study school building from MSA to simplified analysis adopting dispersions proposed in this study compared to those provided in FEMA P58.

Analysing the dispersion in the expected loss ratio curves further in Figure 8.16 shows how the proposed values match the extensive analysis very well in terms of the percentile values around the expected value of loss at each intensity. Comparing this with the results using the FEMA P58 values shows how the overall dispersion tends to be underestimated. This is despite the correlations between different demand parameters being assumed to be fully correlated in FEMA P58, which would tend to increase the overall dispersion of the losses. This results in the dispersion due to record-to-record variability and modelling uncertainty tended to be greatly underestimated with respect to those proposed in this study. This underestimation has the impact of slightly underestimating the expected value of loss and subsequently the EAL ratio.

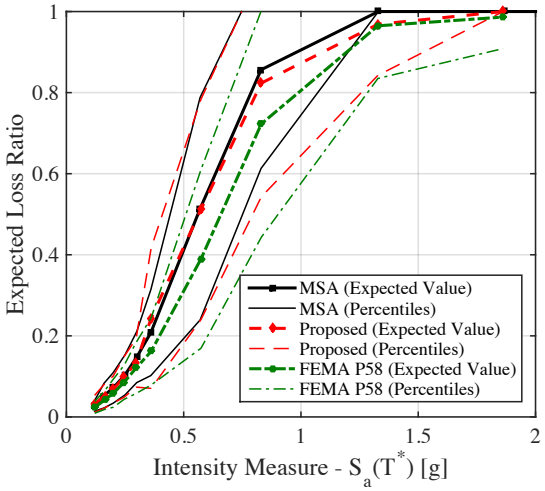

Figure 8.16. Comparison of the dispersion in loss of the case study school building from MSA to simplified analysis adopting dispersions proposed in this study compared to those provided in FEMA P58.

The comparisons outlined above highlight the importance of the proper consideration of dispersion and correlations of demand parameters. It has been shown how the values proposed here match the results of extensive analysis very well whereas those from the existing guidelines do not appear to very appropriate in their application of the Italian GLD RC frames with masonry infill. Again, it is noted this discrepancy is not to suggest that FEMA P58 values are incorrect but to state that their applicability to the structures examined here is limited. It further reinforces the conclusions made regarding the applicability of DBA for more simplified loss estimation, whereby should the median values of demand be estimated reasonably accurately, very good matches in terms of expected loss

ratio curves and EAL can be obtained with the correct consideration of dispersion and correlation, values for which are proposed in previous sections of this thesis.

8.6 SUMMARY AND CONCLUSIONS

This chapter examined the application of the various aspects of loss assessment of GLD RC frames with masonry infills discussed in previous chapters to an existing school building in Italy. The case study building forms part of a larger project that examines the performance of school buildings throughout Italy and involves the detailed investigation of the buildings by performing in-situ surveys of the building's structural and non-structural element composition; in addition to conducting various methods of performance assessment. The building was modelled using the numerical modelling approaches calibrated from older RC frame elements in Chapter 2 in addition to accounting for the masonry infill and potential shear failure of the columns due to excessive overloading when interacting with the masonry infill. Static analysis was performed to characterise the response of the structure, where the typical behaviour such as the significant influence of masonry infills along with soft storey mechanisms forming was observed. This static analysis was used to quantify the different limit states outlined in NTC 2008. The exceedance of these limit states was then quantified in the form of limit state fragility functions using the MSA analysis conducted using a set of hazard consistent GMs records selected for the case study site location.

The quantification of such information regarding the school buildings response with respect to intensity allowed a great deal of information to be determined regarding the overall performance. The first of these involved using the information regarding the exceedance of the various limit states in conjunction with the site hazard information to verify the performance of the school building at the required limit states outlined in NTC 2008. In addition, the collapse safety was also verified using the FEMA P695 approach which illustrated that the collapse fragility of the building is adequately low and thus the non-structural retrofitting approach of Chapter 6 can be explored. These results from extensive analysis then formed the basis for a loss assessment of the school building to examine the performance of the school beyond the code prescribed life safety check in terms of expected losses due to damage to the structural and non-structural elements are considered. This assessment followed much the same structure of that conducted in Chapter 6, where the list of damageable elements in the building was identified through site visits and surveys to generate a representative damageable element inventory. The loss assessment of the school highlighted how the actual loss estimation results showed similar trends to those previously observed in Chapter 6 in terms of the distributions of expected loss in addition to its magnitude. The results of this assessment then allowed for some further comparisons to be conducted.

The first of these comparisons involved examination of the effectiveness of retrofitting the non-structural elements to improve the overall performance of the building, given that the life safety checks have already been satisfied with respect to the prescribed requirements. It was shown that by identifying the prominent sources of non-structural loss within the building and targeting the improved performance of such elements, the overall performance of the school building can be improved considerably with a modest break-even time to implement such a retrofitting strategy. This observation resonates with the discussion of Chapter 6, whereby the retrofitting of non-structural elements was highlighted as a potentially very effective solution to buildings demonstrating satisfactory performance in terms of life safety but characterised by excessive monetary losses at lower return periods, such as the school building outlined in this chapter. The second comparison involved the application and comparison of the simplified approaches to loss estimation discussed in Chapter 7, whereby the proposed empirical values of demand parameter dispersion due to record-to-record variability and modelling uncertainty and correlations were compared with the extensive numerical analysis with hazard consistent GMs. The comparisons show the values proposed in this thesis match the loss estimation results of the extensive analysis very well to provide added confidence in their applicability to Italian GLD RC frames with masonry infill. Furthermore, the same procedure as applied to the case study school using the empirical dispersions and correlations outlined in FEMA P58 where it as demonstrated that these values appear not to be suitable to the structural typologies outlined here as the overall dispersion tends to be underestimated leading to an underestimation on the expected loss ratio. Overall, this chapter has provided some validation and demonstrated the applicability of much of the work presented in this thesis to the structural typologies examined.

9 CONCLUSIONS

9.1 SUMMARY

This thesis has focused on the assessment of existing GLD RC frames with masonry infill in Italy, where an assessment framework analogous to that outlined in FEMA P58 was explored. The first step involved the proposal of tools calibrated with available experimental test data so that the numerical modelling of various structural elements (i.e. beam-column members susceptible to shear failure, weak beam-column joints and the incorporation of the masonry infill modelling) was represented within the OpenSees analysis framework. These calibrated elements, which serve to capture the behaviour of the different behavioural particularities of GLD RC frames were compared with existing modelling approaches to show the improved representation of the proposed models. This is such that the different aspects of strength and stiffness degradation can be incorporated, in addition to simulating the collapse of the structure through excessive drift deformation or shear failure in the columns due to interaction with the masonry infill. Additional assessment tools were also developed in the form of a new programme TOMS, so that more refined damage and loss assessment of existing structures can be considered. The potential benefit of more refined assessment was illustrated by assessing a torsionally sensitive building and highlighting the discrepancy of adopting COM demands versus a more refined approach when evaluating the damage to the different elements.

Through the calibration of the numerical modelling approach with available experimental data, the uncertainty surrounding the modelling parameters was quantified such that the propagation of this uncertainty through to the overall increase in uncertainty in demand parameters typically used in the seismic assessment of existing buildings was quantified. This study resulted in empirical values of modelling uncertainty being proposed for GLD RC frames with masonry infill, where these values were specified in terms of structural typology in addition to the demand parameter and limit state of interest. Furthermore, the effects of modelling uncertainty on the collapse fragility functions were also quantified to result in empirical adjustment factors to the median intensity and overall dispersion of the collapse fragility being quantified. In addition, extensive analysis was conducted on a number of case study GLD RC frame typologies such that the various aspects of the performance of such GLD RC frames were quantified through IDA. Aspects such as the impacts of masonry infills modelling, different infill typologies and the incorporation of a modelling approach, where the potential shear failure of the column members due to infill interaction could be accounted for during analysis, were also investigated. Overall, the

general non-ductile behaviour of such frames was illustrated through the formation of soft storey column sway mechanisms, in addition to the formation of beam-column joint sway mechanisms and the shear failure of the columns in some cases, all of which have been observed when examining the past performance of such buildings during earthquakes in Italy, to highlight the various aspects regarding the modelling of GLD RC frames that ought to be considered. The numerical modelling tools proposed as part of this thesis aim to aid such considerations for the assessment of GLD RC frames with infills studied here.

Using the results of the extensive IDA studies on the various GLD RC frames with infills, loss estimation studies were carried out within a similar scope to that of the FEMA P58 guidelines for the different typologies to not only investigate the performance in terms of expected losses, but also ways in which retrofitting of such structures could be undertaken. This retrofitting was discussed within to context of aiming to ensure a more resilient building when performance was defined as a combination of both collapse safety and resilience to damage during more frequent events described through the building's EAL. This was carried out by first assessing the collapse safety of the buildings for a variety of site locations in Italy followed by the retrofitting of both the structural and non-structural components to highlight their respective impacts on the collapse performance of the building in addition to the EAL. Using these loss estimation results, a further comparison between the actual building performance defined in terms of induced monetary loss and damage at the limit states outlined in NTC 2008 to the actual qualitative definition of building performance described in the building code was outlined.

By considering the various analytical studies conducted in previous chapters collectively, an overall framework for the performance assessment of GLD RC frames with infills was described, where the scope of the discussion resembles that of the FEMA P58 guidelines. Although the main difference is that the numerous aspects of GLD RC frames with infills requiring additional consideration are highlighted with reference to the analysis conducted here, in addition to how one should incorporate them into the procedure, such as the aforementioned consideration of modelling uncertainty and numerical modelling of the structures. In addition, a more simplified method of seismic assessment and loss estimation was outlined through the use of DBA. The DBA methodology was compared to the extensive analysis previously outlined to illustrate that although the general framework works quite well, some key ingredients to the methodology will require further development before a full proposal of the methodology for GLD RC frames with infills can be made. This simplified methodology was outlined and the quantification of the various empirical values of demand parameter dispersion and correlations to be considered were described and compared with existing values provided by FEMA P58. A comparison of the simplified methodology with the more rigorous procedure via a case study application to an existing school building was utilised to illustrate and validate the various proposals and considerations outlined in this thesis with respect to the assessment of GLD

RC frames with infills. This was described using both the rigorous and simplified assessment methodologies, whereby the rigorous approach was conducted using the numerical tools described here, whereas the potential of the simplified methodology was illustrated by utilising the empirical values quantified here also. Both of these approaches are discussed with respect to the existing building being examined in order to quantify the building's overall performance.

9.2 RESEARCH FINDINGS

The following subsections present a compendium for each of the chapters investigated previously, whereby a brief discussion of the work carried out in that chapter is followed by a list of the main findings.

9.2.1 Calibration of a Numerical Modelling Approach

The first chapter of work in this thesis examined the numerical modelling and calibration of older GLD RC frames in Italy within OpenSees using existing experimental data available in the literature. This was conducted to provide an experimentally calibrated and justified basis for which the analysis and quantifications conducted in later chapters could be confidently based. The following paragraphs collect some of the main points concluded from the calibartion for each modelling aspect required to appropriately represent the behaviour of GLD RC frames with masonry infill.

For beam-column elements with smooth bars and poor detailing typical of older GLD RC frames in Italy, a total of 23 experimental test specimens were collected from the literature in order to calibrate the various aspects of the hysteretic backbone behaviour based on the available information. From this, the following findings are noted:

- Existing expressions to compute the moment capacity and yield curvature of the members were validated against the experimental data, whereas existing expressions to compute the post-yield ductility capacity were reviewed. It was shown how existing expressions to compute yield curvature and moment capacity work well, whereas existing expressions to compute the ductility capacity tended to underestimate the capacity of the older GLD frame members.
- The more recent proposal by Melo *et al.* [2015] was shown to give the best comparison with the experimental data and is recommended for use in the numerical modelling of such GLD RC frame members. In addition, a simplified expression to estimate the ductility capacity as a function of axial load ratio was provided. This is based on comparison with the proposal of Melo *et al.* [2015] and experimental data and is intended for use in situations where very little detail is known about member characteristics, such as material properties or reinforcement ratios.

- Following the work of Ibarra and Krawinkler [2005], three key elements to model structural collapse were shown to be the modelling of P-Delta effects along with in-cycle and cyclic degradation. This study looked to consider the post-peak degradation of members and to appropriately simulate the structural collapse of GLD frames due to the exhaustion of the column member's ductility capacity. Based on the limited available experimental data, the in-cycle degradation was calibrated to capture this degradation in post-peak strength and stiffness of the members. The cyclic degradation term was not calibrated due to a lack of available information and is proposed as a future development pending future experimental testing of members. However, the quantification of the post-peak stiffness of members represents a marked improvement on some existing models that rely solely on P-Delta effects to simulate structural collapse. The omission of the cyclic degradation term will possibly result in the slight overestimation of the collapse capacity of GLD frames should the eventual effects of cyclic degradation be found to be significant with respect to the other two, although this difference is not expected to be as significant as if the in-cycle degradation considered here had been omitted.
- The incorporation of the shear hinge element into the beam-column formulation described here allows for the shear response of the frame members to be incorporated. This is particularly important in the analysis of GLD frames as numerous cases of infill interaction causing a brittle shear failure of the member have been noted from past earthquakes in Chapter 1. This definition of shear behaviour has been adopted from a more recent study by Zimos *et al.* [2015] to capture the shear degradation and subsequent failure of RC members. Adopting this approach here has allowed for the investigation of the effect of such shear failure of RC columns interacting with the masonry infill on the overall performance of the structure in terms of response, collapse capacity and monetary losses.
- The numerical modelling of the column shear hinge was also examined in the context of incorporating the influence of the masonry infill on the overall response. It was illustrated via a simple example how the inclusion of such a shear hinge can result in the loss of the columns strength and stiffness should the shear force induced by the masonry infill on the column exceed the column's shear capacity. This is an important consideration in the study of infilled RC frame members as it means that the shear failure of the columns due to interaction with masonry infill can be captured during numerical analysis and means that other compromises such as post-processing of shear failures or other iterative procedures are not required.

Following the calibration of the beam-column member behaviour, another prominent source of structural damage in GLD RC frames noted during past earthquakes in Italy is the vulnerability of beam-column joints. For the calibration of a numerical modelling approach that captures the overall behaviour in addition to the strength degradation of these joints, a total of 15 and 10 experimental test specimens were utilised for the interior and exterior joints, respectively. Using this test data, the calibration of the various coefficients required to represent the joint behaviour was performed by considering the joint principle tensile stresses. From this consideration of the beam-column joint mechanics and subsequent numerical model calibration, the following findings are noted:

- The shear failure of the beam-column joints was calibrated using experimental test data specific to the detailing of GLD RC frame beam-column joints in Italy. That is to say, joints with no transverse shear reinforcement and smooth bars with end-hooks anchored in the joints. This calibration resulted in coefficients to capture the degradation of beam-column joints to simulate the loss of joint shear capacity.
- The computation of the exterior joint shear capacity was also derived by considering the additional shear transfer of the beam to the joint, where a closed-form solution was derived in place of the existing iterative approach outlined in Sharma *et al.* [2011]. The impact of such a refinement was minimal in the overall scheme of this thesis, but an important one nevertheless.

Following the development of the modelling approach with which the various elements of GLD RC frames could be captured, a comparison with a three-storey experimental test specimen subjected to pseudo-static cyclic pushover analysis was carried out. From this comparison, the following findings are noted:

- The proposed numerical model tracked the evolution of deformed shape with every increasing cycle of lateral displacement excellently, where the formation of a shear hinge in the first floor resulting in a spread in deformation over the two adjacent floors was captured.
- The initial stiffness, overall lateral strength and pinching of the cyclic loading was also very well represented by the proposed numerical model. An additional comparison with two alternative numerical modelling approaches, whereby no joint modelling and ductile RC frame members were considered. This was carried out to illustrate what the predicted response would have been if an analyst were to not consider the joint behaviour or the limited ductility of the frame members through the adoption of models typically used to model modern, ductile structures. This was shown to have a very large impact on the model's response, with the overall response mechanism not being captured in addition to the overall global ductility not being well represented at all.

9.2.2 Exploration of More Refined Assessment and Development of Tools

This chapter discussed some of the current limitations with the current state of practice when implementing the PEER PBEE assessment methodology. Issues such as torsional response, generalised handling of modelling uncertainty, unequal bay lengths and inconsistent definitions of drift demand parameters were highlighted to make the case for the development of tools that allow for more complex and irregular structures to be assessed with more confidence. Following the exploration of these various issues and their subsequent impacts in other areas of this thesis, the following comments can be drawn:

- Examining the performance of a torsionally responding building, adopting the COM demands to estimate the damage and subsequent repair costs were shown to be erroneous and can lead to an underestimation of damage and subsequently the direct loss associated with repair costs. This was highlighted through a number of case study buildings both with and without torsional response. The results of IDA showed that for regular and symmetric structures, the use of a single drift at the COM suffices in estimating the damage to the frame members at any location across the building's floor plan. However, in cases where the structure is no longer regular and possesses some torsional irregularity, the use of drift at the COM was seen to be no longer accurate and not only underestimates the damage to the frames members but also provides unconservative estimates of direct loss in the range of 15-30% for the case study buildings examined. While Chapter 3 highlighted this issue for a relatively simple set of case study buildings, its general implications on assessment are more of interest here. This is because practitioners may be faced with the challenge of assessing with using methods and procedures developed primarily for regular structures without any significant torsional response. However, it can be reasonably stated that a vast number of existing structures in Italy tend to have some degree of irregularity that must be accounted for, which the study here has highlighted and the tool developed allows for consideration of.
- In terms of the handling of the modelling uncertainty, the TOMS software tool allows for the specification of the additional dispersion in demands due to modelling uncertainty on a demand parameter basis, as opposed to using a generic value to be applied to all demand parameters. The significance of this aspect was highlighted during the modelling uncertainty quantification study outlined in Chapter 4, where the overall magnitude of the dispersion due to modelling uncertainty for GLD RC frames with masonry infill was seen to be much less for the PFA demands than for the corresponding PSD demands. Therefore, the demand specific consideration of modelling uncertainty allows for a more refined consideration of the effects of modelling uncertainty on the demands.

- The incorporation of more simplified methods of assessment into the TOMS software tool developed here allowed for the user to input median values along with corresponding demand dispersions to account for record-to-record variability and modelling uncertainty. In addition, the specification of the likely correlation between the different demand parameters employed was also required as an input such that the sampling procedure within TOMS that uses the median and dispersions to develop a set of simulated demands can be sampled according to a reasonable correlation between the different demands. Examining the results of the IDA conducted in Chapter 5, Section 7.2.2.2 showed that these correlations vary significantly depending on the demand parameter and intensity. This issue of maintaining a representative correlation between parameters was previously highlighted by Bradley and Lee [2010] and its impact was illustrated in Chapter 8 of this thesis for the case of GLD RC frames. The assumption of a full correlation between demand parameters, which is the assumption in PACT, for example, will tend to overestimate the variance of the expected losses, which can, in turn, lead to an overestimation in the EAL. As such, the simplified expressions to account for demand parameter correlations in GLD RC frames with infill proposed in Section 7.2.2.2 combined with the incorporation of such correlations in the simplified assessment option of TOMS are regarded as a worthwhile contribution.

9.2.3 Quantification of the Modelling Uncertainty

This chapter discussed the quantification of the modelling uncertainty associated with the various demand parameters typically used in the assessment of GLD RC frames with masonry infill in Italy. The study was motivated by the fact that such empirical values used in assessment do not exist for the structural typologies examined in this thesis, as pointed out by Fajfar and Dolšek [2012]. Combining this with the fact that the statistical information regarding the variability of different modelling parameters was available from the calibration carried out in Chapter 2 for GLD RC frames; it was only logical that such a study be carried out here. This quantification study has the benefit that future research on the topic of assessing Italian GLD frames can adopt more refined values of modelling uncertainty, as opposed to adopting default values based on judgement or on similar quantification studies on different typologies, such as ductile RC frames with no infill, for example. In short, this study has directly addressed the comments made by Fajfar and Dolšek [2012] who highlighted the need for these default values of modelling dispersion to be quantified for the assessment of GLD RC frames with masonry infill. Based on this quantification study, the following points are made:

- The effects of modelling uncertainty on the collapse capacity of the structures showed that the median collapse intensity tends to reduce and the dispersion tends to increase. This finding is also in line with previous observations in the literature for different structural typologies. From this, empirical values for the reduction of

the median collapse intensity and the increase in the dispersion for the collapse fragility were provided with respect to structural typology.

- Similarly, the effects of modelling uncertainty on the dispersion of the PSD and PFA of the different structural typologies were investigated, where the uncorrelated SRSS combination of the dispersion due to record-to-record variability and modelling uncertainty was shown to give a reasonable estimate of the overall dispersion, implying that the effects of modelling uncertainty on these demand parameters can be aggregated into the record-to-record dispersion via an SRSS combination. Using this, a set of empirical dispersion values to account for modelling uncertainty were proposed as a function of the different limit states, structural typology and the demand parameter of interest. Comparing these empirical values of modelling uncertainty with those prescribed in FEMA P58, for example, highlighted the significant difference in the overall magnitude of the values to further demonstrate why such values proposed here are required for assessing GLD RC frames with infill and how relying on default values in guidelines such as FEMA P58, which were not developed for older structures with the effects of masonry infill, should not be adopted.

9.2.4 Response Characterisation

This chapter examined the response of a number of different structural typologies typical to GLD RC frames with masonry infill in Italy. The objective of this was to characterise the response of the frame typologies through extensive analysis using the aforementioned numerical modelling approach which allowed the behaviour of the different elements to be captured. Regarding the performance of these typologies, the following findings are reported**:**

- Overall, the GLD RC frames examined exhibited rather non-ductile modes of response such as column-sway mechanisms, column shear failure and beam-column joint mechanisms, which was highlighted during past earthquakes in Italy in Section 1.1. Each of these mechanisms is characteristic to GLD RC frames with masonry infill and differ from modern construction where proper detailing rules and design considerations result in structures with more stable damage mechanisms. As such, assessment of these structures should properly account for this behaviour and recognise that approaches developed for new construction are not necessarily applicable to existing buildings, which was also previously demonstrated in the modelling approach comparison in Chapter 2.
- The modelling of the masonry infill in the frames had a significant effect with respect to those without infill. This was seen not only through the anticipated effects such as the large increase in initial stiffness and peak capacity due to the

diagonal strut action typically observed in SPO analysis but also with regards to the response during IDA. It was shown how, in terms of PSD, the frames modelled with masonry infill exhibited a relatively low level of maximum PSD for the initially low intensities, which is to be expected. Upon examining the record-to-record variability of the infill model frames, however, it is slightly lower for the initial elastic response when compared to that of the frames without infill (e.g. frames without infill have a dispersion of >0.20 typically, where the infilled frames are slightly lower with a dispersion in the range of 0.10 to 0.20). When examining the frames with infill, it was seen that the record-to-record variability tends to increase significantly upon reaching an intensity whereby many of the records begin to push the structure beyond the peak capacity and into the post-peak region. It was seen that this had the impact of notably increasing the dispersion due to some of the records not overcoming the peak force and remaining in a tightly bound elastic drift range, whereas the records that did overcome this peak reported a drastic increase in the maximum PSD, exhibiting what could be described as a sort of peak capacity "cliff". This peak capacity "cliff" was seen to be the cause of larger dispersion due to the record to record variability in the infilled frames at higher intensities, which when compared to other frame typologies such as the frames modelled without infill seem abnormally large. This is a notable observation in terms of the characteristic response of the GLD RC frames with masonry infill.

- The modelling of the aforementioned shear behaviour of the column members to capture the effects of shear damage due to masonry infill interaction on the response was discussed. It was shown how the overall flexibility of the frames tended to increase slightly - increasing the first mode period by up to 15%. In terms of damage mechanism, it was shown via SPO how the failure of the columns in shear for the strong infills resulted in a reduced base shear capacity of the frame along with a reduced overall lateral capacity. This impact of the direct shear hinge modelling was also noted during the collapse assessment where, generally speaking, the inclusion of a double strut infill model with shear hinges in the columns resulted in a decrease of up to 20% in the median collapse intensity.
- Again referring to the incorporation of the column shear hinge in order to capture the potential failure due to the masonry infill strut action overloading, it was shown that in some cases the collapse median actually increased with respect to the model that did not consider the column shear behaviour. This was due to the shear deformation in the columns changing the overall distribution of damage throughout the height of the building with respect to the single strut models. This is an important point to make as it highlights that the potential shear failure of the columns should not be checked for during the post processing of the NRHA results, where the column shear demands are typically compared with the capacity to determine whether a column mechanism would have been expected to form. This is because the above comments show that the overall response mechanism

of the building is not independent of the inclusion of the shear hinge, suggesting that such shear modelling must be incorporated into analysis and methods that aim to account for shear failures by reducing the median collapse intensity and other methods of post-processing, for example, should be avoided.

9.2.5 Assessment and Retrofitting

This chapter conducted a loss assessment study for the various structural typologies examined in this thesis. Retrofitting measures in terms of both the structural and non-structural elements were investigated to examine the relative impact of the different solutions on the overall EAL, provided the collapse prevention criteria have been satisfied. Following this study, the following observations can be summarised:

- Frames modelled without masonry infill tend to accumulate losses from drift sensitive elements in the building whereas frames modelled with infill tend to be dominated by acceleration sensitive losses, which was observed in the case of the L'Aquila City Planning Offices in 2009.
- The inclusion of a shear hinge in the modelling of the structures was shown to increase the vulnerability of the structures through an increased level of damage as a result of the amplified drift and overall flexibility. Despite this increased flexibility, the modelling of the infilled frames with column shear behaviour resulted in around a 30% overall increase in EAL, highlighting the importance of modelling such behaviour in the assessment of GLD RC frames with masonry infill.
- Comparing the expected loss ratio at each of the SLE limit states of NTC 2008 has been shown to be quite substantial when compared to the qualitative description of damage outlined by the codes.
- The retrofitting of the non-structural elements can have a comparative, if not better impact on the EAL than that of structural retrofitting provided that the collapse safety requirements are met. If not, then structural retrofitting ought to be considered; although should the collapse of the building be linked to the shear-induced damage of the masonry infill, appropriate isolation of the infill from the surrounding frame to mitigate interaction may prove to be beneficial also.
- In some cases, the strengthening and stiffening of the building by inserting additional structural elements in order to comply with NTC 2008 drift serviceability limit state requirements worsened the performance of the building when defined in terms of EAL, although it is noted that some of these cases were actually conservatively overstrengthened. This resulted as a combination of the trade-off in the reduction of drift-induced damage with the increase in acceleration-induced damage; in addition to the change of the definition of hazard due to the periods shortening of the building due to the IM employed. This is a noteworthy conclusion as it clearly illustrated that strengthening and stiffening are

not necessarily a good thing when speaking in terms of economical functionality of the building and mitigation of direct losses. It should be noted, however, that the overall collapse performance of these buildings was markedly improved with respect to the existing ones, although improvement of the collapse performance was not actually needed since the collapse prevention criteria had already been satisfied. This observation was also exemplified in the 2016 earthquake in Ecuador, where excessive strengthening measures to existing hospital structures following the 1998 event resulted in extensive non-structural damage to hospital structures resulting in widespread loss of functionality of these essential services following the 2016 earthquake.

9.2.6 Simplified Assessment

This chapter explored the use of more simplified methods of assessing GLD RC frames with masonry infill in Italy. First, the DBA methodology was compared and critiqued alongside the results of the extensive analyses to examine the applicability of current state-of-the-art simplified assessment methods for the structures examined here. Following this, a more simplified approach to loss estimation was outlined where the DBA methodology was highlighted as a method with which practitioners can use simplified methods of analysis in conjunction with empirical values of dispersion and demand parameter correlation. In addition, the use of a more simplified probabilistic methodology to estimate the annual probability of exceeding a given limit state was discussed within the scope of the structures examined here.

In terms of the DBA methodology, the following points can be made:

- In its current state of development, simplified methods such as DBA cannot be applied to existing GLD RC frame buildings with masonry infill in Italy without assuming approximate values of some key parameters. Although, this is due to the absence of some of the vital ingredients required by the method rather than a fundamental limitation of the approach. Comparing this to the methodology outlined in FEMA P58 where elastic analysis is utilised from and elastic structural model to determine the drift demands through a series of empirical correction factors. Not only does such an approach rely on the elastic behaviour of the structural model to predict the inelastic response, it also indirectly neglects the particularities of the GLD RC frames which are typically susceptible to more non-ductile mechanisms that can no longer be approximated by elastic-perfectly-plastic behaviour and elastic analysis procedures.
- In terms of the ability to predict the correct displaced shape required at the various limit states for DBA, it was shown how traditional beam-sway mechanism typically used in new design does not work well for frames with other modes such as column-sway. A recent approach trialled by Saborio Romano [2016] to predict the

displaced shape of GLD frames without masonry infill was evaluated, where the approach, with some minor modification proposed here, worked excellently in predicting the displaced shape at each limit state considered. While this approach worked well for the frames without masonry infill vulnerable to a column-sway mechanism, further work is required to include the effects of beam-column joint behaviour, masonry infills and the shear behaviour of weak columns.

- The prediction of a given damage mechanism backbone response at different limit states was also compared for each of the case study frames, where compared to the SPO curves showed excellent agreement at each of the limit states considered. Further guidance on the correct estimation of the base shear of the governing mechanism was also discussed. It was shown that using the assumption of the storey shear at the critical storey, the total base shear can be underestimated. This is as when the column sway forms at a storey other than the ground floor, as the additional shear contribution of other elastically responding storeys can provide significant increase in the base shear. Using this proposed base shear consideration, excellent matching with SPO analysis was observed when compared to other approaches suggested in the literature, such as that outlined in FEMA P58 that relies on elastic analysis methods and does not capture the post-peak base shear reduction in the frames. The effect of the shear damage to column members also ought to be investigated further as SPO analysis showed a significant modification in the backbone when shear failures on the columns occurred.
- In the final step of DBA, the seismic intensity required to generate a given limit state is computed, which can then be used in methods such as DBLE. Comparisons of the intensities required for each of the limit states considered were compared to those estimated during the extensive NRHA. This comparison showed that the DBA methodology works quite well in estimating the various intensities for the different structures apart from the frames with masonry infill. This was shown to be a consequence of the absence of an adequate EVD relation to account for the additional hysteretic damping provided by the masonry infill. The recently proposed expression by Landi *et al.* [2016] worked reasonably well but was observed to significantly overestimate the damping at lower levels of ductility.

Regarding the use of simplified methods of assessment results to perform loss estimation in conjunction with the empirical values of demand dispersion and correlations, the following remarks are made:

- This thesis has shown how values of dispersion for the frame typologies examined here differ somewhat to typical values available in the literature, which tend to be for seismically frames without masonry infill. As a result, the extensive analysis carried out in this thesis for GLD RC frames was utilised and more refined

empirical values for the record-to-record variability and modelling uncertainty with respect to limit state, demand parameter and frame typology were quantified. In addition, demand parameter correlations were also identified such that the proper correlations between the different demand parameters can be considered when generating simulated demand using the median and dispersion values.

- In terms of actual loss estimation, it has been shown through a case study application to an existing school building in Italy in Chapter 8 that knowing the median response of the structure from a simplified methodology such as DBA, a reasonable estimate of the expected loss curve and EAL can be obtained using the empirical values of dispersion and correlations proposed in this study. Comparing this with the values proposed in the FEMA P58 guidelines are seen to misrepresent expected loss and subsequently underestimate the EAL due to an underestimation of the various dispersions in addition to a misrepresentation of the expected demand correlations that Bradley and Lee [2010] argued were key aspects to be respected. This further reinforces the point that the current FEMA P58 guidelines cannot be simply applied to existing buildings in Italy in their current form, as many of the empirical values outlined in the guidelines have been quantified for ductile buildings in the US through studies such as those seen in this thesis.

Finally, the exploration of the use of a more probabilistic methodology to estimate the MAF of exceedance of a given limit state was examined using the so-called SAC/FEMA approach outlined in Cornell *et al.* [2002]. This was evaluated with respect to the extensive analysis conducted previously for the different case-study buildings and from this, the following comments are made:

- The demand-intensity model that is crucial in linking the median demand parameter of interest to a median intensity has been seen to be fundamentally different in its overall trends for GLD RC frames; such that typical values previously adopted in the literature stemming from work carried out on modern RC frames without masonry infills cannot be adopted.
- The was first apparent in the overall trend of the demand-intensity relationship for the maximum PSD of the case study frames, where two separate regions of response became apparent depending on the response of the masonry infill. This corresponded to whether the masonry infill was responding in the elastic range prior to reaching its peak force or in the post-peak region of response. The trend in overall response of the structure was observed to fundamentally change with respect to this limit state of the masonry infill such that two regions of overall response were defined based on this. It was subsequently shown how a bilinear fit in log space could achieve a much better fit to the data for GLD RC frames with

infills such that a set of empirical coefficients for such a demand-intensity model for the maximum PSD were outlined using this approach.

- Regarding such coefficients, an assumption of 1.0 for the exponent term b in maximum PSD demand-intensity models was shown to be a good assumption for frames without masonry infill and pilotis frames. This agrees with the value suggested in the initial publication of the methodology by Cornell *et al.* [2002] and subsequently adopted in many other studies. However, when applied to infilled frames it was seen how this assumption of 1.0 no longer holds true and can have a significant impact on the overall annual probabilities computed, with an example showing an overestimation of the annual probability of exceedance by a factor of 8.

9.2.7 Framework for the Assessment of GLD RC Frames with Masonry Infill

As a concluding remark, a discussion of a general framework for the assessment of GLD RC frames with masonry infills was outlined in Chapter 7. This was outlined with respect to the procedure highlighted in FEMA P58, where the numerous observations and further quantifications with the context of the GLD frames considered here were discussed. As a result of this discussion, a number of conclusions can be drawn with regards to a framework with which GLD frames can be assessed are given below:

- In its current form, the various details of the FEMA P58 guidelines should not be applied to GLD RC frames with masonry infills in Italy.
- Issues such as the fundamental difference in the actual behaviour of the elements during numerical modelling have been highlighted in Chapter 2, where it was concluded that traditional methods of analysing frames are not necessarily applicable to GLD frames unless special attention has been given to the different aspects of GLD frame response mechanisms.
- The simplified approach to estimating median demands outlined in FEMA P58 should not be applied to GLD frames. Numerous reasons were cited for this where; suffice to say that the method outlined in FEMA P58 was developed for ductile structures in mind that do not contain masonry infills; meaning that it is no longer applicable to the frames described in this thesis.
- The DBA methodology outlined previously was proposed as a suitable substitute as initial comparisons with the extensive analysis carried out here show it to be a promising method for assessing the particular mechanism as associated with these frame typologies.
- The empirical values of dispersion due to modelling uncertainty and record-to-record variability quantified in this thesis were highlighted to significantly differ to

those outlined in FEMA P58 for more ductile frames such that the values quantified here are recommended for GLD RC frames with masonry infill.

- The proper consideration of demand parameter correlation was considered where it was highlighted that assuming full correlations between demands will not only overestimate the variance in the loss but also result in an increase in the expected losses. This is illustrated through a case study application to an existing school building.

9.3 CONCLUSIONS AND CONTRIBUTIONS TO THE STATE-OF-THE-ART

To close, some of the main conclusions of this thesis and the overall contributions to the state-of-the-art with respect to the seismic PBEE assessment of GLD RC frames with masonry infill are noted. These are:

- The numerical modelling of the GLD RC frames has been examined approach to account for the various particularities of the behaviour of such frames calibrated using existing experimental data available in the literature. This represents an important contribution as not only was it shown how some aspects of the behaviour of GLD frames with respect to more modern construction, but applying modelling techniques developed for ductile construction to the typologies studied here were shown to be erroneous when compared to testing of a three storey test specimen. The numerical modelling approach outlined here, on the other hand, showed a very good comparison in terms of both hysteretic response and the representation of the damage mechanisms formed. Further to this, the model developed accounts of for the post-peak strength degradation of the members such that the overall collapse capacity of the structures can be modelled with a greater degree of confidence.
- With regards to the overall damage and subsequent loss assessment, it was shown that the overall damage may be underestimated for torsionally sensitive buildings if more simplified approaches to quantify demand are adopted. The assessment tool developed as part of this thesis allows for proper handling of such behaviour of irregular structures.
- With regard to the response of GLD RC frames with infill, the adverse effects of the shear failure of column members due to overloading by the masonry infill were investigated. It was shown how such failure can not only be incorporated using the modelling techniques described here but also how it impacts the overall assessment. It has been shown that the shear damage suffered by columns members can change the overall damage and eventual collapse mechanism exhibited by the structure such that post-processing of column shear demand and

subsequent comparison with the capacity cannot be deemed reliable as these shear behaviour and overall building response are not independent of one another.

- Within the scope of the loss assessment of the buildings examined here, it was shown how different aspects of the FEMA P58 guidelines are no longer applicable. This was seen in how the modelling uncertainty was quantified for the buildings examined here and when compared to those given in FEMA P58, were shown to be somewhat less. This point regarding the applicability of the FEMA P58 guidelines also applies to the points highlighted previously, where the numerical modelling and handling of demand parameters in assessment listed in the documents have been shown to be not applicable in the case of the GLD RC frames examined here, where the required tools for such a framework have been since been developed in this study.
- In addition, within the scope of more simplified methods of assessment, extensive calibration of the DBA methodology with GLD RC frames has been applied and some specific areas that require further development have been noted. Assuming the eventual developments of these current limitations of DBA, it is shown how that compared with the simplified approach outlined in FEMA P58, the DBA methodology used in conjunction with the empirical values proposed in this study represent a more accurate way of quantifying the performance of GLD RC frames. This was illustrated through a case study application to an existing Italian school building to clearly illustrate the limitations of the FEMA P58 proposed values and the improved performance of those proposed here.
- Lastly, the simplified approach to probabilistic assessment of various limit states outlined by the SAC/FEMA methodology has been outlined with respect to the GLD RC frames examined here. It was shown how typical values for the required coefficients in the demand-intensity relationship to not be applicable to GLD RC frames, with more appropriate values being proposed here. This combined with the various characterisation of anticipated dispersions in the frames allow for the application of this methodology to GLD RC frames with masonry infill, which had not been previously examined.

Overall, the main contribution of this thesis is that it presents the current state-of-the-art PBEE assessment framework outlined by FEMA P58 in the context of Italian GLD RC frames with masonry infill. From this thesis, a better understanding of the various facets of this approach when applied to these structural typologies can be appreciated, with the necessary tools to perform such an assessment outlined here. This was seen through the numerous aspects investigated in this thesis and through the conclusion with an example application to an existing school building in central Italy.

9.4 LIMITATIONS AND FUTURE WORK

As a final remark, some of the limitations of the study outlined in this thesis are noted in addition to suggestions of future work. This arises as a result of the detailed consideration of some of the issues with regards to GLD RC frames with masonry infills such that areas requiring further research can be clearly identified to provide motivation for future work in this area. Some of these issues are listed below:

- Chapter 2 saw the development of a numerical modelling approach in order to characterise the behaviour of the beam-column members in GLD RC frames. In this modelling calibration, the backbone hysteretic behaviour of the elements was identified and post-peak degradation of the elements accounted for by means of an in-cycle strength and stiffness degradation in order to better represent the collapse of the structural typologies examined. However, as noted by Ibarra *et al.* [2005] the collapse of structures requires appropriate modelling of not only the P-Delta effects but also the in-cycle and cyclic degradation of the members. The calibration outlined in this thesis has considered the first two of these, where sufficient experimental data in order to properly quantify the effects of cyclic degradation was seen not to be available. Future work on the experimental testing of such elements should aim to incorporate this cyclic degradation of the GLD RC frame beam-column members through investigation of specimens tested into the post-peak range such that the strength degradation can be quantified and incorporated into future numerical modelling.
- Chapter 3 outlined the development of an assessment tool so that the damage and subsequent loss assessment of GLD RC frames could be performed. It was noted in Chapter 6, however, that this tool did not allow for the combined in-plane and out-of-plane failure of masonry infills, where only the damage due to in-plane response was examined. Recent work by Kohrangi *et al.* [2016] has shown that considering the potential out-of-plane failure of the masonry infills doesn't adversely affect the EAL, meaning that the impact of this limitation on the study conducted in this thesis is not expected to be significant. Nevertheless, such a consideration ought to be considered as part of future work. Initial progress has been made by the author to incorporate this aspect into TOMS, although time constraints mean that it is not included in this thesis, although anticipated to be fully developed in the near future.
- Chapter 5 conducted an extensive assessment using IDA of the case study buildings to characterise their response both with respect to increasing intensity and also collapse. Comparisons of the observed collapse fragility functions with those predicted by the more simplified SPO2IDA tool showed fairly accurate results for the pilotis frames and the frames modelled without masonry infill. However, for infilled frames, it was shown to significantly underestimate the

collapse capacity of the frames. Future work should aim to expand this SPO2IDA tool to incorporate the frames with masonry infill examined here.

- Chapter 7 investigated the application of the DBA methodology to GLD RC frames with masonry infills examined in this thesis. The overall approach of the methodology was investigated and some areas requiring further work were noted. The first of these was the expansion of the displaced shape expression to account for the influence of the beam-column joint behaviour and also the presence of masonry infills. A recent approach to estimating the displaced shape trialled by Saborio Romano [2016] was developed for GLD RC frames to estimate the displaced shape and was further illustrated in this thesis to provide excellent predictions when further evaluated against frames without masonry infill. As such, a similar approach is suggested but with additional consideration of the joints and infills.
- Further work should be conducted into quantifying the EVD contributions of masonry infills for the application of the DBA methodology. Initial work by Landi *et al.* [2016] has proposed a formulation that works reasonably well when compared to the infilled frame structures outlined here, although it was shown to slightly overestimate the EVD at the serviceability limit states. As such, further refinements and verifications should be carried out in this regard such that the EVD can be accurately estimated at all limit states of interest.

REFERENCES

Akguzel, U. [2011] "Seismic Performance of FRP Retrofitted Exterior RC Beam-Column Joints under Varying Axial and Bidirectional Loading," PhD Thesis, University of Canterbury, New Zealand.

Alath, S., Kunnath, S. [1995] "Modeling Inelastic Shear Deformations in RC Beam–Column Joints," *Proceedings of 10th Conferecne on Engineering Mechanics*, Boulder, Colorado, USA.

Ambraseys, N. N., Simpson, K. A., Bommer, J. J. [1996] "Prediction of horizontal response spectra in Europe," *Earthquake Engineering & Structural Dynamics*, Vol. 25, pp. 371–400.

ASCE 7-10. [2010] *Minimum Design Loads for Buildings and Other Structures*, Reston, VA, USA.

ASCE 7-16. [2016] *Minimum Design Loads for Buildings and Other Structures*, Reston, VA, USA.

Aslani, H., Miranda, E. [2005] "Probabilistic Earthquake Loss Estimation and Loss Disaggregation in Buildings," *Blume Report No. 157*, Stanford, CA.

Augenti, N., Cosenza, E., Dolce, M., Manfredi, G., Masi, A., Samela, L. [2004] "Performance of School Buildings during the 2002 Molise, Italy, Earthquake," *Earthquake Spectra*, Vol. 20, No.S1, pp. S257–S270.

Augenti, N., Parisi, F. [2010] "Learning from Construction Failures due to the 2009 L'Aquila, Italy, Earthquake," *Journal of Performance of Constructed Facilities*, Vol. 24, No.6, pp. 536–555.

Baker, J. W. [2015] "Efficient Analytical Fragility Function Fitting Using Dynamic Structural Analysis," *Earthquake Spectra*, Vol. 31, No.1, pp. 579–599.

Baker, J. W., Cornell, C. A. [2006] "Spectral shape, epsilon and record selection," *Earthquake Engineering & Structural Dynamics*, Vol. 35, No.9, pp. 1077–1095.

Baker, J. W., Jayaram, N. [2008] "Correlation of spectral acceleration values from NGA ground motion models," *Earthquake Spectra*, Vol. 24, No.1, pp. 299–317.

Bakir, P. G., Boduroğlu, H. M. [2002] "A new design equation for predicting the joint shear strength of monotonically loaded exterior beam-column joints," *Engineering Structures*, Vol. 24, No.8, pp. 1105–1117.

Barrera, M. J., Przelazloski, K., Filiatrault, A., Sullivan, T. J., Christovasilis, I. P. [2016] "Assessment of the loss of functionality of individual rooms in critical facilities after earthquakes," *Bulletin of Earthquake Engineering*, Springer Netherlands, Vol. Online.

Bedirhanoglu, I., Ilki, A., Pujol, S., Kumbasar, N. [2010] "Behavior of Deficient Joints with Plain Bars and Low-Strength Concrete," *ACI Structura Journal*, Vol. 107, No.3, pp. 300–312.

Benvenuti, G. [2012] "Italy farm lobby lifts quake damage estimate," *Reuters*, <http://www.reuters.com/article/us-italy-quake-business-idUSBRE8550VI20120606> (Jun. 6, 2012).

Bertoldi, S. H., Decanini, L. D., Gavarini, C. [1993] "Telai tamponati soggetti ad azione sismica, un modello semplificato: confronto sperimentale e numerico," *Atti del 6 Convegno Nazionale ANIDIS*, Perugia, Italy.

Beschi, C., Riva, P., Metelli, G., Meda, A. [2014] "HPFRC Jacketing of Non Seismically Detailed RC Corner Joints," *Journal of Earthquake Engineering*, Vol. 19, No.1, pp. 25–47.

Bradley, B. A. [2013] "A critical examination of seismic response uncertainty analysis in earthquake engineering," *Earthquake Engineering & Structural Dynamics*, Vol. 42, No.11, pp. 1717–1729.

Bradley, B. A., Lee, D. S. [2010] "Component correlations in structure-specific seismic loss estimation," *Earthquake Engineering & Structural Dynamics*, Vol. 39, pp. 237–258.

Braga, F., Gigliotti, R., Laterza, M. [2009] "R/C Existing Structures with Smooth Reinforcing Bars: Experimental Behaviour of Beam-Column Joints Subject to Cyclic Lateral Loads," *The Open Construction and Building Technology Journal*, Vol. 3, No.1, pp. 52–67.

Bursi, O. S., Dusatti, T., Pucinotti, R. [2009] *A Reconnaissance report. The April 6, 2009, L'Aquila Earthquake. Italy*.

Calvi, G. M. [2013] "Choices and Criteria for Seismic Strengthening," *Journal of Earthquake Engineering*, Vol. 17, No.6, pp. 769–802.

Calvi, G. M., Magenes, G., Pampanin, S. [2002a] "Relevance of Beam-Column Joint Damage and Collapse in RC Frame Assessment," *Journal of Earthquake Engineering*, Vol. 6, No.Supp 1, pp. 75–100.

Calvi, G. M., Magenes, G., Pampanin, S. [2002b] "Experimental Test on a Three Storey RC Frame Designed for Gravity Only," *12th European Conference on Earthquake Engineering*, London, UK.

Calvi, G. M., Sullivan, T. J., Welch, D. P. [2014] "A seismic performance classification framework to provide increased seismic resilience," *2nd European Conference on Earthquake Engineering and*

Seismology, Istanbul, Turkey.

Calvi, P. M., Sullivan, T. J. [2014] "Estimating floor spectra in multiple degree of freedom systems," *Earthquakes and Structures*, Vol. 7, No.1, pp. 17–38.

Cardone, D. [2016] "Fragility curves and loss functions for RC structural components with smooth rebars," *Earthquakes and Structures*, Vol. 10, No.5, pp. 1181–1212.

Cardone, D., Flora, A. [2014] "Direct displacement loss assessment of existing RC buildings pre- and post-seismic retrofitting: A case study," *Soil Dynamics and Earthquake Engineering*, Vol. 64, pp. 38–49.

Cardone, D., Perrone, G. [2015] "Developing fragility curves and loss functions for masonry infill walls," *Earthquakes and Structures*, Vol. 9, No.1, pp. 257–279.

Cardone, D., Perrone, G. [2016] "Damage and Loss Assessment of Pre-70 RC Frame Buildings with FEMA P-58," *Journal of Earthquake Engineering*, Vol. Online, pp. 1–39.

Carr, A. J. [2007] "RUAUMOKO - User Manual, Theory, and Appendices," <http://www.civil.canterbury.ac.nz/ruaumoko/index.html>.

Celano, F., Cimmino, M., Coppola, O., Magliulo, G., Salzano, P. [2016] "Report dei danni registrati a seguito del terremoto del Centro Italia del 24 Agosto 2016," *ReLUIS Report (Release 1)*.

Celarec, D., Dolšek, M. [2013] "Practice-oriented probabilistic seismic performance assessment of infilled frames with consideration of shear failure of columns," *Earthquake Engineering & Structural Dynamics*, Vol. 42, No.9, pp. 1339–1360.

Celarec, D., Ricci, P., Dolšek, M. [2012] "The sensitivity of seismic response parameters to the uncertain modelling variables of masonry-infilled reinforced concrete frames," *Engineering Structures*, Vol. 35, pp. 165–177.

Celik, O. C., Ellingwood, B. R. [2008] "Modeling Beam-Column Joints in Fragility Assessment of Gravity Load Designed Reinforced Concrete Frames," *Journal of Earthquake Engineering*, Vol. 12, No.3, pp. 357–381.

Celik, O. C., Ellingwood, B. R. [2010] "Seismic fragilities for non-ductile reinforced concrete frames – Role of aleatoric and epistemic uncertainties," *Structural Safety*, Vol. 32, No.1, pp. 1–12.

Charleson, A. [2008] *Seismic Design for Architects - Outwitting the Quake*, Elsevier Ltd, Oxford, UK.

CNR. [2014] "Istruzioni per la Valutazione Affidabilistica della Sicurezza Sismica di Edifici Esistenti," *CNR – Commissione di studio per la predisposizione e l'analisi di norme tecniche relative alle*

costruzioni, CNR-DT 212/2013, Rome, Italy.

Colangelo, F. [2004] "Pseudo-dynamic seismic response of infilled RC frames designed for gravity load," *13th World Conference on Earthquake Engineering*, Vancouver, Canada.

Collins, M. P., Mitchell, D. [1991] *Prestressed Concrete Structures*, Prentice Hall, New Jersey, USA.

Cornell, C. A., Jalayer, F., Hamburger, R. O., Foutch, D. A. [2002] "Probabilistic Basis for 2000 SAC Federal Emergency Management Agency Steel Moment Frame Guidelines," *Journal of Structural Engineering*, Vol. 128, No.4, pp. 526–533.

Cornell, C. A., Krawinkler, H. [2000] "Progress and Challenges in Seismic Performance Assessment," *PEER Center News*.

Crisafulli, F. J., Carr, A. J., Park, R. [2000] "Analytical Modelling of Infilled Frame Structures - A General Review," *Bulletin of the New Zealand Society for Earthquake Engineering*, Vol. 33, No.1, pp. 30–47.

Crowley, H., Pinho, R., Bommer, J. J., Bird, J. F. [2006] "Development of a Displacement-Based Method for Earthquake Loss Assessment," *Report ROSE 2006/01*, IUSS Press, Pavia, Italy.

Decanini, L. D., De Sortis, A., Goretti, A., Langenbach, R., Mollaioli, F., Rasulo, A. [2004] "Performance of Masonry Buildings During the 2002 Molise, Italy, Earthquake," *Earthquake Spectra*, Vol. 20, No.S1, pp. S191–S220.

Decanini, L. D., De Sortis, A., Goretti, A., Liberatore, L., Mollaioli, F., Bazzurro, P. [2004] "Performance of Reinforced Concrete Buildings During the 2002 Molise, Italy, Earthquake," *Earthquake Spectra*, Vol. 20, No.S1, pp. S221–S255.

Decanini, L., Mollaioli, F., Mura, A., Saragoni, R. [2004] "Seismic Performance of Masonry Infilled R/C Frames," *13th World Conference on Earthquake Engineering*, Vancouver, Canada.

Dolce, M., Manfredi, G. [2015] *Libro bianco sulla ricostruzione privata fuori dai centri storici nei comuni colpiti dal sisma dell'Abruzzo del 6 aprile 2009*, Doppiavoce, Napoli, Italy.

Dolšek, M. [2009] "Incremental dynamic analysis with consideration of modeling uncertainties," *Earthquake Engineering and Structural Dynamics*, Vol. 38, No.6, pp. 805–825.

Dolšek, M. [2012] "Simplified method for seismic risk assessment of buildings with consideration of aleatory and epistemic uncertainty," *Structure and Infrastructure Engineering: Maintenance, Management, Life-Cycle Design and Performance*, Vol. 8, No.10, pp. 939–953.

Dolšek, M., Fajfar, P. [2008] "The effect of masonry infills on the seismic response of a four-storey

reinforced concrete frame — a deterministic assessment," *Engineering Structures*, Vol. 30, No.7, pp. 1991–2001.

Eads, L., Miranda, E., Lignos, D. G. [2015] "Average spectral acceleration as an intensity measure for collapse risk assessment," *Earthquake Engineering & Structural Dynamics*, Vol. 44, No.12, pp. 2057–2073.

Eads, L., Miranda, E., Lignos, D. G. [2016] "Spectral shape metrics and structural collapse potential," *Earthquake Engineering & Structural Dynamics*, Vol. 45, No.10, pp. 1643–1659.

EERI. [2009] *The Mw=6.3 Abruzzo, Italy, Earthquake of April 6, 2009*.

Ellingwood, B. R., Celik, O. C., Kinali, K. [2007] "Fragility assessment of building structural systems in Mid-America," *Earthquake Engineering & Structural Dynamics*, Vol. 36, No.13, pp. 1935–1952.

Elnashai, A. S., Pinho, R. [1998] "Repair and Retrofitting of RC Walls Using Selective Techniques," *Journal of Earthquake Engineering*, Vol. 2, No.4, pp. 525–568.

Elwood, K. J. [2004] "Modelling failures in existing reinforced concrete columns," *Canadian Journal of Civil Engineering*, Vol. 31, No.5, pp. 846–859.

Elwood, K. J., Moehle, J. P. [2003] "Shake table tests and analytical studies on the gravity load collapse of reinforced concrete frames," *PEER Report 2003/01*, Berkeley, California.

EN 1998-1:2004. [2004] *Eurocode 8: Design of Structures for Earthquake Resistance - Part 1: General Rules, Seismic Actions and Rules for Buildings*, Brussels, Belgium.

EN 1998-3:2005. [2005] *Eurocode 8: Design of Structures for Earthquake Resistance - Part 3: Assessment and Retrofit of Buildings*, Brussels, Belgium.

EN 1998-3:2009. [2009] *Corrigenda to EN 1998-3*, Brussels, Belgium.

Fajfar, P. [2000] "A Nonlinear Analysis Method for Performance-Based Seismic Design," *Earthquake Spectra*, Vol. 16, No.3, pp. 573–592.

Fajfar, P., Dolšek, M. [2010] "A Practice-Oriented Approach for Probabilistic Seismic Assessment of Building Structures," M. N. Fardis, ed., Springer, pp. 225–233.

Fajfar, P., Dolšek, M. [2012] "A practice-oriented estimation of the failure probability of building structures," *Earthquake Engineering & Structural Dynamics*, Vol. 41, No.3, pp. 531–547.

FEMA P58-1. [2012] *Seismic Performance Assessment of Buildings: Volume 1 - Methodology (P-58-1)*, Washington, DC.

FEMA P58-2. [2012] *Seismic Performance Assessment of Buildings: Volume 2 - Implementation Guide (P-58-2)*, Washington, DC.

FEMA P58-3. [2012] *Seismic Performance Assessment of Buildings Volume 3—Performance Assessment Calculation Tool (PACT) Version 2.9.65 (FEMA P-58-3.1)*, Washington, DC.

FEMA P695. [2009] *Quantification of Building Seismic Performance Factors*, Washington, DC, USA.

Fernandes, C., Melo, J., Varum, H., Costa, A. [2012] "Experimental and Numerical Analysis of the Cyclic Behaviour of RC Beam-Column Connections with Plain Reinforcing Bars," *15th World Conference on Earthquake Engineering*, Lisbon, Portugal.

Filiatrault, A., Sullivan, T. [2014] "Performance-based seismic design of nonstructural building components: The next frontier of earthquake engineering," *Earthquake Engineering and Engineering Vibration*, Vol. 13, No.1, pp. 17–46.

Fox, M. J., Sullivan, T. J. [2015] "Record-to-Record Variability in the Seismic Response of RC Walls Subjected to Ground Motions Matched to the Conditional Spectrum," *COMPDYN 2015 - 5th ECCOMAS Thematic Conference on Computational Methods in Structural Dynamics and Earthquake Engineering*, Crete Island, Greece.

Fox, M. J., Welch, D. P., Sullivan, T. J. [2015] "Examining the Dispersion of Engineering Demand Parameters Relevant to the Assessment of Existing Buildings in Europe," *Developing Information Relating to Simplified Displacement-Based Loss Assessment and Retrofit Approaches*, G. M. Calvi and T. J. Sullivan, eds., RELUIS Report, Pavia, Italy.

Furtado, A., Rodrigues, H., Arêde, A., Varum, H. [2015] "Simplified macro-model for infill masonry walls considering the out-of-plane behaviour," *Earthquake Engineering & Structural Dynamics*, Vol. 45, No.4, pp. 507–524.

Galli, M. [2006] "Evaluation of the Seismic Response of Existing RC Frame Buildings with Masonry Infills," MSc Thesis, IUSS Pavia, Italy.

Del Gaudio, C., De Martino, G., Di Ludovico, M., Manfredi, G., Prota, A., Ricci, P., Verderame, G. M. [2016] "Empirical fragility curves from damage data on RC buildings after the 2009 L'Aquila earthquake," *Bulletin of Earthquake Engineering*, Vol. Online.

Genesio, G. [2012] "Seismic Assessment of RC Exterior Beam- Column Joints and Retrofit with Haunches Using Post-Installed Anchors," PhD Thesis, Universitat Stuttgart, Germany.

Glaister, S., Pinho, R. [2003] "Development of a Simplified Deformation-Based Method for Seismic Vulnerability Assessment," *Journal of Earthquake Engineering*, Vol. 7, No.sup001, pp. 107–140.

Global Risk Miyamoto. [2009] *M6.3 L'Aquila, Italy, Earthquake Field Investigation Report.*

Gokkaya, B. U., Baker, J. W., Deierlein, G. G. [2016] "Quantifying the impacts of modeling uncertainties on the seismic drift demands and collapse risk of buildings with implications on seismic design checks," *Earthquake Engineering & Structural Dynamics*, Vol. 45, No.10, pp. 1661–1683.

Gulkan, P., Sozen, M. A. [1974] "Inelastic Responses of Reinforced Concrete Structures to Earthquake Motions," *ACI Journal*, Vol. 71, No.12, pp. 604–610.

Gunturi, S., Shah, H. [1993] "Building-specific Earthquake Damage Estimation," PhD Thesis, Stanford University, CA.

Hak, S., Morandi, P., Magenes, G., Sullivan, T. J. [2012] "Damage Control for Clay Masonry Infills in the Design of RC Frame Structures," *Journal of Earthquake Engineering*, Vol. 16, No.sup1, pp. 1–35.

Haselton, C. B., Deierlein, G. G. [2007] "Assessing Seismic Collapse of Modern Reinforced Concrete Moment Frame Buildings," *Blume Report No. 156*, Stanford University.

Haselton, C. B., Goulet, C. A., Mitrani Reiser, J., Beck, J. L., Deierlein, G. G., Porter, K. A., Stewart, J. P., Taciroglu, E. [2007] "An Assessment to Benchmark the Seismic Performance of a Code-Conforming Reinforced Concrete Moment-Frame Building," *PEER Report 2007/12*, Berkeley, California.

Haselton, C. B., Liel, A. B., Taylor Lange, S., Deierlein, G. G. [2008] "Beam-Column Element Model Calibrated for Predicting Flexural Response Leading to Global Collapse of RC Frame Buildings," *PEER Report 2007/03*, Berkeley, California.

Hegger, J., Sherif, A., Roesner, W. [2003] "Nonseismic Design of Beam–Column Joints," *ACI Structural Journal*, Vol. 100, No.5, pp. 654–664.

Hwang, S. J., Lee, H. J. [1999] "Analytical Model for Predicting Shear Strength of Exterior RC Beam Column Joints for Seismic Resistance," *ACI Structural Journal*, Vol. 96, No.5, pp. 846–857.

Ibarra, L. F., Krawinkler, H. [2005] "Global Collapse of Frame Structures under Seismic Excitations," *PEER Report 2005/06*, Berkeley, California.

Ibarra, L. F., Medina, R. A., Krawinkler, H. [2005] "Hysteretic models that incorporate strength and stiffness deterioration," *Earthquake Engineering & Structural Dynamics*, Vol. 34, No.12, pp. 1489–1511.

Iervolino, I., Chioccarelli, E., Cito, P. [2015] "REASSESS V1.0: A computationally efficient software

for probabilistic seismic hazard analysis," *COMPDYN 2015 - 5th ECCOMAS Thematic Conference on Computational Methods in Structural Dynamics and Earthquake Engineering*, Crete Island, Greece.

Ioannou, I., Borg, R., Novelli, V., Melo, J., Alexander, D., Kongar, I., Verrucci, E., Cahill, B., Rossetto, T. [2012] *The 29th May 2012 Emilia Romagna Earthquake*, London, UK.

ISTAT. [2011] "Censimento della popolazione e delle abitazioni 2011," *Censimento Popolazione Abitazioni*, <http://dati-censimentopopolazione.istat.it/Index.aspx#> (Oct. 25, 2016).

Jalayer, F., Iervolino, I., Manfredi, G. [2010] "Structural modeling uncertainties and their influence on seismic assessment of existing RC structures," *Structural Safety*, Vol. 32, No.3, pp. 220–228.

Jayaram, N., Lin, T., Baker, J. W. [2011] "A Computationally efficient ground-motion selection algorithm for matching a target response spectrum mean and variance," *Earthquake Spectra*, Vol. 27, No.3, pp. 797–815.

Jeon, J., Park, J., DesRoches, R. [2015] "Seismic fragility of lightly reinforced concrete frames with masonry infills," *Earthquake Engineering & Structural Dynamics*, Vol. 44, No.11, pp. 1783–1803.

Jones, G. [2016] "L'Aquila is grim reminder of struggle facing Italy's quake-hit towns," *Reuters*, <http://www.reuters.com/article/us-italy-quake-reconstruction-idUSKCN1130AO> (Sep. 28, 2016).

Kazantzi, A. K., Vamvatsikos, D. [2015] "Intensity measure selection for vulnerability studies of building classes," *Earthquake Engineering & Structural Dynamics*, Vol. 44, No.15, pp. 2677–2694.

Kazantzi, A. K., Vamvatsikos, D., Lignos, D. G. [2014] "Seismic performance of a steel moment-resisting frame subject to strength and ductility uncertainty," *Engineering Structures*, Vol. 78, pp. 69–77.

Kohrangi, M., Bazzurro, P., Vamvatsikos, D. [2016a] "Vector and Scalar IMs in Structural Response Estimation: Part I – Hazard Analysis," *Earthquake Spectra*, Vol. 32, No.3, pp. 1507–1524.

Kohrangi, M., Bazzurro, P., Vamvatsikos, D. [2016b] "Vector and Scalar IMs in Structural Response Estimation: Part II – Building Demand Assessment," *Earthquake Spectra*, Vol. 32, No.3, pp. 1525–1543.

Kohrangi, M., Vamvatsikos, D., Bazzurro, P. [2016] "Implications of Intensity Measure Selection for Seismic Loss Assessment of 3-D Buildings," *Earthquake Spectra*, Vol. 32, No.4, pp. 2167–2189.

Krawinkler, H. [2005] "Van Nuys Hotel Building Testbed Report: Exercising Seismic Performance

Assessment," *PEER Report 2005/11*, Berkeley, California.

Kumar, M., Rai, D. C., Jain, S. K. [2015] "Ductility Reduction Factors for Masonry-Infilled Reinforced Concrete Frames," *Earthquake Spectra*, Vol. 31, No.1, pp. 339–365.

Kwon, O. S., Elnashai, A. [2006] "The effect of material and ground motion uncertainty on the seismic vulnerability curves of RC structure," *Engineering Structures*, Vol. 28, No.2, pp. 289–303.

Landi, L., Benedetti, A. [2013] "Reinforced Concrete Buildings," *Developments in the Field of Displacement-Based Seismic Assessment*, T. J. Sullivan and G. M. Calvi, eds., IUSS Press, Pavia, Italy.

Landi, L., Tardini, A., Diotallevi, P. P. [2016] "A Procedure for the Displacement-Based Seismic Assessment of Infilled RC Frames," *Journal of Earthquake Engineering*, Vol. 20, No.7, pp. 1077–1103.

Liel, A. B. [2008] "Assessing the Collapse Risk of California's Existing Reinforced Concrete Frame Structures: Metrics for Seismic Safety Decisions," PhD Thesis, Stanford University, CA.

Liel, A. B., Haselton, C. B., Deierlein, G. G., Baker, J. W. [2009] "Incorporating modeling uncertainties in the assessment of seismic collapse risk of buildings," *Structural Safety*, Vol. 31, No.2, pp. 197–211.

Lowes, L. N., Altoontash, A. [2003] "Modeling Reinforced-Concrete Beam-Column Joints Subjected to Cyclic Loading," *Journal of Structural Engineering*, Vol. 129, No.12, pp. 1686–1697.

Lowes, L. N., Mitra, N., Altoonash, A. [2003] "A Beam-Column Joint Model for Simulating the Earthquake Response of Reinforced Concrete Frames," *PEER Report 2003/10*, Berkeley, California.

Lucchini, A., Mollaioli, F., Bazzurro, P. [2014] "Floor Response Spectra for Bare and Infilled Reinforced Concrete Frames Floor Response Spectra for Bare and Infilled," *Journal of Earthquake Engineering*, Vol. 18, No.7, pp. 1060–1082.

Di Ludovico, M., Verderame, G. M., Prota, A., Manfredi, G., Cosenza, E. [2013] "Cyclic Behavior of Nonconforming Full-Scale RC Columns," *Journal of Structural Engineering*, Vol. 140, No.5.

Mathworks. [2014] *Version 8.3.0 (R2014a)*, The Mathworks Inc., Natick, Massachusetts.

McKay, M. D., Beckman, R. J., Conover, W. J. [1979] "A Comparison of Three Methods for Selecting Values of Input Variables in the Analysis of Output from a Computer Code," *Technometrics*, Vol. 21, No.2, pp. 239–245.

McKenna, F., Fenves, G., Filippou, F. C., Mazzoni, S. [2000] "Open System for Earthquake Engineering Simulation (OpenSees)," <http://opensees.berkeley.edu/wiki/index.php/Main_Page>.

Melo, J., Fernandes, C., Varum, H., Rodrigues, H., Costa, A., Arêde, A. [2011] "Numerical modelling of the cyclic behaviour of RC elements built with plain reinforcing bars," *Engineering Structures*, Vol. 33, No.2, pp. 273–286.

Melo, J., Varum, H., Rossetto, T. [2014] "Cyclic behaviour of interior beam-column joints reinforced with plain bars," *Earthquake Engineering & Structural Dynamics*, Vol. 44, No.9, pp. 1351–1371.

Melo, J., Varum, H., Rossetto, T. [2015] "Experimental cyclic behaviour of RC columns with plain bars and proposal for Eurocode 8 formula improvement," *Engineering Structures*, Vol. 88, pp. 22–36.

Melo, J., Varum, H., Rossetto, T., Costa, A. [2012] "Cyclic response of RC beam-column joints reinforced with plain bars : An experimental testing campaign," *15th World Conference on Earthquake Engineering*, Lisbon, Portugal.

Mergos, P. E., Kappos, A. J. [2008] "A distributed shear and flexural flexibility model with shear-flexure interaction for R/C members subjected to seismic loading," *Earthquake Engineering & Structural Dynamics*, Vol. 37, No.12, pp. 1349–1370.

Mergos, P. E., Kappos, A. J. [2012] "A gradual spread inelasticity model for R/C beam–columns, accounting for flexure, shear and anchorage slip," *Engineering Structures*, Vol. 44, pp. 94–106.

Metelli, G., Messali, F., Beschi, C., Riva, P. [2015] "A model for beam–column corner joints of existing RC frame subjected to cyclic loading," *Engineering Structures*, Vol. 89, pp. 79–92.

Mitrani Reiser, J. [2007] "An Ounce of Prevention: Probabilistic Loss Estimation for Performance-Based Earthquake Engineering," PhD Thesis, California Institute of Technology, Pasadena, CA.

Montaldo, V., Meletti, C. [2007] *Valutazione del valore della ordinata spettrale a 1sec e ad altri periodi di interesse ingegneristico. Progetto DPC-INGV S1, Deliverable D3.*

Morales, E., Filiatrault, A., Aref, A. [2017] "Sustainable and Low Cost Room Seismic Isolation for Essential Care Units in Developing Countries," *16th World Conference on Earthquake Engineering*, Santiago, Chile.

Morandi, P., Hak, S., Magenes, G. [2013] *Simplified out-of-plane resistance verification for slender clay masonry infills in RC frames*, *Individual Study Report*, Università degli Studi di Pavia, Italy.

Morandi, P., Hak, S., Magenes, G. [2014] "In-plane Experimental Response of Strong Masonry Infills," *9th International Masonry Conference*, Guimarães, Portugal.

Nievas, C. I., Sullivan, T. J. [2016] "Accounting for directionality as a function of structural typology in performance-based earthquake engineering design," *Earthquake Engineering & Structural Dynamics*, Vol. Online.

NTC. [2008] *Norme Tecniche Per Le Costruzioni*, Rome, Italy.

NZS 3101. [2006] *Concrete Structures Standard: Part 1- The Design of Concrete Structures*, Wellington, New Zealand.

O'Connor, J. S., Morales, E. [2016] *Reconnaissance of damaged structures after the 2016 Muisne-Ecuador Earthquake*, State University of New York at Buffalo (Presentation), Buffalo, NY.

O'Reilly, G. J., Sullivan, T. J. [2015] "Influence of Modelling Parameters on the Fragility Assessment of pre-1970 Italian RC Structures," *COMPDYN 2015 - 5th ECCOMAS Thematic Conference on Computational Methods in Structural Dynamics and Earthquake Engineering*, Crete Island, Greece.

O'Reilly, G. J., Sullivan, T. J. [2016] "Direct Displacement-Based Seismic Design of Eccentrically Braced Steel Frames," *Journal of Earthquake Engineering*, Vol. 20, No.2, pp. 243–278.

O'Reilly, G. J., Sullivan, T. J., Filiatrault, A. [2017] "Implications of a More Refined Damage Estimation Approach in the Assessment of RC Frames," *16th World Conference on Earthquake Engineering*, Santiago, Chile.

Oesterle, R. G., Al., E. [1979] *Earthquake resistant structural walls-tests of isolated walls—phase II.*, Skokie, Illinois, USA.

Olsson, A., Sandberg, G., Dahlblom, O. [2003] "On Latin hypercube sampling for structural reliability analysis," *Structural Safety*, Vol. 25, No.1, pp. 47–68.

Ozcebe, G., Saatcioglu, M. [1989] "Hysteretic Shear Model for Reinforced Concrete Members," *Journal of Structural Engineering*, Vol. 115, No.1, pp. 132–148.

Pagano, M. [1963] *Strutture (Volume I)*, Liguori, Napoli; Italy.

Pampanin, S., Calvi, G. M., Moratti, M. [2002] "Seismic Behaviour of RC Beam-Column Joints Designed for Gravity Loads," *12th European Conference on Earthquake Engineering*, London, UK.

Pampanin, S., Magenes, G., Carr, A. J. [2003] "Modelling of Shear Hinge Mechanism in Poorly Detailed RC Beam-Column Joints," *Concrete Structures in Seismic Regions*, Athens, Greece.

Panagiotakos, M., Fardis, M. N. [1996] "Seismic Response of Infilled RC Frame Structures," *11th World Conference on Earthquake Engineering*, Mexico City, Mexico.

Parducci, A., Mezzi, M. [1980] "Repeated horizontal displacements of infilled frames having different stiffness and connection systems – experimental analysis," *Proceedings of The Seventh World Conference on Earthquake engineering*, Istanbul, Turkey.

Park, R., Paulay, T. [1975] *Reinforced Concrete Structures*, John Wiley & Sons, Ltd., New York.

Paulay, T., Priestley, M. J. N. [1992] *Seismic Design of Reinforced Concrete and Masonry Buildings*, John Wiley & Sons, Ltd.

Pennucci, D., Sullivan, T. J., Calvi, G. M. [2011] "Displacement Reduction Factors for the Design of Medium and Long Period Structures," *Journal of Earthquake Engineering*, Vol. 15, No.Supp 1, pp. 1–29.

Piazza, A. [2013] "Development of a Simpified Displacement-Based Procedure for the Seismic Design and Assessment of RC Frame Structures," MSc Thesis, IUSS Pavia, Italy.

Pinto, P. E., Franchin, P. [2014] "Existing Buildings: The New Italian Provisions for Probabilistic Seismic Assessment," *Perspectives on European Earthquake Engineering and Seismology*, A. Ansal, ed., Springer.

Pires, F. [1990] "Influencia das paredes de alvenaria no comportanmento de estruturas reticuladas de betao armado sujeitas a accoes horizontais," PhD Thesis, LNEC Lisbon, Portugal.

Porter, K. A. [2003] "An Overview of PEER's Performance-Based Earthquake Engineering Methodology," *Proceedings of Ninth International Conference on Applications of Probability and Statistics in Engineering*, San Francisco, CA.

Porter, K. A., Beck, J. L., Shaikhutdinov, R. V. [2002] "Sensitivity of Building Loss Estimates to Major Uncertain Variables," *Earthquake Spectra*, Vol. 18, No.4, pp. 719–743.

Porter, K. A., Beck, J. L., Shaikhutdinov, R. V. [2004] "Simplified Estimation of Economic Seismic Risk for Buildings," *Earthquake Spectra*, Vol. 20, No.4, pp. 1239–1263.

Porter, K. A., Kiremidjian, A. S. [2001] "Assembly-Based Vulnerability of Buildings and Its Uses in Seismic Performance Evaluation and Risk Management Decision-Making," *Blume Report No. 139*, Stanford, CA.

Prevention Web. [2016] "Prevention Web - Serving the information needs of the disaster reduction community," <http://www.preventionweb.net/countries/ita/data/> (Oct. 25, 2016).

Priestley, M. J. N. [1993] "Myths and Fallacies in Earthquake Engineering- Conflicts between design and reality," *Bulletin of the New Zealand Society for Earthquake Engineering*, Vol. 26, No.3, pp. 329–341.

Priestley, M. J. N. [1997] "Displacement-Based Seismic Assessment of Reinforced Concrete Buildings," *Journal of Earthquake Engineering*, Vol. 1, No.1, pp. 157–192.

Priestley, M. J. N. [2003] "Myths and Fallacies in Earthquake Engineering, Revisited," *The 9th Mallet Milne Lecture*, IUSS Press, Pavia, Italy.

Priestley, M. J. N., Calvi, G. M., Kowalsky, M. J. [2007] *Displacement Based Seismic Design of Structures*, IUSS Press, Pavia, Italy.

Priestley, M. J. N., Seible, F., Calvi, G. M. [1996] *Seismic Design and Retrofit of Bridges*, John Wiley & Sons, Ltd.

Priestley, M. J. N., Seible, F., Verma, R., Xiao, Y. [1993] "Seismic Shear Strength of Reinforced Concrete Columns," *Report SSRP-93/06*, San Diego, CA, USA.

Ramamoorthy, S. K., Gardoni, P., Bracci, J. M. [2006] "Probabilistic Demand Models and Fragility Curves for Reinforced Concrete Frames," *Journal of Structural Engineering*, Vol. 132, No.10, pp. 1563–1572.

Ramirez, C. M., Miranda, E. [2009] "Building Specific Loss Estimation Methods & Tools for Simplified Performance Based Earthquake Engineering," *Blume Report No. 171*, Stanford, CA.

Regio Decreto. [1939] *Norme per la l'esecuzione delle opere conglomerato cementizio semplice od armato - 2229/39*, Rome, Italy.

Ricci, P., De Luca, F., Verderame, G. M. [2011] "6th April 2009 L'Aquila earthquake, Italy: reinforced concrete building performance," *Bulletin of Earthquake Engineering*, Vol. 9, No.1, pp. 285–305.

Ruggiero, D. [2015] "The Behaviour of Reinforced Concrete Subjected to Reversed Cyclic Shear," PhD Thesis, University of Toronto, Canada.

Saatcioglu, M., Ozcebe, G. [1988] *Tests of reinforced concrete columns under uniaxial and biaxial load reversals*, Toronto, Canada.

Saborio Romano, D. [2016] "Performance Based and Simplified Displacement Based Assessment of Infilled RC Frame Building in L'Aquila, Italy," MSc Thesis, IUSS Pavia, Italy.

Salvatore, W., Caprilli, S., Barberi, V. [2009] *Rapporto dei Danni Provocati dall'Evento Sismico del 6 Aprile*

sugli Edifici Scolastici del Centro Storico dell'Aquila, Pisa, Italy.

Santarella, L. [1956] *Il cemento armato – La tecnica e la statica.*

Sassun, K. [2014] "A Parametric Investigation into the Seismic Behaviour of Window Glazing Systems," MSc Thesis, IUSS Pavia, Italy.

Sassun, K., Sullivan, T. J., Morandi, P., Cardone, D. [2015] "Characterising the In-Plane Seismic Performance of Infill Masonry," *Bulletin of the New Zealand Society for Earthquake Engineering*, Vol. 49, No.1.

Scholl, R. E., Kutsu, O., Perry, C. L., Zanetti, J. M. [1982] *Seismic Damage Assessment for High-Rise Buildings*, San Francisco, CA.

SEAOC. [1995] *Vision 2000: Performance-based seismic engineering of buildings*, Sacramento, California.

Sezen, H., Moehle, J. P. [2004] "Shear Strength Model for Lightly Reinforced Concrete Columns," *Journal of Structural Engineering*, Vol. 130, No.11, pp. 1692–1703.

Shafaei, J., Zareian, M. S., Hosseini, A., Marefat, M. S. [2014] "Effects of joint flexibility on lateral response of reinforced concrete frames," *Engineering Structures*, Vol. 81, pp. 412–431.

Sharma, A., Eligehausen, R., Reddy, G. R. [2011] "A new model to simulate joint shear behavior of poorly detailed beam–column connections in RC structures under seismic loads, Part I: Exterior joints," *Engineering Structures*, Vol. 33, No.3, pp. 1034–1051.

Shibata, A., Sozen, M. A. [1976] "Substitute-Structure Method for Seismic Design in R/C," *Journal of the Structural Division*, ASCE, Vol. 102, No.1, pp. 1–18.

Singhal, A., Kiremidjian, A. S. [1996] "A Method for Earthquake Motion-damage Relationships with Application to Reinforced Concrete Frames," *Blume Report No. 119*, Stanford, CA.

Stafford Smith, B. [1966] "Behaviour of square infilled frames," *Journal of the Structural Division*, Vol. 92, No.1, pp. 381–403.

Stevens, N. J., Uzumeri, S. M., Collins, M. P. [1991] "Reinforced-Concrete Subjected to Reversed-Cyclic Shear – Experiments and Constitutive Model," *ACI Structura Journal*, Vol. 88, No.2, pp. 135–146.

Stylianidis, K. C. [1998] "Cyclic Behaviour of infilled R/C frames," *Proceedings of 8th Conference IBMAC*, Dublin, Ireland.

Sullivan, T. J., Calvi, G. M. [2011] "Considerations for the Seismic Assessment of Buildings Using

the Direct Displacement-Based Assessment Approach," *Atti del 5 Convegno Nazionale ANIDIS*, Bari, Italy.

Sullivan, T. J., Calvi, G. M., Priestley, M. J. N., Kowalsky, M. J. [2003] "The Limitations and Performances of Different Displacement-Based Design Methods," *Journal of Earthquake Engineering*, Vol. 7, No.S1, pp. 201–241.

Sullivan, T. J., Calvi, P. M., Nascimbene, R. [2013] "Towards improved floor spectra estimates for seismic design," *Earthquakes and Structures*, Vol. 4, No.1, pp. 109–132.

Sullivan, T. J., Priestley, M. J. N., Calvi, G. M. (Eds.). [2012] *A Model Code for the Displacement-Based Seismic Design of Structures - DBD12*, IUSS Press, Pavia, Italy.

Sullivan, T. J., Welch, D. P., Calvi, G. M. [2014] "Simplified seismic performance assessment and implications for seismic design," *Earthquake Engineering and Engineering Vibration*, Vol. 13, No.Supp1, pp. 95–122.

Taghavi, S., Miranda, E. [2003] "Response Assessment of Nonstructural Building Elements," *PEER Report 2003/05*, Berkeley, California.

Tankut, A. T., Fenwick, R. C., Thom, C. W. [1981] *The deformation of reinforced concrete beams subjected to inelastic cyclic loading-experimental results.*, Auckland, New Zealand.

Terzic, V., Schoettler, M. J., Restrepo, J. I., Mahin, S. A. [2015] "Concrete Column Blind Prediction Contest 2010: Outcomes and Observations," *PEER Report 2015/01*, Berkeley, California.

Tsai, K. C., Popov, E. P. [1988] "Steel Beam-Column Joints in Seismic Moment Resiting Frames," *EERC Report No. UCB/EERC/88-19*, Berkeley, California.

Vamvatsikos, D. [2002] "Seismic Performance, Capacity and Reliability of Sructures As Seen Through Incremental Dynamic Analysis," PhD Thesis, Stanford University, Stanford, CA.

Vamvatsikos, D. [2013] "Derivation of new SAC/FEMA performance evaluation solutions with second-order hazard approximation," *Earthquake Engineering & Structural Dynamics*, Vol. 42, No.8, pp. 1171–1188.

Vamvatsikos, D. [2014] "Seismic Performance Uncertainty Estimation via IDA with Progressive Accelerogram-Wise Latin Hypercube Sampling," *Journal of Structural Engineering*, Vol. 140, No.8.

Vamvatsikos, D., Cornell, C. A. [2002] "Incremental dynamic analysis," *Earthquake Engineering & Structural Dynamics*, Vol. 31, No.3, pp. 491–514.

Vamvatsikos, D., Cornell, C. A. [2005] "Direct Estimation of Seismic Demand and Capacity of Multidegree-of-Freedom Systems through Incremental Dynamic Analysis of Single Degree of Freedom Approximation," *Journal of Structural Engineering*, Vol. 131, No.4, pp. 589–599.

Vamvatsikos, D., Fragiadakis, M. [2010] "Incremental dynamic analysis for estimating seismic performance sensitivity and uncertainty," *Earthquake Engineering & Structural Dynamics*, Vol. 39, No.2, pp. 141–163.

Vecchio, F. J., Collins, M. P. [1986] "The Modified Compression-Field Theory for Reinforced Concrete Elements Subjected to Shear," *ACI Journal Proceedings*, Vol. 83, No.2, pp. 219–231.

Verderame, G. M., Fabbrocino, G., Manfredi, G. [2008a] "Seismic response of r.c. columns with smooth reinforcement. Part I: Monotonic tests," *Engineering Structures*, Vol. 30, No.9, pp. 2277–2288.

Verderame, G. M., Fabbrocino, G., Manfredi, G. [2008b] "Seismic response of r.c. columns with smooth reinforcement. Part II: Cyclic tests," *Engineering Structures*, Vol. 30, No.9, pp. 2289–2300.

Verderame, G. M., Iervolino, I., Ricci, P. [2009] *Report on the Damage on Buildings Following the Seismic Event of 6th of April 2009 Time 1:32 - L'Aquila M=5.8*.

Verderame, G. M., Polese, M., Mariniello, C., Manfredi, G. [2010] "A simulated design procedure for the assessment of seismic capacity of existing reinforced concrete buildings," *Advances in Engineering Software*, Vol. 41, No.2, pp. 323–335.

Verderame, G. M., Ricci, P., Manfredi, G., Cosenza, E. [2010] "Ultimate chord rotation of RC columns with smooth bars: some considerations about EC8 prescriptions," *Bulletin of Earthquake Engineering*, Vol. 8, No.6, pp. 1351–1373.

Vidic, T., Fajfar, P., Fischinger, M. [1994] "Consistent inelastic design spectra: Strength and displacement," *Earthquake Engineering & Structural Dynamics*, Vol. 23, No.5, pp. 507–521.

Vona, M., Masi, A. [2004] "Resistenza sismica de telai in c.a. progettati con il R.D. 2229/39," *XI Congresso Nazionale "L'Ingegneria Sismica in Italia,"* Genova, Italia.

Vorechovsky, M., Novak, D. [2003] "Statistical correlation in stratified sampling," *ICAPS 9 Proceedings of International Conference on Applications of Statistics and Probability in Civil Engineering*, A. Der Kiureghian, S. Madant, and J. Pestana, eds., Millpress:, Rotterdam, San Francisco, pp. 119–124.

Welch, D. P. [2016] "Non-structural Element Considerations for Contemporary Performance-Based Earthquake Engineering," PhD Thesis, IUSS Pavia, Pavia, Italy.

Welch, D. P., Sullivan, T. J. [2013] "Nonstructural Considerations for Seismic Serviceability Performance in European Steel Moment Frames," *Giornate Italiane della Costruzione in Acciaio*, Torino, Italia.

Welch, D. P., Sullivan, T. J., Calvi, G. M. [2014] "Developing Direct Displacement-Based Procedures for Simplified Loss Assessment in Performance-Based Earthquake Engineering," *Journal of Earthquake Engineering*, Vol. 18, No.2, pp. 290–322.

Wong, H. F. [2005] "Shear Strength and Seismic Performance of Non-Seismically Designed RC Beam-Column Joints," Hong Kong University of Science and Technology, Hong Kong.

Yang, T. Y., Moehle, J., Stojadinovic, B., Der Kiureghian, A. [2009] "Seismic Performance Evaluation of Facilities: Methodology and Implementation," *Journal of Structural Engineering*, Vol. 135, No.10, pp. 1146–1154.

Yu, X., Lu, D., Li, B. [2016] "Estimating uncertainty in limit state capacities for reinforced concrete frame structures through pushover analysis," *Earthquakes and Structures*, Vol. 10, No.1, pp. 141–161.

Zimos, D. K., Mergos, P. E., Kappos, A. J. [2015] "Shear Hysteresis Model for Reinforced Concrete Elements Including the Post-Peak Range," *COMPDYN 2015 - 5th ECCOMAS Thematic Conference on Computational Methods in Structural Dynamics and Earthquake Engineering*, Crete Island, Greece.

APPENDIX A

This appendix outlines the results of the IDA conducted in Section 5.3 for each of the case study frames examined. The plots below outline the results of each of the IDA conducted for each of the case study frames. These results form the data set that go on to form the median values discussed in Section 5.3, which are then used for various comparisons and validations throughout the thesis. The results are presented in a format whereby for each intensity, the median, dispersion and probability of collapse are provided.

MAXIMUM PEAK STOREY DRIFT

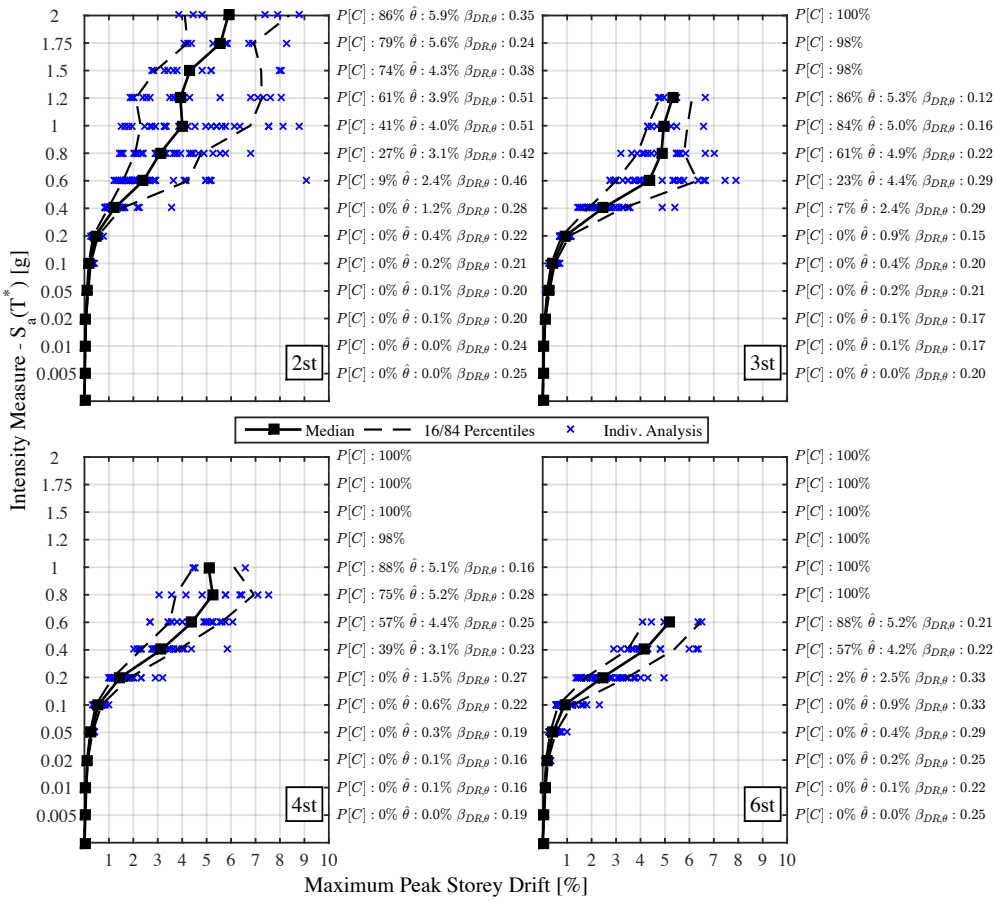

Figure A.1: Maximum PSD for the 2D case study frames modelled without masonry infill.

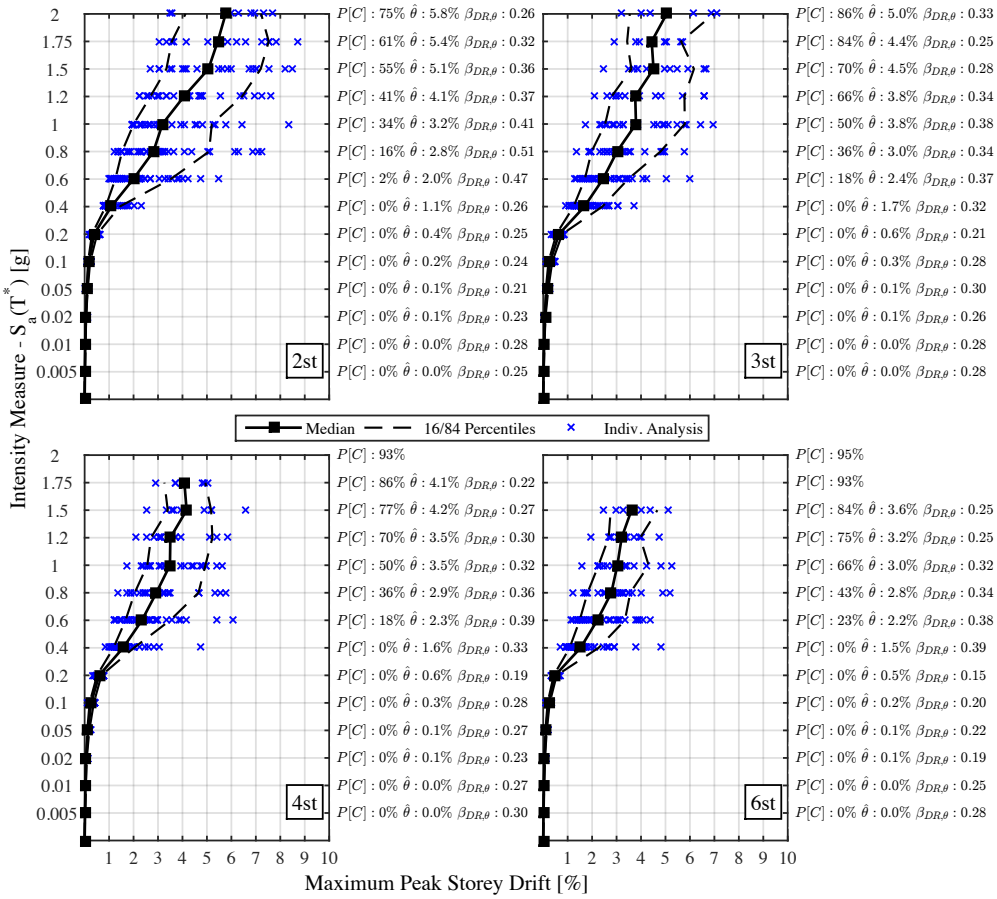

Figure A.2: Maximum PSD for the 2D case study pilotis frames.

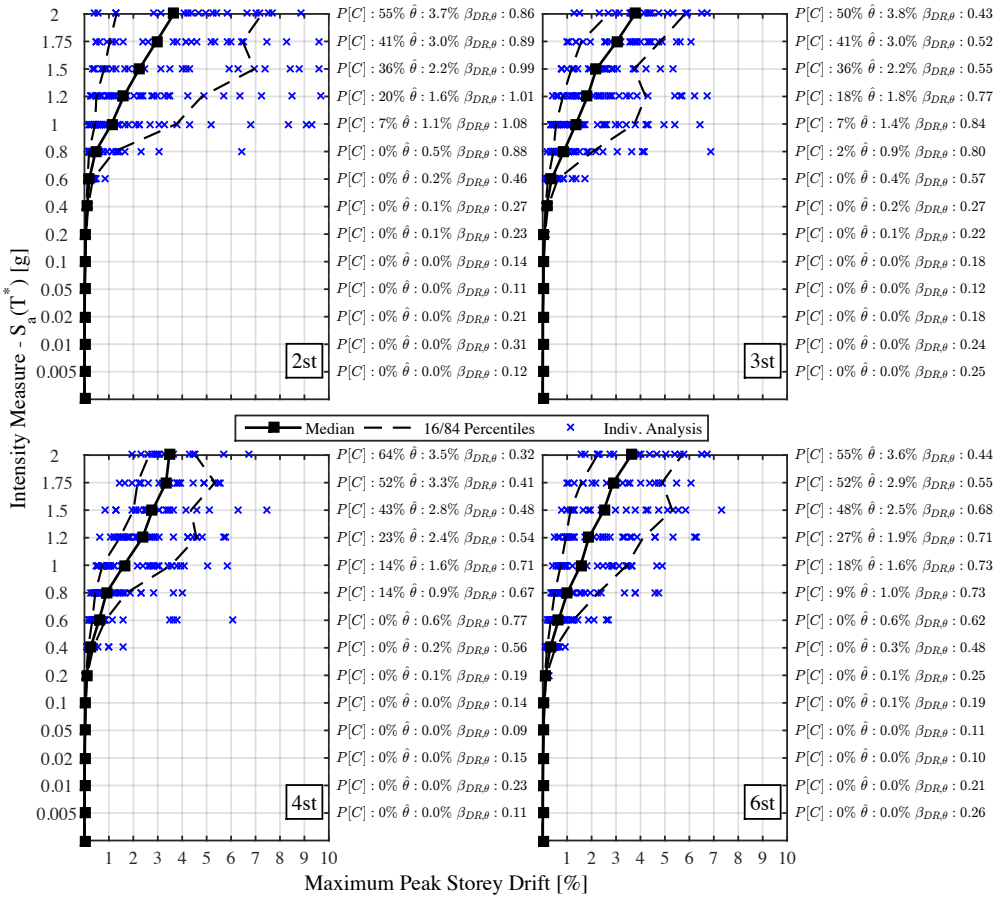

Figure A.3: Maximum PSD for the 2D case study frames with weak infill modelled with single diagonal struts.

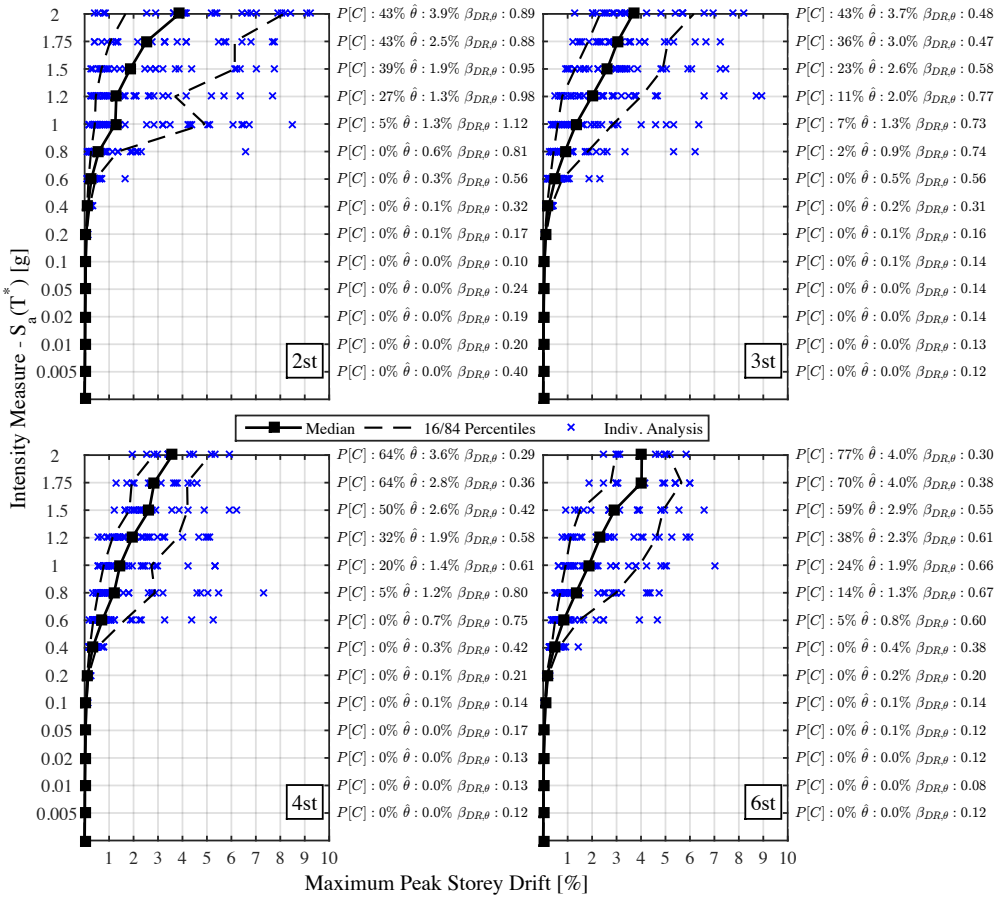

Figure A.4: Maximum PSD for the 2D case study frames with weak infill modelled with double diagonal struts.

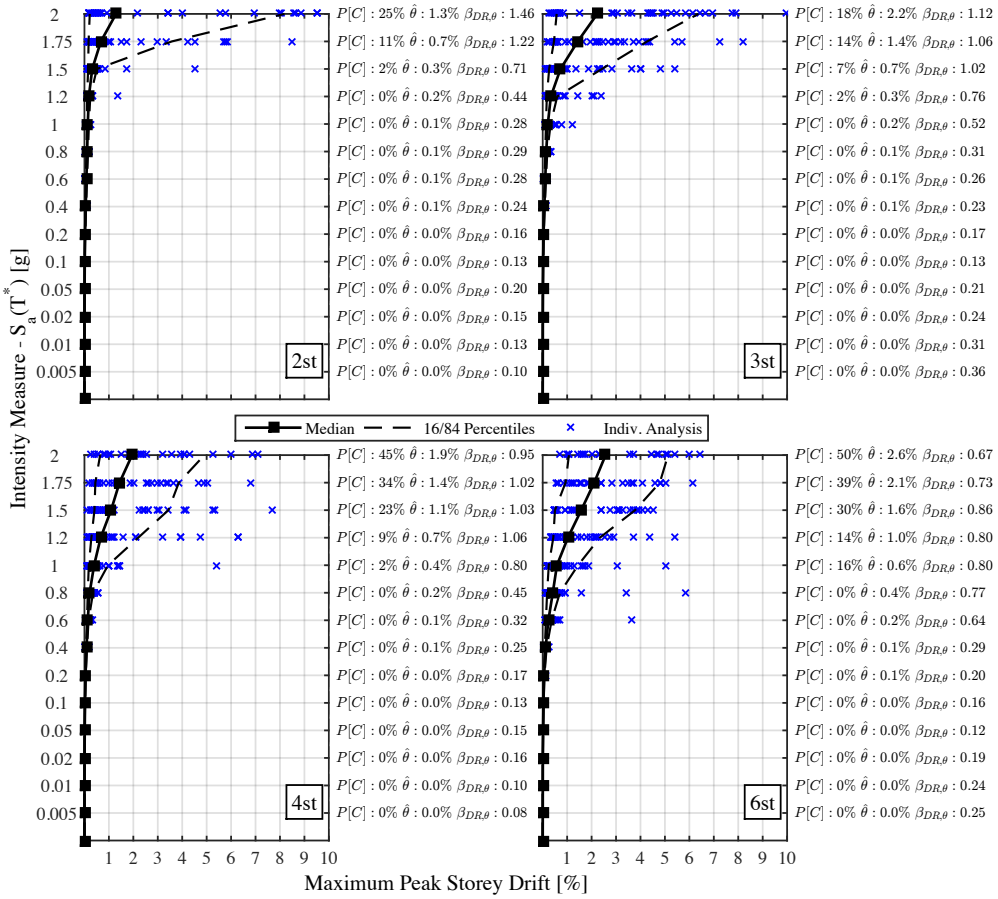

Figure A.5: Maximum PSD for the 2D case study frames with strong infill modelled with single diagonal struts.

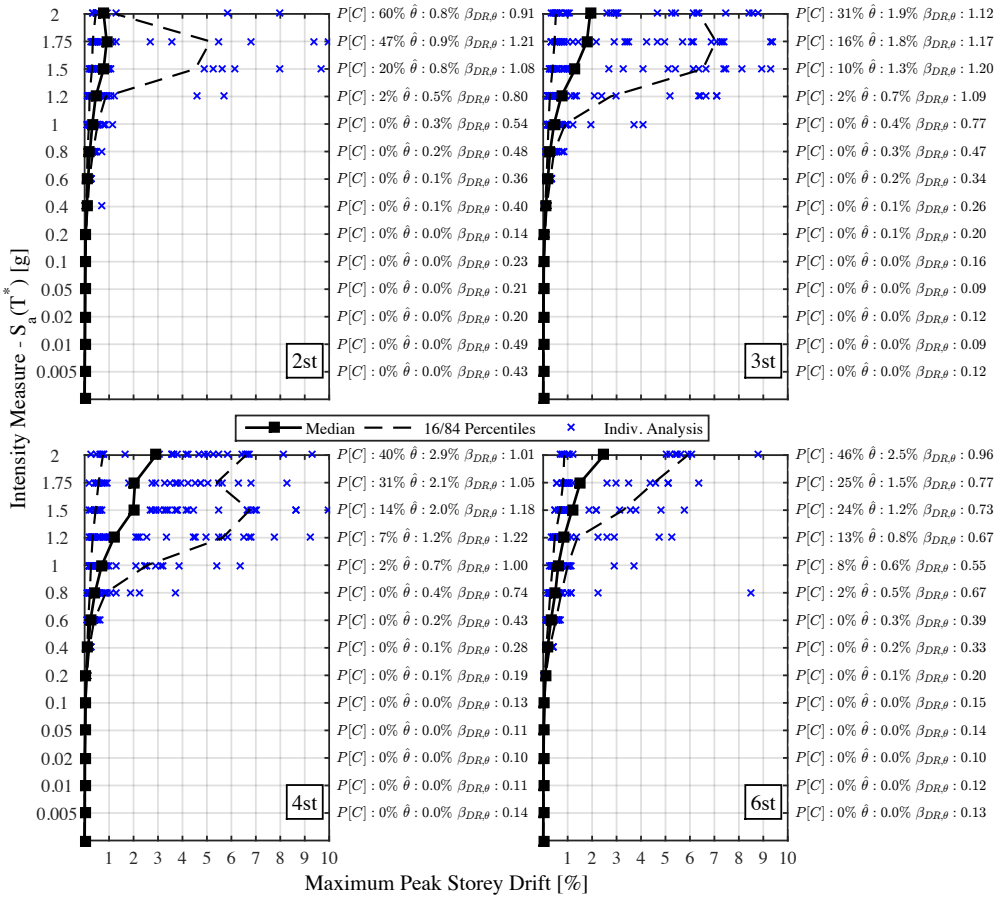

Figure A.6: Maximum PSD for the 2D case study frames with strong infill modelled with double diagonal struts.

MAXIMUM PEAK FLOOR ACCELERATION

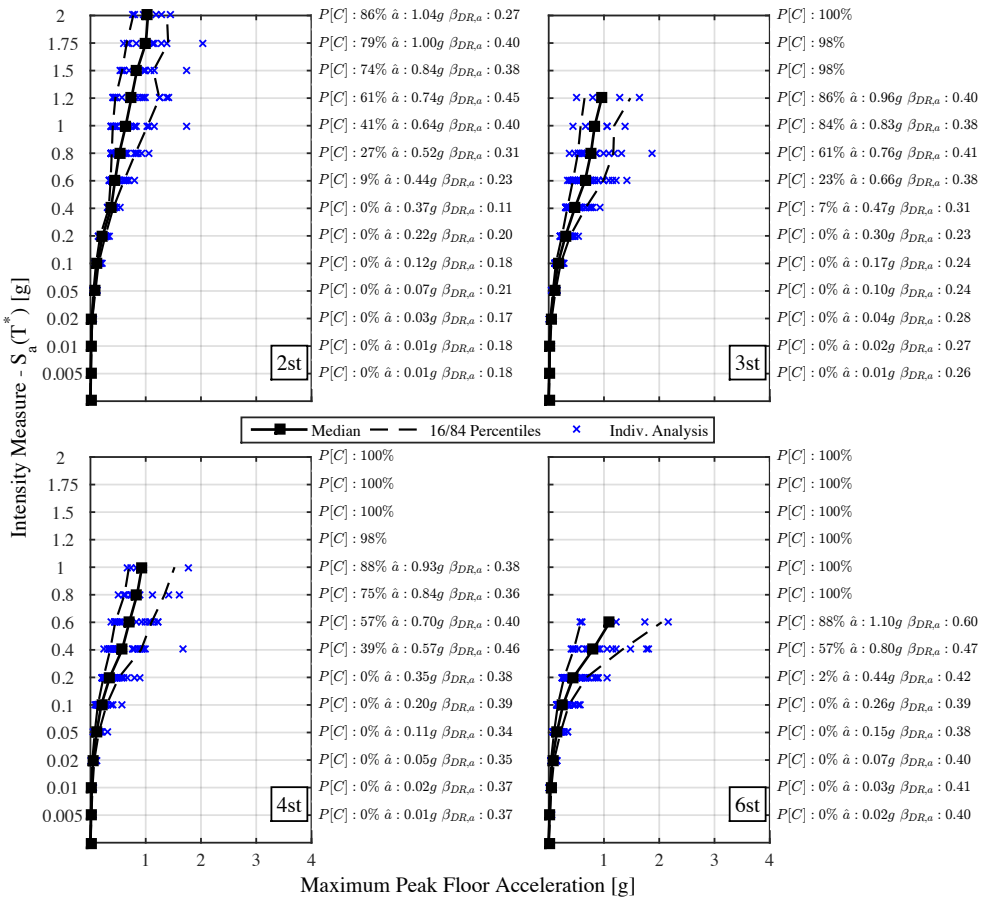

Figure A.7: Maximum PFA for the 2D case study frames modelled without masonry infill.

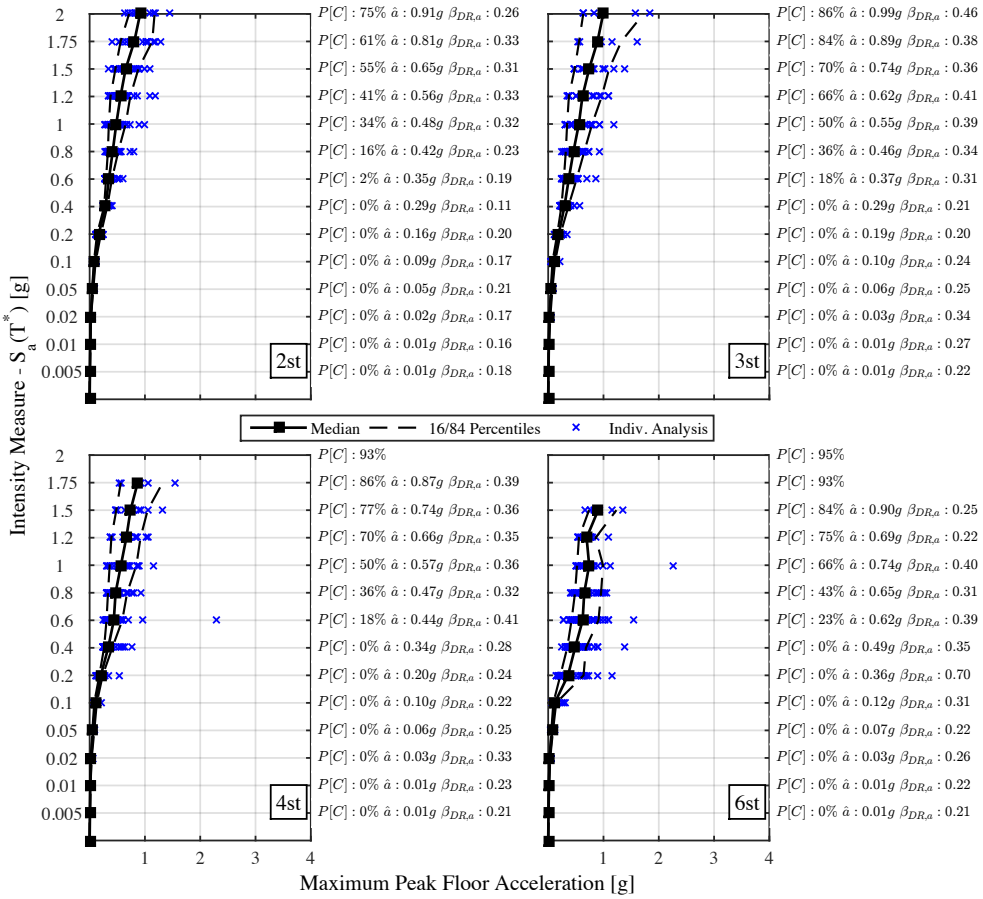

Figure A.8: Maximum PFA for the 2D case study pilotis frames.

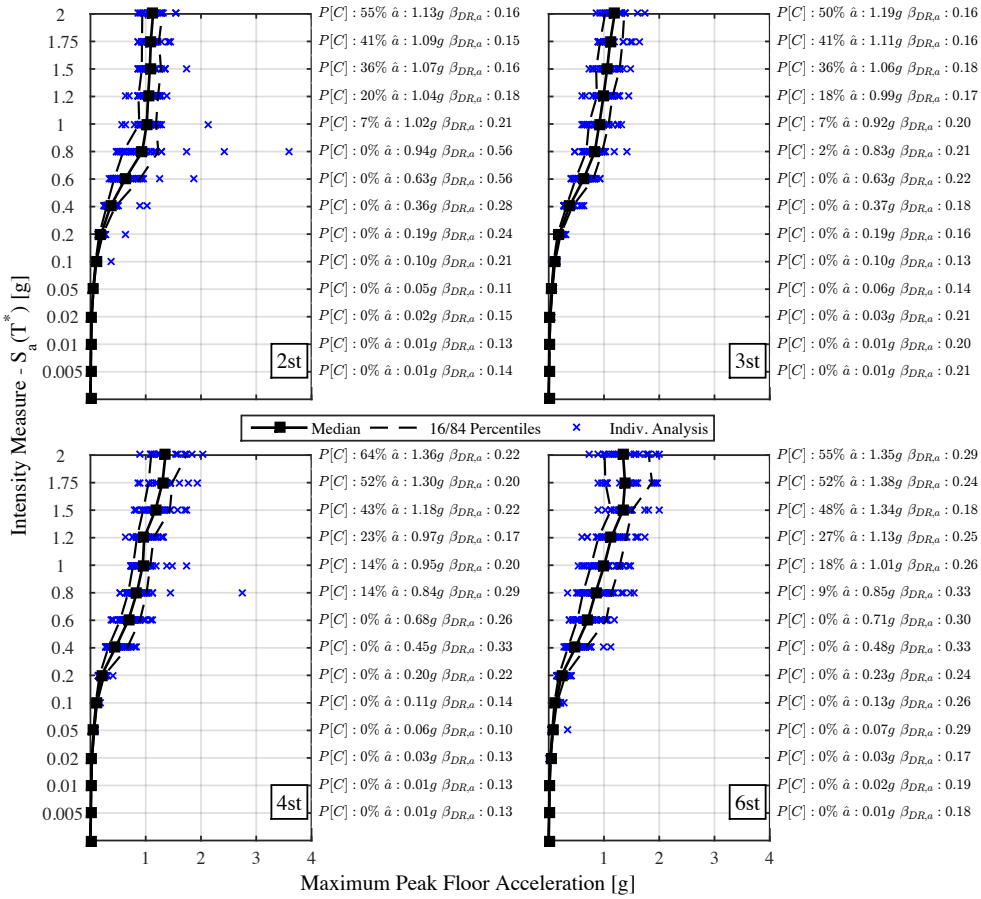

Figure A.9: Maximum PFA for the 2D case study frames with weak infill modelled with single diagonal struts.

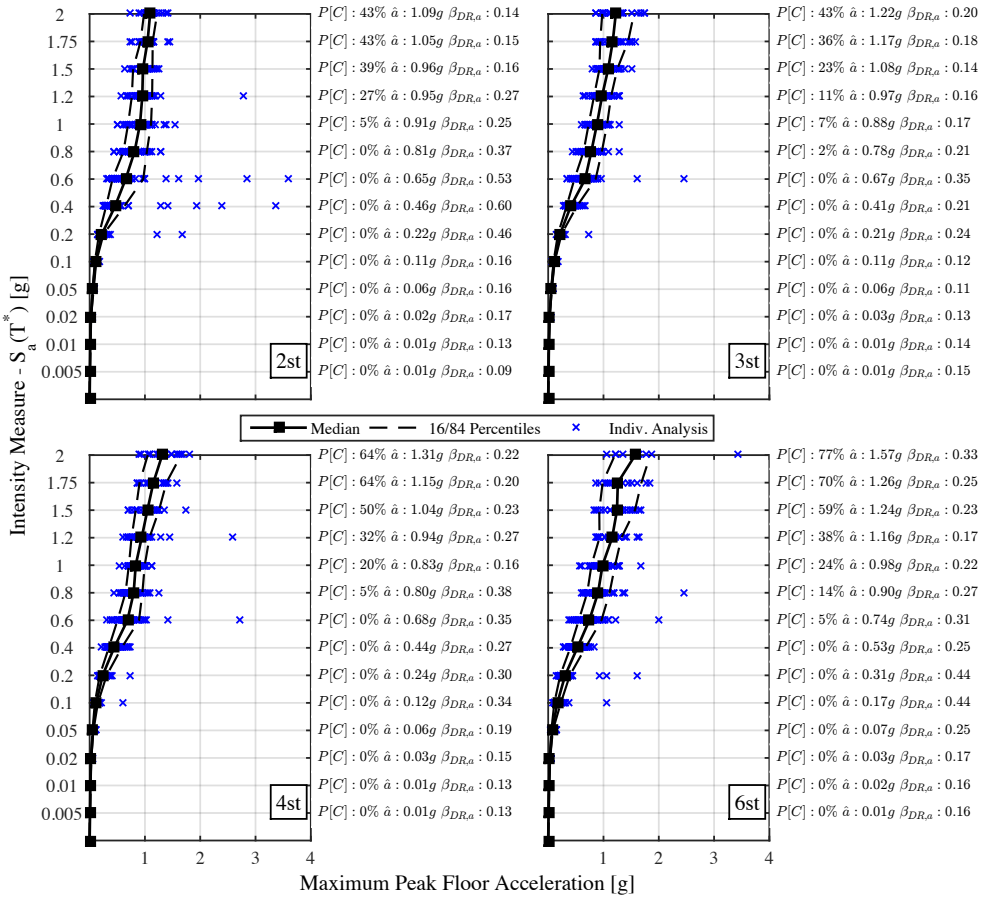

Figure A.10: Maximum PFA for the 2D case study frames with weak infill modelled with double diagonal struts.

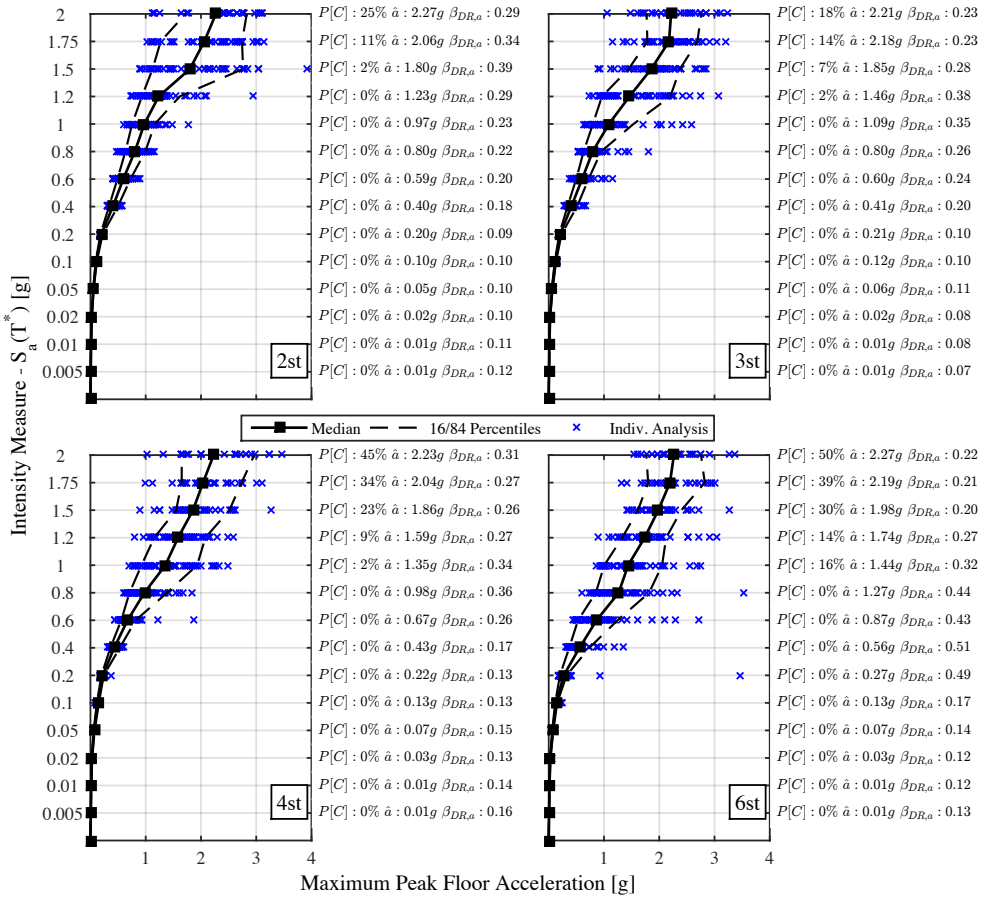

Figure A.11: Maximum PFA for the 2D case study frames with strong infill modelled with single diagonal struts.

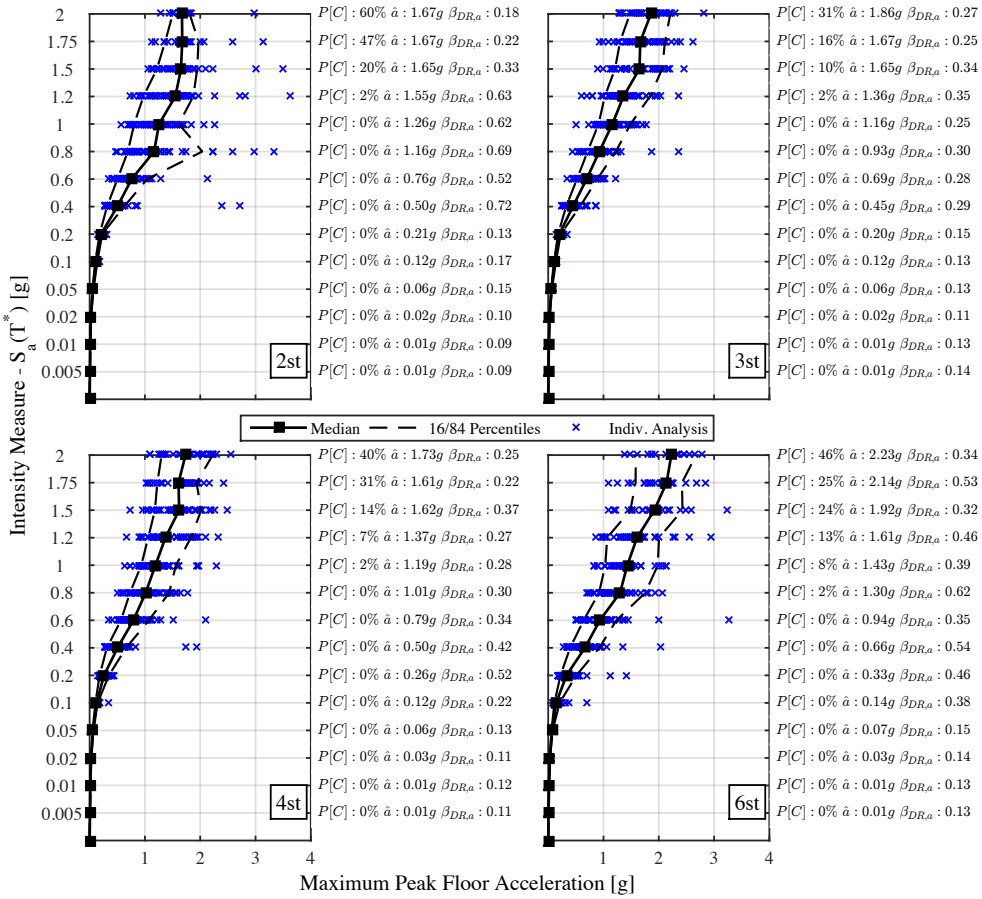

Figure A.12: Maximum PFA for the 2D case study frames with strong infill modelled with double diagonal struts.

LIMIT STATE FRAGILITY FUNCTIONS

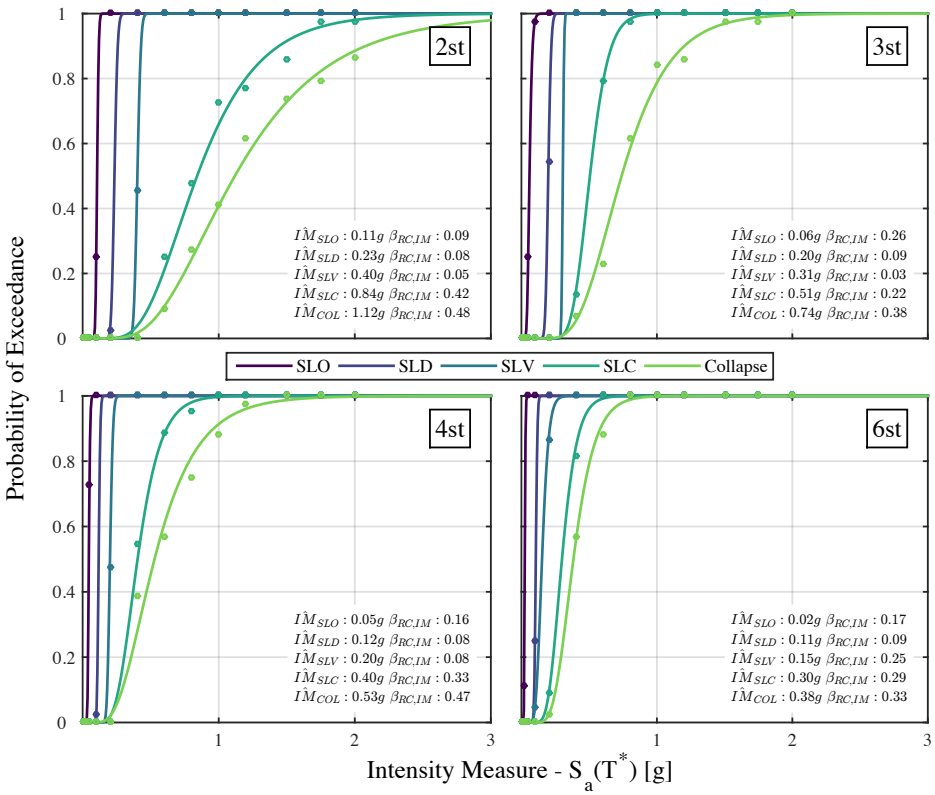

Figure A.13: Limit state fragility functions for the 2D case study frames modelled without masonry infill.

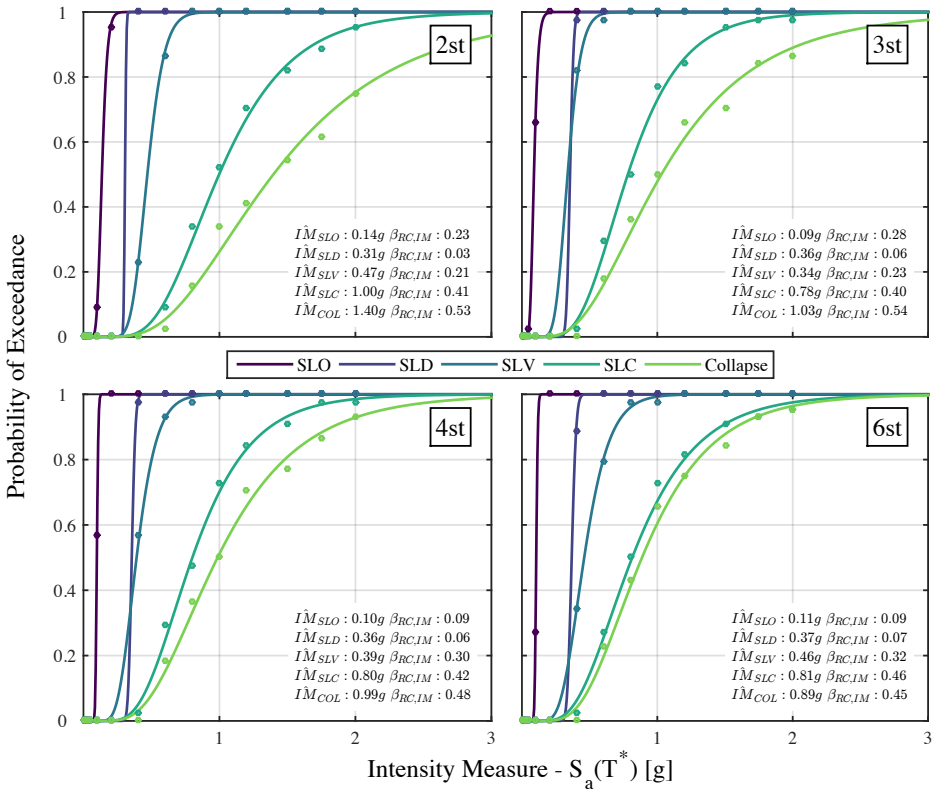

Figure A.14: Limit state fragility functions for the 2D case study pilotis frames.

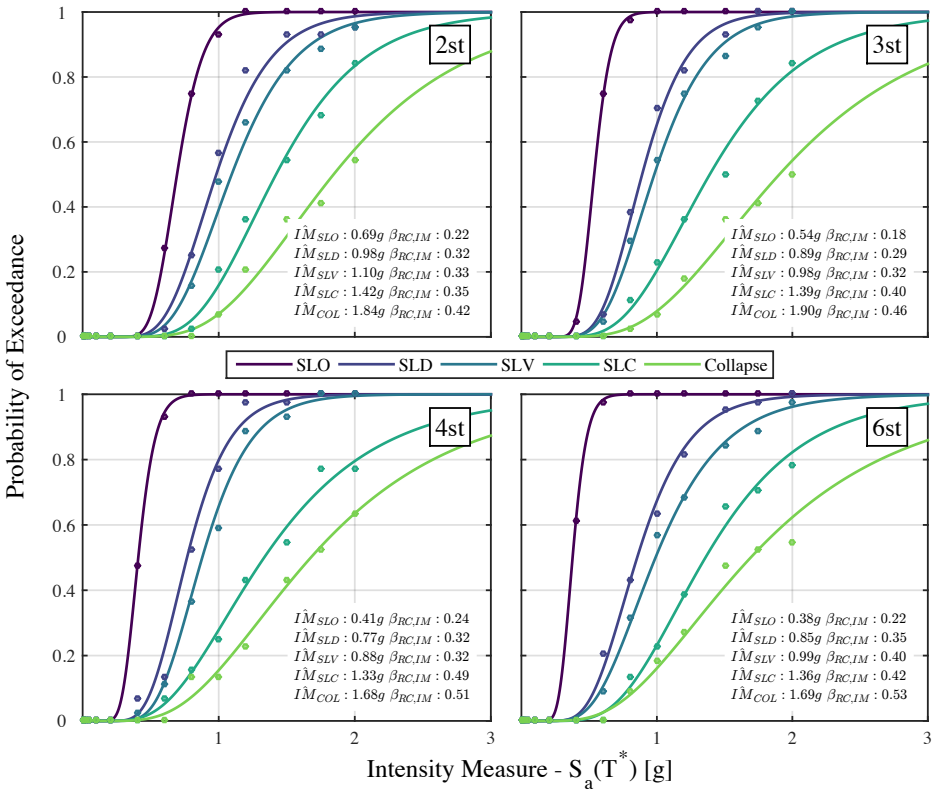

Figure A.15: Limit state fragility functions for the 2D case study frames with weak infill modelled with single diagonal struts.

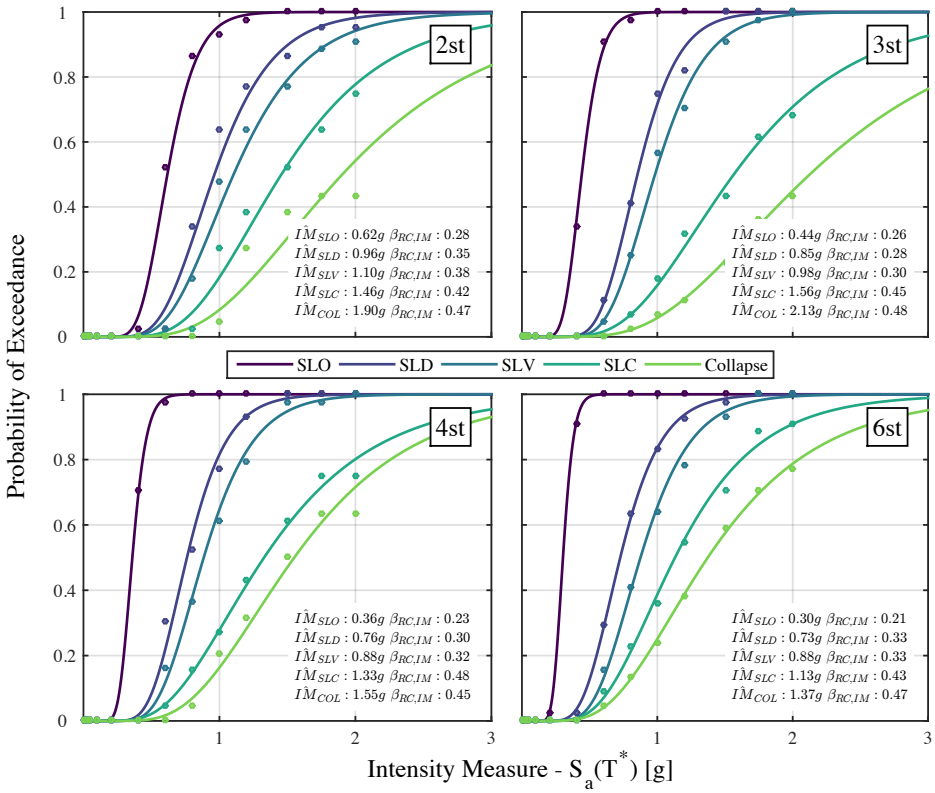

Figure A.16: Limit state fragility functions for the 2D case study frames with weak infill modelled with double diagonal struts.

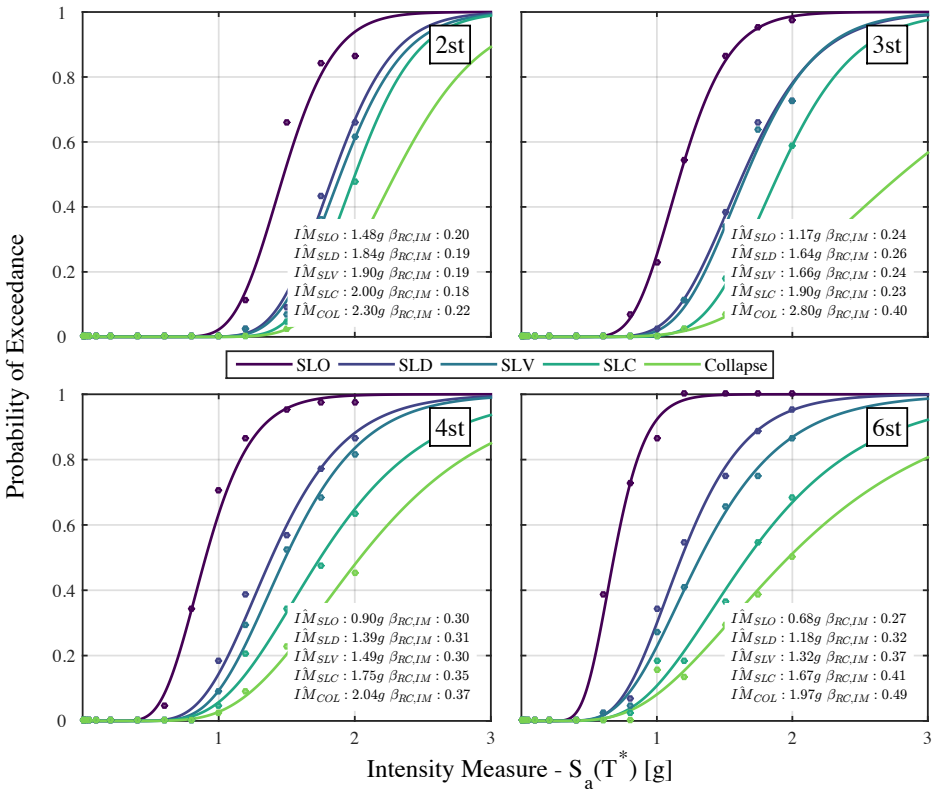

Figure A.17: Limit state fragility functions for the 2D case study frames with strong infill modelled with single diagonal struts.

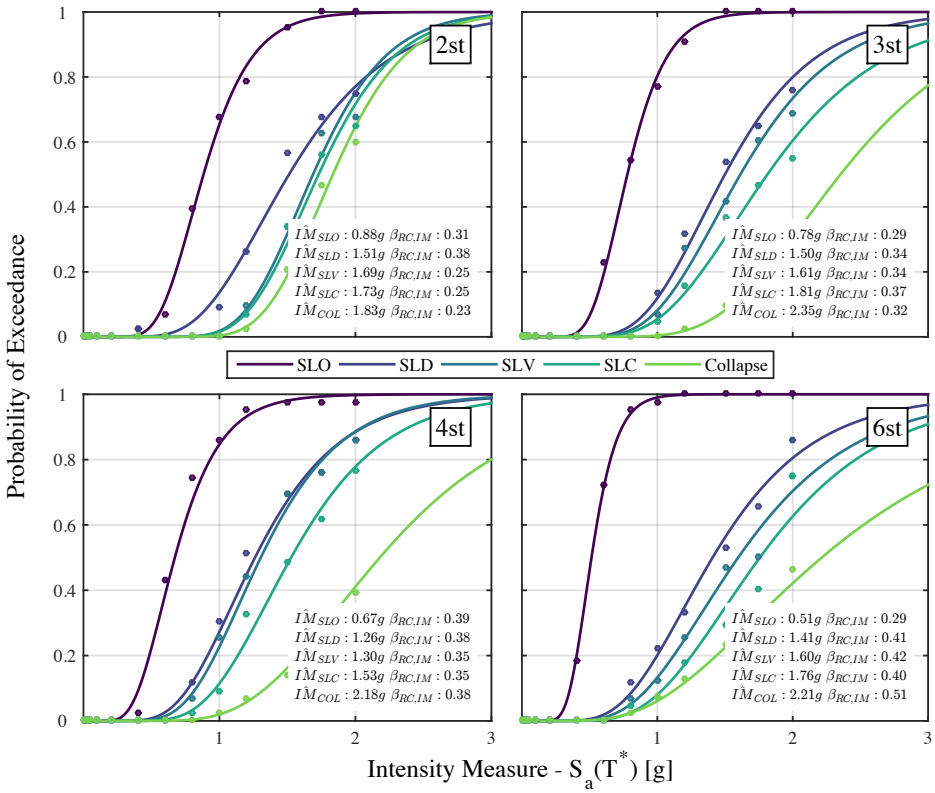

Figure A.18: Limit state fragility functions for the 2D case study frames with strong infill modelled with double diagonal struts.